Air Quality

Edited by Ashok Kumar

Air Quality

edited by
Ashok Kumar

Notice

Statements and opinions expressed in the chapters are these of the individual contributors and not necessarily those of the editors or publisher. No responsibility is accepted for the accuracy of information contained in the published chapters. The publisher assumes no responsibility for any damage or injury to persons or property arising out of the use of any materials, instructions, methods or ideas contained in the book.

We are IntechOpen,
the world's leading publisher of Open Access books
Built by scientists, for scientists

4,200+
Open access books available

116,000+
International authors and editors

125M+
Downloads

151
Countries delivered to

Our authors are among the
Top 1%
most cited scientists

12.2%
Contributors from top 500 universities

CLARIVATE ANALYTICS
BOOK CITATION INDEX
INDEXED

WEB OF SCIENCE™

Selection of our books indexed in the Book Citation Index
in Web of Science™ Core Collection (BKCI)

Interested in publishing with us?
Contact book.department@intechopen.com

Numbers displayed above are based on latest data collected.
For more information visit www.intechopen.com

Meet the editor

Prof. A. Kumar obtained his M. Tech and Ph.D. degree from IIT, Kanpur in Material Science. He had done masters in Physics with Electronics as specialization from Meerut University. His research interest involve Materials Science/Condensed Matter Physics: Polymer Electrolytes and Conducting Polymers. He has been a faculty member of the department of physics since 1999.

Contents

Preface

Air pollution is about five decades or so old field and continues to be a global concern. Therefore, the governments around the world are involved in managing air quality in their countries for the welfare of their citizens. The management of air pollution involves understanding air pollution sources, monitoring of contaminants, modeling air quality, performing laboratory experiments, the use of satellite images for quantifying air quality levels, indoor air pollution, and elimination of contaminants through control. Research activities are being performed on every aspect of air pollution throughout the world in order to respond to public concerns. There are many books that are available on the subject of air pollution. Some books are directed toward undergraduate students, and others are written for environmental professionals and graduate students. This book will be helpful for the second group – professionals and graduate students. Most of the chapters are based upon the ongoing research in the field of air pollution. Some topics are more important to professionals than others, because of their need for information. The book chapters were invited by the publisher on the above topics. The book is grouped in five different sections. Some topics are more detailed than others. The readers should be aware that multi-authored books have difficulty maintaining consistency. A reader will find, however, that each chapter is intellectually stimulating.

The first chapter discusses the sources of anthropogenic air pollution and points out that number of sources are increasing with the rise in population and the growing demand for energy. A brief discussion on air pollution technologies to reduce emission of gaseous pollutants is also given.

The chapters 2 through 6 focus on the difficult task of monitoring air pollutants. Ambient monitoring, satellite monitoring, online monitoring, and biological monitoring are discussed in this section of the book. The multi-pollutant planning procedure for designing an urban air quality monitoring system is given in chapter 2. A new method to design or optimize air quality networks is discussed in chapter 3. The procedure is based on four steps: preliminary evaluation, sampling campaigns, spatial interpolation, and selection of best locations.

A case study to investigate monitoring of spatial and temporal distribution patterns of aerosols in southern Ontario, Canada is discussed in chapter 4. In the age of information technology, it is important to update a monitoring system using the latest technologies. Chapter 5 discusses the use of online monitoring of air pollution concentrations. Active bio-monitoring using moss bags and tree leaves is discussed in chapter 6 for detecting trace elements and radionuclides.

The next section covers four topics related to modeling. Chapter 7 provides the application of receptor models and scanning electron microscopy (SEM) to establish the relationship between ambient air quality and pollutant sources. Another interesting chapter explains the procedure for estimating uncertainty in predicting ground level concentrations using the

equations from the US EPA's model. The concept of ventilation efficiency used in indoor air quality work is applied in order to understand the magnitude of urban air pollution problem. An overview of nonlocal atmospheric boundary layer mixing schemes developed in the last two decades to describe vertical mixing during convective condition is given in chapter 10.

Various air quality data collection methods and associated analyses are discussed in chapters 11 to 13 of this book. Chapter 11 will be helpful for those who are involved in analyzing air quality data for a plant located near a coast or lakeshore. This chapter provides information on collecting data and using models and synoptic weather maps in order to draw conclusions. Analysis of data collected in an outdoor smog chamber, to understand the formation of secondary organic particles from a mixture of volatile organic compounds is given in chapter 12. The next chapter discusses methods to use satellite images to determine the concentration of particulate matter less than 10 microns.

The last part of the book deals with indoor air pollution. The chapter 14 reviews general and local thermal comfort models for controlling indoor ambiences. The author argues the benefits of using new heating, ventilation and air conditioning (HVAC) systems based on their simulations. A new methodology for controlling HVAC systems is discussed in chapter 15. The focus of this study is to lessen the number of unhappy workers and reduce energy consumption. A case history for an automobile assembly plant for studying the indoor air quality and heat stress is given in chapter 16. The last chapter deals with the issue of fungi in medical indoor environments. An outline for preventing and controlling fungal diseases is also given.

Note that all the chapters have been prepared by individuals who are experts in their field. The views expressed in the book are those of the authors and they are responsible for their statements. Efforts have been made to check the accuracy of each chapter by the authors through several iterations. In conclusion, the editor, publisher, and hard-working air quality professionals have put together an air quality book that could be used as a reference book in coming years. Our goal was to provide current information and present a reasonable analysis of air quality data compiled by knowledgeable professionals in the field of air pollution.

Editor

Ashok Kumar
*Department of Civil Engineering, The University of Toledo,
Toledo, OH 43606*

Anthropogenic air pollution sources

Francisc Popescu and Ioana Ionel
University "Politehnica" from Timisoara
Romania

1. Introduction

What one experiences today as atmosphere is a transient snapshot and result of its evolutionary history. Much of the development and present status was explained based both on scientific knowledge, and combined with established facts, even speculation. The planet Earth was formed around 4600 million years ago by the gravitational accretion of relatively small rocks and dust, within the solar nebula. The first evidence of single-celled life, for which tiny oxygen concentration was an essential prerequisite, is shown in the fossil record from around 3000 million years ago. Subsequently, the process of respiration led to a gradual increase in the atmospheric oxygen concentration. This in turn allowed the development of O_3 which is thought to have been a necessary shield against solar UV. Subsequent evolution of the atmosphere has been dominated by the balance between production and consumption of both CO_2 and O_2 (Colls, 2002).

Presently the lower part of the atmosphere is known as *air* and is formed by mainly nitrogen, oxygen and other gases, trace gases and particles. The composition, even if is suspected to major changes, is under the influence of the man kind evolution, both in terms of population number growth, as in industrial and agricultural and household development (in one word civilization). The energy consumption and technical evolution related to these sources is one main cause of the man made pollution, causing modification of the air quality, above limits, stipulated generously in legislation, adapted and modified according the to the level of knowledge, permanently. These anthropogenic pollution sources are exhausting diverse specific species to the free atmosphere and are stressing over the limit the natural possibility of the ecosystem to adapt or to cover these caused concentration augmentation. One has to notice that all the man made sources (from industry, agriculture, transportation, household sources, etc.) are contributing to the air quality level in addition to the natural sources, that existed since the Earth was created and in direct dependence to it.

The population reached presently over 6 billion, is now forecast to reach 7.5 billion by 2020 and will be stabilize at approx. 9 billion by 2050. 90% of the future growth will occur in developing countries, and most of that will be concentrated in urban areas.

By their nature, the air pollution sources can be classified, mainly, as physical, chemical and biological sources, secondly as natural and anthropogenic sources, further on climate change relevant or not. The physical pollution of the atmosphere is a consequence energy input like sound and heat energy. The most relevant physical pollution sources are the direct thermal pollution, natural or anthropogenic. The local climate is changed by heat

(caloric input) generated by industry, household, agricultural and transportation and the air from the lower atmosphere will have an increased local temperature. The indirect thermal pollution is a consequence of greenhouse effect and takes place in the troposphere and is linked to chemical anthropogenic pollution and its evolution in reference to the greenhouse gases.

The chemical pollution of the atmosphere is a consequence of the chemical compounds input, over the natural air constituents and is of natural and artificial origin. However, the natural chemical pollution sources like volcanoes eruption, natural decomposition of organic substances or fire (naturally occurred) are not of major concern as they are part of natural environment equilibrium. However, the anthropogenic chemical pollution is of major concern as their sources are increasing in number and concentration with the increase of global human population and our continuously increase of energy demand.

The anthropogenic chemical pollution has no borders and no matter where the pollutants are released into the atmosphere will have an impact over global environment. The most relevant sources are the incineration of fossil fuels to produce energy (heat and electricity), major industrial processes (like metallurgy industry or cement/construction industry) and transportation. We will classify the anthropogenic chemical pollution sources into two major groups: stationary and mobile sources.

In the chapter one will bring to attention main stationary and mobile sources of anthropogenic chemical pollution, on their causes and formation and not at least on measures to reduce their emissions. The main possibilities to reduce pollution level by correct and active measures, from which most are related to economy and balanced efficient energy use, are also presented.

The four major groups of gaseous air pollutants by historical importance, concentration, and overall effects on plants and animals (including people), are sulphur dioxide (SO_2), oxides of nitrogen (NOx: NO, NO_2), carbon dioxide (CO_2) and ozone (O_3). Sulphur dioxide and nitric oxide (NO) are primary pollutants – they are emitted directly from sources. We shall start by looking at the main sources of these and other primary gases, and also consider some of the methods of control that can be used to reduce emissions and concentrations when required.

The most important groups of anthropogenic air pollution sources are defined by industrial processed, residential heating systems, transportation (terrestrial, naval and aerial) and agricultural systems.

The majority of the pollutants are the direct result of the combustion process in large power plants and piston engines so that the first steps to reduce the pollutants concentration from atmosphere is to control and reduce the emissions from those source groups.

In this chapter we will deal mainly with the pollutants generated from combustion processes in large boilers and piston engines, as a result of the combustion process of fossil fuels.

In the ideal case the combustion process is complete (perfect) and the exhaust gazes are formed only from CO_2 and H_2O. To achieve the complete combustion is necessary to obtain a combustion air-fuel ratio (different for each type of combustion chamber) constant into the whole combustion chamber and this is not possible due to limitations is the construction of the combustion chamber. In figure 1 a short and simplified relation between fuel, combustion, combustion products (pollutants) and air quality is given.
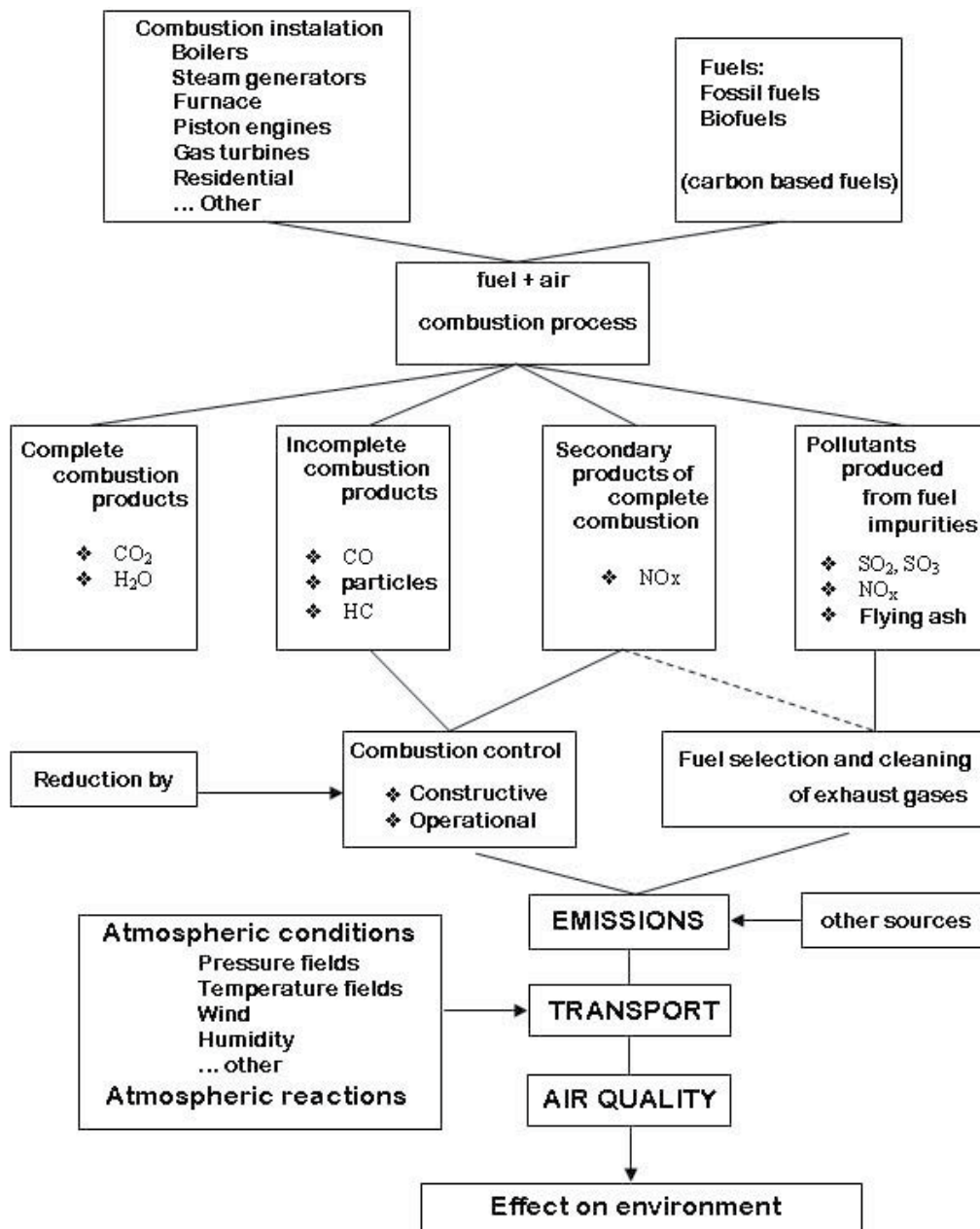
Fig. 1. Sources and products of anthropogenic pollution.

The fossil fuels, solid, liquid or gaseous, are mainly formed by carbon and hydrogen in various ratios. During the combustion of this fuels the carbon and hydrogen reacts with oxygen to form carbon dioxide and water. Due to incomplete combustion or other substances included in fuels, like nitrogen, sulphur, organic compounds, heavy metals and other compounds, besides CO_2 and H_2O other chemical compounds will be formed,

compounds that are dangerous both to humans and environment if their concentrations in ambient air exceeds supportability limits. Equation 1 shows the products of complete combustions of an ideal fuel formed only from carbon and hydrogen.

$$C_n H_m + \left(n + \frac{m}{4} \right) O_2 \rightarrow n CO_2 + \frac{m}{2} H_2 O \qquad 1)$$
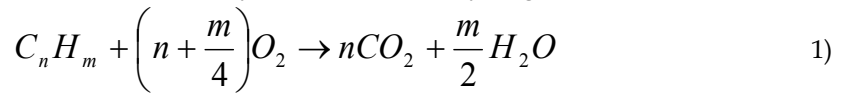
From an ecological point of view we can distinguish between several types of air pollutants, depending on how they affect the ecosystem (Ionel, 2006):

- pollutants that will have a direct impact on human health, like nitrogen oxides (NOx), carbon monoxide (CO), sulphur oxides (SO$_2$) or volatile organic carbon (VOC);
- pollutants with direct impact on vegetation, like nitrogen oxides (NOx), sulphur oxides (SO$_2$) and chemical compounds of chlorine and hydrogen;
- pollutants that will form acids, like (NOx) and sulphur oxides (SO$_2$), especially when they are found in high concentrations and in same time into a humid atmosphere;
- persistent pollutants with a long life cycle and accumulated in soil and by the transfer thru biological plant-animal-human chain or accumulations in human body will have serious consequences on human health;
- pollutants with direct influence over climate, like carbon dioxide (CO$_2$) and methane (CH$_4$) with major impact on global warming issues.

There are many other atmospheric pollutants with anthropogenic origin but those listed above are of higher relevance for us and will be dealt in the next pages.

2. Carbon monoxide (CO)

Carbon monoxide is an odorless, colorless and toxic gas. Because it is impossible to see, taste or smell the toxic fumes, CO can kill you before you are aware it is in your home. At lower levels of exposure, CO causes mild effects that are often mistaken for the flu. These symptoms include headaches, dizziness, disorientation, nausea and fatigue. The effects of CO exposure can vary greatly from person to person depending on age, overall health and the concentration and length of exposure.

Carbon monoxide is mainly produced as an intermediary product of combustion processes in piston engines and boilers. The oxidation of CO into CO$_2$ requires a temperature of minimum 990 K and a sufficient stationary time into the combustion chamber. If the combustion temperature is not high enough or uniform inside the combustion chamber, when the exhaust gases are evacuated some CO will not oxidize. The dependency between some pollutants and oxygen content of fuel mixture and excess air ration is given in figure 2. Ambient CO concentrations in metropolitan areas are orders of magnitude higher than background. These levels are primarily associated with transportation emissions and are closely related to traffic density and meteorological conditions. Highest concentrations occur along major traffic arteries during morning and evening rush hours and decrease relatively rapidly with distance from roadways. Peak levels averaged over 1 h vary from about 5 to more than 10 ppmv in some cities. Elevated CO levels tend to plague cities that have high traffic densities and are located at relatively high altitudes. (Godish, 2004)

CO concentrations are significantly and more important than regulatory concerns would indicate. Carbon monoxide affects tropospheric concentrations of both hydroxyl radical (OH-) and O3 and, as a consequence, the oxidizing potential of the atmosphere. Because CO

and CH_4 (a major greenhouse gas) compete for OH-, CO indirectly affects tropospheric concentrations of CH_4 and stratospheric H_2O vapor (derived from CH_4 oxidation).
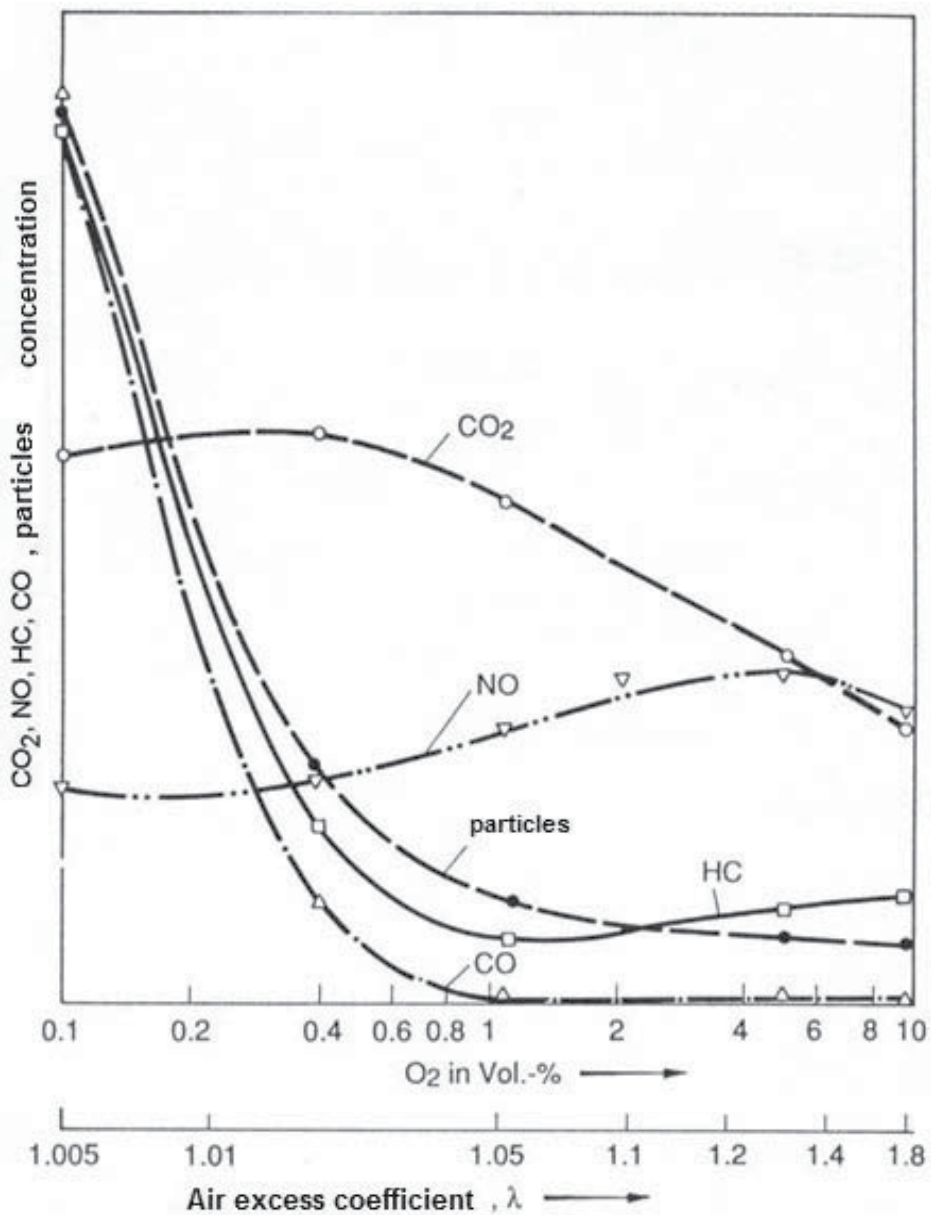
Fig. 2. Dependency of some pollutants to air-fuel ration value inside the combustion chamber

In figure 3 the contribution of key categories to EU-27 emissions of carbon monoxide are presented for year 2006 (EEA, 2008) and in figure 4 the sources of CO emissions, by sector,

for USA in 2005 (US-EPA, 2005). A very important issue is that in the EU-27, emissions of CO decreased by just over 53 % between 1990 and 2006. Decreased emissions were reported in all Member States except Romania. The largest absolute decreases were reported by France, Germany, Italy, Poland, Spain and the United Kingdom; however, these countries remained the largest emitters of CO in absolute terms in 2006. (EEA, 2008)
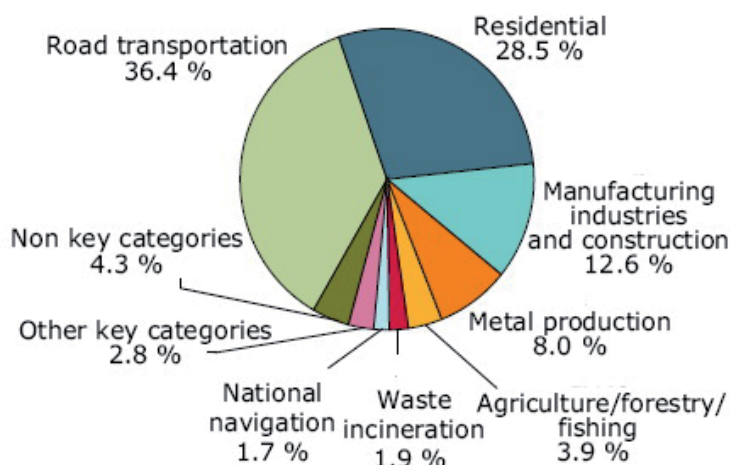
Fig. 3. EU-27 emission sources of carbon monoxide, 2006 (EEA, 2008).
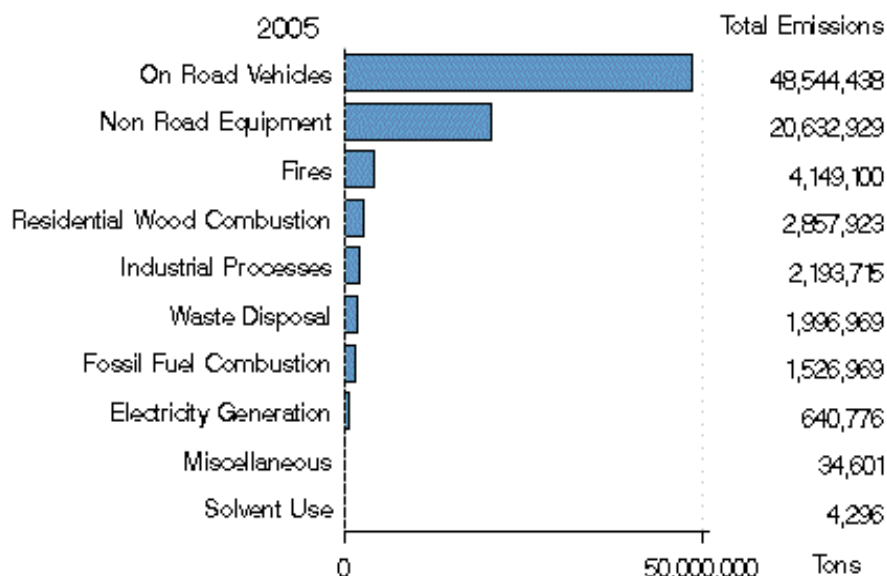
Fig. 4. USA emission sources of carbon monoxide, 2005 (US EPA, 2009).

Carbon monoxide is oxidized in the atmosphere to CO_2 on reaction with OH- radicals:
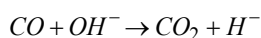
$$CO + OH^- \rightarrow CO_2 + H^-$$ 2)

Subsequent reactions of H- and oxygen O_2 produce the highly reactive hydroperoxyl radical, HO_2-:

$$H^- + O_2 + M \rightarrow HO_2^- + M \qquad\qquad 3)$$

where M is an energy-absorbing molecule, e.g., nitrogen N_2 or O_2. From those to reactions we can conclude:

$$CO + H^- + O_2 \rightarrow CO_2 + HO_2^- \qquad\qquad 4)$$

In the presence of photons of light energy another reaction will occur:

$$CO + O_2 + hv \rightarrow CO_2 + O_3 \qquad\qquad 5)$$

where O_2 is ground-state atomic oxygen and hv is a photon of light energy.
As a result of these reactions, CO is converted to CO_2, with one molecule of O_3 produced for each CO molecule oxidized. As such, CO oxidation in the troposphere is an important (but low-level) source of O_3.

The effects of carbon monoxide on human health are caused due to the fact that CO enters the bloodstream through the lungs and attaches to hemoglobin (Hb), the body's oxygen carrier, forming carboxyhemoglobin (COHb) and thereby reducing oxygen (O_2) delivery to the body's organs and tissues. High COHb concentrations are poisonous. Central nervous system (CNS) effects in individuals suffering acute CO poisoning cover a wide range, depending on severity of exposure: headache, dizziness, weakness, nausea, vomiting, disorientation, confusion, collapse, and coma. At lower concentrations, CNS effects include reduction in visual perception, manual dexterity, learning, driving performance, and attention level. Earlier work is frequently cited to justify the statement that CO exposure sufficient to produce COHb levels of ca. 5% would be sufficient to produce visual sensitivity reduction and various neurobehavioral performance deficits. In a recent literature re-evaluation, however, the best estimate was that (COHb) would have to rise to 15-20% before a 10% reduction in any behavioral or visual measurement could be observed. (Raub, 2002)
Carbon monoxide (CO) may be the cause of more than one-half of the fatal poisonings reported in many countries: fatal cases also are grossly under-reported or misdiagnosed by medical professionals. Therefore, the precise number of individuals who have suffered from CO intoxication is not known.
In conclusion, CO poisoning occurs frequently; has severe consequences, including immediate death involves complications and often is overlooked. Efforts in prevention and in public and medical education should be encouraged. (Raub, 2002)

3. Nitrogen oxides (NOx)

Nitrous oxide concentrations in the atmosphere have been increasing steadily since preindustrial times, from ~280 to ~320 ppbv today. Estimated annual emissions to the atmosphere are 13.8 Tg (tetragrams) N/year, with ~70% being produced by nitrification and denitrification processes in undisturbed terrestrial environments and the world's oceans. About 3 Tg N/year, or ~8%, is associated with agricultural tillage, fertilizer use, and animal wastes.

In case of combustion equipments the NOx are formed during the combustion process at high temperatures by the oxidation of nitrogen content of fuel and combustion air. In a first phase only NO is formed while the NO_2 is mainly formed after the combustion in exhaust process when more O_2 is present and into the atmosphere.

The main anthropogenic sources of nitrogen oxides are road transport and public electricity and heat sector. In figure 5 the contribution of key categories to EU-27 emissions of nitrogen oxides are presented for year 2006 (EEA, 2008) and in figure 6 the sources of NOx emissions, by sector, for USA in 2005 (US-EPA, 2005).
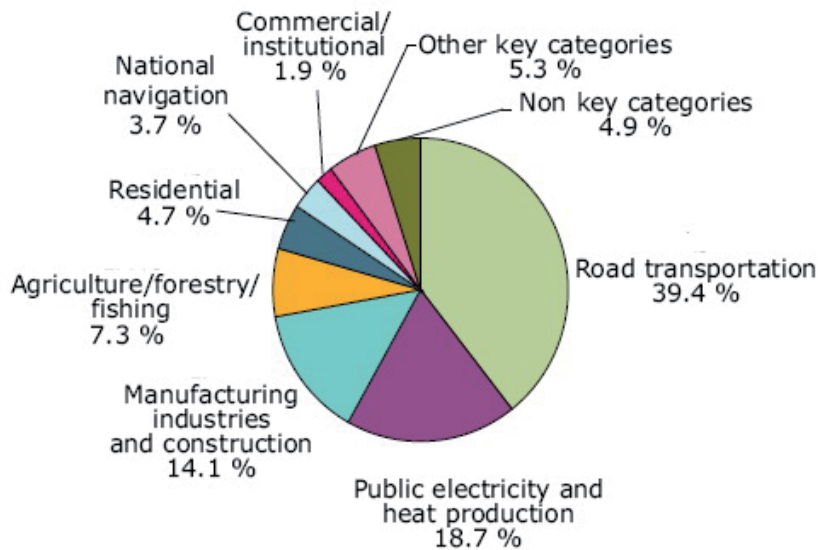

Fig. 5. EU-27 emission sources of nitrogen oxides, 2006 (EEA, 2008).
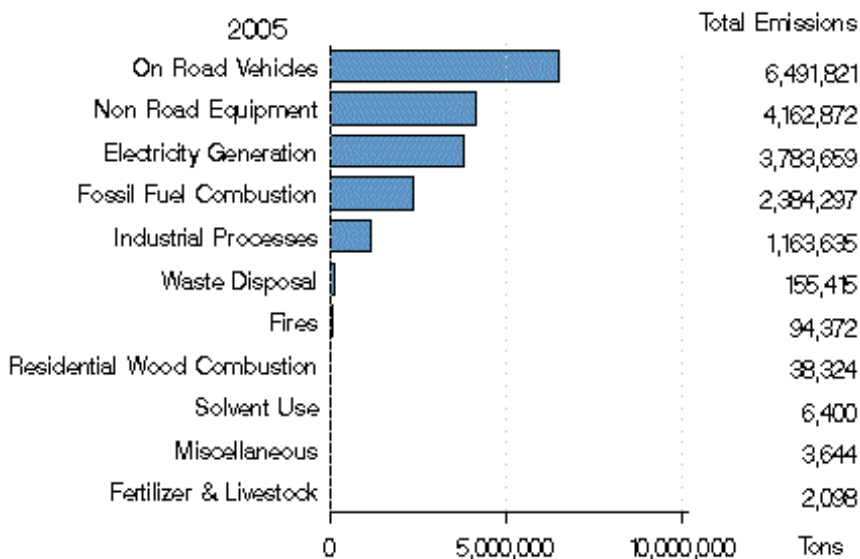
Fig. 6. USA emission sources of nitrogen oxides, 2005 (US EPA, 2009).

Between 1990 and 2006, NO_X emissions decreased in the EU-27 by 35 %. The change of total NOx emissions between 2005 and 2006 was rather small, a decrease of 1.8 %, mainly caused by reductions achieved in Germany, Italy and the United Kingdom. (EEA, 2008)

Increased atmospheric N_2O levels pose two major environmental concerns: stratospheric O_3 depletion and, because of its thermal absorptivity, global warming.

In case of combustions formed nitric oxides three mechanism are present: Thermal mechanism, the prompt mechanism and NOx formation from fuel nitrogen.

3.1. Thermal mechanism of nitrogen oxide formation

The thermal mechanism of nitric oxide formation during combustion was first studied by Zeldovici. The thermal mechanism occurs in combustion chamber in areas with higher oxygen concentration or in exhaust gases when nitrogen reacts with free oxygen atoms.

In areas when the combustion flame has high oxygen content the following reactions take place:

$$O + N_2 \rightarrow NO + N \qquad\qquad 6)$$

$$N + O_2 \rightarrow NO + O \qquad\qquad 7)$$
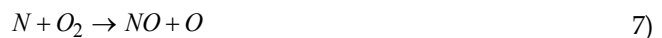
In areas with rich fuel content and at temperatures over 1300 °C another reaction is more probable:

$$N + OH \rightarrow NO + H \qquad\qquad 8)$$

The quantities of nitric oxides produced thru this mechanism are influenced by numerous factor but most relevant are:

- air-fuel excess ration factor (λ);
- combustion temperature;
- air-fuel mixture residence time in combustion chamber areas with high temperatures.

Figure 7 gives an image on how temperature and residence time influences the NO formation during combustion process.

In the case of combustion in steam generators from large power plants, in installation where the ash is evacuated in dry state (particles) the contribution of thermal NOx mechanism to total NOx formation is up to 20%. For installations where ash is evacuated in liquid state the thermal NOx contribution is up to 50%.

In case of piston engines, gas turbines or in any other combustion process at high temperature rate the thermal NOx mechanism is responsible for ~ 50% of total concentrations of NOx exhausted. In these cases a very important role plays the air-fuel ratio (λ). As seen in figure 7, if air-fuel ration is lower then 1 the formation of NO decreases.

3.2. Prompt NO mechanism

In areas where the combustion take place with low oxygen content nitric oxide can be formed by reactions between molecular nitrogen N_2 and radicals like CH and CN. This phenomenon was first discovered by Fenimore. It is widely accepted that reactions described bellow are responsible for NO formation by prompt NOx mechanism.

The majority of scientists agree that the prompt mechanism of NO formation can be neglected because the atomic nitrogen and CN radicals can only be formed in areas with very low air-fuel ratios.

$$CH + N_2 \rightarrow HCN + N \tag{8}$$
$$C + N_2 \rightarrow CN + N \tag{9}$$
$$CN + H_2 \rightarrow HCN + H \tag{10}$$
$$CN + H_2O \rightarrow HCN + OH \tag{11}$$
$$HCN(CN) + O \rightarrow NO + R \tag{12}$$
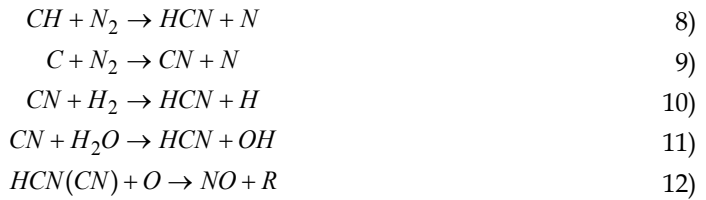
where R is an organic residue.
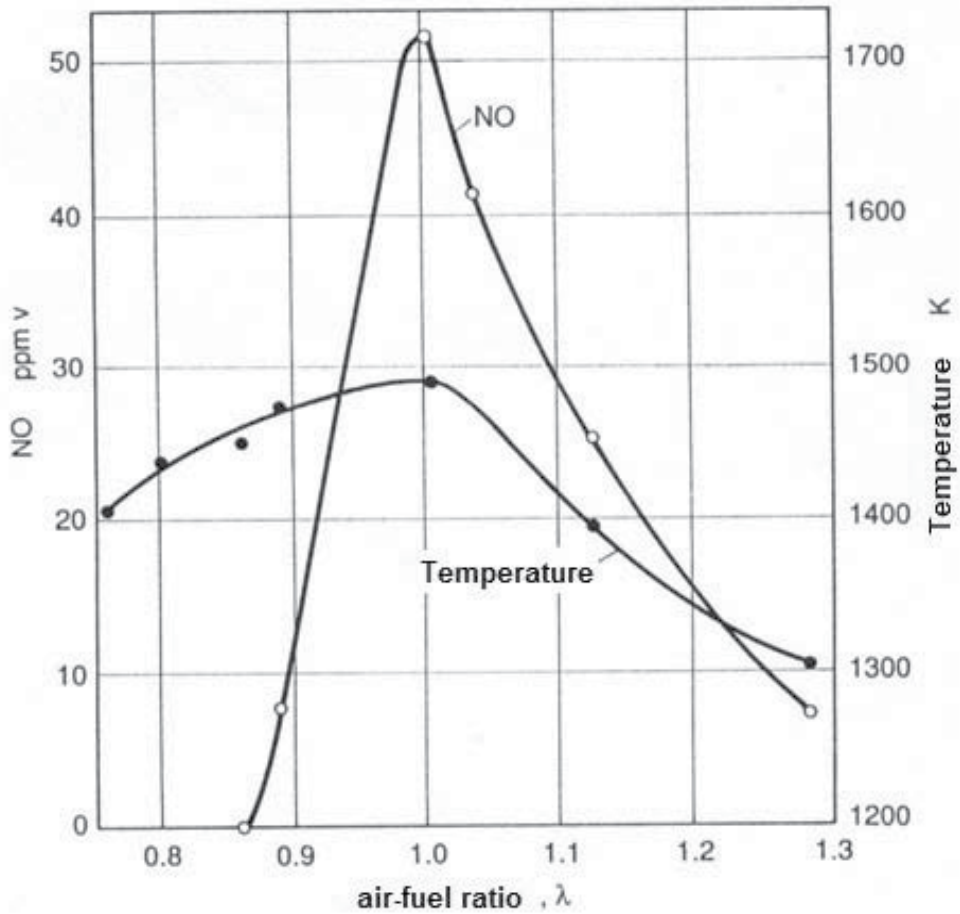
Fig. 7. Dependency between formed NO and combustion temperature and air-fuel ration (λ)

3.3. Fuel NO mechanism

The fuel NOx mechanism is also a flame based one but is more complex then prompt and thermal NOx mechanisms and partially unknown. However, it is known that first CN radicals are formed and their evolution in the presence of oxygen leads to NO formation.

The decisive factors in fuel NOx mechanism are nitrogen content of fuel, oxygen concentration in combustion flame, reaction time and flame temperature.

The thermal NOx mechanism is much slower then prompt mechanism and the fuel NOx mechanism is faster then thermal NOx.

The sources of nitrogen fuel content are mainly the decay of proteins and nucleic acid from fossil material, mainly the aliphatic compounds as first, secondary and tertiary amines (RNH_2, R_1R_2NH, $R_1R_2R_3N$) or aromatic compound like pyridine (C_5H_5N).

The complicated mechanism of fuel NOx formation can be synthesized as follows (Baumbach, 1992):

$$fuel\ N \rightarrow HCN \rightarrow NCO \rightarrow NH_i \begin{array}{l} \rightarrow\ NO \\ \rightarrow\ N_2 \\ \rightarrow\ NO \\ \rightarrow\ N_2 \end{array} \qquad N$$

13)
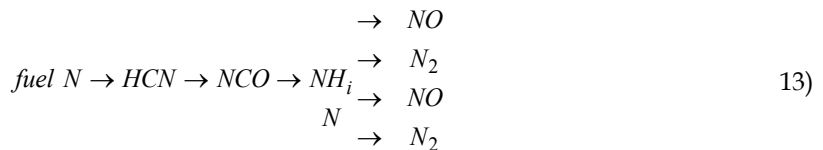
Figure 8 gives an image of the NOx formation mechanisms to combustion temperature.
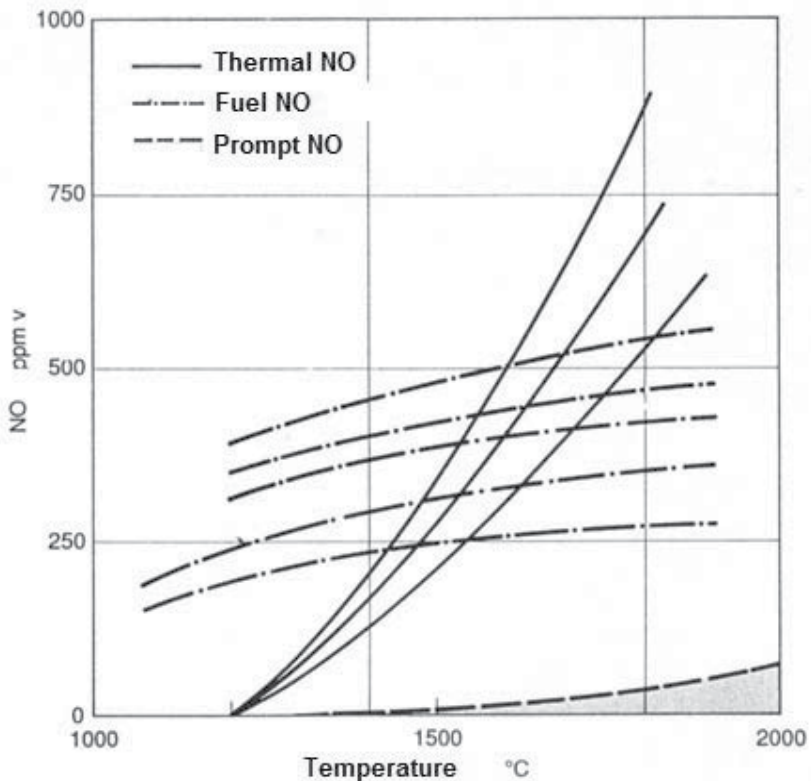
Fig. 8. Dependency between NO formation mechanisms and combustion temperature.

Into exhaust gases the nitric oxides consists only in nitrogen oxide (NO). The oxidation of NO to NO_2 occurs partially in flue gases exhaust channels and in atmosphere, most important reactions are:

$$2NO + O_2 \rightarrow 2NO_2$$

14)

$$NO + O_3 \rightarrow NO_2 + O_2 \qquad \qquad 15)$$

Another important reaction is the one that oxidize NO_2 into nitric acid HNO_3 in gaseous phase, because is a major contributor to acid rain by its diffusion in water droplets.

$$NO_2 + OH + M \rightarrow HNO_3 + M \qquad \qquad 16)$$

where M is a passive reaction partner.

4. Sulphur oxides (SOx)

All fossil fuels contain sulphur, most of which is released as sulphur dioxide during combustion. Almost all the anthropogenic sulphur contribution is due to fossil fuel combustion. Different fuels offer a wide range of sulphur contents (Colls, 2002):

- Oil and its by-products contain between 0.1% sulphur (paraffin) and 3% (heavy fuel oil) in the form of sulphides and thiols. Petrol contains negligible sulphur in the context of overall mass emissions, although there can be an odor problem from conversion to hydrogen sulphide (H_2S) on catalytic converters.
- Coal contains 0.1–4% sulphur, mainly as flakes of iron pyrites (FeS_2). The average sulphur content of European coal reservoirs is 1.7%.
- Natural gas (mainly methane, CH_4) can be up to 40% H_2S when it is extracted from the well. The sulphur is taken out very efficiently at a chemical processing plant before distribution, so natural gas is effectively sulphur free.

Global sulphur dioxide emissions are estimated to have increased from 4 Mt (containing 2 Mt of sulphur) in 1860 to 150 Mt in 1990. The emissions from the US and Europe increased steadily until the 1970s before coming under control. Sulphur emissions from the faster-growing Asian region have continued to increase, due largely to coal combustion. Emissions from China are now comparable to those from the US, and in 1990 emissions from China, US and Russia accounted for over half the global total.

The EU-27 total SO_X emissions in 2006 were 7 946 Gg. This is almost a 70 % reduction compared to the level of emissions reported in 1990. Since 1990, SO_X emissions have increased in only two Member States: Romania (21.9 %) and Greece (11.9 %). Inspection of the time-series trends for some Member States shows some step changes in emission reductions have occurred since 1990. For example, emissions of SO_2 in Slovenia fell considerably in 2001 and again in 2005 due to the introduction of flue gas desulphurization abatement equipment in thermal power plants.

In figure 9 the contribution of key categories to EU-27 emissions of sulphur oxides are presented for year 2006 (EEA, 2008) and in figure 10 the sources of SOx emissions, by sector, for USA in 2005 (US-EPA, 2005).

The natural sources are now heavily outweighed by human ones, principally fossil fuel combustion. Since 90% of the biogenic emission is as dimethyl sulphide, and an even higher proportion of the human emission is as SO_2, we have a clear demarcation between the source types. Since most of the dimethyl sulphide comes from oceans in the southern hemisphere, and most of the human SO_2 from fossil fuel emissions in the northern hemisphere, we also have a geographical split.
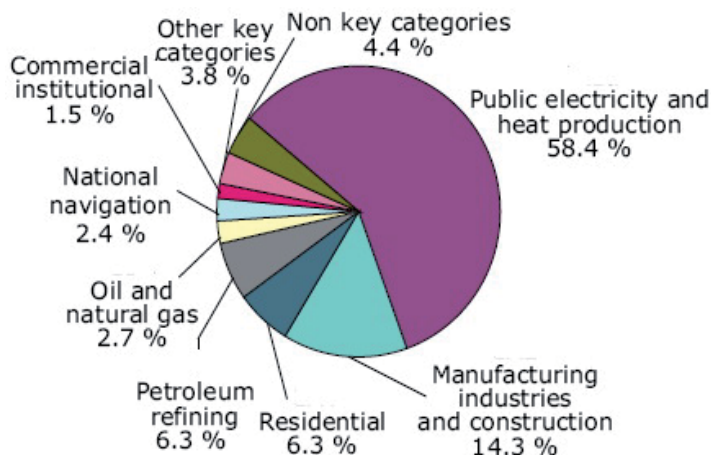
Fig. 9. EU-27 emission sources of sulphur oxides, 2006 (EEA, 2008).
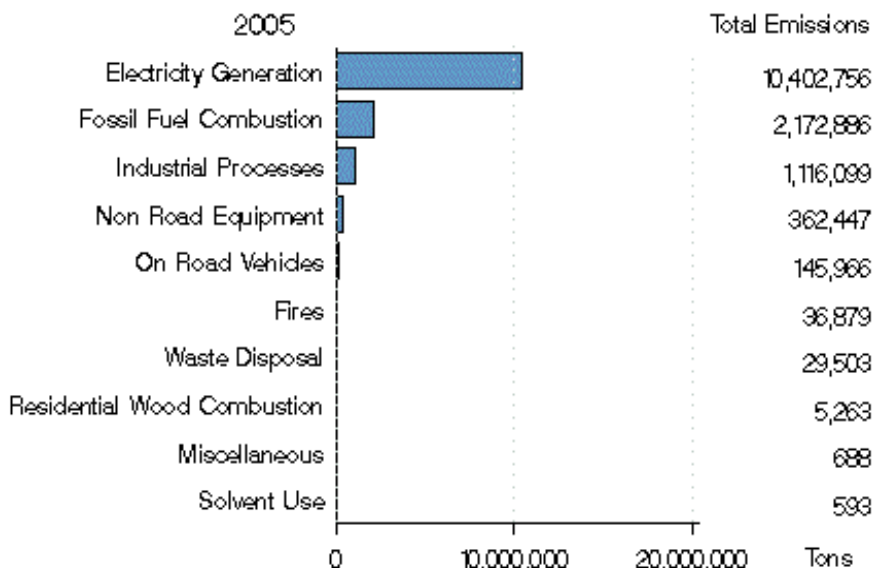
Fig. 10. USA emission sources of sulphur oxides, 2005 (US EPA, 2009).

Anthropogenic SO_2 is almost exclusively formed during the combustion of fossil fuels with relevant sulphur content and most important is coal because the sulfur content of liquid and gaseous fossil fuels can be easily removed before combustion.

If the sulphur content of the fuel is totally combusted SO_2 is formed thru the reaction:

$$CH_3 - SH + 3O_2 \rightarrow SO_2 + CO_2 + 2H_2O \qquad\qquad 17)$$
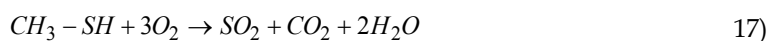
During the incomplete combustion with lack of oxygen elementary sulphur and hydrogen sulphide (H_2S) can form, at high temperatures.

$$CH_3 - SH + 0.5O_2 \rightarrow H_2S + HCHO \tag{18}$$

$$2H_2S + O_2 \rightarrow 2H_2O + 2S \tag{19}$$
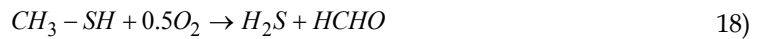
Hydrogen sulphide (H_2S) can occur during the combustion process of low quality coals like lignite or into the piston engines exhaust gases after catalytic reduction if the engine works at high load and low air-fuel ratio.

During the combustion and in exhaust channels the SO_2 can be oxidized to SO_3 who will form with water content of flue gases sulphuric acid H_2SO_4. The SO_2 conversion to SO_3 is increased in the presence of vanadium of iron oxides at temperatures over 800 °C.

Evacuated into the atmosphere SO_2 reacts in proportion of (1 – 2) ‰/hour with oxygen, under the presence of ultraviolet radiation (uvr) and will form SO_3.

$$2SO_2 + O_2 + uvr \rightarrow 2SO_3 \tag{20}$$

Afterwards, the SO_3 will react with water vapors from the atmosphere to form sulphuric acid H_2SO_4. In periods of fog or days with high humidity the transformation rate of SO_3 to H_2SO_4 can be up to 15 %.

$$SO_3 + H_2O \rightarrow H_2SO_4 \tag{21}$$

Figure 11 is an illustrated view of some atmospheric reactions for SO_2 and the historical evolutions of SO_2 emissions into air.
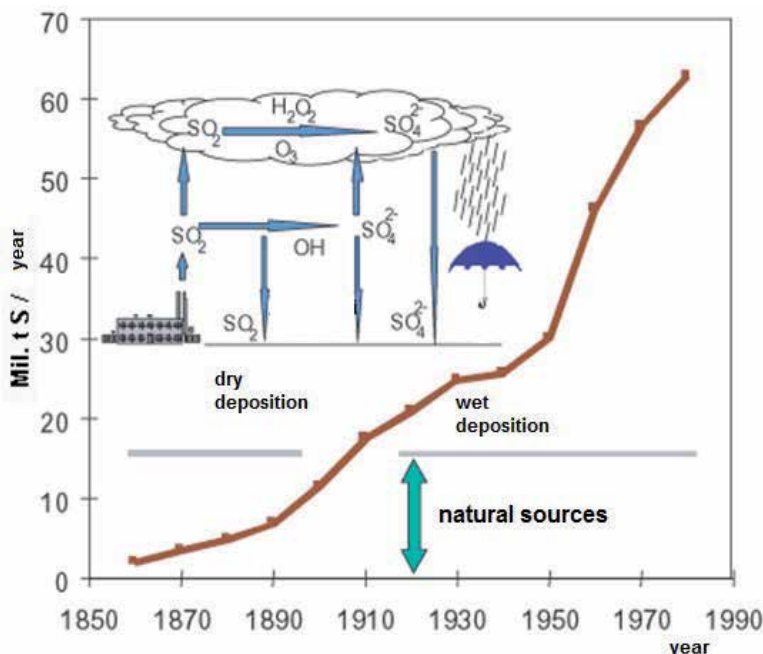
Fig. 11. SO_2 atmospheric reaction and historical emissions. (Popescu, 2009)

5. Particulate matter

Particulate matter is a collective term used to describe small solid and liquid particles that are present in the atmosphere over relatively brief (minutes) to extended periods of time (days to weeks). Individual particles vary in size, geometry, mass, concentration, chemical composition, and physical properties.

They may be produced naturally or as a direct or indirect result of human activities. Of major concern are particles < 10 μm because they can remain suspended in the atmosphere where (depending on actual particle size) they can settle out relatively slowly. Atmospheric aerosol is characterized by these relatively small particles. The formation and increase of atmospheric aerosol by both natural and anthropogenic sources is a major air quality concern because aerosol particles may scatter light, reducing visibility, pose an inhalation hazard to humans and animals, affect climate on a regional and global scale.

Particulate matter can be described as being primary or secondary, based on its origin and processes of formation. Primary particles are emitted directly into the atmosphere from a variety of natural and anthropogenic sources. The natural particle sources include volcanoes, forest fires, ocean spray, biologic sources and the anthropogenic sources of particles are transportation, fuel combustion in stationary sources, a variety of industrial processes, solid waste disposal and miscellaneous sources such as agricultural activities and fugitive emissions from roadways. Secondary particles are formed in the atmosphere as a result of chemical processes involving gases, aerosol particles, and moisture.

In figure 12 the contribution of key categories to EU-27 emissions of particle matter, PM10 fraction, are presented for year 2006 (EEA, 2008) and in figure 13 the sources of particle matter, PM10 fraction, by sector, for USA in 2005 (US-EPA, 2005).
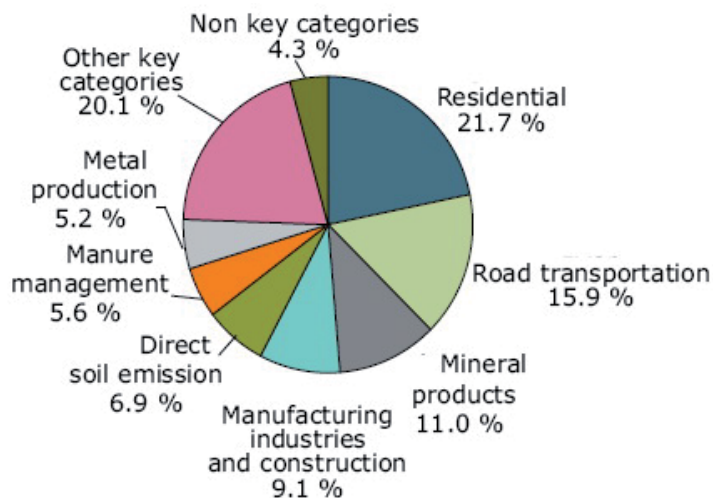
Fig. 12. EU-27 emission sources of PM10, 2006 (EEA, 2008).
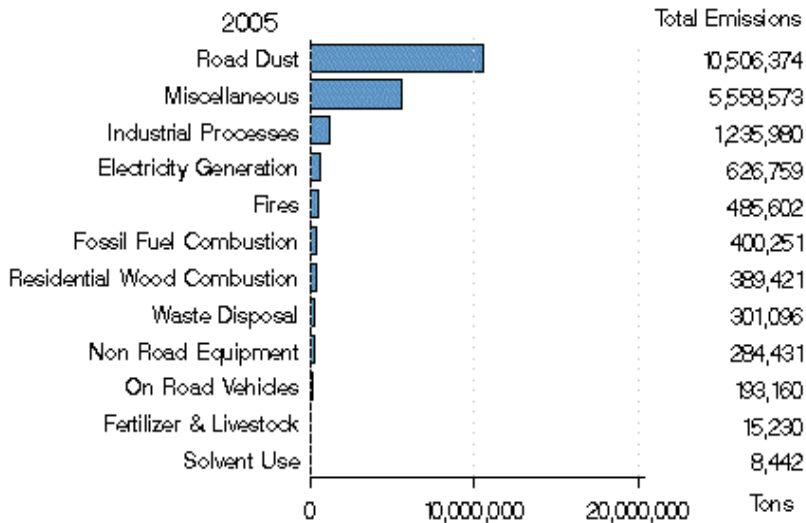
Fig. 13. USA emission sources of PM10, 2005 (US EPA, 2009).

In figure 14 the sources and diameter of representative particle matter fractions, thoracic (PM10), Respirable (PM4.0) and total suspended particles (TSP) are synthesized.
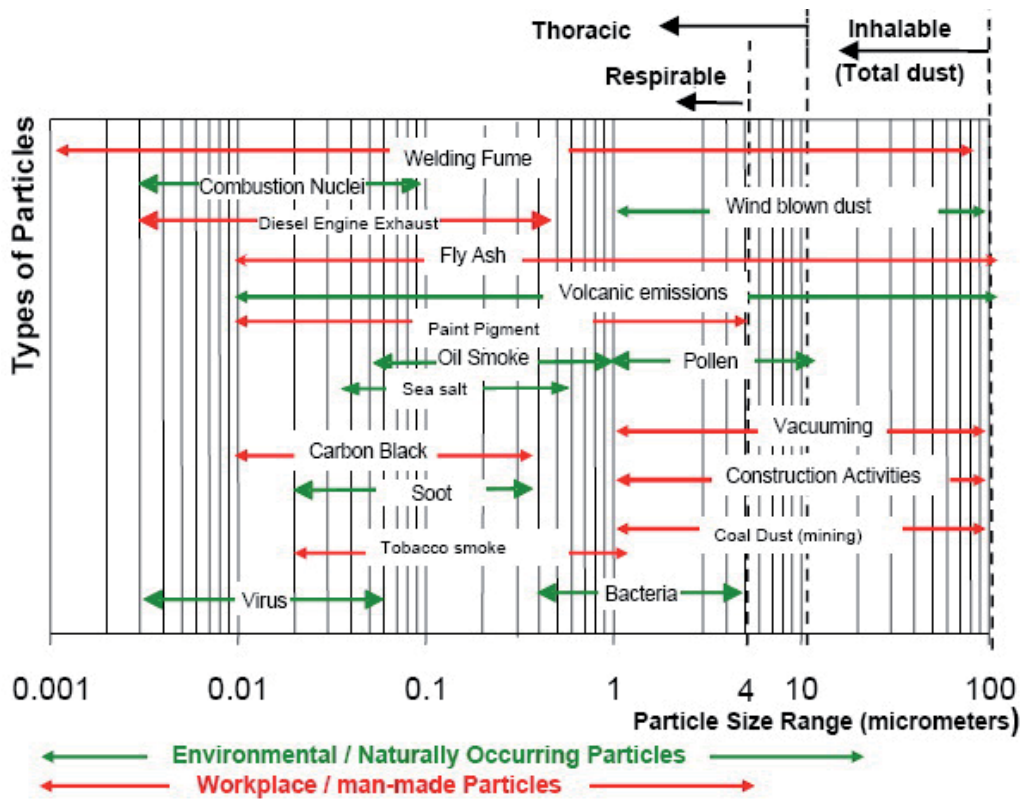
Fig. 14. Type of particles and their sources. (TSI, 2010)

Into the combustion process particles are formed mainly from agglomerations of carbon and partially from hydrocarbons. The particle formation is encouraged by lack of oxygen at flame base and by high temperatures in this phase. The type of fuel is also relevant for particle formation.

During the fuel combustion the particles can form as soot, condensed hydrocarbons, ash or unburned carbon. For example, in the case of coal combustion, when the process starts first the volatile compounds is released while the mineral components are almost completely unburned. Large size particles (from 1 to 20 µm) are formed by mineral inclusions agglomeration on burned soot. During the soot fragmentation up to 5 large ash particles are formed, with a diameter from 10 to 20 µm and a large number of particles with a diameter of 1 to 3 µm. Particles with a diameter lower then 0.1 µm will form mainly due to vaporization and re-condensation of a part of the mineral components that are surrounding the ignited coal. In the combustion conditions of up to 1400 to 1600 ºC appreciatively 1 % of mineral components will vaporize in Na, As, Fe, SiO and Mg vapors. This vapors will then diffuse (nucleation) into combustion chamber extremities where oxygen content is higher and will form a large number of very fine particle with a diameter of maximum 1 µm. All those particles will be then transported in atmosphere by exhaust gases. Figure 15 is a schematic representation of particle formation during fuel combustion.
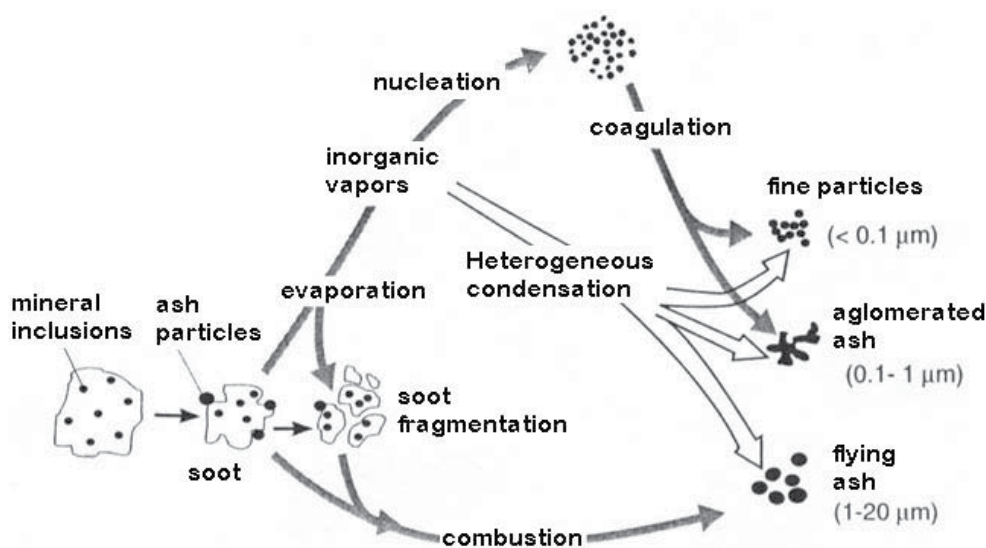
Fig. 15. Formation of particles in the combustion process of pulverized coal.

Before atmospheric particles can cause adverse health effects, they must enter and be deposited in the human respiratory system. Respiratory penetration and deposition depend on the aerodynamic size of particles, respiratory defense mechanisms, and breathing patterns. Particles can be described as inhalable, thoracic or respirable, based on their penetration and potential for deposition. Size ranges and fractional penetration are illustrated in figure 14. Particles with a diameter higher then 10 µm generally do not pass through the nasal hairs and defense mechanisms of the upper respiratory system and are not of a public health concern.

6. Non Methane Volatile Organic Compounds

The anthropogenic fraction of atmospheric VOCs is related to the unprecedented usage of fossil fuels for transport, the production of consumer goods and various industrial processes in the past centuries. The distinction between biogenic and anthropogenic VOCs in the atmosphere is far from straightforward because many VOC species are produced by both sources. Emissions of alkanes and alkenes, for example, are dominated by anthropogenic sources, but are also produced by soils, wetlands and oceans. (Koppmann, 2007)

The larges sources of NMVOC emissions are use of fossil fuel in transportation and chemistry industry. Mobile sources can be divided into emissions from the exhaust and fugitive emissions by evaporation. Stationary emissions from the use of fossil fuel are due to industrial applications (e.g. refineries and chemical sector). Emissions related to production, storage and delivery of fossil fuels predominately occur in those regions where extensive fossil fuel drilling activities exist. However, fugitive emissions can also occur from the transport and distribution of the fuel, such as ships, road tankers and fuel stations.

After their release into the atmosphere, VOCs are oxygenated by photochemical processes, which finally lead to their removal from the atmosphere. For most VOCs the process is initiated by atmospheric radicals like OH, O_3, NO_3 and Cl, with the OH radical being by far the most important reactant. The atmospheric lifetime of an individual VOC species is dependent on its chemical structure, the radical concentration and the intensity of solar radiation. When VOCs are degraded in polluted air masses, NO is oxygenated to NO_2, which then gets photolysed and contributes to the formation of tropospheric ozone, a key issue in air pollution control.

In the EU-27, NMVOC emissions declined by just under 45 % between 1990 and 2006. Twenty-three countries reported reductions (Belgium, Germany, Luxembourg the Netherlands and the United Kingdom have reduced emissions by more than 60 % during this period). The four countries that reported increased NMVOC emissions are Bulgaria, Greece, Poland and Romania.
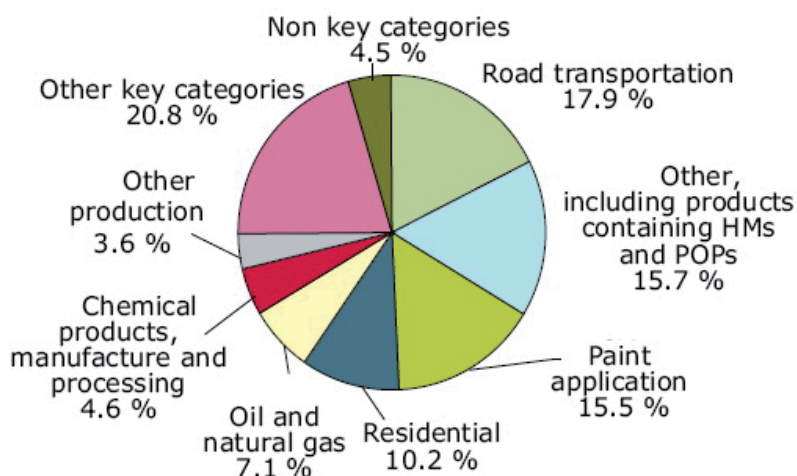
Fig. 16. EU-27 emission sources of NMVOC, 2006 (EEA, 2008).
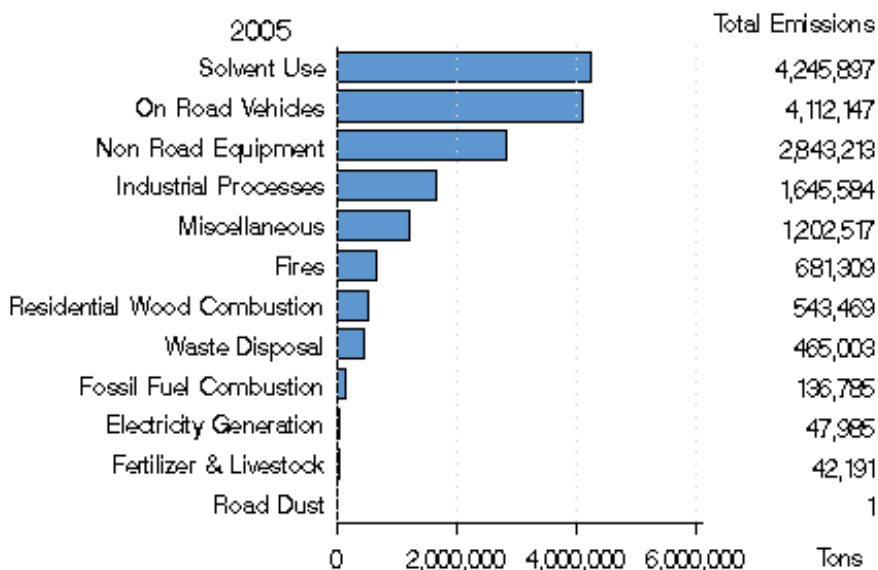
Fig. 17. USA emission sources of NMVOC, 2005 (US EPA, 2009).

The ability of NMVOCs to cause health effects varies greatly from those that are highly toxic, to those with no known health effect. As with other pollutants, the extent and nature of the health effect will depend on many factors including level of exposure and length of time exposed. Eye and respiratory tract irritation, headaches, dizziness, visual disorders, and memory impairment are among the immediate symptoms that some people have experienced soon after exposure to some organics. At present, not much is known about what health effects occur from the levels of organics usually found in homes. Many organic compounds are known to cause cancer in animals; some are suspected of causing, or are known to cause, cancer in humans.

7. Relevant methods to control NOx and SOx emissions from fossil fuel combustion

7.1. NOx control

Two primary categories of control techniques for NOx emissions are combustion control and flue gas treatment. Very often more than one control technique is used in combination to achieve desired NOx emission levels. A variety of combustion control techniques are used to reduce NOx emissions by taking advantage of the thermodynamic and kinetic processes. Some reduce the peak flame temperature; other reduces the oxygen concentration in the primary flame zone while other methods use the thermodynamic balance to reconvert NOx back to nitrogen and oxygen

In the low air-fuel excess ration firing techniques the principle is based on cutting back the amount of excess air, the lower oxygen concentration in the flame zone reduces NOx production. In some cases where too much excess air has become normal practice, thermal efficiency is improved. However, low excess air in the resulting flame may be longer and less stable, and carbon monoxide emissions may increase. Applying advanced optimization systems at four coal-fired power plants resulted in NOx emission reductions of 15 to 55%.

Another widely used method to control NOx emissions is the flue gas recirculation technology, when some of the flue gas, which is depleted in oxygen, is re-circulated to the combustion air. This has two effects: the oxygen concentration in the primary flame zone is decreased, and additional nitrogen absorbs heat, and reduces the peak flame temperature.

Injecting water or steam into the combustion chamber provides a heat sink that reduces peak flame temperature. (Schnelle & Brown, 2002)

Low-NOx burners are designed to stage either the air or the fuel within the burner tip. The principle is similar to overfire air (staged air) or reburn (staged fuel) in a furnace. With staged-air burners, the primary flame is burned fuel rich and the low oxygen concentration minimizes NOx formation. Additional air is introduced outside of the primary flame where the temperature is lower, thereby keeping the thermodynamic equilibrium NOx concentration low, but hot enough to complete combustion. Staged-fuel burners introduce fuel in two locations. A portion of the fuel is mixed with all of the combustion air in the first zone, forming a hot primary flame with abundant excess air. NOx formation is high in this zone. Then additional fuel is introduced outside of the primary flame zone, forming a low-oxygen zone that is still hot enough for kinetics to bring the NOx concentration to equilibrium in a short period of time. In this zone, NOx formed in the primary flame zone reverts back to nitrogen and oxygen.

All those methods are primary methods to reduce NOx formation at the combustion chamber level. Also secondary methods for NOx reduction have been developed, like selective non-catalytic reduction (SNRC) and selective catalytic reduction (SCR).

Selective noncatalytic reduction uses ammonia (NH_3) or urea (H_2NCONH_2) to reduce NOx to nitrogen and water. The overall reactions using ammonia as the reagent are:

$$2H_2S + O_2 \rightarrow 2H_2O + 2S \qquad\qquad\qquad 22)$$
$$8NH_3 + 6NO_2 \rightarrow 7N_2 + 12H_2O \qquad\qquad\qquad 23)$$

The intermediate steps involve amine (NHi) and cyanuric nitrogen (HNCO) radicals.

The critical dependence of temperature requires excellent knowledge of the temperature profile within the furnace for placement of reagent injection nozzles.

In the case that the SNCR process is not controlled efficiently supplementary emissions will occur in exhaust gases, like CO, NH_3 or N_2O, called secondary emissions. In a typical application, SNCR produces about 30 to 50% NOx reduction. Some facilities that require higher levels of NOx reduction take advantage of the low capital cost of the SNCR system, then follow the SNCR section with an SCR system. (Schnelle & Brown, 2002)

In the SCR technology a catalyst bed can be used with ammonia as a reducing agent to promote the reduction reaction and to lower the effective temperature. An SCR system consists primarily of an ammonia injection grid and a reactor that contains the catalyst bed. A variety of catalyst types are used for SCR. Precious metals are used in the low temperature ranges. Vanadium pentoxide on titanium dioxide is a common catalyst for the medium temperature ranges and various aluminum silicates are used as high temperature catalysts.

While the SNCR technology can provide NOx reduction ratios of over 90% has a major disadvantage in economical cost and the necessity to retrofit the combustion facilities.

7.2. SO$_2$ control

SO$_2$ control processes are used for coal-fired industrial boilers. SO$_2$ and HCl controls are required for hazardous and municipal solid waste combustors. Many coal fired power plants use wet limestone scrubbers that have a relatively high capital cost in order to utilize inexpensive limestone reagent. Smaller, industrial-scale facilities typically use more expensive reagents in systems with lower equipment costs. Another solution to control SO$_2$ emissions can be found in combustion of coals (anthracite) with high calorific value and low sulphur content.

The most relevant and used technology to reduce SO$_2$ emissions from coal fired power plants is the combustion of coal with calcium based absorbers. Limestone is an inexpensive rock that is quarried and crushed. It can be used directly as a reagent either in aqueous slurry or by injection into a furnace where the heat decarbonates the limestone. This is a primary reduction process. The parameters that will influence the efficiency of SO$_2$ removal are the type of combustor, the type of coal, the absorber quality and its time of residence into the facility.

The main reactions involved are:

$$CaCO_3 \xrightarrow{\sim 800 grd.C} CaO + CO_2 \qquad (24)$$

$$CaO + SO_2 \rightarrow CaSO_3 \qquad (25)$$

$$CaSo_3 + \frac{1}{2}O_2 \rightarrow CaSO_4 \qquad (26)$$

Other absorbers can also be used, like CaOH$_2$, Na$_2$CO$_3$ or NaOH but they are more expensive than limestone.

The secondary methods for SO$_2$ reduction can be classified as dry procedures, semidry and wet procedures.

A simplified process flow diagram for a coal fired power plant with wet limestone SO$_2$ emission control system is presented in figure 18.
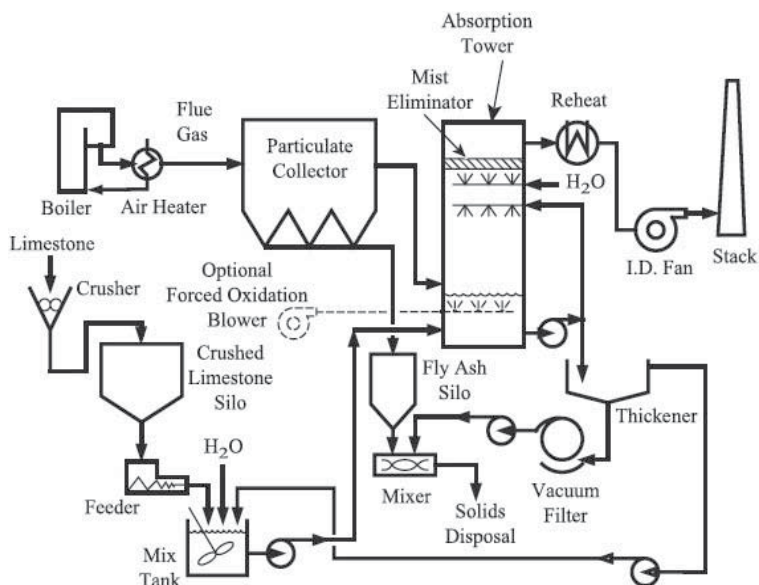
Fig. 18. Simplified wet limestone process flow diagram. (Schnelle & Brown, 2002)

8. References

Baumbach, G. (1992). *Luftreihaltung – 2 auflange*, Springer Verlag, Berlin, Germany

Colls, J. (2002). *Air Pollution – Second Edition,* Spon Press, ISBN 0-20347602-6, UK

EEA, (2008). EEA technical report, no7/2008, *Annual European Community LRTAP Convention emission inventory report 1990–2006*, EEA office for official publication, Copenhagen

Godish, T. (1997). *Air Quality*, CRC Press LLC, ISBN 1-56670-231-3 Boca Raton

Godish, T. (2004). *Air Quality – 4th Edition*, CRC Press LLC, ISBN 0-203-49265-X, Boka Raton, Florida

Ionel, I. et al. (2010). Removal of mercury from municipal solid waste combustion gases, *Journal of Environmental Protection and Ecology*, 11 (1), 2010, ISSN 1311-5065

Ionel, I; Ungureanu C. & Bisorca D. (2006). Thermo energy and environment, Politehnica Press, ISBN (10) 973-625-387-2, Timisoara, Romania

Koppmann, R. (2007). *Volatile organic compounds in the atmosphere*, Blackwell Publishing Ltd, ISBN 978-1-4051-3115-5, Singapore

Popescu, F. (2009). *Alternative fuels. Biodiesel*. Politehnica Press, ISBN 978-973-625-726-1, Timisoara, Romania

Popescu, F. et al. (2009). Ambient air quality measurements in Timisoara. Current situation and perspectives, *Journal of Environmental Protection and Ecology*, 10 (1), 2009, ISSN 1311-5065

Raub, J. A. (2002). Carbon Monoxide and the Nervous System. *Neuroscience and Biobehavioral* Reviews, 26(8), 2002, ISSN 925-940

Raub, J. A. et al. (2000). Carbon Monoxide Poisoning - a Public Health Perspective. *Toxicology* (145):1-14, 2000

Schnelle, K.B & Brown, C.A. (2002). *Air pollution control technology handbook*, CRC Press, ISBN 0-8493-9588-7, Boca Raton. Florida

TSI. (2010). *Type of particles. Technical document*, TSI Incorporated, www.tsi.com

US EPA (2009). United States Environmental Protection Agency, *Air Emission Sources*, November 04, 2009, http://www.epa.gov/air/emissions/index.htm, 2009

Development and application of a methodology for designing a multi-objective and multi-pollutant air quality monitoring network for urban areas

Nicolás A. Mazzeo and Laura E. Venegas
National Scientific and Technological Research Council (CONICET)
National Technological University
Argentina

1. Introduction

Air pollution has been with us since the first fire was lit, although different aspects have been important at different times. Air pollutants are substances which, when present in the atmosphere under certain conditions, may become injurious to human, animal, plant or microbial life, or to property, or which may interfere with the use and enjoyment of life or property. Air pollution is, however enacted on all geographical and temporal scales, ranging from strictly "here and now" problems related to human health and material damage, over regional phenomena like acidification and forest die back with a time horizon of decades, to global phenomena, which over the next centuries can change the conditions for man and nature over the entire globe.

Three classes of factors determine the amount of pollution at a site: a) the nature of relevant emissions, b) the state of the atmosphere and c) topographical aspects.

In this respect the cities act as sources. Cities are by nature concentrations of humans, materials and activities. They therefore exhibit both the highest levels of pollution and the largest targets of impact. Air pollution problems in urban areas generally are of two types. One is the release of primary pollutants and the other is the formation of secondary pollutants. Since a major source of pollutants is motor vehicles, "hot spots" of high concentrations can occur especially near multilane intersections where the emissions are especially high from idling vehicles. The "hot spots" are exacerbated if high buildings surround the intersection, since the volume of air in which the pollution is contained is severely restricted. The combination of these factors results in high concentrations. These cause effects on health and the environment. Increasingly rigorous legislation, combined with powerful societal pressures, is increasing our need for impartial and authoritative information on the quality of the air we all breathe.

Monitoring is a powerful tool for identifying and tackling air quality problems, but its utility is increased when used, in conjunction with predictive modelling and emission assessment, as part of an integrated approach to air quality management (Rao, 2009).

The monitoring of air pollution level is of significance especially to those residents living in urban areas. Planning and location air quality monitoring networks is an important task for environmental protection authorities, involving: a) ensuring that air quality standards are achieved, b) planning and implementing air quality protection and air pollution control strategies, and c) preventing or responding quickly to air quality deterioration. Therefore, environmental protection authorities need to plan and install air quality monitoring networks effectively and systematically. There are no hard and fast rules for air quality network design, since any decisions made will be determined ultimately by the overall monitoring objectives and resource availability.

Before starting the air quality monitoring network design it is essential to establish what problem has to be solved and what constraints have to be imposed on an "ideal" measuring system. The overall objectives of the monitoring network have to be clearly stated. Some of the specific monitoring objectives can be: to quantify ambient air quality and its variation in space and time; to provide data for air pollution control regulations; to provide real-time data for an alert and warning system; to provide trends for identifying future problems or progress against management/control targets; to provide data for development/validation of management tools.

The goals of this study are: a) to develop an objective procedure to determine the monitoring site locations to detect urban background air pollutant concentrations greater than reference concentrations in an urban area, taking into account the consideration of "protection capability" for areas with higher population density, b) to apply the proposed methodology for designing a multi-pollutant (NO_2, CO and PM_{10},) urban air quality network for Buenos Aires city and c) to evaluate "the spatial representativeness" of mean concentrations measured at each monitoring station. The proposed network design methodology is based on the analysis of the results of atmospheric dispersion models; an exceedance score; a population factor and on the application of the t-Student test for comparison air pollutant mean concentrations at different sites.

2. Introduction to Air Quality Monitoring Network Design

Since one cannot expect to monitor air quality at all locations at all times, selection of sites to give a reliable and realistic picture of air quality becomes a problem in the efficient use of limited resources. The selection of monitoring objectives for optimal allocation of air quality monitoring stations may have to cover several design principles. The required design principles usually consist of the considerations of protection capability for regions with higher population density and significant area with higher economic growth as well as the detection capability of higher pollution concentrations, higher frequency of violation of stipulated standards, and the major industrial/traffic sources in an urban region. Moreover, the cost for siting a pollutant-specific monitoring network would be higher than that for a common monitoring network with respect to several pollutants simultaneously. Thus, for practical reasons, most monitoring networks install different detection instruments together in a common monitoring network that could be viewed as more economic and feasible applications.

Even with a clear set of network objectives, there is no universally accepted methodology for implementing such objectives into the network design, with the approaches used being as varied as the regions being managed. Different methodologies on air quality monitoring network design have been reported in the literature. Among them, statistical methods take advantage of the fact that most air quality measurements are correlated either in time at the

same location or in space with other monitors in a network. In this way, networks can be optimized by examining time series correlations from long measurement records or spatial correlations among measurements from many nearby monitors (Munn, 1975, 1981; Elsom, 1978). Various statistical and optimization schemes were applied for designing a representative air quality monitoring network with respect to a pollutant-specific case (Smith & Egan, 1979; Graves et al., 1981; Pickett & Whiting, 1981; Egmond & Onderdelinden, 1981; Handscombre & Elsom, 1982; Husain & Khan, 1983; Nakamori & Sawaragi, 1984; Modak & Lohani, 1985a,b; Liu et al, 1986; Langstaff et al., 1987, Hwang & Chan, 1997). Furthermore, Noll & Mitsutome (1983) developed a method to establish monitor locations based on expected ambient pollutant dosage. This method ranked potential locations by calculating the ratio of a station's expected dosage over the study area's total dosage.

It usually happens that an initial monitoring network evolves over time. Therefore after some time a redesign may be required to maximize its capacity to meet modern demands. In this case, it may be desirable the new network maximizes the amount of information it will provide about the environmental field it is being asked to monitor. Equivalently, it should maximally reduce uncertainty about that field. These ideas can be formalized through the use of entropy that quantifies uncertainty and can be used as an objective function. Caselton et al. (1992) used it to rank monitoring sites for possible elimination, an idea extended by Wu & Zidek (1992). Recently, Ainslie et al. (2009) used the entropy-based approach of Le & Zidek (2006) to redesign a monitoring network in Vancouver (Canada) using hourly ozone concentration.

The consideration of multi-pollutant air quality monitoring network design with respect to different objectives was introduced in a series of papers by Modak & Lohani (1985a,b,c). The design principles of a minimum spanning tree algorithm for single or multiple pollutants with respect to one or two objectives was illustrated in these studies. Kainuma et al. (1990) developed a similar procedure to evaluate several types of siting objectives and used a multi-attribute utility function method to determine optimal locations.

Several methods of air quality monitoring design or optimization also include the analysis of atmospheric dispersion models estimations (Hougland & Stephens, 1976; Koda & Seinfeld, 1978; McElroy et al., 1986; Mazzeo & Venegas, 2000, 2008; Tseng and Chang, 2001; Baldauf et al., 2002; Venegas & Mazzeo; 2003a, 2010). For example, Hougland & Stephens (1976) selected monitoring site locations maximizing coverage factors, such as strength of emission source, distance from the source, and local meteorology for each source included in the study. The basis of this "source oriented" method was to consider for each source and wind direction, the monitor with the largest coverage factor. Koda & Seinfeld (1978) presented a methodology for distributing a number of monitoring stations in a study area in order to obtain the maximum sensitivity of the collected data to achieve the variations in the emissions of the sources of interest. The developed methodology used model estimations of ground level concentrations of pollutants for different meteorological scenarios. McElroy et al. (1986) applied air quality simulation models and population exposure information to produce representative combined patterns and then employed the concept of 'sphere of influence' (SOI) developed by Liu et al. (1986) to determine the minimum number of sites required. The monitor's SOI is defined as the area over which the air quality data for a given station can be considered representative, or can be extrapolated, with known confidence. The site's SOI can be determined using the covariance structure of the concentrations. Thus, a monitor site's SOI comprises those neighbouring sites whose variance can be explained by the original site's variance within a certain degree of confidence.

Tseng & Chang (2001) integrated a series of simulation and optimization techniques for generating better siting alternatives of air quality monitoring stations in an urban environment. The analysis presented used atmospheric dispersion models to estimate air pollution concentrations required in the optimization analysis. Three planning objectives for the minimization of the impacts of the highest concentrations and the highest frequency of violation, as well as the maximization of the highest protection potential of population were emphasized subject to budget, coverage effectiveness (the ratio between effective detection area and total detection area for a monitoring station), spatial correlation, or concentration differentiation constraints. In this case, the concentration differentiation constraints takes into account that the spatial correlation between grids can be high, but the order of magnitude of measured or predicted concentrations between both grids may present significant difference, given the fact that grids are only spatially correlated in terms of concentration pattern.

Baldauf et al. (2002) presented a simple methodology for the selection of a neighbourhood-scale site for meeting either of the following two objectives: to locate monitors at the point of maximum concentration or at a location where a population oriented concentration can be measured. The proposed methodology is based on analyzing middle-scale (from 100 to 500 m) atmospheric dispersion models estimations within the area of interest.

Sarigiannis & Saisana (2008) presented a method for multi-objective optimization of air quality monitoring systems, using both ground-based and satellite remote sensing of the troposphere. This technique used atmospheric turbidity as surrogate for air pollution loading. In their study, Sarigiannis & Saisana (2008) also defined an information function approach combining the values of the violation score, the land-use score, the population density, the density of cultural heritage sites and the cost function. Furthermore, similarities among locations were assessed via the linear correlation coefficient between locations. A gain of information was defined as the product between the correlation coefficient and the information function. The location with the maximum value of the gain information was selected as the best monitoring location.

Elkamel et al. (2008) presented an interactive optimization methodology for allocating the number of sites and the configuration of an air quality monitoring network in a vast area to identify the impact of multiple pollutants. They introduced a mathematical model based on the multiple cell approach to create monthly spatial distributions for the concentrations of the pollutants emitted from different emission sources. These spatial temporal patterns were subject to a heuristic optimization algorithm to identify the optimal configuration of a monitoring network. The objective of the optimization was to provide maximum information about multi-pollutants emitted from each source within a given area.

Pires et al. (2009) applied principal component analysis to identify redundant measurements in air quality monitoring networks. To validate their results, authors used statistical models to estimate air pollutant concentrations at removed monitoring sites using the concentrations measured at the remaining monitoring sites.

Mofarrah & Husain (2010) presented an objective methodology for determining the optimum number of ambient air quality stations in a monitoring network. They developed an objective methodology considering the multiple-criteria, including multiple-pollutants concentration and social factors such as population exposure and the construction cost. The analysis employed atmospheric dispersion model simulations. A multiple-criteria approach in conjunction with the spatial correlation technique was used to develop an optimal air

quality monitoring network design. These authors used triangular fuzzy numbers to capture the uncertain (i.e., assigning weights) components in the decision making process. The spatial area coverage of the monitoring station was also determined on the basis of the concept of a sphere of influence.

3. Proposed Methodology

The purpose is to design a multi-pollutant air quality monitoring network for an urban area, considering two objectives: one is the detection of higher pollutant concentrations and the other is the "protection capability" for areas with higher population density. The first one is analysed measuring the potential of a monitoring site to detect violations of reference concentrations in terms of violation scores.

The proposed approach consists of seven steps. The first step is to select the air pollutants of concern and their reference concentration levels for each averaging time less-equal 24h. The values for different intervals of reference concentrations can be chosen based on air quality guideline values for the selected pollutants. Furthermore, weighing factors are defined to penalize the exceedance of higher reference concentrations with regard to exceedance of lower ones.

The second step is to apply atmospheric dispersion models to compute the time series of pollutant concentrations in each grid cell in which the urban area is divided.

In the third step an exceedance score (ES_k) of pollutant k is computed for each grid cell. ES_k is given by the following equation (Modak & Lohani, 1985b):

$$ES_k = \sum_{i=1}^{N_k} \sum_{j=1}^{n_k} \frac{\left(\omega_{j+1} - \omega_j \right) \left(C_{i,k} - CR_{j,k} \right) Z}{\left(CR_{(j+1),k} - CR_{j,k} \right)} \tag{1}$$

where $C_{i,k}$ is a simulated concentration value of pollutant k, N_k is the number of concentration values ($C_{i,k}$) of pollutant k, ω_j is the weighing factor corresponding to the reference value $CR_{j,k}$, n_k is the number of reference values for each pollutant, Z is a factor defined by

$$Z \begin{cases} 1 & C_{i,k} > CR_{j,k} \\ 0 & C_{i,k} \le CR_{j,k} \end{cases} \tag{2}$$

The fourth step is to evaluate a population factor (PF) for each grid cell, defined by

$$PF = \frac{P}{P_T} 100 \tag{3}$$

where P is the number of inhabitants in the grid cell, P_T is the total population in the urban area.

In the fifth step the total score (TS) defined by Equation (4) is evaluated for each grid cell.

$$TS = PF \sum_{k=1}^{M} ES_k \tag{4}$$

where M is the number of pollutants (if one pollutant has more than one averaging time, each of them has to be considered separately).

In the sixth step the grid cells are ranked according to TS values. The location with the maximum TS value is selected as the best monitoring location. All grid squares located nearer than a given distance (D) (for example, 1 km) to the selected one, are discarded for further site selections. The next site locations are determined according to the same procedure. The number of locations is arbitrary (usually limited by the economical constraint). All grid cells with high TS separated more than distance a D are selected for installing a monitoring station. These selected grid cells constitute the preliminary network.

The seventh step is to evaluate if average concentrations of each pollutant at near selected sites are significantly different. Considering one pollutant at a time, and using the t-Student test, if the difference between mean concentrations at a pair of near sites is statistically significant at the 99% confidence level, both sites remain in the network. Otherwise, the site with less TS can be eliminated from the preliminary network. This procedure is repeated considering all sites. The proposed network is obtained in this step.

Furthermore, "the spatial representativeness" of the monitoring sites of the proposed network can be evaluated. Applying the t-Student test to each pollutant mean concentration, "the spatial representativeness" of each monitoring site can be given by all the near grid cells where mean concentrations are not statistically significant different at the 99% confidence level.

4. Application to the city of Buenos Aires

4.1 The city of Buenos Aires and its surroundings

The city of Buenos Aires (34°35′S – 58°26′W) is the capital of Argentina and is located on the west coast of the de la Plata River. It has an extension of 203km² and 3058309 inhabitants (INDEC, 2008). The city (Fig. 1) is surrounded by the Greater Buenos Aires (24 districts) of 3627km² and 9575955 inhabitants. Both the city of Buenos Aires and the Greater Buenos Aires form the Metropolitan Area of Buenos Aires (MABA), which is considered the third megacity in Latin America following Mexico City (Mexico) and Sao Paulo (Brazil).
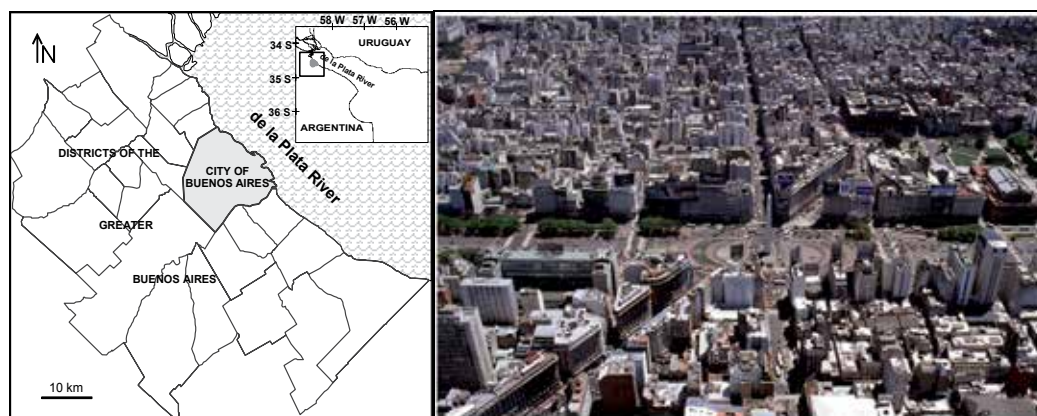

Fig. 1. Location of the city of Buenos Aires and an aerial view of Buenos Aires city.

The MABA is located on a flat terrain with height differences less than 30 m. The de la Plata River is a shallow estuary of 35000km^2, approximately. It is 320km length, and its width varies from 38km to 230km in the upper and lower regions, respectively. In front of the city, the width of the river is about 42km. Mean water temperature varies from 12°C in winter to 24°C in summer. The de la Plata River plain has a temperate climate. The city is hot and humid during summer months (December to February), with a mean high temperature of 27°C. Fluctuating temperatures and quickly changing weather conditions characterise autumn and spring seasons. The winter months (June to August) are mild but humid, with a mean minimum temperature of 6°C. The annual average temperature is 18°C in the city, and it varies between 15-16°C in the suburbs. In the city, frost may occur from June to August, but snowfall is extremely rare. The annual rainfall varies between 900mm and 1600mm, influenced by winds that advect humidity from the Atlantic Ocean. Rainfall is heaviest in March. Winds are generally of low intensity. Strong winds are more frequent between September and March, when storms are more frequent. Annual frequency of winds blowing clean air from the river towards the city is 58%.

The air quality in the city has been the subject of several studies carried out during the last years. Some of these studies analysed data obtained from measurement surveys of pollutants in the urban air (Bogo et al., 1999, 2001, 2003; Venegas & Mazzeo, 2000, 2003b; Mazzeo & Venegas, 2002, 2004; Mazzeo et al., 2005; Bocca et al., 2006). Other studies reported results of the application of atmospheric dispersion models (Venegas & Mazzeo, 2005, 2006). In the Greater Buenos Aires, very few air quality measurements have been made (Fagundez et al., 2001, SAyDS, 2002).

4.2. Emission inventory for the city of Buenos Aires

Mazzeo & Venegas (2003) developed a first version of CO and NO$_x$ (expressed as NO$_2$) emission inventory for Buenos Aires city. Also Pineda Rojas et al. (2007) presented an emission inventory of these pollutants for the Metropolitan Area of Buenos Aires which includes updated emissions for the city of Buenos Aires. An emission inventory of particulate matter (PM$_{10}$) for the city of Buenos Aires has been presented by Venegas & Martin (2004). The inventories for the city of Buenos Aires include: a) area sources: residential, commercial, small industries, aircrafts LTO (landing/take-off) cycles at the domestic airport, and road traffic (cars, trucks, taxis, buses) and b) point sources: stacks of three Power Plants. The spatial resolution of the inventories is 1x1 km and a typical hourly variation. The emission factors used in preparing the emission inventories were derived considering: a) monitoring studies undertaken in Buenos Aires (Rideout et al., 2005); b) the EMEP/CORINAIR Atmospheric Inventory Guidebook (EMEP/CORINAIR, 2001); c) the US Environmental Protection Agency's manual on the Compilation of Air Pollution Emission Factors (EPA, 1995). These factors were applied to fuel consumption, gas supply data and vehicle kilometres travelled within each grid square. Data on traffic flow, fleet composition and bus service frequencies was also available. Aircraft emissions were computed knowing the scheduled hourly flights, the type of aircraft, the information available on LTO (landing/take-off) cycles and emission factors (Romano et al, 1999, EMEP/CORINAIR, 2001). Spatial and temporal dependent NO$_x$ (expressed as NO$_2$), CO and PM$_{10}$ emission distributions in the Buenos Aires Metropolitan Area were obtained.

Figs. 2, 3 and 4 show in diagrammatic form the distribution of annual emission of NO$_x$ (expressed as NO$_2$), CO and PM$_{10}$ by source category, for the city of Buenos Aires. Since the

Power Plants burn natural gas most of the year and consume fuel oil as much as twenty days in wintertime only, they are responsible for approximately, 51.6% of NO_x (expressed as NO_2), 0.02% of CO and 2.3% of PM_{10} total annual emissions in the city. Carbon monoxide and particulate matter are very much associated with emissions from road traffic. Within Buenos Aires city, road traffic is responsible for 43% of NO_x (expressed as NO_2), 99.43% of CO and 94% of PM_{10} annual emissions in the city.
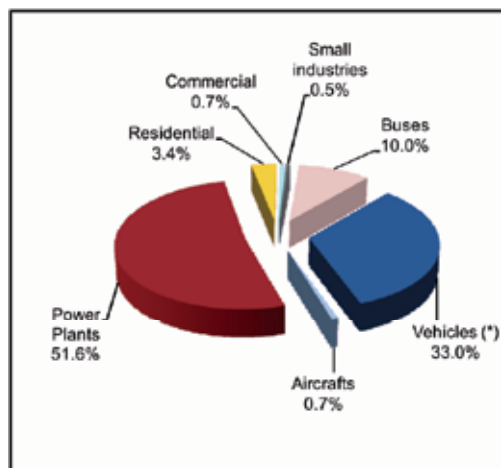
Fig. 2. Estimated emissions of NO_x (expressed as NO_2) by source category. (*) cars, taxis, trucks
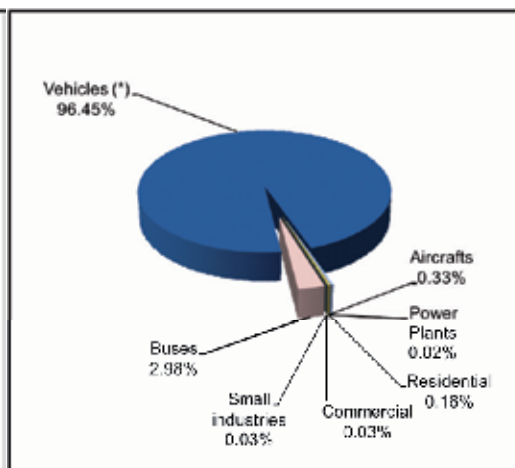
Fig. 3. Estimated emissions of CO by source category. (*) cars, taxis, trucks
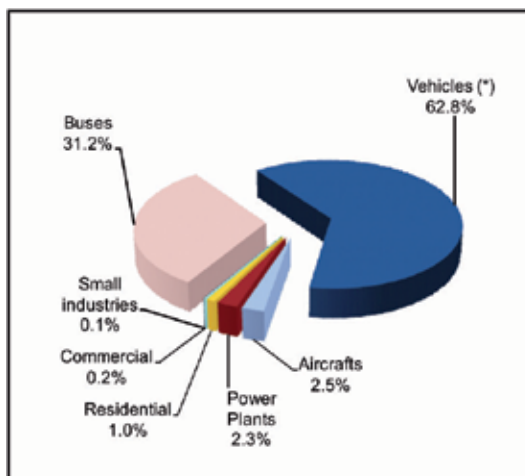
Fig. 4. Estimated emission of PM_{10} by source category. (*) cars, taxis, trucks

4.3. Brief description of the atmospheric dispersion models used in this study

In this work, area sources and point sources contributions to air pollutant concentrations in the city are estimated applying the following atmospheric dispersion models: a) DAUMOD model for urban area sources and b) AERMOD model for urban point sources.

The DAUMOD model
The DAUMOD urban atmospheric dispersion model can be used to estimate background concentrations due to area source emissions. This model has been described elsewhere (Mazzeo & Venegas, 1991; Venegas & Mazzeo, 2002, 2006) however a brief description of it is included. In the development of the DAUMOD model (Mazzeo & Venegas, 1991), a semi-infinite volume of air, bounded by the planes z=0 and x=0 is considered. According with Gifford (1970), for steady-state conditions, with the x-axis in the direction of the mean wind and the z-axis vertical, the concentration [C(x,z)] of pollutants emitted from an area source at the surface, satisfies the bi-dimensional diffusion equation :

$$u(z)\frac{\partial C(x,z)}{\partial x} = \frac{\partial}{\partial z}\left[K(z)\frac{\partial C(x,z)}{\partial z}\right] \tag{5}$$

because only the vertical diffusion contributes significantly to the process. In Equation (5), $u(z)$ is the mean wind speed and $K(z)$ is the vertical eddy diffusivity for contaminants. If the effluents are emitted continuously from the surface level with source strength (Q) expressed as mass per unit area per unit time, the concentration [C(x,z)] satisfies the lower boundary condition:

$$K(z)\left.\frac{C(x,z)}{z}\right|_{z=0} = -Q \tag{6}$$

Another basic assumption is that at a given distance, the vertical extension of the plume of contaminants is h(x), where C(x,h(x)) = 0. Then, there is no transport of mass through the upper limit of the plume, and this can be expressed as:

$$K(z)\left.\frac{C(x,z)}{z}\right|_{z=h} = 0 \tag{7}$$

The boundary condition C(x,h(x))= 0, can be satisfied assuming that the solution of Equation (5) is given by the following polynomial form:

$$C(x,z) = C(x,0)\sum_{j=0}^{6} A_j\left(\frac{z}{h}\right)^j \tag{8}$$

The coefficients A_j have been computed fitting Equation (8) to the results given by the following expression (Pasquill & Smith, 1983):

$$C(x,z) = C(x,0)\exp\left[-4.605\left(\frac{z}{z_m}\right)^s\right] \tag{9}$$

where s is a shape factor which depends on atmospheric stability and surface roughness (Gryning et al., 1987) and z_m is the height at which $C(z_m) = 0.01C(0)$. The height z_m is usually

considered to be the upper limit of the plume, so we assumed h= z_m. Considering different atmospheric stability conditions, the coefficients (A_0, A_1,....A_6) of the polynomial of grade 6 are obtained for each fitting.

Atmospheric stability	Expressions for $A_j(z_0/L)$
$z_0/L < -10^{-2}$	$A_j = A_j(z_0/L=-0.01)$
$-10^{-2} \leq z_0/L < -10^{-4}$	$A_0 = 1.0$ $A_1 = -9.254667 - 0.8043134 \ln(|z_0/L|)$ $A_2 = -26.88303107 - 197.989893 [\ln(1.2146\ |z_0/L|)]^{-1}$ $A_3 = -38.00005 + \exp[4.16612 - 373.1065\ |z_0/L|)]$ $A_4 = -84.48740174 - 333.915544 [\ln(7.5651|z_0/L|)]^{-1}$ $A_5 = -33.25054 + \exp[4.13875 - 289.5308\ |z_0/L|)]$ $A_6 = -14.47563571 - 43.4735075 [\ln(14.5776\ |z_0/L|)]^{-1}$
$-10^{-4} \leq z_0/L \leq 10^{-4}$	$A_0 = 1.0$ $A_1 = 3853.3\ (z_0/L) - 1.461$ $A_2 = -18740\ (z_0/L) - 6.797$ $A_3 = 27740\ (z_0/L) + 26.931$ $A_4 = -16270\ (z_0/L) - 39.652$ $A_5 = 965\ (z_0/L) + 27.781$ $A_6 = 1635\ (z_0/L) - 7.655$
$10^{-4} < z_0/L$	$A_0 = 1.0$ $A_1 = -0.05478233 - 0.0001021171 [\ln[(z_0/L)+1]]^{-1}$ $A_2 = -6.55023478 + 0.02035983\ [\ln(z_0/L)]^3 + 0.00191583[\ln(z_0/L)]^4$ $A_3 = 12.9282233 + \exp[2.917612 - 1007.8064\ (z_0/L)]$ $A_4 = -0.59677391 + 0.05583574\ [\ln(z_0/L)]^3 + 0.00040899[\ln(z_0/L)]^4$ $A_5 = -1.9551195 + \exp[3.5211141 - 1255.2843\ (z_0/L)]$ $A_6 = 2.66883478 + 0.00810494[\ln(z_0/L)]^3 - 0.00053199[\ln(z_0/L)]^4$

Table 1. Expressions of $A_j(z_0/L)$ as functions of (z_0/L)

The fittings of polynomial form given by Equation (8) to the results of Equation (9) are excellent; with coefficients of determination of ≈ 1.0 (the reader can find details of these results in Mazzeo & Venegas, 1991). Coefficients A_j (j=0,...6) depend on surface roughness and atmospheric stability. Plotting the values of A_j vs (z_0/L) (z_0 is the surface roughness length and L is the Monin-Obukhov´s length) the expressions of $A_j (z_0/L)$ included in Table 1 have been obtained

The following expressions are considered for the wind speed and the eddy diffusivity (Arya, 1999):

$$u(z) = \frac{u_*}{k_v} \left[\ln\left(\frac{z}{z_0}\right) + \Psi\left(\frac{z}{L}\right) \right] \tag{10}$$

$$K(z) = \frac{k_v \ u_* \ (z + z_0)}{\varphi\left(\frac{z}{L}\right)} \tag{11}$$

where u_* is the friction velocity, k_v is the von Karman´s constant (=0.41), $\Psi(z/L)$ functions determine stability correction due to stratification and $\varphi(z/L)$ is the dimensionless wind shear (Wieringa, 1980; Gryning et al., 1987):

$$\Psi\left(\frac{z}{L}\right) = \begin{cases} 6.9\dfrac{z}{L} & \dfrac{z}{L} > 0 \\[3mm] 1 - \varphi^{-1}\left(\dfrac{z}{L}\right) & \dfrac{z}{L} < 0 \end{cases}$$

$$\varphi\left(\frac{z}{L}\right) = \begin{cases} 1 + 6.9\dfrac{z}{L} & \dfrac{z}{L} > 0 \\[3mm] \left(1 - 22\dfrac{z}{L}\right)^{-\frac{1}{4}} & \dfrac{z}{L} < 0 \end{cases}$$

$\Psi(0) = 0$ and $\varphi(0) = 1$.

Substituting Equations (8) and (11) into Equation (6) and operating, the following expression for C(x,0) can be obtained:

$$C(x,0) = \frac{Q\ h(x)}{|A_1|\ k_v\ u_*\ z_0} \tag{12}$$

C(x,0) can be estimated from Equation (12) knowing the form of h(x). Therefore, considering the equation of pollutant mass continuity expressed by (Pasquill & Smith, 1983):

$$\int_0^x Q\ dx = \int_{z_0}^h u(z)\ C(x,z)\ dz \tag{13}$$

and Equations (8), (10) and (12) along with the boundary condition C(x,h)=0, the following expression can be obtained when Q= constant:

$$\frac{x}{z_0} = \frac{1}{|A_1| k_v^2}\left(\frac{h}{z_0}\right)^2 G\left(\frac{z_0}{h};\frac{h}{L}\right) \tag{14}$$

The form of $G(z_0/h; h/L)$ is not simple (the complete expression is included in Mazzeo & Venegas, 1991), however the values of (h/z_0) computed from Equation (14) can be fitted with great accuracy (coefficient of determination ≈1) to potential functions (Mazzeo & Venegas, 1991) given by:

$$\frac{h}{z_0} = a\left(\frac{x}{z_0}\right)^b \tag{15}$$

a and b depend on atmospheric stability. The expressions for $a(z_0/L)$ and $b(z_0/L)$ are included in Table 2.

Atmospheric stability	Expressions for $a(z_0/L)$ and $b(z_0/L)$
$z_0/L < -10^{-4}$	$a = 3.618833 + 0.2369076 \ln(|z_0/L|)$
	$b = 0.5356147 + 0.0234187 \ln[(|z_0/L|) + 0.01]$
$-10^{-4} \leq z_0/L \leq 10^{-4}$	$a = -384.73 (z_0/L) + 1.4$
	$b = -130.0 (z_0/L) + 0.415$
$10^{-4} < z_0/L$	$a = 0.6224632 + 7.37387 \times 10^{-5} / \ln[(z_0/L) + 1]$
	$b = 0.5065736 - 1.196137 / \ln[2802.315 + 9 / (z_0/L)]$

Table 2. Expressions of $a(z_0/L)$ and $b(z_0/L)$ as functions of (z_0/L).

Substituting Equation (15) in Equation (12), it becomes:

$$C(x,0) = \frac{a \; Q \; (x/z_0)^b}{|A_1| \, k_v \, u_*} \tag{16}$$

which is the expression for a semi-infinite area source emitting continuously with a uniform strength (Q). The expression for a finite and continuous source located between x= 0 and x= x_1, with strength Q, can be derived from Equation (16) by subtracting the concentration due to a continuous semi-infinite source with strength Q lying through x>x_1, from Equation (16):

$$C(x,0) = \frac{a \; Q \left[x^b - (x - x_1)^b \right]}{|A_1| \, k_v \, z_0^b \, u_*} \tag{17}$$

In an urban area, we may assume horizontal distribution of area sources with strength varying according to a typical square grid pattern. Each grid square has a uniform strength Q_i (i = 0, 1, 2, …, N). The variation of the concentration with x, for x > x_i (i = 0, 1, 2, …, N) is given by:

$$C(x,0) = \frac{a \left[Q_o \, x^b + \sum_{i=1}^{N} (Q_i - Q_{i-1})(x - x_i)^b \right]}{\left(|A_1| \, k_v \, z_o^b u_* \right)} \tag{18}$$

The form of C(x,z) can be obtained substituting Equation (18) into Equation (8),

$$C(x, z) = \frac{a \left[Q_o \, x^b + \sum_{i=1}^{N} (Q_i - Q_{i-1})(x - x_i)^b \right]}{\left(|A_1| \, k_v \, z_o^b u_* \right)} \sum_{j=0}^{6} A_j \left(\frac{z}{h} \right)^j \tag{19}$$

A constant wind direction is required for application of Equations (18) and (19). It has been noted from applications of Equation (18) that estimated concentration at any receptor is mainly originated from the emission in the grid square in which the receptor is located. This is because area source distributions in a city are generally fairly smooth and, the contribution of upstream grid squares (from Equation (18)) rapidly reduces with distance to the receptor. The simplification of assuming that the uniform area source strength Q_i only varies with x (in the wind direction), suppose to consider the "narrow plume" hypothesis.

This assumption has also been included in other simple urban dispersion models (Gifford, 1970, Gifford & Hanna, 1973, Arya, 1999).

The performance of DAUMOD model in estimating background concentrations has been evaluated comparing estimated and observed concentration data from several cities. Results for Bremen (Germany), Frankfurt (Germany) and Nashville (USA) have been reported in Mazzeo & Venegas (1991) and for Copenhagen (Denmark) can be found in Venegas & Mazzeo (2002). The validation of the application of DAUMOD to estimate NO_x, CO and PM_{10} in Buenos Aires City can be found in Mazzeo & Venegas (2004), Venegas & Mazzeo (2006) and Venegas & Martin (2004). Results show that the performance of the model in estimating short-term concentrations (hourly and daily) is good and it improves when estimating long averaging time values (monthly and annual).

At present, photochemical transformations involving NO, NO_2 and O_3 are not included in DAUMOD model. However, output concentrations of NO_2 are calculated on the basis of an empirical relationship between NO_2 and NO_x (Derwent & Middleton, 1996; Dixon et al., 2001; Middleton at al., 2008). The concentration of NO_2 is calculated using the polynomial expression (Derwent & Middleton, 1996, CERC, 2003):

$$[NO_2] = 2.166 - [NO_x] (1.236 - 3.348\ B + 1.933\ B^2 - 0.326\ B^3)$$

where $B = \log_{10}([NO_x])$ and $[NO_x]$ is hourly-averaged concentration in ppb.

The AERMOD model

AERMOD (EPA, 2004) is a steady-state plume dispersion model for assessment of pollutant concentrations from a variety of sources. AERMOD simulates transport and dispersion from multiple point, area or volume sources based on an up-to-date characterization of planetary boundary layer (PBL). AERMOD's concentration formulations consider the effects from vertical variations in wind, temperature and turbulence. These profiles are represented by "effective" values constructed by averaging over the layer through which plume material travels directly from the source to receptor. Sources may be located in rural or urban areas, and receptors may be located in simple or complex terrain. The model employs hourly sequential pre-processed meteorological data to estimate concentrations for averaging times from one hour to one year (also multiple years). AERMOD is designed to operate in concert with two pre-processor codes: AERMET processes meteorological data for input to AERMOD, and AERMAP processes terrain elevation data and generates receptor information for input to AERMOD. AERMOD is applicable to primary pollutants and continuous releases of toxic and hazardous waste pollutants. Chemical transformation is treated by simple exponential decay. A more complete description of AERMOD model can be found in EPA (2004) and Cimorelli et al. (2005).

In stable boundary layer (SBL), the concentration distribution is assumed to be Gaussian, both vertically and horizontally. During stable conditions (i.e., stable and neutral stratifications, when $L > 0$), AERMOD estimates concentrations (C_s) from:

$$C_S(x,y,z) = \frac{Q_p}{\sqrt{2\pi}\,\tilde{u}\,\sigma_{zs}} F_y$$

$$x \sum_{m=-\infty}^{\infty} \left\{ \exp\left[-\frac{\left(z - h_{es} - 2mz_{ieff}\right)^2}{2\sigma_{zs}^2} \right] + \exp\left[-\frac{\left(z + h_{es} + 2mz_{ieff}\right)^2}{2\sigma_{zs}^2} \right] \right\}$$

(20)

where, Q_P is the point source emission rate, $\tilde{u}$ is the effective wind speed, z_{ieff} is the effective mechanical mixing height, σ_{zs} is the total vertical dispersion, h_{es} is the plume height (Weil, 1988; Cimorelli et al, 2005) and F_y is the lateral distribution functions.

In the convective boundary layer (CBL), the horizontal distribution is assumed to be Gaussian, but vertical distribution is described with a bi-Gaussian probability density function (Willis & Deardoff, 1981; Briggs, 1993). In CBL the transport and dispersion of a plume is characterized as the superposition of three modelled plumes: the direct plume (from the stack), the indirect plume, and the penetrated plume, where the indirect plume accounts for lofting of a buoyant plume near the top of boundary layer, and the penetrated plume accounts for the portion of a plume that, due to its buoyancy, penetrates above the mixed layer, but can disperse downward and re-enter the mixed layer. In the CBL, plume rise is superposed on the displacements by random convective velocities (Weil et al, 1997).

The total concentration (C_c) in the CBL is found by adding the contribution from three sources: a "direct" source, an "indirect" source and a "penetrated" source (above the CBL top). For the horizontal plume state,

$$C_c(x,y,z) = C_d(x,y,z) + C_r(x,y,z) + C_p(x,y,z) \tag{21}$$

The concentration (C_d) due to the direct plume is given by

$$
\begin{aligned}
C_d(x,y,z) = {} & \frac{Q_P\, f_p}{\sqrt{2\pi}\tilde{u}\sigma_y} \exp\left[-\frac{y^2}{2\sigma_y^2}\right] \\
& \times \sum_{j=1}^{2}\sum_{m=0}^{\infty}\frac{\lambda_j}{\sigma_{zj}}\left\{\exp\left[-\frac{(z-\Psi_{dj}-2mz_i)^2}{2\sigma_{zj}^2}\right]+\exp\left[-\frac{(z+\Psi_{dj}+2mz_i)^2}{2\sigma_{zj}^2}\right]\right\}
\end{aligned}
\tag{22}
$$

where $\Psi_{dj} = h_s + \Delta h_d + \overline{w_j}\, x/\tilde{u}$ is the height of the direct source plume, $\tilde{u}$ is the effective wind speed, Z_i is the mixing height, Δh_d is the plume rise and $\overline{w_j}$ is the vertical velocity. The subscript j is equal to 1 for updrafts and 2 for downdrafts with λ_j defined as the weighting coefficient for each distribution:

$$\lambda_1 = \frac{\overline{w_2}}{\overline{w_2}-\overline{w_1}} \tag{23}$$

$$\lambda_2 = -\frac{\overline{w_1}}{\overline{w_2}-\overline{w_1}} \tag{24}$$

Equation (22) uses an image plume to handle ground reflections by assuming a source at $z = -h_s$. All subsequent reflections are handled by sources at $z=2z_i+h_s$, $-2z_i - h_s$, $4z_i + h_s$, $-4z_i-h_s$ and so on. The factor f_p accounts for the fraction of source material that does not penetrate the top of the CBL.

The concentration (C_r) due to the indirect source is calculated from

$$C_r(x,y,z) = \frac{Q_P f_p}{\sqrt{2\pi}\tilde{u}\sigma_y} \exp\left[-\frac{y^2}{2\sigma_y^2}\right]$$

$$x \sum_{j=1}^{2} \sum_{m=0}^{\infty} \frac{\lambda_j}{\sigma_{zj}} \left\{ \exp\left[-\frac{\left(z+\Psi_{rj}-2mz_i\right)^2}{2\sigma_{zj}^2}\right] + \exp\left[-\frac{\left(z-\Psi_{rj}+2mz_i\right)^2}{2\sigma_{zj}^2}\right] \right\}$$

(25)

where σ_{zj} and F_y are the same as defined for the direct source, the plume height $\Psi_{rj} = h_s + \Delta h_r + \overline{w}_j\, x/\tilde{u}$ (j=1,2) with $\Delta h_r = \Delta h_d - \Delta h_i$ and Δh_i is the indirect source plume rise.

For the penetrated source, the vertical and lateral concentration distributions have a Gaussian form, such that the concentration (C_p) is given by

$$C_p(x,y,z) = \frac{Q_P(1-f_p)}{\sqrt{2\pi}\tilde{u}\sigma_{yp}\sigma_{zp}} \exp\left[-\frac{y^2}{2\sigma_{yp}^2}\right]$$

$$x \sum_{m=-\infty}^{\infty} \left\{ \exp\left[-\frac{\left(z-h_{ep}-2mz_{ieff}\right)^2}{2\sigma_{zp}^2}\right] + \exp\left[-\frac{\left(z+h_{ep}+2mz_{ieff}\right)^2}{2\sigma_{zp}^2}\right] \right\}$$

(26)

where h_{ep} is the height of the penetrated plume height and z_{ieff} is the height of the upper reflecting surface in a stable layer.

For flow in complex terrain, AERMOD incorporates the concept of a dividing streamline (Snyder et al., 1985), and the plume is modelled as a combination of terrain-following and terrain-impacting states. This approach has been designed to be physically realistic and simple to implement while avoiding the need to distinguish among simple, intermediate and complex terrain. As result, AERMOD removes the need for defining complex regimes; all terrain is handled in a consistent and continuous manner that is simple while still considering the dividing streamline concept in stably-stratified conditions.

The model considers the influence of building wakes and it enhances vertical turbulence to account for the "convective like" boundary layer found in night-time urban areas.

4.4. Annual concentration distributions in the city of Buenos Aires

Hourly urban background concentrations of NO_2, CO and PM_{10} at each grid square (1 x 1 km) in which the city of Buenos Aires has been divided, are estimated applying the two atmospheric dispersion models described above. DAUMOD model is applied to compute area source emissions contribution and AERMOD to estimate point sources contribution. Hourly data registered at the meteorological station of the domestic airport (located in the city) and the emissions inventory for Buenos Aires city (Section 4.2.) have been used in calculations. Figs. 5, 6 and 7 show the horizontal distributions of computed mean annual NO_2, CO and PM_{10} concentrations within the city of Buenos Aires. High concentration values can be found downtown and near the main train stations in the city, where there are usually more activity and traffic. The NO_2, CO and PM_{10} concentration patterns show large spatial variability that is mainly related to the distribution of area sources emissions. Higher concentration values are related to higher traffic density area.
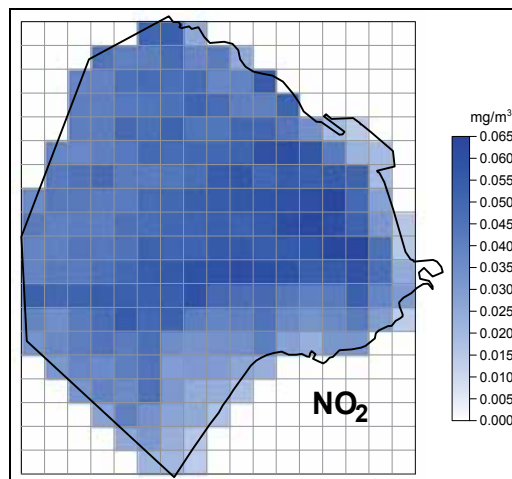
Fig. 5. Mean annual background concentrations of NO_2 in Buenos Aires city.
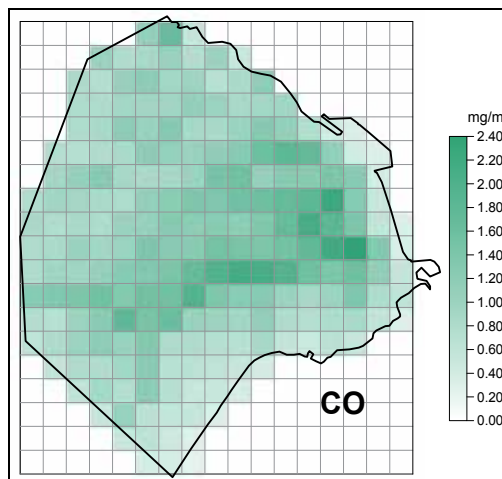
Fig. 6. Mean annual background concentrations of CO in Buenos Aires city.
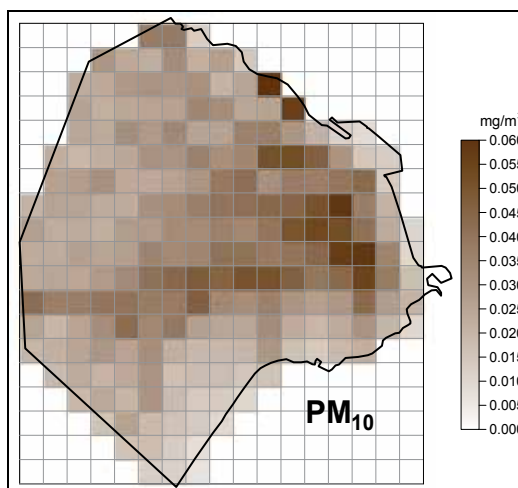
Fig. 7. Mean annual background concentrations of PM_{10} in Buenos Aires city.

4.5. Application of the methodology for designing the air quality monitoring network

The site selection proposed methodology described in Section 3 has been applied to determine the site locations for monitoring 1-h average NO_2 concentration (k=1), 1-h (k=2) and 8-h (k=3) average CO concentrations and 24-h average PM_{10} concentration (k=4) in the atmosphere of the city of Buenos Aires, greater than reference concentration levels.

Reference concentration levels have been selected considering the Air Quality Guidelines established by the World Health Organization (W.H.O., 2000, 2006). A weighing factor (ω_j) of 1 is assigned to the Air Quality Guideline levels. Table 3 presents the reference concentration levels and the corresponding weighing factors for the three pollutants considered. According to the proposed methodology, in this application, M=4 and n_k=7.

Weighing factor (ω_j)	NO$_2$ (averaging time: 1h)	CO (averaging time: 1h)	CO (averaging time: 8h)	PM$_{10}$ (averaging time: 24h)
	mg/m^3	mg/m^3	mg/m^3	mg/m^3
0.5	0.10	15	5	0.025
0.7	0.14	21	7	0.035
0.9	0.18	27	9	0.045
1.0	0.20	30	10	0.050
1.2	0.24	36	12	0.060
1.5	0.30	45	15	0.075
2.0	0.40	60	20	0.100

Table 3. Reference concentration levels and weighing factors (ω_j) for NO$_2$ (averaging time: 1h), CO (averaging times: 1h and 8h) and PM$_{10}$ (averaging time: 24h).

The values of 1-h average NO$_2$ concentrations, 1-h and 8-h average CO concentrations and 24-h average PM$_{10}$ concentrations ($C_{i,k}$) are estimated for each grid square in which the city has been divided applying DAUMOD and AERMOD atmospheric dispersion models.

Using model estimations of ($C_{i,k}$) and data on Table 3, the values of the exceedance score ES$_k$ (Equation (1)) for each combination (air pollutant, averaging time) (k=1,...,4) are estimated for each grid square. Fig. 8 presents the horizontal distribution of the total exceedance score (ES= ES$_1$ + ES$_2$ + ES$_3$ + ES$_4$) in the urban area.

In order to evaluate the population factor (PF) given by Equation (3), the horizontal distribution of population density (inhab/km^2) in the city has been elaborated using the information of the last National Census (INDEC, 2008). Fig. 9 shows the horizontal distribution of the population factor (PF) in the city of Buenos Aires.
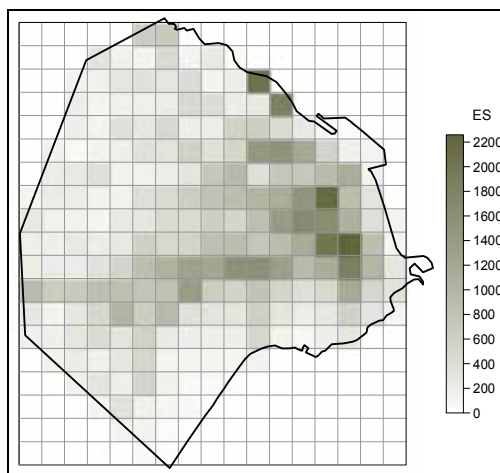
Fig. 8. Horizontal distribution of the total exceedance score ($ES = \sum_{k=1}^{4} ES_k$) in the city of Buenos Aires.
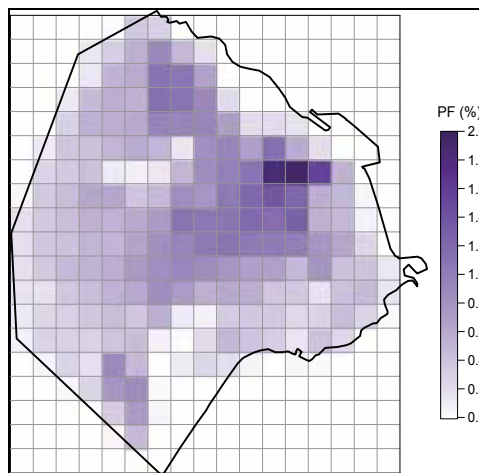
Fig. 9. Horizontal distribution of the population factor (PF) in the city of Buenos Aires.

In this way, knowing the total exceedance score (ES) and the population factor (PF) for each grid square, the horizontal distribution of the total score (TS= PFxES) (Fig. 10) is estimated using Equation (4). A preliminary monitoring network configuration is defined considering a budget constraint that limits the number of monitoring sites to twelve. The location of the 12 stations is obtained maximizing TS and considering a minimum distance of D=1km between two sensors of the same pollutant. Fig. 11 shows the monitoring sites of the preliminary network.
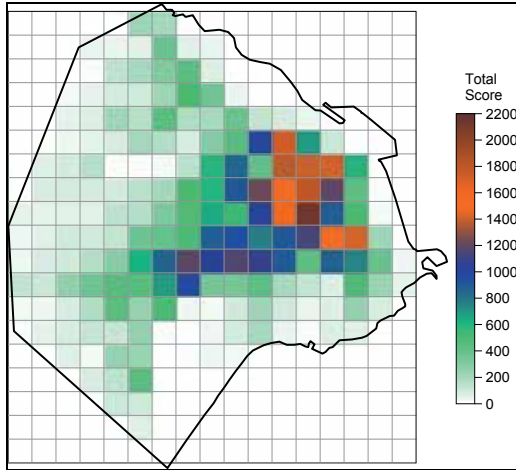
Fig. 10. Horizontal distribution of the Total Score (TS) in the urban area.
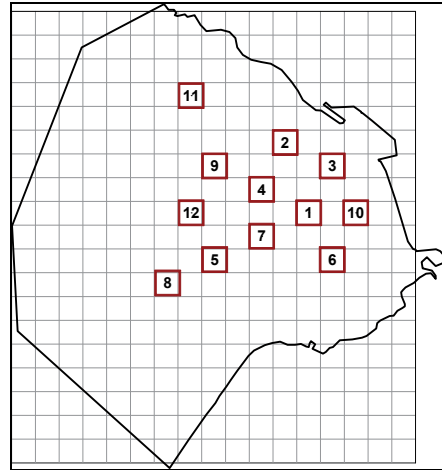
Fig. 11. Monitoring locations selected considering the total score and the distance constraint (preliminary configuration).

The final configuration of the proposed monitoring network is defined comparing the mean concentration of each pollutant at near preliminary sites, using the t-test. If the difference between average concentrations at two nearby sites is statistically significant at the 99% confidence level, both sites remain in the final network configuration. Otherwise, the site with lower TS can be discarded. Tables 4 and 5 show if the difference between average concentrations at a pair of near sites is statistically significant at the 99% (Yes:Y, No: N).

NO₂	1	2	3	4	5	6	7	8	9	10	11	12
1		Y	Y	Y		Y	Y			Y		
2			Y	Y			Y		Y			
3				Y		N			Y			
4					N		Y		Y		Y	Y
5						Y	Y	Y	Y			Y
6							N		Y			
7								N				Y
8												Y
9										Y	Y	
10												
11												N

CO	1	2	3	4	5	6	7	8	9	10	11	12
1		Y	Y	Y		Y	Y			Y		
2			Y	Y					Y		Y	
3				Y		N			N			
4					Y		Y		Y		Y	Y
5						Y	Y	Y	Y			Y
6							N		N			
7								N				Y
8												Y
9											Y	Y
10												
11												Y

Table 4. It is indicated if the difference between the average concentrations at two nearby monitoring locations is statistically significant at the 99% confidence level (Y: yes; N: no)

PM$_{10}$	1	2	3	4	5	6	7	8	9	10	11	12
1		N	Y	Y		Y	Y			Y		
2			Y	Y					Y	Y		
3				N		Y			Y			
4					N		Y		Y		Y	Y
5						N	Y	Y	Y			Y
6							Y			N		
7									N			Y
8												Y
9											Y	Y
10												
11												N

Table 5. It is indicated if the difference between the average concentrations at two nearby monitoring locations is statistically significant at the 99% confidence level (Y: yes; N: no)

Fig. 12 shows the proposed monitoring sites and the pollutants to be measured at each site according to results on Tables 4 and 5.
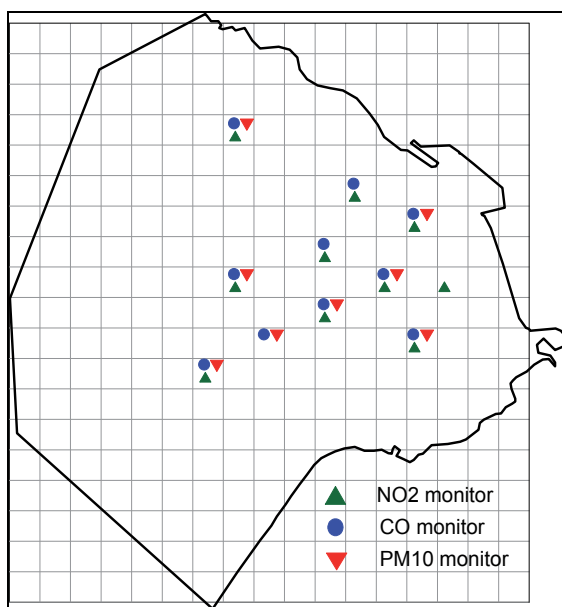
Fig. 12. Sites chosen to locate an air quality monitoring station and pollutants to be measured.

Once the proposed network (Fig. 12) is in operation, the environmental authority of the city may be interested to know the horizontal extension of the "spatial representativeness" of mean concentration values registered at each monitoring site. Figs. 13, 14 and 15 shows the areas near each monitoring site where the NO$_2$, CO and PM$_{10}$ mean concentrations cannot be considered statistically significant different at the 99% confidence level, obtained after the application of the t-Student test.
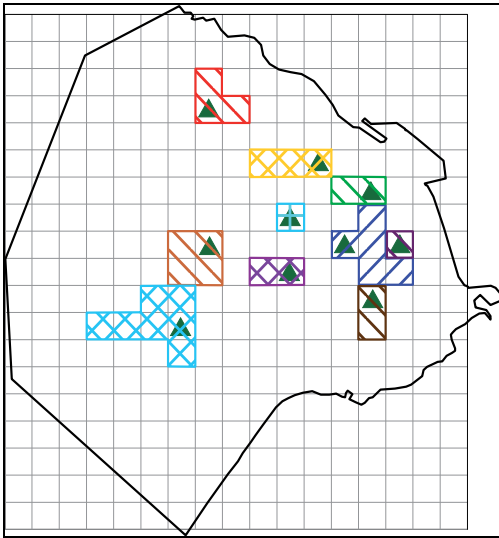
Fig. 13. "Spatial representativeness" for NO$_2$ monitoring stations (▲).
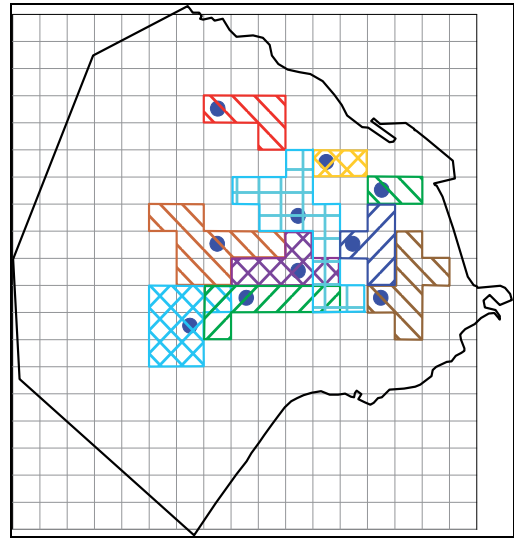
Fig. 14. "Spatial representativeness" for CO monitoring stations (●).
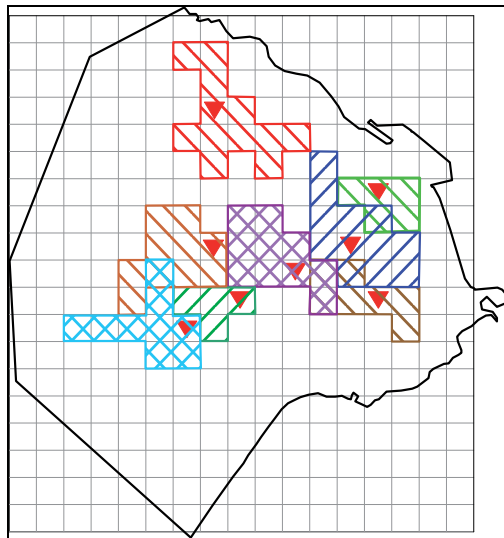
Fig. 15. "Spatial representativeness" for PM$_{10}$ monitoring stations (▼).

5. Conclusion

A multiple objective and multi-pollutant planning procedure for designing an urban air quality monitoring network is presented in this study. The considered monitoring objectives are to maximize the "detection capability" of higher pollutant concentrations and the "protection capability" for areas with higher population density. The design methodology is based on the analysis of air pollutant concentrations estimated by atmospheric dispersion

models. It simultaneously considers an exceedance score and a population factor. A statistical analysis is used for optimization.

The methodology is applied to design a NO_2, CO and PM_{10}, monitoring network for the city of Buenos Aires considering a spatial resolution (for the emission inventory and model estimations) of 1 x 1km. Air pollutant concentrations in the city have been estimated using the DAUMOD and AERMOD atmospheric dispersion models, that evaluate the contribution of area and point sources, respectively.

The optimal alternative of the proposed network can be summarized as: a) seven locations for monitoring NO_2, CO and PM_{10}; b) two sites for NO_2 and CO; c) one location for CO and PM_{10} and d) one station for NO_2 only. The "spatial representativeness" of mean concentrations at monitoring sites varies with each pollutant: a) for NO_2, between 1-7km^2; b) for CO between 2-11km^2 and c) for PM_{10}, between 4-12km^2.

It must be noted that the ultimate decision in site selection is left to the air quality monitoring authority.

Future studies could be focused on: a) the evaluation of how sensitive is the proposed methodology for air quality network design to slight changes in the input data (e.g. the weighing factors, the spatial resolution) and b) the inclusion of other optimization objectives (e.g. land use, frequency of violations of air quality standards, protect damage to vulnerable receptors as historic and/or artistic valuable property).

6. References

Ainslie, B., Reuten, C., Steyn, D.G., Le, N.D. & Zidek, J.V. (2009). Application of an entropy-based Bayesian optimization technique to the redesign of an existing monitoring network for single air pollutants. *Journal of Environmental Management*, Vol. 90, pp. 2715–2729.

Arya S. P. (1999). *Air Pollution Meteorology*. Oxford University Press. New York

Baldauf, R., Wiener, R.W. & Heist, D.K. (2002). Methodology for Siting Ambient Air Monitors at the Neighborhood Scale. *Journal of Air & Waste Management Association*, Vol. 52, pp. 1433–1442.

Bocca, B., Caimi, S., Smichowski, P., Gómez, D. & Cairoli, S. (2006). Monitoring Pt and Rh in urban aerosols from Buenos Aires, Argentina. *Science of the Total Environment*, Vol. 358, pp. 255-264.

Bogo, H., Negri, R.M. & San Román, E. (1999). Continuous measurement of gaseous pollutants in Buenos Aires city. *Atmospheric Environment*, Vol. 33, pp. 2587-2598.

Bogo, H., Gómez, D. R., Reich, S. L., Negri, R. M. & San Román, E. (2001). Traffic pollution in downtown of Buenos Aires City. *Atmospheric Environment*, Vol. 35, pp. 1717-1727.

Bogo, H., Otero, M., Castro, P., Ozafrán, M. J., Kreiner, A., Calvo, E. J. & Negri, R. M. (2003). Study of atmospheric particulate matter in Buenos Aires city. *Atmospheric Environment*, Vol. 37, pp. 1135-1147.

Briggs, G. A. (1993) Plume dispersion in convective boundary layer. Part II: Analysis of CONDORS field experiment data. *Journal of Applied Meteorology*, Vol. 32, pp. 1388-1425.

Caselton, W.F., Kan, L. & Zidek, J.V. (1992) Quality data networks that minimize entropy. In: *Statistics in the Environmental and Earth Sciences*. Walden, A. & Guttorp, P. (Eds.), pp. 10-38, Halsted Press, New York.

CERC (2003). *ADMS-Urban. An Urban Air Quality Management System. User Guide. Version 2.0.* Cambridge Environmental Research Consultants Ltd., Cambridge.

Cimorelli, A. J., Perry, S. G., Venkatram, A., Weil, J. C. , Paine, R. J., Wilson, R. B., Lee, R. F., Peters, W. D. & Brode, R. W. (2005). AERMOD: A dispersion model for industrial source applications Part I: General model formulation and boundary layer characterization. *Journal of Applied Meteorology*, Vol. 44, pp. 682-693.

Derwent, R.G. & Middleton, D.R. (1996). An empirical function for the ratio NO_2:NO_x. *Clean Air*, Vol. 26, pp. 57-62.

Dixon, J., Middleton, D.R. & Derwent, R.G. (2001). Sensitivity of nitrogen dioxide concentrations to oxides of nitrogen controls in the United Kingdom. *Atmospheric Environment,* Vol. 35, pp. 3715-3728.

Egmond, N.D.V. & Onderdelinden, D. (1981). Objective analysis of air pollution monitoring network data: spatial interpolation and network density. *Atmospheric Environment,* Vol. 15, pp. 1035–1046.

Elkamel, A., Fatehifar, E., Taheri, M., Al- Rashidi, M.S. & Lohi, A. (2008). A heuristic optimization approach for Air Quality Monitoring Network design with the simultaneous consideration of multiple pollutants. *Environmental Management*, Vol. 88, pp. 507-516.

Elsom, D.M. (1978). Spatial correlation analysis of air pollution data in an urban area. *Atmospheric Environment*, Vol. 12, pp. 1103–1107.

EMEP/CORINAIR. (2001). *Atmospheric Emission Inventory Guidebook,* Third Edition, European Environment Agency, Copenhagen.

EPA. (1995). *Compilation of Air Pollution Emission Factors*, AP-42, 5th ed., United States Environmental Protection Agency, Research Triangle Park, NC.

EPA. (2004). *User's Guide for the AMS/EPA Regulatory Model-AERMOD,* EPA-454/B-03-001. United States Environmental Protection Agency, Research Triangle Park, NC.

Fagundez, L. A., Fernández V. L., Marino T. H., Martín I., Persano D. A., Rivarola y Benítez M., Sadañiowski I. V., Codnia J. & Zalts A. (2001). Preliminary air pollution monitoring in San Miguel, Buenos Aires. *Environmental Monitoring and Assessment*, Vol. 71, pp. 61-70.

Gifford, F.A. (1970). *Atmospheric Diffusion in an Urban Area*, NOAA Research Lab. Nº 33. Oak Ridge, N. C.

Gifford, F.A. & Hanna, S.R. (1973). Modelling urban air pollution. *Atmospheric Environment,* Vol. 7, pp. 131-136.

Graves, R.J., Lee, T.D. & McGinnis, L.F.J. (1981). Air Monitoring Network Design: case study. *Journal of Environmental Engineering ASCE*, Vol. 107, pp. 941-955.

Gryning, S.E., Footslog, A.A.M., Irwin, J.S. & Sivertsen, B. (1987). Applied dispersion modelling based on meteorological scaling parameters. *Atmospheric Environment*, Vol. 21, pp. 79-89.

Handscombe, C.M. & Elsom, D.M. (1982). Rationalisation of the National Survey of Air Pollution Monitoring Network of the United Kingdom using spatial correlation analysis: a case study of the Greater London area. *Atmospheric Environment*, Vol. 16, pp. 1061-1070.

Hougland, E.S. & Stephens, N.T. (1976). Air Pollutant Monitor Siting by Analytical Techniques. *Journal of the Air Pollution Control Association*, Vol. 26, pp. 51-53.

Husain, T. & Khan, S.M. (1983). Air Monitoring Network Design Using Fisher's Information Measures—A Case Study. *Atmospheric Environment*, Vol. 17, pp. 2591–2598.

Hwang, J.S. & Chan, Ch.Ch. (1997). Redundant measurements on urban air monitoring networks in air quality reporting. *Journal of Air & Waste Management Association*, Vol. 47, pp. 614-619.

INDEC (2008). *Estimaciones de población total por departamento y año calendario. Período 2001-2010*. Serie Análisis Demográfico. Nº 34. Instituto Nacional de Estadística y Censos. (www.indec.gov.ar) (in Spanish)

Kainuma, Y., Shiozawa, K, & Okamoto, S. (1990). Study of the Optimal Allocation of Ambient Air Monitoring Stations. *Atmospheric Environment*, Vol. 24B, pp. 395–406.

Koda, M. & Seinfeld, J.H. (1978). *Air monitoring siting by objective.* EPA-600/4-7-036, United States Environmental Protection Agency, Las Vegas, Nevada.

Langstaff, J., Seigneur, C. & Liu, M.K. (1987) Design of an optimum air monitoring network for exposure assessment. *Atmospheric Environment*, Vol. 21, pp. 1393-1410.

Le, N.D. & Zidek, J.V. (2006). *Statistical Analysis of Environmental Space–Time Processes*. Springer, New York.

Liu, M. K., Avrin, J., Pollack, R. I., Behar, J. V., & McElory J.L. (1986) Methodology for designing air quality monitoring networks. *Environmental Monitoring and Assessment*, Vol. 6, pp. 1-11.

Mazzeo, N. A. & Venegas, L. E. (1991). Air pollution model for an urban area. *Atmospheric Research*, Vol. 26, pp. 165-179.

Mazzeo, N. A. & Venegas, L. E. (2000). Practical use of the ISCST3 model to select monitoring site locations for air pollution control. *International Journal of Environment and Pollution*, Vol. 14, pp. 246-259.

Mazzeo, N. A. & Venegas, L. E. (2002). Estimation of cumulative frequency distribution for carbon monoxide concentration from wind-speed data, in Buenos Aires (Argentina). *Water, Air and Soil Pollution, Focus*, Vol. 2, pp. 419-432.

Mazzeo, N. A. & Venegas, L. E. (2003). Carbon monoxide and nitrogen oxides emission inventory for Buenos Aires City (Argentina). *Proceedings of the Fourth International Conference on Urban Air Quality – Measurement, Modelling and Management*, pp. 159-162. Prague, Czech Republic, March 2003. University of Hertfordshire, Hatfield.

Mazzeo, N. A. & Venegas, L. E. (2004). Some aspects of air pollution in Buenos Aires city. I*nternational Journal of Environment and Pollution*, Vol. 22, pp. 365-378.

Mazzeo, N. A., Venegas, L. E. & Choren, H. (2005). Analysis of NO, NO_2, O_3 and NO_x concentrations measured at a green area of Buenos Aires City during wintertime, *Atmospheric Environment*, Vol. 39, pp. 3055-3068.

Mazzeo, N.A. & Venegas, L.E. (2008). Design of an air quality surveillance system for Buenos Aires city integrated by a NO_x monitoring network and atmospheric dispersion models. *Environmental Modeling and Assessment*, Vol. 13, pp. 349-356.

McElroy, J.L., Behar, J.V., Meyers, T.C. & Liu, M.K. (1986). Methodology for designing Air Quality Monitoring Networks: II. Application to Las Vegas, Nevada, for carbon monoxide. *Environmental Monitoring and Assessment*, Vol. 6, pp. 13-34.

Middleton, D.R., Jones, A.R., Redington, A.L., Thomson, D.J., Sokhi, R.S., Luhana, L. & Fisher, B.E.A. (2008). Lagrangian modelling of plume chemistry for secondary pollutants in large industrial plumes. *Atmospheric Environment*, Vol. 42, pp. 415-427.

Modak, P.M. & Lohani, B.N. (1985a). Optimization of ambient Air Quality Monitoring Networks: Part I. *Environmental Monitoring and Assessment*, Vol. 5, pp. 1–19.

Modak, P.M. & Lohani, B.N. (1985b). Optimization of ambient Air Quality Monitoring Networks: Part II. *Environmental Monitoring and Assessment*, Vol. 5, pp. 21–38.

Modak, P.M. & Lohani, B.N. (1985c). Optimization of ambient Air Quality Monitoring Networks: Part III. *Environmental Monitoring and Assessment*, Vol. 5, pp. 39–53.

Mofarrah A. & Husain T. (2010). A Holistic Approach for optimal design of Air Quality Monitoring Network Expansion in an Urban Area. *Atmospheric Environment,* Vol. 44, pp. 432-440.

Munn, R.E. (1975). Suspended particulate concentrations: Spatial correlations in the Detroit-Windsor area. *Tellus*, Vol. XXVII, pp. 397–405

Munn, R.E. (1981). *The Design of Air Quality Monitoring Networks*. MacMillan, London.

Nakamori, Y. & Sawaragi, Y. (1984) Interactive Design of Urban Level Air Quality Monitoring Network. *Atmospheric Environment,* Vol. 18, pp. 793–799.

Noll, K.E. & Mitsutome, S. (1983) Design methodology for optimum dosage air monitoring site selection. *Atmospheric Environment,* Vol. 17, pp. 2583–2590.

Pasquill, F. & Smith, F.B. (1983). *Atmospheric Diffusion,* John Wiley & Sons, New York.

Pickett, E.E. & Whiting, R.G. (1981). The design of cost-effective Air Quality Monitoring Networks. *Environmental Monitoring and Assessment*, Vol. 1, pp. 59-74.

Pineda Rojas, A.L., Venegas, L.E. & Mazzeo, N.A. (2007). Emission inventory of carbon monoxide and nitrogen oxides for area sources at Buenos Aires Metropolitan Area (Argentina). *Proceedings of the Sixth International Conference on Urban Air Quality*, Cyprus, March 2007, University of Hertfordshire, Hatfield.

Pires, J.C.M., Pereira, M.C., Alvim-Ferraz, M.C.M. & Martins, F.G. (2009). Identification of redundant air quality measurements through the use of principal component analysis. *Atmospheric Environment*, Vol. 43, pp. 3837–3842.

Rao, S. T. (2009). Environmental Monitoring and Modeling Needs in the 21st Century, *EM*, October, pp. 3-4.

Rideout, G., Gourley, D. & Walker, J. (2005). *Measurement of in-service vehicle emissions in Sao Paulo, Santiago and Buenos Aires*. ARPEL Environmental Report Nº25, Environmental Services Association of Alberta, Edmonton.

Romano, D., Gaudioso, D. & De Lauretis, R. (1999). Aircraft emissions: a comparison of methodologies based on different data availability. *Environmental Monitoring and Assessment*, Vol. 56, pp. 51-74.

Sarigiannis, D.A. & Saisana, M. (2008). Multi-objective optimization of air quality monitoring. *Environmental Monitoring and Assessment*, Vol. 136, pp. 87-99.

SAyDS. (2002). *Estudio o línea de base de concentración de gases contaminantes en atmósfera en el área de Dock Sud en Argentina.* Agencia de Cooperación Internacional del Japón en Argentina y Secretaría de Desarrollo Sustentable y Política Ambiental, Buenos Aires. www.medioambiente.gov.ar/dock_sud/default.htm (in Spanish)

Smith, D.G. & Egan, B.A. (1979). Design of monitor networks to meet multiple criteria, *Journal of Air and Waste Management Association,* Vol. 29, pp. 710-714.

Snyder, W. H., Thompson, R. S., Eskridge, R. E., Lawson, R. E., Castro, I. P., Lee, J. T., Hunt, J. C. R. & Ogawa, Y. (1985). The structure of the strongly stratified flow over hills: Dividing streamline concept. *Journal of Fluid Mechanics,* Vol. 152, pp. 249-288.

Tseng, C.C. & Chang, N.B. (2001). Assessing relocation strategies of urban air quality monitoring stations by GA-based compromise programming. *Environment International*, Vol. 26, pp. 523-541.

Venegas, L.E. & Martin, P.B. (2004). Particulate Matter Concentrations in the City of Buenos Aires, *Proceedings of the 14th Congreso Argentino de Saneamiento y Medio Ambiente*, Buenos Aires, November 2004, AIDIS-Argentina, Buenos Aires (in Spanish).

Venegas, L.E. & Mazzeo, N.A. (2000). Carbon monoxide concentrations in a street canyon at Buenos Aires City (Argentina). *Environmental Monitoring & Assessment*, Vol. 65, pp. 417-424.

Venegas, L.E. & Mazzeo, N.A. (2002). An evaluation of DAUMOD model in estimating urban background concentration. *Water, Air and Soil Pollution: Focus*, Vol. 2, pp. 433-443.

Venegas, L.E. & Mazzeo, N.A. (2003a). Design methodology for background air pollution monitoring site selection in an urban area. *International Journal of Environment and Pollution*, Vol. 20, pp. 185-195.

Venegas, L.E. & Mazzeo, N.A. (2003b). Air quality in an area of Buenos Aires City (Argentina), *Proceedings of the III Congresso Interamericano de Qualidade do Ar*, Canoas, Brasil, July 2004, Asociación Interamericana de Ingeniería Sanitaria y Ambiental –Asociacion Brasileira de Engenharia Sanitaria e Ambiental, Seçao, Rio Grande do Sul. (in Spanish).

Venegas, L.E. & Mazzeo, N.A. (2005). Application of atmospheric dispersion models to evaluate population exposure to NO_2 concentration in Buenos Aires. *International Journal of Environment and Pollution*, Vol. 25, pp. 224-238.

Venegas, L. E. & Mazzeo, N. A. (2006). Modelling of urban background pollution in Buenos Aires city (Argentina). *Environmental Modelling & Software*, Vol. 21, pp. 577-586.

Venegas, L.E. & Mazzeo, N.A. (2010). An ambient air quality monitoring network for Buenos Aires city. *International Journal of Environment and Pollution*, Vol. 40, pp. 184-194.

Weil J. C. (1988). Dispersion in the convective boundary layer. In: *Lectures on Air Pollution Modeling*. Venkatram, A. & Wingaard, J.C. (Eds.), pp. 167-227, American Meteorological Society, Boston.

Weil, J. C., Corio, L. A. & Brower, R. P. (1997). A PDF dispersion model for buoyant plumes in the convective boundary layer. *Journal of Applied Meteorology*, Vol. 36, pp. 982-1003.

W.H.O. (2000). *Air Quality Guidelines for Europe*, World Health Organization Regional Publications, European Series Nº91, Copenhagen.

W.H.O. (2006). *Air Quality Guidelines. Global Update 2005*. Particulate matter, ozone, nitrogen dioxide and sulphur dioxide, World Health Organization, Geneve.

Wieringa, J. (1980). A revaluation of the Kansas mast influence on measurements of stress and cup anemometer overspeeding. *Boundary-Layer Meteorology,* Vol. 18, pp. 411-430.

Willis, G. E. & Deardorff, J. W. (1981). A laboratory study of dispersion in the middle of the convectively mixed layer. *Atmospheric Environment*, Vol. 15, pp. 109-117.

Wu, S. & Zidek, J.V. (1992). An entropy based review of selected NADP/NTN network sites for 1983-86. *Atmospheric Environment*, Vol. 26A, pp. 2089-2103.

Optimization of the design of air quality monitoring networks and its application to NO$_2$ and O$_3$ in Seville, Spain

Antonio Lozano[a], José Usero[b] , Eva Vanderlinden[b], Juan Raez[a],
Juan Contreras[c], Benito Navarrete[b] and Hicham El Bakouri[b]

[a] *The Environmental Management Company (EGMASA), Seville, Spain*
[b] *Department of Chemical and Environmental Engineering, University of Seville, Spain*
[c] *Environmental Council of the Junta de Andalucía, Seville, Spain*

1. Introduction

Air quality monitoring networks are used in order to obtain objective, reliable and comparable information on the air quality of a specific area. This makes it possible to take the requisite measures to protect the environment, to assess the results of such actions and to ensure that the public is properly informed about the state of the air quality.

The approval and publication of Council Directive 1996/62/EC (1996) on ambient air quality assessment and management and its daughter directives, 1999/30/EC (1999), 2000/69/EC (2000), 2002/3/EC (2002) and 2004/107/EC (2005), gave rise to an important change in air quality monitoring systems in Europe. Recently, in the interests of clarity, simplification and administrative efficiency, the above-mentioned European directives were replaced by the single Directive 2008/50/EC (2008) on ambient air quality and cleaner air for Europe with no change to existing air quality objectives for nitrogen dioxide (NO$_2$) and ozone (O$_3$). With the aim of being as up-to-date as possible, references to the law will be made to Directive 2008/50/EC (2008).

The present work describes a new method to design or optimize air quality networks, particularly to monitor nitrogen dioxide and ozone in compliance with the legislation. The proposed method consists of four steps for choosing the best locations for the monitoring stations: (1) preliminary evaluation; (2) sampling campaigns with passive diffusion samplers; (3) spatial interpolation; (4) selection of best locations for the monitoring stations.

The first step in the optimization process is the preliminary evaluation of air quality based on historical data. This evaluation makes it possible to establish the minimum number and characteristics of the stations needed in each zone as set forth in Directive 2008/50/EC (2008). The location of the monitoring stations depends on the distribution of the contamination levels of pollutants, as the stations need to record representative levels for the entire zone.

The second step of the method consists of sampling campaigns with a large number of diffusive samplers to determine the concentration of nitrogen dioxide and ozone in the

studied area. In a diffusion sampler, the gas molecules are transported only by molecular diffusion, which is a function of air temperature and pressure. This independence allows the time-weighted average ambient concentration to be calculated using Fick's laws of diffusion (UNEP, 2004). Diffusive sampling has been increasingly used for the assessment of environmental exposure to criteria pollutants, such as O_3, NO_2, SO_2, NH_3 and COV (Hangartner et al., 1989; Koutrakis et al., 1993; Liu et al., 1995; Krupa & Legge, 2000 and Thöni et al., 2003). The benefits of passive sampling devices include simplicity of sampling, low operating costs, high correlation results as compared to continuous monitors and deployment in areas where there is no electricity. A large number of units can be used simultaneously, gathering information on the spatial distribution of the pollutants. Diffusive sampling can be used if the average, instead of the real-time, and pollutant concentration is adequate for the purpose of monitoring (Krupa & Legge, 2000 and De Santis et al., 2003).

To assign a contamination value to every point in the zone, spatial interpolations (step 3) of the information obtained in the sampling campaign are made by use of Geographical Information Systems (GIS), which are becoming increasingly popular to estimate the distribution of environmental phenomena (Spokas et al., 2000 and Duc et al., 2000). Also Directive 2008/50/EC (2008) states that modelling techniques should be applied where possible to enable point data to be interpreted in terms of geographical distribution of concentration. The result map obtained by GIS is used to define the best sites for placing the control stations of the air quality monitoring network. In this last step for the design or optimization of the monitoring network a selection of the best locations for the sampling stations is made, obtaining a spatial distribution that ensures compliance with the micro- and macroscale location criteria established in the legislation.

Every few years, new sampling campaigns are carried out to verify the improvement of the optimized network and to make sure that the chosen locations for the stations are still representative of the air quality in the area.

The method proposed in this article for optimization of the design of air quality monitoring networks and its application to NO_2 and O_3 was carried out in Seville, a city located in Andalucia, southern Spain. The area considered in this study is Seville city and the most densely populated part of its metropolitan area. Seville city has a population of 703 206 inhabitants, and covers a superficies of 140.8 km². Its metropolitan area is composed by 46 municipals and includes a population of About 1 500 000 inhabitants, occupying a superficies of 4900 km². Traffic is the most important source of air pollution in Seville, followed by households. The mining industry of Seville area is the principal source of SO_2 pollution. The sunny climate in the study area favours the photochemical reactions that originate smog.

2. Materials and methods

The method developed in this study consists of four steps that make it possible to choose the best locations for the stations of the monitoring network, in compliance with the legislation. Additionally, a fifth step is included for verification of the optimized monitoring network.

2.1. Preliminary evaluation

This first step for optimising or designing an air monitoring network includes zonification, classification of the zones and determination of the minimum number of control stations needed.

The zonification of the study area consists in subdividing the territory into different zones with similar air quality. The division is based on studies of topography, population, economic activities, weather, land use, situation of nature parks and emission into the atmosphere. A zone with a population in excess of 250 000 inhabitants is considered an agglomeration. The possible types of zones are city (agglomeration), industrial or rural area (Annex XV of Directive 2008/50/EC, 2008).

Each zone is classified in terms of the level of recorded pollutants. The upper and lower assessment thresholds (UAT and LAT) for nitrogen dioxide (NO_2) are determined in Annex II of Directive 2008/50/EC (2008) (Table 1). The zones are classified as follows:
- The level of the pollutant is higher than the UAT;
- The level is between the LAT and the UAT;
- The level is lower than the LAT.

	Hourly limit value for the protection of human health (NO_2)	Annual limit value for the protection of human health (NO_2)	Annual critical level for the protection of vegetation and natural ecosystems (NO_X)
Upper assessment threshold	70 % of limit value (140 µg/m^3, not to be exceeded more than 18 times in any calendar year)	80 % of limit value (32 µg/m^3)	80 % of critical level (24 µg/m^3)
Lower assessment threshold	50 % of limit value (100 µg/m^3, not to be exceeded more than 18 times in any calendar year)	65 % of limit value (26 µg/m^3)	65 % of critical level (19.5 µg/m^3)

Table 1. Upper and lower assessment thresholds for nitrogen dioxide and oxides of nitrogen as expressed in Annex II of Directive 2008/50/EC.

The classification of each zone or agglomeration in relation to the assessment thresholds must be reviewed at least every five years. Classification must be reviewed earlier in the event of significant changes in activities relevant to ambient concentrations (Directive, 2008). The minimum number of sampling points for the fixed measurement of NO_2 concentration in ambient air is given in annex V of Council Directive 2008/50/EC (2008) and depends on the classification of the zone. The minimum number of sampling points for fixed continuous measurements of ozone (O_3) concentration to assess air quality for compliance with the target values, long-term objectives and information and alert thresholds where continuous measurement is the sole source of information is indicated in Annex IX of Directive 2008/50/EC (2008). Table 2 resumes the minimum number of sampling points needed for NO_2 and O_3.

Population of agglomeration or zone (thousands)	NO₂		O₃	
	Maximum concentrations exceed UAT	Maximum concentrations between UAT and LAT	agglomeration	Other zones (urban and suburban)
0-249	1	1	--	1
250-499	2	1	1	2
500-749	2	1	2	2
750-999	3	1	2	2
1000-1499	4	2	3	3
1500-1999	5	2	3	4
2000-2749	6	3	4	5
2750-3749	7	3	5	6
3750-4749	8	4	1 additional station per 2 million inhabitants	
4750-5999	9	4		
>6000	10	5		

Table 2. Minimum number of sampling points (for fixed measurement) needed for NO_2 and O_3 depending on the classification of the zone

2.2. Sampling campaigns with passive diffusion samplers

Once the evaluation requirements are known, the most appropriate sites for placement must be determined. Areas with high pollution levels but representative of the zone must be ascertained. In the proposed method, sampling campaigns with passive diffusion samplers are planned in order to determine the spatial distribution of the concentrations and to find the locations within each zone that have the best characteristics for continuous monitoring of air quality.

For purposes of taking into account the influence of weather conditions on the contamination levels of nitrogen oxide, two sampling campaigns are carried out, one in winter and one in summer. As the formation of ozone is a photochemical reaction, a large difference in ozone concentrations could be expected between winter and summer, with higher ozone values in summer. Therefore, this pollutant is only measured during a summer campaign (Guicherit & Van Dop, 1977 and Beck et al., 1998). Each sampling campaign consisted of a series of biweekly sampling periods. The average of the periods determines the campaign value. The annual behaviour of the pollutants is estimated from the values of the winter and summer campaigns. In accordance with Annex I of Directive 2008/50/EC (2008), the indicative measurement of nitrogen dioxide needs a minimum time coverage of 14% which means one measurement a week at random, evenly distributed over the year, or eight weeks evenly distributed over the year. For ozone, the minimum time coverage for indicative measurements should be more than 10% during summer.

To determine the best siting for the air quality monitoring stations in Seville, two NO_2 campaigns were carried out, one in winter (December 1999-April 2000) and one in summer

(June 2000-October 2000). Both campaigns included eight biweekly sampling periods. For O_3, a summer campaign of 7 biweekly periods was carried out from June 2000 until September 2000.

Different kind of passive samplers can be used to determine the studied pollutants. In this study, Ogawa badges were used. They consist of a cylindrical Teflon surface, whose approximate dimensions are 19 mm in external diameter and 30 mm in length. The cylinder is comprised of two chambers separated by a solid segment. The following components are placed in each chamber of the Ogawa tub, beginning at the innermost part: a solid pad, a pad-retaining ring, a stainless steel grid, a fibre-glass filter impregnated with the absorbent reagent, another grid of stainless steel and the diffuser cap at the outer end (Ogawa, 1998 and Ogawa, 2001).

The diffusive sampling technique is based on the principle that the pollutant is absorbed into a specific sorbent at a rate controlled by molecular diffusion of the gaseous pollutant in the air. The theoretical rate at which the diffusive sampler collects the pollutant from the atmosphere is described by Fick's first law of diffusion (Perkauskas & Mikelinskiene, 1998). The concentration C of the pollutant is given by $C=m/(U \cdot t)$, where m is the collected mass of pollutant, t is the averaging time and U is the uptake rate.

For the adsorption of NO_2, the filters are impregnated with triethanolamine (TEA) (Palmes et al., 1976 and Atkins et al., 1986). Many chemicals can be used in diffusive sampling badges for the determination of O_3 concentrations, although studies have shown that sodium nitrite is a better one (Zhou & Smith, 1997). Nitrite impregnated filters were used in this work. Research has shown that when using passive samplers to determine ozone concentrations, measurements are not affected by temperature and humidity and, under ambient conditions, co-pollutant interference is negligible (Koutrakis et al., 1993).

The passive diffusion samplers are placed in such a manner that the measurements represent the concentrations of their environment. Geographic Information Systems (GIS) are used to select the sampling sites. The siting criteria established in the legislation are implied in these systems to obtain those sites susceptible to get a diffusion sampler. Annexes III and VIII of Directive 2008/50/EC (2008) list the macroscale and microscale siting criteria to consider for sampling of NO_2 and O_3 respectively.

To minimize the effect of wind, rain and direct solar radiation, the tubes were protected by rain shields. Different models are available, ceramic rain shields giving the best results in this study. This protection was attached to wooden blocks (5 cm), fastened to posts and placed between 1.5 and 2.5 m from the ground, using urban furniture. Duplicates (10% of the exposed tubes) were used to determine reproducibility, and field blanks (10% of the exposed tubes) were placed to determine the background reagent contamination and interference during the analytical process. Samplers were sent to and from the field in sealed plastic recipients.

A large number of diffusive samplers were used in this study, taking advantage of low operating costs and ease of use. They were located at 139 sites, representing a total area of 1109.3 km², which makes the average radius of representativeness per sampler 1.59 km.

The municipals included in the study area are: Seville (53 sites), Alcalá de Guadaira, Dos Hermanas, La Rinconada, Coria del Río, Bormujos, Santiponce, La Algaba, Gelves, Mairena del Alcor, Mairena del Aljarafe, Camas, Carmona, Castilleja de Guzmán, Espartinas, Gines, Palomares del Río, La Puebla del Río, Salteras, Tomares, Utrera and Valencina de la Concepción. Figure 1 shows how the urban nucleus and the most populated part of the metropolitan area was covered by a large number of samplers.
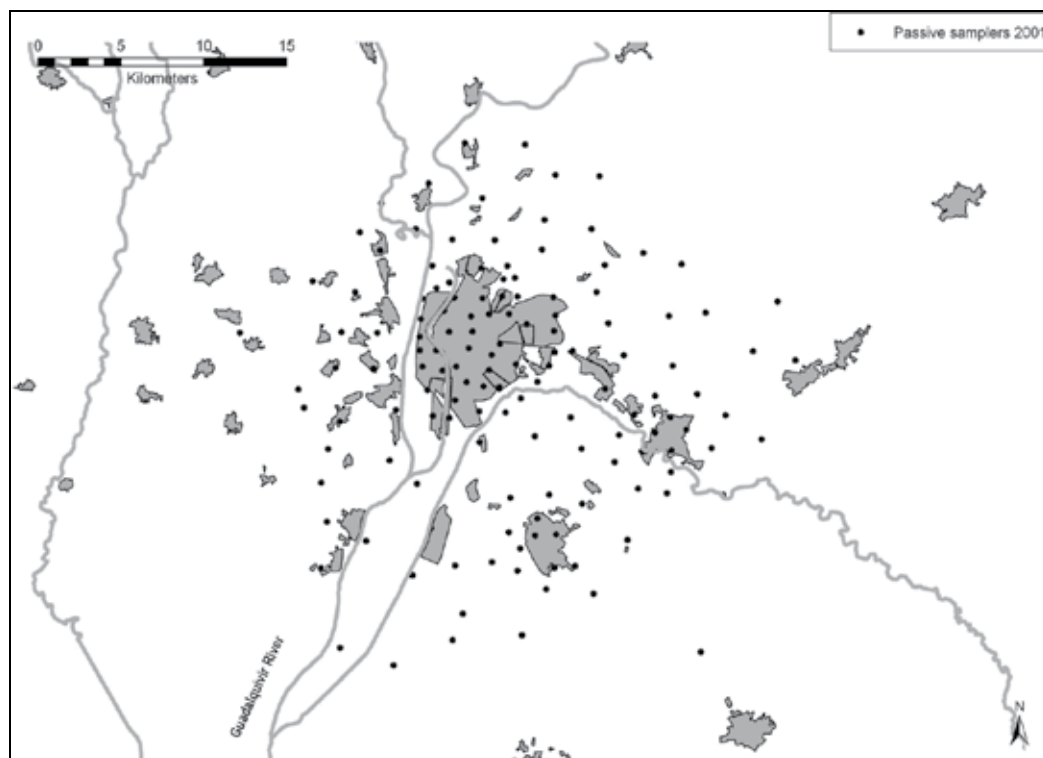
Fig. 1. Location of the diffusive samplers in the Seville sampling campaign 2000

During the sampling period, the nitrogen dioxide was adsorbed and accumulated in the diffusion sampler as nitrite ion after reaction with triethanolamine (TEA), the adsorbent reagent (Palmes et al., 1976). After the sampling period, the captures were sent to the Andalusian Reference Laboratory for Air Quality Monitoring (LARCA), where the analyses were carried out. The analysis of this ion was performed with UV-spectrophotometry at 545 nm, using the Griess-Saltzmann method (UNEP/WHO, 1994). A Shimadzu spectrophotometer model UV-1203 with double beam and 1 cm cuvettes was used. The accuracy of the obtained results was confirmed using a t test. Experimental values of t were less than the critical value at 5% level which means that there were no significant differences between the obtained values.

The technique used for the determination of ozone concentrations was based on the oxidation reaction of nitrite (NO_2) with ozone O_3 producing nitrate (NO_3) (Koutrakis et al., 1993), followed by ion chromatography of the produced nitrate (Palmes et al., 1976). The analyses were also done at the Andalusian Reference Laboratory for Air Quality Monitoring

(LARCA), using a Dionex DX 120 chromatograph with a conductivity detector, Ion-Pack AS9-HC anion separation column (4 x 250 mm), CS12A suppressor column and a graphic recorder connected by a PC to the chromatograph. The effluent used was Na_2CO_3 12 mM, loop: 100 µL. The accuracy of the obtained results was also less than 5%.

2.3. Spatial interpolations

The concentration values obtained were spatially interpolated to assign a contamination value to every point of the studied area. The campaigns used for the determination of urban and suburban pollution were characterized by a large number of significantly concentrated sampling points, and therefore the Inverse Distance Weighted (IDW) method for spatial interpolation was used (Watson & Philip, 1985). This method is based on the assumption that the interpolating surface will be influenced most by the nearby points and less by the more distant points. The interpolating surface is a weighted average of the scatter points and the weight assigned to each scatter point diminishes as the distance from the interpolation point to the scatter point increases. The IDW interpolation does not need any kind of assumption about the distribution and behaviour of the measurements. The result of this method is exact at the sampling points and behaves smoothly without abrupt changes between the points of measurement (Burrough & McDonell, 1998).

2.4. Selection of the best locations

The sampling points directed at the protection of human health shall be sited in such a way as to provide data on the areas within zones and agglomerations where the highest concentrations occur to which the population is likely to be directly or indirectly exposed for a period which is significant in relation to the averaging period of the limit value(s).The sampling points should also provide data on levels in other areas within the zones and agglomerations which are representative of the exposure of the general population.

The control stations must be chosen according to the macro- and microscale siting requirements in Annexes III and VIII of Directive 2008/50/EC (2008) for the measurement of nitrogen dioxide and ozone, respectively.

By macroscale siting requirements is meant that areas within a zone or agglomeration with the highest concentrations to which the population is likely to be exposed need to be covered by a monitoring station, thus avoiding measuring very small micro-environments. Urban background locations should be sited so that their pollution level is influenced by all sources upwind of the station. Insofar as practicable, some of the microscale siting criteria that should apply are following: the flow around the inlet sampling probe should be unrestricted without any obstructions affecting the airflow in the vicinity of the sampler; the inlet sampling point should be between 1.5 m and 4 m above the ground and away from the immediate vicinity of sources in order to avoid the direct intake of emissions unmixed with ambient air, etc.

First, areas meeting the macrositing criteria are selected, using Geographical Information Systems (GIS). Then, microscale criteria are applied.

2.5. Validation of the relocation of the monitoring stations

To verify the improvement of the optimized network, a new sampling campaign was carried out from May 2005 until May 2006 to make sure that the chosen locations for the

stations were still representative of the air quality in the area. The method used was the same as the one described in sections 2.1 to 2.3. If it seems necessary to relocate some stations, the method described in section 2.4 should be used.

3. Results and discussion

3.1. Preliminary evaluation

Before the optimization of the air quality assessment network, Seville city had six stations in the urban area and two in the suburban area to assess NO_2 pollution.

A comparison was made between the recorded historical values of NO_2 between 1988 and 2000 and the assessment thresholds established in the applicable legislation, Directive 2008/50/EC (2008), which establishes 40 µg/m³ as annual limit value for NO_2. 200 µg/m³, not to be exceeded more than 18 times a calendar year, is set as hourly limit value for NO_2. The historical data were obtained from the eight fixed monitoring stations and three campaigns with mobile units. At seven locations the annual concentration value for NO_2 exceeded the upper assessment threshold (80% of the limit value) and at one location the lower assessment threshold was exceeded (65% of the limit value). The upper assessment threshold for the hourly limit value (70% of limit value) was exceeded at six locations, and the lower assessment threshold (50% of limit value) at two locations.

This, together with the number of inhabitants, makes a minimum of two monitoring station for NO_2 necessary, as established in Annex V of Directive 2008/50/EC (2008), overtaken in Table 2. One station should be urban background and the other one traffic-orientated. Two stations for fixed measurement of ozone concentrations are necessary, as the population of the studied agglomeration is between 500 000 and 1 000 000 inhabitants (Table 2) (Annex IX of Directive 2008/50/EC, 2008).

The same exercise was done for Alcalá de Guadaira, Dos Hermanas and Aljarafe region, the most populated areas of the metropolitan area (Table 3).

area	Superficies (km²)	inhabitants	n° of stations necessary		Existing stations before	Existing stations after
			NO_2	O_3		
Seville	141	703 206	2	2	8	7
Alcalá de Guadaira	285	70 155	1	1	2	1
Dos Hermanas	159	122 943	1	1	0	1
Aljarafe	1136	338 532	1	1	0	1

Table 3. Number of assessment stations necessary and present before and after optimization of the quality network.

Before the optimization of its air quality assessment network, Seville city had eight assessment stations, but it only needs two NO_2 orientated and two O_3 orientated assessment stations to comply legislation. In the target metropolitan area, Alcalá de Guadaira, Dos Hermanas and Aljarafe need each a NO_2 and an O_3 assessment station. Before adaptation of the assessment network, only Alcalá de Guadaira counted with air quality assessment stations. After optimization, one stations is located in each area, assessing both NO_2 and O_3.

3.2. Sampling campaigns with passive diffusion samplers

To determine the best siting for the stations of the air quality monitoring network in Seville, two sampling campaigns were carried out using passive diffusion samplers located at 139 sites, as indicated in Figure 1. The average NO_2 concentration for Seville area in 2000 was 23.7 µg/m^3, and 7.6 and 52.1 µg/m^3 were the minimum and maximum values, respectively. This agrees with the measurement of NO_2 in 363 cities of the United Kingdom (Campbell et al., 1994), which shows average concentration levels varying from 17.5 until 87.5 µg/m^3. Moreover the obtained values for nitrogen dioxide in Seville vary considerably between summer and winter, with average values of 18.1 µg/m^3 and 29.4 µg/m^3 respectively. In winter they are higher because of the greater stability of the atmosphere in that season and because of NO_2 involvement in the formation of ozone in summer. The same is observed in other cities in Europe (Perkauskas & Mikelinskiene, 1998 and Karppinen et al., 2000).

The average ozone concentration for the summer campaign in 2000 was 71.6 µg/m^3. The lowest average concentration recorded was 42.0 µg/m^3, while the highest was 93.2 µg/m^3. These concentrations are comparable with those measured by Klumpp et al. (2006) during summer 2001 at many sites in studies conducted in 11 European cities.

3.3. Spatial interpolations

To get a better view of the distribution of pollutant concentrations, the obtained values were spatially interpolated using the Inverse Distance Weighted (IDW) method. Figure 2 shows the annual average for NO_2 in Seville.
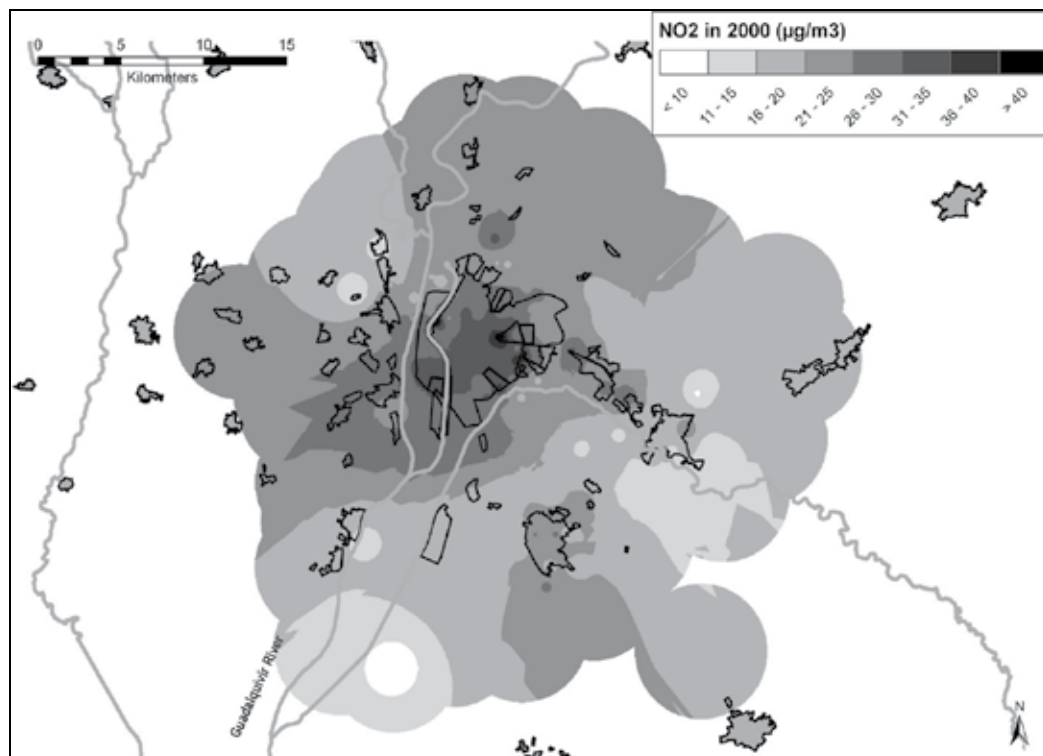
Fig. 2. The annual average concentrations for NO_2 in Seville (2000)

The city centre is characterized by concentration between 26 and 35 µg/m³. The maximum NO₂ values were found in the new city centre, where they reached concentrations of more than 36 µg/m³. This is due to intense traffic circulation, which is the principal responsible for nitrogen dioxide emissions. Lowest values were found in the outskirts of the city, with the lowest concentrations in the northwest and southeast. A study in Vilnius (Perkauskas & Mikelinskiene, 1998) and another in Antwerp (Stranger et al., 2008) commented the same phenomenon; NO₂ average rates depend strongly on traffic and are highest in crossroads and lowest at the background suburban layer.

The dense populated municipals in the Aljarafe region present NO₂ values between 21 and 30 µg/m³. Dos Hermanas is characterized by values between 21 and 25 µg/m³ while Alcalá de Guadaira presents values between 16 and 20 µg/m³ and some higher values in the western part of the community.

The distribution of the ozone concentrations measured in the summer campaign can be seen in Figure 3.
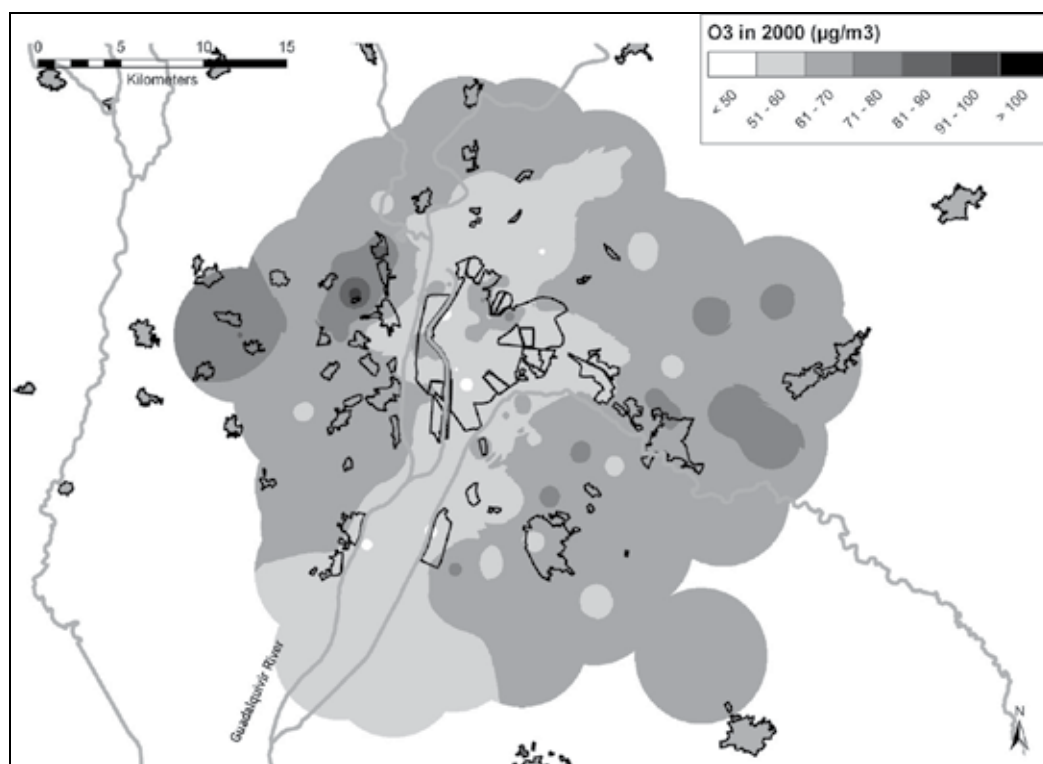
Fig. 3. The average concentrations for O₃ in the summer campaigns in Seville (2000)

The highest levels are found in the suburban regions, situated at a certain distance from the area of maximum pollutant emissions. During the transport of NO₂, principally emitted in the centre of the studied zone, reactions that generate ozone take place, obtaining the highest concentrations in the suburban regions. The samplers situated in the eastern and western part of the studied area recorded the highest concentrations (>61 µg/m³, locally >71

μg/m³), while the city centre of Seville showed lower ozone concentrations (<60 μg/m³). The population of the municipals in the Aljarafe, Dos Hermanas and Alcalá de Guadaira is exposed to higher ozone levels than the inhabitants of Seville city.

3.4. Selection of the locations for the monitoring network in Seville
Figure 4 represents the location of the monitoring stations before and after the optimization of the monitoring network in Seville and its metropolitan area.

Fig. 4. Location of monitoring stations before and after optimization of the monitoring network in Seville

Before the optimization of the air quality assessment network, Seville city had six stations in the urban area and two in the suburban area to assess NO$_2$ pollution. Five of the urban stations were traffic-orientated (Ranilla, Enramadilla, Macarena, Torneo, Reina Mercedes) and one urban background-orientated (Principes). One of the suburban stations was also background-orientated (Santa Clara) and the other one was industrial-orientated (San Jeronimo).
In the preliminary evaluation of Seville city it was concluded that this agglomeration needs only two monitoring stations for nitrogen dioxide assessment. It was decided to keep all monitoring stations but part of them was relocated. After applying macro- and microscale siting requirements using Geographical Information Systems, it was decided to move station Enramadilla to Aljarafe where it will function as a suburban background station. Station Macarena was moved to Bermejales where it will function as an urban background station.

Reina Mercedes moves to Centro where it will take the function of urban background station. One of the stations of Alcalá de Guadaira is moved to Dos Hermanas.

Although only two NO$_2$ monitoring stations are obligatory by law, Seville counts with seven monitoring stations after adapting the assessment network. Two stations are traffic-orientated (Ranilla, Torneo) and tree are urban background-orientated (Principes, Bermejales, Centro). The two suburban stations keep their function (Santa Clara background-orientated and San Jeronimo industrial-orientated). The urban and suburban monitoring stations will not only measure NO$_2$ concentrations but are also chosen for O$_3$ assessment.

Aljarafe area, Dos Hermanas and Alcalá de Guadaira count each with one fixed moninitoring station to assess NO$_2$ and O$_3$ after redesigning the assessment network.

3.5. Validation of the relocation of the monitoring stations

From May 2005 until April 2006, a new sampling campaign was carried out in Seville to make sure that the chosen locations for the stations were still representative of the air quality of the zone. Figure 5 gives the average NO$_2$ values in the 2005-2006 sampling campaign. The figure was obtained by the same method as used in the 2000 sampling campaign. The results are very similar to those obtained in 2000. The monitoring stations were correctly located for the assessment of NO$_2$ as they record values representative for the areas they cover within the agglomeration.
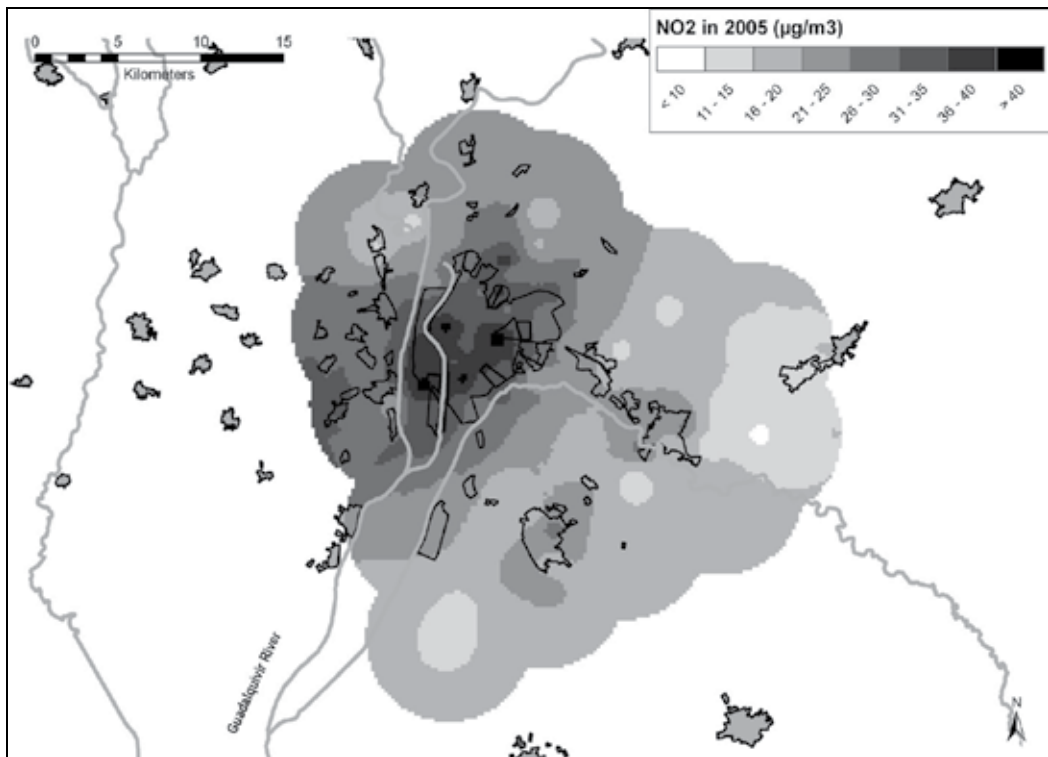
Fig. 5. Annual average concentrations for NO$_2$ in Seville (2005-2006)

Figure 6 shows the average values for O_3 in the 2005-2006 sampling campaign. The figure was obtained by the same method as used for the 2000 sampling campaign. The average O_3 concentrations are higher than those registered in the 2000 sampling campaign. A significant difference is found in the western part of Seville city. The location with high ozone concentrations is situated between two industrial parks and an important confluence of highways. More traffic and polluting industry comparing to 2000 can explain this difference. The general higher values are explained by metrological differences between 2000 and 2005 and a general increase of pollution (traffic).
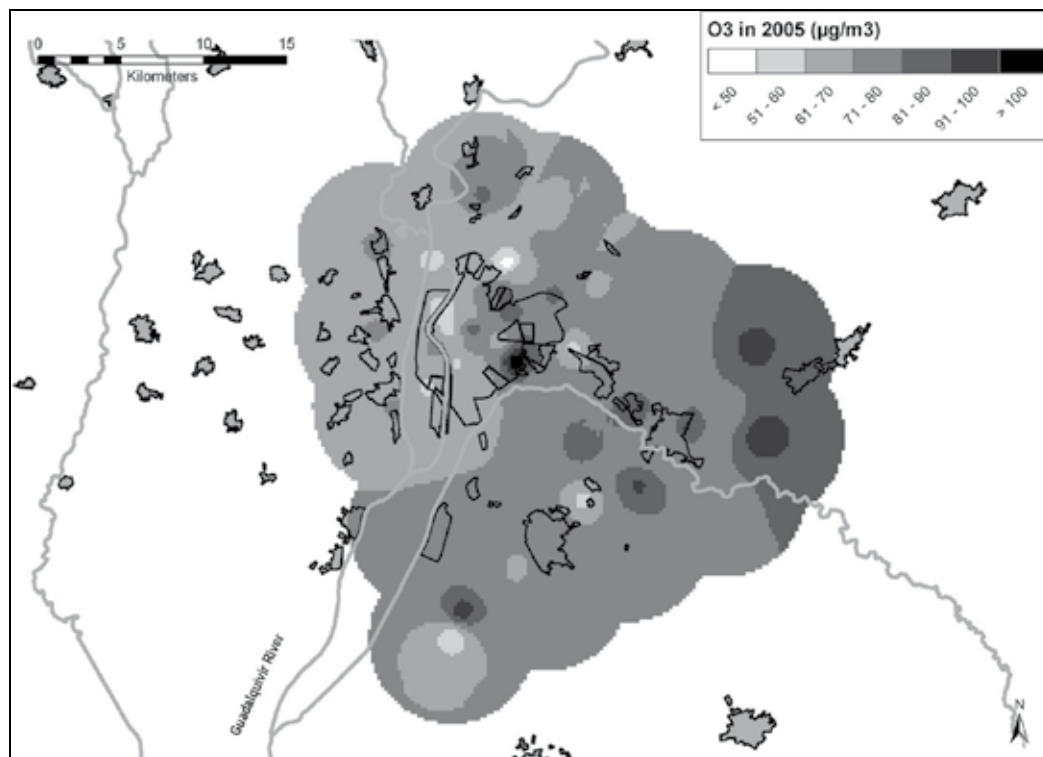
Fig. 6. The average concentrations for O_3 in Seville (2005-2006)

To better assess the O_3 pollution in this part of Seville city, it is desirable to locate a monitoring station at this location. However, it has to be outlined that the high concentrations are apparently very local and the recorded values would not be representative for the whole study area.

4. Conclusions

The method described was applied to the optimization of the air quality assessment network in Seville city and the most populated metropolitan municipals, more precisely for monitoring nitrogen dioxide and ozone. The completion of the four steps described in this method for designing and optimizing air quality monitoring networks made it possible to determine that two control station for NO_2 assessment and two for O_3 assessment were

necessary in Seville city according to the legislation. Even so one station for NO_2 and for O_3 were necessary in the metropolitan areas Aljarafe, Alcalá de Guadaira and Dos Hermanas. Following the described method it was possible to find the right locations for the monitoring stations, in compliance with the macro- and microscale siting requirements established in the European legislation.

The sampling campaigns in 2000 revealed an average concentration of 23.7 $\mu g/m^3$ NO_2 with maximum values up to 52.1 $\mu g/m^3$ in the new Seville city centre, characterized by intense traffic. The highest average ozone concentrations were recorded in the eastern and western part of the studied area, reaching 93.2 $\mu g/m^3$; the average O_3 value in Seville was 61.6 $\mu g/m^3$.

In 2005-2006 another sampling campaign was carried out to verify whether the locations of the monitoring stations were still representative for the area's air quality. The results were affirmative for NO_2 and showed that an extra O_3 assessment station in the west of Seville city could be interesting.

5. Acknowledgement

6. References

Atkins, D.H.F.; Sandalls, J.; Law, D.V.; Hough, A.M. & Stevenson, K. (1986). *The measurement of nitrogen dioxide in the outdoor environment using passive diffusion tube samplers*, Report AERE-R 12133. Harwell laboratory, ISBN 9780705811439, Oxfordshire, United Kingdom

Beck, J.P.; Krzyzanowski, M. & Koffi, B. (1998). *Tropospheric Ozone in the European Union "The Consolidated Report"*, European Environment Agency, November 1998. ISBN 9282856720, Copenhagen

Burrough, P.A. & McDonell, R.A. (1998). *Principles of geographical information systems,* Oxford University Press, ISBN 9780198233657, Oxford, UK

Campbell, G.W.; Stedman, J.R. & Stevenson, K. (1994). A survey of nitrogen dioxide concentrations in the United Kingdom using diffusion tubes, July-December 1991, *Atmospheric Environment*, Vol. 28 (3) 477-486

Council Directive 1996/62/EC of 27 September 1996 on ambient air quality assessment and management, Official Journal of the European Union, L 296, 21/11/1996, 55-63

Council directive 1999/30/EC of 22 April 1999 relating to limit values for sulphur dioxide, nitrogen dioxide and oxides of nitrogen, particulate matter and lead in ambient air, Official Journal of the European Union, L 163, 29/06/1999, 41-60

De Santis, F.; Vazzana, C.; Menichelli, S.; Allegrini, I. & Morimoto, S. (2003). Ozone monitoring in the polar troposphere using a new diffusive sampler. *Physics and Chemistry of the Earth*, Vol. 28 (28-30) 1213-1216

Directive 2000/69/EC of the European Parliament and of the Council of 16 November 2000 relating to limit values for benzene and carbon monoxide in ambient air, Official Journal of the European Union, L 313, 13/12/2000, 12-21

Directive 2002/3/EC of the European Parliament and of the Council of 12 February 2002 relating to ozone in ambient air, Official Journal of the European Union, L 67, 09/03/2002, 14-30

Directive 2004/107/EC of the European Parliament and of the Council of 15 December 2004 relating to arsenic, cadmium, mercury, nickel and polycyclic aromatic hydrocarbons in ambient air, Official Journal of the European Union, L 23, 26/01/2005, 3-16

Directive 2008/50/EC of the European Parliament and of the Council of 21 May 2008 on ambient air quality and cleaner air for Europe, Official Journal of the European Union, L 152, 11/6/2008, 1-44

Duc, H.; Shannon, I. & Azzi, M. (2000). Spatial distribution characteristics of some air pollutants in Sydney. *Mathematics and Computers in Simulation*, Vol. 54 (1) 1-21

Guicherit, R. & Van Dop, H. (1977). Photochemical production of ozone in Western-Europe (1971-1975) and its relation to meteorology. *Atmospheric Environment*, Vol. 11 (2) 145-155

Hangartner, M.; Burri, P. & Monn, C. (1989). Passive sampling of nitrogen dioxide, sulfur dioxide and ozone in ambient air, *Proceedings of the eight World Clean Air Congress*, The Hague, Holland

Karppinen, A.; Kukkonen, J.; Elolähde, T.; Konttinen, M. & Koskentalo, T. (2000). A modelling system for predicting urban air pollution: comparison of model predictions with the data of an urban measurement network in Helsinki, *Atmospheric Environment*, Vol. 34 (22) 3735-3743

Klumpp, A.; Ansel, W.; Klumpp, G.; Calatayud, V.; Garrec, J.P.; He, S.; Peñuelas, J.; Ribas, A.; Ro-Poulsen, H.; Rasmussen, S.; Sanz, M.J. & Vergne, P. (2006). Ozone pollution and ozone biomonitoring in European cities, Part I: Ozone concentrations and cumulative exposure indices at urban and suburban sites, *Atmospheric Environment*, Vol. 40 (40) 7963-7974

Koutrakis, P.; Wolfson, J.M.; Bunyaviroch, A.; Froehlich, S.E.; Hirano, K. & Mulik, J.D. (1993). Measurement of ambient ozone using a nitrite coated filter. *Analytical Chemistry*, Vol. 65 (3) 209-214

Krupa, S.V. & Legge, A.H. (2000). Passive sampling of ambient, gaseous air pollutants: an assessment from an ecological perspective. *Environmental Pollution*, Vol. 107 (1) 31-45

Liu, L.S.; Koutrakis, P.; Leech, J. & Broder, I. (1995). Assessment of ozone exposures in the greater metropolitan Toronto area. *Journal of the Air & Waste Management Association*, Vol. 45 (4) 223-234

Ogawa (1998). *NO, NO2, NOX and SO2 sampling protocol using the Ogawa sampler,* fourth revision, Ogawa & Company, USA, 1998

Ogawa (2001). *Protocol for ozone measurement using the ozone passive sampler badge*, third revision, Ogawa & Company, USA, 2001

Palmes, E.D.; Gunnison, A.F.; DiMattio, J. & Tomczyk, C. (1976). Personal sampler for nitrogen dioxide, *American Industrial Hygiene Association Journal*, Vol. 37 (10) 570-577

Perkauskas, D. & Mikelinskiene, A. (1998). Evaluation of SO2 and NO2 concentration levels in Vilnius (Lithuania) using passive diffusion samplers. *Environmental Pollution*, Vol. 102 (1) 249-252

Spokas, K.; Graff, C.; Morcet, M. & Aran, C. (2000). Implications of the spatial variability of landfill emission rates on geospatial analyses. *Waste Management*, Vol. 23 (7) 599-607

Stranger, M.; Krata, A.; Kontozova-Deutsh, V.; Bencs, L.; Deutsh, F.; Worobiec, A.; Naveau, I.; Roekens, E. & Van Grieken, R. (2008). Monitoring of NO_2 in the ambient air with passive samplers before and after a road reconstruction event, *Microchemical Journal*, Vol. 90 (2) 93-98

Thöni, L.; Seitler, E.; Blatter, A. & Neftel, A. (2003). A passive sampling method to determine ammonia in ambient air. *Journal of Environmental Monitoring*, Vol. 5 (1) 96-99

UNEP/WHO (United Nations Environmental Program and World Health Organization). (1994). GEMS/AIR Methodology Reviews Vol. 1: *Quality Assurance in Urban Air Quality Monitoring*, United Nations Environmental Program, WHO/EOS/94.1, UNEP/GEMS/94.A.2, Nairobi

United Nations Environmental Program (UNEP). (2004). *Guidance for a Global Monitoring Programme for Persistent Organic Pollutants*, first edition, Switzerland

Watson, D.F. & Philip, G.M. (1985). A refinement of inverse distance weighting interpolation. *Geo-Processing*, Vol. 2 (4) 315-327

Zhou, J. & Smith, S. (1997). Measurement of ozone concentrations in ambient air using a Badge-type passive monitor, *Journal of the Air & Waste Management Association*, Vol. 47 (6) 697-703

Monitoring spatial and temporal variability of air quality using satellite observation data: A case study of MODIS-observed aerosols in Southern Ontario, Canada

DongMei Chen and Jie Tian
Department of Geography, Queen's University
Canada

1. Introduction

Aerosol refers to solid or liquid particles suspended in the air. Aerosol particles mostly originate from the earth surface and are well mixed within the atmospheric boundary layer of the atmosphere. Aerosols scatter and/or absorb solar radiation as well as emitted and reflected radiation from the earth (Ichoku *et al.*, 2004). As a consequence, aerosol particles can significantly affect radiative forcing of climate (Feczkó *et al.*, 2002), and play a key role in atmospheric physics and chemistry (Figueras i Ventura and Russchenberg, 2008; Han *et al.*, 2008). Moreover, the aerosols near the ground are one of the air pollutants responsible for human health hazard. Exposure to aerosols, both short-term and long-term, may cause considerable negative health effects. Accurate mapping of those parameters and their spatial and temporal changes is important for the evaluation of the current air dispersion modeling, air pollution control regulations, and other environmental and climate change related activities (Dockery *et al.*, 1993).

A crucial step toward the understanding of the complex effects of aerosols is to study aerosol properties and distribution (Haywood and Boucher, 2000). Aerosol optical depth (AOD), a dimensionless measure of atmospheric extinction of solar radiation by aerosols, is one of the most important aerosol properties. AOD can be measured *in situ* or estimated by remote sensing. Ground-based sunphotometers can provide direct measurement of AOD. The AOD data measured by this means is very accurate with a high temporal resolution. However, the limited spatial coverage of such data largely hampers the in-depth understanding of aerosol distribution, especially for the regions with few or no sunphotometers. Remote sensing provides an alternative data resource that is prominent in studying air quality. AOD can be derived from the spectral information sensed by certain relatively new satellites such as Moderate Resolution Imaging Spectroradiometer (MODIS) and Multi-angle Imaging SpectroRadiometer (MISR) (Remer *et al.*, 2006; Martonchik *et al.*, 2002). Satellite remote sensing of aerosol is advantageous on several aspects, including its extensive and continuous spatial coverage and lower cost for acquisition. However, the

MODIS-derived AOD is subject to weather condition and has lower accuracy and lower temporal frequency (once a day) than the sunphotometer measurements.

A number of studies have been conducted to address the spatial and temporal variability of aerosols. Early research mainly focused on a group of cities that hold an Aerosol Robotic Network (AERONET) site (equipped with a sunphotometer). For instance, Masmoudi *et al.* (2003) found higher spatial variability of AOD and AE for the central African sites than the Mediterranean ones. The central African sites showed a lower variation with the smallest values of their measured AE due to the presence of very large dust particles. Remotely-sensed data have also been used in the analysis of aerosol loading distribution in recent years. By mapping AOD over Europe at a continental scale, Koelemeijer *et al.* (2006) clearly identified Northern Italy, Southern Poland, and the Belgium/Netherlands/Ruhr area as major aerosol source regions. Frank *et al.* (2007) used the data from MISR for an inter-annual analysis of AOD variation over the Mojave desert of southern California. The authors suggested that AOD varies significantly across the desert and therefore the AERONET site at Rogers Dry Lake (within the desert) cannot be used to represent the aerosol conditions over the entire study area. However, the relationship between aerosol distribution and land use structure/topography has not been examined in previous studies.

This chapter reviews the algorithms used to extract AOD from MODIS data and presents a case study of using MODIS AOD data to investigate the spatial-temporal distribution patterns of aerosols in southern Ontario, Canada. The relationship between land-use structure and AOD has been analyzed through a correlation analysis and discuss the impacts of topography on the aerosol distribution.

2. Aerosal Retrieval from MODIS data

The Moderate Resolution Imaging Spectroradiometer (MODIS) is onboard the Earth Observing System (EOS) Terra and Aqua, with daytime equator crossing times of late morning (10:30am) and early afternoon (1:30pm), respectively. It is an optical scanner that observes the Earth in 36 channels covering visible, near, and shortwave infrared from 0.4μm to 14.5μm with spatial resolution ranging from 250 m to 1 km. Since launched in 1999, the Moderate Resolution Imaging Spectroradiometer (MODIS) has provided an unprecedented opportunity to monitor aerosol (or particulate matter) status and events, and examine the role of aerosols in the earth-atmosphere system. MODIS is designed to produce a wide variety of information about the three spheres that human life depends on: geosphere, hydrosphere, and atmosphere. The MODIS science team has correspondingly developed three groups of data products (Atmosphere, Ocean, and Radiometric/Geolocation).

The MODIS Atmosphere products are provided in data level 2 (5-minute swath granules) and data level 3 (global grid maps) according to the Distributed Active Archive Center (DAAC) data level scheme. In particular, the MODIS atmosphere product (level 2) provides retrieved Aerosol Optical Depth (AOD), representing columnar aerosol loading of the atmosphere, at a typical spatial resolution of 10 km. Two separate algorithms are applied for the retrieval of aerosols over land (Kaufman *et al.*, 1997a) and ocean (Tanre *et al.*, 1997). Over land, the retrieval is made at two wavelengths independently: 0.47 μm and 0.66 μm with the

aid of additional information from the 2.12 µm channel. The strategy for retrieving AOD over land from MODIS is introduced by Kaufman *et al.* (1997a). The satellite-measured reflectance ρ_λ^* at a particular wavelength can be approximated by:

$$\rho_\lambda^*(\theta_o, \theta, \phi) = \rho_\lambda^\alpha(\theta_o, \theta, \phi) + \frac{F_\lambda(\theta_o)T_\lambda(\theta)\rho_\lambda^s(\theta_o, \theta, \phi)}{1 - S_\lambda \rho_\lambda^s(\theta_o, \theta, \phi)} \tag{1}$$

where ρ_λ^α is the atmospheric path reflectance. F_λ represents the normalized downward flux for zero surface reflectance. S_λ is the atmospheric backscattering ratio. ρ_λ^s is the angular spectral surface reflectance. $\theta o, \theta$, and ϕ denote solar zenith angle, satellite zenith angle, and solar/satellite relative azimuth angle, respectively. Each term on the right hand side of Equation (1), except for the surface reflectance, is a function of the aerosol type and loading (AOD).

The reflectance sensed by the satellite sensor is separated into the surface reflectance and atmospheric path reflectance. Dark objects (e.g. vegetated and dark soil surfaces) are selected for AOD retrieval for their relatively low reflectance (at the visible bands). The older versions of the retrieval algorithm over land (e.g. C004-L) assume that aerosol is transparent in the 2.12 µm channel. The empirical relationships (correlation) between the surface reflectance at 0.47 µm/0.66 µm and 2.12 µm wavelengths have been recognized by Kaufman *et al.* (1997b). The physical reason for the correlation was found to be the combination of absorption of visible light by chlorophyll and infrared radiation by liquid water in healthy vegetation (Kaufman *et al.*, 2002). Therefore, the surface reflectance at 0.47 µm and 0.66 µm can be estimated based on the satellite-measured reflectance at 2.12 µm. In contrast, the surface reflectance in the most recent version of the algorithm over land (C005-L) is not only a function of the surface reflectance at 2.12 µm, but also a function of the scattering angle and the "greenness" (a parameter like the well-known Normalized Difference Vegetation Index) of the surface in the mid-Infrared spectrum (Levy *et al.*, 2007). Moreover, the C005-L algorithm also assumes that the 2.12 µm channel contains information about coarse mode aerosol as well as the surface reflectance. Assuming that a small set of aerosol types and loadings can describe the range of global aerosol, the MODIS aerosol retrieval algorithm relies on a lookup table (LUT) procedure (instead of real-time calculation). Radiative transfer calculations are pre-computed for a set of aerosol and surface parameters. The satellite measured radiance and the estimated surface reflectance are used as input into the LUT to retrieve AOD at 0.47 µm and 0.66 µm. The strategy of the algorithm is to examine the LUT to determine the conditions that can best mimic the MODIS-observed spectral reflectance, and retrieve the associated aerosol properties including AOD. The AOD at 0.55 µm can then be obtained by interpolating the values at 0.47 µm and 0.66 µm using the Ångström exponential (AE) coefficient, which is given by

$$\alpha = -\frac{\log\frac{\tau_1}{\tau_2}}{\log\frac{\lambda_1}{\lambda_2}} \tag{2}$$

where $\tau 1$ and $\tau 2$ represent the AOD values at the wavelengths of $\lambda 1$ and $\lambda 2$, respectively.

The global validation of the MODIS AOD collection 5 products shows a MODIS/AERONET regression line of y=1.01x+0.03, r=0.9 (Levy et al., 2007). It should be noted that surface reflectivity has impact on accuracy of MODIS-derived AOD as the relationships between

visible reflectance and mid-infrared are used in the MODIS aerosol retrieval algorithm to derive AOD over land. For very dark surfaces, the surface reflectance in the red channel may be overestimated, resulting in an underestimate in the derived AOD. Moreover, the highest latitude of the study area is below 47°N so that the solar elevation is high enough to allow retrieval of AOD by the algorithm, even in the mid-winter period.

3. Study Area

The study area of this research is Southern Ontario, the key agricultural and industrial area of Canada and home to nearly 12 million people based on 2006 demographics (Statistics Canada, 2007). Extending over southern Ontario is mainly the physiographic region of the Great Lakes-St Lawrence Lowerlands (Bone, 2005). Figure 1 shows the location of the study area. A continental climate affects this temperate mid-latitude region. The climate is highly modified by the influence of the Great Lakes: the addition of moisture from them increases precipitation amounts. The spatial and temporal distributions of both anthropogenic and natural aerosols are of particular concern due to their consequences on local climate and impacts on the local residents' health. The latest studies indicate that areas of southern Ontario often experience the highest levels of PM2.5 concentration in eastern Canada. Ontario is burdened with $9.6 billion in health and environmental damages each year due to the impact of ground-level fine PM and ozone (Yap *et al.*, 2005), which are generally attributed to the formation of smog. It therefore becomes a continuing priority for environmental researchers and government agencies (e.g. the Ontario Ministry of Environment) to develop a better understanding of the distributional patterns of these pollutants at multiple scales. There are only three AERONET sites (Windsor, Toronto, and Egbert) located in Ontario. It has therefore been a challenge for researchers to fully understand how aerosols are distributed across space in terms of concentration and size. Moreover, the increase of anthropogenic aerosols due to changes in land use and industrial activity has been found to have a significant impact on both the radiation budget and the hydrological cycle (Figuerasi Ventura and Russchenberg, 2008). The possible relationship between aerosol distribution and land use structure/topography has not been explicitly studied.

Fig. 1. Location map of the study area of southern Ontario

4. Data and Method

In this study, the MODIS aerosol product files (collection 5 data) from both Terra and Aqua have been collected for southern Ontario to cover the entire calendar year 2004. The collection 5 was chosen as its products were produced based on the most recent version of the retrieval algorithm. In total, over eight hundred MODIS aerosol image products of level 2 were collected from each platform (Terra and Aqua). These data were stored and provided in a standard hierarchical data format (HDF), which is a multi-object file format for sharing scientific data in multi-platform distributed environments. MATLAB programs have been developed to read the MODIS HDF files systematically and extract the parameters of AOD at 0.47µm and AE over land. The utility of MODIS-derived AOD data was first checked based on the frequency of valid measurements and the effective data coverage in different months. Both the AOD data and the AE data were binned into a 0.1°×0.1° grid. Typically, there are about 40 valid measurements (for both AOD and AE) available per grid cell for the study period. The number of valid MODIS-derived AOD values for each cell varies across space and time, so there will be some random differences associated with the observation frequency. The MODIS-derived AOD measurements were sampled to ensure a minimum of one day interval between the AOD values chosen for any averaging processing over each grid cell. This is mainly to reduce the possible temporal autocorrelation between the pixel values taken within a small time window (*e.g.* 3 hours). Yearly averaging and monthly averaging were performed for the grid cells and the municipal regions, respectively. The overall average and the standard deviation of AOD were calculated from the sampled AOD values for each month to reveal the seasonal variation.

The sampled AOD values were also aggregated by municipal regions, which often delimit the study area for local climate, air quality analyses. The monthly AOD means for the municipal regions were examined to capture seasonal distribution patterns. In space, the cities with a population greater than 100,000 have been selected and a statistical *t*-test was performed to find out those cities distinguishable from the general study area as a whole.

A detailed land use map and a digital elevation model were also collected as ancillary data for the study area. The land-use structure within the municipal regions and their corresponding AOD mean were also compared. Yet, only the municipal regions with land-use information were incorporated in our analysis due to the fact that complete land-use data were unavailable for the entire study area. The land-use types were aggregated into three major classes: Built-up Area, Vegetation Area, and Water Body. The yearly AOD means of the municipal regions were subsequently plotted against the fractions of the aggregated land uses within them. A correlation analysis was then performed to provide a quantitative description of the land use-AOD relationship. In addition, the digital elevation model (DEM) of southern Ontario was compared to its AOD distribution to help understand the impacts of the local topography on the aerosol dispersion or transportation.

5. Results and Discussion

5.1 Overall analysis

The observation of the collected data shows that, in southern Ontario, AOD generally varies between 0 to about 2.2 (unitless) and has an overall mean of 0.211 with a standard deviation

of 0.225. The frequency distribution of the collected AOD is shown in Fig. 2a. The availability of the valid AOD data from MODIS is highly season-dependent for southern Ontario. Due to the extremely limited number of valid AOD values (see Fig. 2b) and the lack of coverage for a great portion of the study area, MODIS can hardly provide a complete or unbiased picture of AOD for southern Ontario in January, February, March, or December. The data in these winter months were therefore excluded from the mean calculation to facilitate cross-space comparison. In other words, the yearly mean in the present study represents the AOD average over April though November.
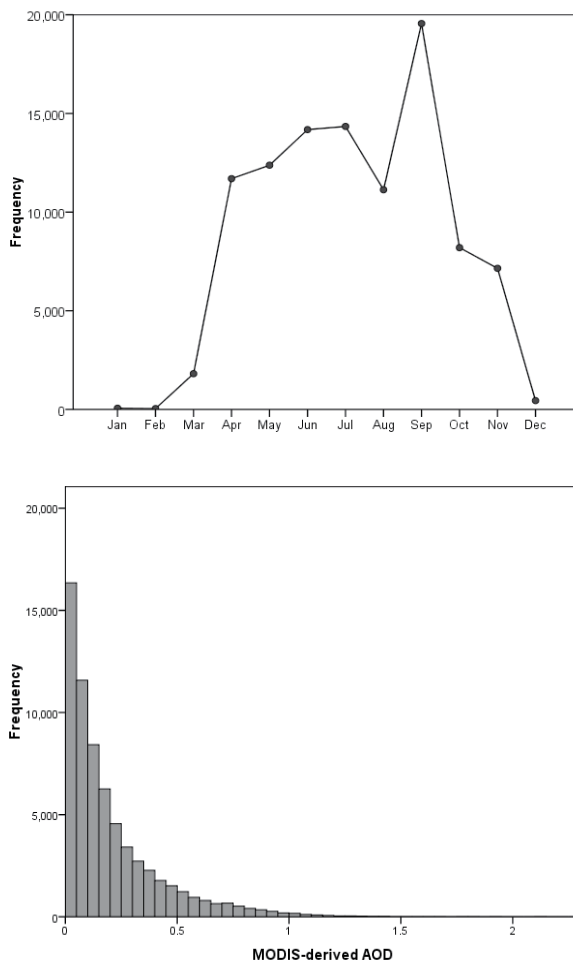
Fig. 2. Frequency distribution of valid MODIS-derived AOD measurements for the entire study period (a) and their utility for the different months (b) in southern Ontario.

Fig. 3 displays a heterogeneous distribution of the 2004 yearly AOD mean across southern Ontario. Relatively high AOD means are found in the densely populated and industrialized areas. Urban and industrial areas are considered to be the major sources of various anthropogenic aerosols, which often result in haze weather. Particularly high values are

found for Greater Toronto Area (A in Fig. 3), the belt connecting Niagara Falls, Hamilton, and London (B in Fig. 3), and the Greater Windsor Area (C in Fig. 3). This is largely attributed to their inherent high productivity of aerosol particles from manufacturing industry, heavy traffic, and geographic proximity to some U.S. cities (*e.g.* Detroit, Buffalo). Caution should be exercised when interpreting some high-AOD cells at the land/water boundaries, as applying the land algorithm to the pixels with sub-pixel water may lead to higher estimates than actual AOD values (Chu et al. 2003).
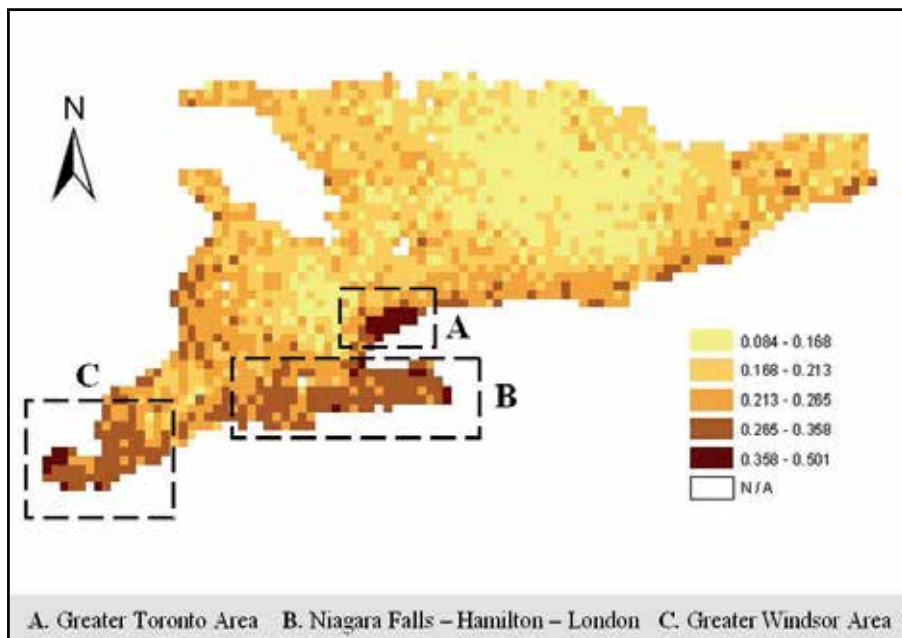
Fig. 3. Distribution of MODIS-derived aerosol optical depth (AOD) mean for the period from April to November (2004) in southern Ontario.

MODIS-derived AOD varies greatly over seasons. Fig. 4 presents the AOD mean and standard deviation as a function of month, revealing a seasonal pattern with a higher AOD level during the spring and summer months, and a lower AOD level during the fall and winter months. Accordingly, there seems to be larger variances in AOD during the spring and summer months. This is largely explained by the seasonality of atmospheric motion over the area. During summer months, weather conditions in southern Ontario are generally dominated by the Maritime Tropical air mass (highly unstable with strong turbulence) originating from the Gulf of Mexico and Caribbean Sea, bringing aerosols sourced in the U.S. In contrast, the Continental Polar air mass in winter moves over the area, bringing clean and stable air from the north and producing heavy lake-effect snows. Extensive snow cover is the main reason causing the inability to retrieve AOD in winter (Power et al., 2006). In addition, higher air temperatures tend to hold more water vapor that feeds aerosol to grow (Masmoudi et al., 2003). This is another reason causing the higher AOD levels in the summer time.
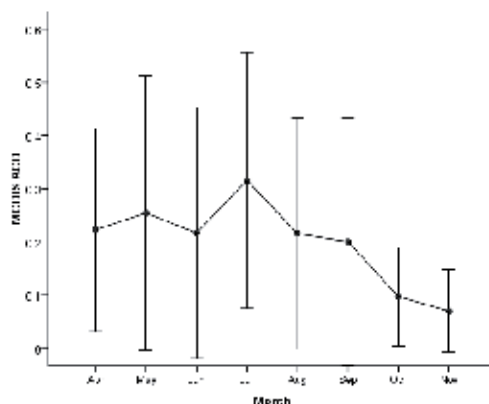
Fig. 4. Mean (point) and one standard deviation (bar) of monthly AODs for southern Ontario in 2004 (Note: January, February, March, and December are not presented because there were very few valid AOD values in these months).
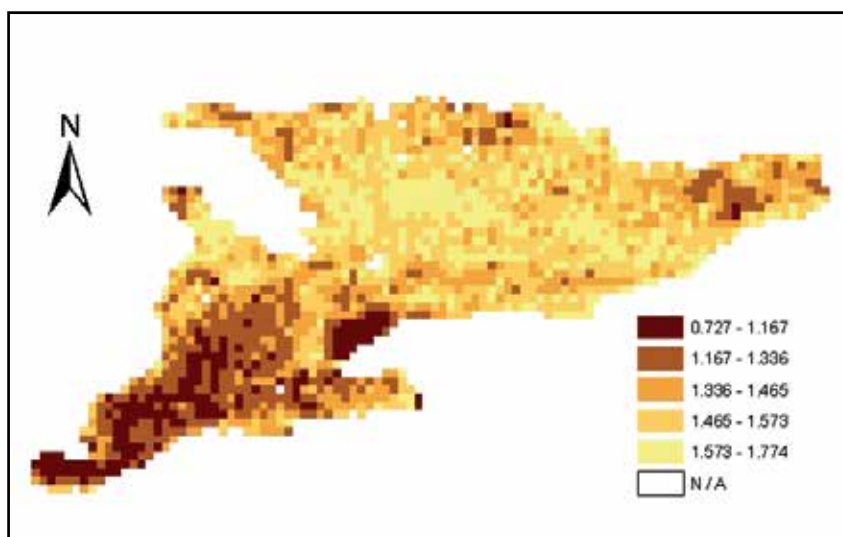
Fig. 5. Distribution of MODIS-derived Ångström exponent (AE) for the period from April to November (2004) in southern Ontario.

Fig. 5 depicts the distribution of the 2004 yearly AE mean across southern Ontario. In general, Southwestern Ontario and the Golden Horseshoe area appear to have smaller means (<1.34) of AE, indicating relatively larger sizes of the aerosols suspended over these areas. Such relatively coarser aerosols may originate and assemble from anthropogenic sources including industrial/constructional dust, soot, etc. Both the Canadian cities (local sources) located in the areas, and the U.S. cities across the Great Lakes (aerosol plumes can be transported downwind) are considered the contributors. There are large areas of concentrated agricultural lands in Southwestern Ontario. Physically produced agricultural dust is believed to account for the larger aerosol size over the area. Traffic emissions are perhaps another major source. In comparison, the northern areas (dominated by larger AE

means) are believed to be loaded with aerosols more from natural sources (*e.g.* sulfates from
biogenic gases and organic matter from biogenic volatile organic compounds). Yet the result
should be interpreted with caution because the AE here is a secondary derivative from
MODIS AOD. MODIS-derived AE is not very accurate by comparison to AERONET AE
(Remer et al. 2006); it may be biased for specific surface types or seasons (Koelemeijer et al.
2006).

5.2 Region-based analysis

The municipal regions with a low yearly AOD (0-0.2) were found to be spatially clustered,
forming mainly two 'clean' zones (see A and B in Fig. 6). These regions are recognized as
being more inland and including nearly no industrial or urban areas (further discussion is
provided in Section 2.3.3). In contrast, the municipal regions with a relatively higher yearly
AOD (0.2-0.3) are distributed around these two zones and take up most of the remaining
portions in southern Ontario. Particularly Southwestern Ontario was recognized as having
almost all the municipal regions with a relatively high yearly AOD. Moreover, there are
some 'hot' regions (AOD>0.3) that can be clearly identified, including the Greater Toronto
Area, the Niagara Falls Area, and the Greater Windsor Areas (see C, D, and E in Fig. 6,
respectively).
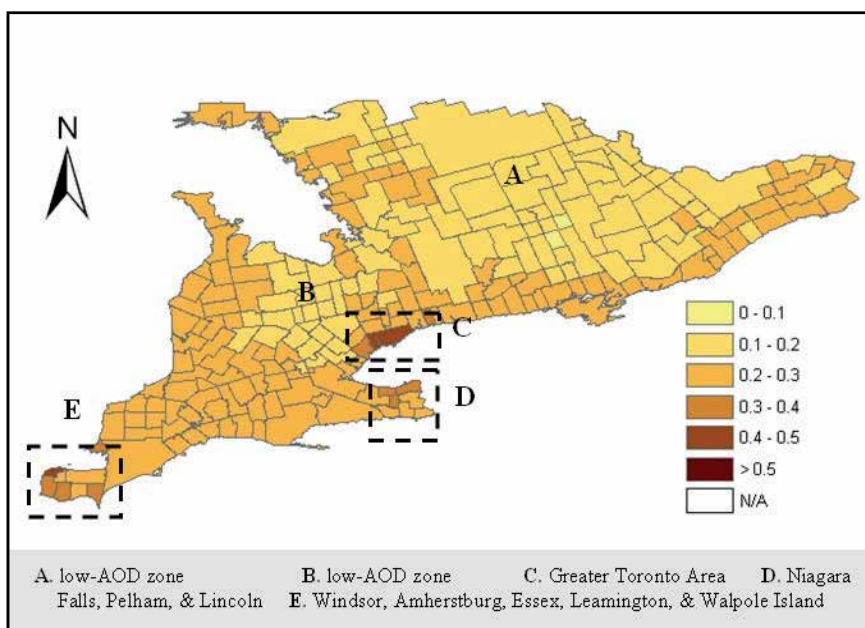
Fig. 6. 2004 yearly AOD mean over the municipal regions in southern Ontario.

Paired *t*-test between the monthly AOD for the entire southern Ontario and for each of the
17 cities with a population greater than 100,000 was conducted to determine which cities are
significantly different from the study area average. A difference is considered to be
significant when the associated *p*-value is less than 0.05. As can be seen in Table 1, Toronto,

Mississauga, Hamilton, and Windsor show to be significantly higher ($t>0$) than the area average, while Ottawa and Cambridge are lower ($t<0$). The relatively low AOD level for Ottawa, the national capital, may be explained by the large fraction of suburban and rural areas included within its municipal boundary. It is understandable that there exist significant spatial variations of AOD within such regions that hold both highly urbanized or industrialized areas and considerable suburban and agriculture/forest lands. The mean AOD over a municipal region like Ottawa tends to even off these differences and only represent the averaged level.

Municipal Regions	t	p	r
Toronto	5.768	0.001	0.969
Ottawa	-1.487	0.181	0.939
Mississauga	5.364	0.001	0.970
Hamilton	3.670	0.008	0.968
London	2.329	0.053	0.711
Brampton	2.872	0.024	0.938
Markham	2.263	0.058	0.830
Windsor	5.694	0.001	0.925
Kitchener	3.191	0.015	0.899
Vaughan	2.856	0.024	0.893
Burlington	1.765	0.121	0.861
Oakville	2.143	0.069	0.809
Oshawa	2.152	0.068	0.795
Richmond Hill	2.001	0.086	0.976
Kingston	1.768	0.120	0.882
Cambridge	-.305	0.769	0.662
Chatham-Kent	3.376	0.012	0.897

Table 1. Results of the paired t-test between the monthly AOD means of the cities with a population greater than 100,000 and those of the entire southern Ontario
Note: t = t-value. $p<0.05$ indicates sample means are statistically different from the study area means. r represents the correlation coefficient to the study area mean.

The spatial-temporal variability of MODIS-derived AOD has been investigated by mapping the monthly AOD mean of the municipal regions over April through November (Fig. 7). As there was very limited data coverage for January, February, March, and December (statistically sound mean could not be obtained for most municipal regions), their monthly AOD maps are not presented. It is clear that MODIS can not be relied upon for the aerosol data acquisition for southern Ontario during these four months. Again, this is mainly due to the extensive snow cover in winter, which greatly hampers the usability of the MODIS algorithm for AOD retrieval over land. Although there was relatively much more data available than the other winter months, data for the north part of the study area (approximately above 45°N) was widely missed in March.
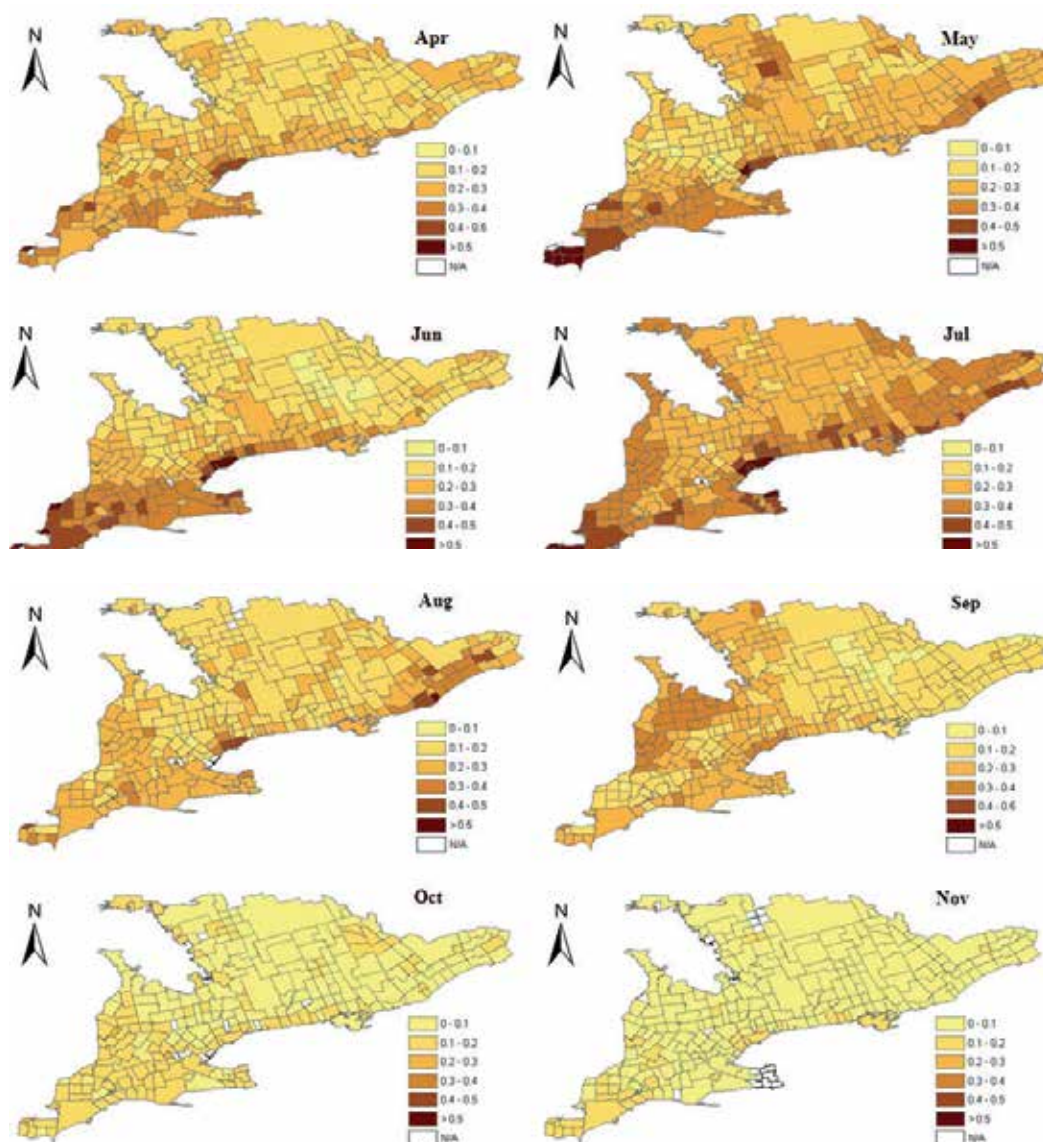
Fig. 7. Spatial and temporal variations of the monthly AOD mean over the municipal regions in southern Ontario

Visual examination of Fig. 7 showed that April experienced a moderate level of AOD overall (also supported by Fig. 4). May and June presented similar distribution patterns in Southwestern Ontario. The difference lies in that higher levels of AOD are observed for many municipal regions in Central and Eastern Ontario in May, compared with June. The reason for this remains unclear especially for some small towns with particularly high aerosol loading such as Huntsville. The Greater Toronto Area and Southwestern Ontario remain to be the areas with higher aerosol loadings in these two months, despite the inner-

section distributions of AOD were somewhat different. July exhibited the highest level of AOD in the year for most of the municipal regions. The monthly AOD mean for a large number of cities or towns reached a level of >0.4 in this month. The coastal regions and the regions in Eastern Ontario widely experienced an elevated AOD level of 0.3-0.4. Due to the scope of this research, the discussion for such a phenomenally high level of AOD in July is not covered in the present paper. The AOD level dropped to its normal summer level for most municipal regions in August. The presence of relatively high levels of AOD at Eastern Ontario in July and August may be related to aerosol emissions sourced from major Québec cities such as Montréal. Although the spatial distribution of monthly AOD across the municipal regions differed in August and September, the overall study area mean remained at similar levels (0.2-0.22) for these two months (Fig. 4). Moreover, September seems to be a transition period towards a different meteorological air pollution regime at the synoptic scale, although more quantification may be needed in terms of air mass change. October and November exhibited a distinctly low level of AOD. More specifically, October saw no municipal regions with a monthly AOD of >0.3. Almost all the regions became dramatically reduced with their monthly AOD levels at this time. The overall AOD level appeared to be even lower in November, when only few municipal regions experienced a monthly AOD of 0.1-0.2, leaving the remaining regions to all have a value of <0.1. The above spatial-temporal distribution of AOD over months calls for a physical explanation. We tentatively suggest that the explanation may lie in the mesoscale meteorological processes.

As expected, the MODIS-derived AOD data appears to be patchy and lacks a consistent spatial coverage. This has greatly restricted its use in more detailed analysis, such as detection of short-term (*e.g.* one week) clusters of the municipal regions that were heavily loaded with aerosols. Attempts have been made to produce daily, weekly, and biweekly maps of AOD mean. Unfortunately, none of them have steady coverages with sufficient observations for each municipal region, even for the data-rich month of September.

5.3 Relate MODIS-derived AOD to land use and topography

Fig. 8 displays the land-use map (fully covering 62 municipal regions) available for the present study. The map was overlaid with the municipal region map for a zonal analysis of land-use structure. Descriptive statistics showed that the fraction of Built-up Areas (FBA) ranges from 0.1% to 78% for the municipal regions with land-use information. As can be seen from Fig. 9, regardless of seasonal changes, a municipal region's yearly AOD mean seems to be positively correlated ($r = 0.7$) with its FBA. A fitted linear regression model between the two variables is able to explain almost 50% of the variability in AOD. Meanwhile, a municipal region's yearly AOD declines with the increase of its fraction of its Vegetation, although this negative correlation ($r = -0.6$) is not as strong as that of the FBA-AOD relationship. These observations, to some extent, suggest that local and anthropogenic aerosols are a large contributor to the aerosol loading in southern Ontario. The urban heat island effect may be another reason; the lower albedo, higher heat capacity, and internal energy generated as a result of human activities in urban areas often causes atmospheric circulations towards the urban centers at urban/rural fringes, bringing in exogenous aerosols.
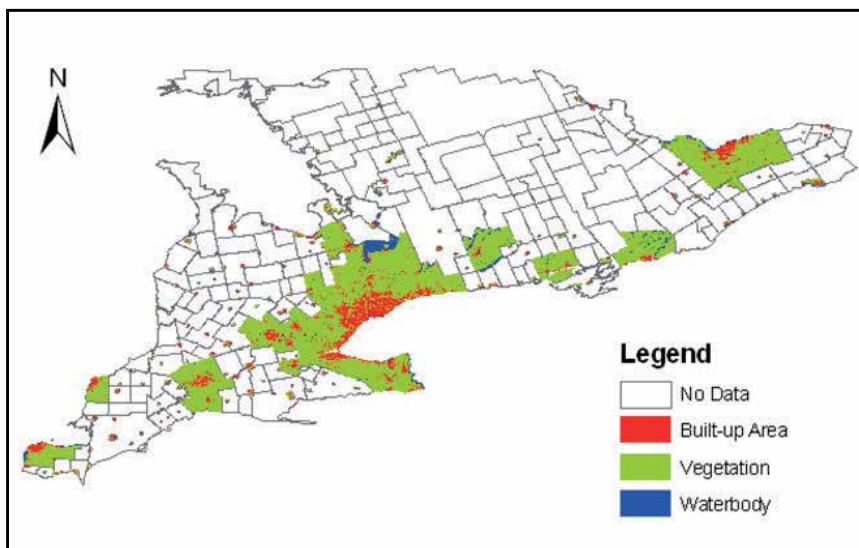
Fig. 8. Land use/cover map of certain municipal regions in southern Ontario.
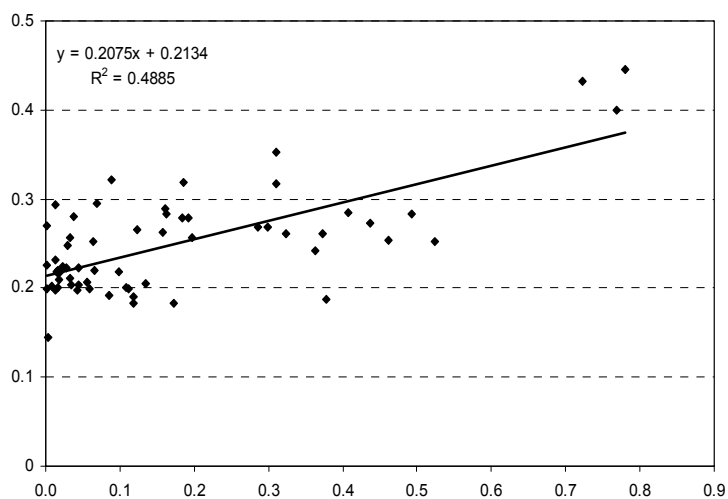
Fig. 9. Scatter plot of yearly AOD mean versus fraction of Built-up Areas (FBA) for the municipal regions.

Ideally, the land use/cover data should be weighted by their productivity of aerosols. More detailed information including road density, traffic volume, and pollution inventory are necessary in order to estimate such productivity. Another limitation with the current analysis is its exclusion of large areas of rural lands due to the lack of accurate land use/cover data for these areas. In summers, occurrences of forest fires in these areas may produce smoke aerosols and lead to short-time event-induced high levels of AOD. Such

aerosols are non-anthropogenic and can dominate the aerosol composition during the event period.

When compared with the digital elevation model (Fig. 10), the AOD distributions in southern Ontario seemed to be susceptible to topography. Interestingly, it is found that the low-AOD zones basically resemble the higher elevation upland areas (brown areas). The possible reasons to account for this observation include: (1) there are much less human activities or anthropogenic processes for aerosol production in these areas due to historic settlement; (2) the air circulations, either thermally induced (*e.g.* valley breeze) or mechanically forced (*e.g.* lee waves) by uplands, can possibly impel uptake of aerosols by posing more flux towards vegetated land surfaces, and the aerosol concentration can therefore degrades rapidly. The AOD values in these zones reflect the background aerosol loading level in southern Ontario, and may be valuable to the estimation of the net increase or decrease of local aerosol emissions.
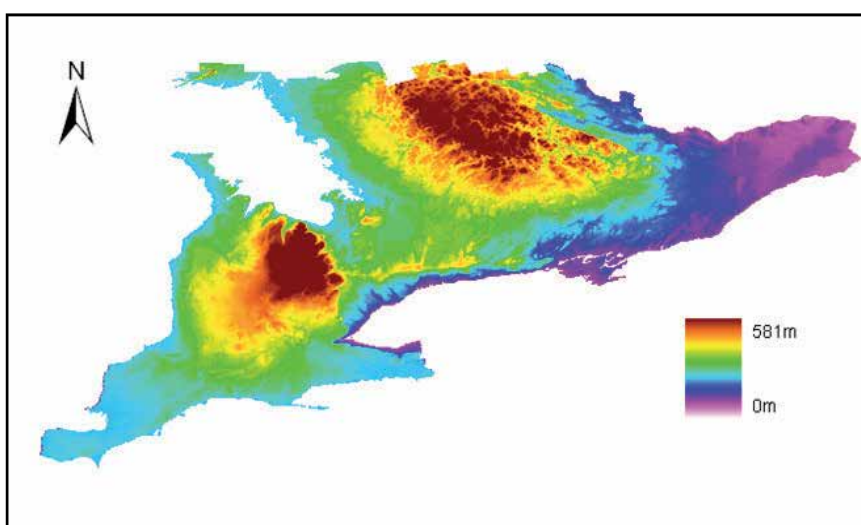
Fig. 10. The digital elevation model of southern Ontario.

6. Summary

This study has investigated the spatial-temporal distribution patterns of aerosols over a year in southern Ontario. It has been found that MODIS-derived AOD varies greatly across space and time in the region. In general, the Greater Toronto Area and the Greater Windsor Area experience the highest level of yearly AOD average. Summer months relate to elevated levels of AOD and stronger variations, compared to the other months. Among cities with a population greater than 100,000, Toronto, Hamilton, Mississauga, and Windsor experience a significantly higher yearly AOD than the study area average. Aerosols in Southwestern Ontario are mainly composed of relatively larger particles, resulting smaller values of Ångström exponent. The regional topography is also found to have a role to play in affecting the aerosol distribution. The two low-AOD zones identified clearly resemble the two major high elevation upland areas in southern Ontario. Moreover, AOD seems to be related with the underlying land-use structure: a higher fraction of built-up area within a

municipal region tends to correspond to a higher value of AOD. This somewhat proves the local and anthropogenic nature of a large portion of aerosols in southern Ontario, especially for the urbanized and/or industrialized areas, and can inform land-use management aiming to improve aerosol-oriented air quality. An in-depth understanding of the aerosol distribution across municipal regions in southern Ontario is expected to support decision-making for regional air quality protection or the establishment of compensation under transboundary air pollution agreements. This study is based on one year MODIS-derived AOD data in 2004. A multi year analysis should be conducted in the future to confirm or modify findings in this study.

Acknowledgement

7. References

Albrecht, B.A. (1989). Aerosols, cloud microphysics and fractional cloudiness. Science, 245(4923): 1227-1230.

Chu, D.A., Kaufman, Y.J., Zibordi, G., Chern, J.D., Mao, J., Li, C. and Holben, B.N. (2003). Global monitoring of air pollution over land from EOS-Terra MODIS. Journal of Geophysical Research, 108(D21): 4661 doi:10.1029/2002JD003179.

Dockery, D.W., Pope, C.A., Xu, X., Spengler, J.D., Ware, J.H., Fay, M.E., Ferris, B.G. and Speizer, F.E. (1993). An association between air pollution and mortality in six U.S. cities. The New England Journal of Medicine, 329(24): 1753-1759.

Feczkó, T., Molnár, A., Mészáros, E. and Major, G. (2002). Regional climate forcing of aerosol estimated by a box model for a rural site in Central Europe during summer. Atmospheric Environment, 36(25): 4125-4131.

Figueras i Ventura, J. and Russchenberg, H.W.J. (2008). Towards a better understanding of the impact of anthropogenic aerosols in the hydrological cycle: IDRA, IRCTR drizzle radar. Physics and Chemistry of the Earth, Parts A/B/C, In Press.

Frank, T.D., Di Girolamo, L. and Geegan, S. (2007). The spatial and temporal variability of aerosol optical depths in the Mojave Desert of southern California. Remote Sensing of Environment, 107(1-2): 54-64.

Han, Y., Dai, X., Fang, X., Chen, Y. and Kang, F. (2008). Dust aerosols: a possible accelerant for an increasingly arid climate in North China. Journal of Arid Environments, 72(8): 1476-1489.

Haywood, J.M. and Boucher, O. (2000). Estimates of the direct and indirect radiative forcing due to tropospheric aerosols: a review. Review of Geophysics, 38: 514- 543.

Holben, B.N., Eck, T.F. and Fraser, R.S., (1991). Temporal and spatial variability of aerosol optical depth in the Sahel region in relation to vegetation remote sensing. International Journal of Remote Sensing, 12(6): 1147 - 1163.

Ichoku, C., Kaufman, Y.J., Remer, L.A. and Levy, R. (2004). Global aerosol remote sensing from MODIS. Advances in Space Research, 34(4): 820-827.

Kaufman, Y.J., Setzer, A., Ward, D., Tanre, D., Holben, B.N., Menzel, P., Pereira, M.C. and Rasmussen, R. (1992). Biomass burning airborne and spaceborne experiment in the Amazonas (BASE-A). Journal of Geophysical Research, 97: 14581–14599.

Kaufman, Y.J., Tanre, D., Remer, L.A., Vermote, E.F., Chu, A. and Holben, B.N., (1997). Operational remote sensing of tropospheric aerosol over land from EOS moderate resolution imaging spectroradiometer. Journal of Geophysical Research, 102(D14): 17051-17067

Kaufman, Y. J., Gobron, N., Pinty, B., Widlowski, J.L., Verstraete, Michel M., (2002). Relationship between surface reflectance in the visible and mid-IR used in MODIS aerosol algorithm-theory, Geophysical Research Letters, 29(23): 2116, doi:10.1029/2001GL014492.

Koelemeijer, R.B.A., Homan, C.D. and Matthijsen, J. (2006). Comparison of spatial and temporal variations of aerosol optical thickness and particulate matter over Europe. Atmospheric Environment, 40(27): 5304-5315.

Levy, R.C., Remer, L.A., Mattoo, S., Vermote, E.F. and Kaufman, Y.J.(2007). Secondgeneration operational algorithm: retrieval of aerosol properties over land from inversion of Moderate Resolution Imaging Spectroradiometer spectral reflectance. Journal of Geophysical Research, 112(D13211): doi:10.1029/2006JD007811.

Martonchik, J.V., Diner, D.J., Crean, K.A. and Bull, M.A. (2002). Regional aerosol retrieval results from MISR. IEEE Transactions on Geoscience and Remote Sensing, 40(7): 1520-1531.

Masmoudi, M., Chaabane, M., Tanré, D., Gouloup, P., Blarel, L. and Elleuch, F. (2003). Spatial and temporal variability of aerosol: size distribution and optical properties. Atmospheric Research, 66(1-2): 1-19.

Power, H.C., Sheridan, S.C. and Senkbeil, J.C.(2006). Synoptic climatological influences on the spatial and temporal variability of aerosols over North America. International Journal of Climatology, 26(6): 723-741.

Remer, L.A., Tanré, D. and Kaufman, Y. (2006). Algorithm for remote sensing of tropospheric aerosol from MODIS: collection 5. MODIS Algorithm Theoretical Basis Document. Available at <http://modis-atmos.gsfc.nasa.gov/MOD04_L2/atbd.html>.

Savtchenko, A., Ouzounov, D., Ahmad, S., Acker, J., Leptoukh, G., Koziana, J. and Nickless, D.(2004). Terra and Aqua MODIS products available from NASA GES DAAC. Advances in Space Research, 34(4): 710-714.

Statistics Canada (2007). Population and dwelling counts, for Canada, provinces and territories, 2006 and 2001 censuses, Catalogue no. 97-550-XWE2006002, Ottawa.

Tanre, D., Kaufman, Y.J., Herman, M. and Mattoo, S. (1997). Remote sensing of aerosol properties over oceans using the MODIS/EOS spectral radiances. Journal of Geophysical Research, 102(D14): 16971-16988.

Methods for online monitoring of air pollution concentration

Ionel Ioana and Francisc Popescu
"Politehnica" University of Timisoara
Romania

1. Introduction

In this chapter some major considerations of an environmental management by direct on line monitoring of the air quality, illustrated by examples, as experienced by the authors, are discussed. First the *standard (reference) methods* for the main pollutants are indicated, further some *non-standard methods*.

Atmospheric pollution is a major problem facing all nations of the world. Rapid urban and industrial growth has resulted in vast quantities of potentially harmful waste products being released into the atmosphere. The atmosphere is the largest imaginable chemical reactor in which pollutants may be converted into more harmful or harmless substances. Societies have been reluctant to accept, or have simply failed to recognise the limitations of the cleaning properties of the atmosphere and self-adaptation of the ecosystem Planet, with no remnant damages or preventing a non-equilibrium status. The consequences has been that air pollution has affected the health and wellbeing of people, has caused widespread damage to vegetation, crops, wildlife, materials, buildings and climate, and has resulted in depletion of the scarce natural resources needed for long-term economic development. In the past, the earth was considered virtually infinite, and little thought was given to the polluting effects of our dumping wastes. The atmosphere felt to be so vast that it could absorb any amount. However, over the past decades, several factors have come together to bring this attitude into sharp question. Along with the realisation that we are on an all too finite spaceship - the earth - the *increasing population* and *technological base for our way of life* and the *increased sensitivity of our instruments for measuring pollution* have all played a role in bringing about an awareness regarding the environment and its quality.

Air pollution adversely affects soil, water, crops, vegetation, human-made materials, buildings, animals, wildlife, weather, climate, and transportation, as well as reduce economic values, personal comfort and well being. More and more, in the present time of the society of knowledge, the population and the policy makers are convinced and engaged for preserving the biodiversity that is fundamental to human welfare and economic development, and plays a critical role in meeting human needs by maintaining the ecological processes on which our survival depends. Broad-scale ecological systems provide benefits such as clean air and fresh water that are needed by everyone, whether in urban or rural settings.

As main sources for the pollution of air one recognises: *the natural sources*, and the *man-made sources*, in direct dependency to the energy consumption that is driven from the standard of comfort and industrial development, being influenced by the number of population, as well. It is not difficult to see that all of us are either directly or indirectly polluters and all of us share the disadvantages and cleanup costs of pollution generating activities, although often not in an equal and equitable manner.

In order to keep control over the quality of air the policy makers, in international co-operation mostly, decided to introduce specific regulations attesting the maximum admitted values as well the alert values. Thus, one controls both the emissions and the air quality, that represents a result of the transport in the air of the pollutants, in direct dependence to the topography and the weather conditions. *Primary pollutants* are those released directly from the source into the air in a harmful form. They are mostly result from combustion of classic C - containing non-renewable fuels, and not only even the combustion is perfect, according to thermodynamic concepts. *Secondary pollutants*, by contrast, are modified to a hazardous form after they enter the air or are formed by chemical reactions as components of the air mix and interactive. *Fugitive emissions* are those that do not go through a smokestack. By far the most massive example of this category is dust from soil erosion, strip mining, rock crushing, and building construction (and destruction). Fugitive industrial emissions are also an important source of air pollution.

2. Present state of art

2.1 Significance of the locations and sampling

When carrying out air quality measurements it is important to define the problem precisely (measuring plan) and to choose accordingly the site locations, measuring stations and methods. Applying the most expensive measuring instrument is of no use if, e.g., the pollutant to be investigated is influenced during its sampling to such a degree that it either cannot reach the measuring instrument at all or not in its original state. When measuring pollutant gases in the air a difference between mobile measurements and stationary measurements stations is necessary. Mobile stations (laboratories) are measuring at random and changing locations, according to a plan, to determine the spatial distribution of the air pollutants, whereas stationary measurements continuously record the temporal distribution in few fixed points of a certain area. Stationary measurements must be carried out at representative points of the investigated area. It is recommended to know the spatial dis-tribution of the ambient air pollutants which might be determined only with mobile measurements at the corner points of a 1 x 1 km grid over the area to be investigated (Erste allg., 1986). Special guidelines have been drawn up so that the site locations for automatic measuring stations are chosen according to standardized criteria. Selection of the right sampling site can be of great importance for stationary as well as for mobile measurements.

Guidelines have been drawn up so that in the measuring networks the site locations for automatic measuring stations are chosen according to standardized criteria. These guidelines are very important especially when planning on line in real time air quality measuring networks, i.e., when data are continuously transferred to a central station (RdSchr, 1983). Thus, selecting the site locations for ambient air quality measuring stations means to respect important guidelines in order to meet the general goal that the ambient air meaning that sample is representative of the area (Immissionsmessnetze in der

Bundesrepublik Deutschland, 1987), (Projektgruppe Bayern, GSF-Bericht 25/87). Generally speaking, these conditions are specified by legislation, in each country, but general rules are at their origin. Some of these general rules refer to: (i) distance of measuring site to the closest flow obstacle must be twofold height or width of the obstacle's, (ii) sample suction should be placed below half of the mean building height, (iii) influence of local emission sources must be kept low meaning the distance to sources (industry, domestic furnaces, streets with heavy traffic) should be more than regularly 20 m, and special investigation when industrial sources are situated nearby, are necessary. Further, a free flow accessibility of the sampling systems within a radius of less than 10 m and no flow obstacles such as trees or buildings must be assured, excluding by this mean the influence on measuring site by topographically caused local circulation. EU guideline requires that special aggressive pollutant gases (i.e. NO), must be measured continuously, particularly in locations with the suspected highest load risk, i.e., also near roads with heavy traffic, in street canyons, etc. The sampling system for gaseous pollutants consists generally of a sampling nozzle, a guidance tube, a central sampling tube, sampling connections leading from the central sampling tube to the individual measuring instruments and a fan or a pump. The sampling nozzle might be constructed as a pre-separator for particles and precipitation. The sampling line should extend generally 1 m beyond the station roof. In the standard measuring stations particle filtering in the sampling system is not provided in order to avoid possible reactions of the gases on the filters. Particle filters are only installed at the input of the instruments themselves (Laskus & Bake 1976).

Within air quality investigations, pollutant concentration profiles must frequently be measured. Examples for this are the determinations of pollutant concentrations in and over special sites at different altitudes (Baumbach et al., 1987), (Kost & Baumbach, 1985) or the registration of the concentration decline in the vicinity of streets, industrial areas with heavy traffic or intensive emissions (Esser, 1982), (Baumann, 1987). To be able to simultaneously or quasi-simultaneously measure the gas concentrations at several locations there is the possibility of sucking the air in via tubes and to conduct it to a set of measuring instruments with the help of a measuring gas change-over in short periods of alternation.

During measuring the gas (air) probe is sucked in through tubes, and an influencing of gaseous substances is generally to be expected even if the tube wall material is inert, e.g., from Teflon. Also it is best to use warmed up tubes, in order to avoid the condensation of vapor. This depends on the reactivity of the gases to be investigated. Examinations with long tube lines have shown that the component ozone is most prone to losses in the tube system whereby a clear dependency on the rate of flow through the tube is to be observed. The air sucked in must be filtered to avoid dust depositions on the admission section.

According to national standards and general international methods the main pollutants to be measured are: NO_x (NO, NO_2), CO, SO_2, PM10, O_3, TOC (Total organic carbon) respectively VOC (Volatile organic compounds).

Fig. 1 shows a scheme of a set-up of such a measuring station. The measuring gas suction hoods and different meteorological measuring instruments are installed on a 10 m high altitude. The management and working methods are respecting the international standards SR EN ISO/CEI 17025:2005 (General features and competences), according to the fundamentals and definitions imposed by SR EN ISO 9000:2006. In addition to the instruments for the specific measurement of pollutants there are numerous other instruments for the recording of meteorological parameters such as wind direction and wind

speed, temperatures, global radiation, duration of rain and bedewing, amount of rain etc., as well as an electronic controlled computer, to record, calculate and memorise the values. The computer also controls the valve timing and correctly stores the measured values according to the given valve position. Half-hourly mean values (or other mean values) are calculated and are stored in the memory or/and printed out. Further evaluation of the data is then carried out on a larger computing system. Some measuring stations work with direct data transmission to a central computing station. For reasons of safety the measured values are additionally recorded by multi-channel continuous-line recorders or multipoint recorders independently of the computer controlled measured value recording system. If the computer breaks down these recorder graphs can be evaluated if necessary.
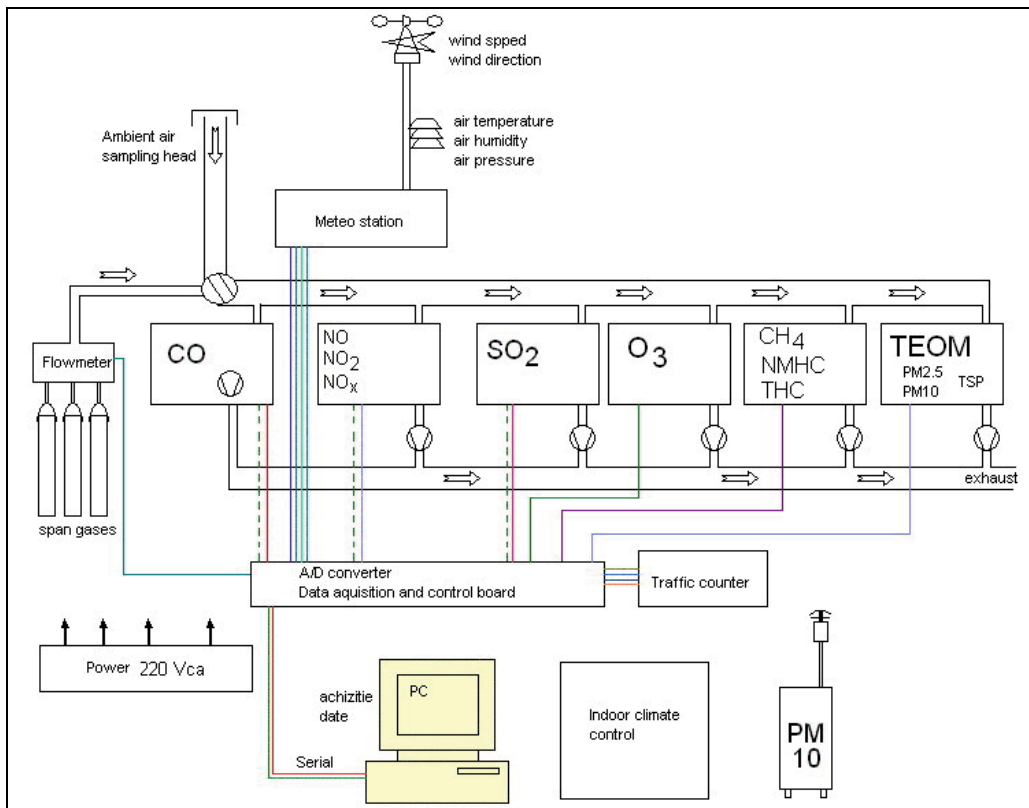
Fig. 1. Set-up of the sampling system of an air quality station with air suction through tubes and with calibration gas switching (www.mediu.ro).

In the example (Fig. 1.) also an optic open path device is included; this is an option not compulsory, for supplementary measuring possibilities, according non standardised methods. Monitors for NO_x detection from ambient air, based on the chemiluminescence's principle, according ISO 7996/1985, Monitor for the SO_2 ambient air concentration, working in UV by applying the fluorescence method, according ISO/FDIS 10498, instruments for CO detection applying ND spectroscopy in IR, according ISO 4224, Sampling analyser LVS3 for the PM10 specie, based on the filtration and mass determination of a specific suspension by

means of gravimetric principles, according EN 12341 are the basic standard main components. Mostly available are also an O_3 measuring devices applying as measurement principle the UV photometry, according reference method: EN 14625:2005, and CH_4, NMHC and THC instruments using the measurement principle of FID (flame ionization detection), reference method EN 12619:2002.

Calibration and adjusting are of major importance for the correctness of the measurements. *Adjusting* means setting or trimming a measuring instrument as accurately as possible, while calibrating signifies determining the deviation measured as compared to the accurate value or the value considered as such (DIN 1319, 1985). In air pollution measurements calibration conditions are set up with the help of *calibration* (ready made by special companies) *gas mixtures.* These are gas or gas mixtures having a composition predetermined with sufficient certainty by measuring basic parameters such as mass, volume, time, amount of substance (molar number) by applying independent analysis methods (Hartkamp et al., 1983). During calibration the calibration gas are entered into the measuring setup (measuring instrument), the values indicated are read and compared with the values of the calibration gases assumed correct, then the deviations are recorded. Frequently, calibrating a measuring instrument is accompanied by other measures such as maintenance, function control, trimming and others.

According (Hartkamp et al., 1983) the total of all calibration processes consists either of basic calibration, or routine calibration, and control calibration. The basic calibration provides the fundamental relationship between given calibration gas concentrations and recorded signals, and is called calibration function. In many instruments linear calibration functions are indicated. Routine and control calibrations ensure the validity of the calibration data of the basic calibration. This control verifies whether the data obtained by the basic calibration carried out last are still valid. The results of routine and control calibrations are yes-no-decisions. The principle of calibration gas production is based on the procedure of adding a known amount of the gas of interest to a known volume or volume flow of carrier gas (mostly N_2 or air) in certain amount. The most convenient way of calibrating is with commercially available calibration gases in pressure gas cylinders (produced with static methods).

Basically, the instruments are connected to a common sample line and the measurements are taking place in the same time and for the same spot for all species. Because of the instruments high precision and accuracy the station must be equipped with calibration gases with a minimum of ± 1% uncertainty. The numeric values provided be instruments are collected by an PC data acquisition system and stored continuously for interpretation. The station indoor environment must be controlled in order to maintain a constant temperature for instruments.

The data acquisition system of the station is automatic and the data are stored in an ASCI file type format. The operator is using the data mainly to perform graphics for each pollutant and to compare their concentration with law regulated concentrations.

2.2 Physical and Chemical Measuring Principles

For the *physical measuring methods* a specific physical property of the pollutant is made use of as quantity to be measured. The air sample does not change materially during its measurement. Specific physical properties of the substances to be investigated are applied to which other components of the sample do not contribute. In *chemical measuring methods* the quantity to be

measured is transformed into a condition with characteristic; measurable properties by a chemical reaction; during this chemical reaction the measured quantity changes.

Measuring processes based on a physical principle can generally be automated better for continuous processes, chemical methods usually being suitable for discontinuous measurements. Chemo-physical measuring principles are also applied. An essential principle which is primarily applied in the continuous measurement of gaseous pollutants is the *excitation of molecules* by adding energy. Excitation can be caused by exposure to radiation in different wave lengths, by generating high temperatures, e.g., via combustion, or by chemical reactions. Either the energy used for excitation or the energy released in another form is exploited for measurement. There are still further methods of excitation, e.g., excitation by electric, magnetic or nuclear forces. Methods of this type can be used for laboratory analyses of air pollutant samples collected. They are used less frequently, however, for direct measuring.

Passive sampling methods provide reliable, cost-effective air quality analysis, which gives a good *indication* of average pollution concentrations over a period of weeks or months. Passive samplers are so-called because the device does not involve any pumping. Instead the flow of air is controlled by a physical process, such as diffusion. Active sampling methods use *physical or chemical methods* to collect polluted air, and analysis is carried out later in the laboratory. Typically, a known volume of air is pumped through a collector (such as a filter, or a chemical solution) for a known period of time. The collector is later removed for analysis.

2.3 Units

A number of different units are used in expressing the concentrations of various species in the atmosphere (Ionel, 2000).

For gas phase species, the most commonly used units are *parts per million (ppm)*, *parts per hundred million (pphm)*, *parts per billion (ppb)*, and *parts per trillion (ppt)*. These units express the number of molecules of pollutant found in a million (10^6), a hundred million (10^8), a billion (an *American billion is 10, a^9 British billion* is 10^{12}) or a trillion (10^{12}) molecules of air, respectively (Finlayson-Pitts & Pitts, 1986).

Alternatively because numbers of molecules (or moles) are proportional to their volumes according to the ideal gas law *(pV = mRT*, where *p* – pressure in Pa, *V* - volume in m^3, *m* - mass in kg, *R* is the gas constant expressed in J/(kg K), *T* - temperature in K)*, one uses also the ***mass concentration***. The conversion is carried out as follows:

$$1\,mg/m^3 = 1\,cm^3/m^3 \cdot \rho = 1 \cdot \frac{cm^3\,pollutant \cdot mg\,pollutant}{m^3\,air \cdot cm^3 \cdot pollutant}$$

$$\rho = gas\,density = \frac{m}{V}\,kg/m^3$$

$$\rho = \frac{molar\,mass}{molar\,volume}\,kg/m^3\,or\,g/l\,or\,mg/cm^3$$

$$\rho = \frac{molar\,mass}{22.4}\,kg/m^3\,or\,mg/cm^3\,(at\,0\,°C, 1{,}013\,mbar)$$

$$\rho = \frac{molar\,mass}{24}\,kg/m^3\,or\,mg/cm^3\,(at\,20\,°C, 1{,}013\,mbar)$$

The molar mass is specific to each chemical gas specie, according to its chemical formula. The molar volume is depending on the pressure and temperature values, considered by law as reference.

3. Standard Measuring Methods for Air Pollutants

3.1 Photometry

Photometry uses the absorption of infrared (IR), visible (VIS) or ultraviolet (UV) radiation by the gases as measuring effect. Wave length ranges are: IR (1,000 - l0,000 nm), VIS (400 - 800 nm), UV (approx. 200 - 400 nm). In the visible and UV electrons are excited by radiation, in the IR range predominantly molecule vibrations but also rotations are activated. During this, the gases absorb energy in certain wave length ranges (absorption bands). The loss of radiation intensity caused by this is consequently measured.

Fig.2 shows the principle of a photometer that consists of a radiation source (lamp), having a focused beam of light falling through a cell on a radiation detector. The latter transforms the beam into an electric signal of proportional intensity. The loss of radiation intensity due to the absorption of the measuring gas is - when frame conditions are constant - a measure for its concentration.

The interrelationships of radiation absorption are described by the Lambert-Beer law:

$$I = I_0 \cdot e^{-\varepsilon \cdot C \cdot 1} \tag{1}$$

$$\frac{I}{I_o} = T = \frac{1}{E} \tag{2}$$

$$E = \ln\frac{I_o}{I} = \varepsilon \cdot C \cdot l \tag{3}$$

where I_0 is the intensity of entering radiation (intensity of light for the reference), I the intensity of exiting radiation (intensity of light for the sample), T stands for the transmission, ε for the extinction coefficient (dependent on wave-length), C for the concentration of gas or pollutant, l for optical path-length of the cell measurement, E for extinction (non-dimensional) of the absorbing substance inverse logarithm of the transmission T.

Most *IR photometers* function as so-called non-dispersive instruments (NDIR), i.e., radiation is emitted in the entire IR range. There is no spectral splitting of the IR radiation emitted by the radiation source. Selectivity is achieved by installing a radiation detector filled with the component to be measured. This type of detector is possible only in the IR range, as the lifespan of the molecules excited by IR radiation is so long that the excitation energy can be released via molecule collisions as thermal energy.
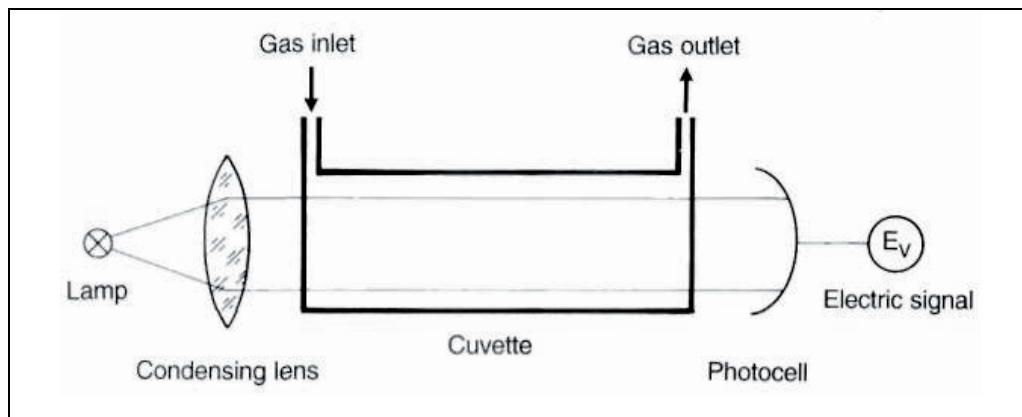
Fig. 2. Principle of a photometer (Baumbach, 1997).

Extinction E as a measure of the radiation absorption of a gas (or also of a liquid) is thus dependent on the properties of the gas (extinction coefficient epsilon), on the concentration c and on the optical path-length l which the beam of light must pass through. If ambient conditions are constant, e for a gas is constant. If l is also kept constant, then extinction E is directly dependent on the concentration of the gas to be measured.

In practice it is not sufficient to form the logarithm of the ratio of intensity I_0 in and intensity I out and to thus determine extinction E. Even without the presence of the component to be measured the instruments absorb radiation, e.g., via optical windows and the gases to be investigated. Thus, even without the presence of the component to be measured, radiation in is not equal to radiation I_0 out. This blank absorption must generally be determined experimentally.

NDIR instruments are primarily used for emission measurements; analyzers are mainly suitable for the determination of the gases CO, CO_2 ,NO, SO_2, H_2O,CH4, C_2H_6, and many other hydrocarbons. For CO and CO_2, NDIR photometry is the most commonly used measuring technique, which is also unrivalled in its application for the measurement of these gases in the ambient air range.

As shown in the Fig. 3, the instruments for CO measurements uses the modulation effect that occurs with infrared absorption of sample gas itself when sample gas and zero gas are alternately sent to its cell at a certain flow rate using a solenoid valve which is actuated at a frequency of 1 Hz. Unless the gas concentration of the measured component is changed in the cell, the output from the detector essentially becomes zero, therefore, the zero drift dose not occur. Since the instrument also uses the AS-type detector, extremely high-accuracy results are obtained without any effect of the interference component.

The radiation source is an infrared radiation emitter. The radiation - modulated by a chopper - passes a chamber containing the probe and in parallels a chamber containing a reference gas. To reduce the influence of interfering gases optical filters are used. The content of the measurement cell receives periodically infrared radiation with different strength, which results in different temperature and pressure effects. The pressure effects are hence transferred to electrical signals by a sensor, and this signal correlates to the measured CO concentration. Some systems use the pressure waves for detection, while others use directly the IR receiving an optical detector to measure the CO concentration.
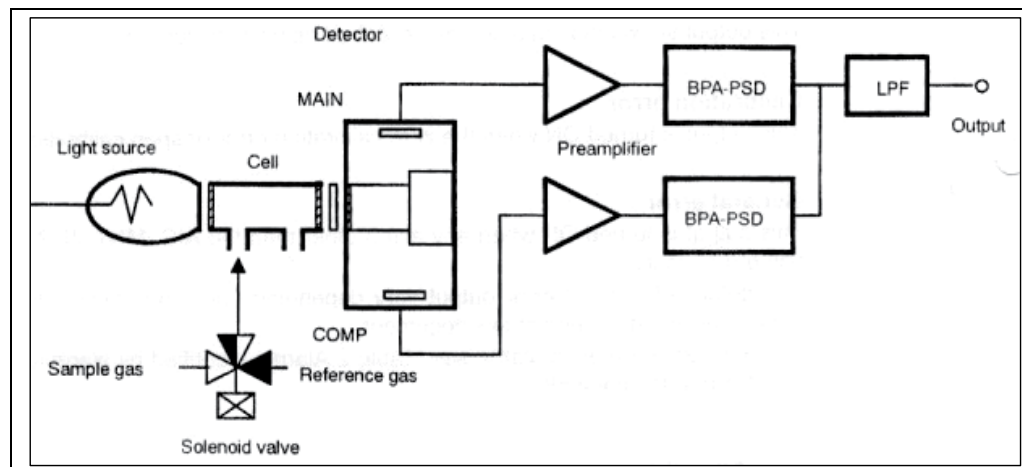
Fig. 3. CO monitoring device schematic (Horiba, User manual)

There are gases with relatively narrow UV absorption bands, e.g., NO and NH_3. Other gases, however, absorb UV radiation in a wider band. To be able to obtain selective measurements certain stratagems are to be applied. A first selection is made by choosing the right UV lamp. Depending on their metal or gas fillings UV lamps have certain emission spectra. Therefore one uses lamps with emission bands which best correspond to the absorption bands of the measuring components or which lie within the absorption bands as clearly defined lines. Besides soiled cells and lamps with fluctuating intensities, they also lead to high and fluctuating reference values l_0 of the radiation and thus to high blank values of extinction. There are different possibilities of compensating for the blank extinctions and of receiving corrected reference radiation intensity I_0 and will be outlined using the example of UV-photometric measurement of NO.

An UV absorption photometer for NO was developed as shown schematically in Fig. 4 (Hartmann & Braun, 1982), (FVLR, 1979). In a hollow cathode lamp filled with nitrogen and oxygen at reduced pressure, excited NO molecules are formed in an electrical discharge. The energy of the excited molecules is dissipated by emission of characteristic luminescence radiation. The source of radiation is selective; it produces an emission range which corresponds precisely to the absorption range of NO in the measuring cell. This is called resonance absorption. One peculiarity of the radiation excited by electrical discharge is that two groups of NO-specific lines are emitted, i.e.: (i) "cold" emission lines - this is the group absorbed by the NO to be determined in the measuring cell (measuring radiation), (ii) "hot" emission lines - that group of radiation showing lines in the neighboring range and meeting the detector not influenced by NO (reference radiation).

The radiation is modulated by a chopper wheel and passed through the measuring cell via a condensing lens. It reaches the radiation detector, a photomultiplier, via an interference filter where interfering radiation is removed. If NO is present in the measuring cell, then the radiation is reduced by resonance absorption (extinction E) according to the Lambert-Beer law. For this measuring technique the blank value of extinction E_0 is compensated for by alternately setting the chopper wheel to a position where all radiation (hot and cold emission lines) is passed through and to a position with a gas filter.
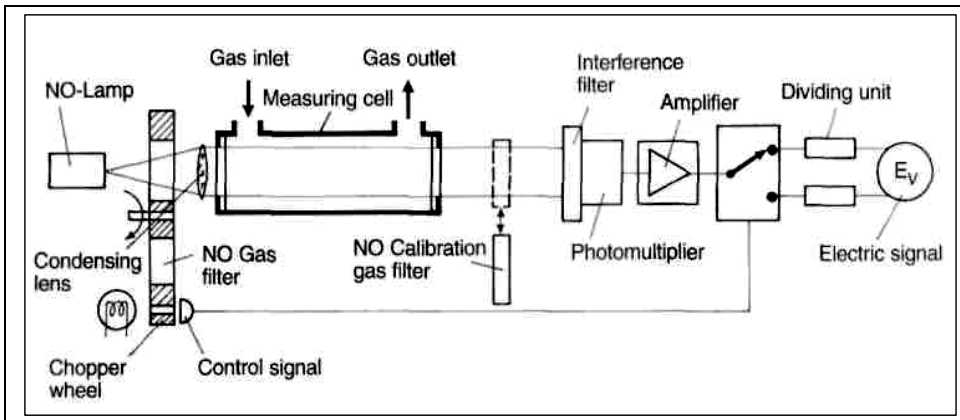
Fig. 4. Diagram of a UV gas analyzer for the detection of NO with blind value compensation by wavelength comparison (FVLR, 1979).

The gas filter contains NO in high concentrations which completely absorbs the cold emission lines. The hot emission lines, however, which are in the immediate neighborhood range, pass through it as reference radiation. Just like the measuring radiation they are influenced by the in-line optics, by the cell windows but mainly by the wide-banded interfering components to produce the intensity reference value I_0 at the photomultiplier.

Fig 5 presents an ozone instrument that performs a dry analysis of ozone, on continuous basis.
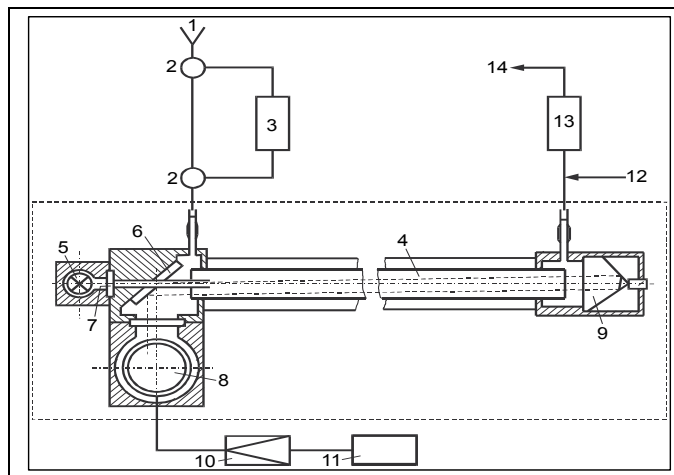
Fig. 5. O_3 monitoring device schematic (Horiba, User manual) 1 - Sample intake, 2 - Three way valve, 3 - Ozone generator (internal calibration), 4 - Measurement cell, 5 - Hg-Low pressure lamp, Mirror, 6 - Interference filter, 7 - Photo multiplier, 8 - Quartz - triple prisms, 9 – Amplifier, 10 – Display, 11 - Exit gas sample, 12 – Charcoal, 13 - Excess air exit.

3.2 UV Fluorescence
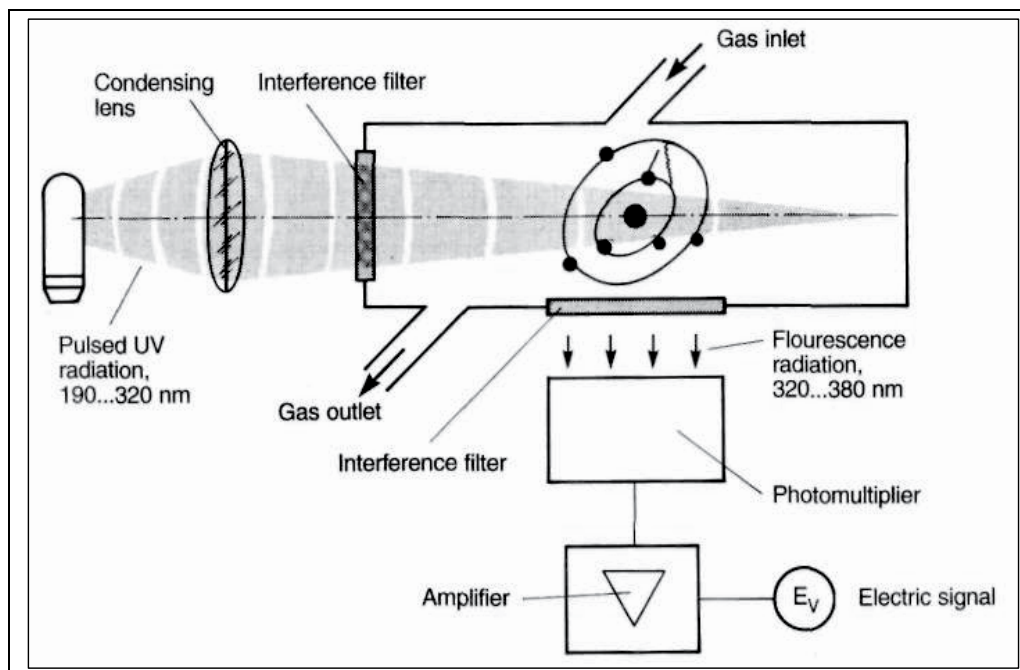
Fig. 6. Principle of UV fluorescence measurement (Zolner, 1984).

UV fluorescence is a measuring technique related to photometry. The measuring gas is also exposed to radiation. However, it is not the radiation absorption which is measured but a luminous phenomenon (fluorescence) which is caused by the excitation of molecules through UV radiation of a certain wavelength. The measuring principle is, e.g., applied in SO_2 ambient air measurement, presented in Fig. 6.

The air sample is exposed to UV radiation in the wavelength range of 190-320 nm. If present, SO_2 gives off a fluorescence radiation of 320-380 nm. Due to an interference filter only a radiation of this wavelength is recorded by the detector (photomultiplier); thus, the measuring principle is strictly selective. The higher the SO_2 concentration, the greater the fluorescence.

One interference in this measuring technique is that other components can absorb the energy of the excited SO_2 molecules, thus reducing the fluorescence yield. This interfering effect is known particularly from water vapor and hydrocarbons. By interposing a permeation gas exchanger an elimination of the interfering components from the measuring gas is attempted. Measuring instruments operating according to this principle are used for both SO_2 air quality measurements as well as for SO emission measurements. In emission measurements the interferences are higher due to the higher concentrations of the interfering components. Air quality measurement instruments operate very stably as far as zero point and sensitivity drift are concerned and as long as the intensity of the UV lamp remains constant.

The reference method for SO_2 measurements is the ultraviolet fluorescent method (UVF).

When a sample is irradiated with ultraviolet ray (215 nm), SO_2 emits the light of a different wavelength (peak: 320 nm, range: 240 nm to 420 nm) from that irradiated. The former, irradiated light is referred to as excitation light, and the later, emitted light is referred to as fluorescence. The method to obtain sample concentrations by measuring the fluorescence intensity is called the fluorescence method. In the fluorescence method, fluorescence, which radiates in all directions, is usually detected at the right angles to the excitation light in order to' prevent interference by the excitation light.

When excitation light is irradiated and absorbed following processes take place:

Process 1: Absorbing and process excitation.

$$SO_2 + hv_1 \rightarrow SO_2* \tag{4}$$

There are three ways by which the SO_2* loses its excitation energy.

Process 2: Fluorescence process: Excitation energy is emitted as fluorescence.

$$SO_2{}^* \xrightarrow{\;kf\;} SO_2 + Kv_2 \tag{5}$$

Process 3: Dissociation process: Excitation energy is used for dissociation.

$$SO_2{}^* \xrightarrow{\;kd\;} SO + O \tag{6}$$

Process 4: Quenching process: Excitation energy is lost by collision with surrounding molecules, M.

$$SO_2{}^* + M \xrightarrow{\;kq\;} SO_2 + M \tag{7}$$

Practically, the excitation energy is lost resulting from the confluence of these three processes. Fig. 7 presents the schematic diagram of a SO_2 measurement device.

The sample gas is continuously drawn into a cylindrical Teflon-coated reaction cell at near ambient pressures. The atmospheric gas is irradiated by UV light that has been mechanically modulated and filtered to 214 nm. The fluorescent secondary emission of the SO2 molecules present in the gas is measured by a photo-multiplier tube (PMT). The PMT is located at 90° from the UV lamp source on the axial centre line of the reaction cell. The filtered UV light passes through a collimating lens that focuses the light energy at the centre of the cell. The PMT is optically tuned to measure the fluorescent emission and outputs the signal through an amplifier to a synchronous demodulator. Simultaneously, the UV light source constancy is measured by a reference photo-detector tube, located directly across the reaction cell from the lamp. The light travel down an optically-designed dump to the photo tube, whereupon is output is amplified and processed through a nearly identical synchronous demodulator. The mixer board electronics then uses this signal to compensate for any variation in the UV light source.
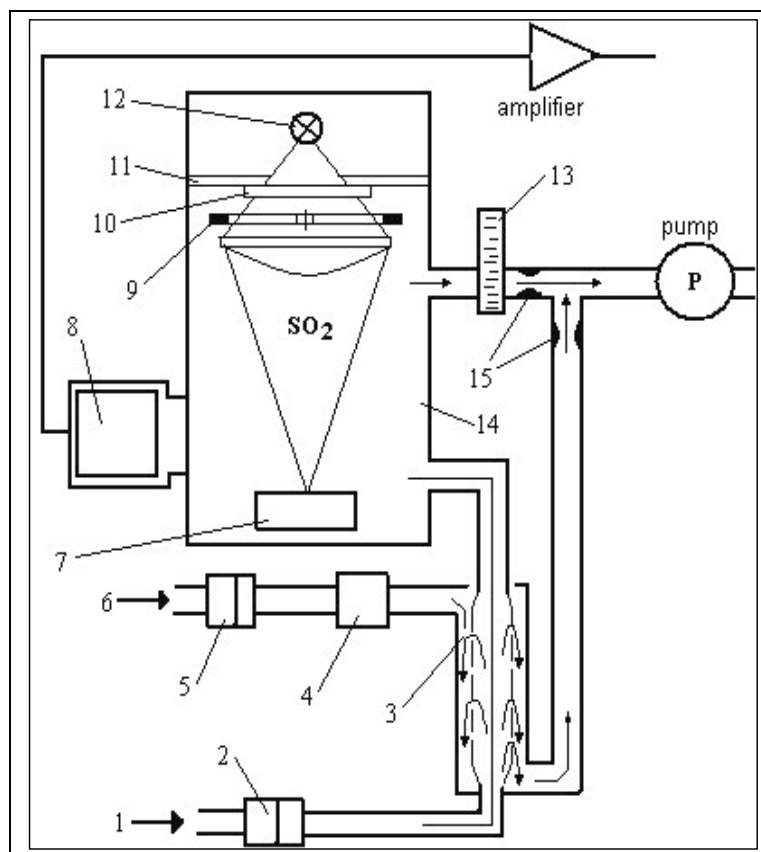
Fig. 7. SO$_2$ monitoring device schematic according UV fluorescence principle (Baumbach, 1997).

3.3 Chemiluminescence

Chemiluminescence is related to UV fluorescence. The difference between the two is that in chemiluminescence molecules are not excited by UV radiation, but are excited by a chemical reaction. Thus, the measuring principle is a chemo-physical one. The intensity of the radiation created is a measure for the concentration of the reacting gas in a mixture of gases, if the external conditions (pressure, temperature and volume flow of the measuring gas) are kept constant. Just as is the case in UV fluorescence, the radiation created is recorded by a photomultiplier acting as radiation detector and is transformed into an electric signal. This method is used mainly for measuring NO, NO+NO$_2$ (i.e., NO$_x$) and O$_3$.

To measure the NO and NO$_2$ concentration into the atmosphere the TÜV (EU) and U.S. EPA requirements are fulfilled only by chemiluminescence's method. The instrument must provide continuous and unattended monitoring of NO, NO$_2$ and NO$_x$ with individual determinations and high reliability and accuracy. An internal NO$_2$ to NO converter permit NO$_x$ analysis and an integral ozone supply system which puts filtered, dehumidified ambient air through an ozonator to generate the ozone necessary for reaction with NO to give chemiluminescence's reaction. The instrument must have a flow-chopping modulation system to give continuous NOx and NO analysis. With this system, the sample gas is divided into two separate lines. One sample gas line passes through the N0$_2$ to NO

converter, while the other leads directly to the detector. Also a permeation tube in which only moisture is passed through is used for the sample line is needed. This tube functions so that an influence from the moisture is reduced by minimizing difference of moisture concentration between sample gas and reference gas.

Inside the reaction chamber NO reacts with ozone to form NO. The NO_2 is excited to a higher electronic state. This chemiluminescence's is measured through an optical filter by a photodiode. The modulated hybrid signal from the detector is demodulated to give continuous NO_x and NO signals at the same time. The NO_2 concentration is given by subtraction of NO from NO_x.

$$NO + O_3 \rightarrow NO_2{}^* + O_2 \tag{8}$$

$$NO_2{}^* \rightarrow NO_2 + hv \tag{9}$$

Filtered sample gas is divided into lines 1 and 2. In line 1, the sample gas flows through an integral converter which reduces NO_2 to NO. In line 2, the sample gas remains as it is. The sample gas is switched to NO line, reference line, NO line and to reference line again by the solenoid valve with 0.5 sec interval. Then it is introduced into respective reaction chamber. Luminescence due to reaction of the sample and O_3 occurred in the chamber is detected by a photodiode. By electrically processing the output of photodiode, it is possible to take out continuous signal in NO line and NO line respectively. Flow to the detector unit is controlled by capillaries. Ozone is supplied to the reaction chamber at a constant rate by an internal ozonator which uses dehumidified ambient air as feed gas. The dryer unit has two dryer cylinders. When one cylinder is under operation, the other is regenerated. For regeneration, first heat the tube to 120°C for 135 minutes to evaporate all the water, and then cool the tube for 45 minutes. It is possible to perform continuous drying by changing over the line of use and regeneration every 180 minutes.

According to the same chemiluminescence reaction as in the case of the NO measurement, ozone could be measured by its reaction with NO. A better and more inexpensive reaction partner for ozone, however, is ethane (C_2H_4):

$$O_3 + C_2H_4 \rightarrow O_2 + C_2H_4O^* \tag{10}$$

$$C_2H_4O^* \rightarrow C_2H_4O + hv \quad (300...600nm) \tag{11}$$
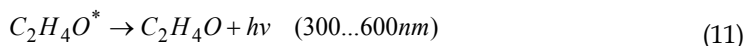
During this reaction chemiluminescence radiation is once again formed to be measured analogous to NO determination. The sole disadvantage of this ozone measuring technique is that ethane is required which is only available from a gas cylinder. As it is a flammable gas, this measuring technique is regarded with disfavor in air quality measuring stations and has given way increasingly to UV photometry. In the matter of interference and susceptibility to faults the chemiluminescence method is superior to UV photometry.

Fig. 8 gives the basic schematic of one NO_x analyzer.
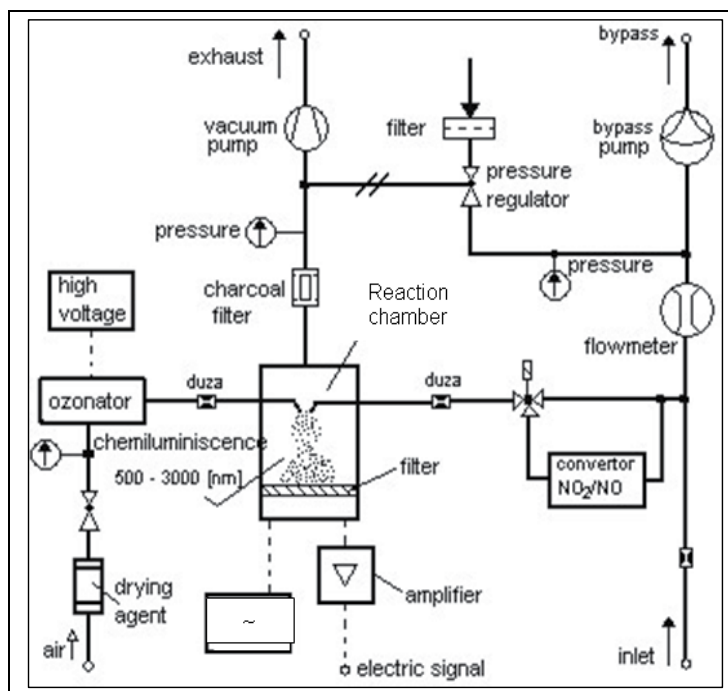
Fig. 8. NO$_x$ monitoring device schematic (HORIBA AP370 User manuals).

3.4 Flame Photometry and Ionization

In flame-photometry atoms are excited in a flame and made to luminescence. The spectral line of the atom of interest is filtered out from the radiation of the flame via an interference filter and measured with a photomultiplier. In gas analyses this process is used mainly for sulfur measurements, but it is also suitable for measuring phosphorous compounds. In sulfur measurement, however, the flame-photometric effect is not based on an atom emission but on a recombining of sulfur atoms whereby excited S^*_2 molecules are formed which pass into their basic state under a light emission of approx. 320 nm - 460 nm. With an optical filter a wave length of 394 nm is chosen for sulfur detection (Birkle, 1979).

The total sulfur content of the air, mainly H$_2$S and SO$_2$, is primarily measured. If individual compounds are to be identified, then single gases must be removed by absorption and adsorption filters prior to measuring. This process is distinguished by a high sensitivity (low detection limit!) and by a very brief response time. Therefore measuring devices working on this principle are used, e.g., for air quality measurements with aircraft (Paffrath, 1985). Owing to the fact that hydrogen is required as an auxiliary gas for generating the flame inside the device the flame photometer is used less frequently in stationary air quality measuring stations. It is not common practice to use it for emission measurements as the concentrations to be measured are too high and there are too many interfering components (quenching).

Gases can be ionized more or less easily by the addition of energy. For gas analyses the ionization of organic molecules in flames (flame ionization) has gained the greatest significance. Ionization by radiation of radioactive substances in detectors, e.g., in gas chromatography, is also applied (Kaiser, 1965).
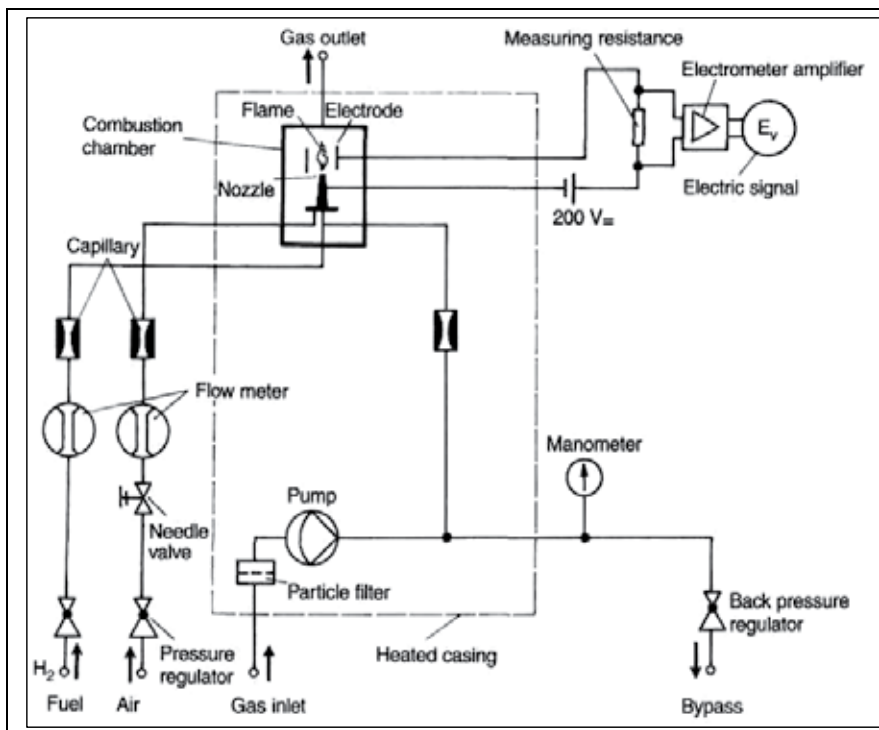
Fig. 9. Diagram of a flame ionization detector (FID) (Kaiser, 1965).

The so-called flame-ionization detector (FID) was originally developed for gas chromatography. Nowadays, it is also used as the most important measuring device for the continuous recording of organic substances in exhaust gases or in ambient air.

The measuring principle of the FID is classic and will be summarized here with the help of Fig 9.

The hydrogen flame burns out of a metal nozzle which simultaneously represents the negative electrode of an ionization chamber. The positive counter-electrode is fixed above the flame, e.g., as a ring. Between the two electrodes direct voltage is applied. The ion current is measured as a voltage drop above the resistor W. The measuring gas is added to the burning gas shortly before entering the burner nozzle. The air required for combustion flows in through a ring slot around the burner nozzle.

For stable measuring conditions it is essential that all gases - combustion gas, combustion air and measuring gas - are conducted into the flame in constant volume flows. For this, all gas flows are conducted via capillaries. Constant pressures before the capillaries ensure a constant flow. Sensitive pressure regulators for combustion gas and combustion air are used to achieve this fine-tuning. The measuring gas is pumped past the capillary in the bypass in a great volume flow. Pressure is kept constant by the back pressure regulator, so that a constant partial flow reaches the flame via the capillary. Most FID's operate with overpressure, i.e., the measuring gas pump is located before the capillary. To avoid condensation of the hydrocarbons to be measured almost all instruments can be heated to 150-200 °C. Heating includes the particle filter and the measuring gas pump; in most cases,

particularly with warm exhaust gases, a heated sampling line is also used from measuring gas sampling to the measuring instrument.

Hydrocarbon compounds are oxidized in the flame with ions being formed as an intermediate product. In a certain range of the accelerating voltage the strength of the ionization current is in first approximation directly proportional to the amount of C atoms of the burned substance. Thus, an FID basically responds to all hydrocarbons and measures their total sum. Corresponding to the number of carbon atoms, larger molecules with many C atoms produce a higher signal than smaller molecules with a small number of C atoms. Ionization energy does not only stem from the flame's energy, but mainly from the oxidation energy of the carbon. Accordingly partially oxidized hydrocarbons provide a weak detector signal, completely oxidized hydrocarbons no signal at all; HCHO, CO and CO_2, e.g., are not detected. If exhaust gases predominantly consist of mixtures of pure, i.e., non-oxidized or halogenated hydrocarbons, the FID provides a signal nearly proportional to the carbon miss content of the exhaust gas.

The reference method for HC (hydrocarbons) measurements (including CH_4 methane and NMHC – non-methane hydrocarbon) is the flame ionization method (FID). The principle of this method is represented in figure 10.
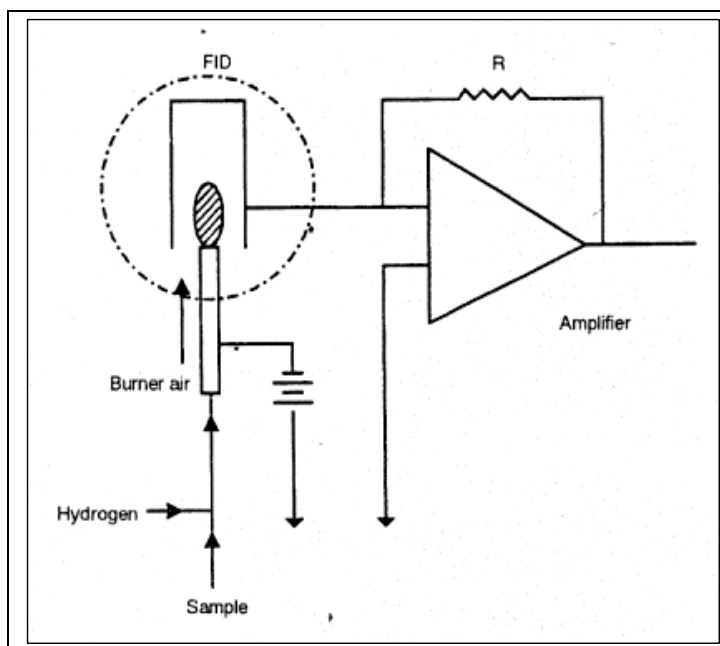
Fig. 10. FID monitoring device schematic for (Horiba, User manual)

When hydrocarbon is introduced to hydrogen flame, the high-temperature energy at the jet nozzle tip ionizes the hydrocarbon molecules. In this time, applying a direct-current voltage between two electrodes that face each other across the flame generates a minute ion current, proportional to the carbon number of the ionized hydrocarbon. The total hydrocarbon can be measured by passing this ion current through a high resistance to convert it to voltage. The sampled gas is divided in two flows: one is used for CH_4 concentration measurement by removing HC other than CH_4. The other is used for THC concentration measurement

directly. These two sample gases and zero gas are sent to the analyzer alternately to measure CH_4 and THC concentrations. Besides, NMHC concentration is obtained by subtracting CH_4 from THC.

3.5 Measuring Methods for Particulate Matter

When examining particulate matter in ambient air the following factors must be taken into account: (i) total mass concentration of the particulate matter, (ii) concentration of fine particles, (iii) size distribution, (iv) chemical composition.

In the air quality range particle sedimentation as well as non-sediment suspended particulate matter is of interest, particularly the latter, as it is respirable and can thus carry pollutants into the human body.

Particulate matter (PM) is a medium which consists of a lot of different substances regarding chemical composition and size distribution. Relevant for human health are PM with an aerodynamic diameter smaller 10 µm (PM10) with a tendency to smaller sizes, e.g. PM2.5.

PM's could be measured with many techniques but the most relevant are TEOM devices and SMPS (Scanning Mobility Particle Seizer) gravimetric techniques.

The TEOM instrument is a true "gravimetric" instrument that draws ambient air through a filter at a constant flow rate, continuously weighing the filter and calculating near real time mass concentrations.

When the instrument samples, the ambient air stream first passes through an optional size-selective inlet, and continues down the heated sample tube to the mass transducer. Inside the mass transducer, this sample stream passes through a filter made of Teflon-coated borosilicate glass. The instrument measures the mass of this filter every 1.68 seconds. The difference between the filter´s initial weight (as automatically measured by the instrument when data collection begins) and the current mass of the filter gives the total mass of the collected particulate. These instantaneous readings of total mass are then averaged using a user selectable averaging time to reduce noise. Next, the mass rate is calculated by computing the increase in the averaged total mass between the current reading and the immediately preceding one, and expressing this as a mass rate in g/sec. This mass rate is smoothed to reduce noise. Finally, the mass concentration in µg/m³ is computed by dividing the mass rate by the flow rate. Internal temperatures in the instrument are controlled in order to minimise the effects of changing ambient conditions. The sample stream is preheated before entering the mass transducer (usually to 50° C) so that the sample filter always collects under conditions of very low (and therefore relatively constant) humidity.
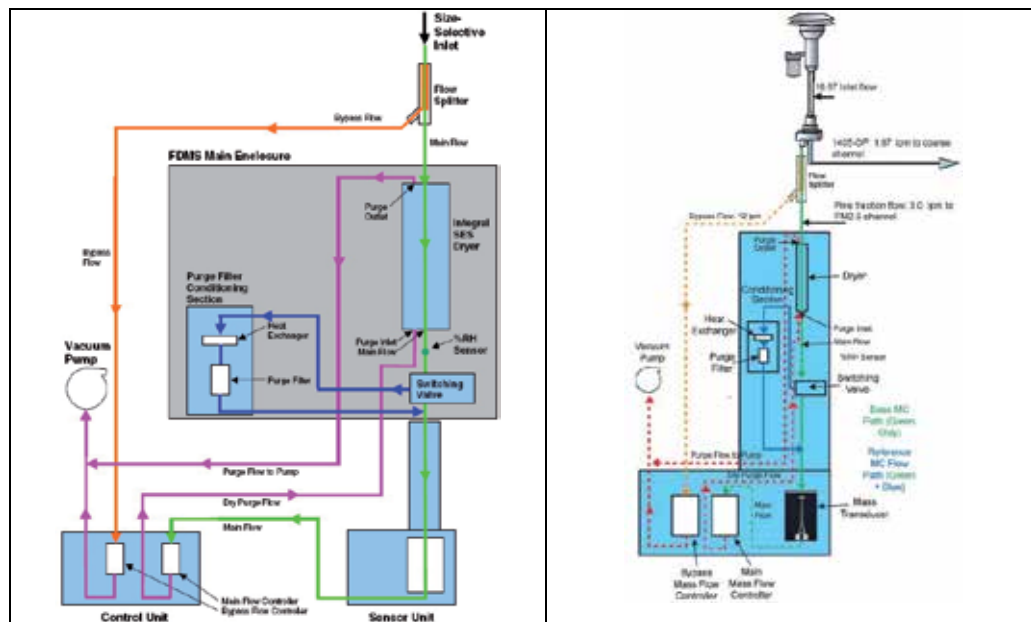
Fig. 11. PM measurement device TEOM (Thermo Scientific, User manual TEOM Monitor, Series 1400ab)

Fig. 11 is a schematic diagram showing the flow of the sample stream through the instrument in the case of a PM-10 configuration. The TEOM Monitor measures PM-10 or PM-2.5 mass concentrations and consists of a TEOM mass sensor and control unit in a network ready configuration.

The particle size separation at 10 μm diameter takes place as the sample proceeds through the PM-10 inlet. The flow splitter separates the total flow (16.7 l/min) into two parts: a main flow of 3l/min that enters the sensor unit through the sample tube, and the bypass flow of 13.7 l/min. The main flow passes through the exchangeable filter in the mass transducer, and then proceeds through an air tube and in-line filter to a mass flow controller. The bypass flow is filtered in the bypass fine particulate filter and again in an in-line filter before it enters a second mass flow controller. A single pump provides the vacuum necessary to draw the sample stream through the system.

The weighing principle used in the TEOM mass transducer is fundamentally different from that on which most other weighing devices are based. The tapered element at the heart of the mass detection system is a hollow tube, clamped on one end and frees to vibrate at the other. An exchangeable filter cartridge is placed over the tip of the free end. The sample stream is drawn through this filter, and then down the tapered element. This flow is maintained at a constant volume by a mass flow controller that is corrected for local temperature and barometric pressure. The tapered element vibrates precisely at its natural frequency, much like the tine of a tuning fork. An electronic control circuit senses this vibration and, through positive feedback, adds sufficient energy to the system to overcome losses. An automatic gain control circuit maintains the vibration at constant amplitude. A precision electronic counter measures the frequency with a 1.68 second sampling period. The tapered element is in essence a hollow cantilever beam with an associated spring rate

and mass. As in any spring-mass system, if additional mass is added the frequency readout on the screen of the computer.

4. Non standard Remote Sensing Monitoring

Some detectors measure the optical properties of the gas, and have been designed so that the reflected or transmitted signal is received after an extended path-length through the air. This arrangement offers the advantages of eliminating the possibility of sample degradation during passage to and through an instrument, and of integrating the concentration over a region of space rather than sampling at one point.

Remote sensing devices offer a number of advantages over competing technologies such as electro-chemical sensors or closed path optical systems, including flexibility of deployment, and avoidance of extractive sampling. The value of ROMT instrumentation has already been proven in applications including transport, power generation, chemical processing and air quality monitoring, to monitor gaseous emissions for the protection of the environment, or the safety of citizens. However the use of these instruments for formal monitoring purposes, e.g. to comply with the requirements of European directives on air quality, is hampered by the lack of instrument performance standards against which products could be certified. Remote or open-path optical systems are explicitly excluded from current gas sensing and environmental monitoring standards. This is partly owing to the difficulties in defining performance requirements which take into account the environmental factors which affect the instruments use in the field.

Remote sensing systems are now often used for detection of airborne pollutants. These systems deliver information about the concentrations in a certain region which is covered from a light beam between emitter and receiver. This results in an average value which represents mostly better the pollution level in a particular area then a point measurement. In addition they can be used for "fence-line" monitoring at industrial sites. The path length can vary from some cm to some hundreds of meters. The measurement can be done in the atmosphere in the so called "open-path" mode, or in a gas cell (White cell) in the so called "extractive" mode. The methodology is based on the analyses of the spectra of a light beam which passes through the ambient air (open-path) or through the White-cell (extractive). The relationship between the absorbed amount of light and the number of molecules is described by the Beer-Lambert absorption law. Due to the fact that each gas has its own typical absorption profile (finger print), it is possible to detect the concentrations of multiple gases in the same light beam either simultaneously, or one after the other.

4.1 LIDAR

In addition to the point measurements, the author propose to investigate air quality and specific thermodynamic and meteorological parameters, on line, by one simultaneous use of LIDAR (Light Detection and Ranging) systems, as presented by Fig. 12 (Vetres et al., 2010).
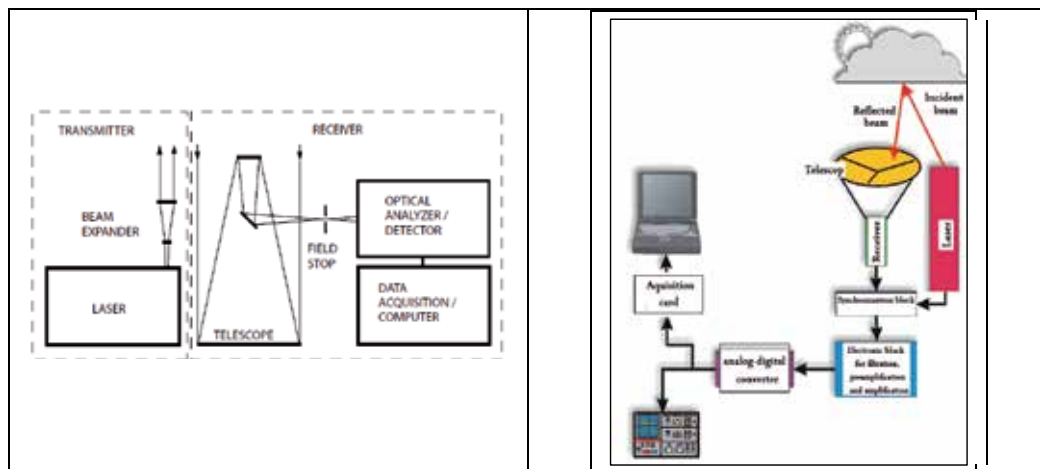
Fig. 12. Principles of functioning for LIDAR systems (Vetres, 2009).

LIDAR effectively detects and characterizes air contaminants, with best spatial and temporal resolution, locates the pollution sources and take correct actions to correct the problems while also helping in developing perspective strategies. Complementary, by applying a trajectory model or different dispersion models, one can characterize, at regional scale, the pollution regime, as well as the dynamics of the pollutants. The most obvious use is to track the evolution of a pollutant over time. Urban monitoring might be thus completed by on line LIDAR measurements, in a very modern way, in accordance to recent technical developments worldwide. Other relevant results might be analyzed from LIDAR systems are well suited for the remote measurement of pollutants, with numerous applications depending on the purpose. The most obvious use is to track the evolution of a pollutant over time. If the LIDAR laser beam is oriented vertically, the device acts as a profiler. If one changes the vertical angle of the laser beam a succession of alignments is generated that, with the proper interpolation, can define a concentration plane. The profiler is the usual configuration of the LIDAR systems, providing very valuable information, such as the depth of the planetary boundary layer and the evolution of the concentration.

Light detection and ranging (LIDAR) describes a family of active remote sensing methods. The most basic technique is long-path absorption, in which a beam of laser light is reflected from a distant retro reflector and returned to a detector which is co-located with the source. The wavelength of the radiation is chosen so that it coincides with an absorption line of the gas of interest. The concentration of that gas is found by applying the Beer–Lambert law to the reduction in beam flux density over the path length. No information is obtained on the variation in density of the gas along the path length; if the gas is present at twice the average concentration along half the path, and zero along the other half, then the same signal will be received as for uniform distribution at the average concentration.

The scheme in Fig. 13 represents the configuration of the LIDAR from the Timisoara location, as designed in order to realize analysis for the western part of Romania.
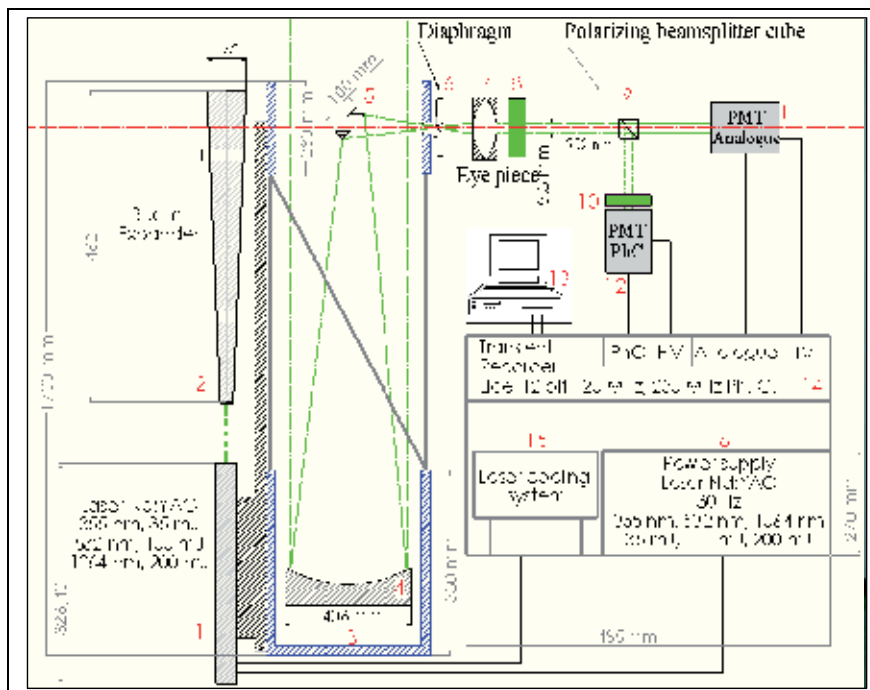
Fig. 13. Scheme of the LIDAR system (Vetres et al., 2009), (Vetres et al., 2009)

The system that has been developed is configured by following components:

-       Nd:YAG 30 Hz pulsed laser (35 mJ at 355 nm, 100 mJ at 532 nm, 200 mJ at 1064 nm);
-       Newtonian telescope of 406 mm in diameter of primary mirror;
-       Licel transient recorder acquisition cards;
-       Analogue photo detector and Photon counting photo detector.

The acquisition for the Lidar system is based on 2 channels, 532 nm analogue and photon-counting (depolarization). The Licel transient recorder is a TR 20 model, with a 7.5 m spatial resolution. Because of the powerful 30 Hz YAG laser, the instrument is proper to be used in air scattering applications, the acquisition being triggered by the laser and it can record up to 30 profiles every second.

4.2 Differential Absorption LIDAR (DIAL)

Pulses from a tunable laser are directed into the air at two wavelengths, and the backscattered signals from the air molecules, gas molecules and particles are measured by a cooled detector. One laser wavelength (min) is just to one side of an absorption band for the gas of interest, and calibrates the backscatter of the LIDAR system for molecular (Rayleigh) and aerosol (Mie) scattering that occurs whether the gas of interest is present or not. The second laser wavelength (max) is tuned to an absorption band, so that the difference between the two can be used to derive absorption due to the gas alone. The ratio of the scattered flux density at the two wavelengths is given by (Popescu et al., 2009):

$$\frac{I(\lambda_{\max})}{I(\lambda_{\min})} = \exp(-2RN\sigma)$$

(10)

where σ is the absorption cross section of the target species at wavelength λ_{max}, R is the range and N is the number concentration of the gas.

Molecule	Peak absorption [wavelength/nm]	Absorption [cross section/10^{-22} m^2]
Nitric oxide	226.8; 253.6; 289.4	4.6; 11.3; 1.5
Benzene	250.0	1.3
Mercury	253.7	56000
Sulphur dioxide	300.0	1.3
Chloride	330.0	0.26
Nitrogen dioxide	448.1	0.69

Table 1. Absorption wavelengths and cross sections for dye lasers.

By measuring the time for the back-scattered signal to return, the range can also be determined to within a few meters over a distance of 2000 m. The technique has been used for studying plume dispersion and vertical concentration profiles, as well as spatial distribution in the horizontal plane. The most widely used sources are CO_2 lasers emitting in the 9.2–12.6 m band, within which they can be tuned to emit about 80 spectral lines. For example, O_3 absorbs strongly at 9.505 m, and NH_3 at 10.333 m. In the UV-visible, dye lasers pumped by flash lamps or by laser diodes are used. By using different dyes, they are tunable over the whole visible band. Some examples of the wavelengths used are given in Table 1 (Popescu et al., 2009).

4.3 Differential optical absorption spectroscopy (DOAS)

The instrument consists in a detector at one end of an atmospheric path (typically 200–10 000 m in length) scans across the waveband of a UV/visible source, such as a high-pressure xenon arc lamp that has a known broad spectrum, at the other end. The physical arrangement can be bi-static (with the receiver at one end and the transmitter at the other) or monostatic (a retro reflector returns the beam to the receiver, which is co-located with the transmitter). Gases that are present on the optical path absorb radiation according to the Beer-Lambert Law, and the absorption varies differently with wavelength for each gas. Variations across the spectrum are compared to stored reference spectra for different gases, and the equivalent amounts and proportions of the gases adjusted in software until the best match is achieved (Popescu et al., (2009). The main wavelength range used is 250–290 nm, in the UV, with typical spectral resolution of 0.04 nm. Several different gases can be measured simultaneously. Sensitivity is high, and 0.01% absorption can be detected, equivalent to sub-ppb concentrations of many gases over a path length of 1 km. Detectable gases include SO_2, NO, NO_2, O_3, CO_2, HCl, HF, NH_3, Cl_2, HNO_2 and many organic compounds (aldehydes, phenol, benzene, toluene, xylenes, styrene and cresol). The method is appropriate for obtaining the average concentrations of a pollutant across an urban area or along the length of an industrial plant boundary.
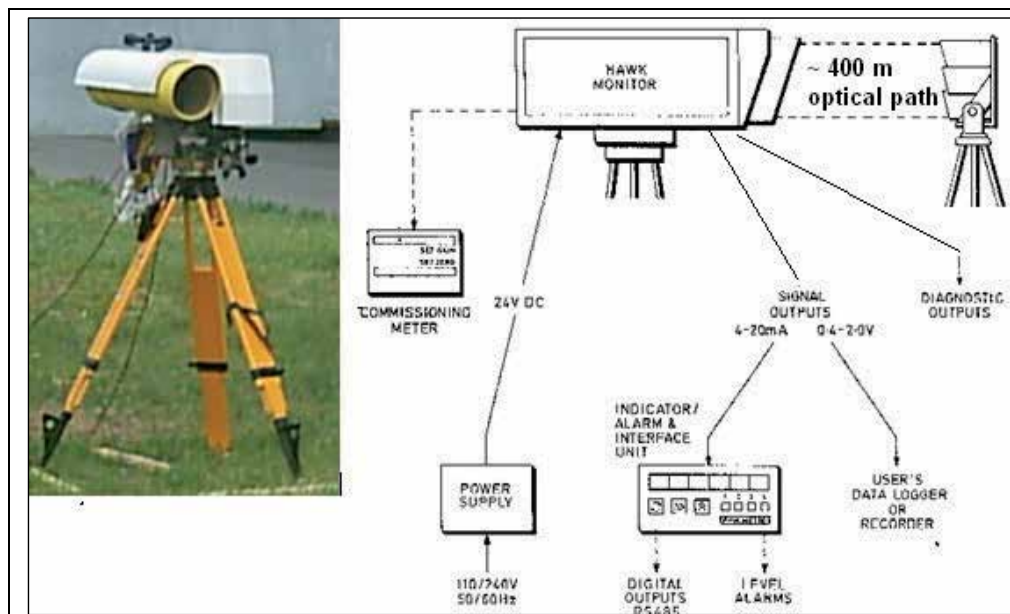
Fig. 14. Schematic of the HAWK flow diagram (Siemens Hawk Technical Manual).

An example of one DOAS instrument is given in Fig. 14. The Siemens HAWK instrument is used to measure the CO concentration over a 400 meters length optical path, in an intersection with intense road traffic. In addition one reference NDIR (Non - disperse Infrared) cross-flow Horiba APMA350 instrument is used to validate the DOAS measurements.

4.4 Fourier transform infrared (FTIR) absorption spectroscopy

This is the most optically sophisticated remote sensing technique, using a scanning Michelson interferometer to detect the entire spectral region at once, and therefore capable of measuring many gases simultaneously. The wavebands used are within the atmospheric absorption windows of 8.3 - 13.3 or 3.3 - 4.2 m. However, sensitivity is generally limited to a few tens or hundreds of ppb (depending on the gas) over a 200 m path length; the technique is therefore more appropriate to perimeter monitoring for gas escapes from an industrial site than to general ambient monitoring (Popescu et al., 2009).

Infrared spectroscopy has been used for several decades, initially developed for the detection of atmospheric CO_2 by non-dispersive instruments. Instruments based on Fourier transform spectroscopy can measure a lot of species by means of multiple reflection cells (White cells) as well as in open-path mode, and has been improved during the last years from a laboratory instrument to an instrument for in-situ emission and/or air quality measurements.

All polyaromatic molecules and heteronuclear diatomic molecules absorb infrared radiation. The absorption changes the molecular rotation and vibration. The pattern of absorption therefore depends on the physical properties of the molecule such as the number and type of atoms, the bond angles, and the bond strengths. This means that each spectrum differs from all others and may be considered the molecular "signature" (finger-print). Monatomic gases such as radon and homonuclear diatomic molecules such as N_2 and O_2 do not have infrared bands and therefore must be measured with non-infrared means. Diatomic molecules such a

NO, CO, HCl, and HF have a single major band that is an array of individual lines, each with a width of about 0.2 cm^{-1}. Linear polyatomic molecules like CO_2, N_2O, and C_2H_2 also show arrays of individual lines. Non-linear polyatomic molecules like O_3, SO2, NH_3, H_2CO, CH_4, and H_2O have many apparent "lines" that is in fact small bundles of lines, with the widths of the bundles varying from 0.2 cm^{-1} to many cm^{-1}. For larger polyatomic molecules at atmospheric pressure there are so many lines overlapping each other that the spectral features are broad and smooth, except for occasional "spikes" (Nicolae & Cristescu, 2006).

The big advantage of "open-path" measurements can be found in the detection of emissions from diffusive sources, e.g. a lot of small sources in industrial plants, waste deposits, waste water facilities, or at fence-line monitoring, where a possible pollution transport over particular boundaries has to be monitored, e.g. prevention of losses of hazardous pollutants.

5. Examples and Comments of Air Quality Monitoring Results

The examples that are following are given in the idea to complete the theoretical information from previous, and to give realistic data concerning on line monitoring campaigns. Two main episodes were selected, referring to two locations: (i) an airport), and (ii) urban area. Also for the first episode parallel measurements have been recorded, by two independent laboratories (http://inoe.inoe.ro/RADO).

Following pollutants have been continuously measured, with 10 sec resolution, over the entire measuring episode with high precision equipment (Ionel et al., 2008):

- **SO_2** measured with two Horiba APSA370 instruments, measurement principle is UV fluorescence, reference method: EN 14212:2005. The combined measurement uncertainty is $U = 1.76$ % for recorded values;

- **NO**, **NO_2** and **NO_x** measured with two Horiba APNA370 instruments, measurement principle is chemiluminescences, reference method: EN 14211:2005. The combined measurement uncertainty is $U = 2.06$ % for recorded values;

- **O_3** measured with two Horiba APOA370 instruments, measurement principle is UV photometry, reference method: EN 14625:2005. The combined measurement uncertainty is $U = 6.98$ % for recorded values;

- **CO** measured with two Horiba APMA370 instruments, measurement principle is NDIR (Non Dispersive Infrared), reference method EN 14626:2005. The combined measurement uncertainty is $U = 4$ % for recorded values;

- **CH_4, NMHC** and **THC** measured with two Horiba APHA370 instruments, measurement principle is FID (flame ionization detection), reference method EN 12619:2002. The combined measurement uncertainty is $U = 0.9$ % for recorded values;

- Other gases have been measured with DOAS Instruments
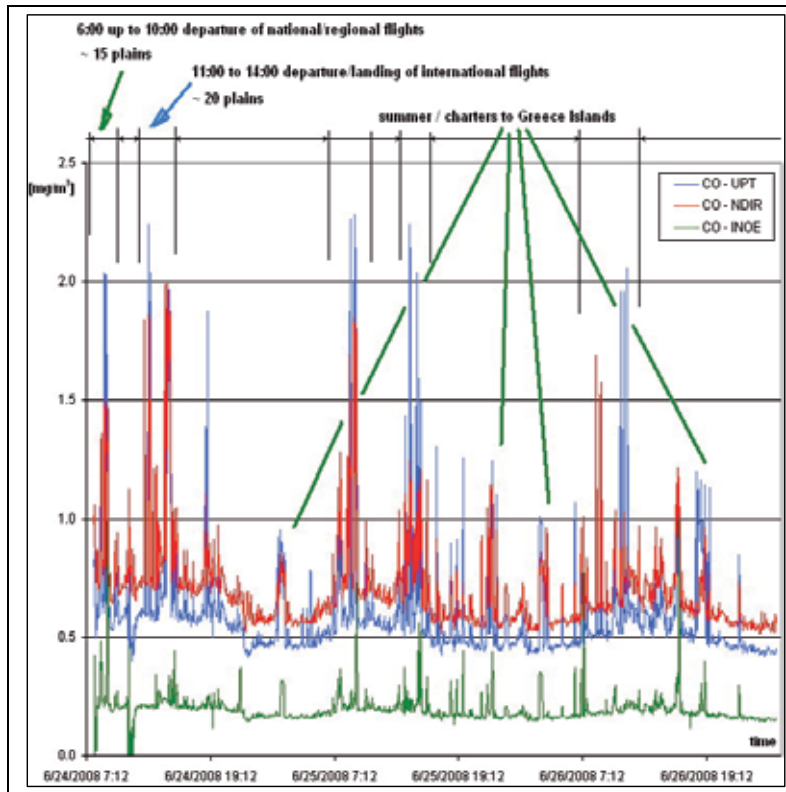
Fig. 15. CO measurements and airplanes traffic.

Fig. 15 shows the carbon monoxide CO recorded values, measured with 3 different instruments: two reference NDIR point measurement instruments and one DOAS-IR Siemens-Hawk instrument.

The different methods used for CO measurements have given same result; the high concentration recorded values and background concentration values are similar for point and open path instruments. The CO-INOE measurements are in the same trend but the measured values are with ~ 0.4 mg/m³$_N$ lower than the other instruments. This could be caused by an error in span gas calibration. On top of the figure 2 are drafted the departures and arrivals of national/regional, international and charters corroborated with the carbon monoxide measured values. The dependency between aircraft traffic on the apron and the CO measured values is visible in figure 2, the higher values for CO have only been recorded during the departure or landing of the aircrafts. This result is important because it demonstrates that the selected placement of the mobile air laboratories near the airport facilities and apron is ideal for depicting the air quality and the measured values can be considered representatives for the airport facilities surroundings.

The measured values for carbon monoxide are much lower than the 10 mg/m³ limit value, regulated by 2000/69/EC Directive. The measured values were normal because the airport location is far-off from the city or any main road and the only CO source is represented by the aircrafts.

Fig. 16 shows the mean measured values of sulfur dioxide SO_2, measured by two instruments.
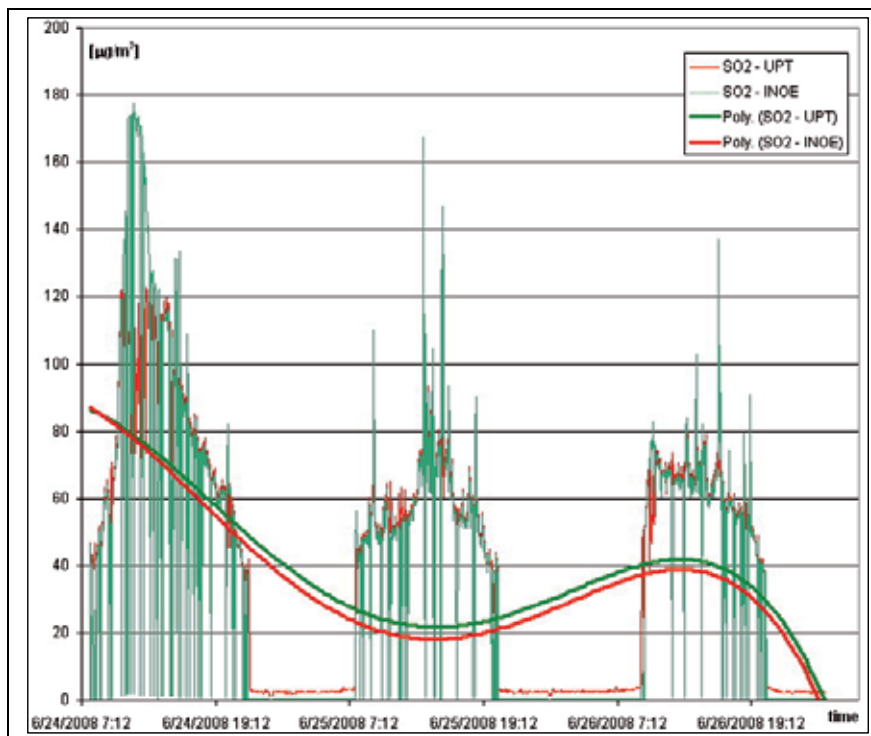
Fig. 16. SO_2 measurements and polynomial (4 degree) trend lines.

The SO_2 concentration in air is continuously measured and recorded (one value every second) and mediated every 3 minutes. Because the SO_2 - INOE instrument has given high variations (in short term intervals) two 4th degrees polynomial trend lines are added to the graph, one for the recorded values of each instrument. The correlation between the instruments is acceptable, just differences of about 5 $\mu g/m^3_N$ are recorded, differences that can be considered equivalent within the measurement uncertainty.

The recorded values for SO_2 are not higher then the 350 $\mu g/m^3_N$ limit value regulated by 1999/30/EC Directive but they are about 10 times higher then the background values (7 $\mu g/m^3_N$). The 3 minutes mean value have been used for an easy observation of the influence of airplanes traffic on pollutants concentration, that is the main purpose of this study. The SO_2 concentrations below 150 $\mu g/m^3$ have only moderate (and reversible) irritant effect on human respiratory system, but in synergy with NO_x and high air humidity can cause permanent pulmonary impairment (according to CCOHS - Canadian Centre for Occupational Health and Safety). The only possible source responsible for the SO_2 high values is the airplane fuel because there are no other possible emission sources of SO_2 in the airport vicinity (no main road traffic or industrial areas). The ground support vehicles are limited in number (5 busses and 2 passenger cars) and their contribution to airport emissions is insignificant (Ionel et al., 2010).
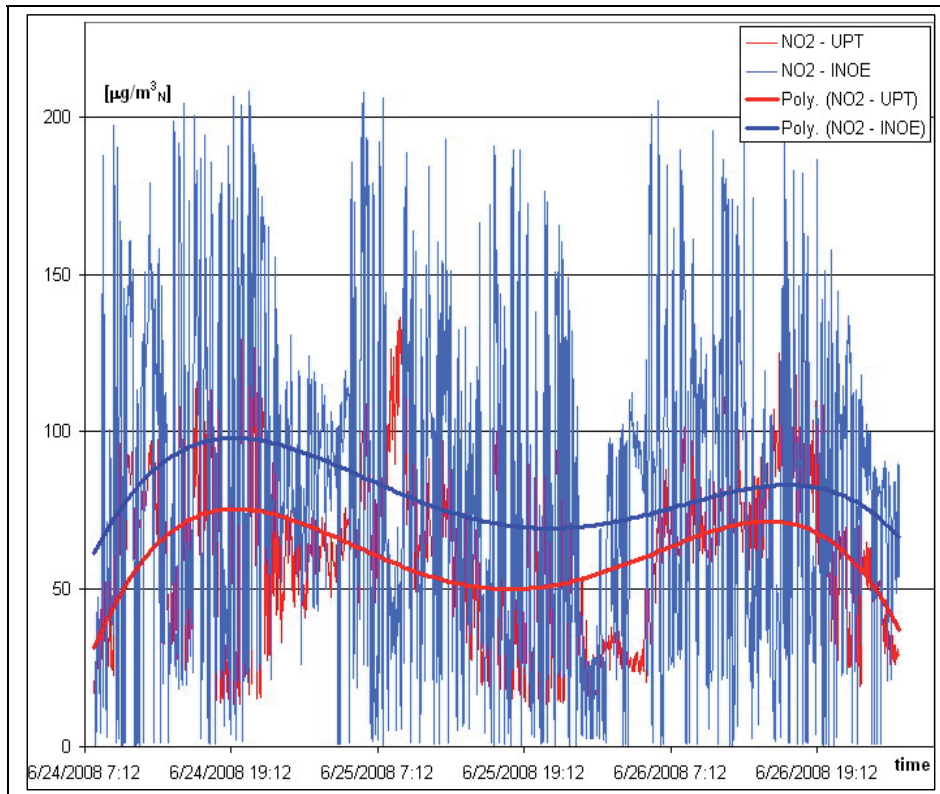
Fig. 17. NO$_2$ measurements and polynomial (4 degree) trend lines.

Fig. 17 shows the measured values for nitrogen dioxide NO$_2$, with two identical instruments. The correlation between the instruments is good, polynomial trend lines have been added for better resolution. The recorded values are similar for both instruments and higher then the 200 µg/m^3_N limit value regulated by 1999/30/EC Directive. Because the highest measured values is overlapping airplane traffic on apron it is clear that the only possibility to reduce NO$_2$ concentration is to manage more efficient airplane taxiing procedures.

Figure 18 shows the measured values for methane CH$_4$, non-methane hydrocarbon NMHC (VOC) and total hydrocarbon THC, with one FID (flame ionization detection) instrument. The recorded values for methane are higher that the global background (1.7 ppm) with only 0.4 ppm. The values recorded for volatile organic compounds are up to 3 mg/m^3_N in periods with high airplane traffic. These values are representing a serious concern for the passenger health, knowing that some on these volatile compounds (like benzene) are causing cancer (www.epa.gov/). VOCs include a variety of chemicals, some of which may have short- and long-term adverse health effects. Key signs or symptoms associated with exposure to VOCs include conjunctival irritation, nose and throat discomfort, headache, allergic skin reaction, dyspnea, declines in serum cholinesterase levels, nausea, emesis, epistaxis, fatigue, dizziness. As with other pollutants, the extent and nature of the health effect will depend on many factors including level of exposure and length of time exposed. The measured values for VOCs are up to 3 mg/m^3 (3000 µg/m^3). These values emerge not only during airplanes departure or arrivals, but mostly when the airplanes are fueled.
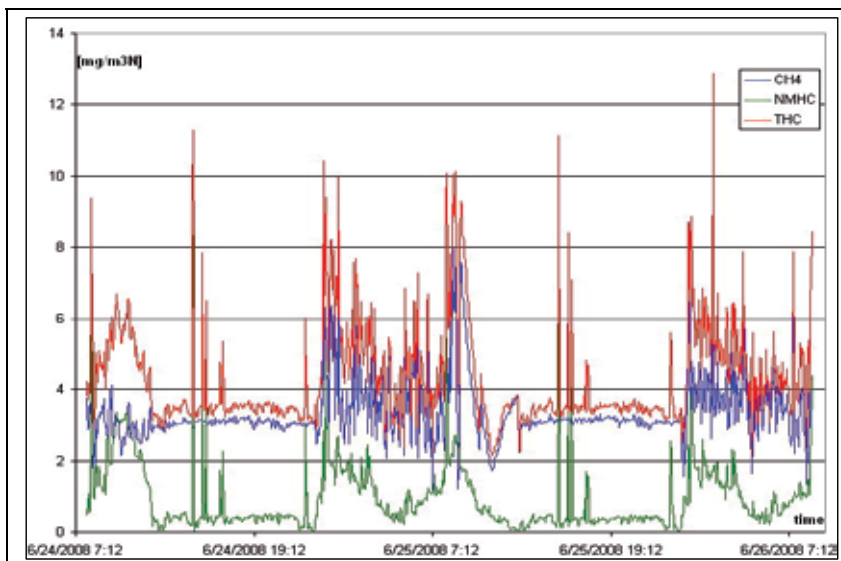
Fig. 18. CH₄, NMHC (VOC) and THC measurements, 3 minutes mean value.

The most relevant values recorded with INOE DOAS instrument are presented in figures 19 to 22. Very high values have been recorded for acrolein and tert-butil. Also significant values were recorded for benzen, toluen, benzaldehyde, O-cresol, O-xylen, (2, 5) – dimethyl, and also for P-tolylaldehyde.
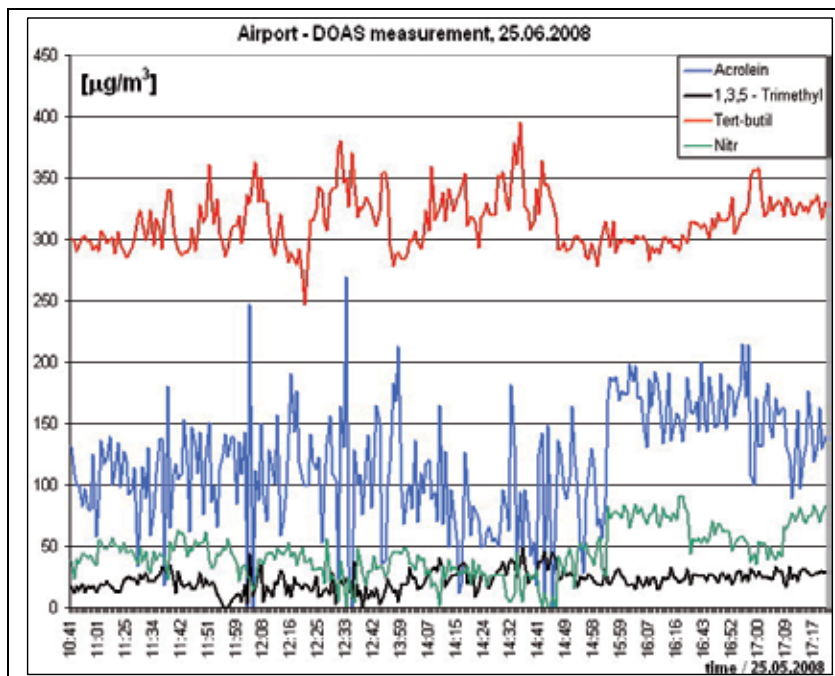
Fig. 19. DOAS measurements. Several species for the episode 25.06.2008, 3 minutes mean value.
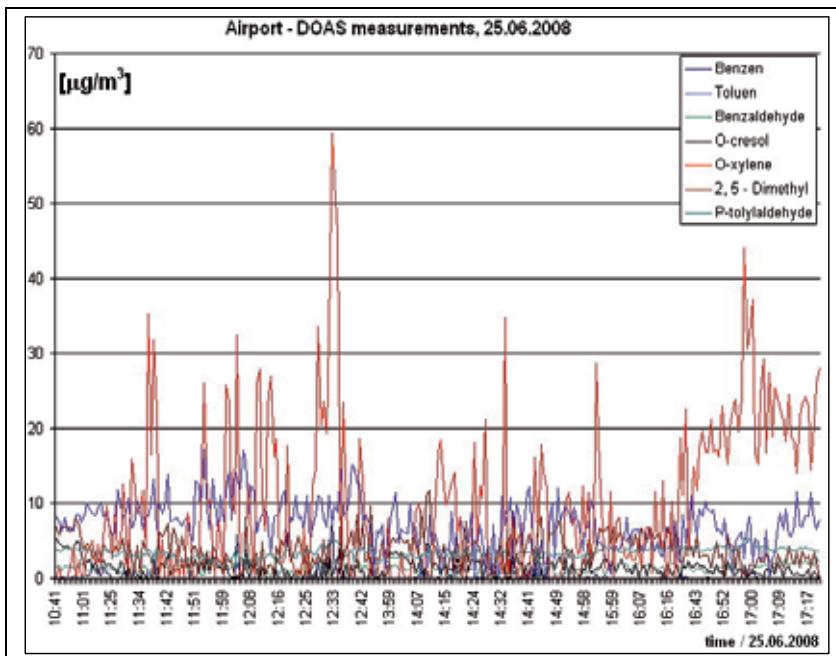
Fig. 20. DOAS measurements of several species for the episode 25.06.2008 , 3 minutes mean value.
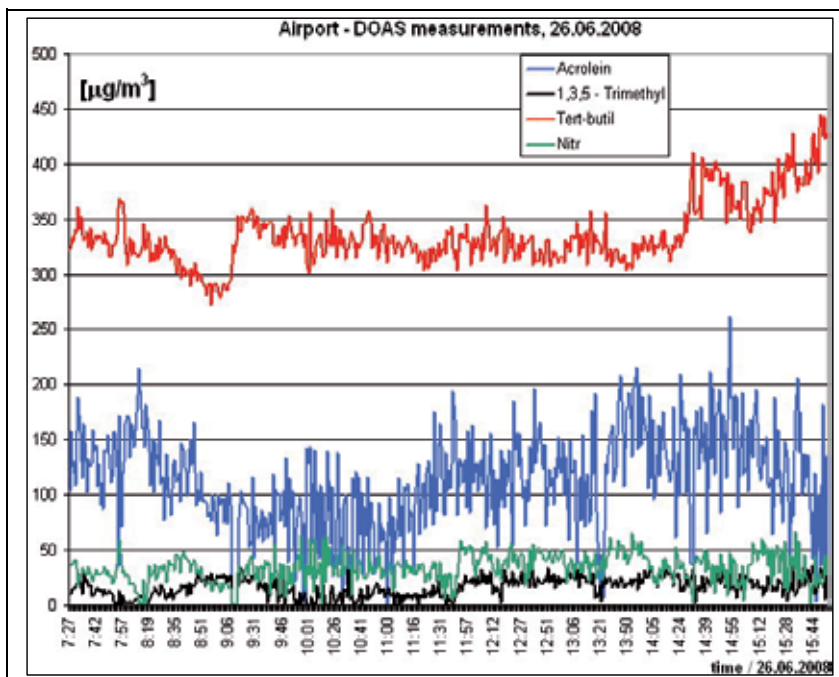
Fig. 21. DOAS measurements of several species for the episode 26.06.2008 , 3 minutes mean value.
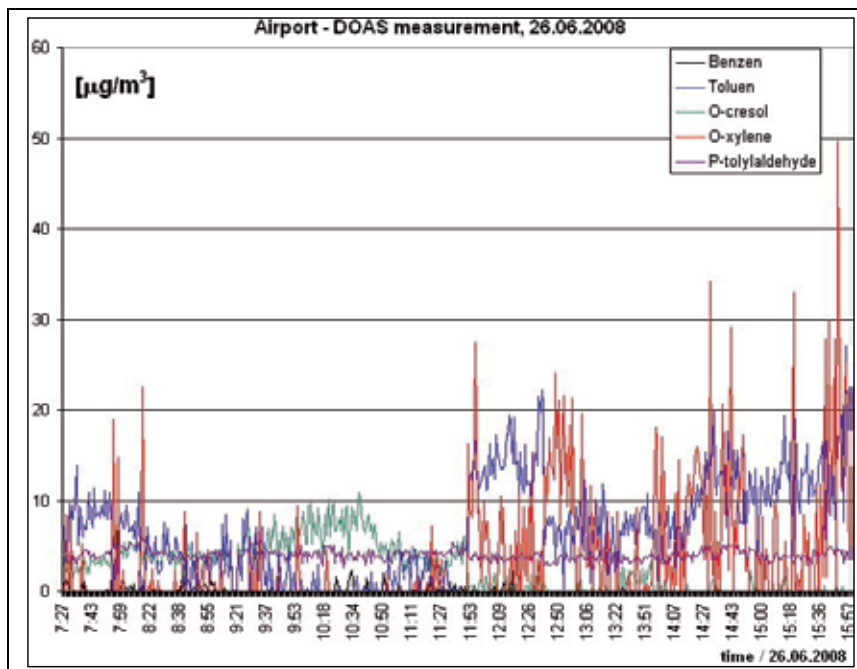
Fig. 22. DOAS measurements of several species during 26.06.2008, 3 minutes mean value.

It is well known that acrolein may be released to the environment in emissions and effluents from its manufacturing and use facilities, in emissions from combustion processes (including cigarette smoking and combustion of petrochemical fuels), from direct application to water and waste water as a slimicide and aquatic herbicide, as a photooxidation product of various hydrocarbon pollutants found in air (including propylene and 1,3-butadiene), and from land disposal of some organic waste materials. Acrolein is a reactive compound and is unstable in the environment (Popescu, 2009). In ambient air, the primary removal mechanism for acrolein is predicted to be reaction with photochemically generated hydroxyl radicals (half-life, 15–20 hours). Products of this reaction include carbon monoxide, formaldehyde, and glycolaldehyde. In the presence of nitrogen oxides, eroxynitrate and nitric acid are also formed. Small amounts of acrolein may also be removed from the atmosphere in precipitation. Insufficient data are available to predict the fate of acrolein in indoor air (Nicolae et al., 2007). But experimental data indicate that reaction of acrolein with ozone in specific conditions ($k = 2.8 \times 10^{-19} cm^3/molecules$-sec at 25 °C; half-life, 59 days) or nitrate radicals ($k = 5.9 \pm 2.8 \times 10^{-16} cm^3/molecules$-sec at 25 °C; half-life, 16 days) in the troposphere would be too slow to be environmentally significant (Nicolae & Cristescu, 2006), (Wang et al., 2009), (Ionel et al., 2010).

The second range of examples is comparisons between urban episodes from two EU cities, one in Romania (Timisoara - TM), one in Austria (Graz - GdB).

When considering carbon monoxide (C0) the maximum hourly mean value shows differences in the order of five to ten (Fig. 23). As Graz don Bosco is already the traffic hot spot of Graz the main reason of this difference can only be found in the difference of the technical standards of the vehicle fleet. The Austrian vehicle fleet consists of gasoline vehicles with three way catalytic converters and of diesel cars. Both groups have very small

CO concentrations. This is not the case for the vehicle fleet of Timisoara. Cars and domestic heating contribute strongly to the high CO level.

Figure 24 depicts the NO, NO_2 and SO_2 concentrations; again the maximum hourly value is shown. NO and NO_2 are in most – but not all – cases in Timisoara higher than in Graz don Bosco. A clear picture is given only for SO_2 – which is a tracer for emissions from industry and private households. In Graz there is almost no SO_2 concentration measured, whereas Timisoara shows levels up to 50 $\mu g/m^3$, but well below the threshold of 200 $\mu g/m^3$.
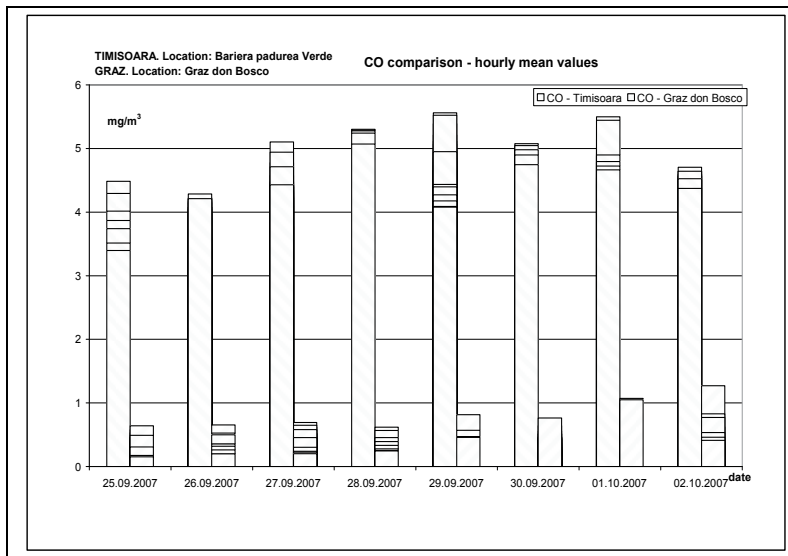
Fig. 23. Comparative CO one hour mean values.
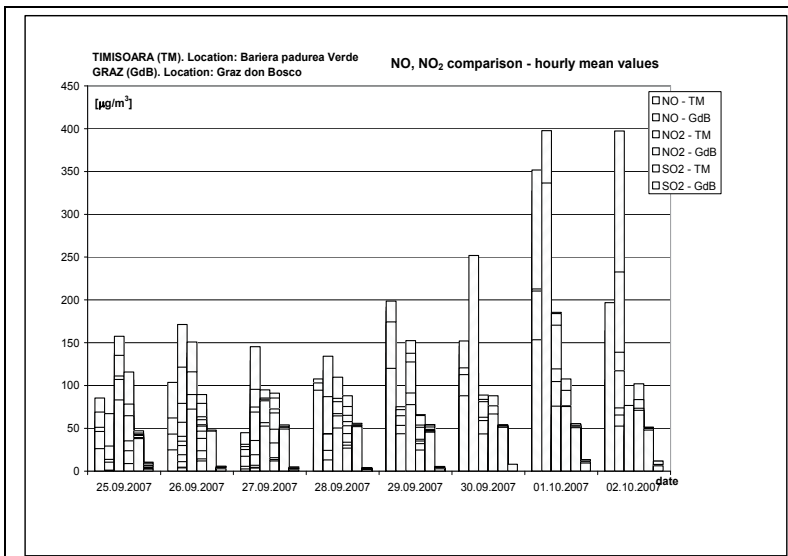
Fig. 24. Comparative NO, NO_2, SO_2 one hour mean values.

The comparison between AQ online monitoring data in two European cities (even no mega-cities) proofs that despite the fact that the same EU legislation and monitoring methods are applied, the results are quite different.

Finally new results taken by the LIDAR system of the RADO (***Romanian Atmospheric 3D research Observatory Project***) consortium project in Romania are presented by Fig. 25. Thus the Range Corrected Signal from April 22-th, 2010, evening, is presented, indicating that the volcanic cloud is observed already starting from 3 km high, with an ascendant tendency, and that at 4.5 km approximately the clouds are formed. Combining LIDAR observations with in situ measurements and models is a strong complementary support for monitoring of different atmospheric parameters over various space-time scales, promoting the remote-sensing approaches in environmental applications. The Romanian Atmospheric research 3D Observatory (RADO) is an ambitious facility that aims to improve modelling of physical, chemical, and biological processes, to assess the effects of climate change, and to quantify and reduce uncertainties in evaluating the hydrological cycle and its influence on natural resources. Over the last five years, environmental research has focused increasingly on remote sensing of the atmosphere. The station is able to monitor a number of atmospheric parameters, including trace gases and aerosols, as well as meteorological ones. Microwave spectroscopy and mass spectrometry are the latest techniques to be implemented at this site.
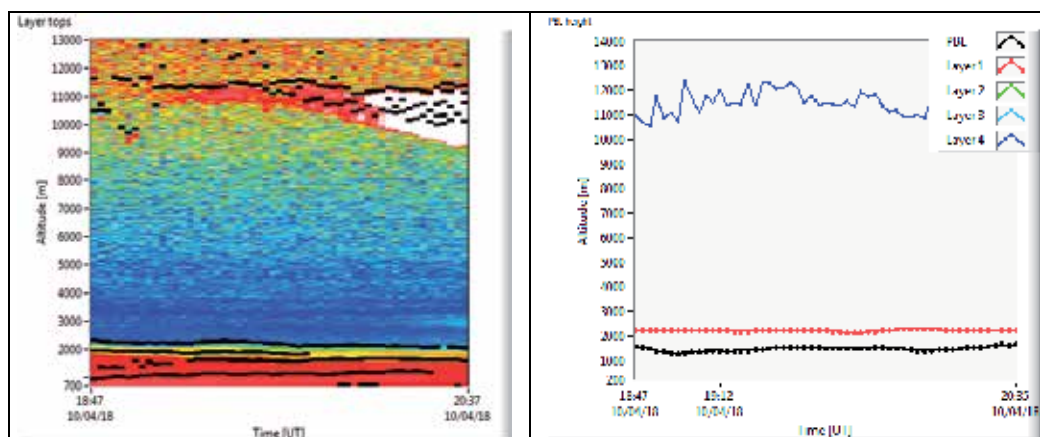
Fig. 25. Range corrected signal from April 22-th, 2010, evening, presenting the Cloud and volcanic layer formation (http://inoe.inoe.ro/RADO).

6. Conclusion

Air pollution is a global environmental problem that represents a measure of the potential of the climate change rate influenced by local pollution sources, although its scale has a strong regional or local orientation. Improvements in technology supported by policy measures have lead to reduced pollution levels, but still, especially in new member states, more activity is needed. In developed countries advanced low pollution technique is applied in order to reduce the pollution levels However, in developing countries the relatively high economic growth rates increase the incomes but also the global (regional or local) pollution level, and hence contribute as long range transported pollution to air quality problems in regions far away. Reaching the stringent AQ levels remains to be the challenge for all

countries and especially for urban areas. This calls for an intensive cooperation between all cities, in developed or developing countries, in terms of research collaboration, technology transfer, knowledge exchange and dissemination.

There are many ways to measure air pollution, basic they are referring either to standard methods or to acceptable one, with both simple chemical and physical methods and with more sophisticated electronic techniques, in addition to modelling possibilities, according special tailored programs, according emission factors and pollutant inventory, for real or probable meteorological conditions (Ionel, & Popescu, 2009), (Varga et al., 2010). *Automatic methods* produce high-resolution measurements of hourly pollutant concentrations or better, at a single point. Pollutants analyzed include ozone, nitrogen oxides, sulphur dioxide, carbon monoxide and particulates. The samples are analyzed using a *variety of methods including spectroscopy*. The sample, once analyzed is downloaded in real-time, providing very accurate information. *Remote optical, long path analyzers* use spectroscopic techniques, make real-time measurements of the concentrations of a range of pollutants.

7. References

Apascaritei, M.; Popescu, Fr. & Ionel, I. (2009). Air pollution level in urban region of Bucharest and in rural region, *SSE'09 Proceedings of the 11th WSEAS International Conference on Sustainability in Science Engineering*, pp. 330 – 335, ISBN 978-960-474-080-2, Timisoara, Romania

Baumann, K. (1987). Schadstoffausbreitung im Nahbereich einer Autobahn, *Institut für Verfahrenstechnik und Dampfkesselwesen der Universität Stuttgart*, Abt. Reinhalt. Luft, Bericht Nr. 8

Baumbach, G.; Baumann, K. & Dröscher, F. (1987). Luftverunreinigungen in Wäldern, *Institut für Verfahrenstechnik und Dampfkesselwesen der Universität Stuttgart*, Abteilung Reinhalt. Luft, Bericht Nr. 5

Birkle, M. (1979). Messtechnik für den Immissionsschutz — Messen der gas- und partikelförmigen Luftverunreinigungen. München Wien: Oldenburg

DIN 1319, (1985) Teil 1: Grundbegriffe der Messtechnik - Allgemeine Grundbegriffe. Berlin: Beuth 6

Erste allg. (1986) Verwaltungsvorschrift zum Bundes-Immissionsschutzgesetz (Technische Anleitung zur Reinhaltung der Luft - TA Luft), GMBI, S.95f

Esser, J. (1982). Schadstoffkonzentration im Nahbereich von Autobahnen in Abhängigkeit von Verkehr und Meteorologie. *In: Kolloquiumsbericht „Abgasbelastungen durch den Kraftfahrzeugverkehr im Nahbereich verkehrsreicher Straßen"*, TÜV Rheinland und Umwelt 3/82, S. 158-164, Köln, Germany

Finlayson-Pitts, B. & Pitts, J. (1986). *Atmospheric chemistry: fundamentals and experimental techniques*, John Wiley & Sons, p.10, ISBN: 978-0471882275, University of Michigan

FVLR (1979). Institut für Reaktionskinetik: Messgerät zum Nachweis von Stickstoffoxiden. Exponatbeschreibung, Stuttgart, Germany

Hartkamp, H.; Buchholz, N.; Klukas, F. & Münch, J. (1983). Ermittlung und Erprobung von Kalibrierverfahren für Immissionsmessnetze, *Umweltforschungsplan des Bundesministers des Innern*, Forschungsbericht 104 02 216, UBA-FB 83 - 034, Materialien 3/83, Berlin: Erich Schmidt

Hartmann & Braun AG. (1982). NDUV - Betriebsphotometer Radas 1G. Gebrauchsanweisung 42/20-22-1 bzw. Listenblatt 20-1.53, Frankfurt

HORIBA GmbH Process & Environmental, *AP 370 User manuals*, http://www.horiba.com/process-environmental/products/ambient/

http://www.epa.gov/iaq/schools/tfs/guidem.html, *United States Environmental Protection Agency*, IAQ TfS Action Kit

http://www.mediu.ro, *Laboratory for Fuel Analyses, Environmental Investigations and Pollutants Dispersion*

http://www.thermoscientific.com/wps/portal/ts/HOME , Thermo Scientific, User manual TEOM Monitor

http://inoe.inoe.ro/RADO/#, Romanian Atmospheric 3D research Observatory Project

Immissionsmessnetze in der Bundesrepublik Deutschland (Stand 1987). In: *Monatsberichte aus dem Messnetz 8/87*, Umweltbundesamt Berlin, Germany

Ionel, I.; Nicolae, D.; Popescu, Fr.; Talianu, C.; Belegante, L. Apostol, G. (accepted paper for publication in 2010) http://www.nipne.ro/rjp/accepted_papers.htm. Measuring Air Pollutants in an International Romanian Airport with Point and Open Path Instruments, *Romanian Journal of Physics*, Publishing House of the Romanian Academy

Ionel, I. & Popescu, Fr. (2009). Data acquisition system in a mobile air quality monitoring station, *5th International Symposium on Applied Computational Intelligence and Informatics*, IEEE Catalog Number: CFP0945C - CDR, pp. 547-552, ISBN: 978-1-4244-4477-9, Timisoara, Romania

Ionel, I.; Ionel, S.; Popescu, Fr.; Padure, G.; Dungan, L. & Bisorca, D. (2008). Method for determination of an emission factor for a surface source, *Optoelectronics and Advance Materials – Rapid Communication Journal,* Vol 2 (12), pp.851 - 854, ISSN 1842-6573

Ionel, I., (2000). *Dispersia noxelor. Teorie si aplicații*. Editura Politehnica, Timişoara, ISBN:973-9389-58-9

Kaiser, R. (1965). Chromatographie in der Gasphase. *Teil 4: Quantitative Auswertung. Mannheim:* Bibliographisches Institut

Kost, W. & Baumbach, G. (1985). Messung der vertikalen Konzentrationsgradienten der Spurengase NO, NO_2, SO_2 und O_3 in Waldbeständen im Schönbuch und Schwarzwald. *VD1 Ber. 560*, S. 205 -239, Düsseldorf, Germany

Laskus, L. & Bake, D. (1976). Erfahrungen bei der Korngrößenanalyse von Luftstäuben mit dem Andersen-Kaskadenimpaktor, *Staub-Reinhalt. Luft 36*, Nr. 3, S. 102-106

Nicolae, D.; Talianu, C.; Carstea, E. & Radu, C. (2007). Using classification to derive aerosol number density from lidar measurements, *Journal Optoelectronics and Advanced Materials*, Vol.9 (11), pp.3518-3521, ISSN 1454-4164

Nicolae, D. & Cristescu, C., P. (2006). Laser remote sensing of tropospheric aerosol, *Journal Optoelectronics and Advanced Materials*, Vol. 8 (5), pp.1781-1795, ISSN 1454-4164

Paffrath, D. (1985). DFVLR - Messsystem zur Erfassung der räumlichen Verteilung von Umweltparametern in der Atmosphäre mit mobilen Messträgern. *Forschungsbericht 85-09. DFVLR Institut für Physik der Atmosphäre*. Oberpfaffenhofen

Popescu, Fr.; Ionel, I.; Lontis, N.; Calin, L. & Dungan L. (accepted paper for publication in 2010) http://www.nipne.ro/rjp/accepted_papers.htm. Air Quality Monitoring in an Urban Agglomeration, *Romanian Journal of Physics*, Publishing House of the Romanian Academy

Popescu, Fr. (2009). Advantages in the use of Biodiesel in an urban fleet. Case study: major cross-roads in the Timisoara city, *Journal of Environmental Protection and Ecology*, Vol.10 (1), pp.182-191, ISSN 1311-5065

Popescu, Fr.; Ionel, I. & Ungureanu, C. (2009). Ambient air quality measurements in Timisoara. Current situation and perspectives, *Journal of Environmental Protection and Ecology*, Vol.10 (1), pp.1-13, ISSN: 1311-5065

Popescu, Fr.; Ionel, I.; Pavlovic, M. & Pavlovic. Al. (2009). Air pollution monitoring, *Proceedings of the 4th Symposium "Recycling technologies and sustainable development"*, Zbornik Radova Proceeding, p.451-462, ISBN: 978-86-80987-73-6, Bor, Serbia

Projektgruppe Bayern zur Erforschung der Wirkung von Umweltschadstoffen (PBWU): Atlas der Immissionsmessstationen Europas, 2. *Aufl. Gesellschaft für Strahlen- und Umweltforschung*, GSF-Bericht 25/87, München, Germany

RdSchr. (1983) des Bundesministers des Innern betreffend Bundeseinheitliche Praxis bei der Überwachung der Emissionen und Immissionen -UI8 - 556134/4 - , *II. Richtlinien für die Wahl der Standorte und die Bauausführung automatischer Messstationen in telemetrischen Immissionsmessnetzen*, GMB1. S. 76-78

Varga, L.; Apascaritei, M.; Ionel, I. & Popescu Fr. (2010). Contribution to air quality monitoring in the eastern part of Timisoara city, *Revista Metalurgia International*, No.6, Editura Stiintifica F.M.R., pp.40-45, ISSN: 1582-2214

Vetres, I.; Ionel, I.; Popescu Fr.; Nicolae, D.; Talianu, C. & Dungan, L. (accepted paper for publication in 2010). Lidar. Systems implementation and development in Timisoara urban area. *Digest Journal of Nanomaterials and biostructures*, Published NIMP-Bucharest, ISSN: 1842-3582

Vetres, I.; Ionel, I.; Padureanu, I. & Lontis, N. (2009). Sistemul Lidar pentru investigarea aerosolului atmosferic, *Revista Metalurgia*, Editura Stiintifica F.M.R., Nr.11, pp.22-27

Vetres, I.; Ionel, I.; Popescu, Fr. & Dungan, L. (2009). Air Pollution Analysis, in Western Romania and Necessity of Complementary Vertical Resolved LIDAR Observation, *Proceedings of the 3rd Workshop on Optoelectronic Techniques for Environmental Monitoring*, Published by INOE, pp.32-36, ISSN: 2066-851, Bucharest, Romania

Wang, Y., W.; Yang, J. & Jiang, W., M. (2009). Impact of large cities' expansion on air pollution, *Proceedings of the International workshop on Geoscience and Remote Sensing*, Vol. 1, pp.393-396, ISBN 978-0-7695-3563-0

Zolner, W.J.; Cieplinski, E.W. & Dunlap, D.V. (1984). *Measurement of Ambient Air SO_2 Concentration using a pulsed Fluorescent Analyzer.* Themo Electron Corporation, Waltham USA; deutsche Vertretung. Duisburg. Firmenprospekt

Trace elements and radionuclides in urban air monitored by moss and tree leaves

Dragana Popović[1], Dragana Todorović[2], Mira Aničić[3],
Milica Tomašević[3], Jelena Nikolić[2] and Jelena Ajtić[1]
[1]University of Belgrade, Faculty of Veterinary Medicine, Serbia
[2]Institute of Nuclear Sciences Vinča, Belgrade, Serbia
[3]University of Belgrade, Institute of Physics, Belgrade, Serbia

1. Introduction

In urban areas, air quality is strongly influenced by numerous anthropogenic activities. High population density, heavy traffic and domestic heating in winters in the centre, and various industrial activities at the outskirts, influence atmospheric concentrations of trace elements and radionuclides. Consequently, large population is exposed to possible adverse effects arising from the altered urban air composition. Therefore, air quality monitoring has become one of the standard quality control procedures in urban areas.

1.1 Trace elements and radionuclides in air

Due to changed atmospheric concentrations of trace elements, their availability and cycling has changed, too. Numerous studies showed that trace metals as persistent, widely dispersed and interacting with different natural components, cause threat to human health and environment (Seinfeld & Pandis, 1998). Trace elements in urban areas (such as Cu, Zn, and Pb) are mainly emitted by traffic, including exhaust emissions and vehicle wear products (Harrison et al., 2003). Even though the use of leaded gasoline has been drastically reduced, our understanding of the effects of whole lead emission to air is far from sufficient (Van der Gon & Appelman, 2009). As reported recently, though atmospheric Pb had declined by a factor of 7 from 1980 to 2007, atmospheric deposition is still recognised as a major pathway of Pb to vegetation and topsoil (Hovmand et al., 2009). Since it offers a practical approach for monitoring deposition of atmospheric trace elements on the surface environment (Azimi et al., 2003; Tasić et al., 2008), collection of atmospheric deposition using bulk sampling devices has been extensively used. However, instrumental studies on atmospheric contamination are often limited by high cost and difficulties in carrying out extensive monitoring surveys in time and space, and do not offer reliable information about an impact of atmospheric pollutants on the living systems.

Among the naturally occurring radionuclides in air, beryllium-7, radon and its short lived progenies are most significant, while caesium-137 is of major interest among the fission products. Long-lived radionuclides, potassium-40, uranium and thorium, found in

significant quantities in soils, are usually not detectable in air, thus, if found on leaves, they are mainly resuspended from soils (Vandenhove et al., 2009). The soil-to-plant transfer factor above 1.0 is reported for ^{40}K, while values for uranium and thorium are much lower (10^{-4}) (Uchida et al., 2007). In higher plants, the distribution of the radionuclides is uneven. In tropical forest plants, for example, the highest ^{40}K concentrations are found in stem, and the lowest in root, while ^{137}Cs is mostly accumulated in root (Somashekarappa et al., 1996).

Beryllium-7 (half-life 53.28 days) is produced by cosmic rays in spallation processes with light elements (nitrogen, oxygen, carbon) in the upper troposphere and lower stratosphere. Its production depends on the Earth's magnetic field, and the variations in its annual mean concentrations are a good indicator of changes in the atmospheric production rate caused by cosmic ray intensity. The ^{7}Be seasonal patterns are correlated to the stratosphere–to–troposphere exchange processes. The ^{7}Be concentration in ground level air in the midlatitudes has the maximum during spring and summer (e.g., Ajtić et al., 2008), caused by a seasonal thinning of the tropopause which allows the ^{7}Be rich stratospheric masses to enter the troposphere (Gerasopoulos et al., 2003).

Lead-210 (half-life 22.3 years) is an effective tracer of continental surface air masses history and often used to identify soil aerosols sources. It mostly originates from the decay of uranium-238 in the Earth's crust, but anthropogenic sources (uranium ores sintering, coal combustion, production or use of phosphate fertilizers) also contribute to the total ^{210}Pb in air (UNCEAR, 1988). Deposition of ^{210}Pb varies with season and geographical position. The ^{210}Pb concentration maxima in fall could be attributed to an enriched emanation of radon. Radon emanation, and therefore concentration of ^{210}Pb in air, is affected by atmospheric pressure, temperature inversions, covering vegetation, snow and ice ground coverage, etc. Furthermore, important factors influencing the ^{210}Pb concentrations in air are soil geology, continental and areas masses distribution, conditions of surface air layers, etc. (Delfanti et al., 1999).

Due to its half-life of 30 years, ^{137}Cs is a good indicator of nuclear weapon atmospheric tests and nuclear power plant accidents on global scale. Since 1986, ^{137}Cs in ground level air has mainly originated from the Chernobyl nuclear accident, with concentrations of the order of μBq/m^3, and with one or two maxima in summer and winter. The ^{137}Cs winter maxima are attributed to the inversion weather conditions and to soil dust air resuspension from the Chernobyl fallout (Todorovic et al., 1999).

1.2 Moss and tree leaves as biomonitors

For several decades, air quality biomonitoring has been widely applied to detect and monitor the effects of trace elements pollution (Bargagli, 1998; Markert et al., 2003). Mosses and lichens are recognised as the most appropriate biomonitors of atmospheric trace elements and radionuclides contamination. Many studies have demonstrated the ability of moss to absorb and accumulate trace elements in their tissue. Due to the absence of root and cuticle, mosses uptake their nutritive elements from wet and dry atmospheric deposition (Rühling & Tyler, 1968). Mosses have also been recognised as valuable biomonitors in the assessment of temporal trends in trace metal accumulation (Harmens et al., 2008), and in spatial variations across national boundaries (Schröder et al., 2008).

Mosses are also highly efficient in accumulating radionuclides and have been widely used as reliable bioindicators of radioactive contamination of the environment since the late 1960's (Sumering, 1984; Steinnes, 2008; Frontaseyeva et al., 2009; Aničić et al., 2007; Barandovski et al., 2008; Guillén et al., 2009). Due to their continuous accumulation of elements, mosses offer

information about the sources of pollution long after the pollution episode itself took place (Golubev et al., 2005). Being globally spread, mosses are an important tool in mapping global distribution of radionuclides following nuclear weapon atmospheric tests and in radioactivity monitoring in the vicinity of nuclear and coal power plants (Delfanti et al., 1999; Uğur et al., 2003). In 1986, mosses and lichens proved to be reliable indicators of environmental contamination after the nuclear plant accident in Chernobyl (Papastefanou et al., 1989; Hofmann et al., 1993). In the late 1990's, mosses and lichen were used to estimate the level of contamination caused by the military use of depleted uranium (DU) in the Balkans (UNEP, 2002; Loppi et al., 2003; Frontasyeva et al., 2004; Popovic et al., 2008a).

Since naturally growing mosses are often rare or absent in urban areas, the "moss bags technique'' (*active biomonitoring*) has been developed in order to spatially and/or temporally assess deposition of trace elements in highly polluted areas (Goodman & Roberts, 1971; Vasconcelos & Tavares, 1998; Fernandez et al., 2004; Culicov & Yurukova, 2006). The technique offers several advantages compared to naturally growing mosses: one can precisely limit the time of exposure, acquire data on the concentrations of different elements in the sample prior to the exposure, and choose a most suitable site for moss transplantation. The *Sphagnum* moss species are especially recommended for active biomonitoring for their large surface area and a number of protonated anionic functional groups (ion exchange sites) in the form of uronic acids. However, moss bags tend to dry out and thus their efficiency in retaining elements varies with the environmental conditions, especially humidity (Al-Radady et al., 1993). Until now, only a few quantitative comparisons of biomonitoring methods with the standard measurements of atmospheric deposition have been published (Berg & Steinnes, 1997; Thöni et al., 1996; Aničić et al., 2009a,b). Moreover, the exact relationship between the element content in moss and the actual atmospheric deposition is not yet well understood, though some studies have given evidence of possible quantitative conversion with unsedimentable dry deposited particles (<0.8 µm) (Vasconcelos & Tavares, 1998).

In urban and industrial areas, however, where lichens and mosses are often not found, higher plants could replace them. In areas with high atmospheric pollutant loads, plants may provide information, not only about quality/quantity of air pollutants, but also about effects on ecosystems. Leaves of both evergreen and deciduous tree species have been recognised as valuable accumulative biomonitors of atmospheric elements and radionuclides in urban areas. Tree leaves are also very efficient in trapping atmospheric particles (Freer-Smith et al., 2005; Peachey et al., 2009; Qiu et al., 2009), and they have a special role in reducing the level of "high risk" respirable particulates possibly harmful to the environment and human health (Beckett et al., 2000). There are numerous studies searching for sensitive tree species, and their validity for urban air quality biomonitoring (Alfani et al., 1996; Monaci et al., 2000; Piczak et al., 2004; Mingorance & Oliva, 2006; De Nicola et al., 2008). Some species show a good response to atmospheric trace elements pollution, e.g. *Q. ilex* may be appropriate for biomonitoring in urban areas where it is naturally present and widely distributed (Gratani et al., 2008). A significant correlation was reported between the Cu and Fe contents in inhalable atmospheric particles (PM_{10}) and in leaves of *Nerium oleander* (Espinosa & Oliva, 2006). According to Bargagli (1998), the species of *Tilia* genus could be used as biomonitors of trace elements in urban and industrial environments, while Baycu et al. (2006) reported that, compared to other urban tree species, *A. hippocastanum* accumulated the highest Pb concentrations in leaves.

Plants are also an important link in the transport and distribution of radionuclides from the source of pollution to man and can be used as biomonitors of atmospheric pollution by radionuclides (Djuric and Popovic, 1994). Radionuclides can be deposited on plants from air (foliar deposition) where they appear from fallouts or by natural sources, or can be taken through soil root system. Most of the air borne radionuclides are quickly attached to aerosols, and their concentration in air is manly due to behaviour of aerosols in the atmosphere. Thus, the rate of their removal from the atmosphere and deposition on ground and vegetation depends on the size of particles they are attached on (Djuric and Popovic, 1994). Foliar deposition and absorption of radionuclides from air to leaves are closely associated not only with morphological characteristics of leaves, but also with local climate (moisture, concentrations of dust particles, wind velocity and direction, amount of precipitation, etc). Thus, some authors found radionuclides concentrations in leaves to be of an order of magnitude or two less than those in stem or roots (Somashekarappa et al., 1996). Accumulation of radionuclides by plants, e.g. estimation of soil-to-plant transfer factors, foliar deposition rate and root uptake, has been in focus of investigations of many authors, but mainly for agricultural plants, cereals and vegetables, in laboratory and/or in field conditions (Djuric et al., 1996; Djuric & Popovic, 1994; Golmakani et al., 2008; Koranda & Robison, 1978). The main problem in assessing the contribution of air pollution compared to root uptake is the fact that soil-to-plant/leaves transfer factors are found in the large range of values (10^{-3}–10^{-1}) due to numerous factors, mainly characteristics of soils and leaves/plant morphology (IAEA, 1994). Solubility, pH, acidity, organic matter content, etc., play a vital role to radionuclides availability by plants (Golmakani et al., 2008). Still, some studies found similar seasonal variation pattern of ^7Be and ^{210}Pb between leaves and aerosol samples, high in spring and low in summer (Sugihara et al., 2008).

Trace elements in Belgrade air are mostly bound to the particulates of the mixed road origin (Rajšić et al., 2008). As reported previously for the area, the leaves of *A. hippocastamum* and *Corulys colurna* showed a distinguished seasonal accumulation of some elements (Cu, Zn and Pb). Among the two, *A. hippocastanum* seems a more suitable biomonitor, not only by the leaf content, but also because it was found that a level of the Pb accumulation reflected marked changes in the atmospheric Pb concentrations (Tomašević et al., 2008).

Active biomonitoring with the moss bag (MB, *Sphagnum girgensohnii* Russow, Russia) and bulk deposition (BD) measurements were performed for trace elements (Al, V, Cr, Mn, Fe, Ni, Cu, Zn, As, Cd, Pb) atmospheric deposition in the urban area of Belgrade in 2005 – 2006. The aim of the research was to evaluate trace element accumulation in the moss bags, and to examine its relationship to the atmospheric bulk deposition measurements. In order to assess the actual responses of moss to trace element concentrations in air, and to investigate the role of water supply on the moss accumulation ability, experiments with dry and irrigated (wet) moss bags were carried out. The content of natural and fallout radionuclides (^7Be, ^{210}Pb, ^{40}K and ^{137}Cs) in moss bags was also determined, with an aim to assess the validity of the method for radioactivity monitoring and control in ground level air.

The trace elements (Cr, Fe, Ni, Zn, Pb V, As, and Cd) accumulation and the temporal trends were also assessed in leaves of the trees common for the city of Belgrade: *Aesculus hippocastanum* (horse chestnut) and *Tilia spp.* (linden), over a period of five years (2002 – 2006). The relationship between the trace elements concentration in the leaves and the instrumental measurements of atmospheric bulk deposition was also examined. The contents of radionuclides in leaves in comparison with their activities in ground level were determined, too.

2. Experimental

2.1 Study area

The study was conducted in Belgrade (44° 49′ N, 20° 27′ E; 117 m a.s.l.), the capital of Serbia, with about 2 million inhabitants, situated at the confluence of the rivers Sava and Danube. The climate is moderate continental with fairly cold winters and warm summers. In winter, severe air pollution as aerosol smog occurs frequently in the central city area, particularly during meteorologically calm and stable conditions. The number of vehicles is around 500,000, including heavy-duty trucks and over 1,000 city buses run on diesel. The average age of passenger cars is more than 15 years, and leaded gasoline is still widely used. There are many old buses and trucks in the city traffic, which could be the major source of ambient particulates. The city is heated with a number of heating plants run on natural gas or crude oil, but there are still individual houses heated with coal (Todorović et al., 2005; Todorovic et al., 2007). Natural gas has only been introduced in the last few years.

The moss bags measurements were carried out at three representative sites in heavy traffic areas: the Faculty of Veterinary Medicine (VF), the Rector's Office Building of the Belgrade University (RB), and the Public Health Institute (HI). The tree leaves samples were collected in the parks adjacent to those three locations. Trace elements and radionuclides accumulation was investigated in dry and wet moss bags and tree leaves (in May and September), while bulk deposition and aerosols were collected on a monthly basis at the same places and time. The map of Belgrade central area, with the sampling sites, is presented in Fig.1.

Fig. 1. Map of Belgrade central city area with the sampling sites: A) the Rector's Office building of the Belgrade University RB, B) the Public Health Institute HI, and C) the Faculty of Veterinary Medicine VF.

2.2 Moss sampling, bag preparation and analysis

2.2.1 Trace elements

Moss (*Sphagnum girgensohnii* Russow) was collected in June 2005 from a pristine wetland area near Dubna, Russia (56° 44' N, 37° 09' E; 120 m a.s.l.), and cleaned from soil particles and other matter. About 3 g of moss was packed in (10 x 10) cm² nylon net bags (1 mm mesh size). The bags, with and without irrigation (WET and DRY MB) were exposed at the same time at the three sampling sites (Fig.1). Wet moss bags were placed on the top of cellulose sponge with the bottom immersed in distilled water, and the setup was put in a polyethylene box. Distilled water was added every several days, depending on meteorological conditions (precipitation and temperature) (Aničić et al., 2009a). Using specially constructed holders (1.5 m high) on platforms 5–10 m above the street level, two dry (hung freely in the air) and two wet moss bags were exposed for five 3-month periods, between July 2005 and October 2006. After the exposure, the moss was removed from the net, homogenised and dried to a constant weight at 40 °C for 24 h.

The concentrations of Al, V, Cr, Mn, Fe, Ni, Zn, and As were determined by instrumental neutron activation analysis (detection limit 0.01–10 μg/g). Short-term irradiation (2 min) was applied for short-lived radionuclides (Al, V, and Mn). The long irradiation (100 h) was applied to determine elements associated with long-lived radionuclides (Na, Cr, Fe, Ni, Zn, and As). The concentrations of Cu, Cd, and Pb in moss were analysed by flame atomic absorption spectrometry. Quality control was performed using the standard reference material: Lichen (IAEA–336), Tomato Leaves (SRM–1573a) and Coal Fly Ash (SRM–1633b).

2.2.2 Radionuclides

Moss (*S. girgensohnii*) was packed in nylon net bag (total mass 255 g), and exposed on the VF site (Fig. 1) for one year (May 2006 – May 2007). The site is in the vicinity of a highway, and is one of the pollution "black spots" in the city. It is also the sampling site for air radioactivity monitoring by filter paper method (Todorovic et al., 2007).

Prior to exposure, the moss was dried and cleared of soil and other material. After the exposure, the sample was divided into eight subsamples of 25–36 grams to examine the uniformity of radionuclides' distribution within the sample (Popović et al., 2009b).

The activities of [7]Be, ^{210}Pb, [40]K and ^{137}Cs were determined on an HPGe detector (Canberra, relative efficiency 23%) by standard gamma spectrometry. Geometric calibration was performed using the standard reference radioactive material IAEA-373 (grass, with [134]Cs, ^{137}Cs, [40]K and ^{90}Sr, total activity of 15 kBq d.w. on 31.12. 1991). Counting time was 58,000 s, with the total standard error of 16% for [40]K, 20% for ^{210}Pb, and 10% for [137]Cs (Popović et al., 2009b).

2.3 Tree leaves sampling and analysis

Leaves were sampled from *Aesculus hippocastanum* L. (horse chestnut), and *Tilia spp.* (linden: *Tilia tomentosa* L. and *Tilia cordata* Mill.), at the beginning (May) and the end (September) of the vegetation seasons from 2002 to 2006. Five subsamples (10 to 15 fully developed leaves) were taken randomly from several crowns 2 m above the ground (Tomašević et al., 2008). Leaves were washed with bidistilled deionised water, dried at 40 °C for 24 h, and pulverised with agate mortars prior to analyses. About 0.4 g of leaves were digested for 2 h in a microwave digester with 3 ml of 65% HNO_3 (Suprapure, Merck) and 2 ml of 30% H_2O_2, and then diluted with distilled water to a total volume of 25 ml. The content of Cr, Fe, Ni, Cu,

Zn, and Pb was determined by inductively coupled plasma optical emission spectrometry, and V, As, and Cd by inductively coupled plasma mass spectrometry. Quality control was performed using the standard reference material Lichen-336 (IAEA).

For radionuclide analysis, the samples of leaves were collected in the identical fashion (Tomašević et al., 2008). In addition, samples of soils were also collected in the three sites. Soils and leaves were measured in native state, leaves were dried up to 105 °C. Aerosols were also sampled and analysed for the contents of radionuclides by standard procedures (Todorović et al., 2005; Todorovic et al., 2007).

2.4 Sampling and analysis of bulk deposition

Bulk depositions were collected monthly, in open polyethylene cylinders (29 cm x 40 cm) fixed in baskets at the measuring sites, from the beginning of 2002 to the end of 2006. The samples were evaporated to dryness and digested with 50 ml of 0.1 N HNO_3 on an ultrasonic bath. The content of Al, V, Cr, Mn, Fe, Ni, Cu, Zn, As, Cd, and Pb was determined by flame atomic absorption spectrometry (Perkin Elmer AA 200) and graphite furnace atomic absorption spectrometry (Tasić et al., 2009). For calibration, standard solutions containing all metals of interest were prepared using Merck certified atomic absorption stock standard solutions.

2.5 Trace elements data analysis

Data analysis included the basic statistics (mean/average, correlation, and t-test) for Al, V, Cr, Mn, Fe, Ni, Cu, Zn, As, Cd, and Pb concentrations measured in DRY and WET MB, the tree leaves and the monthly BD samples. To assess the element accumulation in moss, the relative accumulation factors (RAF) were calculated as the ratio of the moss content of element after and before the exposure ($C_{exposed}$ - $C_{initial}$), and before the exposure ($C_{initial}$):

$$RAF = (C_{exposed} - C_{initial}) / C_{initial} \qquad (1)$$

3. Results and Discussion

3.1 Trace elements in moss bags

The initial (background) content of elements plays a crucial role in obtaining the relative accumulation level in biomonitoring studies. For most of the examined elements, the initial values in *S. girgensohnii*, used for active biomonitoring in Belgrade (Aničić et al., 2009a,b), were significantly lower than those from other sites (Adamo et al., 2003; Djingova et al., 2004; Culicov & Yurukova, 2006) or in other *Sphagnum spp*. (Djingova et al., 2004). The initial element concentrations in *S. girgensohnii* were even lower than the values proposed by Markert (1992) as "reference plant values" used to compare elements accumulation among the different species. This points to the variation in natural *Sphagnum* element content from different areas and, consequently, to a necessity to determine the background (control) levels prior to each biomonitoring study. The advantage of low background levels is the higher method sensitivity in areas with low atmospheric deposition (Culicov et al., 2005).

Significant accumulation of the majority of examined elements in the *S. girgensohnii* moss bags were observed over the 3-month exposure periods (Table 1) indicating that this species is an efficient trace element accumulator (Aničić et al., 2009a). Higher element content was

measured in the WET MB (except for Mn) which is in agreement with other studies (Al-Radady et al., 1993). One of the differences between the WET and DRY MB is that deposited particles are trapped in higher quantities on wet surfaces. Furthermore, WET MB could incorporate the elements in its tissues, whereby being less susceptible to rinsing and thus better reflecting the atmospheric conditions (Astel et al., 2008). This is in agreement with findings of Berg & Steinnes (1997) that atmospheric humidity and precipitation are important factors for moss accumulation.

To compare the element accumulation in DRY and WET moss bags, relative accumulation factors RAF (Eq. 1) were calculated. The RAF values, which are inherently insensitive to the influence of the initial element content, have been used to compare accumulation between different monitoring species (Adamo et al., 2003; Culicov & Yurukova, 2006). The most accumulated elements in DRY MB, according to the RAF value were V (22), followed by Cr (11) > Cu (9) > Pb (8) > As (5) > Al (4) > Fe (3) > Ni (3) ≈ Zn (2.5) > Mn (0.9) > Cd (0.5). In WET MB, the order for the most accumulated elements was somewhat different: Cu (68) > V (26) > Cr (21) > Pb (13) > Al (6.5) > As (6) > Fe (5) > Zn (4.5) > Ni (4) > Cd (1) > Mn (0.2) (Aničić et al., 2009b). The accumulation of Cu in WET MB was about eight times higher than for DRY MB. Likewise, the content of Cr was about twice as high in WET MB. Other elements, such as Pb, Al, Fe, and Zn, were slightly more accumulated in WET MB than in DRY MB. In some moss bags, both dry and wet, a loss of Mn, compared to the initial material, was evident (10% and 80%, respectively). The loss of Mn caused by washing out and leaching from moss, was described in Couto et al. (2004). The RAF values, obtained in this study, are significantly higher than the literature data (Adamo et al., 2003; Culicov & Yurukova, 2006). This is most likely related to higher atmospheric pollution in Belgrade urban area, and to lower initial concentration of the elements in used *S. girgensohnii* moss.

	S. g.	*S. girgensohnii* (DRY MB)			*S. girgensohnii* (WET MB)		
Element	Initial	Min	Max	Median	Min	Max	Median
Al	254	659	1960	1363	802	3523	1870
V	0.54	2.9	112	13	2.9	69	14
Cr	0.25	2.0	6.8	3.1	3.7	8.3	5.8
Mn	113	92	322	215	77	212	134
Fe	297	732	2496	1219	1026	4810	1682
Ni	2.4	1.9	41	8.7	4.5	30	12
Cu	2.1	10	49	20	42	476	144
Zn	20	44	105	71	85	264	113
As	0.11	0.38	2.2	0.67	0.53	5.4	0.80
Cd	0.18	0.19	0.36	0.27	0.25	0.50	0.36
Pb	2.2	7.0	38	20	14	63	31

Table 1. Trace elements (µg g⁻¹ of dry weight) in DRY and WET MB of *S. girgensohnii* exposed in Belgrade urban area.

3.1.1 Trace elements accumulation in moss bags *vs.* bulk deposition

To compare the element accumulation in moss bags with the bulk deposition data, the moss element concentrations (µg g^{-1}) were expressed as the deposition fluxes (µg m^{-2} day^{-1}) and the Spearman rank correlation coefficients (r) were calculated to estimate a relationship between the element deposition flux in DRY MB/WET MB and BD. The correlation between the element BD and the element deposition flux in WET MB was high for V (r=0.87), As (r=0.74), Fe (r=0.73), Al (r=0.71), and Ni (r=0.68). No correlation was found for Cd, Mn, and Zn. The DRY MB *vs.* BD highest correlation was found for Cu (r=0.85). Lower, but still significant correlation (r > 0.50), was obtained for Pb, Cr, and Zn (Aničić et al., 2009a).

In general, trace elements may be deposited onto the moss surface either as dry particulates or dissolved and/or suspended in precipitation. The elements may be retained by particulate entrapment, physicochemical processes such as ion exchange or by passive and active intracellular uptake (Tyler, 1990). Therefore, moss is not a mere passive filter. Poor correlation for some element deposition fluxes in moss samples and BD probably indicates more complex mechanisms of element accumulation in moss. Furthermore, due to splash effect and irregular surfaces, it is difficult to estimate the exact atmospheric deposition fluxes in moss bags. Nevertheless, the concentrations of some elements (e.g., V, Fe, Co, As, Mo, Cd, Sb, and Pb) were found to be significantly correlated in moss and wet deposition (Couto et al., 1994; Berg & Steinnes, 1997). The rate of element uptake by moss increased markedly, but not regularly, with atmospheric humidity and precipitation, whereas their atmospheric level decreased (wet deposition), preventing the possibility of establishing a conversion factor for wet weather conditions (Vasconcelos & Tavares, 1998).

Studies on the capture of atmospheric particles by moss have demonstrated that standardised active biomonitoring with moss bags provides a better capture efficiency of particles over 20 µm in diameter (sedimentable particles) less influenced by abiotic conditions like wind speed. Therefore, it was suggested that particles trapped by bryophytes may be a major source of poorly water-soluble elements, and that moss content can reflect recent environmental conditions for dry and coarse depositions, especially for active biomonitoring experiments in highly polluted areas (Amblard-Gross et al., 2002).

3.1.2 Seasonal variations of trace elements in moss

Trace elements content in moss bags was also analysed for the summer (May – October) and winter (November – April) seasons. Seasonal variations in both DRY and WET MB samples were observed for all of the elements except Pb, Al, and Mn. At all three sites, the highest variations were noticed for V and Ni, whose content was two and three times higher in winter than in summer, respectively (Fig. 2).

The content of As and Fe in moss bags were 1.5 times higher in winter than in summer. This was not unexpected as these elements are markers for oil and coal combustion. However, concentrations of Cu were increased in summer, especially in WET MB. Moreover, the concentrations of Zn and Cd in WET and DRY MB were slightly higher in summer than in winter period. These elements are markers for traffic sources, but our results point to some other local sources, more expressed during the warm period (Aničić et al., 2009a).

Seasonal variations were also found for the elements in the bulk deposition, being higher in winter season (except for Pb, which was increased during summer time). In winter, much higher contents of V, Ni, As, and Fe were found in the bulk deposits.

3.2 Radionuclides in moss bags

Fission product ^{137}Cs and naturally occurring [40]K and ^{210}Pb were detected in all of the eight subsamples of moss bags, while [7]Be was detected only in one, with the activity of 60 Bq/kg.
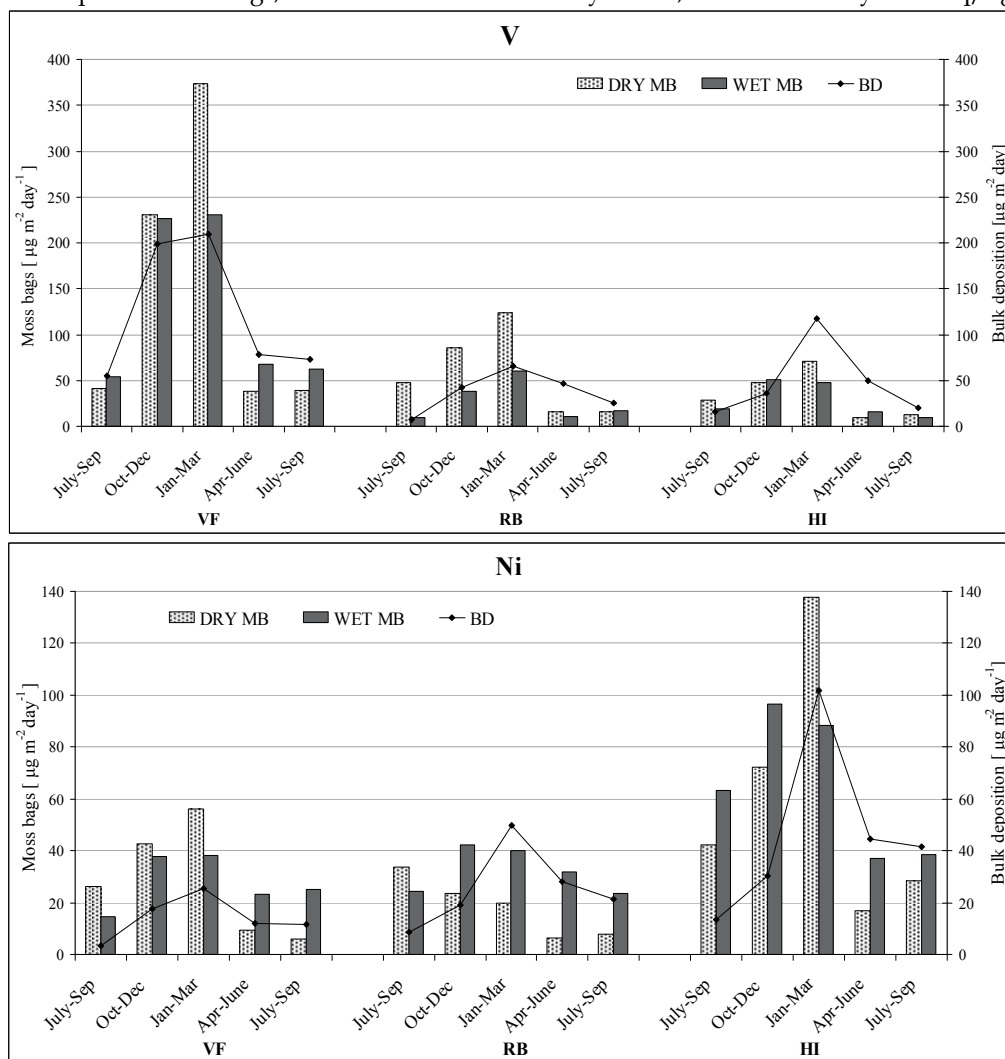
Fig. 2. Seasonal variation of V and Ni daily fluxes (mg m^{-2} day^{-1}) for DRY MB and WET MB, and BD for 3-month periods in 2005/2006 at the study sites (VF, RB, and HI).

The absence of [7]Be in the subsamples could be explained by its decay, since the period between the sample arrival in the laboratory and the analysis was nearly 60 days. Taking into account the standard uncertainty of the method and the volume of the composite sample, the distribution of the activities of the detected radionuclides in the eight subsamples was rather uniform with the differences not exceeding 30% (Popović et al., 2009b). The level of the annual activities of the radionuclides implied that the exposure time could be reduced to a month, and that would enable monitoring seasonal variations in the content of radionuclides in air. The mean activities with standard deviations of [40]K, ^{210}Pb, and ^{137}Cs in moss bags (*S. girgensohnii*),

are given in Table 2. For comparison, the content of these radionuclides in naturally growing mosses (*Hypnum cupressiforme*) in Southern Serbia (Borovac) are also presented in the table.

Location	Activity (Bq/kg)			
	^{40}K	^{210}Pb	^{137}Cs	^{7}Be
Belgrade	245 ± 34	315 ± 25	28 ± 4	/
Borovac	298 ± 42	210 ± 52	226 ± 22	228 ± 34

Table 2. Activities of the radionuclides in moss bags (*S. girgensohnii*) exposed in Belgrade (Popović et al., 2009b) and in *H. cupressiforme*, Borovac (Popovic et al., 2008b).

The activity ratio $^{210}Pb/^{40}K$ of 1.30 was calculated. The ratio could provide a sound basis for the ^{210}Pb activity estimation by solely measuring the activity of ^{40}K, which is more easily detected, and with a lesser uncertainty than ^{210}Pb (Popović et al., 2009b). The mean activities of the detected radionuclides in moss bags were in the range of the values reported for the local moss (*H. cupressiforme*) in the region (Krmar et al., 2007; Popovic et al., 2008b), with differences arising from the species, the method, local climate and soil characteristics. Krmar et al. (2007) found measurable, even significant concentrations of ^{7}Be in *H. cupressiforme*, with an increase in summer and autumn (up to 920 Bq/kg), but the sampling in the study took place over a 14-month period. Beryllium-7 was also found in naturally growing moss (*H. cupressiforme*) in the rural area of Southern Serbia (Popovic et al., 2008b) (Table 2).

As can be seen from Table 2, there are no significant differences in the content of ^{40}K in naturally growing mosses in Southern Serbia and in the urban area of Belgrade. On the other hand, higher concentrations of ^{210}Pb in Belgrade indicate a contribution of anthropogenic air pollution sources. Significantly higher activities of ^{137}Cs, as well as the detectable amount of ^{7}Be, in mosses sampled in Southern Serbia are due to a longer, undefined exposure period (in the Belgrade study, the exposure period of one year was precisely defined). Hence, the observed differences mirror the differences in the accumulation period.

Before the Chernobyl nuclear plant accident in 1986, the concentrations of ^{137}Cs in moss and lichen in Serbia were under 1 Bq/kg (Djuric & Popovic, 1994). Immediately after the accident and later, the contents of ^{137}Cs in mosses and lichens, sampled in a mountainous region, was in the range of 8–18 kBq per kg of dry weight (Djuric et al., 1992, 1996; Popović et al., 1996). In 1997, the activities of ^{137}Cs in the naturally growing mosses in a region in Serbia were up to 3 kBq/kg, while the soil-to-moss transfer factors calculated for the same region in 2000 were in the range of 3.0–10.0 (Popović et al., 2009a). High transfer factors for ^{137}Cs and ^{210}Pb from soil to mosses were also found in Southern Serbia, in the range of 1–10 and 4–10, respectively (Popovic et al., 2008a).

Still, as already mentioned, naturally growing mosses are unlikely to be found in urban areas, and the active moss monitoring is therefore a suitable alternative technique for monitoring contents of radionuclides in urban air. Furthermore, this method solves some of the problems in monitoring using naturally growing mosses, such as intercalibration of different species of mosses and transformation of concentrations in moss to absolute deposition rate (Steinnes, 2008).

Frontasyeva et al. (2009) proposed a linear correlation between the concentrations of ^{137}Cs in mosses A_{moss} and in air A_{air}:

$$A_{air} \ (Bq/m^3) = \ 3.3 \times 10^{-8} \ (kg/m^3) \times A_{moss} \ (Bq/kg) \qquad (2)$$

When applying this relationship to the activity of ^{137}Cs in moss obtained in our study, the calculated ^{137}Cs activity in air is 0.924×10^{-6} Bq/m^{3}, which is under the lower limit of detection in our measurements (1×10^{-6} Bq/m^{3}).

To conclude, since the Belgrade study showed that the exposure time for the moss bags technique could be reduced to a month, the technique could be used to monitor the level of radionuclides' contents in air, as well as to follow their seasonal variations.

3.3 Trace elements in tree leaves

Seasonal accumulation trends of elements' concentration in leaves have been well known and reported for many plant species (Kim & Fergusson, 1994; Bargagli, 1998; Piczak et al., 2003). In Belgrade urban area, the elements' concentration were determined in leaves of *A. hippocastanum* and *Tilia spp.* at the beginning (May) and the end (September) of the vegetation seasons over a period of 2002 – 2006. An increase of the element concentrations (*p<0.001)* from May to September, i.e. seasonal element accumulation, was evident in all of the *A. hippocastanum* samples throughout the investigated years for V, Cr, Fe, As, Ni, Zn, and Pb (Fig. 3). However, in *Tilia spp.* leaves the elements' increase was not regular (Fig. 4).

On the other hand, in *A. hippocastanum* leaves there was no regularity in the seasonal accumulation of Cu (*p<0.15)* and in *Tilia spp.* leaves for Cu (*p<0.2)* and Zn (*p<0.09)*. For *A. hippocastanum,* such seasonal discrepancy in the Cu and Zn concentrations was previously noted by Kim & Fergusson (1994), who pointed out that these elements concentrations were the highest in new leaves, and decreased over the vegetation season. Thus, variations in seasonal accumulation of Cu and Zn in some samples of *A. hippocastanum* and *Tillia spp.* may be a result of the fact that these elements are essential constituents of plant tissue. It is considered that the Cu remobilisation to non-senescent parts occurs before the senescence, and leaf fall takes place. In walnut trees, the concentration of Cu in old leaves was just 8 % of the maximum Cu value in younger mature leaves (Drossopoulos et al., 1996). Moreover, some recent data for the black spruce needles supported the previous hypothesis and confirmed that an active translocation of essential metals, particularly Cu, takes place from senescent to non-senescent parts of a plant. However, the results for Pb, as a nonessential metal, were in accordance with a hypothesis that the passive sequestration of toxic metals was attained in the senescing foliage as a detoxification process (Aznar et al., 2009).

3.3.1 Spatial and temporal trace elements' variation in leaves *vs.* bulk deposition

Evaluation of biomonitoring validity is a complex process and, apart from the accumulation level, requires other data, such as temporal trend consistency in accumulation capability. Moreover, the biomonitor should be in correspondence with instrumental monitoring data. Following the previous assumptions, the obtained elements concentration in leaves was compared to the bulk deposition data. From 2002 to 2006, the Pb concentrations in leaves of *A. hippocastanum* at the beginning and the end of vegetation seasons showed a decreasing trend at all sites (Figs. 3 and 4). Temporal decrease of the Pb concentrations in leaf tissue of both species, observed in Belgrade urban area, might be a consequence of a diminishing use of leaded gasoline over the period. This is in accordance with the data reported for other European countries (Dmuchowski & Bytnerowicz, 2009). Furthermore, as shown by a long-term study of Hovmand et al. (2009), though atmospheric Pb declined by a factor of 7 from 1980 to 2007, airborne Pb is still considered a major pathway to vegetation and topsoil.

Fig. 3. Median concentrations (μg g^{-1}) of Cd, As, V, Cr, Ni, Pb*, Cu*, Zn*, and Fe** in the leaves of *A. hipposctanum*, sampled from the urban area of Belgrade in May and September from 2002 to 2006.

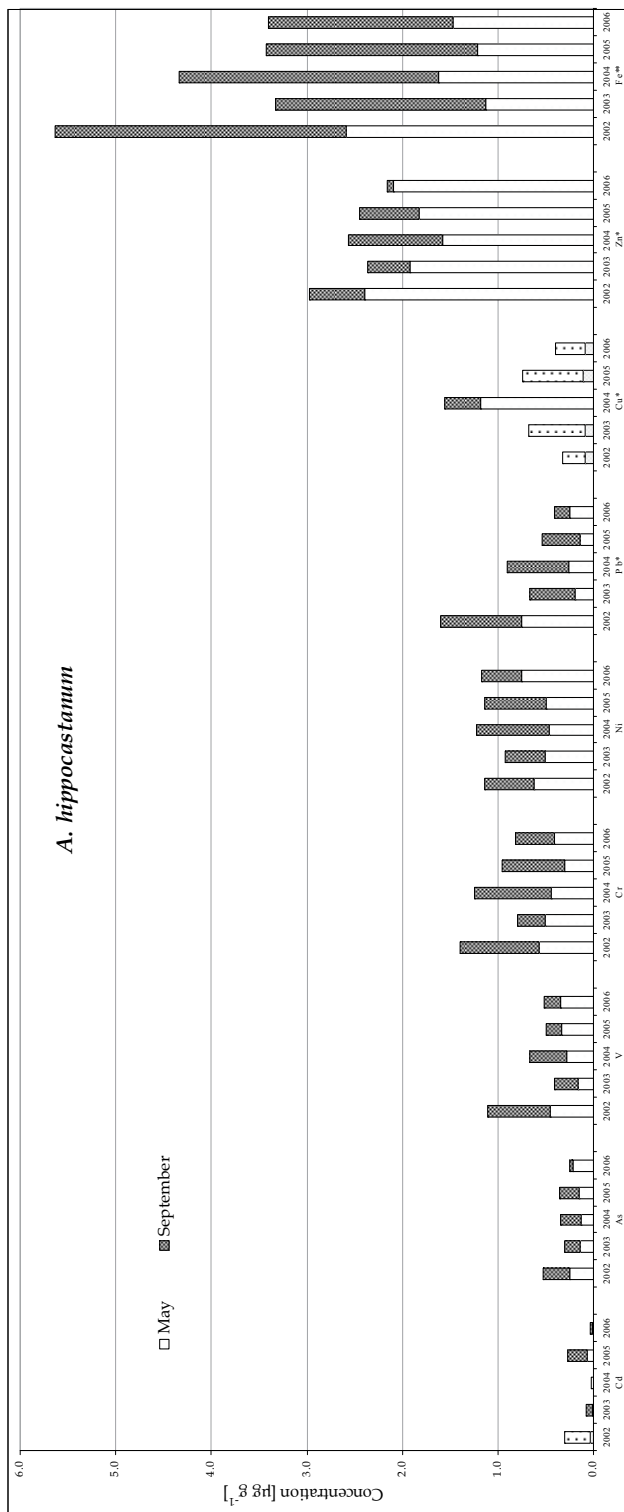Note: Concentrations of Pb*, Cu* and Zn* are divided by 10 and Fe** by 100 to clearly present the results on the graph

Fig. 4. Median concentrations (µg g⁻¹) of Cd, As, V, Cr, Ni, Pb*, Cu*, Zn*, and Fe** in the leaves of *Tilia spp.*, sampled from the urban area of Belgrade in May and September from 2002 to 2006.
Note: Concentrations of Pb*, Cu* and Zn* are divided by 10 and Fe** by 100 to clearly present the results on the graph
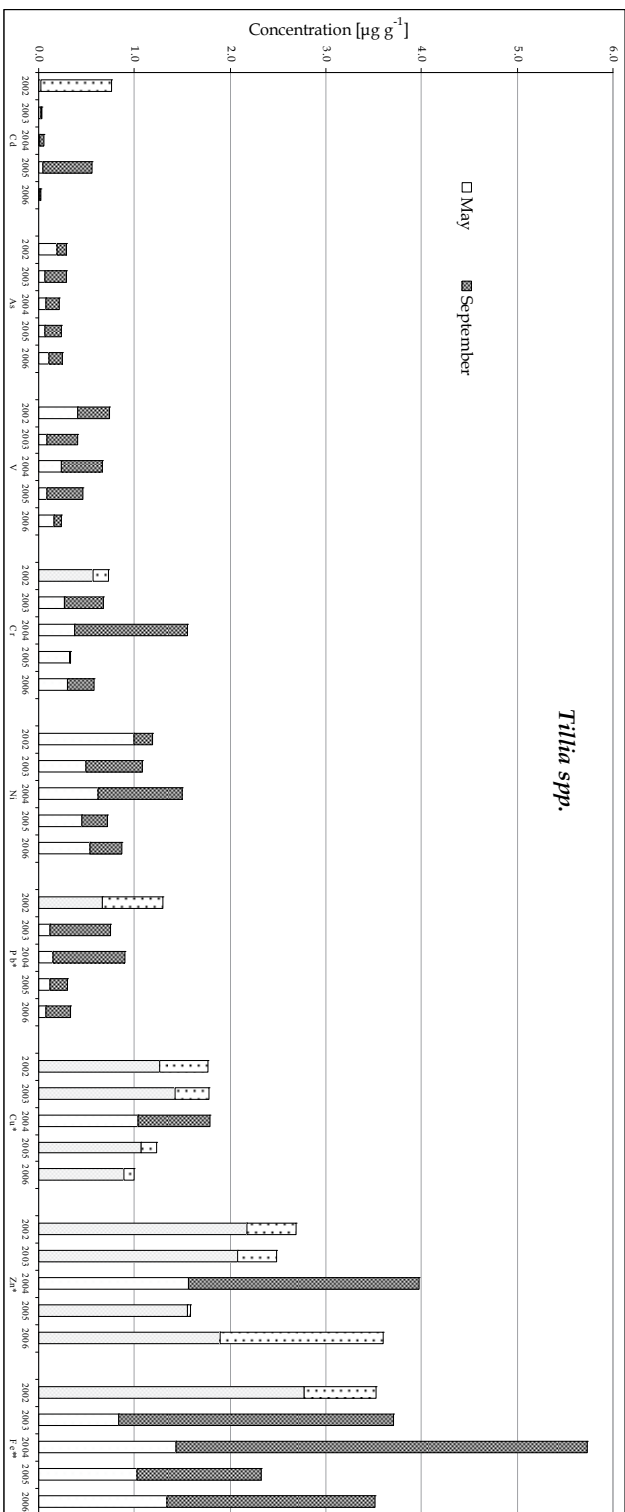
Uncertainty in element uptake pathways has generally been seen as a disadvantage for the use of the vascular plant leaves as biomonitors of trace element atmospheric pollution. However, Hovmand et al. (2009) investigated the origin of Pb in leaves and showed that less than 2 % of the Pb content of needles and twigs of Norway spruce comes from root uptake, i.e. approximately 98 % is of atmospheric origin. Tomašević et al. (2008) showed that in the Belgrade urban area there was a good correlation between the Pb leaf content of *A. hippocastanum* with a significantly increased level of atmospheric Pb in suspended particles during two successive years (1996 and 1997). Therefore, the Pb concentration in the leaves of *A. hippocastanum* reflected changes in atmospheric Pb pollution.

Among the sites, Cu concentrations were obtained at significantly higher level at the RB site, which was also shown by some instrumental monitoring techniques: BD, PMs (Rajšić et al., 2008) and active moss biomonitoring (Aničić et al., 2009a,b) pointing to an additional local source. Through the investigated years, the observed Cu concentration at this site showed a decreasing trend, a more regular one for *A. hippocastanum* (Fig. 5) than for *Tilia spp.* Presumably, a local Cu emitter (metal arts and crafts manufacturing) contributed to a much higher atmospheric Cu levels in 2002, 2003 and 2004 at the RB site, tending to decrease throughout the years until it closed down. Namely, at this site the Cu concentration was the highest in September 2002, and the accumulation level was about nine times higher in *A. hippocastanum* leaves (88 µg g^{-1}) than in the "reference plant" (10 µg g^{-1}, given by Markert, 1992). At the same time, Cu concentrations in bulk deposition were 3–4 time higher in the first than in the final year of the study (Fig. 5). Thus, the temporal trend for Cu accumulation in *A. hippocastanum* leaves follows the Cu contents in the BD for the RB site. The Cu content in *Tilia spp.* leaves did not show a clear seasonal nor temporal dependence.
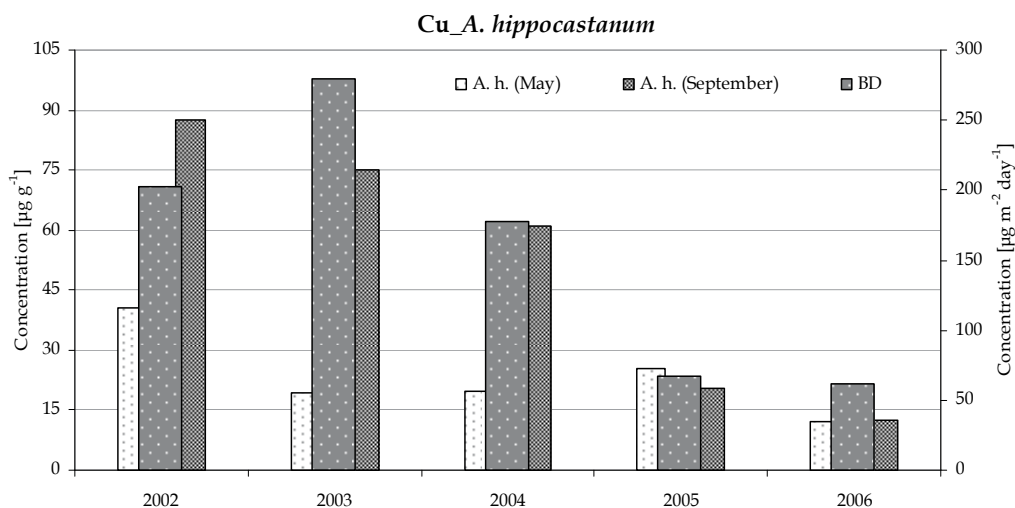
Fig. 5. The Cu concentrations in *A. hipposactanum* leaves in May and September (2002 – 2006), and bulk deposition (BD) at the RB site.

The soil Cu concentration at the RB site also decreased from 98 µg g^{-1} in 2002 (Tomašević et al., 2004) to 50 µg g^{-1} in 2008 (Marjanović et al., 2009). However, the presence of the elements in soil does not imply that they are available to plants, as plant-to-soil concentration ratio is

far from a linear one (Bargagli, 1998). The results of Chojnacka et al. (2005) showed that there is a low correlation between the transfer factors of metals from polluted soils to plants. Moreover, the pH of the soil samples at the RB site was 8.8, and it is not likely that the element availability for the root uptake would be considerable. Consequently, it may be concluded that in our study the Cu content in leaves was mainly of atmospheric origin.

Temporal trends of V and As in the investigated years were slightly decreasing (Figs. 3 and 4), but no correlation with the bulk deposition was observed. However, there was no substantial variation in the accumulated content of Cr, Fe, Ni, Zn, and Cd thought the years, and no agreement in temporal trends with the bulk deposition measurements.

3.4 Radionuclides in tree leaves

The mean activities and standard deviations for the radionuclide contents in soils in Belgrade urban area are given in Table 3. The measured activities are within the range reported for the region and elsewhere (Djuric et al., 1992; RA Report, 2002; Todorovic et al., 2005) with no significant differences among the sites.

Site	Activity (Bq/kg)						
	^{226}Ra	^{232}Th	^{40}K	^{137}Cs	^{238}U	^{235}U	^{210}Pb
VF	39 ± 5	33 ± 5	402 ± 40	21 ± 2	15 ± 5	2.9 ± 0.3	/
HI	33 ± 3	34 ± 4	395 ± 35	31 ± 3	27 ± 9	1.6 ± 0.3	/
RB	26 ± 3	27 ± 4	378 ± 30	35 ± 2	16 ± 10	/	/
Mean ± SD	32 ± 4	32 ± 4	392 ± 35	29 ± 2	16 ± 8	1.7 ± 0.3	51 ± 10

Table 3. Radionuclides in soils in Belgrade urban area. Lead-210 in soils was estimated using two measuring episodes (4 samples).

Soil-to-leaves transfer factors (TF) were calculated as a ratio of an element's activity in leaves and its activity in soil (IAEA, 1994). The results for ^{40}K, ^{210}Pb and ^{137}Cs are presented in Table 4. The high TFs for ^{40}K show that its predominant route of accumulation in *Tilia spp.* and *A. hippocastanum* leaves is by root uptake, which could also be concluded for Pb, although, considering the scarcity of the Pb data in soils (Table 3), this result should be taken with caution.

The activities of radionuclides in leaves of *Tilia spp.* and *A. hippocastanum* (in Bq/kg) and aerosols (in Bq/m^3) in Belgrade parks, over the period 2002 – 2008 are presented in Table 5. The presented results include the mean, standard deviation and the coefficient of variation (in %) (Todorović et al., 2009).

Species	Transfer factor		
	^{40}K	^{210}Pb	^{137}Cs
Tilia spp.	1.29	0.90	0.09
A.hippocastanum	1.26	0.90	0.03
Tilia spp. & *A.hippocastanum*	1.27	0.90	0.06

Table 4. Transfer factors soil–to–leaves for *Tilia spp.* and *A. hippocastanum* in Belgrade.

The coefficient of variation, calculated as a ratio of standard deviation and the mean, shows dispersion of the mean activity for a detected radionuclide. The dispersion is the lowest for ^{40}K, the radionuclide generally uptaken from soil through roots. The seasonal variations, therefore, are not expected to be pronounced. The seasonal variations for ^{210}Pb are higher than for ^{7}Be, which can be explained by an additional input, resulting from coal burning and traffic, in winters. The variations in the ^{137}Cs activity, on the other hand, are very high. They are mainly influenced by low measurable quantities of this radionuclide, a very limited data set, and a large standard error. The concentrations of ^{137}Cs in Belgrade air before the Chernobyl nuclear plant accident were of an order 10^{-5} Bq/m^3, increased to 0.39 Bq/m^3 immediately after the accident, and decreased to 9.5×10^{-5} Bq/m^3 in 1988 (Popović et al., 2009a).

Activity variations in leaves of *Tilia spp.* and *A. hippocastanum* show a very similar behaviour (Table 5). In turn, these variations resemble those in air, thus confirming that ^{7}Be and ^{137}Cs are mainly deposited in leaves by foliar deposition. Since the ^{210}Pb variations are higher in plants than in air, Pb accumulation is influenced by root uptake and by foliar deposition.

Species	Activity in leaves (Bq/kg) and in aerosols (Bq/m³)			
	^{40}K	^{210}Pb	^{137}Cs	^{7}Be
Tilia spp.	504 ± 196 (39)	46 ± 29 (63)	2.6 ± 2.2 (85)	131 ± 56 (43)
A. hippocastanum	494 ± 184 (37)	46 ± 34 (74)	1.0 ± 0.8 (80)	121 ± 60 (49)
Tilia spp. & A. hippocast.	499 ±191 (38)	46 ± 31 (67)	1.7 ± 1.6 (94)	126 ± 57 (45)
Aerosols	/	$(5.6 ± 2.7) \times 10^{-4}$ (48)	$(2.5 ± 1.8) \times 10^{-6}$ (94)	$(2.9 ± 1.2) \times 10^{-3}$ (41)

Table 5. Activity of radionuclides in leaves of *Tilia spp.* and *A. hippocastanum* and aerosols in Belgrade, 2002 – 2008 (the mean and standard deviation, and the coefficient of variation (in %) in the parenthesis).

To estimate the concentrations of radionuclides in air due to resuspension, we applied the following equation (SRS, 2006):

$$C_{air/res} (Bq/m^3) = RF(m^{-1}) \times C_{soil} (Bq/m^2) \tag{3}$$

where $C_{air/res}$ is concentration of radionuclides in air due to resuspension (Bq/m^3), RF is the resuspension factor (estimated to 10^{-7} for urban and non-agricultural soils, and to 10^{-5} for agricultural soils), and C_{soil} is the surface concentrations. It was calculated using (SRS, 2006):

$$C_{soil} (Bq/m^2) = C_s \times \rho_s \times d_s \tag{4}$$

where d_s is the mean depth (15 cm), ρ_s is the density of soils (global average 1.6 g/cm^3), and C_s is the average annual concentration in soils (in Bq/kg). Thus, the calculated global average for $\rho_s \times d_s$ is 240 kg/m^2. The results for the calculated concentrations of radionuclides in air caused by resuspension, together with the annual mean concentrations measured in air (C_{air}), are presented in Table 6.

The correlation coefficients for the content of radionuclides in aerosols and leaves of *Tilia spp.* and *A. hippocastanum* were calculated (Table 7). The lack of linear correlation between [7]Be in air and leaves could be explained mainly by leaching (rainfalls) effects and short half-life of [7]Be. There is a low correlation for ^{210}Pb, for both *Tilia spp.* and *A. hippocastanum*, but the uptake of lead by plants is due to many factors and is more complex than for [7]Be.

	Concentration (Bq/m^3)		
	^{40}K	^{210}Pb	^{137}Cs
$C_{air/res}$	94.08x10^{-4}	12.24x10^{-4}	6.96x10^{-4}
C_{air}	(0.9-1.5)x10^{-4}	5.6x10^{-4}	2.5x10^{-5}

Table 6. Concentrations of radionuclides in air caused by resuspension from soil in Belgrade, 2002 – 2008. The activity of ^{40}K in air was estimated from the measurements with a new pump, with higher air flow capacity (average flow 30–50 m^3/h and volume up to 40,000 m^3).

Species	Correlation coefficient	
	^{7}Be	^{210}Pb
Tilia spp.	-0.266	0.302
A.hippocastanum	-0.241	0.347
Tilia spp. and *A. hippocastanum*	-0.139	0.311

Table 7. Correlations coefficients for the ^{7}Be and ^{210}Pb activities in leaves and in aerosols.

3.4.1 Seasonal variations of radionuclides in tree leaves

The seasonal variations of the radionuclides' activities in leaves of *Tilia spp.* and *A. hippocastanum* in Belgrade urban area, from 2002 – 2008, are presented in Fig. 6. The concentrations of ^{40}K and ^{137}Cs are the highest over the spring–summer periods, probably caused by a higher accumulation in young leaves. For ^{137}Cs, this conclusion should be taken with caution since there were only a few measurable episodes in the data set (up to 2005), and very low concentrations of this radionuclide were detected both in leaves and air. Concentrations of ^{210}Pb were the highest in autumn, and concentrations of ^{7}Be in summer, and both follow the pattern of seasonal variations of those radionuclides in air (Popovic et al., 2008b; Todorovic et al., 1999, 2000, 2005, 2007; Todorović et al., 2005; Sugihara et al., 2008). Thus, for these two radionuclides, leaves of higher plants could be used to monitor their concentrations and seasonal variations in air in urban areas.

4. Conclusion

Moss biomonitoring study in the urban area of Belgrade showed that most of the analysed trace elements (Al, V, Cr, Mn, Fe, Ni, Cu, Zn, As, Cd, Pb) were significantly accumulated in *Sphagnum girgensohnii* bags exposed in five consecutive 3-month periods. The highest relative accumulation factors were obtained for V, Cr, Cu, and Pb in both wet and dry moss bags. However, in general, higher element contents were noticed in the wet moss bags. Significant correlations were found between the element bulk deposition fluxes and elements concentration in dry (Cu, V, Zn, Fe, Pb, As, Cr) and wet (V, As, Fe, Al, Ni, Cu)

moss bags. It may be concluded that active moss biomonitoring with *S. girgensohnii* could be used for screening monitoring of atmospheric trace element pollution in urban areas.
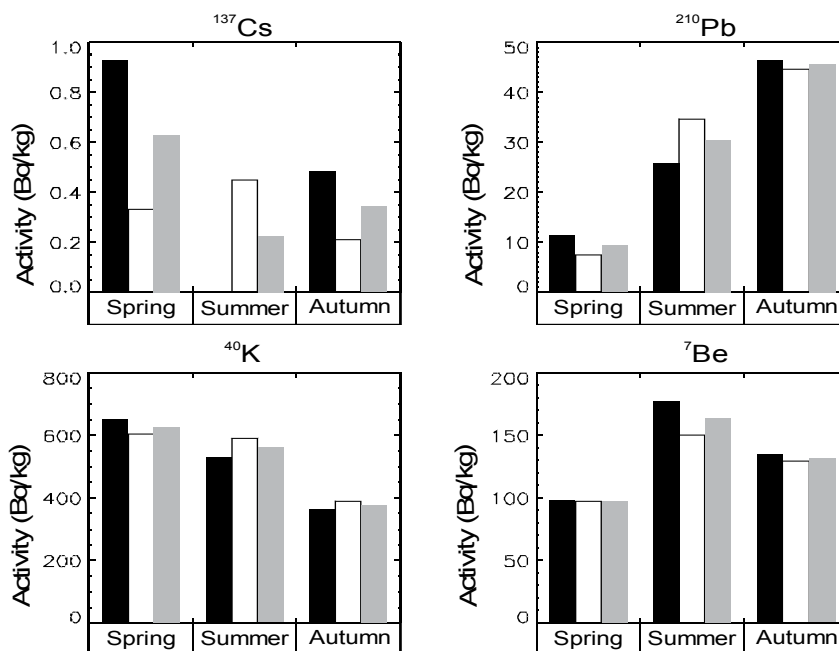

Fig. 6. Seasonal variations of radionuclides' activities in leaves of *Tilia spp.* and *A. hippocastanum* in Belgrade, 2002 – 2008 (the mean value for *Tilia spp.* is given in black, for *A. hippocastanum* in white, and the mean for *Tilia spp.* and *A. hippocastanum* in grey).

The mean activities of the detected radionuclides in *S. girgensohnii* were in the range of the values reported for other local naturally growing moss species in the region, with differences arising from the species, the method, local climate and soil characteristics. For the long lived ^{40}K there were no significant differences in its content in naturally growing mosses in a rural region of Southern Serbia and in the urban area of Belgrade. On the other hand, higher concentrations of ^{210}Pb in Belgrade indicate a contribution of anthropogenic air pollution sources. Significantly higher activities of ^{137}Cs, as well as the detectable amount of ^7Be, in mosses sampled in Southern Serbia are a consequence of a longer, unknown exposure period, while in the Belgrade study, the exposure period was limited to exactly one year. Hence, the observed differences mirror the differences in the accumulation period. Since naturally growing mosses are unlikely to be found in urban areas, the active moss monitoring proved to be a suitable alternative technique for monitoring contents of radionuclides in urban air. Furthermore, the exposure period in the moss bags technique could be reduced to one month, thus nominating the technique as an efficient means to monitor the level of radionuclides' contents in air, as well as to follow their seasonal variations.

Seasonal accumulation of the examined trace elements in leaves of *Aesculus hippocastanum* L. and *Tilia spp.* (*Tilia tomentosa* L. and *Tilia cordata* Mill.) was evident for V, Cr, Fe, Ni, As, and Pb, and it was more regular for *A. hippocastanum*. Considering the temporal trends of the

trace elements content in leaves, some elements displayed a variation throughout the investigated years. The most obvious was the Pb variation, showing a decreasing trend from 2002 to 2006, in accordance with the lead trend in bulk atmospheric deposition measurements. Likewise, the temporal concentration trend for Cu in *A. hippocastanum* was decreasing, similarly to the Cu trends seen in the bulk atmospheric deposition at the site with the high atmospheric Cu loading. No agreement was observed between the accumulation trend of V and As in leaves and bulk deposition, although they exhibited decreasing temporal trends, as well as Cr, Fe, Ni, and Zn. The results implied that those elements' content in leaves could not reflect atmospheric deposition directly. Therefore, due to its higher accumulation capability, temporal trend consistency, and better agreement with the bulk deposition measurements, *A. hippocastanum* may be suggested as a more appropriate biomonitor of the trace elements atmospheric deposition than *Tilia spp*. The lead leaf content clearly reflected the atmospheric Pb contamination, and it may as well be assumed for Cu in highly polluted areas.

As for the examined radionuclides, the study showed that the predominant route of ^{40}K accumulation in *Tilia spp.* and *A. hippocastanum* leaves is by root uptake. The accumulation pathways for lead seem more complex, although, according to Hovmand et al. (2009), less than 2 % of Pb content comes from root uptake and 98 % is of atmospheric origin. The dispersions of the mean activities of the radionuclides in leaves were the lowest for ^{40}K, which is generally uptaken from soil by roots. Its seasonal variations, therefore, were not expected to be pronounced. The seasonal variations for ^{210}Pb were higher than for ^{7}Be. This could be explained by an additional ^{210}Pb input, e.g., coal burning and more traffic, in winter. The ^{137}Cs variations, on the other hand, were very high. They were influenced by low measurable quantities of ^{137}Cs, a limited data set, and a large standard error. Variations of ^{7}Be and ^{137}Cs in air and in leaves of *Tilia spp.* and *A. hippocastanum* showed similar behaviour, confirming that these radionuclides are mainly deposited on leaves by foliar deposition. Since the ^{210}Pb variations are higher in plants than in air, lead accumulation is influenced both by root uptake and by foliar deposition. The comparison of the radionuclides' content in aerosols and leaves of *Tilia spp.* and *A. hippocastanum* showed no linear correlation for ^{7}Be, which could be explained mainly by leaching effects and short half-life of ^{7}Be. There was a low correlation for ^{210}Pb, for both *Tilia spp.* and *A. hippocastanum*, but the uptake of lead by plants is influenced by many factors and is more complex than for beryllium-7.

The seasonal variations of the radionuclides' activities in leaves of *Tilia spp.* and *A. hippocastanum* in Belgrade urban area, from 2002 – 2008, showed that the concentrations of ^{40}K and ^{137}Cs were the highest over the spring–summer periods, probably caused by a higher accumulation of young leaves. For ^{137}Cs, this conclusion should be taken with caution as there were only a few measurable episodes in the data set (up to 2005), and the content of ^{137}Cs was generally very low in leaves and air. The concentrations of ^{210}Pb were the highest in autumn, those of ^{7}Be in summer. Both ^{210}Pb and ^{7}Be in leaves follow the pattern of their seasonal variations in air. Thus, leaves of *Tilia spp.* and *A. hippocastanum* could be used to monitor concentrations and seasonal variations of these radionuclides in air in urban areas.

Acknowledgements

5. References

Adamo, P.; Giordano, S.; Vingiani, S.; Castaldo Cobianchi, R. & Violante, P. (2003). Trace element accumulation by moss and lichen exposed in bags in the city of Naples (Italy). *Environmental Pollution*, 122, 91–103, 0269-7491

Ajtić, J.; Todorović, D.; Filipović, A. & Nikolić, J. (2008). Ground level air beryllium-7 and ozone in Belgrade. *Nuclear Technology & Radiation Protection*, 23, 2, 65-71, 1451-3994

Alfani, A.; Maisto, G.; Iovieno, P.; Rutigliano F. A. & Bartoli, G. (1996). Leaf contamination byatmospheric pollutants assessed by elemental analysis of leaf tissue, leaf surface deposit and soil. *Journal of Plant Physiology*, 148, 243–248, 0176-1617

Al-Radady, A. S.; Davies, B. E. & French, M. J. (1993). A new design of moss bag to monitor metal deposition both indoors and outdoors. *Science of the Total Environment*, 133, 275-283, 0048-9697

Amblard-Gross, G.; Ferard, J. F.; Carrot, F.; Bonnin-Mosbah, M.; Maul, S.; Ducruet, J. M.; Coddeville, P.; Beguinel, P. & Ayrault, S. (2002). Biological fluxes conversion and SXRF experiment with a new active biomonitoring tool for atmospheric metals and trace element deposition. *Environmental Pollution*, 120, 47–58, 0269-7491

Aničić, M.; Frontasyeva, M.; Tomašević, M. & Popović, A. (2007). Assessment of Atmospheric Deposition of Heavy Metals and Other Elements in Belgrade Using the Moss Biomonitoring Technique and Neutron Activation Analysis. *Environmental Monitoring and Assessment*, 129, 1-3, 207-219, 0167-6369

Aničić, M.; Tasić, M.; Frontasyeva, M. V.; Tomašević, M.; Rajšić, S.; Mijić, Z. & Popović, A. (2009a). Active moss biomonitoring of trace elements with *Sphagnum girgensohnii* moss bags in relation to atmospheric bulk deposition in Belgrade, Serbia. *Environmental Pollution,* 157, 673–679, 0269-7491

Aničić, M.; Tasić, M.; Frontasyeva, M. V.; Tomašević , M.; Rajšić, S.; Strelkova, L. P.; Popović, A. & Steinnes, E. (2009b). Active biomonitoring with wet and dry moss: a case study in an urban area. *Environmental Chemistry Letters*, 7, 55-60, 1610-3653

Astel, A.; Astel, K. & Biziuk, M. (2008). PCA and multidimensional visualization techniques united to aid in the bioindication of elements from transplanted *Sphagnum palustre* moss exposed in Gdan´sk city area. *Environmental Science and Pollution Research*, 15, 1, 41–50, 0944-1344

Azimi, S.; Ludwig, A.; Thevenot, D. R. & Colin, J. L. (2003). Trace metal determination in total atmospheric deposition in rural and urban areas. *Science of the Total Environment*, 308, 247-254, 0048-9697

Aznar, J. C.; Richer-Laflèche, M.; Bégin, C. & Bégin, Y. (2009). Lead Exclusion and Copper Translocation in Black Spruce Needles. *Water, Air & Soil Pollution*, 203, 139-145, 0049-6979

Barandovski, L.; Cekova, M.; Frontasyeva, M. V.; Pavlov, S. S.; Stafilov, T.; Steinnes, E. & Urumov, V. (2008). Atmospheric deposition of trace element pollutants in Macedonia studied by the moss biomonitoring technique. *Environmental Monitoring and Assessment*, 138, 1-3, 107-118, 0167-6393

Bargagli, R. (1998). *Trace Elements in terrestrial Plants: An Ecophysiological Approach to Biomonitoring and Biorecovery*, Springer-Verlag Berlin, Heidelberg, NY

Baycu, G.; Tolunay, D.; Ozden, H. & Sureyya, G. (2006). Ecophysiological and seasonal variations in Cd, Pb, Zn and Ni concentrations in the leaves of urban deciduous trees in Istanbul. *Environmental Pollution,* 143, 545–554, 0269-7491

Beckett, K. P.; Freer-Smith, P. H. & Taylor, G. (2000). Effective tree species for local air quality management. *Journal of Arboriculture*, 26, 12–19, 02785-226

Berg, T. & Steinnes, E. (1997). Use of mosses (*Hylocomium splendens* and *Pleurozium schrebery*) as biomonitors of heavy metal deposition: from relative to absolute deposition values. *Environmental Pollution,* 98 (I), 61–71, 0269-7491

Chojnacka, K.; Chojnacki, A.; Gorecka, H. & Gorecki, H. (2005). Bioavailability of heavy metals from polluted soils to plants. *Science of the Total Environment,* 337, 175-182, 0048-9697

Couto, J. A.; Fernandez, J. A.; Aboal, J. R. & Carballeira, A. (2004). Active biomonitoring of element uptake with terrestrial mosses: a comparison of bulk and dry depositions. *Science of the Total Environment*, 324, 211–222, 0048-9697

Culicov, O. A.; Mocanu, R.; Frontasyeva, M. V.; Yurukova, L. & Steinnes, E. (2005). Active moss biomonitoring applied to an industrial site in Romania: Relative accumulation of 36 elements in moss-bags. *Environment Monitoring and Assessment*, 108, 229-240, 0167-6369

Culicov, O. A. & Yurukova, L. (2006). Comparison of element accumulation of different moss and lichen-bags, exposed in the city of Sofia (Bulgaria). *Journal of Atmospheric Chemistry*, 55, 1–12, 0167-7764

Delfanti, R.; Papucci, C. & Benco, C. (1999). Mosses as indicators of radioactivity deposition around a coal-fired power station. *Science of the Total Environment*, 227, 1, 49-56, 0048-9697

De Nicola, F.; Maisto, G. M.; Prati, V. & Alfani, A. (2008). Leaf accumulation of trace elements and polycyclic aromatic hydrocarbons (PAHs) in *Quercus ilex* L. *Environmental Pollution*, 153, 376-383, 0269-7491

Djingova, R.; Kuleff, I. & Markert, B. (2004). Chemical fingerprinting of plants. *Ecological Research*, 19, 3–11, 0912-3814

Djuric, G.; Popovic, D.; Smercerovic, M.; Sarvajic, A.; Vankovic, S. & Misic, N. (1992). Exposures and doses at honey bee pastures at Mt. Tara, *Veterinary Courier* 46, 9, 491-497, 0350-2457

Djuric, G. & Popovic, D. (1994). Radioactive Contamination of Plants. *Ecologica* I, 2, 19-24, 0354-3285

Djuric, G.; Popovic, D. & Todorovic, D. (1996). Activity variations and concentration factors for natural radionuclides in a "soil-plant-honey" system. *Environment International*, 22, Supplement 1, 361-363, 0160-4120

Dmuchowski, W. & Bytnerowicz, A. (2009). Long-term (1992–2004) record of lead, cadmium, and zinc air contamination in Warsaw, Poland: Determination by chemical analysis of moss bags and leaves of Crimean linden. *Environmental Pollution*, 157, 3413-3421, 0269-7491

Drossopoulos, B.; Kouchaji, G. & Bouranis, D. (1996). Seasonal dynamics of mineral nutrients and carbohydrates by walnut tree leaves. *Journal of Plant Nutrition*, 19, 493-516, 0190-4167

Espinosa, F. A. J. & Oliva, S. R. (2006). The composition and relationships between trace element levels in inhalable atmospheric particles (PM10) and in leaves of *Nerium oleander* L. and *Lantana camara* L. *Chemosphere*, 62, 1665-1672

Fernandez, J. A.; Aboal, J. R. & Carballeira, A. (2004). Identification of pollution sources by means of moss bags. *Ecotoxicology and Environmental Safety,* 59, 76–83, 0147-6513

Freer-Smith, P. H.; Beckett, K. P. & Taylor, G. (2005). Deposition velocities to *Sorbus aria*, *Acer campestre*, *Populus deltoides* X *trichocarpa* 'Beaupre', *Pinus nigra* and X *Cupressocyparis leylandii* for coarse, fine and ultra-fine particles in the urban environment. *Environmental Pollution*, 133, 157-167, 0269-7491

Frontasyeva, M. V.; Galinskaya, T. Ye.; Krmar, M.; Matavuly, M.; Pavlov, S. S.; Povtoreyko E. A.; Radnovic, D. & Steinnes, E. (2004). Atmospheric deposition of heavy metals in northern Serbia and Bosnia-Herzegovina studied by moss biomonitoring, neutron activation analysis and GIS technology. *Journal of Radioanalytical and Nuclear Chemistry*, 259, 1, 141-147, 0236-5731

Frontasyeva, M. V.; Aleksiayenak, Yu. V.; Steinnes, E.; Florek, M.; Sukora, I.; Teshovsky, M.; Ramatllape, J. & Faauhof, A. (2009). Moss biomonitoring of the long-lived radionuclides: 20 years after Chernobyl. 22nd Task Meeting of ICP Vegetation Group, February 2009, Braunschweig, Germany. http://icpvegetation.ceh.ac.uk

Gerasopoulos, E.; Zerefos, C. S.; Papastefanou, C.; Zanis, P. & O'Brien, K. (2003). Low-frequency variability of beryllium-7 surface concentrations over the Eastern Mediterranean. *Atmospheric Environment*, 37, 13, 1745-1756, 1352-2310

Golmakani, S.; Vahabi Moghaddam, M. & Hosseini, T. (2008). Factors affecting the transfer of radionuclides from the environment to plants. *Radiation Protection Dosimetry*, 130, 3, 368-375, 0144-8420

Golubev, A. V.; Golubeva, V. N.; Krylov, N. G.; Kuznetsova, V. F.; Mavrin, S. V.; Aleinikov, A. Yu.; Hoppes, W. G. & Surano, K. A. (2005). On monitoring anthropogenic airborne uranium concentrations and $^{235}U/^{238}U$ isotopic ratio by Lichen – bio-indicator technique. *Journal of Environmental Radioactivity*, 84, 3, 333-342, 0265-931X

Goodman, G. T. & Roberts, T. M. (1971). Plants and soils as indicators of metals in the air. *Nature*, 231, 287–292, 0028-0836

Guillén, J.; Baeza, A.; Ontalba, M. A. & Miguez, M. P. (2009). ^{210}Pb and stable lead contents in fungi: its transfer from soil. *Science of the Total Environment*, 407, 14, 4320-4326, 0048-9697

Harmens, H.; Norris, D. A.; Koerber, G. R.; Buse, A.; Steinnes, E. & Ruhling, A. (2008). Temporal trends (1990–2000) in the concentration of cadmium, lead and mercury in mosses across Europe. *Environmental Pollution*, 151, 368–376, 0269-7491

Harrison, R. M.; Tilling, R.; Romero, M. S. C.; Harrad, S. & Jarvis, K. (2003). A study of trace metals and polycyclic aromatic hydrocarbons in the roadside environment. *Atmospheric Environment*, 37, 2391-2402, 1352-2310

Hofmann, W.; Attarpour, N.; Lettner, H. & Turk, R. (1993). ^{137}Cs Concentrations in Lichen Before and After the Chernobyl accident. *Health Physics*, 64, 1, 70-73, 0017-9078

Hovmand, M. F.; Nielsen, S. P. & Johnsen, I. (2009). Root uptake of lead by Norway spruce grown on ^{210}Pb spiked soils. *Environmental Pollution*, 157, 404–409, 0269-7491

IAEA (1994). *Handbook of Parameter Values for the Prediction of Radionuclides Transfer in Temperate Environment, Tech Report Series 364*, IAEA, 92-0-101094X, Vienna

Kim, N. D. & Fergusson, J. E. (1994). Seasonal variations in the concentrations of cadmium, copper, lead and zinc in leaves of the horse chestnut (*Aesculus hippocastanum* L.). *Environmental Pollution*, 86, 89-97, 0269-7491

Koranda, J. J. & Robison, W. L. (1978). Accumulation of Radionuclides by Plants as a Monitor System. *Environmental Health Perspectives*, 27, December 1978, 165-179, 0091-6765

Krmar, M.; Radnović, D.; Rakic, S. & Matavuly, M. (2007). Possible use of terrestrial mosses in detection of atmospheric deposition of [7]Be over large areas. *Journal of Environmental Radioactivity*, 95, 1, 53-61, 0265-931X

Loppi, S.; Riccobono, F.; Zhang, Z. H.; Savic, S.; Ivanov, D. & Pirintsos, S. A. (2003). Lichens as biomonitors of uranium in the Balkan Area. *Environmental Pollution*, 125, 2, 277-280, 0269-7491

Marjanović, M.; Vukčević, M. M.; Antonović, D. G.; Dimitrijević, S. J.; Jovanović, Đ. M.; Matavulj, M. N. & Ristić, M. Đ. (2009). Heavy metals concentrations in soils from parks and green areas in Belgrade. *Journal of the Serbian Chemical Society*, 74, 6, 697-706, 0352-5139

Markert, B. (1992). Establishing of "Reference Plant" for inorganic characterization of different plant species by chemical fingerprinting. *Water, Air & Soil Pollution*, 64, 533-538, 0049-6979

Markert, B. A.; Breure, A. M. & Zechmeister, H. G. (2003). (Eds.) *Bioindicators and Biomonitors*. Elsevier, 0-08-044177-7, Amsterdam

Mingorance, M. D. & Oliva, S. R. (2006). Heavy metals content in *N. oleander* leaves as urban pollution assessment. *Environmental Monitoring and Assessment*, 119, 57–68, 0167-6393, 0167-6369

Monaci, F.; Moni, F.; Lanciotti, E.; Grechi, D. & Bargagli, R. (2000). Biomonitoring of airborne metals in urban environments: New tracers of vehicle emission, in place of lead. *Environmental Pollution,* 107, 321–327, 0269-7491

Papastefanou, C.; Manolopoulou, M. & Sawidis, T. (1989). Lichens and Mosses: Biological Monitors of Radioactive Fallout from the Chernobyl Reactor Accident. *Journal of Environmental Radioactivity*, 9, 3, 199-207, 0265-931X

Peachey, C. J.; Sinnett, D.; Wilkinson, M.; Morgan, G. W.; Freer-Smith, P. H. & Hutchings, T. R. (2009). Deposition and solubility of airborne metals to four plant species grown at varying distances from two heavily trafficked roads in London. *Environmental Pollution*, 157, 2291-2299

Piczak, K.; Lesnievicz, A. & Zyrnicki A. (2004). Metal concentrations in deciduous tree leaves from urban areas in Poland. *Environmental Monitoring and Assessment*, 86, 273-287, 0167-6393

Popovic, D.; Djuric, G. & Todorovic, D. (1996). Chernobyl fallout radionuclides in soil, plant and honey of a mountain region. *Proceedings of the International Conference "A Decade After Chernobyl"*, pp. 432-437, 1011-4289, Vienna, April 1996, IAEA, Vienna

Popovic, D.; Todorovic, D.; Frontasyeva, M.; Ajtic, J.; Tasic, M. & Rajsic, S. (2008a). Radionuclides and heavy metals in Borovac, Southern Serbia. *Environmental Science & Pollution Research*, 15, 6, 509-520, 0944-1344

Popovic, D.; Todorovic, D.; Spasic-Jokic, V. & Djuric, G. (2008b). Air Radioactivity Monitoring In Serbia, In: *Environmental Technologies – New Developments*, Burcu, E. & Gungor, O. (Ed.), 147-166, I-Tech Education and Publishing, 978-3-902613-10-3, Vienna

Popović, D.; Spasić-Jokić, V. & Đurić, G. (2009a). *Chernobyl: More than an accident? Consequences of the nuclear accident at Chernobyl power plant in 1986*, Faculty of Technical Sciences, 978-86-7892-155-1, Novi Sad

Popović, D.; Todorović, D.; Ajtić, J. & Nikolić, J. (2009b). Active biomonitoring of air radioactivity in urban areas. *Nuclear Technology & Radiation Protection*, 24, 2, 100-103, 1451-3994

Qiu, Y.; Guan, D.; Song, W. & Huang, K. (2009). Capture of heavy metals and sulphur by foliar dust in urban Huizhou. *Chemosphere*, 75, 447-452, 0045-6535

Rajšić, S.; Mijić, Z.; Tasić, M.; Radenković, M. & Joksić, J. (2008). Evaluation of the levels and sources of trace elements in urban particulate matter. *Environmental Chemistry Letters*, 6, 95-100, 1610-3653

RA Report (2002). *Radioactivity in the Environment in the Republic of Serbia in 2002*, Simic, S. (Ed.), Ministry of the Environmental Protection of the Republic of Serbia, April 2002, Belgrade

Rühling, Å. & Tyler, G. (1968). An ecological approach to the lead problem. *Botaniska Notiser*, 122, 248–342,0006-8195

Schröder, W.; Pesch, R.; Englert, C.; Harmens, H.; Suchara, I.; Zechmeister, H. G.; Thöni, L.; Maňkovská, B.; Jeran, Z.; Grodzinska, K. & Alber, R. (2008). Metal accumulation in mosses across national boundaries: uncovering and ranking causes of spatial variation. *Environmental Pollution*, 151, 377-388, 0269-7491

Seinfeld, J. H. & Pandis, S. N. (1998). Atmospheric chemistry and physics, In: *From Air Pollution to Climate Change*. John Wiley & Sons, Inc., NY, pp. 1326

Somashekarappa, H. M.; Narayana, Y.; Radhakrishna, A. P.; Karunakara, N.; Balakrishna, K. M. & Siddappa, K. (1996). Bioindicators in the tropical forest of Kaiga environment. *Journal of Environmental Radioactivity*, 31, 2, 189-198, 0265-931X

SRS (2006). Dose Reconstruction Report: Food chain transport – uptake of radionuclides by plants and animals. Savannah River Site Dose reconstruction Report, August 2006. http:/www.cdc.gov/nceh/radiation/Savannah/docs/ExecSummary-083006.pdf

Steinnes, E. (2008). Use of mosses to study atmospheric deposition of trace elements: contributions from investigations in Norway. *International Journal of Environmental Pollution*, 32, 4, 499-508, 0957-4352

Sugihara, S.; Efrizal; Osaki, S.; Momoshima, N. & Maeda, Y. (2008). Seasonal variation of natural radionuclides and some elements in plant leaves. *Journal of Radioanalytical and Nuclear Chemistry*, 278, 2, 419-422, 0236-5731

Sumerling, T. J. (1984). The use of mosses as indicators of airborne radionuclides near a major nuclear installation. *Science of the Total Environment*, 35, 3, 251-265, 0048-9697

Tasić, M.; Mijić, Z.; Rajšić, S.; Stojić, A.; Radenković, M. & Joksić, J. (2009). Source apportionment of atmospheric bulk deposition in the Belgrade urban area using Positive Matrix factorization. 2nd Int. Workshop on Nonequilibrium Processes in Plasma Physics and Science, IOP Publishing, *Journal of Physics: Conference Series* 162, 012018, doi:10.1088/1742-6596/162/1/012018, 1742-6588

Thöni, L.; Schnyder, N. & Krieg, F. (1996). Comparisons of metal concentrations in three species of mosses and metal freights in bulk precipitations. *Fresenius Journal of Analytical Chemistry*, 354, 703–708, 0937-0633

Todorovic, D.; Popovic, D. & Djuric, G. (1999). Concentration measurements of [7]Be and ^{137}Cs in ground level air in the Belgrade City area. *Environment International*, 25, 1, 59-66, 0160-4120

Todorovic, D.; Popovic, D.; Djuric, G. & Radenkovic, M. (2000). [210]Pb in ground-level air in Belgrade city area. *Atmospheric Environment*, 34, 19, 3245-3248, 1352-2310

Todorovic, D.; Popovic, D.; Djuric, G. & Radenkovic, M. (2005). [7]Be to ^{210}Pb concentration ratio in ground level air in Belgrade area. *Journal of Environmental Radioactivity*, 79, 3, 297-307, 0265-931X

Todorović, D.; Radenković, M.; Popović, D.; Tasić, M. & Rajšić, S. (2005). Ground Level Air Radiaoctivity Monitoring In Belgrade Urban Area. In: *Recent Advances In Multi-disciplinary Applied Physics,* Mendey-Vilas, A. (Ed.), 479-486, Elsevier, 0-08-044648-5, Amsterdam

Todorovic, D.; Popovic, D.; Rajsic, S. & Tasic, M. (2007). Radionuclides and Particulate Matter in Belgrade Air, In: *Environmental Research Trends*, Cato, M. A. (Ed.), 271-301, Nova Science Publishers Inc., 978-1-60021-556-8, New York

Todorović, D.; Ajtić, J.; Popović, D. & Nikolić, J. (2009). Radionuclides in plants in urban areas, *Proceedings of the XXV Serbia and Montenegro Radiation Protection Society Symposium*, pp. 39-42, 978-86-7306-112-2, Kopaonik, September 2009, Institute of Nuclear Sciences Vinca and Serbia and Montenegro Radiation Protection Society, Belgrade

Tomašević, M.; Vukmirović, Z.; Rajšić, S.; Tasić, M. & Stevanović, B. (2008). Contribution to biomonitoring of some trace metals by deciduous tree leaves in urban areas. *Environmental Monitoring and Assessment,* 137, 16, 393-401, 0167-6393

Tyler, G. (1990). Bryophytes and heavy metals: a literature review. *Botanical Journal of the Linnean Society*, 104, 231–253, 0024-4074

Uğur, A.; Özden, B.; Saç, M. M. & Yener, G. (2003). Biomonitoring of [210]Po and ^{210}Pb using lichens and mosses around a uraniferous coal-fired power plant in western Turkey. *Atmospheric Environment*, 37, 16, 2237-2245, 1352-2310

UNCEAR (1988). *Sources, Effects and Risks of Ionizing Radiation*. United Nation Committee for the Effects of Atomic Radiation, 92-1-1-142143-8, New York

UNEP (2002). *Report: Post-Conflict Environmental Assessment Report On Depleted Uranium In Serbia and Montenegro*. United Nations Environment Programme, 92-807-2146-1, Geneva

Uchida, S.; Tagami, K. & Hirai, I. (2007). Soil-to-Plant Transfer Factors of Stable Elements and Naturally Occurring Radionuclides (1) Upland Field Crops Collected in Japan. *Journal of Nuclear Science and Technology*, 44, 4, 628-640, 0022-3131

Vandenhove, H.; Olyslaegers, G.; Sanzharova, N.; Shubina, O.; Reed, E.; Shang, Z. & Velasco, H. (2009). Proposal for new best estimates of the soil-to-plant transfer factor of U, Th, Ra, Pb and Po. *Journal of Environmental Radioactivity*, 100, 9, 721-732, 0265-931X

Van der Gon, H. D. & Appelman, W. (2009). Lead emissions from road transport in Europe. *Science of the Total Environment*, 407, 5367-5372, 0048-9697

Vasconcelos, M. T. S. D. & Tavares, H. M. F. (1998). Atmospheric metal pollution (Cr, Cu, Fe, Mn, Ni, Pb and Zn) in Oporto city derived from results for low-volume aerosol samplers and for the moss Sphagnum auriculatum bioindicator. *Science of the Total Environment*, 212, 11–20, 0048-9697

Characteristics and application of receptor models to the atmospheric aerosols research

Zoran Mijić[a], Slavica Rajšić[a], Andrijana Žekić[b],
Mirjana Perišić[a], Andreja Stojić[a] and Mirjana Tasić[a]

[a]Institute of Physics, University of Belgrade, 11080, Belgrade, Serbia
[b]Faculty of Physics, University of Belgrade, 11000, Belgrade, Serbia

1. Introduction

Atmospheric aerosols can be defined as solid and liquid particles suspended in air. Due to their confirmed role in climate change (IPCC, 2001), impact on human health (Dockery and Pope, 1994; Schwartz et al., 1996; Schwartz et al., 2001; WHO, 2002, 2003; Dockery and Pope, 2006), role on the radiative budget (IPCC, 2007), effects on ecosystems (Niyogi et al., 2004; Bytnerowicz et al., 2007), and local visibility they are of major scientific interest. The human activities in various aspects cause a change in the natural air quality. This change is more marked in very inhabited areas with high industrialization. Epidemiological research over the past 15 years has revealed a consistent statistical correlation between levels of airborne particulate matter (PM) and adverse human health effects (Pope et al., 2004; Dockery and Stone, 2007). Airborne particulate matter contains a wide range of substances, such as heavy metals, organic compounds, acidic gases, etc. Chemical reactions occurring on aerosols in the atmosphere can transform hazardous components and increase or decrease their potential for adverse health effects. Especially organic compounds react readily with atmospheric oxidants, and since small particles have a high surface-to-volume ratio, their chemical composition can be efficiently changed by interaction with trace gases such as ozone and nitrogen oxides. The impact of atmospheric aerosols on the radiative balance of the Earth is of comparable magnitude to greenhouse gases effect (Anderson et al., 2003). Atmospheric aerosol in the troposphere influences climate in two ways: directly, through the reflection and absorption of solar radiation, and indirectly through the modification of the optical properties and lifetime of clouds. Estimation of the radiative forcing induced by atmospheric aerosols is much more complex and uncertain compared with the well-mixed greenhouse gases because of the complex physical and chemical processes involved with aerosols and because of their short lifetimes which make their distributions inherently more inhomogeneous.

In order to protect public health and the environment i.e. to control and reduce particulate matter levels, air quality standards (AQS) were issued and target values for annual and daily mean PM_{10} (particles with aerodynamic diameter less than 10 μm) and $PM_{2.5}$ (particles with aerodynamic diameter less than 2.5 μm) mass concentrations were established. For the first stage, the EU Directive (EC, 1999) required an annual limit of 40 μg m^{-3} and a 24h limit

of 50 μg m^{-3} (not to be exceeded more than 35 times in a calendar year) for PM$_{10}$ to be met by 2005. In the spring 2008 EU decided on the future PM$_{10}$ regulations and the conclusions are that PM$_{10}$ regulations have been somewhat relaxed despite the fact that the numerical values of the limits have not changed (EC, 2008). The annual PM$_{2.5}$ limit value was set on 25 μg m^{-3}, to be met in 2015 (WHO, 2006). The discussion of these limit values, regulations and relations of new EU standards to US EPA standards can be found elsewhere (Brunekreef and Maynard, 2008). Many epidemiology studies related to the adequacy of the new cut off values were published (Pope et al., 2002; Laden et al., 2006). Although current regulations only target total mass concentrations, future regulations could be focused on to the specific components that are related to inducing the adverse health effects.

One of the main difficulties in air pollution management is to determine the quantitative relationship between ambient air quality and pollutant sources. Source apportionment is the process of identification of aerosols emission sources and quantification of the contribution of these sources to the aerosol mass and composition. The term "source" should be considered short for "source type" because this more general term accounts for the potential that there could be a cluster of sources within short distances of each other and/or there could be multiple sources along the wind flow pattern reaching the receptor thereby creating source types. Identification of pollutant sources is the first step in the process of devising effective strategies to control pollutants. After sources are identified, characterization of the source's emission rate and emission inventory can be followed by the development of a control strategy including the possibility of revised or new regulations.

Although significant improvements have been made over the past decades in the mathematical modelling of the dispersion of pollutants in the atmosphere, there are still many instances where the models are insufficient to permit the full development of effective and efficient air quality management strategies (Hopke, 1991). These difficulties often arise due to incomplete or inaccurate source inventories for many pollutants. Therefore it is necessary to have alternative methods available to assist in the identification of sources and the source apportionment of the observed pollutant concentrations. These methods are called receptor-oriented or receptor models since they are focused on the behaviour of the ambient environment at the point of impact as opposed to the source-oriented dispersion models that focus on the transport, dilution, and transformations that begins at the source and continue until the pollutants reach the sampling or receptor site. The problem is, using the data measured at the receptor site alone, to estimate the number of sources, to identify source composition and most importantly, from a regulatory point of view, to asses the source contributions to the total mass of each sample.

This paper will briefly review the most popular receptor models that have been applied to solve the general mixture problem and link ambient air pollutants with their sources. Some of these models will be applied on originally PM data set from Belgrade and the results will be discussed. Atmospheric monthly deposition fluxes for Belgrade urban area already determined were also used to demonstrate the applicability of receptor modelling for pollution source apportionment. Deposition fluxes were calculated from monthly sampled bulk deposits composed from dry and wet atmospheric deposition.

2. Receptor Modelling

The fundamental principle of receptor modelling is that the mass conversation can be assumed and a mass balance analysis can be used to identify and apportion sources of airborne particulate matter. In order to obtain data set for receptor modelling individual chemical measurements can be performed at the receptor site what is usually done by collecting particulate matter on a filter and analyzing it for the elements and other constituents. Electron microscopy can be used to characterize the composition, size and shape of particles as well. If we assume that N samples are analyzed for n species which come from m sources a mass balance equation can be written as

$$C_{ij} = \sum_{k=1}^{m} a_{jk} S_{ik} + e_{ij} \quad i = 1,...N; j = 1,...n \tag{1}$$

where C_{ij} is the concentration of the j-th species in the i-th sample. The mass fraction of species j in source k is a_{jk} (e.g. source composition) and S_{ik} is the total mass of material from source k in the i sample (e.g. source contribution). Obviously, equation above represents the general mixture problem and includes errors e_{ij} which may be the result of analytical uncertainty and variations in the source composition. It is well known that there are insufficient numbers of constraints to define a unique solution, therefore this problem is related to the class of so called ill-posed problems. There is variety of ways to solve equation (1) depending on some physical constraints (like non negativity of source composition and contribution) and a priori knowledge about sources (Henry et. al., 1984; Kim and Henry, 2000).

From a receptor point of view, pollutants can be roughly categorized into three source types: source known, known source tracers (i.e. pollutant is emitted with another well characterized pollutant) and source unknown. One of the main differences between models is the degree of knowledge required about the pollution sources prior to the application of receptor models. The two main extremes of receptor models are chemical mass balance (CMB) and multivariate models.

The chemical mass balance method requires knowledge of both the concentrations of various chemical components of the ambient aerosol and their fractions in source emissions. A complete knowledge of the composition of emissions from all contributing sources is needed and if changes of the source profiles between the emitter and the receptor may be considered as minimal, CMB can be regarded as the ideal receptor model. This method assumes a priori that certain classes of sources are responsible for ambient concentrations of elements measured at the receptor. Furthermore it is assumed that each source under consideration emits a characteristic and conservative set of elements. However, these requirements are almost never completely fulfilled, and thus, pure CMB approaches are often problematic. For sources that have known tracers but do not have complete emission profiles, factor analysis tools such as Principal Component Analysis (PCA), UNMIX, Positive Matrix Factorization (PMF) can be used to identify source tracers. These are commonly used tools, because software to perform this type of analysis is widely available and detailed prior knowledge of the sources and source profiles is not required. There are many related published papers (Poirot et al., 2001; Song et al., 2001; Azimi et al., 2005; Elbir et al., 2007; Olson et al., 2007; Brown et al., 2007; Song et al., 2008; Duan et al., 2008; Nicolas et al., 2008; Marković et al., 2008; Aničić et al., 2009). Principal component and factor

analyses attempt to simplify the description of a system by determining a minimum set of basis vectors that span the data space to be interpreted. PCA derives a limited set of components that explain as much of the total variance of all the observable variables (e.g., trace element concentrations) as possible. An alternative approach called Absolute Principal Components Analysis (APCA) (Thurston and Spengler, 1985) has also been used to produce quantitative apportionments.

For pollutant sources that are unknown, hybrid models that incorporate wind trajectories (Residence Time Analysis, Potential Source Contribution Function (PSCF), Concentration Weighted Trajectory (CWT) can be used to resolve source locations. Hybrid models combine the advantages and reduce the disadvantages of CMB and factor analysis. The multilinear engine (ME) can solve multilinear problems with the possibility of implementing many kinds of constraints using a script language. Receptor models offer a powerful advantage to the source attribution process as their results are based on the interpretation of actual measured ambient data, what is especially important when ubiquitous area sources exist (e.g., windblown dust). Dispersion models can estimate point source contributions reliably if the source and atmospheric conditions are well characterized. From a mathematical point of view none of these models can give a unique solution but only solutions physically acceptable with different probability levels. These models therefore must be integrated by an at least indicative knowledge of the source profiles and/or by specific analyses such as the determination of the dimensional and morphological characterizations of the particulate matter. The comparison of source apportionment results from different European regions is very complex and many recent publications focus on this issue (Viana et.al, 2008). The combined application of different types of receptor models could possibly solve the limitations of the individual models, by constructing a more robust solution based on their strengths. Each modelling approach was found to have some advantages compared to the others. Thus, when used together, they provide better information on source areas and contribution than it could be obtained by using only one of them.

When evaluating the European publications (Vianna et. al. 2008) PCA was the most frequently used model up to 2005, followed by back-trajectory analysis. Other models commonly used were PMF, CMB and mass balance analysis. Data from 2006–2007 show a continued use of PCA (50% of the new publications) and an increase in the use of PMF and Unmix. Investigation of uncertainty estimates for source apportionment studies as well as quantification of natural emission sources and specific anthropogenic sources is of growing interest, therefore the US Environmental Protection Agency supported development user friendly software for some receptor models which is widely available.

The capabilities of some of the most commonly used models (PMF, Unmix, PSCF and CWT) will be demonstrated using original data set obtained in Belgrade and the fundamentals of these models are described below.

2.1 Unmix

The latest version of Unmix is available from the US Environmental Protection Agency (U.S. EPA, 2007). The concepts underlying Unmix have already been presented in geometrical and intuitive manner (Henry, 1997) and mathematical details are presented elsewhere (Henry, 2003). If the data consist of many observations of n species, then the data can be plotted in an n-dimensional data space where the coordinates of a data point are the observed concentrations of the species during a sampling period. The problem is to find the

vectors (or points) that represent the source composition. In the case of two sources the data are distributed in a plane through the origin. If one source is missing from some of the data points, then these points will lie along a ray defined by the composition of the single, remaining source. Points that have one source missing are the key for solving the mixture problem. The appropriate number of these vectors (also called factors) is determined using computationally intensive method known as the NUMFACT algorithm (Henry et. al., 1999). If there are N sources, the data space can be reduced to an $N-1$-dimensional space. Fig. 1 illustrates the essential geometry of multivariate receptor models for three sources of three species, the most complex case that can be easily graphed. It is assumed that for each source there are some data points where the contribution of the source is not present or small compared to the other sources. These are called edge points and Unmix works by finding these points and fitting a hyperplane through them; this hyperplane is called an edge (if $N = 3$, the hyperplane is a line). For any number of sources and species, the relative source composition can be identified if there are sufficient edge points for each source to define identified edges in the data space. The source vectors are plotted in the direction of the source compositions and the open circles are observed data. The non-negativity constraints on the data and the source compositions require that the vectors and data lie in the first quadrant. Furthermore, the non-negativity of the source contributions requires that all the open circles lie inside the region bounded by the source vectors. This is made easier to see by projecting the data and source vectors from the origin into a plane. The source vectors are the vertices of a triangle in this plot and the projected data points are the filled circles. The solution to the multivariate receptor modelling problem can now be seen as finding three points that represent the source compositions that form a triangle that encloses the data points and lie in the first quadrant, thus guaranteeing the nonnegativity constraints are satisfied. The edge-finding algorithm developed for Unmix is completely general and can be applied to any set of points in a space of arbitrary dimension. Unmix itself can be applied to any problem in which the data are a convex combination of underlying factors. The only restriction is that the data must be strictly positive.

Some special features of Unmix are the capability to replace missing data and the ability to estimate large numbers of sources (the current limit is 15) using duality concepts applied to receptor modelling (Henry, 2005). Unmix also estimates uncertainties in the source compositions using a blocked bootstrap approach that takes into account serial correlation in the data.
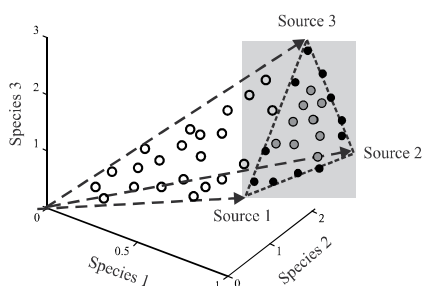

Fig. 1. Plot of three sources and three species case: the grey dots are the raw data projected to a plane, and the solid black dots are the projected points that have one source missing (edge points)

2.2 Positive Matrix Factorization (PMF)

Positive Matrix Factorization (PMF) has been shown to be a powerful receptor modelling tool and has been commonly applied to particulate matter data (Song et al., 2001; Pollisar et al., 2001; Chuenita et. al., 2000) and recently to VOC (volatile organic compounds) data (Elbir et al., 2007; Song et al., 2008). To ensure that receptor modelling tools are available for use in the development and implementation of air quality standards, the United States Environmental Protection Agency's Office of Research and Development has developed a version of PMF with the name of EPA PMF1.1 that is freely available (Eberly, 2005).

PMF solves the general receptor modelling equation using a constrained, weighted, least-squares approach (Paatero, 1993; Paatero and Tapper, 1993; Paatero and Tapper, 1994, Paatero, 1997; Paatero, 1999; Paatero, et. al., 2005; Paatero and Hopke, 2003). The general model assumes there are p sources, source types or source regions (termed factors) impacting a receptor, and linear combinations of the impacts from the p factors give rise to the observed concentrations of the various species.

The model can be written as

$$x_{ij} = \sum_{k=1}^{p} g_{ik} f_{kj} + e_{ij} \tag{2}$$

where x_{ij} is the concentration at the receptor for the j-th species on the i-th sample, g_{ik} is the contribution of the k-th factor to the receptor on the i-th sample, f_{kj} is the fraction of k factor that is species j or chemical composition profile of factor k and e_{ij} is the residual for the j-th species on the i-th sample. The objective of PMF is to minimize the sum of the squares of the residuals weighted inversely with error estimates of the data points. Furthermore, PMF constrains all of the elements of G and F to be non-negative. The task of PMF analysis can thus be described as to minimize Q, which is defined as

$$Q = \sum_{i=1}^{n} \sum_{j=1}^{p} \left(\frac{x_{ij} - \sum_{k=1}^{p} g_{ik} f_{kj}}{s_{ij}} \right)^2 \tag{3}$$

where s_{ij} is uncertainty of the j-th species measured in i-th sample.

In this study the robust mode has been used for analyzing element concentrations in bulk atmospheric deposition data set. The robust mode was selected to handle outlier values (that is any data that significantly deviates from the distribution of the other data in the data matrix) meaning that outliers are not allowed to overly influence the fitting of the contributions and profiles. This can be achieved by a technique of iterative reweighing of the individual data values, thus, the least-squares formulation becomes to

$$Q = \sum_{i=1}^{n} \sum_{j=1}^{m} \left(\frac{e_{ij}}{h_{ij} s_{ij}} \right)^2 \tag{4}$$

where

$$h_{ij}^2 = \begin{cases} 1 & \text{if } \left| e_{ij} / s_{ij} \right| \le \alpha, \\ \left| e_{ij} / s_{ij} \right| / \alpha & \text{otherwise} \end{cases}$$

The parameter α is called the outlier threshold distance and the value $\alpha = 4$ was used in this analysis. One of the most important advantages of PMF is the ability to handle missing and below detection limit data by adjusting the corresponding error estimates. In this analysis missing values were replaced with the geometrical mean of the measured concentrations for each chemical species, and large error estimates were used for them.

2.3. Potential Source Contribution Function (PSCF)

The potential source contribution function (PSCF) was originally presented by Ashbaugh et. al. (1985) and Malm et.al. (1986). It has been applied in a series of studies over a variety of geographical scales (Gao et. al., 1993; Cheng et.al., 1993). Air parcel back trajectories, ending at the receptor site, are represented by segment endpoints. Each endpoint has two coordinates (latitude, longitude) representing the central location of an air parcel at a particulate time. To calculate PSCF, the whole geographic region of interest is divided into an array of grid cells whose size is dependent on the geographical scale of the problem so that PSCF will be a function of locations as defined by the cell indices i and j. The construct of the potential source contribution function can be described as follows: if a trajectory end point lies at a cell of address (i, j), the trajectory is assumed to collect material emitted in the cell. Once aerosol is incorporated into the air parcel, it can be transported along the trajectory to the receptor site. The objective is to develop a probability field suggesting likely source locations of the material that results in high measured values at the receptor site.

Let N be the total number of trajectory segment endpoints during the whole study period. If segment trajectory endpoints fall into the ij-th cell (represented by n_{ij}) the probability of this event is given by

$$P[A_{ij}] = \frac{n_{ij}}{N} \tag{5}$$

where $P[A_{ij}]$ is a measure of the residence time of a randomly selected air parcel in the ij-th cell relative to the total time period. In the same ij cell there is a subset of m_{ij} segment endpoints for which the corresponding trajectories arrive at the receptor site at the time when the measured concentration are higher than a pre-specified criterion value. The choice of this criterion values has usually based on trial and error and in many applications, the mean value of the measured concentration was used. In some publications the use of the 60th and 75th percentile criterion produced results that appeared to correspond better with known emission source locations. Thus, the probability of this high concentration event is given by

$$P[B_{ij}] = \frac{m_{ij}}{N} \tag{6}$$

where $P[B_{ij}]$ is subset probability related to the residence time of air parcel in the ij-th cell for the contaminated air parcel. Finally, the potential source contribution function is defined as

$$PSCF_{ij} = P[B_{ij} \mid A_{ij}] = \frac{m_{ij}}{n_{ij}} \tag{7}$$

where $PSCF$ is the conditional probability that an air parcel which passed through the ij-th cell had a high concentration upon arrival at the receptor site. A sufficient number of endpoints should provide accurate estimates of the source location. Cells containing emission sources would be identified with conditional probability close to 1, if the trajectories that have crossed over the cells effectively transport the emitted contaminant to the receptor site. One can draw the conclusion that PSCF model provides a map of source potential of geographical areas, but it can not apportion the contribution of the identified source area to the measured concentration at the receptor site. Thus, the potential source contribution function can be interpreted as a conditional probability describing the spatial distribution of probable geographical source locations inferred by using trajectories arriving at the sampling site. Cells related to the high values of potential source contribution function are the potential source areas. However, the potential source contribution function maps do not provide an emission inventory of a pollutant but rather show those source areas whose emissions can be transported to the measurement site. To reduce the effect of small values of n_{ij}, an arbitrary weight function $W(n_{ij})$ is multiplied into the PSCF value to better reflect the uncertainty in the values for these cells.

2.4. Concentration Weighted Trajectory (CWT)

In the current PSCF method, grid cells having the same PSCF values can result from samples of slightly higher than the criterion concentrations or extremely high concentrations. As a result, larger sources can not be distinguished from moderate sources. According to this problem, a method of weighting trajectories with associated concentrations (CWT - concentration weighted trajectory) was developed (Hsu et. al, 2003). In this procedure, each grid cell gets a weighted concentration obtained by averaging sample concentrations that have associated trajectories that crossed that grid cell as follows:

$$C_{ij} = \frac{1}{\sum_{l=1}^{M} \tau_{ijl}} \sum_{l=1}^{M} C_l \tau_{ijl} \tag{8}$$

C_{ij} is the average weighted concentration in the grid cell (i,j), C_l is the measured PM concentration observed on arrival of trajectory l, τ_{ijl} is the number of trajectory endpoints in the grid cell (i,j) associated with the C_l sample, and M is the total number of trajectories. Similar to PSCF model, a point filter is applied as the final step of CWT to eliminate grid cells with few endpoints. Weighted concentration fields show concentration gradients across potential sources. This method helps determine the relative significance of potential sources.

3. Experimental Methods and Procedures

3.1 Studies Sites and Sampling

Sampling of particulate matter PM_{10} and $PM_{2.5}$ started in the very urban area of Belgrade in June 2002 and has continued afterwards. Belgrade, (Hs = 117 m, $\varphi = 44^0\,44^{'}$ N and $\lambda = 20^0\,27^{'}$ E) the capital of Serbia, with about 2 million inhabitants, is situated at the confluence of the Sava and Danube rivers. The sampling site was the platform above the entrance steps to the Faculty of Veterinary Medicine (FVM) at a height of about 4 m from the ground, 5 m away from a street with heavy traffic and close to the big Autokomanda junction with the main state highway. This point can be considered as traffic-exposed. During the sampling, meteorological parameters including temperature, relative humidity, rainfall, wind direction and speed were provided by the Meteorological Station of the Hydro-Meteorological Institute of the Republic of Serbia located inside the central urban area, very close (≈ 200 m) to the Autokomanda sampling site.

Suspended particles were collected on preconditioned and pre-weighed Pure Teflon filters (Whatman, 47 mm diameter, 2 μm pore size) and Teflon-coated Quartz filters (Whatman, 47 mm diameter) using two MiniVol air samplers (Airmetrics Co. Inc., 5 l min^{-1} flow rate) provided with PM_{10} and $PM_{2.5}$ cutoff inlets. Particulate matter mass concentration was determined by weighting of the filters using a semi-micro balance (Sartorius, R 160P), with a minimum resolution of 0.01 mg. Loaded and unloaded filters (stored in Petri dishes) were weighed after 48 hours conditioning in a desiccator, in the clean room at a relative humidity of 45-55% and a temperature of 20 ± 2 ˚C. Quality assurance was provided by simultaneous measurements of a set of three ''weigh blank'' filters that were interspersed within the pre- and post- weighing sessions of each set of sample filters and the mean change in "weigh blank" filter mass between weighing sessions was used to correct the sample filter mass changes. After completion of gravimetric analysis, PM samples were digested in 0.1 N HNO3 on an ultrasonic bath. An extraction procedure with dilute acid was used for the evaluation of elements which can become labile depending on the acidity of the environment. This procedure gives valid information on the extractability of elements, since the soluble components in an aerosol are normally dissolved by contact with water or acidic solution in the actual environment. Details on sampling procedures and PM analysis are given in detail elsewhere (Rajšić et al., 2004; Tasić et al., 2005; Rajšić et al., 2008, Mijić et. al., 2009).

The bulk deposition (BD) collection was performed using an open polyethylene cylinder (29 cm inner diameter and 40 cm height) fitted on a stand at about 2 m above the ground. The devices collected both rainwater and the fallout of particles continuously for one month periods from June 2002 to December 2006 at FVM site. The collection bottles were filled before each sampling period with 20 ml of 10% acidified (HNO3 65% (Suprapure, Merck) ultra pure water. Precautions were taken to avoid contamination of samples in both the field and laboratory. Details on studied sites and sampling procedures are given by Tasić et al (2008; 2009).

The elemental composition (Al, V, Cr, Mn, Fe, Ni, Cu, Zn, Cd, and Pb) of the aerosol samples and bulk deposition, was measured by the atomic absorption spectroscopy (AAS) method. Depending on concentration levels, samples were analyzed for a set of elements by flame (FAAS) (Perkin Elmer AA 200) and graphite furnace atomic absorption spectrometry (GFAAS) using the transversely-heated graphite atomizer (THGA; Perkin Elmer AA 600) with Zeeman-effect background correction.

3.2 Scanning Electron Microscopy

Scanning electron microscopy (SEM) coupled with Energy-Dispersive X-ray analysis (EDX) was used for the characterization (size, size distribution, morphology and chemistry of particles) of suspended atmospheric particulate matter in order to improve source identification (US-EPA, 2002).

Approximately 0.5x0.5 cm^2 of the quartz filter was cut off and mounted onto an copper SEM stub using carbon conducting tap and then coated with a thin gold film (<10 nm) using JFC 1100 ion sputterer in order to get a higher quality secondary electron image. The measurements were carried out by the JEOL 840A instrument with INCAPentaFETx3 energy dispersive X-ray microanalyzer at the Faculty of Physics, Belgrade. The electron beam energy was 0-20 keV, probe current of the order of 100 μA and magnification up to 10 000. Analyzing SEM images we determined the particle size distribution in relation to heating and non-heating period. Further more, shape factor (SF) defined as

$$SF = 4\pi \frac{A}{P^2} \qquad (9)$$

where, A is the particle area and P is the particle perimeter was determined. The perimeter refers to the circumference of the projected area and the area refers to the projected area of a particle. Both parameters are derived from SEM images. For a perfect circle SF equals one, and SF decreases as the circle is more and more distorted (for example SF equal to 0.785 for square like and 0.436 for oblong). The SF was determined for all particles analyzed and SF-size distributions were established based on these data. Shape factor distribution can reveal the dominant shape groups of the particles and thus contribute to identification of source emission.

3.3 Receptor Models Application

In the current study, the Unmix model and PMF have been used to analyze a 2-years PM$_{2.5}$ data set and 5-years element bulk depositions respectively for source apportionment purpose. The analysis generated source profiles and overall percentage source contribution estimates for source categories.

Demonstration of PSCF and CWT usage was presented on five years PM$_{10}$ data set (2004-2008) continuously recorded by the Institute of Public Health of Belgrade and Trajstat software (Wang et al., 2008). The PSCF value can be interpreted as the conditional probability that the PM concentrations greater than the criterion level (in this case PM average value for the investigated period) are related to the passage of air parcels through the ij-th cell during transport to the receptor site. Cells with high PSCF values are associated with the arrival of air parcels at the receptor site that have concentrations of the PM higher than the criterion value. These cells are indicative of areas of high potential contributions for the PM. Air masses back trajectories were computed by HYSPLIT (HYbrid Single Particle Lagrangian Integrated Trajectory) model (Draxler, 2010; Rolph, 2010) throw interactive READY system. Backward trajectories started at different heights traverse different distances and pathways. For longer range transport (>24h), trajectories that started at different heights may vary significantly. If this occurs, PSCF modelling results might also be different. Daily back trajectories were evaluated for 2 days and different heights (m) above ground level (300, 500, 1000, 1500, 2000, 3000). The grid covers area of interest with cells 0.5^{0}x0.5^0 latitude and longitude.

4. Results and Discussion

4.1 Unmix Model – PM$_{2.5}$

Descriptive statistic for daily mass and trace element concentrations in PM$_{2.5}$ sampled in urban Belgrade, during the period from June 2003 through July 2005, is given in details by Rajšić et al (2008). Unmix receptor model was run with 50 observations of 10 input variables (Al, V, Cr, Mn, Fe, Ni, Cu, Zn, Cd, and Pb). Three factors were chosen as the optimum number for the Unmix model, details of which are discussed as follows. The element profiles of the sources for PM $_{2.5}$ are given in Table 1.

The first profile extracted by Unmix is the **fossil fuel combustion** source having the high loadings of Ni and V, which are the fingerprint elements for fuel oil burning. It also includes high loadings of Cu and Cr which are also characteristics of emissions by vehicles using diesel fuel and local industry. This source most probably reflects urban region where residual oils are common fuels for utility and industrial sources and it has average contribution of 40%.

The second Unmix profile has high loadings of Cd that is typical for emission of high temperature combustion processes such as **metallurgical industry** and fossil fuel combustion. This factor having also low loadings of Fe accounts for 13% of the total and can be indicated as industry source.

The third Unmix profile is dominated by Al, Zn, Fe, Mn and Cr with average contribution of 47%. Its bulk matrix is soil, while correlations with other metals indicate some other sources, such as tire treat, brake-drum abrasion etc. This factor is interpreted as **resuspended road dust**, which includes soil dust mixed with traffic related particles.

Scatter-plots of measured and Unmix predicted PM$_{2.5}$ element (Zn, Mn, Al, Cd) concentrations are presented in Fig. 2. The correlation coefficients are in the range of 0.7-0.94. The results of Unmix modelling on PM$_{2.5}$ samples indicate that resuspended road dust and fossil fuel combustion play the most significant role.

	Fossil fuel combustion	Metallurgical industry	Resuspended road dust
Pb	5.36	1.53	16.70
Cu	30.10	0	0
Zn	60.40	0	1900
Mn	2.97	0	13.40
Fe	0	288	852
Cd	0	0.75	0.02
Ni	72.60	0	0
V	69.30	0	0
Al	0	0	1740
Cr	3.00	0	2.07

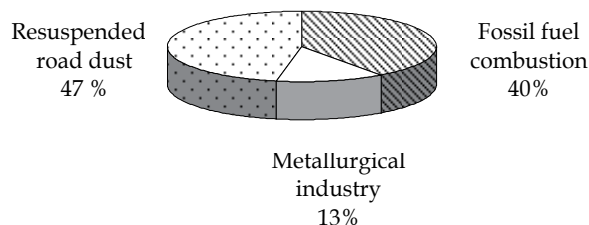Table 1. The element profile of the sources for PM$_{2.5}$ resolved by Unmix

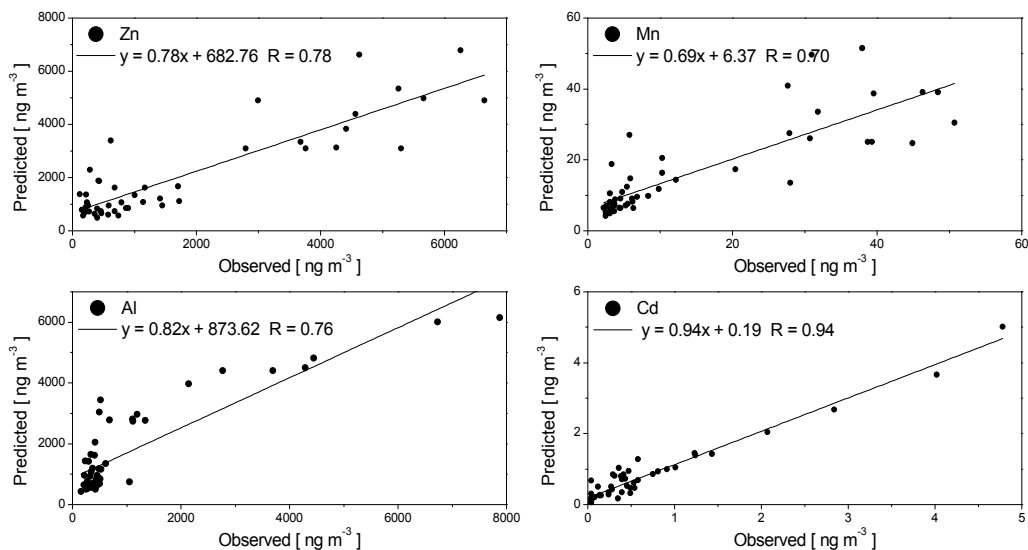Fig. 2. Unmix resolved source contribution in PM$_{2.5}$

Fig. 3. Scatter-plots of measured and Unmix predicted PM$_{2.5}$ element concentrations

4.2 PMF - Total Deposition

A total of 53 atmospheric deposit samples were collected monthly from June 2002 to December 2006 at FVM site, and element (Al, V, Cr, Mn, Fe, Ni, Cu, Zn, Cd, and Pb) monthly fluxes were calculated. The statistical results of monthly element bulk deposition fluxes (BD), annual bulk deposition fluxes and seasonal variation are presented in detail by Tasić et al (2009). For source apportionment purpose, the PMF model was applied on element BD data set and resulted in six factors which have been identified as possible sources. The identified source profiles and time series plots of estimated monthly contributions for bulk depositions are presented on Fig 4.
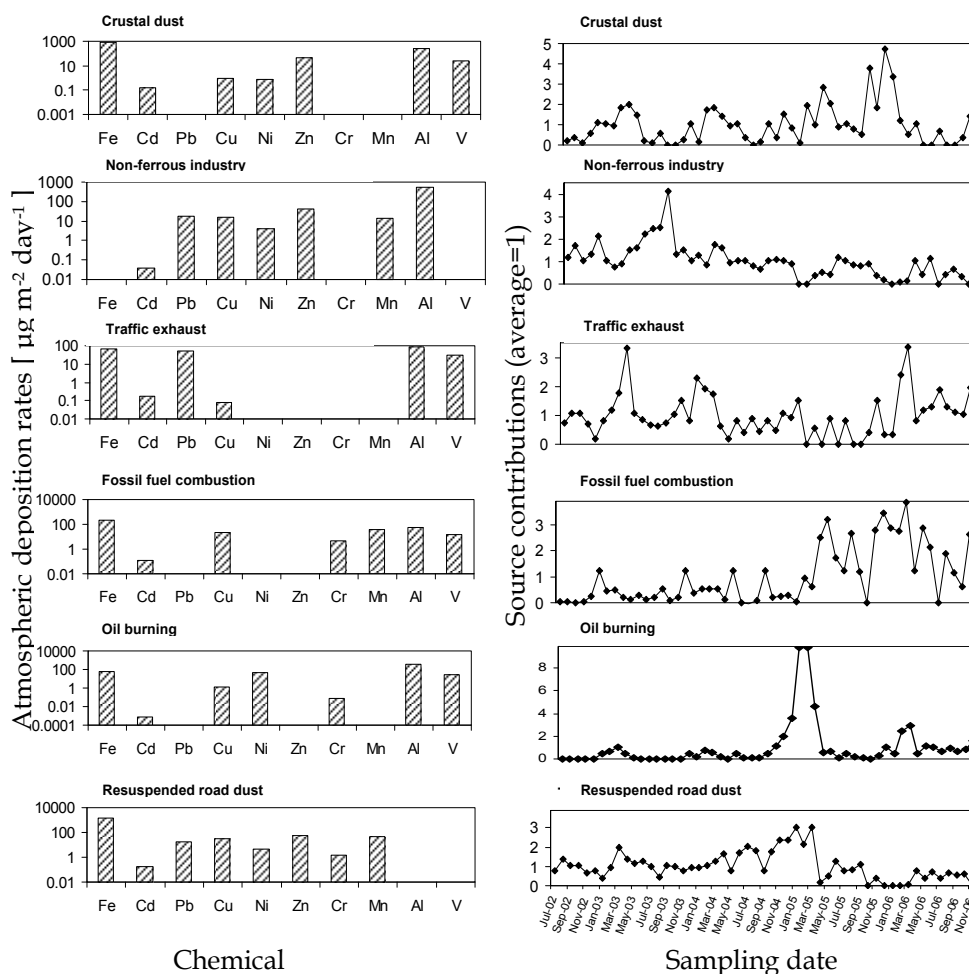
Fig. 4. Source profiles and time series plot of source contribution resolved from bulk deposition by PMF
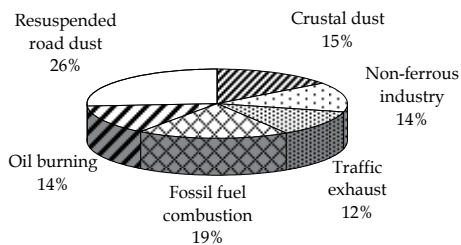

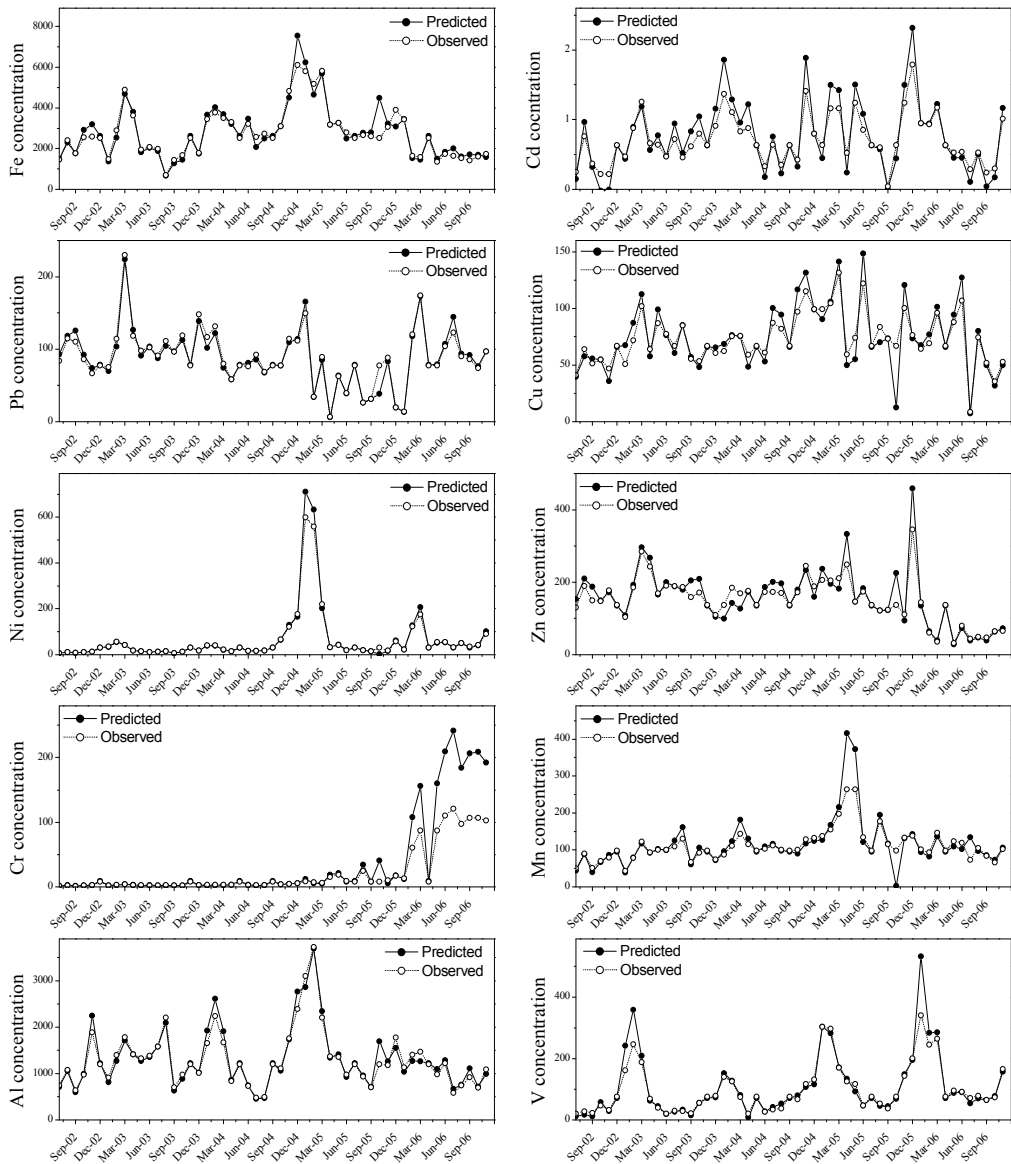Fig. 5. PMF source contribution in bulk deposition

Fig. 6. Time series plot of observed and PMF predicted element bulk deposition in Belgrade

The first factor dominated by Fe, Zn, Al, V and Cd accounted for 15% of the total variance and can be attributed to **crustal dust** contaminated with traffic related particles. Fe and Al are typical crustal elements; Zn is also one of the most common elements in the Earth crust. The second factor with high loadings of Al, Zn, Mn, Cu and Pb is related to **non ferrous metal industry** with contribution of 14%. The third factor resolved from the BD data is attributed to **traffic exhaust** source mostly loaded with Pb, V and Cd with overall contribution of 12 %. Pb probably comes from exhaust emission, since road vehicles use loaded gasoline or diesel fuel while Cd is related to fossil fuel combustion. The fourth factor

characterized by Cr, Cu, Cd, Mn and V. The greatest influence of Cr, can be attributed to the emission from **fossil fuel combustion**, probably mostly coal combustion. Manganese, typically dominated by crustal contributions, has been identified in the atmosphere from fossil fuel combustion and industrial emission sources as well. Emissions of chromium are mostly associated with particles emitted when burning fossil fuels, which includes power stations, cars and trucks. The emissions largely depend on the chromium content of the fuel, which varies with both the fuel type and source. Specific sources of chromium include metal smelting and foundries, cement production, etc. This factor contributes with 19% to the total data set. The fifth factor has high loadings of Ni and V, which are the fingerprint elements for fuel **oil burning** and most probably reflects urban region where residual oils are common fuels for utility and industrial sources. This factor associated to heavy oil burning has contribution of 14%. The sixth factor dominated by Fe, Mn, Cu, Zn, Pb, Cd and Cr has contribution of 26%. Fe and Mn are typical crustal elements, which may have been present in dust resuspended by traffic; Pb, Zn, and Cu are indicator elements of traffic emission; Cu, Fe and Zn are present in resuspended brake wear particles; Fe is also related to heavy-duty diesel emissions; the high Mn concentrations are related to motor vehicles that burn gasoline with the Mn additive. This factor was identified as **resuspended road dust**.

4.3 PSCF and CWT Results

Additional insights into the nature of the identified Unmix PM sources are provided through a trajectory based evaluation of the upwind locations associated with high concentrations of these sources. Five year PM_{10} data set (2004-2008) has been used in PSCF and CWT modelling. PM_{10} data were separated for summer and winter period, and then divided into the two groups, greater and lower of average values for specific period. Calculated PSCF values were subdivided into four categories: very weak (0.0–0.20), weak (0.20–0.40), intermediate (0.40–0.60) and strong (0.60–1.0). The results of PSCF are presented in Fig 7 (left). Based on the analysis of the whole trajectory data set, the most frequently arriving directions are west, north-west and south-west thus suggesting the sampling site might be under influence of several source regions. It can be seen that the highest PSCF values are from the west during summer period as well as during winter period. In addition, higher PSCF values are observed from north and south-east during winter period.

The CWT method evenly distributes concentration along the trajectories similar to PSCF as presented on Fig. 7 (right). However, this method has an advantage over PSCF in that CWT distinguishes major sources from moderate ones by calculating concentration gradients. PSCF shows probabilities of potential sources based on samples with concentrations higher than the criterion, which does not distinguish between moderate and major sources. The results suggest that the major contribution to atmospheric PM_{10} concentrations comes from local and regional sources. There is evident a long – range transport from western countries which is sporadically (mostly in spring and summer) associated with African dust outbreaks in levels of both PM_{10} and $PM_{2.5}$ (Kubilay et al., 2000; Perez et al., 2008).
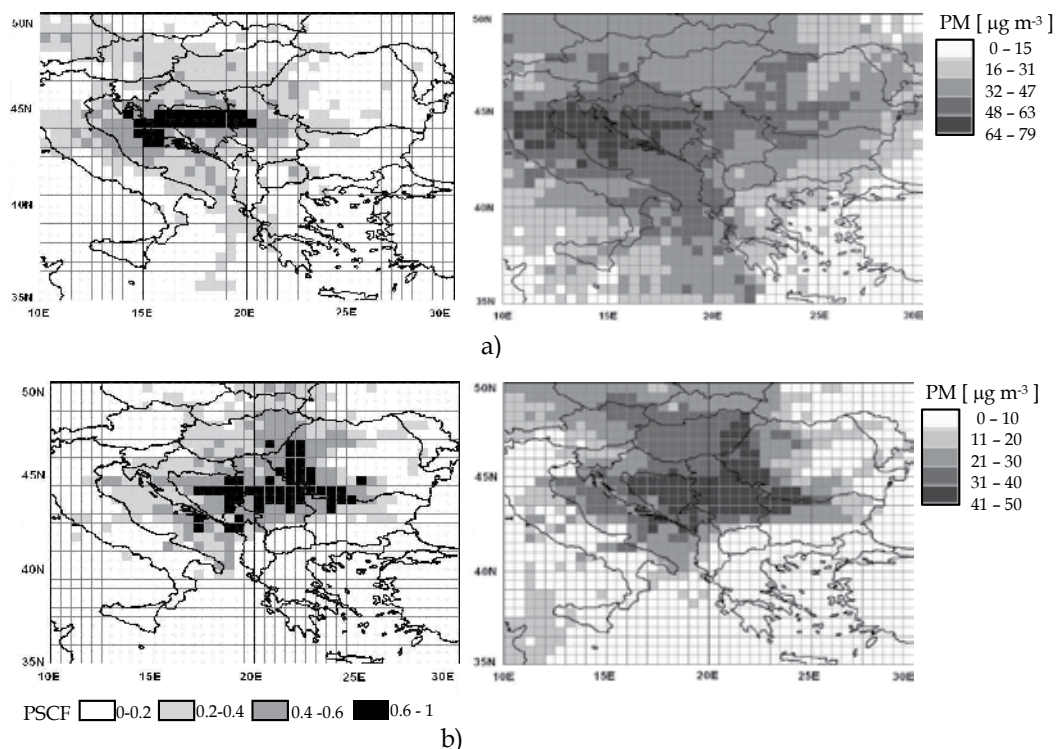
Fig. 7. Distribution of PSCF (left) and CWT (right) for PM$_{10}$ during a) summer and b) winter period 2004-2008.

4.4 SEM / EDX Characterization of Particles

Atmospheric particulate matter sampled in the urban area of Belgrade was analyzed with scanning electron microscopy coupled with energy-dispersive X-ray analysis. Particles were distinguished in terms of both particle morphology (rounded particles, mineral grains, etc.) and composition (determined by qualitative EDS analysis). Tens photomicrographs were arbitrarily taken under low resolution conditions and about 500 particles per PM sample were assessed for morphology and about 30 particles for the X-ray spectral analysis.

As the result of SEM images analysis particle size and shape distributions were determined for non-heating and heating periods and presented on Fig. 8.
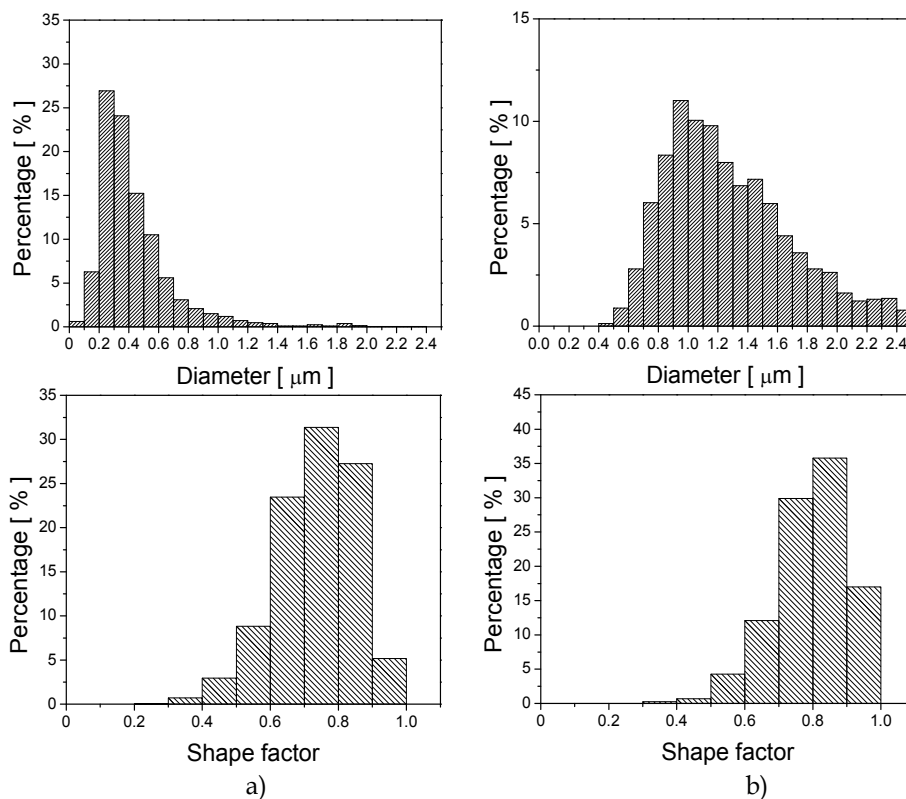
Fig. 8. Particle size distribution and shape factor of PM$_{2.5}$ samples in the a) non-heating and b) heating period.

The particle size distribution spans wider in the heating period than in the non-heating period with more coarse mean size value. Mean size value observed during heating period is 1.32 μm with standard deviation of 0.52 μm, while mean size value observed during non-heating period is 0.44 μm with standard deviation of 0.27 μm. Particles shape group with SF close to 1 (sphere like shape) obviously increase during the heating period and in the non-heating period more particles are square like. According to the morphology, two main particle categories were observed: particles of natural sources that include materials of organic origin (pollen, bacteria, fungal spores etc.) and anthropogenic particles.
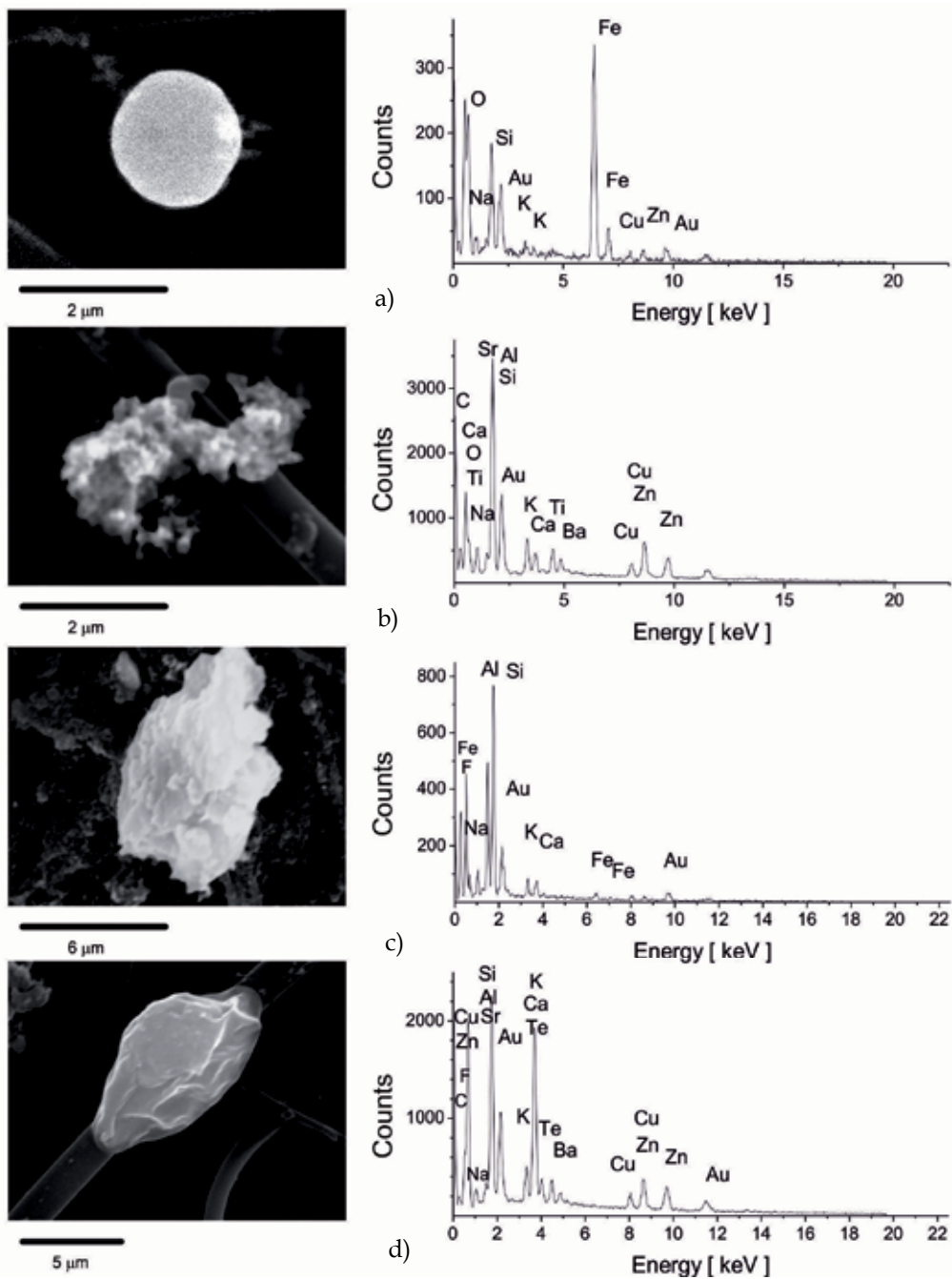
Fig. 9. SEM images of characteristic aerosol particles shape and corresponding X-ray spectra in Belgrade: (a) sphere; (b) soot agglomerate; (c) irregular; d) stick

This category also includes suspended soil dust (mostly minerals) such as the angular-shaped material. Particles from anthropogenic sources, mostly emitted from high

temperature combustion processes are characterized by their spherical shapes and smooth surfaces. This type of particles occurs as individual particles but also in an aggregate form, as agglomerates of similar-sized particles and individual large particles carrying several smaller attached particles (Tasić et al., 2006).

The elemental composition of selected particles in the secondary electron images was deduced from an energy dispersive X-ray spectrum in the energy range of 0 – 20 keV, collected from the selected particles for a spectrum acquisition time of 100 s. The elements observed were: Al, Si, C, S, N, Cl, P, K, Ca, Na, Mg, Cr, Fe, Cu, Zn, Ni, Cd, As, Ti, Te, Sr, F and V. The presence of Au lines on all spectra is due to Au coated samples. The SEM photomicrographs of some characteristic particles and their X-ray spectra are presented in Fig. 9 (a, b, c, d).

Rounded particles of complex compositions were interpreted as anthropogenic 'fly ash' particles, formed by high-temperature combustion processes. In most of the samples analysed, the spherical particles were mainly composed of Al-silicates and oxides of Fe, Zn, Cu, Ni, Pb, Ti. (Fig.9a).

Carbonaceous particles have been known to make up 50% of the aerosol in urban areas (Pandis et al., 1995) and principally consist of soot aggregates with irregular morphology of various shapes (Fig. 9b). Soot is present as agglomerates of many fine spherical primary particles originating mainly from petrol and diesel exhausts and contain C, O, Na, Si, Al, Cu, Zn, Sr, Ba, and Ti.

The most of silica particles (probably Si oxides) and aluminosilicates (containing Al, Si, K, Ca, Fe, F and Na) present in the coarse fractions have irregular forms and come from soil (Fig. 9c).

Sulphates are characterized by a strong S line in the X-ray spectrum and mostly by the presence of Ca, or Fe, Pb and K. These particles are formed as a result of the reaction in the atmosphere between sulphur compounds and other substances. Sulphate clusters, often with sharp edges are mainly composed of Ca sulphates.

Many particles, which could not be classified into one of these groups, in the coarse particle range, were mixed aggregates, irregularly shaped, consisting of soil and road dust: Si, Al with minor constituents such as C, Ca, Ba, K, Zn, Cu, Te, F and Sr, (Fig.9d).

5. Conclusion

In the field of atmospheric sciences receptor models aim to re-construct the impacts of emissions from different sources of atmospheric pollutants based on ambient data measured at the monitoring sites. The information provided by receptor models is key to the design of effective mitigation strategies of the pollutant on the local and meso-scale. In addition, many epidemiological and health-related studies used the results obtained by receptor modelling. Because of widespread need there is growing information available on receptor modelling results from different countries, the type of models applied and the input data utilised. Short review of most popular receptor models used in source apportionment studies was presented in this paper.

Several receptor models (Unmix, PMF, PSCF, CWT) were applied to PM data set and bulk deposition fluxes in Belgrade urban area for pollution source apportionment. The Unmix model identified three sources of particulate matter $PM_{2.5}$: fossil fuel combustion (40%), metallurgical industry (13%) and resuspended road dust (47%). PSCF method indicates that

the most frequently arriving directions of PM_{10} transport are west, north-west and south-west thus suggesting the sampling site might be under influence of several source regions while the results of CWT analysis suggest that the major contribution to atmospheric PM_{10} concentrations comes from local and regional sources. The PMF analysis on bulk deposition fluxes resolved six sources: crustal dust, non ferrous industry, traffic exhaust, fossil fuel combustion and oil combustion.

Both methods, Unmix and PMF followed by characterization of individual particles by SEM/EDX analysis suggested that the road traffic, fossil fuel combustion and industry are the major sources of heavy metals in the Belgrade urban atmosphere.

Receptor models, of both the mathematical (PMF and Unmix) and trajectory (PSCF and CWT) types promise to be helpful tools for source attribution for atmospheric pollution ($PM_{2.5}$ and BD). The mathematical techniques objectively identify sources of influence on the data, but a good deal of subjective judgment is inevitably required in the interpretation of what these identified sources actually represent. The ensemble trajectory techniques produce only qualitative indications of predominant transport patterns and can be highly sensitive to the subjective metrics calculated from the gridded results.

The future direction should be related to the investigation of compatibility between receptor models and combination of back trajectory modelling with source apportionment analysis in order to improve the understanding of source receptor relationships, the confidence in the individual model results, and develop a better understanding of the underlying aerosol data. Models such as PMF, ME and Unmix are able to provide uncertainty estimates by applying a bootstrapping method. Such uncertainty estimations should thus be applied in future source apportionment studies.

6. Acknowledgment

7. References

Anderson, L.T.; Charlson, J.R.; Schwartz, E.S.; Knutti, R.; Boucher, O.; Rodhe, H. & Heintzenberg, J. (2003). Climate Forcing by Aerosols--a Hazy Picture. *Science*, 300, 1103-1104

Aničić, M.; Tomašević, M.; Tasić, M.; Rajšić, S.; Popović, A.; Frontasyeva, M.V.; Lierhagen, S. & Steinnes, E. (2009). Monitoring of trace element atmospheric deposition using dry and wet moss bags: Accumulation capacity versus exposure time. *Journal of Hazardous Materials* 171, 182-188

Ashbaugh, L.L.; Malm, W.C. & Sadeh, W.Z. (1985). A residence time probability analysis of sulfur concentration at ground canyon national park. *Atmospheric Environment,* 19, 1263-1270

Azimi, S.; Rocher, V.; Muller, M.; Moilleron, R. & Thevenot, S. (2005). Sources, distribution and variability of hydrocarbons and metals in atmospheric deposition in an urban area (Paris, France). *Science of the Total Environment*, 337, 223-239

Brown, S.; Frankel, A. & Hafner, H. (2007). Source apportionment of VOCs in the Los Angeles area using positive matrix factorization. Atmospheric Environment, 41, 227-237

Brunekreef, B. & Maynard, L. R. (2008). A note on the 2008 EU standards for particulate matter. *Atmospheric Environment*, 42, 6425-6430

Bytnerowicz A; Omasa K & Paoletti E (2007). Integrated effects of air pollution and climate change on forests: a northern hemisphere perspective. *Environmental Pollution*, 147, 438–445

Chueinta, W.; Hopke, P.K. & Paatero, P. (2000). Investigation of sources of atmospheric aerosol at urban and suburban residential areas in Thailand by positive matrix factorization. *Atmospheric Environment,* 34, 3319-3329

Cheng, M.D.; Hopke, P.K. & Zeng, Y.A. (1993). A receptor methodology for determining source regions of particle sulphate composition observed at Dorset, Ontario. *Journal of Geophysical Research,* 98, 16839-16849

Dockery, D.W. & Pope III, C.A. (1994). Acute respiratory effects of particulate air pollution. *Annual Review of Public Health*, 15, 107-132

Dockery, D.W. & Pope III, C.A. (2006). Critical Review: Health Effects of Fine Particulate Air Pollution: Lines that Connect. *Journal of the Air & Waste Management Association*, 56, 709-742

Dockery D.W, & Stone PH. Cardiovascular risks from fine particulate air pollution (2007)**.** *The New England Journal of Medicine*, 356, 511–513

Draxler, R.R. & Rolph, G.D. (2010). HYSPLIT (HYbrid Single-Particle Lagrangian Integrated Trajectory) Model access via NOAA ARL READY Website (http://ready.arl.noaa.gov/HYSPLIT.php). NOAA Air Resources Laboratory, Silver Spring, MD.

Duan, J.; Tan, J.; Yang, L.; Wu, S. & Hao, J. (2008). Concentration, sources and ozone formation potential of volatile organic compounds (VOCs) during ozone episode in Beijing. Atmospheric Research, 88, 25-35

EC 1999 Air Quality Directive 1999/30 EC of the European Parliament and of the Council of 22 April 1999 relating to limit values for SO2, NO2 and NOx, particulate matter and lead in ambient air. Off J Eur Communities L163, Brussels

EC 2008 Directive 2008/50/EC of the European Parliament and of the Council of 21 May 2008 on ambient air quality and cleaner air for Europe

Eberly, S. (2005) EPA PMF 1.1 user guide. Research Triangle Park, NC: USEPA National Exposure Research Laboratory.

Elbir, T.; Cetin, B.; Cetin, E.; Bayram, A.; Odabasi, M. & Crow, D. (2007). Characterization of volatile organic compounds (VOCs) and their sources in the air of Izmir, Turkey. *Environmental Monitoring and Assessment,* 133, 149–160

Gao, N.; Cheng, M-D. & Hopke, P.K. (1993). Potential source contribution function analysis and source apportionment of sulphur species measured at Rubidoux, CA during the Southern CaliforniaAir Quality Study, 1987. *Analitica Chimica Acta*, 277,369-380

Hsu, Y-K; Holsen, M.T. & Hopke, K.P. (2003). Comparison of hybrid receptor models to locate PCB sources in Chicago. *Atmospheric Environment*, 37, 545-562

Henry, R.C.; Lewis, C.W.; Hopke, P.K. & Williamson, J.H. (1984). Review of the receptor model fundamentals. *Atmospheric Environment*, 18, 1507-1515

Henry, R.C. & Kim, B.-M. (1990). Extension of Self-Modeling Curve Resolution to Mixtures of More Than Three Components. Part 1: Finding the Basic Feasible Region. *Chemometrics and Intelligent Laboratory Systems,* 8, 205–216

Henry, R.C. (1997). History and Fundamentals of Multivariate Air Quality Receptor Models. *Chemometrics and Intelligent Laboratory Systems*, 37, 525–530

Henry, R.C.; Park, E.S. & Spiegelman, C.H. (1999). Comparing a New Algorithm with the Classic Methods for Estimating the Number of Factors. *Chemometrics and Intelligent Laboratory Systems,* 48, 91–97

Henry, R.C. (2003). Multivariate receptor modeling by N-dimensional edge detection. *Chemometrics and intelligent laboratory systems*, 65, 179 – 189

Henry, R.C. (2002). Multivariate receptor models- current practices and future trends. *Chemometrics and intelligent laboratory systems*, 60, 43- 48

Henry R.C. (2005). Duality in multivariate receptor models. Chemometrics and Intelligent Laboratory Systems, 77, 59–63

Hopke, P.K.; Ito, K.; Mar, T.; Christensen, W.F.; Eatough, D.J.; Henry, R.C.; Kim, E.; Laden, F.; Lall, R.; Larson, T.V.; Liu, H.; Neas, L.; Pinto, J.; Stolzel, M.; Suh, H.; Paatero, P. & Thurston, G.D. (2006). PM source apportionment and health effects: 1. Intercomparison of source apportionment results. *Journal of Exposure Science and Environmental Epidemiology*, 16, 275-286

Hopke, K.P. (2003). Recent developments in receptor modelling. *Journal of chemometrics*, 17 255-265

Hopke, K. (1991). *Receptor modelling for air quality management,* Eslevier, Amsterdam

IPCC 2001 Intergovernmental Panel on Climate Change, Third Assessment Report. Cambridge University Press. Cambridge UK

IPCC. Climate change 2007: the physical science basis. Contribution of Working Group I to the Fourth Assessment Report of the IPCC (ISBN 978 0521 88009-1 Hardback; 978 0521 70596-7 Paperback); 2007.

Kim, B-M. & Henry, R.C. (2000). Application of the SAFER Model to Los Angeles PM_{10} Data. *Atmospheric Environment*, 34, 1747–1759

Kim, E.; Hopke, P.K. & Edgerton, E.S. (2003). Source Identification of Atlanta Aerosol by Positive Matrix Factorization. *Journal of Air & Waste Management Association,* 53, 731-739

Kubilay, N.; Nickovic, S.; Moulin, C. & Dulac, F. (2000). An Ilulustartion of the transport and deposition of mineral dust onto the eastern Mediterranen. *Atmospheric Environment*, 34, 1293-1303

Laden, F.; Schwartz, J.; Speizer, F.E. & Dockery, D.W. (2006). Reduction in fine particulate air pollution and mortality: extended follow-up of the Harvard six cities study. *American Journal of Respiratory and Critical Care Medicine*, 173 (6), 667–672

Lewis, C.W.; Norris, G. & Henry, R. (2003). Source Apportionment of Phoenix PM2.5 Aerosol with the Unmix Receptor Model. *Journal of the Air & Waste Management Association*, 53, 325-338

Malm, W.C.; Johnson, C.E. & Bresch, J.F. (1986). Application of principal component analysis for purposes of identifying source-receptor relationship, In: *Receptor Methods for Source Apportionment,* 127-148, Pace, T.G. (Ed), Air Pollution Control Association, Pittsburgh, PA

Marković, M.D.; Marković, A.D., Jovanović, A.; Lazić, L. & Mijić, Z. (2008). Determination of O_3, NO_2, SO_2, CO and PM_{10} measured in Belgrade urban area. *Environmental monitoring and assessment,* 145, 349-359

Mijić, Z.; Tasić, M.; Rajšić, S. & Novaković, V. (2009). The statistical character of PM_{10} in Belgrade. *Atmospheric Research*, 92, 420-426

Mukerjee, S.; Norris, G.A.; Smith, L.A.; Noble, C.A.; Neas, L.M.; Ozkaynak, A.H. & Gonzales M. (2004). Receptor model comparisons and wind direction analyses of volatile organic compounds and submicrometer particles in an arid, binational, urban air shed. Environmental science & technology, 38(8), 2317-2327

Nicolas, J.; Chiari, M.; Crespo, J.; Garcia, I..; Lucarelli, F.; Nava, S.; Pasto, C. & Yubero, E. (2008). Quantification of Saharan and local dust impact in an arid Mediterranean area by the positive matrix factorization (PMF) technique. *Atmospheric Environment,* 42, 8872-8882

Niyogi, D.; Chang, H.-I; Saxena, V.K.; Holt, T.; Alapaty, K.; Booker, F.; Chen, F.; Davis, K.J.; Holben, B.; Matsui, T.; Meyers, T.; Oechel, W.C.; Pielke, R.A., Sr.; Wells, R.; Wilson, K. & Xue, Y. (2004). Direct observations of the effects of aerosol loading on net ecosystem CO2 exchanges over different landscapes. *Geophysical Research Letters*, 31, 1–5

Olson, D.A.; Norris, G.A.; Seila, R.L.; Landis, M.S.& Vette, A. F. (2007). Chemical characterization of volatile organic compounds near the World Trade Center: Ambient concentrations and source apportionment. *Atmospheric Environment*, 41, 5673–5683

Paatero, P. (1993). Least squares formulation of robust non-negative factor analysis. *Chemometrics and Intelligent Laboratory Systems*, 37, 23-35

Paatero, P. & Tapper, U. (1993). Analysis of different modes of factor analysis as least square fit problems. *Chemometrics and Intelligent Laboratory Systems*, 18, 183-194

Paatero, P. & Tapper, U. (1994). Positive matrix factorization: a non-negative factor model with optimal utilization of error-estimates of data values. *Envirometrics*, 5, 111-126

Paatero, P. (1997). Least Squares Formulation of Robust Non-Negative Factor Analysis. *Chemometrics and Intelligent Laboratory Systems* ,37, 23-35

Paatero, P. (1999). The Multilinear Engine – A Table-Driven, Least Squares Program for Solving Multilinear Problems, Including the n-Way Parallel Factor Analysis Model. *Journal of Computational and Graphical Statistics*, 1, 854-888

Paatero, P.; Hopke & Philip K. (2003). Discarding or downweighting high-noise variables in factor analytic models. *Analytica Chimica Acta,* 490, 277-289

Paatero, P.; Hopke, P.K.; Begum, B.A. & Biswas, S.K. (2005). A graphical diagnostic method for assessing the rotation in factor analytical models of atmospheric pollution. *Atmospheric Environment*, 39,193-201

Pandis, S.N.; Wexler, A.S.; Seinfeld, J.H.; (1995). Dynamics of tropospheric aerosols. *Journal of Physical Chemistry*, 99 (24), 9646-9659

Perez, N.; Pey, J.; Querol, X.; Alastuey, A.; Lopez, J.M. & Viana, M. (2008). Portioning of major and trace components in PM_{10}-$PM_{2.5}$-PM_1 at an urban site in Southern Europe. *Atmospheric Environment*, 42, 1677-1691

Polissar, V.A.; Hopke, K.P. & Poirot, L.R. (2001). Atmospheric Aerosol over Vermont: Chemical Composition and Sources. *Environmental Science and Technology*, 35, 4604-4621

Poirot, R.L.; Wishinski, P.R; Hopke, P.K & A.V. Polissar (2001). Comparative Application of Multiple Receptor Methods to Identify Aerosol Sources in Northern Vermont. *Environmental Science & Technology*, 35, 4622-4636

Pope, III, C.A.; Burnett, R.T.; Thun, M.J.; Calle, E.E.; Krewski, D.; Ito, K.; Thurston, D.G. (2002). Lung cancer, cardiopulmonary mortality, and long-term exposure to fine particulate air pollution. *The Journal of American Medical Association,* 287 (9), 1132–1141

Pope, III, C.A.; Burnett, R.T.; Thurston, G.D.; Thun, M.J.; Calle, E.E.; Krewski, D. Godleski, J.J. (2004). Cardiovascular mortality and long-termexposure to particulate air pollution. epidemiological evidence of general pathophysiological pathways of disease. *Circulation*, 109, 71–77

Rajšić, F.S.; Tasić, D.M.; Novaković; T.V. & Tomašević, N.M. (2004). First Assessment of the PM_{10} and $PM_{2.5}$ Particulate Level in the Ambient Air of Begrade City. *Environmental Science and Pollution Research*,11, 158-164

Rajšić, S.; Mijić, Z.; Tasić, M.; Radenković, M. & Joksić, J. (2008). Evaluation of the Levels and Sources of Trace Elements in Urban Particulate Matter. *Environmental Chemistry Letters*, 6, 95-100

Rolph, G.D. (2010). Real-time Environmental Applications and Display sYstem (READY) Website (http://ready.arl.noaa.gov). NOAA Air Resources Laboratory, Silver Spring, MD.

Song, X.-H.; Polissar, A.V.; Hopke, P.K. (2001). Sources of fine particle composition in the northeastern US. *Atmospheric Environment*, 35, 5277-5286

Song, Y.; Dai, W.; Shao, M.; Liu, Y.; Lu, S.; Kuster, W. & Goldan, P. (2008). Comparison of receptor models for source apportionment of volatile organic compounds in Beijing, China. *Environmental Pollution*, 156, 174-183

Schwartz, J.; Ballester, F.; Saez, M.; Perez-Hoyos, S.; Bellido, J.; Cambra, K.; Arribas, F.; Canada, A.; Perez-Boillos, M.J. & Sunyer, J. (2001). The concentration-response relation between air pollution and daily deaths. *Environmetal Health Perspective,* 109 1001-1006

Schwartz, J., Dockery, D.W., Neas, L.M. (1996) Is daily mortality associated specifically with fine particles? *Journal of the Air & Waste Management Association*, 46, 927-939

Tasić, D.M.; Rajšić, F.S.; Novaković, T.V.; Mijić, R.Z. & Tomašević, N.M. (2005). PM_{10} and $PM_{2.5}$ Mass Concentration Measurements in Belgrade Urban Area. *Physica Scripta*, T118, 29-30

Tasić, M.; Djurić-Stanojevic, B.; Rajšić, S.; Mijić, Z. & Novaković, V. (2006). Physico-Chemical Characterization of PM_{10} and $PM_{2.5}$ in the Belgrade Urban Area. *Acta Chimica Slovenica*, 53, 401-405

Tasić, M.; Mijić, Z.; Rajšić, S.; Stojić, A.; Radenković, M. & Joksić, J. (2009). Source apportionment of atmospheric bulk deposition in the Belgrade urban area using Positive Matrix factorization. 2nd Int. Workshop on Nonequilibrium Processes in Plasma Physics and Science, IOP Publishing, Journal of Physics: Conference Series 162, 012018 doi:10.1088/1742-6596/162/1/012018

Tasić, M.; Rajšić, S.; Tomašević, M.; Mijić, Z.; Aničić, M.; Novaković, V.; Marković, M.D.; Marković, A.D.; Lazić, L.; Radenković, M. & Joksić, J. (2008). Assessment of Air Quality in an Urban Area of Belgrade, Serbia, In: *Environmental Technologies, New Developments*, Burcu Ozkaraova Gungor, E. (Ed.) page numbers (209-244), I-Tech Education and Publishing, ISBN 978-3-902613-10-3, Vienna, Austria

Thurston, G.D. & Spengler, J.D. (1985). A quantitative assessment of source contributions to inhalable particulate matter pollution in metropolitan Boston. *Atmospheric Environment,* 19, 9-25

U.S. Environmental Protection Agency, 2007. EPA Unmix Version 6.0, available from http://www.epa.gov/heasd/products/unmix/unmix.html

Viana, M; Kuhlbusch, T.A.J; Querol, X.; Alastuey, A.; Harrison, R.M.; Hopke, P.K.; Winiwarter, W.; Vallius, M.; Szidat, S.; Prevot, A.S.H.; Hueglin, C.; Bloemen, H.; Wahlin, P.; Vecchi, R.; Miranda, A.I.; Kasper-Giebl, A.; Maenhhaut, & W.; Hitzenberger, R. (2008). Source apportionment of particulate matter in Europe: A review of methods and results. *Aerosol Science* 39, 827-849

Wang, Y.Q.; Zhang, X.Y. & Draxler, R. (2008). TrajStat: GIS-based software that uses various trajectory statistical analysis methods to identify potential sources from long-term air pollution measurement data. *Environmental Modelling & Software*, 24, 938-939

WHO - World Health Organization (2002). Air quality Guidelines for Europe

WHO - World Health Organization (2006). WHO Air quality guidelines for particulate matter, ozone, nitrogen dioxide and sulphur dioxide, Global update 2005. (accesses April 9th, 2010)

World Health Organization (WHO): (2003) Health aspects of air pollution with particulate matter, ozone and nitrogen dioxide. Report on a WHO Working Group, Regional Office for Europe; Bonn, Germany 13–15 January 2003. EUR/03/5042688. Available also at http://www.euro.who.int/document/e79097.pdf.

US-EPA (2002). Guidelines for the Application of SEM/EDX Analytical Techniques to Particulate Matter Samples. EPA-600/R-02-070

Estimation of uncertainty in predicting ground level concentrations from direct source releases in an urban area using the USEPA's AERMOD model equations

Vamsidhar V Poosarala, Ashok Kumar and Akhil Kadiyala
Department of Civil Engineering, The University of Toledo, Toledo, OH 43606

Abstract

One of the important prerequisites for a model to be used in decision making is to perform uncertainty and sensitivity analyses on the outputs of the model. This study presents a comprehensive review of the uncertainty and sensitivity analyses associated with prediction of ground level pollutant concentrations using the USEPA's AERMOD equations for point sources. This is done by first putting together an approximate set of equations that are used in the AERMOD model for the stable boundary layer (SBL) and convective boundary layer (CBL). Uncertainty and sensitivity analyses are then performed by incorporating the equations in Crystal Ball® software.

Various parameters considered for these analyses include emission rate, stack exit velocity, stack exit temperature, wind speed, lateral dispersion parameter, vertical dispersion parameter, weighting coefficients for both updraft and downdraft, total horizontal distribution function, cloud cover, ambient temperature, and surface roughness length. The convective mixing height is also considered for the CBL cases because it was specified. The corresponding probability distribution functions, depending on the measured or practical values are assigned to perform uncertainty and sensitivity analyses in both CBL and SBL cases.

The results for uncertainty in predicting ground level concentrations at different downwind distances in CBL varied between 67% and 75%, while it ranged between 40% and 47% in SBL. The sensitivity analysis showed that vertical dispersion parameter and total horizontal distribution function have contributed to 82% and 15% variance in predicting concentrations in CBL. In SBL, vertical dispersion parameter and total horizontal distribution function have contributed about 10% and 75% to variance in predicting concentrations respectively. Wind speed has a negative contribution to variance and the other parameters had a negligent or zero contribution to variance. The study concludes that the calculations of vertical dispersion parameter for the CBL case and of horizontal distribution function for the SBL case should be improved to reduce the uncertainty in predicting ground level concentrations.

1. Introduction

Development of a good model for decision making in any field of study needs to be associated with uncertainty and sensitivity analyses. Performing uncertainty and sensitivity analyses on the output of a model is one of the basic prerequisites for model validation. Uncertainty can be defined as a measure of the 'goodness' of a result. One can perform uncertainty analysis to quantify the uncertainty associated with response of uncertainties in model input. Sensitivity analysis helps determine the variation in model output due to change in one or more input parameters for the model. Sensitivity analysis enables the modeler to rank the input parameters by their contribution to variance of the output and allows the modeler to determine the level of accuracy required for an input parameter to make the models sufficiently useful and valid. If one considers an input value to be varying from a standard existing value, then the person will be in a position to say by how much more or less sensitivity will the output be on comparing with the case of a standard existing value. By identifying the uncertainty and sensitivity of each model, a modeler gains the capability of making better decisions when considering more than one model to obtain desired accurate results. Hence, it is imperative for modelers to understand the importance of recording and understanding the uncertainty and sensitivity of each model developed that would assist industry and regulatory bodies in decision-making.

A review of literature on the application of uncertainty and sensitivity analyses helped us gather some basic information on the applications of different methods in environmental area and their performance in computing uncertainty and sensitivity. The paper focuses on air quality modeling.

Various stages at which uncertainty can be obtained are listed below.

   a) Estimation of uncertainties in the model inputs.
   b) Estimation of the uncertainty in the results obtained from the model.
   c) Characterizing the uncertainties by different model structure and model formulations.
   d) Characterizing the uncertainties in model predicted results from the uncertainties in evaluation data.

Hanna (1988) stated the total uncertainty involved in modeling simulations to be considered as the sum of three components listed below.

   a) Uncertainty due to errors in the model.
   b) Uncertainty due to errors in the input data.
   c) Uncertainty due to the stochastic processes in the atmosphere (like turbulence).

In order to estimate the uncertainty in predicting a variable using a model, the input parameters to which the model is more sensitive should be determined. This is referred to as sensitivity analysis, which indicates by how much the overall uncertainty in the model predictions is associated with the individual uncertainty of the inputs in the model [Vardoulakis et al. (2002)]. Sensitivity studies do not combine the uncertainty of the model inputs, to provide a realistic estimate of uncertainty of model output or results. Sensitivity analysis should be carried out for different variables of a model to decide where prominence should be placed in estimating the total uncertainty. Sensitivity analysis of dispersion parameters is useful, because, it promotes a deeper understanding of the phenomenon, and helps one in placing enough emphasis in accurate measurements of the variables.

The analytical approach most frequently used for uncertainty analysis of simple equations is variance propagation [IAEA (1989), Martz and Waller (1982), Morgan and Henrion (1990)]. To overcome problems encountered with analytical variance propagation equations,

numerical methods are useful in performing an uncertainty analysis. Various approaches for determining uncertainty obtained from the literature include the following.

1) Differential uncertainty analysis [Cacuci (1981), and Worley (1987)] in which the partial derivatives of the model response with respect to the parameters are used to estimate uncertainty.

2) Monte Carlo analysis of statistical simplifications of complex models [Downing et al. (1985), Mead and Pike (1975), Morton (1983), and Myers (1971), Kumar et al. (1999)].

3) Non-probabilistic methods [for example: fuzzy sets, fuzzy arithmetic, and possibility theory [Ferson and Kuhn (1992)].

4) First-order analysis employing Taylor expansions [Scavia et al. (1981)].

5) Bootstrap method [Romano et al. (2004)].

6) Probability theory [Zadeh (1978)].

The most commonly applied numerical technique is the Monte Carlo simulation (Rubinstein, 1981).

There are many methods by which sensitivity analysis can be performed. Some of the methods are listed below.

1) Simple regression (on the untransformed and transformed data) [Brenkert et al. (1988)] or visual analysis of output based on changes in input [(Kumar et al. (1987), Thomas et al. (1985), Kumar et al. (2008)].

2) Multiple and piecewise multiple regression (on transformed and untransformed data) [Downing et al. (1985)].

3) Regression coefficients and partial regression coefficients [Bartell et al. (1986), Gardner et al. (1981)].

4) Stepwise regression and correlation ratios (on untransformed and transformed data).

5) Differential sensitivity analysis [Griewank and Corliss (1991), Worley (1987)].

6) Evidence theory [Dempster (1967), Shafer (1976)].

7) Interval approaches (Hansen and Walster, 2002).

8) ASTM method [(Kumar et al. (2002), Patel et al. (2003)].

Other studies that discuss the use of statistical regressions of the randomly selected values of uncertain parameters on the values produced for model predictions to determine the importance of parameters contributing to the overall uncertainty in the model result include IAEA (1989), Iman et al. (1981a, 1981b), Iman and Helton (1991), and Morgan and Henrion (1990).

Romano et al. (2004) performed the uncertainty analysis using Monte Carlo, Bootstrap, and fuzzy methods to determine the uncertainty associated with air emissions from two electric power plants in Italy. Emissions monitored were sulfur dioxide (SO_2), nitrogen oxides (NO_X), carbon monoxide (CO), and particulate matter (PM). Daily average emission data from a coal plant having two boilers were collected in 1998, and hourly average emission data from a fuel oil plant having four boilers were collected in 2000. The study compared the uncertainty analysis results from the three methods and concluded that Monte Carlo method gave more accurate results when applied to the Gaussian distributions, while Bootstrap method produced better results in estimating uncertainty for irregular and asymmetrical distributions, and Fuzzy models are well suited for cases where there is limited data availability or the data are not known properly.

Int Panis et al. (2004) studied the parametric uncertainty of aggregating marginal external costs for all motorized road transportation modes to the national level air pollution in

Belgium using the Monte Carlo technique. This study uses the impact pathway methodology that involves basically following a pollutant from its emission until it causes an impact or damage. The methodology involves details on the generation of emissions, atmospheric dispersion, exposure of humans and environment to pollutants, and impacts on public health, agriculture, and buildings. The study framework involves a combination of emission models, and air dispersion models at local and regional scales with dose-response functions and valuation rules. The propagation of errors was studied through complex calculations and the error estimates of every parameter used for the calculation were replaced by probability distribution. The above procedure is repeated many times (between 1000 and 10,000 trails) so that a large number of combinations of different input parameters occur. For this analysis, all the calculations were performed using the Crystal Ball® software. Based on the sensitivity of the result, parameters that contributed more to the variations were determined and studied in detail to obtain a better estimate of the parameter. The study observed the fraction high-emitter diesel passenger cars, air conditioning, and the impacts of foreign trucks as the main factors contributing to uncertainty for 2010 estimate.

Sax and Isakov (2003) have estimated the contribution of variability and uncertainty in the Gaussian air pollutant dispersion modeling systems from four model components: emissions, spatial and temporal allocation of emissions, model parameters, and meteorology using Monte Carlo simulations across ISCST3 and AERMOD. Variability and uncertainty in predicted hexavalent chromium concentrations generated from welding operations were studied. Results showed that a 95 percent confidence interval of predicted pollutant concentrations varied in magnitude at each receptor indicating that uncertainty played an important role at the receptors. AERMOD predicted a greater range of pollutant concentration as compared to ISCST3 for low-level sources in this study. The conclusion of the study was that input parameters need to be well characterized to reduce the uncertainty.

Rodriguez et al. (2007) investigated the uncertainty and sensitivity of ozone and $PM_{2.5}$ aerosols to variations in selected input parameters using a Monte Carlo analysis. The input parameters were selected based on their potential in affecting the pollutant concentrations predicted by the model and changes in emissions due to distributed generation (DG) implementation in the South Coast Air Basin (SoCAB) of California. Numerical simulations were performed using CIT three-dimensional air quality model. The magnitudes of the largest impacts estimated in this study are greater and well beyond the contribution of emissions uncertainty to the estimated air quality model error. Emissions introduced by DG implementation produce a highly non-linear response in time and space on pollutant concentrations. Results also showed that concentrating DG emissions in space or time produced the largest air quality impacts in the SoCAB area. Thus, in addition to the total amount of possible distributed generation to be installed, regulators should also consider the type of DG installed (as well as their spatial distribution) to avoid undesirable air quality impacts. After performing the sensitivity analysis, it was observed from the study that the current model is good enough to predict the air quality impacts of DG emissions as long as the changes in ozone are greater than 5 ppb and changes in $PM_{2.5}$ are greater than $13\mu g/m^3$.

Hwang et al. (1998) analyzed and discussed the techniques for model sensitivity and uncertainty analyses, and analysis of the propagation of model uncertainty for the model used within the GIS environment. A two-dimensional air quality model based on the first order Taylor method was used in this study. The study observed brute force method, the most straightforward method for sensitivity to be providing approximate solutions with

substantial human efforts. On the other hand, automatic differentiation required only one model run with minimum human effort to compute the solution where results are accurate to the precision of the machine. The study also observed that sampling methods provide only partial information with unknown accuracy while first-order method combined with automatic differentiation provide a complete solution with known accuracy. These techniques can be used for any model that is first order differentiable.

Rao (2005) has discussed various types of uncertainties in the atmospheric dispersion models and reviewed sensitivity and uncertainty analysis methods to characterize and/or reduce them. This study concluded the results based on the confidence intervals (CI). If 5% of CI for pollutant concentration is less than that of the regulatory standards, then remedial measures must be taken. If the CI is more than 95% of the regulatory standards, nothing needs to be done. If the 95% upper CI is above the standard and the 50th percentile is below, further study must be carried out on the important parameters which play a key role in calculation of the concentration value. If the 50th percentile is also above the standard, one can proceed with cost effective remedial measures for risk reduction even though more study needs to be carried out. The study concluded that the uncertainty analysis incorporated into the atmospheric dispersion models would be valuable in decision-making.

Yegnan et al. (2002) demonstrated the need of incorporating uncertainty in dispersion models by applying uncertainty to two critical input parameters (wind speed and ambient temperature) in calculating the ground level concentrations. In this study, the Industrial Source Complex Short Term (ISCST) model, which is a Gaussian dispersion model, is used to predict the pollutant transport from a point source and the first-order and second-order Taylor series are used to calculate the ground level uncertainties. The results of ISCST model and uncertainty calculations are then validated with Monte Carlo simulations. There was a linear relationship between inputs and output. From the results, it was observed that the first-order Taylor series have been appropriate for ambient temperature and the second-order series is appropriate for wind speed when compared to Monte Carlo method.

Gottschalk et al. (2007) tested the uncertainty associated with simulation of NEE (net ecosystem exchange) by the PaSim (pasture simulation model) at four grassland sites. Monte Carlo runs were performed for the years 2002 and 2003, using Latin Hypercube sampling from probability density functions (PDF) for each input factor to know the effect of measurement uncertainties in the main input factors like climate, atmospheric CO_2 concentrations, soil characteristics, and management. This shows that output uncertainty not only depends on the input uncertainty, but also depends on the important factors and the uncertainty in model simulations. The study concluded that if a system is more environmentally confined, there will be higher uncertainties in the model results.

In addition to the above mentioned studies, many studies have focused on assessing the uncertainty in air quality models [Freeman et al. (1986), Seigneur et al. (1992), Hanna et al. (1998, 2001), Bergin et al. (1999), Yang et al. (1997), Moore and Londergan (2001), Hanna and Davis (2002), Vardoulakis et al. (2002), Hakami et al. (2003), Jaarsveld et al. (1997), Smith et al. (2000), and Guensler and Leonard (1995)]. Derwent and Hov (1988), Gao et al. (1996), Phenix et al. (1998), Bergin et al. (1999), Grenfell et al. (1999), Hanna et al. (2001), and Vuilleumier et al. (2001) have used the Monte Carlo simulations to address uncertainty in regional-scale gas-phase mechanisms. Uncertainty in meteorology inputs was studied by Irwin et al. (1987), and Dabberdt and Miller (2000), while the uncertainty in emissions was observed by Frey and Rhodes (1996), Frey and Li (2002), and Frey and Zheng (2002).

Seigneur et al. (1992), Frey (1993), and Cullen and Frey (1999) have assessed the uncertainty for a health risk assessment.

From the literature review, it was observed that uncertainty and sensitivity analyses have been carried out for various cases having different model parameters for varying emissions inventories, air pollutants, air quality modeling, and dispersion models. However, only one of these studies [Sax and Isakov (2003)] reported in the literature discussed such application of uncertainty and sensitivity analyses for predicting ground level concentrations using AERMOD equations. This study tries to fill this knowledge gap by performing uncertainty and sensitivity analyses of the results obtained at ground level from the AERMOD equations using urban area emission data with Crystal Ball® software.

2. Methodology

This section provides a detailed overview of the various steps adopted by the researchers when performing uncertainty and sensitivity analyses over predicted ground level pollutant concentrations from a point source in an urban area using the United States Environmental Protection Agency's (U.S. EPA's) AERMOD equations. The study focuses on determining the uncertainty in predicting ground level pollutant concentrations using the AERMOD equations.

2.1 AERMOD Spreadsheet Development

The researchers put together an approximate set of equations that are used in the AERMOD model for the stable boundary layer (SBL) and convective boundary layer (CBL). Note that the AERMOD model treats atmospheric conditions either as stable or convective. The basic equations used for calculating concentrations in both CBL and SBL are programmed in a spreadsheet. The following is a list of assumptions used while deriving the parameters and choosing the concentration equations in both SBL and CBL.

1) Only direct source equation is taken to calculate the pollutant concentration in CBL. However, there is only one equation for all conditions in the stable boundary layer.
2) The fraction of plume mass concentration in CBL is taken as one. This assumes that the plume will not penetrate the convective boundary layer at any point during dispersion and plume is dispersing within the CBL.
3) The value of convective mixing height is taken by assuming a value for each hour i.e., it is not computed using the equations given in the AERMOD manual.

2.1.1 Stable Boundary Layer (SBL) and Convective Boundary Layer (CBL) Equations

This section presents the AERMOD model equations that are incorporated in to the AERMOD spreadsheet for stable and convective boundary layer conditions.

2.1.1a Concentration Calculations in the SBL and CBL*

For stable boundary conditions, the AERMOD concentration expression (C_s in equation 1a) has the Gaussian form, and is similar to that used in many other steady-state plume models. The equation for Cs is given by,

$$C_s(x,y,z) = \frac{Q}{\sqrt{2\pi}.u.\sigma_z} \cdot F_y \cdot \sum_{m=-\infty}^{\infty} \left[exp\left(-\frac{(z - h_{es} - 2.m.z_{ieff})^2}{2.\sigma_z{}^2} \right) + exp\left(-\frac{(z + h_{es} + 2.m.z_{ieff})^2}{2.\sigma_z{}^2} \right) \right]$$

(1a)

For the case of m = 1 (i.e. m= -1, 0, 1), the above equation changes to the form of equation 1b.

$$C_s(x,y,z) = \frac{Q}{\sqrt{2\pi}.u.\sigma_z} \cdot F_y \cdot \left\{ \left[exp\left(-\frac{(z - h_{es} - 2.z_{ieff})^2}{2.\sigma_z{}^2} \right) + exp\left(-\frac{(z + h_{es} + 2.z_{ieff})^2}{2.\sigma_z{}^2} \right) \right] + \left[exp\left(-\frac{(z - h_{es})^2}{2.\sigma_z{}^2} \right) + \right. \right.$$
$$\left. \left. exp\left(-\frac{(z + h_{es})^2}{2.\sigma_z{}^2} \right) \right] + \left[exp\left(-\frac{(z - h_{es} + 2.z_{ieff})^2}{2.\sigma_z{}^2} \right) + exp\left(-\frac{(z + h_{es} - 2.z_{ieff})^2}{2.\sigma_z{}^2} \right) \right] \right\}$$

(1b)

The equation for calculation of the pollutant concentration in the convective boundary layer is given by equation 2a.

$$C_d(x,y,z) = \frac{Q.f_p}{\sqrt{2\pi}.u} \cdot F_y \cdot \sum_{j=1}^{2} \sum_{m=0}^{\infty} \frac{\lambda_j}{\sigma_z} \left[exp\left(-\frac{(z - \varphi_{dj} - 2.m.z_i)^2}{2\sigma_z^2} \right) + exp\left(-\frac{(z + \varphi_{dj} + 2.m.z_i)^2}{2\sigma_z^2} \right) \right]$$

(2a)

for m = 1 (i.e. m= 0, 1) the above equations changes to the form of equation 2b.

$$C_d(x,y,z) = \frac{Q.f_p}{\sqrt{2\pi}.u} \cdot F_y \cdot \sum_{j=1}^{2} \frac{\lambda_j}{\sigma_z} \left\{ \left[exp\left(-\frac{(z - \varphi_{dj})^2}{2\sigma_z^2} \right) + exp\left(-\frac{(z + \varphi_{dj})^2}{2\sigma_z^2} \right) \right] + \left[exp\left(-\frac{(z - \varphi_{dj} + 2.z_i)^2}{2\sigma_z^2} \right) + \right. \right.$$
$$\left. \left. exp\left(-\frac{(z + \varphi_{dj} + 2.z_i)^2}{2\sigma_z^2} \right) \right] \right\}$$

(2b)

The symbols are explained in the Nomenclature section at the end of the Chapter.

2.1.1b Friction Velocity (u∗) in SBL and CBL

The computation of friction velocity (u∗) under SBL conditions is given by equation 3.

$$u_* = \frac{C_D.u_{ref}}{2} \cdot \left[-1 + \left(1 + \frac{4.u_0^2}{C_D u_{ref}^2} \right)^{\frac{1}{2}} \right]$$

(3)

where, $u_0^2 = \frac{\beta_m.z_{ref}.g.\theta_*}{T_{ref}}$ [Hanna and Chang (1993), Perry (1992)]   (4)

$$C_D = \frac{K}{\ln\left(\frac{z_{ref}}{z_0}\right)}$$ [Garratt (1992)]   (5)

$$\theta_* = 0.09.(1 - 0.5.n^2)$$

Substituting equations 4 and 5 in equation 3, one gets the equation of friction velocity, u_* for SBL conditions, as given by equation 6.

$$u_* = \frac{k.u_{ref}}{\ln\left(\frac{z_{ref}}{z_0}\right)} . \left[-1 + \left(1 + \frac{4.\beta_m.z_{ref}.g.\theta_*.\ln\left(\frac{z_{ref}}{z_0}\right)}{T_{ref}.k.u_{ref}^2}\right)^{\frac{1}{2}}\right] \tag{6}$$

The computation of friction velocity u_* under CBL conditions is given by equation 7.

$$u_* = \frac{k.u_{ref}}{\ln\left(\frac{z_{ref}}{z_0}\right)} \tag{7}$$

2.1.1c Effective Stack Height in SBL
The effective stack height (h_{es}) is given by equation 8.

$$h_{es} = h_s + \Delta h_s \tag{8}$$

where, Δh_s is calculated by using equation 9.

$$\Delta h_s = 2.66.\left(\frac{F_b}{N^2.u}\right)^{1/3} . \left[\frac{N'.F_m}{F_b}.\sin\left(\frac{N'.x}{u}\right) + 1 - \cos\left(\frac{N'.x}{u}\right)\right]^{\frac{1}{3}} \tag{9}$$

where, $N'=0.7N$,

$$N = \left[\frac{g}{\theta}.\frac{\partial\theta}{\partial z}\right]^{\frac{1}{2}} \tag{10}$$

$\frac{\partial\theta}{\partial z} = 10^{-5}$ (K m^{-1}) is potential temperature gradient.

$$F_m = \left(\frac{T}{T_s}\right).w_s^2.r_s^2 \tag{11}$$

$$F_b = \left(\frac{\Delta T}{T_s}\right).g.w_s.r_s^2 \tag{12}$$

2.1.1d Height of the Reflecting Surface in SBL
The height of reflecting surface in stable boundary layer is computed using equation 13.

$$z_{ieff} = MAX[(h_{es} + 2.15.\sigma_{zs}; z_{im})] \tag{13}$$

where,

$$\sigma_{zs} = \left(1 - \frac{h_{es}}{z_i}\right).\sigma_{zgs} + \left(\frac{h_{es}}{z_i}\right).\sigma_{zes} \tag{14}$$

$$\sigma_{zes} = \frac{\sigma_{wt}.\left(\frac{x}{u}\right)}{\left(1 + \frac{x}{2.u.T_{lzs}}\right)^{1/2}} \tag{15}$$

$$\sigma_{zgs} = \sqrt{\frac{2}{\pi}.\left(\frac{u_*.x}{u}\right)\left(1 + 0.7\frac{x}{L}\right)^{-\frac{1}{3}}} \tag{16}$$

$$T_{lzs} = \frac{l}{\sigma_{wt}} \qquad\qquad \text{[Venkatram et.al., 1984]} \tag{17}$$

$l = \frac{1}{\left(\frac{1}{l_n} + \frac{1}{l_s}\right)}$

$l_n = 0.36.h_{es}$ and $l_s = 0.27.(\frac{\sigma_{wt}}{N})$, $z_i = z_{im}$.

2.1.1e Total Height of the Direct Source Plume in CBL

The actual height of the direct source plume will be the combination of the release height, buoyancy, and convection. The equation for total height of the direct source plume is given by equation 18.

$$\psi_{dj} = h_s + \Delta h_d + \frac{w_j.x}{u} \tag{18}$$

$$\Delta h_d = \left(\frac{3.F_m}{\beta_1^2.u^2} + \frac{3}{2.\beta_1^2} + \frac{F_b.x^2}{u^3}\right)^{\frac{1}{3}} \tag{19}$$

$w_j = a_j.w_*$ where, subscript j is equal to 1 for updrafts and 2 for the downdrafts.
λ_j in equation 2 is given by λ_1 and λ_2 for updraft and downdraft respectively and they are calculated using equations 20 and 21 respectively.

$$\lambda_1 = \frac{a_2}{a_2 - a_1} \tag{20}$$

$$\lambda_2 = -\frac{a_1}{a_2 - a_1} \tag{21}$$

$$a_1 = \frac{\sigma_{wt}}{w_*}\left(\frac{\alpha.S}{2}\right) + \frac{1}{2}\left(\alpha^2 S^2 + \frac{4}{\beta}\right) \tag{22}$$

$$a_2 = \frac{\sigma_{wt}}{w_*}\left(\frac{\alpha.S}{2}\right) - \frac{1}{2}\left(\alpha^2 S^2 + \frac{4}{\beta}\right) \tag{23}$$

$\alpha = \dfrac{1+R^2}{1+3.R^2}$ and $\beta^2 = 1+R^2$

R is assumed to be 2 [Weil et al. 1997], $S = \dfrac{\left(\frac{w^3}{w_*^3}\right)}{\left(\frac{\sigma_{wt}}{w_*}\right)^3}$

where, the fraction of $\dfrac{w^3}{w_*^3}$ is decided with the condition given below.

$\dfrac{w^3}{w_*^3} = 0.125$; for $H_p \geq 0.1z_i$ and $\dfrac{w^3}{w_*^3} = 1.25. \dfrac{H_p}{z_i}$ for $H_p < 0.1z_i$

$z_i = \text{MAX}[z_{ic}, z_{im}]$.

2.1.1f Monin-Obukhov length (L) and Sensible heat flux (H) for SBL and CBL
Monin-Obukhov length (L) and Sensible heat flux (H) are calculated using equations 24 and 25 respectively.

$$L = -\frac{\rho.c_p.T_{ref}.u_*^3}{k.g.H} \tag{24}$$

$$H = -\rho.c_p.u_*.\theta_* \tag{25}$$

Product of u_* and θ_* can be taken as 0.05 m s^{-1} K [Hanna et al. (1986)].

2.1.1g Convective velocity scale (w$_*$) for SBL and CBL
The equation for convective velocity (w$_*$) is computed using equation 26.

$$W_* = \left(\frac{g.H.z_{ic}}{\rho.c_p.T_{ref}}\right)^{\frac{1}{3}} \tag{26}$$

2.1.1h Lateral distribution function (F$_y$)
This function is calculated because the chances of encountering the coherent plume after travelling some distance will be less. Taking the above into consideration, the lateral distribution function is calculated. This equation will be in a Gaussian form.

$$F_y = \frac{1}{\sqrt{2\pi}.\sigma_y} exp\left(-\frac{y^2}{2\sigma_y^2}\right) \tag{27}$$

σ_y, the lateral dispersion parameter is calculated using equation 28 as given by Kuruvilla et.al. (2005).

$$\sigma_y = 0.27063 \left(\frac{\sigma_v . x}{u} \right)^{0.7} \tag{28}$$

$\sigma_v = \sqrt{0.35. w_*^2 + 0.25}$ which is the lateral turbulence.

2.1.1i Vertical dispersion parameter (σ_z) for SBL and CBL
The equation for vertical dispersion parameter is given by equation 29.

$$\sigma_z = \sqrt{ \left(2. \sigma_{wt} . \frac{x}{u} \right)^{\frac{0.0023}{\left(\frac{\sigma_{wt}}{w_*} \right)^6}} + 0.8 } \tag{29}$$

$$\sigma_{wt} = \sqrt{ 1.6 w_*^2 . \left(\frac{z}{z_{ic}} \right)^{\frac{2}{3}} + 1.69 u_*^2 . \left(1 - \frac{z}{z_i} \right) } \tag{30}$$

Table 1 presents the list of parameters used by AERMOD spreadsheet in predicting pollutant concentrations and Table 2 presents the basic inputs required to calculate the parameters.

Source Data	Meteorological Data	Surface Parameters	Other Data and Constants
Height of stack (h_s)	Ambient temperature (T_a)	Monin-Obukhov length (L)	Downwind distance (x)
Radius of stack (r_s)	Cloud cover (n)	Surface heat flux (H)	Acceleration due to gravity (g)
Stack exit gas temperature (T_s)	Surface roughness length (z_o)	Mechanical mixing height (z_{im})	Specific heat (c_p)
Emission rate (Q)		Convective mixing height (z_{ic})	Density of air (ρ)
Stack exit gas velocity (w_s)		Wind speed (u)	Time (t)
		Brunt-Vaisala frequency (N)	Van Karman constant (k = 0.4)
		Temperature scale (θ_*)	multiple reflections (m)
		Vertical turbulence (σ_{wt})	$\beta_m = 5$
			$\beta_t = 2$
			$\beta = 0.6$
			R = 2

Table 1. Different Parameters Used for Predicting Pollutant Concentration in AERMOD Spreadsheet.

Parameters	Basic Inputs
Plume buoyancy flux (F_b)	T_a, T_s, W_s, r_s
Plume momentum flux (F_m)	T_a, T_s, W_s, r_s
Surface friction velocity (u_*)	u, z_{ref}, z_o
Sensible heat flux (H)	u, z_{ref}, z_o, n
Convective velocity scale (w_*)	u, z_{ref}, z_o, n, z_{ic}, T_{ref}
Monin-Obukhov length (L)	u, z_{ref}, z_o, n, T_{ref}
Temperature scale (θ_*)	N
Lateral turbulence (σ_v)	u, z_{ref}, z_o, n, z_{ic}, T_{ref}
Total vertical turbulence (σ_{wt})	u, z_{ref}, z_o, n, z_{ic}, T_{ref}, z_i
Length scale (l)	u, z_{ref}, z_o, n, z_{ic}, T_{ref}, z_i, T_a, T_s, W_s, h_s, r_s
Brunt-Vaisala frequency (N)	T_a
Mechanical mixing height	u, z_{ref}, z_o, t
Convective mixing height	u, z_{ref}, z_o, n, T_a
Potential temperature	T_a

Table 2. Basic Inputs Required to Calculate the Parameters.

After programming all the above equations into EXCEL spreadsheet, they are then incorporated into Crystal ball® software to perform uncertainty and sensitivity analyses. Refer to Poosarala et al. (2009) for more information on the application and use of AERMOD spreadsheet. The output from this spreadsheet was compared with the actual runs made using the AERMOD model for a limited number of cases. The concentrations from both AERMOD model and AERMOD equations are calculated using source data (refer to Tables 3, 4, and 5) and metrological data from scalar data for the three days (February 11, June 29, October 22 of 1992) for Flint, Michigan. The predicted concentration values from the AERMOD model are taken and divided into two groups as CBL and SBL based on the Monin-Obukhov length (L) i.e. if L > 0 then it is SBL and vice versa. These results are then compared with AERMOD spreadsheet predicted concentrations for each boundary layer condition. For this comparison, three different cases considering varying emission velocities and stack temperatures for 40 meter, 70 meter, and 100 meter stacks are used for analyzing both the convective and stable atmospheric conditions.

The source data for the comparison of concentrations are taken in sets (represented by set numbers – 1, 2, and 3). In the first set of source group (1-1, 1-2, 1-3 in Tables 3-5), height of stack is kept constant, while exit velocity of the pollutant, stack temperature, and diameter of the stack are changed as shown in Tables 3, 4, and 5. For sets two and three, stack temperature and exit velocity are kept unchanged respectively. The study found results for comparison of predicted concentrations from AERMOD spreadsheet to vary in the range of 87% - 107% when compared to predicted concentrations from AERMOD model. Hence, one can say that the approximate sets of equations used in AERMOD spreadsheet were able to reproduce the AERMOD results.

Sets	Height of Stack (m)	Diameter of Stack (m)	Stack Exit Temperature (^{o}K)	Stack Exit Velocity (ms^{-1})	Emission Rate (gs^{-1})
1-1	100	8	300	15	20
1-2	100	8	346	10	20
1-3	100	8	373	5	20
2-3	100	8	373	15	15
3-1	100	8	373	15	17.4

Table 3. Source Data for Evaluation of AERMODSBL and AERMODCBL Test Cases for 100 m Stack.

Sets	Height of Stack (m)	Diameter of Stack (m)	Stack Exit Temperature (^{o}K)	Stack Exit Velocity (ms^{-1})	Emission Rate (gs^{-1})
2-2	70	6	373	10	15
3-2	70	6	346	15	17.4
4-1	70	6	300	5	20

Table 4. Source Data for Evaluation of AERMODSBL and AERMODCBL Test Cases for 70 m Stack

Sets	Height of Stack (m)	Diameter of Stack (m)	Stack Exit Temperature (^{o}K)	Stack Exit Velocity (ms^{-1})	Emission Rate (gs^{-1})
2-1	40	4	373	10	15
3-3	40	4	346	15	17.4
4-2	40	4	300	5	20

Table 5. Source Data for Evaluation of AERMODSBL and AERMODCBL Test Cases for 40 m Stack

Next, the above sets of equations are incorporated in the Crystal Ball® software for performing the uncertainty and sensitivity analyses. To perform these analyses in calculating the predicted concentrations using AERMOD equations, first the forecasting cell and assumption cells are to be defined. Pollutant concentration is designated to be the

forecasting cell, and parameters such as emission rate, stack exit velocity, stack temperature, wind speed, lateral dispersion parameter, vertical dispersion parameter, weighting coefficients for both updraft and downdraft, total horizontal distribution function, cloud cover, ambient temperature, and surface roughness length are defined as assumption cells. Their corresponding probability distribution functions, depending on the measured or practical values are assigned to get the uncertainty and sensitivity analyses of the forecasting cell in both convective and stable conditions (refer to Table 6). In addition to the above input values, convective mixing height is also taken as another assumption cell in CBL as the value of convective mixing height is directly taken, rather than calculating it using its integral form of equation. Convective mixing height governs the equation of total vertical turbulence, which is used for calculating the vertical dispersion parameter. An accepted error of ±10% of the value is applied for the parameters in both assumption and forecasting cells while performing uncertainty and sensitivity analyses in predicting ground level concentrations.

For each set of data, the analyses are carried at different downwind distances. In the case of height of stacks being constant, uncertainty and sensitivity analyses were performed at three different downwind distances: distance near the maximum concentration value, next nearest distance point to the stack coordinates, and a farthest point. For the other cases where the range for parameters wind speed, Monin-Obukhov length, and ambient temperature are considered, the hour with the lowest and highest value from range are taken (refer to Table 7) and the predicted concentrations from that hour are considered for uncertainty and sensitivity analysis. These values are applicable for the days considered. For CBL condition, separate case is considered by taking two values of surface roughness length (0.03 m for urban area with isolated obstructions and 1 m for urban area with large buildings).

Parameter	Probability Distribution Function		Reference
	CBL	SBL	
Lateral distribution (σ_y)	Gaussian	Gaussian	Willis and Deardorff (1981), Briggs (1993)
Vertical distribution (σ_z)	bi-Gaussian	Gaussian	Willis and Deardorff (1981), Briggs (1993)
Wind velocity (u)	Weibull	Weibull	Sathyajith (2002)
Total horizontal distribution function (F_y)	Gaussian	Gaussian	Lamb (1982)
Weighting coefficients for both updraft and downdraft (λ_1 and λ_2)	bi-Gaussian	NA	Weil et al. (1997)
Stack exit temperature (T)	Gaussian	Gaussian	Gabriel (1994)
Stack exit velocity (W_s)	Gaussian	Gaussian	
Emission rate (Q)	Gaussian	Gaussian	Eugene et al. (2008)

Table 6. Assumption Cells and Their Assigned Probability Distribution Functions.

Parameter	SBL		CBL	
	Lowest	Highest	Lowest	Highest
Wind speed (ms^{-1})	1.5	9.3	3.6	8.2
Ambient temperature (^{o}K)	262.5	294.9	267.5	302
Monin-Obukhov length (m)	38.4	8888	-8888	-356

Table 7. Summary of Parameters Considered for Uncertainty and Sensitivity Analyses.

3. Results and discussion

3.1 Uncertainty Analysis

3.1.1a 100 m Stack

The predicted concentrations from 100 m high stacks for the defined assumption cells have shown an uncertainty range of 55 to 80% for an error of ± 10% (i.e., uncertainty of the concentration equations to calculate ground level concentration within a range of 10% from the predicted value) for all the parameters in convective boundary layer (CBL) for surface roughness length (Z_o) value of 0.03 meter. When Z_o is 1 meter, the uncertainty ranged between 72 and 74%. In the case of stable boundary layer, the uncertainty ranged from 40 to 45% for the defined assumption cells. Bhat (2008) performed uncertainty and sensitivity analyses for two Gaussian models used by Bower et al. (1979) and Chen et al. (1998) for modeling bioaerosol emissions from land applications of class B biosolids. He observed uncertainty ranges of 54 to 63% and 55 to 60% for Bowers et al. (1979) and Chen et al. (1998) models respectively, for a ground level source.

Figures 1 through 6 present the uncertainty charts for both convective and stable atmospheric conditions at different downwind distances. It was observed that the atmospheric stability conditions influenced the uncertainty value. The uncertainty value decreased as the atmospheric stability condition changed from convective to stable.
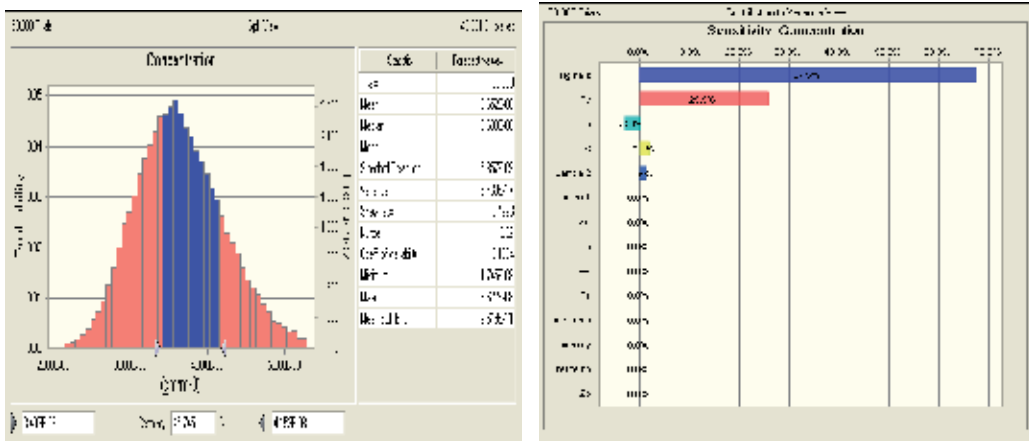
Fig. 1. Uncertainty and Sensitivity Charts for 100 m Stack at 1000 m in CBL (Z_0 = 1 m).
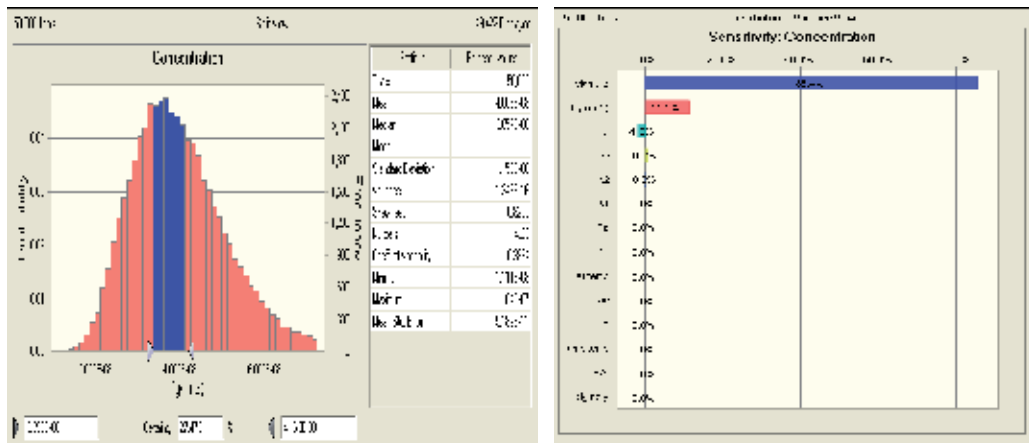
Fig. 2. Uncertainty and Sensitivity Charts for 100 m Stack at 1000 m in CBL (Z_0 = 0.03 m).
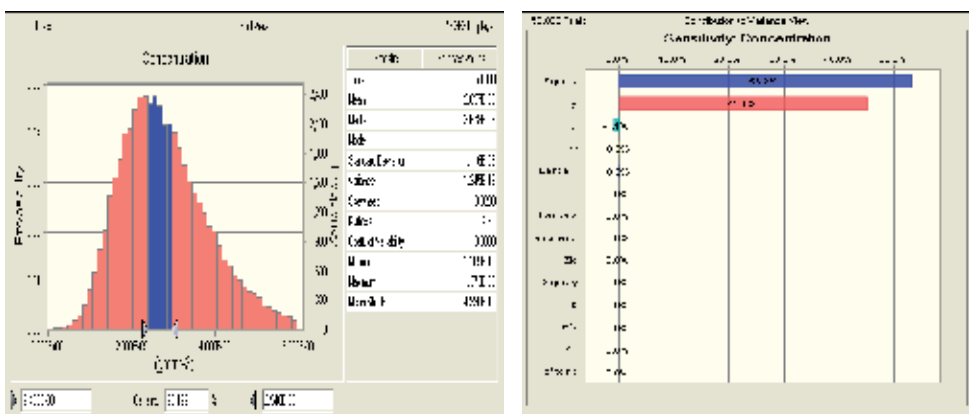
Fig. 3. Uncertainty and Sensitivity Charts for 100 m stack at 10000 m in CBL (Z_0 = 1 m).

Fig. 4. Uncertainty and Sensitivity Charts for 100 m stack at 10000 m in CBL (Z_0 = 0.03 m).

Fig. 5. Uncertainty and Sensitivity Charts for 100 m stack at 1000 m in SBL.

Fig. 6. Uncertainty and Sensitivity Charts for 100 m stack at 10000 m in SBL.

The uncertainty analysis was also carried out for a 70 m and 40 m stack and the results obtained are summarized below.

3.1.1b 70 m Stack

The predicted concentrations from a 70 m stack for the defined assumption cells have shown an uncertainty range of 72 to 77% for an error of ± 10% for all the parameters in CBL for Z_o = 0.03 m, and for the cases where Z_o = 1 m, the uncertainty varied between 72 and 76%.i.e. there is only 23 to 28% certainty that the predicted concentration will lie within the range of 10% from the actual concentration. In the case of SBL, an uncertainty range of 41 to 48% was observed for the defined assumption cells concluding that the certainty of predicting concentration is almost 52 to 59%.

3.1.1c 40 m Stack

The predicted concentrations from the 40 m stack for the defined assumption cells have shown an uncertainty range of 70 to 77% and 70 to 76% for an error of ± 10% for all the parameters in CBL for Z_o = 0.03 m and Z_o = 1 m respectively. In other words, the prediction of concentration for 40 m stack is 27 to 30% times within the 10% range from observed concentration. In the case of SBL, an uncertainty range of 41 to 47% was observed for the defined assumptions cells.

From the above results it is clear that the prediction of concentration is less uncertain in stable case as compared to the convective cases. The spreadsheet predict shows more certainty in predicting concentrations in SBL as compared to that in CBL. Uncertainty ranges for SBL and the case of CBL representing an urban area with large buildings were found to be similar irrespective of the stack height considered. However, the uncertainty ranges varied for the case of CBL representing an urban area with isolated buildings. The influence of surface roughness is found to be more pronounced for a tall stack of 100 m where a much wider range of uncertainty was observed as compared to 40 m and 70 m stack height cases. The uncertainty in concentration results is not influenced by surface roughness for 70 m and 40 m stacks.

3.1.2 Uncertainty Analysis Summary

Table 8 provides a summary of the uncertainty ranges observed from the uncertainty charts for the cases with the lowest and highest value of the parameters from the range of values for the three days taken for analysis.

Parameter	SBL				CBL					
	Low Value	Uncertainty Range	High Value	Uncertainty Range	Low Value	Uncertainty Range for $Z_0 = 1$ m	Uncertainty Range for $Z_0 = 0.03$ m	High Value	Uncertainty Range for $Z_0 = 1$ m	Uncertainty Range for $Z_0 = 0.03$ m
Wind Speed (ms^{-1})	1.5	38% to 40%	9.3	40% to 77%	3.6	73% to 76%	73% to 75%	8.2	71% to 76%	71% to 76%
Ambient Temperature (K)	263	34% to 37%	294.9	39% to 42%	267.5	72% to 76%	71% to 76%	302	54% to 63%	53% to 63%
Monin-Obukhov length (L)	38.4	38% to 40%	8888	40% to 77%	-8888	71% to 75%	71% to 76%	-356	67% to 77%	68% to 73%

Table 8. Summary of Uncertainty Ranges for Wind Speed, Ambient Temperature, and Monin-Obukhov Length from the Three Stack Heights Considered.

One can observe the uncertainty ranges to be different for both CBL and SBL in Table 8. Considering the case of wind speed, the averaged uncertainty value and range are observed to be same for both the cases of wind speed being low and high irrespective of the surface roughness length values in CBL. However, in the case of SBL, lower uncertainty range and values are observed at low wind speed compared to high wind speed. On studying the case of ambient temperature in SBL, less uncertainty was observed at lower ambient temperatures as compared to higher ambient temperatures. In the case of a CBL, uncertainty was observed to be more at lower ambient temperatures as compared to the uncertainty observed at higher ambient temperatures irrespective of the surface roughness length considered. Looking into the case of Monin-Obukhov length for stable atmosphere conditions, one can observe less uncertainty and lower uncertainty range for lower value of Monin-Obukhov length as compared to higher value of Monin-Obukhov length. In the case of a CBL, lower values of Monin-Obukhov length produced higher uncertainty as compared to higher Monin-Obukhov length values irrespective of surface roughness length.
Considering the case of low value of the parameters in SBL, one can observe similar uncertainty ranges for wind speed and Monin-Obukhov length that is higher than the uncertainty range observed in the case of ambient temperature. Similar trend can be observed in the case of parameters with high value in SBL from Table 8. In the case of a CBL, lower value for all the three parameters considered have shown similar uncertainty ranges irrespective of surface roughness length. However, the uncertainty ranges for the cases of higher value in CBL varied with each parameter. An ascending order of uncertainty range and value in order of ambient temperature, Monin-Obukhov length, and wind speed can be observed from Table 8 irrespective of surface roughness length values considered. One can also observe the uncertainty values and ranges to be similar at any given low or high value

of wind speed, ambient temperature, and Monin-Obukhov length in CBL irrespective of the surface roughness length,

Hence, it can be inferred that the output of the AERMOD model is sensitive to the changes in ambient temperature and Monin-Obukhov length for convective cases. However, one needs to provide accurate wind speed, ambient temperature, and Monin-Obukhov length rather than estimating the parameters so that uncertainty in the result is decreased.

Height of Stack (m)	U (ms-1)	L (m)	T$_a$ (ºK)	Uncertainty
40	3.1	366.6	274.9	47%
			287.5	44%
		401.3	274.9	44%
			287.5	48%
	5.1	1821.5	265.9	46%
			273.8	44%
		1838.3	265.9	70%
			273.8	72%
70	3.1	366.6	274.9	46%
			287.5	42%
		401.3	274.9	48%
			287.5	43%
	5.1	1821.5	265.9	50%
			273.8	50%
		1838.3	265.9	70%
			273.8	74%
100	3.1	366.6	274.9	34%
			287.5	39%
		401.3	274.9	38%
			287.5	42%
	5.1	1821.5	265.9	54%
			273.8	51%
		1838.3	265.9	76%
			273.8	72%

Table 9. Uncertainty Values for Different Heights of Stack at Point of Maximum Ground Level Concentration in Stable Boundary Layer (SBL).

Table 10 presents the uncertainty obtained for different cases of parameters in a CBL. There are two uncertainty values for each combination of parameters considered that represent different surface roughness lengths considered. It can be observed from Table 10 that uncertainty ranges were found to be similar for both surface roughness length cases, and there is not much difference in the uncertainty value for any combination of the parameters considered. For 40 m and 100 m stacks, one can observe the uncertainty to decrease with an increase in wind speed regardless of increase or decrease in the values of other parameters for both surface roughness lengths considered. However, similar trend could not be observed in a 70 m stack and mixed results were observed. This concludes that stack height is also a factor that can be responsible for sensitivity of the concentration prediction. There is

need to calculate the uncertainty in calculations due to stack height variation. It can also be seen from Table 10 that irrespective of the ambient temperature, uncertainty observed for a combination of lower values of wind speed and Monin-Obukhov length is more compared to uncertainty observed for a combination of higher values of wind speed and Monin-Obukhov length. Hence, one can infer the uncertainty to be more at lower parameter values than higher parameter values for CBL conditions.

Height of stack (m)	U (ms^{-1})	L (m)	T_a (^{o}K)	Uncertainty	
				Z_o = 0.03 m	Z_o = 1 m
40	4.1	-2423.7	267.5	73%	70%
			295.9	73%	75%
		-356	267.5	75%	72%
			295.9	73%	68%
	6.7	-3345.8	268.1	68%	68%
			302	65%	60%
		-957.2	268.1	58%	63%
			302	54%	53%
70	4.1	-2423.7	267.5	73%	73%
			295.9	70%	68%
		-356	267.5	70%	68%
			295.9	70%	69%
	6.7	-3345.8	268.1	75%	72%
			302	68%	63%
		-957.2	268.1	72%	76%
			302	63%	75%
100	4.1	-2423.7	267.5	76%	70%
			295.9	75%	74%
		-356	267.5	63%	62%
			295.9	54%	59%
	6.7	-3345.8	268.1	68%	70%
			302	60%	70%
		-957.2	268.1	63%	58%
			302	53%	54%

Table 10. Uncertainty Values for Different Heights of Stack at Point of Maximum Ground Level Concentration in Convective Boundary Layer (CBL).

Irrespective of the stack heights considered, one can infer the uncertainty to be more at higher wind speed, Monin-Obukhov length, and ambient temperature for stable boundary conditions. An opposite trend is observed for CBL conditions, i.e., uncertainty was observed to be more at lower wind speed, Monin-Obukhov length, and ambient temperature. One can observe

3.2 Sensitivity Analysis

Sensitivity analysis determines the response of the AERMOD model to change in the values of internal parameters. This helps us to determine how precisely and accurately the ground level concentration (a particular parameter) could be calculated. The analysis is done using the sensitivity charts that provide the percentage contribution to variance by the parameters considered to the output of the AERMOD model. The parameters that have been considered to perform sensitivity analysis are emission rate, stack exit velocity, stack temperature, wind speed, lateral dispersion parameter, vertical dispersion parameter, weighting coefficients for both updraft and downdraft, total horizontal distribution function, cloud cover, ambient temperature, and surface roughness length. The contributions to variance by various parameters considered at different downwind distances are tabulated in Table 11. The parameters that contributed to variance are vertical dispersion parameter, horizontal distribution (lateral dispersion parameter), emission rate, wind speed and weighting coefficients. It should be noted that all the parameters considered for the sensitivity analysis and that have zero contribution to the variance are not tabulated in Table 11. From the sensitivity charts shown in Figures 1 to 6, one can observe wind speed to be having a negative value for contribution to variance indicating that it is oppositely correlated, i.e., wind speed has an inverse effect on concentration. All other parameters had a positive contribution to variance. The sensitivity analysis charts for predicted concentrations show that vertical dispersion parameter and total horizontal distribution function have the maximum influence to variance.

Condition	Parameter	Contribution to variance in CBL (%)				Contribution to variance in SBL (%)	
		$Z_o = 1$ m		$Z_o = 0.03$ m			
		1000 m	10000 m	1000 m	10000 m	1000 m	10000 m
100 meter stack	σ_z	67.5	53.2	85.4	87.5	22.4	10.8
	F_y	25.9	45.1	11.5	10	64.5	76.1
	Q	2.1	0.3	0.8	0.6	4	4.5
	u	-3	-1.1	-1.9	-1.3	-9	-8.6
	λ_1	-	0.3	-	-	-	-
	λ_2	1.5	-	0.5	0.6	-	-
70 meter stack	σ_z	84.4	86.4	84.9	86.4	33.3	14.9
	F_y	12.1	10.5	11.7	10.4	53.9	68
	Q	1.2	1	1.3	1.3	5.6	7.6
	u	-1.7	-1.6	-1.6	-1.4	-7.2	-9.5
	λ_1	0.6	0.4	0.5	0.4	-	-

40 meter stack	σ_z	82.1	85.9	81.9	85.7	28.4	15.9
	F_y	13.6	11.1	14.1	11.1	58.2	66.2
	Q	1.6	1.1	1.6	1.2	6.3	6.7
	u	-2.1	-1.4	-2	-1.6	-7.1	-11.2
	λ_1	-	0.5	-	0.5	-	-
	λ_2	0.6	-	0.4	-	-	-
Low wind speed	σ_z	85.9	89.2	86	89.2	0	0.1
	F_y	11.7	8.7	11.4	9.1	84.1	83.9
	Q	0.7	0.4	0.8	0.5	4.6	5.1
	u	-1.1	-1.4	-1.3	-0.8	-11.3	-10.8
	λ_1	0.5	0.3	0.5	0.3	-	-
High wind speed	σ_z	84.3	89.4	83.3	89.4	5.2	4.7
	F_y	13.8	8.7	13.4	8.4	78.8	79.7
	Q	1	0.5	0.8	0.6	1.2	4.7
	u	-0.4	-1.1	-2	-1.2	-2.5	-10.8
	λ_1	0.4	0.3	0.5	0.3	-	-
Low ambient temperature	σ_z	84.3	88.8	84.2	88.9	0.1	1.2
	F_y	12.4	8.9	12.6	8.9	84.2	82.9
	Q	0.8	0.6	0.8	0.7	5	4.9
	u	-1.9	-1.3	-1.9	-1.2	-10.7	-11
	λ_1	0.6	0.3	0.5	0.4	-	-
High ambient temperature	σ_z	49.2	70.9	49.5	71.5	34.4	1.2
	F_y	41.6	23.5	40.4	23.2	55.7	83.1
	Q	2.3	1.4	2.7	1.5	3.2	4.9
	u	-5.5	-3.3	-5.7	-3	-6.6	-10.9
	λ_1	1.5	0.9	1.6	0.9	-	-

Low Monin-Obukhov length	σ_z	83.7	89.1	83.6	89.0	0	0.1
	F_y	13.1	8.9	13.2	8.7	84.1	83.9
	Q	0.9	0.4	0.9	0.5	4.6	5.1
	u	-1.7	-1.2	-1.8	-1.3	-11.3	-10.8
	λ_1	0.5	0.4	0.5	0.4	-	-
High Monin-Obukhov length	σ_z	76.9	84.3	77.5	87.5	5.2	4.7
	F_y	18.8	9.4	18.1	9.7	78.8	79.7
	Q	1	0.6	1.0	0.7	1.2	4.7
	U	-2.7	-5.3	-2.6	-1.5	-2.5	-10.8
	λ_1	0.6	0.4	0.8	0.5	-	-

Table 11. Contribution to Variance by Parameters in Calculation of Concentration at Different Downwind Distances.

The contributions to variance of parameters in both CBL and SBL for 1000 m and 10000 m downwind distance are tabulated in Table 11. In CBL, contribution to variance by vertical dispersion parameter is more than the contribution from horizontal distribution function which is a function of lateral dispersion parameter, indicating pollutant concentration to be more sensitive to vertical dispersion parameter than lateral dispersion parameter. However, it is the opposite in SBL, i.e., pollutant concentration is more sensitive to lateral dispersion parameter than vertical dispersion parameter. Wind speed parameter had a negative contribution to variance irrespective of the boundary layer conditions at both downwind distances. The contribution to variance by weighting coefficients is found to be negligible in all the conditions.

For the condition considering stack heights from Table 11, the pollutant concentration sensitiveness increased with downwind distance for vertical dispersion parameter and wind speed, but decreased for the remaining parameters in CBL for both surface roughness lengths considered. In SBL, contribution to variance by vertical dispersion parameter reduced with increase in downwind distance and increased for all other parameters considered for analysis.

For the condition considering low and high wind speeds from Table 11, in CBL, the pollutant concentration sensitiveness increased with downwind distance for vertical dispersion parameter. Pollutant concentration sensitiveness varied with surface roughness. For the case of Z_0 being 1 m pollutant concentration sensitiveness decreased with increase in downwind distance and the opposite trend is observed for the case of Z_0 being 0.03 m. For all other parameters pollutant concentration sensitiveness decreased with increase in downwind distance. In SBL, pollutant concentration sensitiveness decreased for vertical dispersion parameter as downwind distance increased and one can note that for lower wind speed, the contribution to variance by vertical dispersion parameter is zero at both 1000 m and 10000 m.

For the condition of ambient temperature in CBL, the contribution of variance by vertical dispersion parameter and wind speed increased with downwind distance and decreased for all other parameters for both the surface roughness lengths considered. Similar pattern can be observed in SBL for the condition of lower ambient temperature with the exception that wind speed showed an opposite trend to that observed in CBL. However, for the case of higher ambient temperature, in SBL, the contribution to variance increases for horizontal distribution and emission rate, and decreases for vertical dispersion parameter and wind speed with increase in downwind distance. For both high and low values of ambient temperature, the contribution by wind speed was significant in SBL compared to CBL. Thus, one can state that the concentrations are more sensitive to higher temperatures and wind speed in SBL than in CBL.

The sensitiveness in Monin-Obukhov length condition showed similar behavior to that of wind speed condition. It was observed that emission rate had more contribution to variance than vertical dispersion parameter in SBL for the cases having lower values of Monin-Obukhov length, wind speed, and ambient temperature. The remaining parameters defined in the assumption cells have negligible contribution to variance when compared to vertical dispersion parameter and total horizontal distribution function.

4. Conclusions

The objective of the study was to perform uncertainty and sensitivity analyses in predicting the concentrations from the AERMOD equations. As it is difficult to perform uncertainty and sensitivity analyses using the original AERMOD model, an approximate set of AERMOD equations were programmed in Excel. The predicted concentrations from the AERMODCBL and AERMODSBL models were compared to the predicted concentrations from AERMOD model. The comparison has shown that the predicted concentration values from the spreadsheet ranged between 87% and 107%, as compared to the predicted concentration values from the AERMOD model. This showed that the predicted concentrations obtained by the modeled equations can be relied upon to perform uncertainty and sensitivity analyses for both atmospheric conditions.

Uncertainty and sensitivity analysis has been performed for different cases taken into consideration by varying stack height, wind speed, Monin-Obukhov length, and ambient temperature for three days and source data as summarized in Tables 3, 4, and 5. The conclusions made from the study are listed below.

1. A user-friendly tool [60], that can calculate downwind contaminant concentrations under different boundary layer conditions has been developed using the AERMOD equations.

2. The uncertainty range varies between 67% and 75% for convective conditions on averaging the uncertainty values from all the considered cases, while in stable conditions, it ranged from 40% to 47%. This means the predictions are less certain in convective cases.

3. The contribution to variance by vertical dispersion parameter (σ_z) is found to be 82% under convective conditions i.e. the predicted concentrations are highly influenced by σ_z. In the case of horizontal distribution (F_y), the contribution to variance was found to be 75% in the stable case.

4. In SBL, for low values of wind speed, Monin-Obukhov length, and ambient temperature, the contribution to variance by emission rate (Q) is considerably more than that of vertical dispersion parameter (σ_z).

5. In CBL, concentration predictions are sensitive to vertical dispersion (σ_z) and horizontal distribution (F_y), i.e. σ_y regardless of stack height and surface roughness.

6. In SBL, concentration predictions are sensitive to horizontal distribution (F_y), i.e. σ_y and vertical dispersion (σ_z) regardless of the stack heights.

7. The predicted concentration equation is sensitive to vertical dispersion parameter (σ_z), horizontal distribution (F_y) (lateral dispersion parameter (σ_y)), and emission rate. Other parameters have negligible or no influence on sensitivity with the exception of wind speed that has a negative correlation.

5. Acknowledgements

6. References

Bartell, S.M.; Breck, J.E.; Gardner, R.H.; Brenkert, A.L. Individual parameter perturbation and error analysis of fish bioenergetics models. *Can. J. Fish. Aquat. Sci*. 1986, 43, 160-168.

Bergin, M.S.; Noblet, G.S.; Petrini, K.; Dhieux, J.R.; Milford, J.B.; Harley, R.A. Formal uncertainty analysis of a lagrangian photochemical air pollution model. *J. Environ. Sci. Technol.* 1999, 33, 1116–1126.

Bhat, A.S. Development and evaluation of a screening type dispersion model for bioaerosols emission from land application of Class B biosolids. Master's Thesis, The University of Toledo. 2008, 78 pp

Bowers, J.F.; Bjorkland J.R.; Cheney C.S. (1979).Industrial Source Complex (ISC) dispersion model user's guide. U.S. Environmental Protection Agency Report. EPA 450/4-79-030.

Brenkert, A.L.; Gardner, R.H.; Bartell, S.M.; Hoffman, F.O. In Reliability of Radioactive Transfer Models; Desmet, G.; Ed.; Uncertainties associated with estimates of radium accumulation in lake sediments and biota. Elsevier Applied Science: London, UK, 1988; pp 185-192.

Briggs, G.A. Plume dispersion in the convective boundary layer. Part II: analysis of CONDORS field experiment data. *J. Appl Meteorol.* 1993, 32, 1388-1425.

Cacuci, D.G. Sensitivity theory for nonlinear systems. Part I and II. *J. Math. Phys*. 1981, 22, 2794-2812.

Chen Y.; Dwaine B.; Steven H. Development of model of dispersion parameters for odour transmission from agricultural sources. *J. Agr. Eng.* 1998, 69, 229-238.

Cullen, A.C.; Frey, H.C. (1999). Probabilistic techniques in exposure assessment: a handbook for dealing with variability and uncertainty in risk analysis. New York: Plenum Press.

Dabberdt, W.F.; Miller, E. Uncertainty, ensembles, and air quality dispersion modeling: applications and challenges. *J. Atmos. Environ.* 2000, 34, 4667–4673.

Dempster, A.P. Upper and lower probabilities induced by a multi-valued mapping. *Ann. Math. Statistics*. 1967, 38, 325–339.

Derwent, R.; Hov, Ø. Application of sensitivity and uncertainty analysis techniques to a photochemical ozone model. *J. Geophys. Res.* 1988, 93, 5185–5199.

Downing, D.J.; Gardner, R.H.; Hoffman, F.O. An examination of response-surface methodologies for uncertainty analysis in assessment models. *Technometrics*. 1985, 27, 151–163.

Eugene, Y.; Fue-Sang, L.; Andrew, K.; D'Amours, R. Bayesian inversion of concentration data: source reconstruction in the adjoint representation of atmospheric diffusion. *J. Wind. Eng. Ind. Aerodyn*. 2008, 96, 1805-1816.

Ferson, S. Kuhn, R. In Computer Techniques in Environmental Studies IV; Zannetti, P.; Ed.; Propagating uncertainty in ecological risk analysis using interval and fuzzy arithmetic. Elsevier Applied Science: London, UK, 1992; pp 387-401.

Freeman, D.L.; Egami, R.T.; Robinson, N.F.; Watson, J.G. A method for propagating measurement uncertainties through dispersion models. *J. Air. Pollut. Control. Assoc.* 1986, 36, 246–253.

Frey, H.C. Separating variability and uncertainty in exposure assessment: motivations and method. Paper No. 93-79.01. Proceedings of the 86th Annual Meeting of Air and Waste Management Association. June 1993.

Frey, H.C.; Li, S. Methods for quantifying variability and uncertainty in AP-42 emission factors: case studies for natural gas-fueled engines. Emissions inventories — partnering for the future. Proceedings of the EPA 11th International Emission Inventory Conference. April 15–18, 2002.

Frey, H.C.; Rhodes, D.S. Characterizing, simulating, and analyzing variability and uncertainty: an illustration of methods using an air toxics example. *J. Hum. Ecol. Risk. Assess*. 1996, 2, 762–797.

Frey, H.C.; Zheng, J. Method for development of probabilistic emission inventories: example case study for utility NO_x emissions. Emissions inventories — partnering for the future. Proceedings of the EPA 11th International Emission Inventory Conference. April 15–18, 2002.

Gabriel, G.K. A model for sensible heat flux probability density function for near-neutral and slightly stable atmospheric flows. *Bound. Lay. Meteorol*. 1994, 71, 1-20.

Gao, D.; Stockwell, W.R.; Milford, J.B. Global uncertainty analysis of a regional-scale gas-phase chemical mechanism. *J. Geophys. Res*. 1996, 101, 9107–9119.

Gardner, R.H.; O'Neill, R.V.; Mankin, J.B.; Carney, J.H. A comparison of sensitivity analysis and error analysis based on a stream ecosystem model. *Ecol. Model*. 1981, 12, 177-194.

Garratt, J.R. The Atmospheric Boundary Layer; Cambridge University Press: New York, NY, 1992, 334 pp.

Gottschalk, P.; Wattenbach, M.; Neftel, A.; Fuhrer, J.; Jones, M.; Lanigan, G.; Davis, P.; Campbell, C.; Soussana, J.F.; Smith, P. The role of measurement uncertainties for the simulation of grassland net ecosystem exchange (NEE) in Europe. *Agricult. Ecosys. Environ.* 2007, 121, 175–185

Griewank, A.; Corliss, H. (1991). Automatic differentiation of algorithms: theory, implementation, and application. Philadelphia: Society for Industrial and Applied Mathematics.

Grenfell, J.L.; Savage, N.H.; Harrison, R.M.; Penkett, S.A. ; Forberich, O. ;Comes, F.J. ; Clemitshaw, K.C. ; Burgess, R.A. ; Cardenas, L.M. ; Davison, B.; McFadyen, G.G. Tropospheric box-modelling and analytical studies of the hydroxyl (OH) radical and related species: comparison with observations. *J. Atmos. Chem*. 1999, 33, 183–214.

Guensler, R.; Leonard, J.D. Monte Carlo technique for assessing motor vehicle emission model uncertainty. Proceedings of the Transportation Congress. Part 2 (of 2), October 22–26, 1995. New York, NY.

Hakami, A.; Odman, M.T.; Russell, A.G. High-order, direct sensitivity analysis of multidimensional air quality models. *J. Environ. Sci. Technol*. 2003, 37, 2442–2452.

Hanna, S.R. Air quality model evaluation and uncertainty. *J. Air Pollut. Control Assoc.* 1988, 38, 406–412.

Hanna, S.R.; Chang, J.S. Hybrid Plume Dispersion Model (HPDM), improvements and testing at three field sites. *J.Atmos. Environ*. 1993, 27A, 1491-1508.

Hanna, S.R.; Chang, J.C.; Fernau, M.E. Monte Carlo estimates of uncertainties in predictions by a photochemical grid model (UAM-IV) due to uncertainties in input variables. *J. Atmos. Environ*. 1998, 32, 3619–3628.

Hanna, S.R.; Davis, J.M. Evaluation of a photochemical grid model using estimates of concentration probability density functions. *J. Atmos. Environ.* 2002, 36, 1793–1798.

Hanna, S.R.; Weil, J.C.; Paine, R.J. Plume model development and evaluation-hybrid approach. EPRI Contract No. RP-1616-27, Electric Power Research Institute, Palo Alto, California, 1986.

Hanna, S.R.; Zhigang, L.; Frey, H.C.; Wheeler, N.; Vukovich, J.; Arunachalam, S.; Fernau, M.; Hansen, D.A. Uncertainties in predicted ozone concentrations due to input uncertainties for the UAM-V photochemical grid model applied to the July 1995 OTAG domain. *J. Atmos. Environ*. 2001, 35, 891–903.

Hansen, E.; Walster, G.W. (2004). Global optimization using interval analysis. Second Ed. New York: Marcel Dekker.

Hwang, D.; Karimi, H.A.; Byun, D.W. Uncertainty analysis of environmental models within GIS environments. *Comput. Geosci*. 1998, 24, 119-130.

Iman, R.L.; Helton, J.C. The repeatability of uncertainty and sensitivity analyses for complex probabilistic risk assessments. *Risk. Anal*. 1991, 11, 591-606.

Iman, R.L.; Helton, J.C.; Campbell, J.E. An approach to sensitivity analysis of computer models, Part 1. Introduction, input variable selection and preliminary variable assessment. *J. Qual. Technol*. 1981a, 13, 174-183.

Iman, R.L.; Helton, J.C.; Campbell, J.E. An approach to sensitivity analysis of computer models, Part 2. Ranking of input variables, response surface validation, distribution effect and techniques synopsis. *J. Qual. Technol*. 1981b, 13, 232-240.

Int Panis, L.; De Nocker, L.; Cornelis, E.; Torfs, R., An uncertainty analysis of air pollution externalities from road transport in belgium in 2010. *J.Sci. Total Environ*. 2004, 334-335, 287-298.

International Atomic Energy Agency (IAEA). (1989). Evaluating the reliability of predictions made using environmental transfer models. Vienna, Austria: IAEA Safety Series 100.

Irwin, J.S.; Rao, S.T.; Petersen, W.B.; Turner, D.B. Relating error bounds for maximum concentration estimates to diffusion meteorology uncertainty. *J. Atmos. Environ*. 1987, 21, 1927–1937.

Jaarsveld, J.A.V.; Van Pul, W.A.J.; De Leeuw, F.A.A.M. Modeling transportation and deposition of persistent organic pollutant in european region. *J. Atmos. Environ.* 1997, 31, 1011–1024.

Kumar, A.; Thomas, S.T.; Kong, S. Local sensitivity analysis of a long range transport model. Meteorology of Acid Deposition, Vol. 2, APCA Transactions TR-8, Air Pollution Control Association, 1987, pp. 158-168.

Kumar, A.; Manocha, A.; Shenoy, T. Sensitivity and uncertainty analysis of a regulatory risk model. Paper No. 219. Proceedings of the 89th Annual Meeting of Air and Waste Management Association. June 1996.

Kumar, A.; Mahurkar, A.; Joshi, A. Sensitivity analysis of an instantaneous box release model with surface heat transfer. Paper No. 42755. Proceedings of the 95th Annual Meeting of Air and Waste Management Association. June 2002.

Kumar, A.; Varadarajan, C.; Bhardwaj, K. Chapter 8, In Air Quality in the 21st Century**;** Romano, G.C.; Conti, A.G.; Ed.; Sensitivity of land use parameters and population on the prediction of concentration using the AERMOD model for an urban area. Nova Science: Hauppauge, NY, 2009.

Kuruvilla, S.A.; Kumar, A.; Varadarajan, C.; Vijayan, A. Development of a spreadsheet to model releases from continuous volume sources. *Environ. Prog*. 2005, 24, 349-353.

Lamb, R.G. In Atmospheric Turbulence and Air Pollution Modeling; Nieuwstadt, F.T.M.; Van Dop, H.; Eds.; Diffusion in the convective boundary layer. Reidel: Boston, MA, 1982; pp 159-229.

Martz, H.F.; Waller, R.A. (1982). Bayesian Reliability Analysis. New York: John Wiley & Sons.

Mead, R.; Pike, D.J. A review of response surface methodology from a biometric viewpoint. *Biometrics*. 1975, 31, 803-851.

Moore, G.E.; Londergan, R.J. Sampled Monte Carlo uncertainty analysis for photochemical grid models. *J. Atmos. Environ*. 2001, 35, 4863–4876.

Morgan, M.G.; Henrion, M. (1990). Uncertainty: A guide to dealing with uncertainty in quantitative risk and policy analysis. New York: Cambridge University Press.

Morton, R.H. Response Surface Methodology. *Math. Sci*. 1983, 8, 31-52.

Myers, R.H. (1971). Response surface methodology. Boston: Allyn and Bacon.

Patel, I.; Kumar, A.; Manne, G. Sensitivity analysis of CAL3QHC roadway intersection model. *J. TRB*. 2003, 1842, 109-117.

Perry, S.G. CTDMPLUS: A dispersion model for sources in complex topography. Part I: technical formulation. *J. Appl. Meteorol*. 1992, 31, 633-645

Phenix, B.D.; Dinaro, J.L.; Tatang, M.A.; Tester, J.W. ; Howard, J.B. ; McRae, G.J. Incorporation of parametric uncertainty into complex kinetic mechanisms: application to hydrogen oxidation in supercritical water. *Combust. Flame*. 1998, 112, 132–146.

Poosarala, V. V.; Kumar, A.; Kadiyala, A. Development of a spreadsheet for computing downwind concentrations based on the USEPA's AERMOD model. *Environ. Prog. & Sustainable Energy*. 2009, 28, 185-191.

Rao, S.K. Uncertainty analysis in atmospheric dispersion modeling. *Pure Appl. Geophys.* 2005, 162, 1893-1917.

Rodriguez, M.A.; Brouwer, J.; Samuelsen, G.S.; Dabdub, D. Air quality impacts of distributed power generation in the south coast air basin of california 2: model uncertainty and sensitivity analysis. *J. Atmos. Environ.* 2007, 41, 5618–5635

Romano, D.; Bernetti, A.; De Lauretis, R. Different methodologies to quantify uncertainties of Air Emissions. *Environ. Int.* 2004, 30, 1099-1107

Rubinstein, R.Y. (1981). Simulation and the Monte Carlo Method. John Wiley & Sons.

Sathyajith, M.; Pandey, K.P.; Kumar, A.V. Analysis of wind regimes for energy estimation. *Renew. Energ.* 2002, 25, 381-399.

Sax, T.; Isakov, V. A case Study for assessing uncertainty in local scale regulatory air quality modeling applications. *J. Atmos. Environ.* 2003, 37, 3481-3489

Scavia, D.; Powers, W.F.; Canale, R.P.; Moody, J.L. Comparison of first-order error analysis and monte carlo simulation in time-dependent lake eutrophication models. *Water. Resour. Res.* 1981, 17, 1051-1059.

Seigneur, C.; Constantinou, E.; Permutt, T. Uncertainty analysis of health risk estimates. Document No. 2460-009-510, Electric Power Research Institute, Palo Alto, California, 1992.

Shafer, G. (1976). A mathematical theory of evidence. New Jersey: Princeton Univ. Press.

Smith, R.I.; Fowler, D.; Sutton, M.A.; Flechard, C.; Coyle, M. Regional estimation of pollutant gas dry deposition in the UK: model description, sensitivity analyses and outputs. *J. Atmos. Environ.* 2000, 34, 3757–3777.

Thomas, S.T.; Kumar, A.; Vangipuram, R.N. Sensitivity analysis of a statistical type long range transport model. Paper No. 85-5.8. 78th Annual Meeting of Air Pollution Control Association. June 1985.

Vardoulakis, S.; Fisher, B.E.A.; Gonzalez-Flesca, N.; Pericleous, K. Model sensitivity and uncertainty analysis using roadside air quality measurements. *J. Atmos. Environ.* 2002, 36, 2121-2134.

Venkatram, A.; Strimaitis, D.G.; Dicristofaro, D. A semiemperical model to estimate vertical dispersion of eleveated releases in the stable boundary layer. *J. Atmos. Environ.* 1984, 18, 923-928

Vuilleumier, L.; Bamer, J.T.; Harley, R.A.; Brown, N.J. Evaluation of nitrogen dioxide photolysis rates in an urban area using data from the 1997 southern california ozone study. *J. Atmos. Environ.* 2001, 35, 6525–6537.

Weil, J.C.; Corio, L.A.; Brower, R.P. A PDF dispersion model for buoyant plumes in the convective boundary layer. *J. Appl Meteorol.* 1997, 36, 982-1002.

Willis, G.E.; Deardroff, J.W. A laboratory study of dispersion in the middle of the convectively mixed layer. *J. Atmos. Environ.* 1981, 15, 109-117.

Worley, B.A. (1987). Deterministic uncertainty analysis. ORNL-6428. Oak Ridge National Laboratory, Oak Ridge, Tennessee.

Yang, Y.J.; Wilkinson, J.G.; Russell, A.G. Fast, direct sensitivity analysis of multidimensional models. *J. Environ. Sci. Technol.* 1997, 31, 2859–2868.

Yegnan, A.; Williamson, D.G.; Graettinger, A.J. Uncertainty analysis in air dispersion modeling. *J. Environ. Modell. Softw.* 2002, 17, 639-649.

Zadeh, L. Fuzzy sets as a basis for a theory of possibility. *Fuzzy. Set. Syst.* 1978, 1, 3-28.

Nomenclature

$C_d(x,y,z)$	ground level concentration from the direct source (CBL) (g m^{-3})
$C_s(x,y,z)$	ground level concentration (SBL) (g m^{-3})
c_p	specific heat at constant pressure (= 1004 J g^{-1} K^{-1})
C_D	neutral drag coefficient (cal g^{-1} ^{o}C^{-1})
F_b	plume buoyancy flux (m^4 s^3)
F_y	total horizontal/lateral distribution function (m^{-1})
F_m	plume momentum flux (m^{4}s^2)
f_p	fraction of plume mass contained in CBL = (1 - penetration factor) (dimensionless)
g	acceleration due to gravity (9.81 m s^{-2})
H	sensible heat flux (W m^{-2})
H_p	plume centroid height (m)
h_s	stack height corrected for stack tip downwash (m)
h_{es}	plume rise for the stable source (m)
Δh_d	plume rise for the direct source (m)
Δh_s	plume rise for the stable source (m)
k	Von Karman constant k = 0.4 (dimensionless)
l	length used in determining the Lagrangian time scale (m)
l_n	neutral length scale – a component of l (m)
l_s	stable length scale – a component of l (m)
L	Monin-Obukhov length (m)
m	multiple reflections of plume (dimensionless)
N	Brunt-Vaisala frequency (s^{-1})
n	cloud cover (fractional)
Q	source emission rate (g s^{-1})
R	solar insolation (W m^{-2})
r_s	stack radius (m)
S	skewness factor (dimensionless)
T	ambient temperature (^{o}K)
T_{lzs}	vertical lagrangian time scale for the SBL (sec)
T_{ref}	ambient temperature - at reference temperature height (^{o}K)
T_s	stack gas temperature (^{o}K)
t	time (sec)
ΔT	difference between stack gas and ambient temperature (K)
u	wind speed (m s^{-1})
u_{ref}	wind speed at reference height (m s^{-1})
u_*	surface friction velocity (m s^{-1})
w_j	mean vertical velocity for the updraft (j = 1) and the downdraft (j = 2) distributions (m-s^{-1})
w_s	stack exit gas velocity (m-s^{-1})
w_*	convective velocity scale (m-s^{-1})
x	downwind distance to a receptor (m)
y	receptor location on the y axis
z	z_r and z_p in the horizontal and terrain following states
z_r	height of the receptor above local source base (m)

z_p	receptor "flagpole" height - the height of a receptor above local terrain (m)
z_i	mixing height (m): $z_i = $ MAX $[z_{ic}; z_{im}]$ in the CBL and $z_i = z_{im}$ in the SBL
z_{ic}	convective mixing height (m)
z_{ie}	equilibrium height of stable boundary layer
z_{ieff}	height of the reflecting surface in the SBL or in the stable layer above the CBL (m)
z_{im}	mechanical mixing height (m)
z_o	surface roughness length (m) (0.03 m for open flat terrain, grass, few obstacles; 1 m for more obstacles)
z_{ref}	reference height for wind (m)
θ	potential temperature (^{o}K)
θ_*	temperature scale (^{o}K)
λ_j	weighting coefficient for the updraft (j = 1) and downdraft (j = 2) distributions
ρ	density of air (Kg m^{-3})
σ_v	lateral turbulence (m s^{-1})
σ_{wt}	total vertical turbulence (m s^{-1})
σ_y	total lateral dispersion parameter for the direct source (m)
σ_z	total vertical dispersion parameter for the direct source (m)
σzas	ambient dispersion for the stable source (m)
σzes	elevated portion of σzas (m)
σzgs	surface portion of σzas (m)
σ_{zj}	total vertical dispersion for the updrafts and downdrafts (j=1, 2 respectively)
σ_{zs}	total dispersion for the stable source (m)
τ	time constant controlling the temporal interpolation of zim (sec)
ψ_{dj}	total height of the direct source plume (i.e. release height + buoyancy + convection) (m)
β_m	5
φ_{dj}	height of the direct source plume

Modeling of Ventilation Efficiency

Mahmoud Farghaly Bady
Assiut University
Egypt

1. Introduction

There are two types of pollution sources: high level sources such as tall stacks and low level sources such as automobile stacks. With respect to high level sources, Gaussian Plume Model (GPM) (Chock, 1977 and Kanda, 2006) is usually applied to estimate the pollutant concentrations, where the obstacles (such as buildings) little influence the diffusion characteristics of pollutants at such levels. In the case of low-level stacks, it is not appropriate to estimate the pollutant concentrations using GPM due to the effect of surrounding obstacles which make the pollutant removal efficiency by the applied wind vary from location to another in the same domain. In addition, the GPM do not take some architectural factors such as the form of building, the configuration of building, street widths, and relative positions of pollution source into account. Therefore, this model is not generally applicable to the built environment. Practically, in order to predict the concentration of pollutants in urban space, wind tunnel experiments and CFD simulation are used to estimate the pollutants concentration for this type of sources.

Many researchers have studied the distribution of pollutants inside urban domains such as street canyons (Xiaomin et al., 2005; Tsai et al., 2004; Baker et al., 2001; Ahmad et al., 2005) and densely built-up areas (Ahmad et al., 2005, Bady et al., 2008). However, based on these studies, it is thought that the determination of pollutant concentrations alone is insufficient to obtain a complete picture of the air quality in urban domains. In other words, if the pollutant source changes, the concentration distributions will also change. In such case, it is difficult to comprehend the removal capacity of pollutants by the wind within urban domains. In order to obtain a complete evaluation for the removal efficiency of pollutants by the natural wind within such domains, other parameters have to be considered in addition to the concentration. Consequently, there is a need to set an index (or a group of indices) that completely describes the air quality of the domain. Such index (or indices) may be used as a guide while designing new areas, or when the evaluation of air quality for urban domains is needed. At the same time, there is a concept of ventilation efficiency (VE) for indoor environments, which indicates the removal capacity of pollutants within indoor domains. This concept is thought to be suitable for evaluating the air quality of urban domains as well. Indeed, the air flow characteristics within outdoor environments are different from those of indoor environments as a result of the unsteadiness caused by fluctuations of wind in both speed and direction. This means that; some additional indices might be needed to evaluate outdoor air quality due to wind variations. In another study by

our group (Bady et al., 2008), the fluctuations of wind conditions within urban sites is considered and investigated using the exceedance probability concept. Such probability was introduced as a parameter or as a measure of the ventilation performance of the applied wind within a domain when the wind conditions of the site are varying.

The air quality of indoor domains in terms of VE indices has been studied by many researchers, such as (Sandberg, 1992; Ito et al., 2000; Kato et al., 2003). With respect to outdoor environments (Uehara et al., 1997) studied experimentally the diffusion of pollutants emitted from a line source located within an urban street canyon and they defined a concept similar to purging flow rate (PFR). More recently, it was confirmed that the ventilation efficiency indices of enclosed environments are also effective in evaluating the air quality of urban domains, as mentioned by (Huang et al., 2006).

2. Ventilation Efficiency Indices

Before presenting the ventilation efficiency indices, it is worth mentioning the fact that the distribution of pollutant concentrations in urban areas is not uniform, which represents a problem when analyzing the removal capacity of pollutants within urban domains. At the same time, the accuracy of the calculated VE indices depends on the uniformity of the pollutant generation strength within the considered local domain (local domain is a term introduced in order to represent a partial zone within the whole urban space such as a pedestrian zone). Thus, the VE indices were estimated in this study based on average values.

Ventilation efficiency indices can be evaluated mainly through CFD simulations since they are principally based on spatial distribution characteristics of pollutants (tracer diffusion). Until now, it is difficult to use wind tunnel experiments to obtain such indices. The problem is that the data needed to evaluate the VE indices is very difficult to be obtained through wind tunnel experiments. For example, to be independent of the source location within the study domain, a uniform generation rate is required, a condition which is difficult to satisfy using wind tunnel experiments. Another difficulty is that to calculate the visitation frequency of the pollutants, the total inflow flux to the study domain is needed which is difficult to estimate experimentally.

In addition to the above difficulties, there are many problems that reduce the chance of achieving successful experimental results. These problems include:

1) Symmetrical condition along the sides of the flow field is not easy to satisfy in wind tunnel experiments due to the lateral flow of wind to the domain.

2) The assumption of steady wind flow is wholly impractical.

3) The assumed boundary layer profile is over-simplistic compared with reality.

4) Fluctuations in the applied wind direction are not considered in the analysis.

These problems make the process of evaluating the VE indices experimentally very difficult. However, many trials were conducted by the authors of this study to estimate purging flow rate and visitation frequency experimentally, but unfortunately the results of these experiments were not readily useable. One way to generate the pollutant uniformly within the considered domain was through the use of four movable point sources which were adjusted in a certain manner to cover the total volume of the domain and then applying the principle of superposition to estimate the domain's average concentration. This low number of release points was selected based on the fact that the greater the presence of gas release

points within the domain, the more wind flow characteristics are affected. The behaviour of the plumes from the four point sources was totally different from those which were emitted from the whole volume. In addition, the measured data showed that the averaged domain concentration is quite sensitive to the source location. This led to inaccurate results.

There are different indices such as the age theory (Sandberg, 1983), purging flow rate, visitation frequency (Kato et al., 2003) and the six indices SVE1-6 (Kato et al., 1992) that are used to assess the air quality of a room or a domain located within an enclosed environment. Among these indices, three indices were adopted to implement the present study, i.e. purging flow rate (PFR), visitation frequency (VF), and pollutant residence time (TP).

Values of VE indices for a domain are of practical importance in reflecting the effect of the geometrical characteristics of such domain, i.e. the PFR value for a domain represents the local ventilation effectiveness of such domain. A small purging flow rate means that this domain is weakly ventilated. Also, higher values for the visitation frequency and residence time of pollutants are indications of poor removal efficiency of the pollutants by the applied wind. In the following section, definitions of the three indices will be explained in details.

2.1 Purging flow rate

The purging flow rate is the most important index for defining the ventilation efficiency of a local domain. It can be considered as the local ventilation efficiency. For a domain, PFR is defined as the effective airflow rate required to remove/purge the air pollutants from that domain (Kato et al., 2003). In other words, the purging flow rate can be considered as the net rate by which the pollutants are flushed out of the domain. It reflects the capacity at which the wind removes the pollutant from the domain. The following equation is used to calculate PFR:

$$PFR = \frac{q_p}{c_p} = \frac{q_p}{c \times \rho} \tag{1}$$

where:

q_P denotes pollutant generation rate (kg/s).

c_P is the domain-averaged concentration (= $c \times \rho$) (kg/m³).

ρ is the air density (kg/m³).

c is the mass concentration (kg/kg).

It is important to mention that PFR can be defined for a source point, not for the whole domain, but in this study, it is defined as common to the domain. Moreover, in addition to average concentrations, PFR can be estimated using the peak concentration of the domain. In such cases, the calculated PFR reflects dilution properties more than removal properties.

2.2 Visitation frequency

There are many parameters which affect the diffusion characteristics of pollutants within urban areas. These factors can be related to wind characteristics itself such as wind speed and direction, and it can be related to the geometry of the urban area such as obstacles dimensions, obstacles exits, and variable pollutant sources and strengths. So, it is important to study not only the level of the pollutant concentration but also the pollutant behaviour within these domains, including how many returns, circulates and stays inside it.
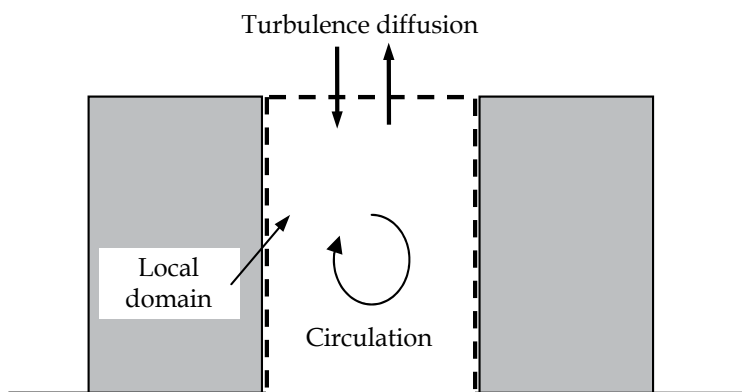
Fig. 1. Pollutant circulation

The index that can describe the pollutant history within a domain is the visitation frequency VF, which represents the number of times a particle enters the domain and passes through it. VF = 1 means that after being generated, a particle stays only one time in the domain. VF = 2 means that a particle stays in the domain for the first time, is transported to the outside and then returns again to the domain, due to recirculation flow for only one time. A schematic of pollutant circulation within a domain is illustrated in Fig. 5. In order to calculate VF, the following equation is applied, as mentioned by (Kato et al., 2003):

$$VF = 1 + \frac{\Delta q_p}{q_P} \tag{2}$$

where:

$$\Delta q_p = \rho \sum_{i=1}^{n} A_i \left(uc + \overline{u'c'} \right) \tag{3}$$

$$q_p = V \times S$$

where:
Δq_p is the inflow flux of pollutants into the domain (kg/s).
A_i is the inflow area of a face i (m²).
u is the inflow wind speed (m/s).
c is pollutant concentration at the boundary of the face i (kg/kg).
n is the number of faces subjected to flow.
V is the domain volume (m³).
u′ is the velocity fluctuation (m/s)
c′ is the concentration fluctuation (kg/kg).
uc together with ρA_i represents the convection part of the inflow flux (kg/s).

$\overline{u'c'}$ together with ρA_i represents the diffusion part of the inflow flux (kg/s).
S is the uniform generation source strength (kg/m³/s).
Visitation frequency can be calculated using the particle tracking method based on Large Eddy Simulation (LES) or by using the passive pollutant flux method based on the Reynolds

Averaged Navier–Stokes (RANS). Although large-eddy simulation (LES) models attract much interest, their use is restricted because it is computationally expensive. For this reason, RANS models are widely used in urban flows and dispersion research. In the present study, calculation of VF based on RANS method was applied.

2.3 Average residence time

One of the most promising parameters being used as an indication of the ventilation performance is the average residence time of pollutants in a domain. It represents the average residence times of all particles inside the domain. For one particle, the residence time is defined as the time the particle takes from once coming (or being generated) into the domain to its leaving (Kato et al., 2003).

Average residence time of domain pollutants is a measure of the air freshness and thus the dilution capability of wind inside such domain (Hui et al., 1997). It is calculated according to the equation:

$$TP = \frac{V}{PFR \times VF} \tag{4}$$

Applying the principle of average values, the multiplication of the visitation frequency by the particle residence time (VF × TP) indicates the average residence time of all particles within the considered domain.

3. Method of calculating the ventilation efficiency indices

Ventilation efficiency indices are estimated using dynamically passive pollutants, which means that the flow field is not influenced by the pollutants. This makes it possible to calculate the flow field at first and then this calculated flow field is used in estimating the VE indices. Thus, the first step is to solve the flow filed. Second, after the flow filed is calculated, the pollutant concentration is calculated through the solution of the convective-diffusion equation for a passive scalar (Ferzigere & Peric, 1997):

$$\frac{\partial(\rho u_i c)}{\partial x_i} = \frac{\partial}{\partial x_i}\left(K\frac{\partial c}{\partial x_i}\right) + S \tag{5}$$

where:
K is the mass diffusivity coefficient for the concentration (kg/m/s);
x_i is the Cartesian coordinates (m);
u_i is the Cartesian components of the velocity (m/s).

A uniform generation rate within the study domain is considered to be independent of the source location within the domain. In the third step, the pollutant average concentration within the domain is estimated and PFR is calculated according to Equation (1). Finally, the total domain inlet flux is calculated and VF is estimated from Equation (2), while TP is obtained according to Equation (5).

It is worth mentioning here the fact that the numerical simulation for diffusion is sometimes inaccurate. This can be attributed to two main reasons: insufficient spatial resolution and the steep concentration gradients that exist within the same calculation domain. These steep

gradients are explained as follows: upwind of a source, the pollutant concentration is zero, while in the region closest to the source; the concentration is at a maximum and decreases as the plume travels downwind of the source. Accordingly, there is a significant variation occur in the concentration values between adjacent cells which lead to steep concentration gradients. To overcome these two problems, a huge number of cells is needed to produce gradual concentration gradients, which is computationally expensive. In this study, in order to overcome the problem of insufficient spatial resolution, a grid-convergence analysis has been carried out during the design of the mesh systems of the building models and in each case; a reasonable number of grids was attained.

Another important matter to be mentioned here relates to the diffusivity coefficient K which is a function of the turbulent Schmidt number ($K = v_t / Sc_t$). It is known that the value of Sc_t is not constant and varies from one location to another within the same calculation domain. In high concentration regions –which means high concentration gradients– the turbulent Schmidt number is less than one, while in low concentration regions –which means that the mixing of pollutants with ambient fluid is almost finished– its value is sometimes greater than one. This means that the diffusivity coefficient is not equal to the eddy diffusivity of the momentum. However, in this work, Sc_t is assumed to be constant. This assumption has been applied in many of the previous studies (Xiaomin et al. 2005; Tsai et al., 2004). The authors consider that this simplification is accepted at this stage of the research.

4. Numerical simulations

Numerical simulations for wind environments in urban areas were performed using CFD code STAR-CD. The standard k-ε model was considered to simulate the turbulence effects. Steady-state analysis was adopted, and the Monotone Advection and Reconstruction Scheme (MARS) was applied to the spatial difference (He et al., 1997).

At the inflow boundary, the turbulent kinetic energy was set to be constant as given by Equation (6), while the turbulent dissipation rate was calculated according to Equation (7), which arises from the assumption of local equilibrium (Lien et al., 2004).

$$k \cong 1.5 \left(u \times I \right)^2 \tag{6}$$

$$\varepsilon \cong C_\mu^{1/2} \times k \times \frac{\partial u}{\partial z} \tag{7}$$

where k is the turbulent kinetic energy (m^2/s^2), I is the turbulent intensity of the applied flow, and C_μ is a constant (= 0.09).

Free slip condition was applied to the top and side boundaries. The logarithmic law with the parameter E = 9 was applied to the boundaries at ground level; (i.e. streets and traffic roads) and for building walls, as smooth surfaces. Table (1) summarizes all parameters used in the simulations together with the applied boundary conditions.

Turbulent Model	The standard k-ε model
Differential scheme	MARS scheme [18]
Inflow conditions	$u = u_o (z/z_o)^{0.25}, u_o = 1\,m/s \& z_o = 74.6\,m$ $k = 1.5(u \cdot I)^2$ $\varepsilon = C_\mu^{1/2} \cdot k \cdot \dfrac{\partial u}{\partial z}, \ C_\mu = 0.09$
Sides and sky	Free slip
Building walls and ground	Generalized logarithmic law

Table 1. CFD simulation parameters together with applied boundary conditions

5. Examples of Applying the Ventilation Efficiency Indices

Urban street width and street building heights are considered the most important parameters in controlling the air quality of the pedestrian level domain (Bady et al., 2008). Also, the arrangement of building arrays within urban areas is very important in controlling the air quality of the pedestrian level domains by enhancing more wind to these domains. Thus, it is worth investigating the effects of these parameters on the air quality of urban domains in terms of the ventilation efficiency indices, in a way that explains the method of applying such indices. Indeed, there are other parameters which may influence the air quality of urban domains such as wind direction, wind velocity, and building roof geometry, etc., but in the present study only the above parameters are considered.

A wind environment containing two buildings of dimensions 5 (L) × 25 (W) × (H) m, was simulated and a street was considered to have one building on each side. The study domain has the dimensions (D × 10 × H) and occupies the mid-third of the whole domain of the street. An isometric view of the model configurations is presented in Fig. 2, while Fig. 3 shows the wind flow domain around the buildings together with the applied boundary conditions.
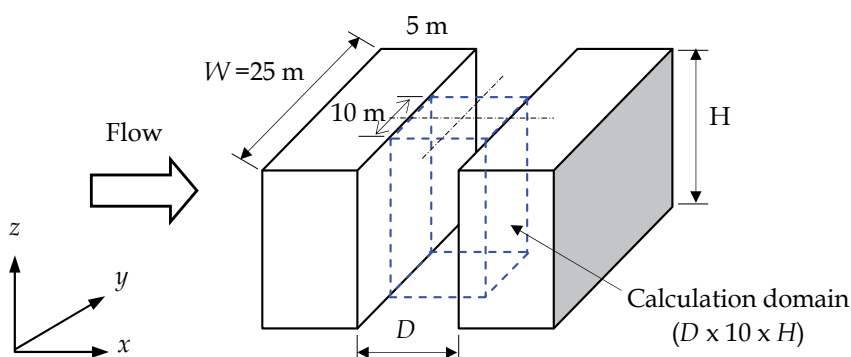
Fig. 2. Building model.
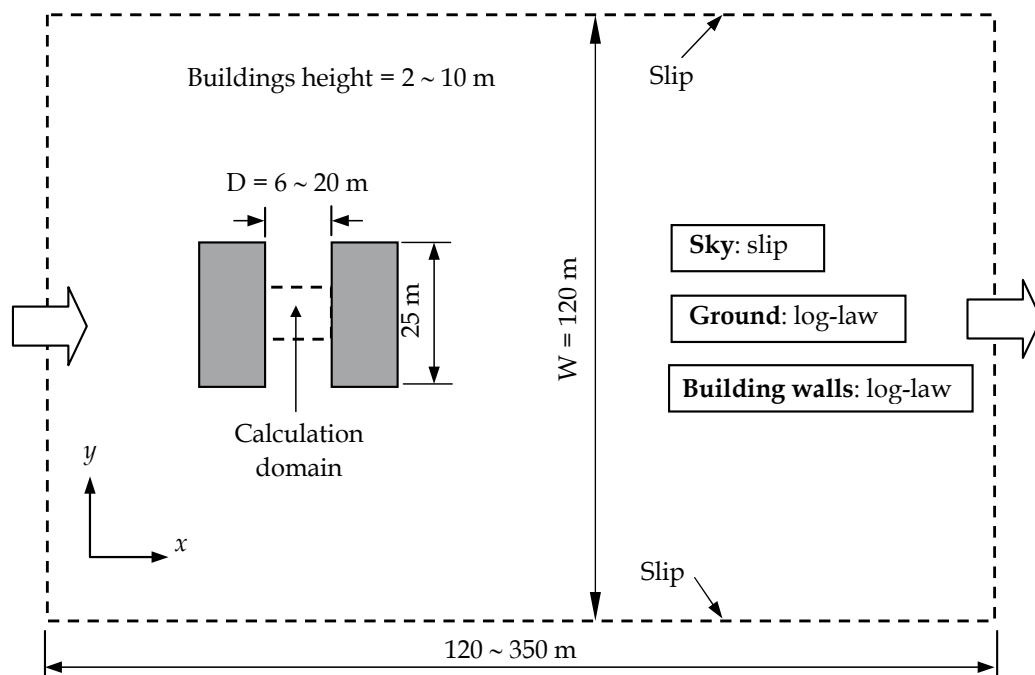
Fig. 3. Calculation conditions and boundary conditions of the wind flow domain.

5.1 Effect of street width (D)

Effects of varying the street width (D) on the wind flow patterns and ventilation efficiency indices are displayed in Figs. 4-7. Figure 4 shows the wind flow field within the mid section of the street for four selected cases of D/H (i.e. D/H = 0.6, 1.0, 1.5 and 2.0).

In the subplot (a), nearly there is no vortex circulation occurred inside the domain which is reflected in a small rotating speed which in turn leads to difficulty in removing the pollutants out of the domain. In Fig 4(b), a small vortex circulation covers the upper right hand side of the domain was generated. The domain average wind speed in this case is greater than that of case (a), which was resulted in a lower average concentration compared with the previous case. In the cases of D/H = 1.5 and 2.0 which are illustrated in Figs. 4(c) and (d), clockwise vortex circulations are generated within the domain when the wind is blown across the shear layer at the buildings height level. These vortices have large rotating velocities and hence transport the pollutant outside the domain from the windward side of the buildings.
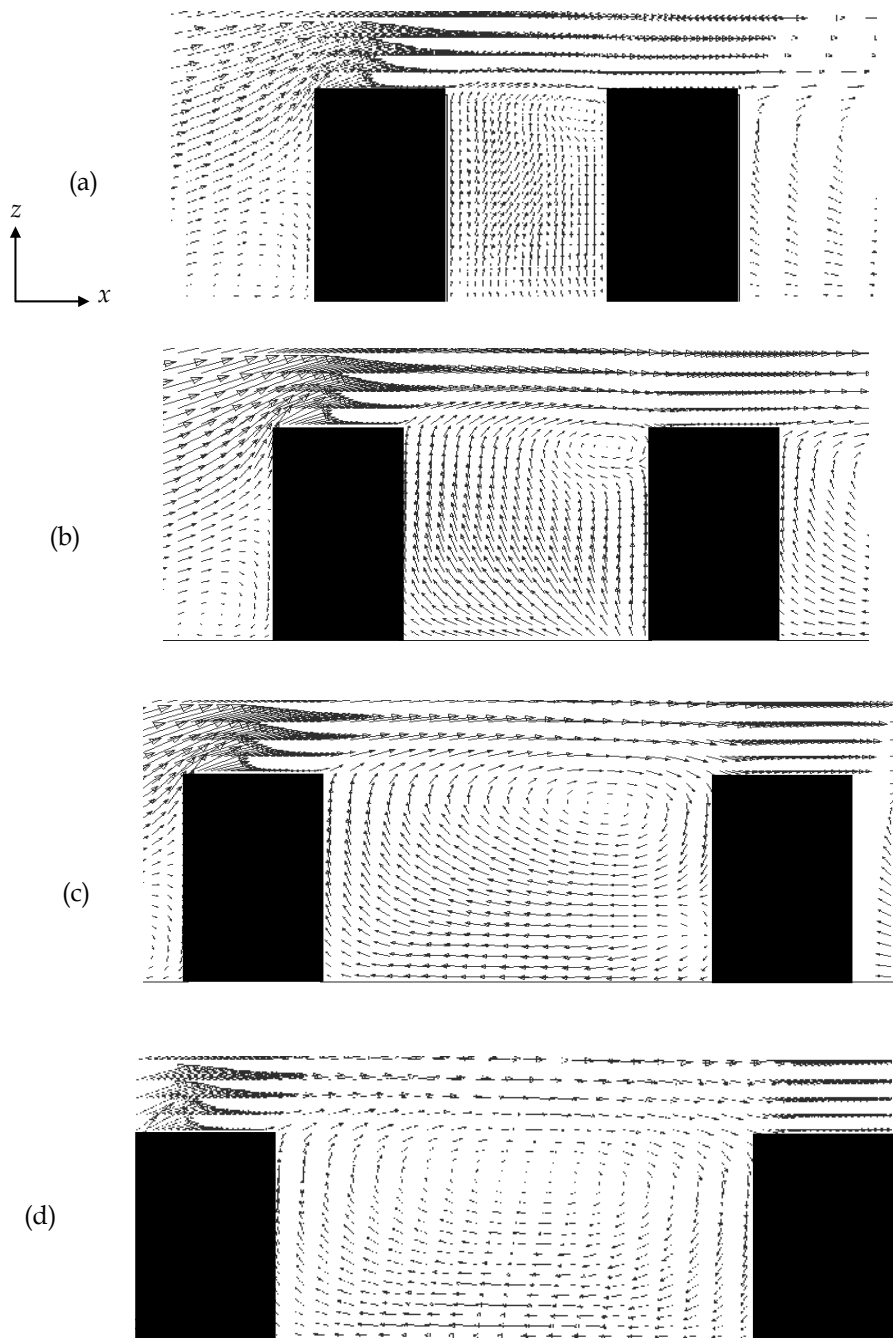
Fig. 4. Influence of street width on the wind flow pattern within the domain (y/W = 0.5)
(a) D/H = 0.6 (b) D/H = 1.0 (c) D/H = 1.5 (d) D/H = 2.0
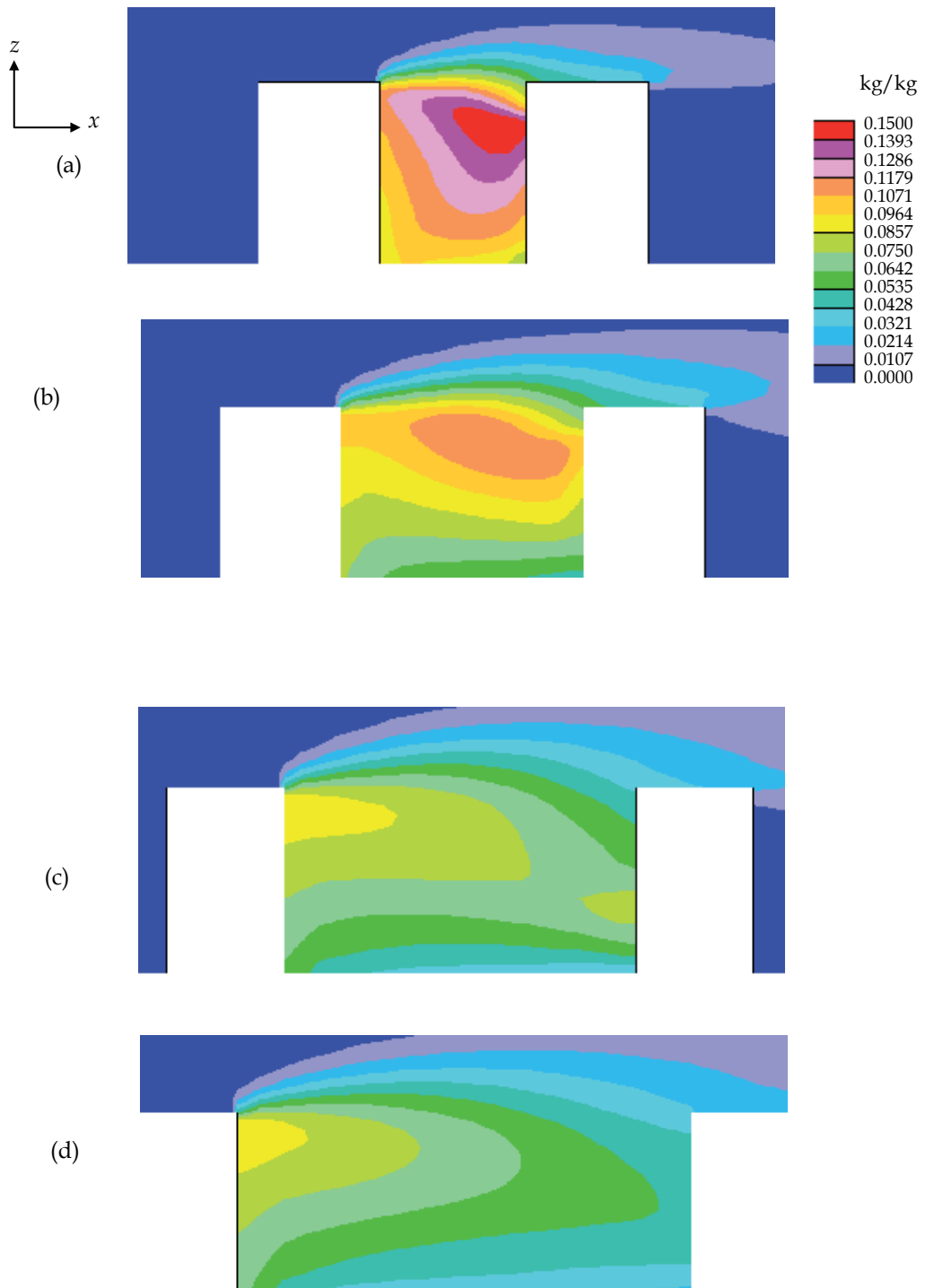
Fig. 5. Concentration fields for different widths of the street domain (y/W = 0.5).
(a) D/H = 0.6   (b) D/H = 1.0   (c) D/H = 1.5   (d) D/H = 2.0

Figure 5 shows the concentration fields within the study domain for the same values of D/H. The figure shows that the level of pollutants within the domain was decrease as D increased, due to the variation of the wind flow characteristics within the street domain with the variation of its width as explained above. Also, the figure shows that the size of the region of influence (Mfula et al., 2005) at which the pollutants disperse becomes larger as the street widens. The wide spread of such region is referred to the increase of the circulation strength (which is generated inside the domain), which improves the wind removal efficiency for purging the pollutants towards the domain exit (Bady et al., 2008).

Effect of street width on the average concentration within the domain is shown in Fig. 6. From this figure, it is obvious that the increase of D has a desirable effect on the concentration, since the concentration decreases as the street widens.

As the street width becomes 20 m (i.e. D/H = 2.0), the concentration level was reduced by about 50 % of its value at D/H = 0.6. This note reflects the fact that the street width is very important parameter in controlling the air quality of urban domains. However, increasing the widths of urban streets depends primarily on the space availability of the construction sites.
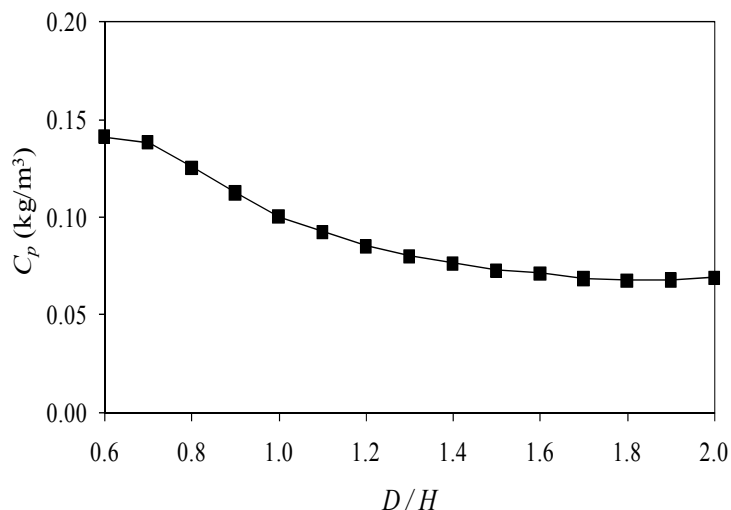
Fig. 6. Effect of street width D on the domain averaged concentration.

Figure 7 shows the influence of D on the wind removal efficiency for the domain's pollutants in terms of the ventilation efficiency indices. The figure shows the normalized PFR and also the air exchange rate which represents the rate at which the total volume of air inside the study domain is replaced with fresh air (AER is calculated through dividing PFR by the volume of the corresponding domain, AER = PFR/V).

As mentioned previously, PFR represents how much fresh air is supplied to the domain which means that PFR has strong dependence on the domain size. Consequently, it is expected that increasing the domain volume increases PFR. This conclusion agrees exactly with the simulation result as shown in Fig. 7, where PFR increases in nearly a linear way with the domain volume.

The second index of the ventilation efficiency indices is the visitation frequency. Figure 7(c) shows that, increasing the width of the street decreases the visitation frequency of the pollutants to it. The trend of VF can be interpreted as follows: the increase of D increases the area subjected to the inlet flux from the boundaries of the domain, which increases the domain inlet fluxes. As a first thinking, increasing the total inlet flux is expected to increase the value of VF as given by Equation (2). This conclusion is not absolutely true because the value of VF depends on the value of the inlet flux as well as the value of the domain volume. The ratio between these two quantities determines the value of VF.

Regarding the residence time of pollutants, Fig. 7(d) shows that the greater the street width, the smaller the time the pollutants stay within the domain. This behaviour is referred to the increased purging capability of the domain wind for pushing the pollutants towards the outside as its volume increases, which reduces the time it takes towards the exit.

The above results for the VE indices supported absolutely that increasing urban streets widths purposefully reduces the air pollution levels (and hence improves the air quality) in the most heavily used streets by enhancing ventilation from the prevailing winds (Bady et al., 2008).

(a)

(b)
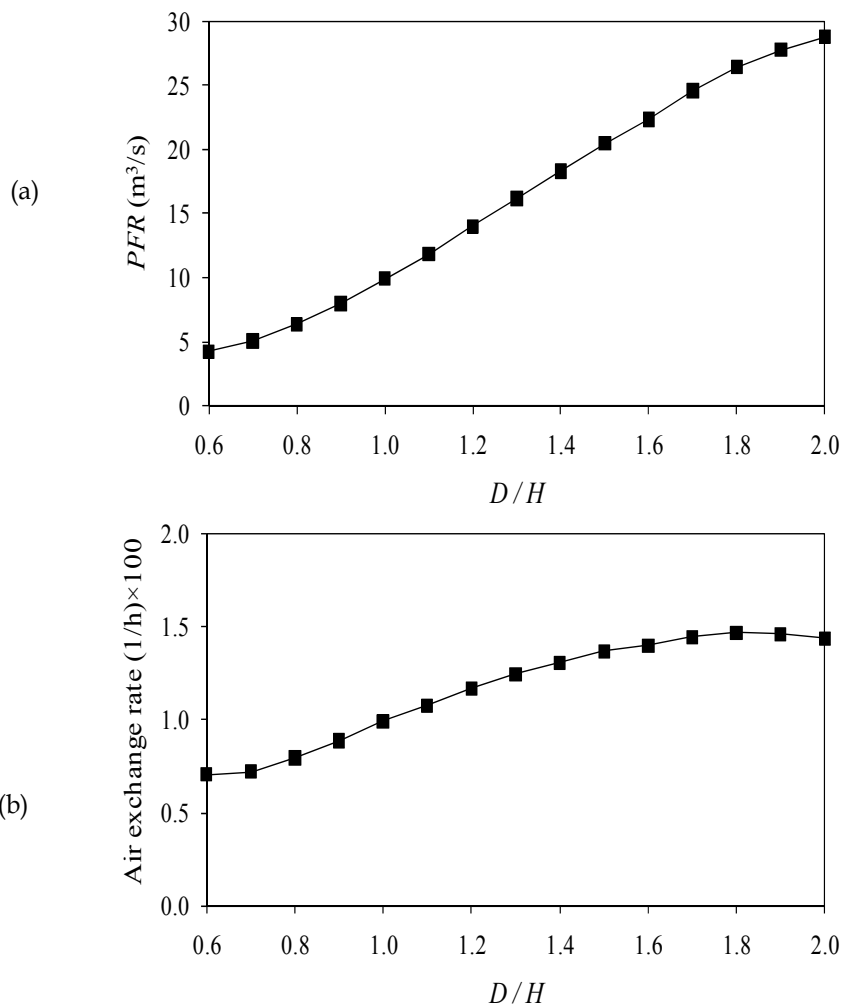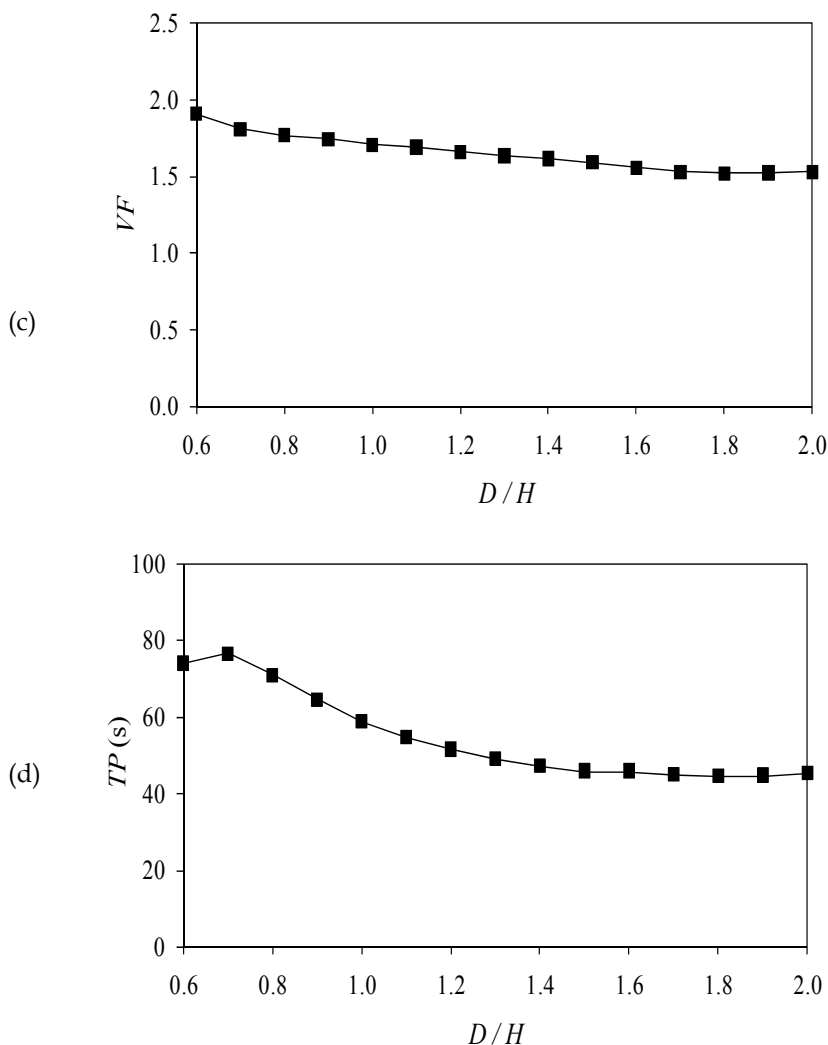
Fig. 7. Effect of street width on the VE indices within the study domain (H = 10 m).
(a) Purging flow rate; (b) Air exchange rate; (c) Visitation frequency; (d) Residence time

5.2 Effect of street buildings height (H)

The other parameter that affects the air flow characteristics in urban domain is the height of street buildings. Figure 8 displays the configuration of the velocity field for four selected cases of H/D (D = 5 m). It can be observed that, as the buildings height increases, a large clockwise vortex circulation is generated along the void between the buildings. The airflow at the center of the vortex circulation is slow and it becomes faster when it approaches the wall of the buildings and the ground level. Changing the height H affects the characteristics of the vortex circulation inside the domain, which in turn affects the diffusion process of the pollutants.
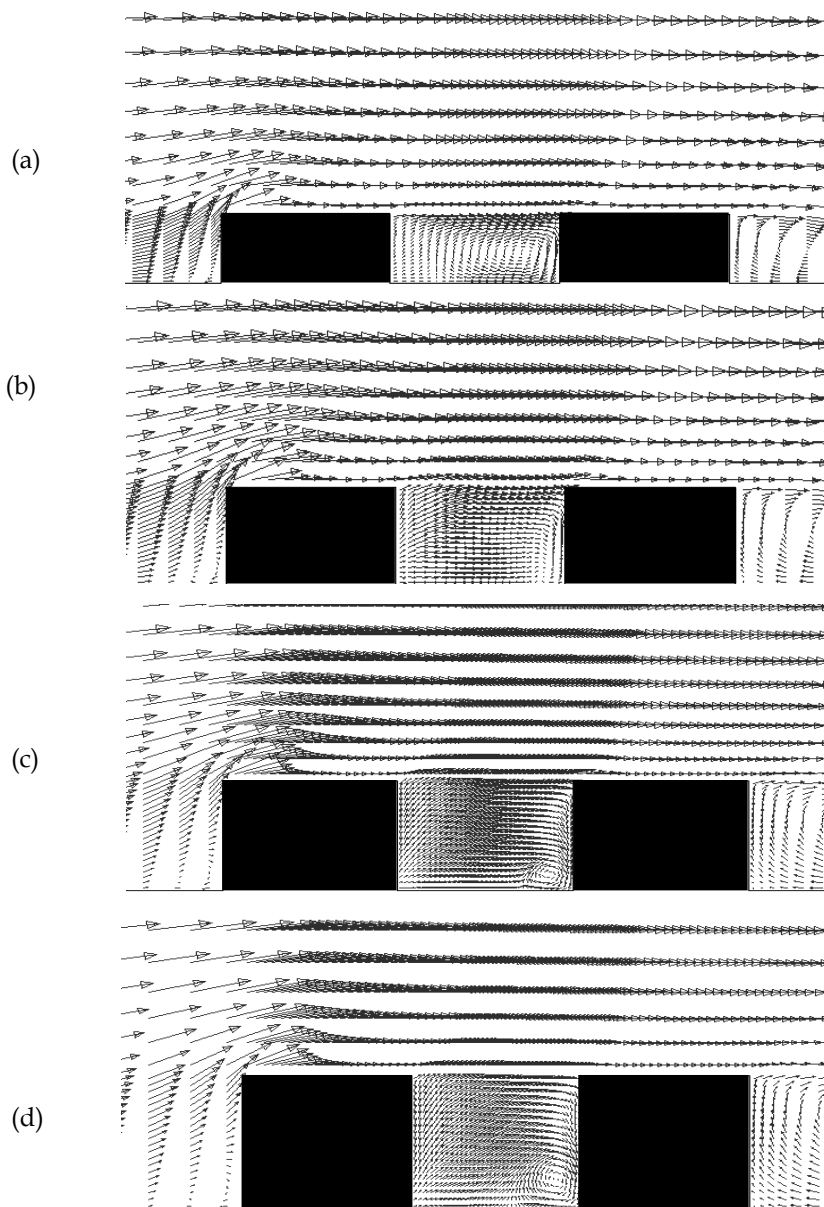
Fig. 8. Influence of building height on the flow pattern within the domain (y/W = 0.5)
(a) H/D = 0.4   (b) H/D = 0.6   (c) H/D = 0.8   (d) H/D = 1.0

Figure 9 shows the concentration fields inside the street at different values of H. In the subplot (a), the pollutant in the study domain is well dispersed and diluted, and the concentration value in such case is the lowest among the four cases. When H increases as shown in the subplots (b) and (d) (i.e. H/D = 0.6 and 0.8), the pollutant dispersion is limited and high concentration zones are observed within the study domain. With the further

increased H (i.e. H/D = 1.0), the high concentration zone increased and covered a large area between the two buildings.
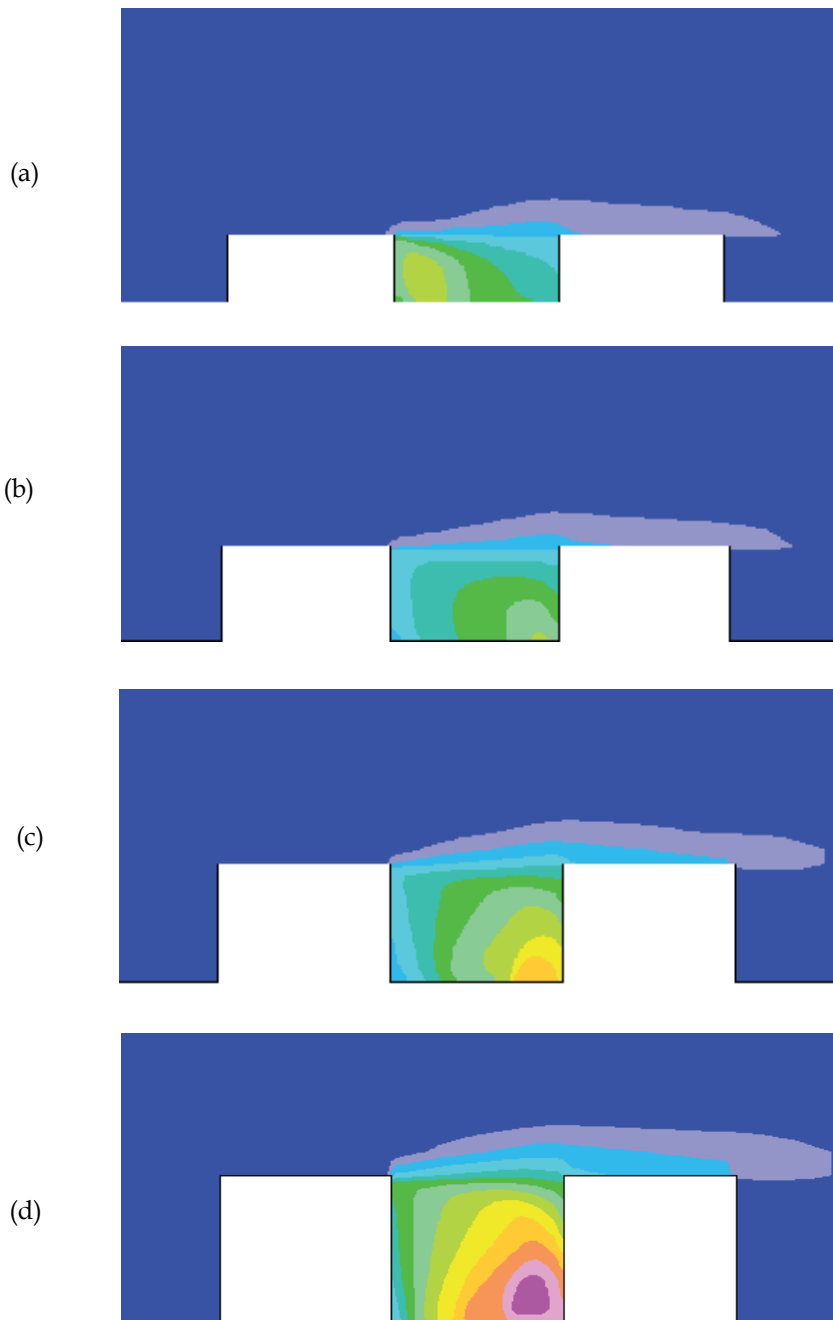
Fig. 9. Concentration fields for different heights of the street buildings (y/W = 0.5).
(a) H/D = 0.4   (b) H/D = 0.6   (c) H/D = 0.8   (d) H/D = 1.0

Figure 10 shows the effect of increasing the street buildings height H on the air quality parameters. As shown, the average concentration increases as the height of the buildings increases which in turn decreases the air exchange rate within the domain. Such effect is attributed to the fact that; increasing the height H weakens the street wind and decreases its ability to purge the pollutants outside the domain as illustrated in Fig. 10; in other words, the pollutants were trapped along the lower part of the domain. The figure shows also that the greater H, the greater the VF values. This can be referred to the increased domain inlet flux with increasing H. Also, the figure shows that the values of VF are greater than one which means that the return or circulation of pollutants is confirmed in the study domain. The relation between the residence time and the building height H is illustrated also in Fig. 10, in which TP increases with the increase of H. This behaviour reflects bad removal efficiency of the wind inside the domain due to the lower vortex strength as the street buildings height increases.

(a)

(b)

(c)

(d)
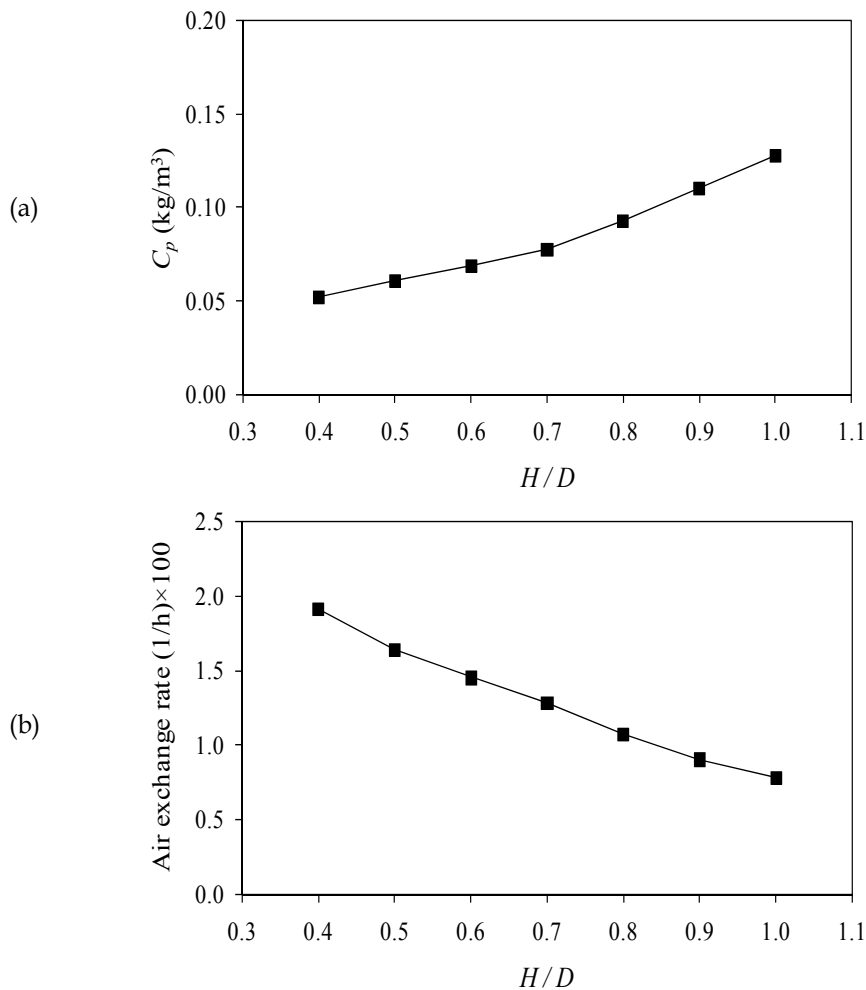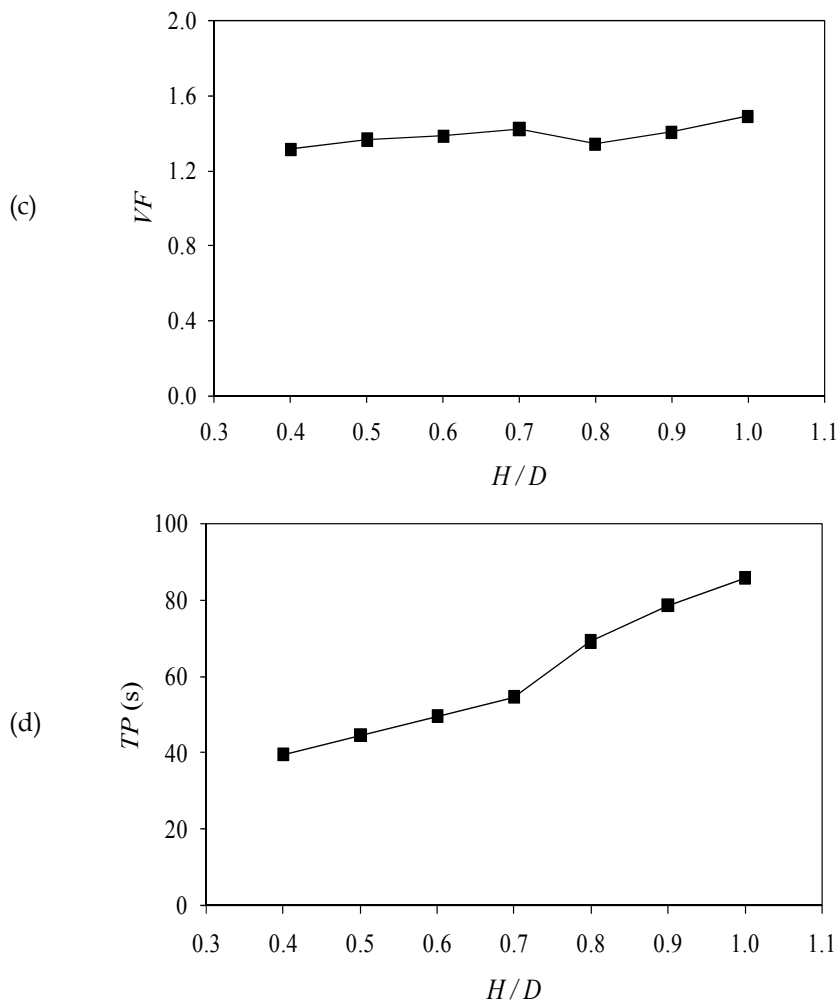
Fig. 10. Effect of street building's height on the air quality parameters within the study domain (D = 5 m); (a) Domain averaged concentration, (b) Air exchange rate, (c) Visitation frequency, (b) Average residence time

5.3 Effect of wind direction

Figure 11 presents the wind vector fields for the five inlet wind directions. According to the incident wind direction, simulated flows can be classified into three patterns regarding the characteristics of the flow circulation generated behind the upwind building (Kim et al., 2004). The first flow pattern appears when the inlet wind angle is 0°. In such case, the horizontal distribution of the wind vector shows symmetric separation located at each lateral side of the upwind building. The figure shows that, there is apparently no motion in the y-direction which reflects a bad removal efficiency of the domain local wind against the pollutant.

The second pattern appears when the flowing wind angle is located in the range 0° < θ < 90°. This pattern appears in the cases of θ = 30°, 45°, 60° in the above figure. For such pattern,

only one vortex appears at the right edge of the upwind building as the incoming wind enters from that side. As the angle θ increases, the vortex size decreases and the flow towards the domain exit in the y-direction increases. This pattern shows an improvement in the domain wind removal efficiency compared with the case of normal wind.
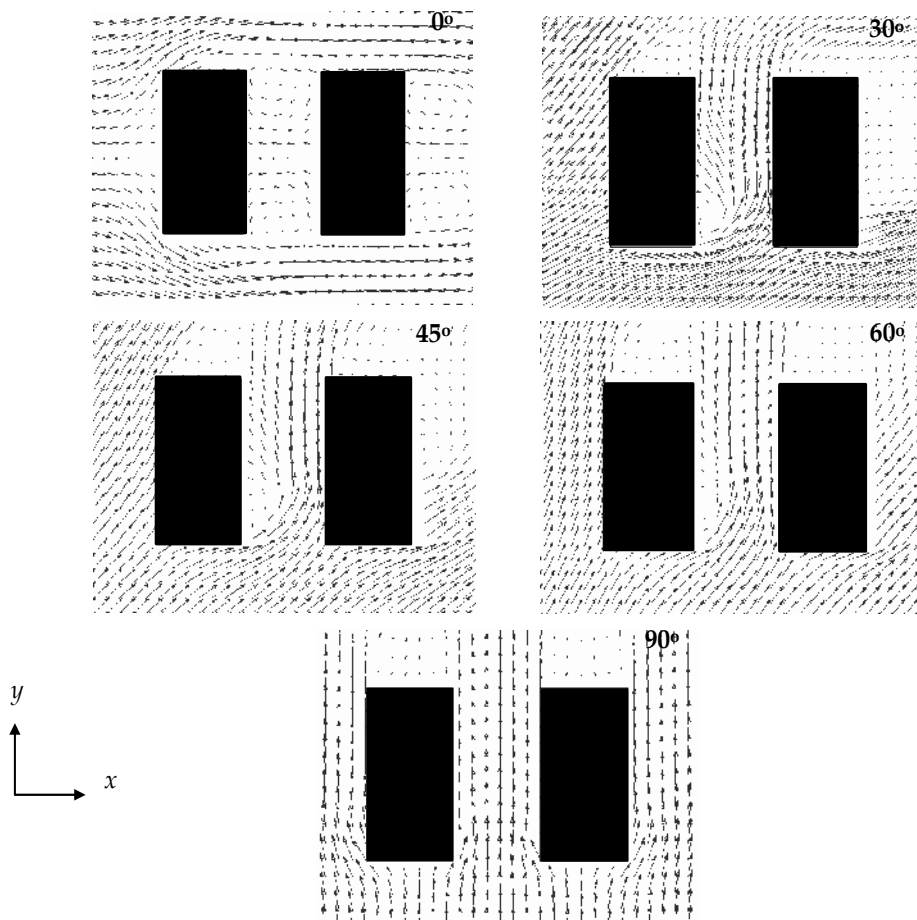
Fig. 11. Horizontal wind vector fields at different wind directions (z = 0.05 m).

The third pattern appears when the wind flows with an angle of 90°. The vortex in that case diminishes and the wind flows smoothly towards the domain exit, which indicates that the removal efficiency of the domain local wind in that that pattern is the best over the above two patterns. Results of the numerical approach for the pollutant concentration inside the street canyon are displayed in Fig. 12. The figure shows the concentration fields at z = 0.05 m for the five wind directions. In the case of normal wind, the concentration field shows symmetry around the central section of the street. It is observed that, high concentration regions appear inside the street canyon, while very low concentration regions appear outside it. That note means that the domain local wind has no ability to carry the pollutants outside the canyon.
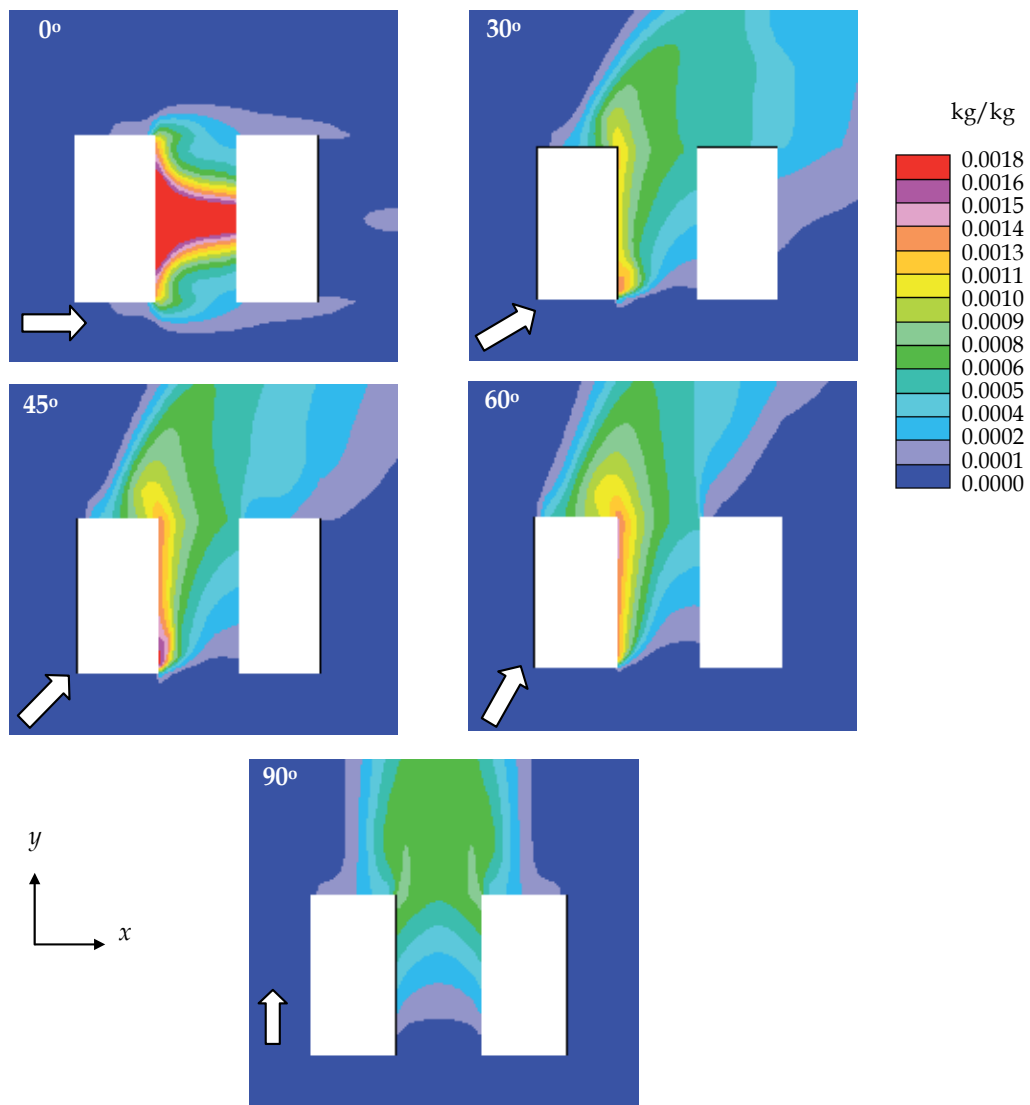
Fig. 12. Concentration fields for different wind directions (z = 0.05 m).

In the cases θ = 30º, 45º, and 60º, the concentration field increased to cover a wide area outside the study domain due to pollutant diffusion towards the outside in the same wind direction. As the maximum concentration area decreases with increasing θ, the canyon averaged concentrations are expected to be lower than the concentration of the case of normal wind as clean air continuously comes into the canyon from outside and dilutes the domain polluted air. Also, it is observed that, very low concentrations exist in the lower part of the figure where clean air arrives. In the case of θ = 90º, a large percentage of the maximum concentration area is shifted outside the canyon, which indicates that the domain average concentration in this case has the lowest value among all of the cases.

The three figures below presents the effects of the applied wind direction on the domain average wind speed, domain pollutant concentrations and on the PFR, inside the study domain. All quantities were normalized by the similar quantities evaluated at the case of normal wind. Figure 13 displays the variation of the air quality parameters with the inflow wind angle. The concentration decrease significantly to about 80% of its value as the flowing wind angle changes from 0º to 90º. That behaviour can be attributed to the increased domain average wind speed. That figure indicates that the domain average speed increases as the wind angle increases it reaches to about 2.5 times as the flow becomes parallel. As the average concentration inside the study domain decrease with increasing the applied wind angle, while the domain volume is kept constant, the PFR is expected to increase. The figure shows that the PFR increases by more than 6 times as the wind flow changes from 0º to 90º. In addition, the trends of VF and TP demonstrate that the ventilation effectiveness within the domain increases as the inflow wind angle increases.

(a)

(b)

(c)

(d)
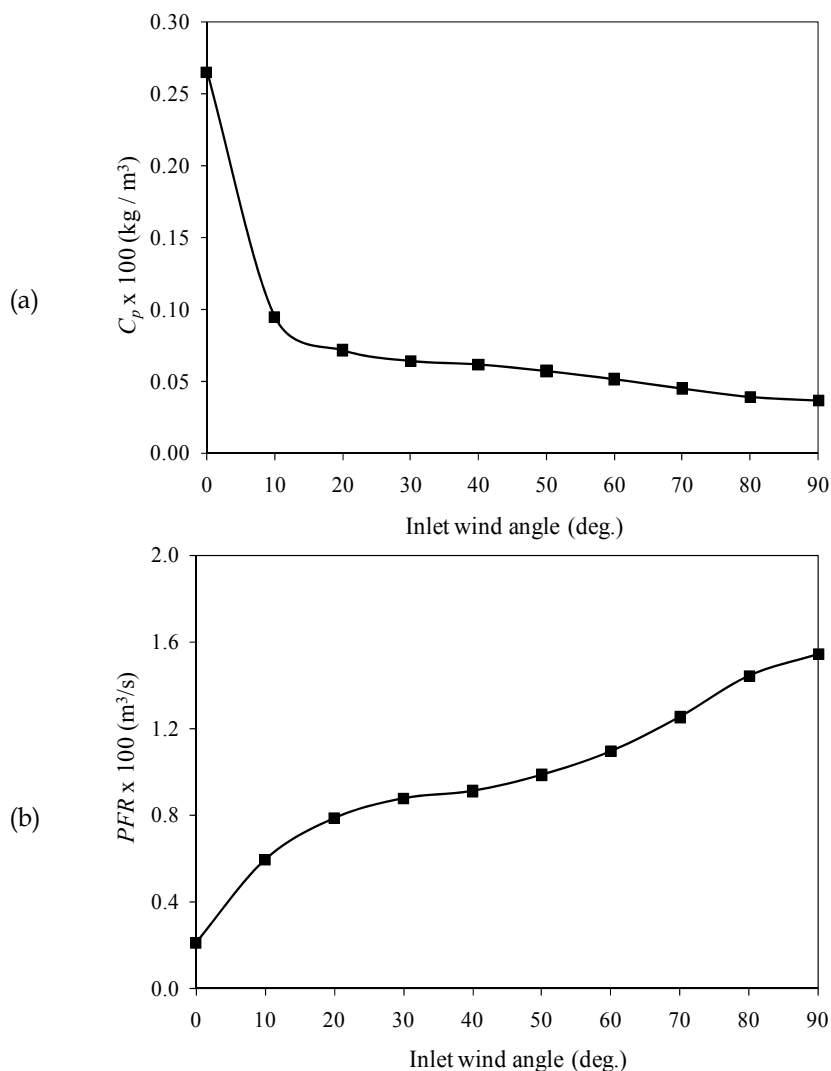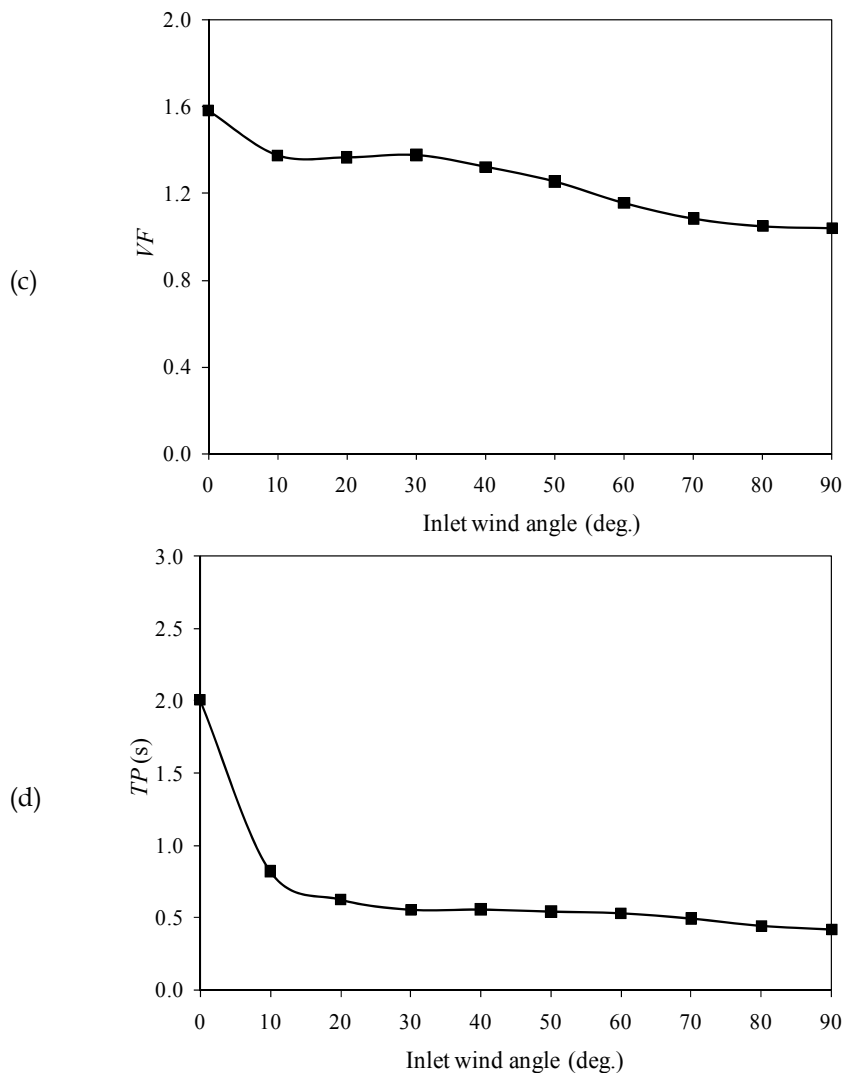
Fig. 13. Air quality parameters within the study domain for variable wind directions; (a) Domain averaged concentration, (b) Purging flow rate, (c) Visitation frequency, (d) Average residence time

5.4. Effect of computational domain height (h)

This section is concerned with investigating the effect of the computational domain height (h) on the VE indices of such domain. The height of the domain was started from 2 m and increased gradually until 10 m, while the width D and the building height H were kept constant at 6 m and 10 m respectively. Figure 14 shows the concentration fields within the street domain for four selected values of h/H (i.e. h/H = 0.2, 0.5, 0.8 and 1.0). Also, Fig. 15 shows the VE indices for different values of the domain height h. In these figures, it is clear that the average concentration increases as the height of the computational domain increases, which in turn decreases the air exchange rate within the domain. In the same time, the

variation of h has no considerable influence on the visitation frequency of the pollutants to the domain. This can be attributed to the fact that both the domain inflow flux and domain's volume are increasing in nearly the same linear way, which is reflected in small changes in the value of VF according to Equation (2). With the increase of domain's volume, the residence time is expected to become higher since the pollutants take more time to be flushed out of the domain.
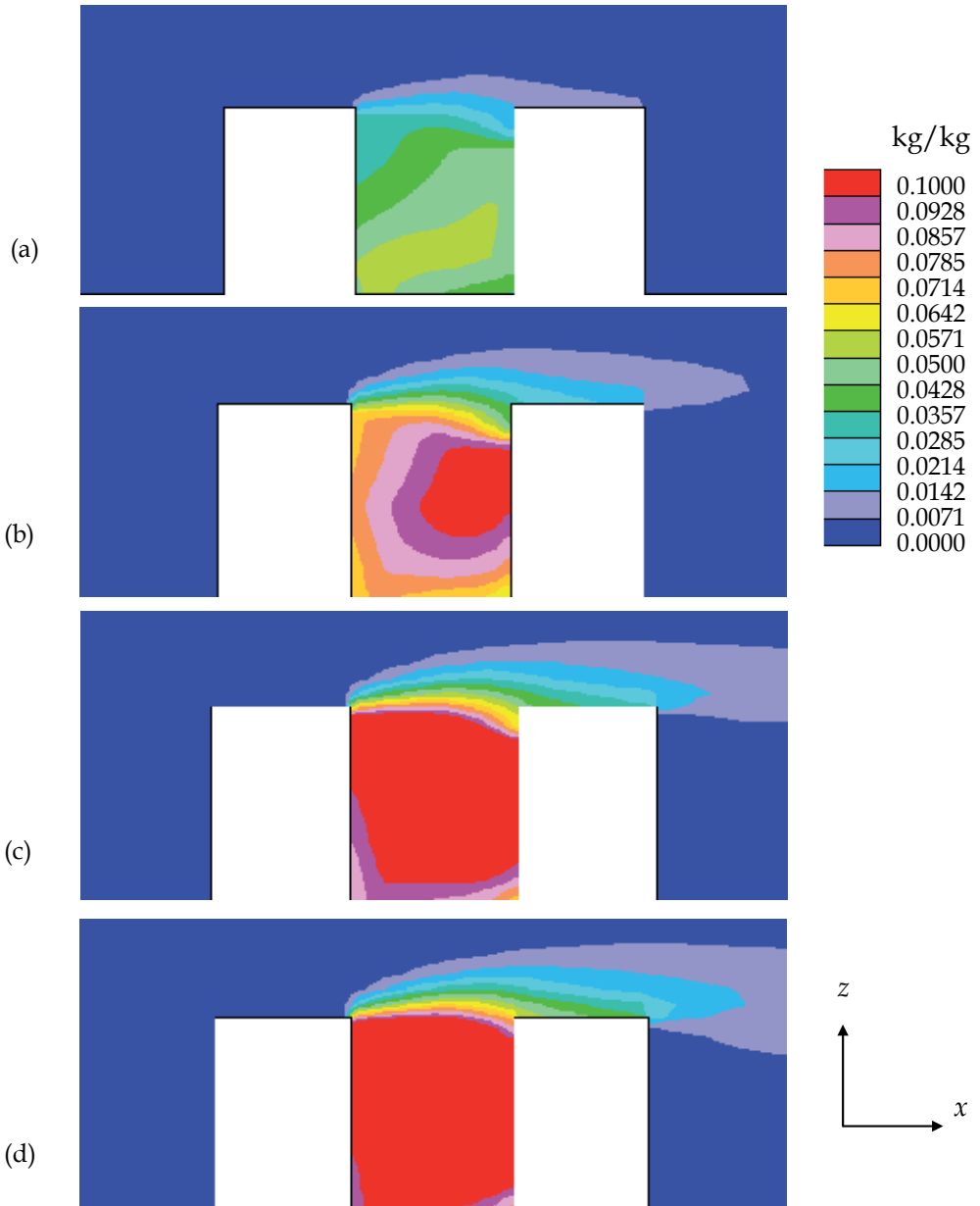
Fig. 14. Concentration fields within the street for different heights of the computational domain (y/W = 0.5); (a) h/H = 0.2, (b) h/H = 0.5, (c) h/H = 0.8, (d) h/H = 1.0

(a)

(b)

(c)

(d)
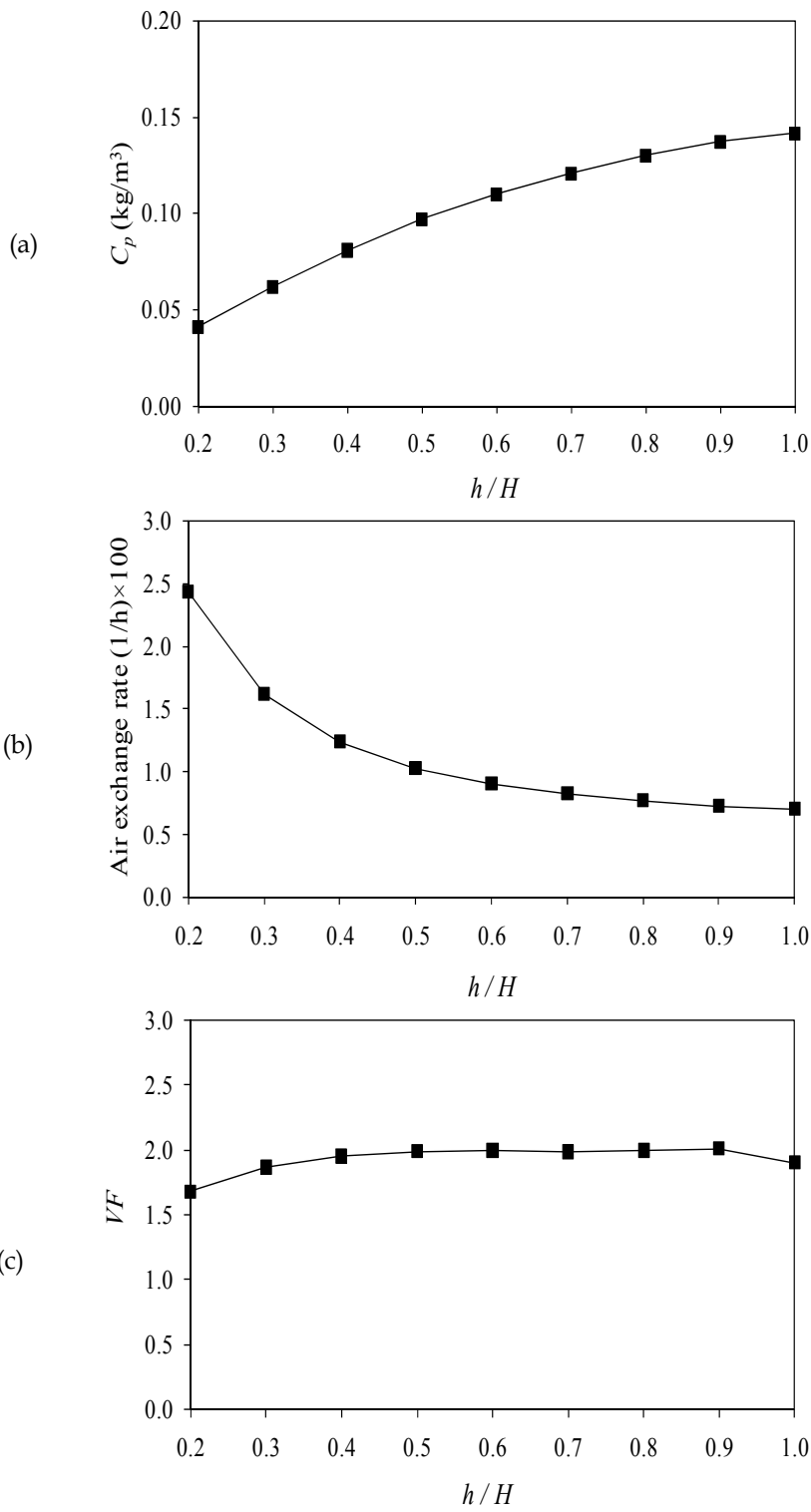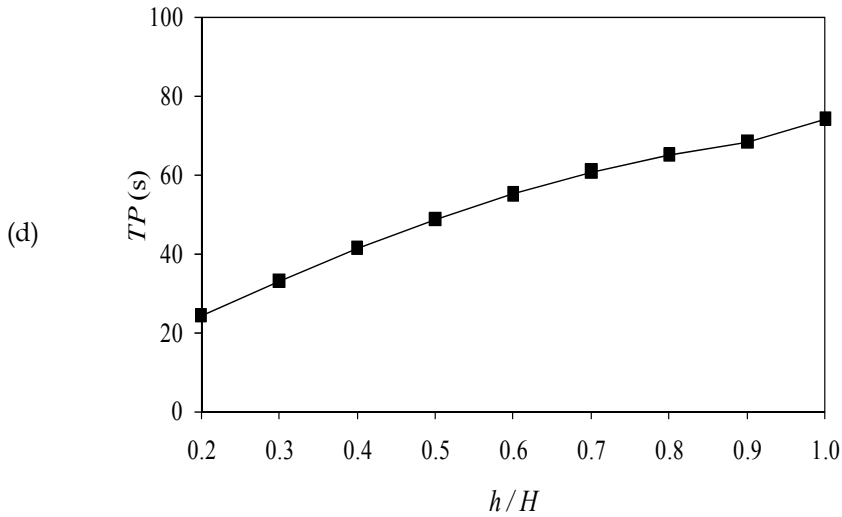
Fig. 15. Effect of computational domain height on the VE indices (D = 6 m, H = 10 m); (a) Domain averaged concentration, (b) Air exchange rate, (c) Visitation frequency, (d) Average residence time.

5.5 Effect of building array configurations

In this section, CFD simulations of the wind flow in densely urban areas – as an example of applying the VE indices in evaluating the air quality of urban domain – are presented. In this example, the VE indices are applied to one of the previously published works (Davidson et al., 1996). Figure 16 shows two building array configurations – aligned and staggered. The two configurations are fundamentally different as the staggered array diverts flow onto neighbouring obstacles whereas the aligned array presents channels through which the flow can pass (Davidson et al., 1996). The aligned array has 42 blocks, while the staggered array is composed of 39 blocks. The dimensions of each block are: 2.3 m height (H), 2.2 m width (W), and 2.45 m breadth (B).

To compare the wind ventilation performance for the two building patterns, seven domains were considered within these arrays, domain (1 ~ 7), as shown in Fig. 16. Wind flow fields were calculated for two directions of 0° and 45°. Figure 17 shows the flow fields around the building patterns for the two directions.

(a)

(b)
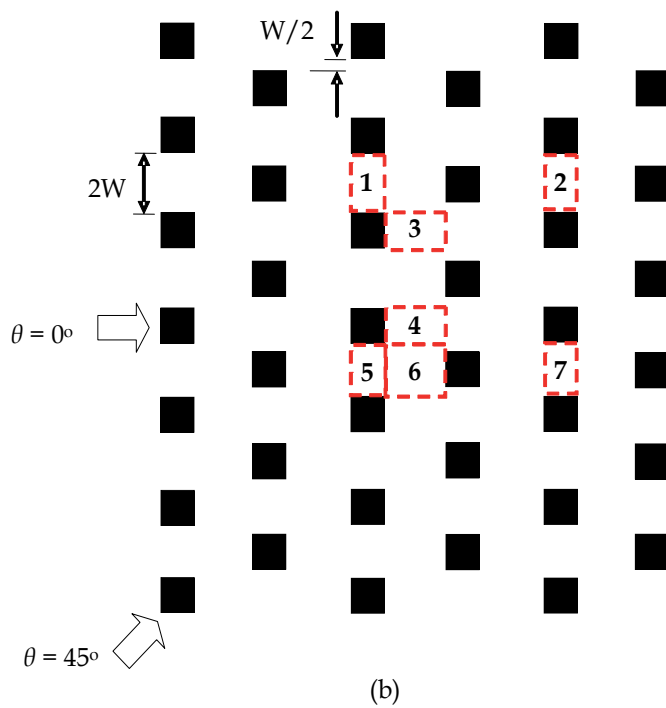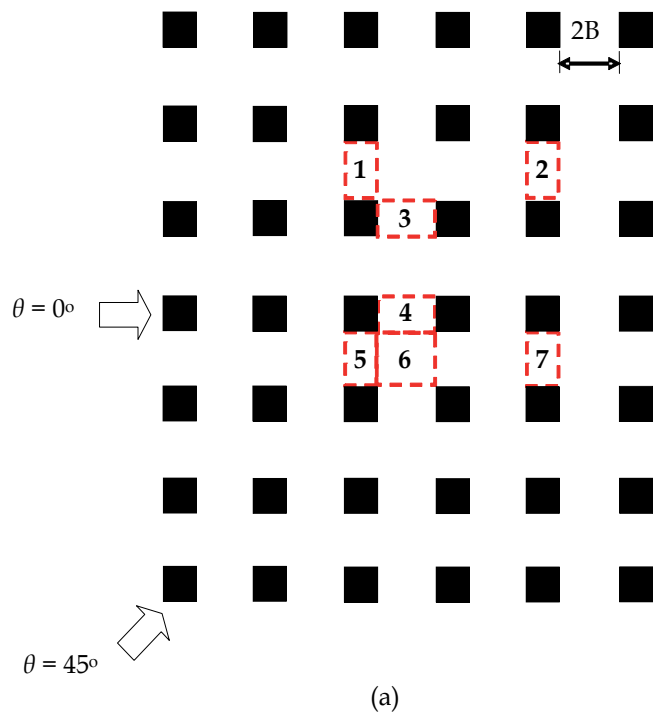
Fig. 16. Schematic of two different building arrays showing the selected domains; (a) aligned, (b) staggered.

The calculated VE indices for the seven domains are shown in Fig. 18. The figure show large variation in the air quality parameters. In the case of $\theta = 0^o$, the staggered array shows undesirable air quality conditions within the selected domains compared with the case of aligned blocks except for domains 3 and 4. High pollutant concentrations and low air exchange rates are observed in this case. Additionally, the purging capability of the natural wind for the staggered distribution was lower than that of the aligned one, reflected by high values for VF and TP. This can be referred to the fact that the staggered distribution of blocks prevents the direct flow between the blocks, which decreases the wind capability in removing the pollutants. On the other hand, the smooth flow of the wind within the aligned array at such wind direction dilutes the pollutant concentrations, and hence improves the air

(a)

(b)
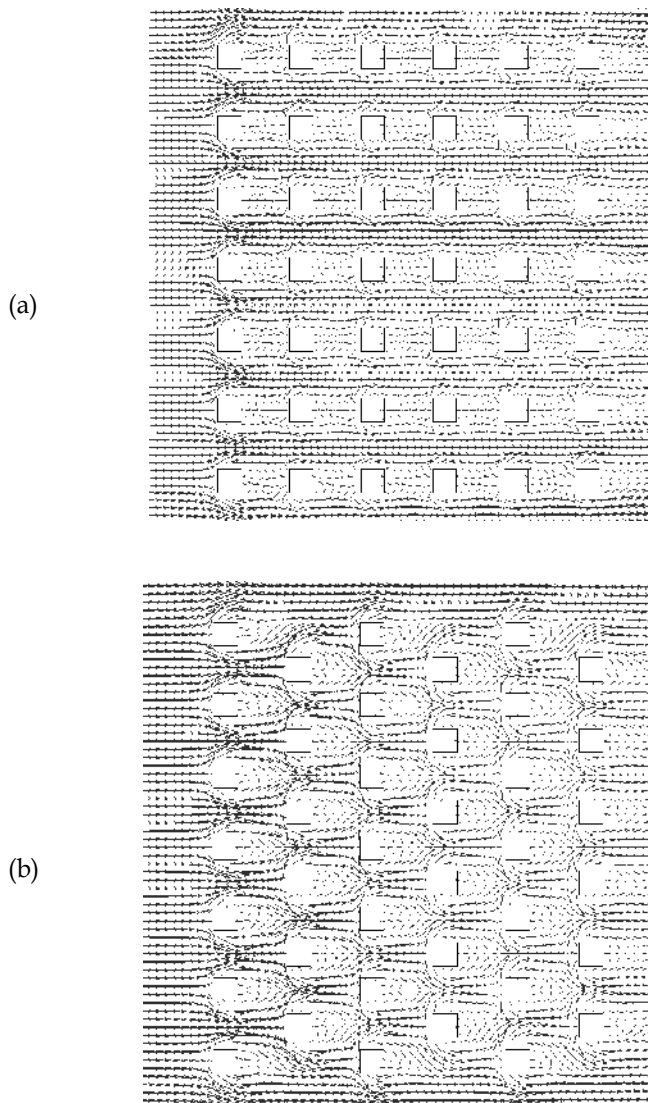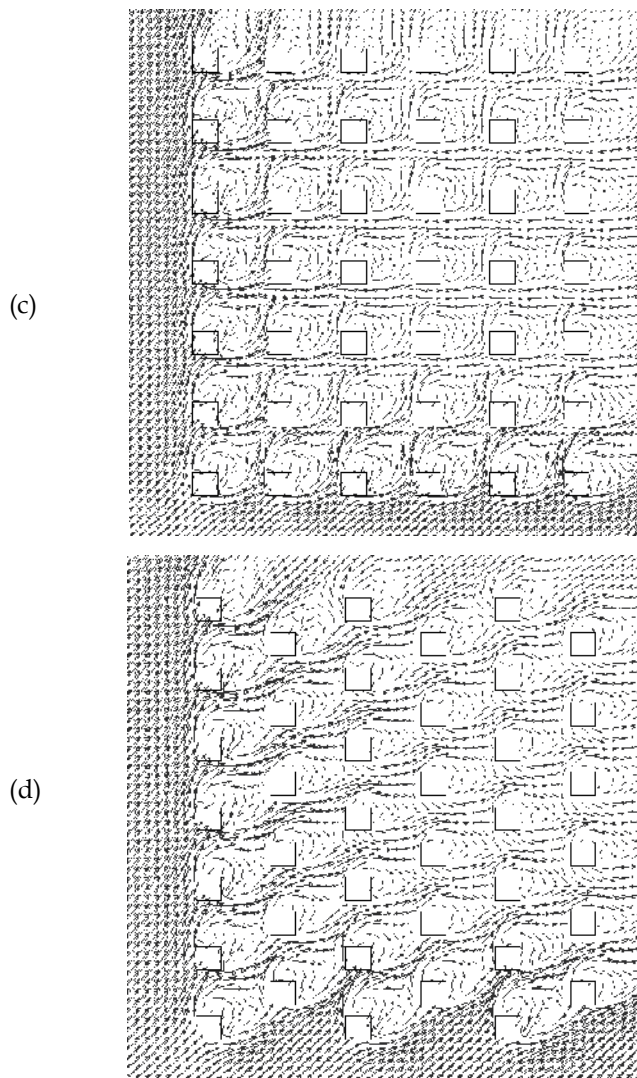
Fig. 17. Wind flow fields around the two building arrays for the two directions (z/H = 0); (a) aligned 0º, (a) staggered 0º, (a) aligned 45º, (a) staggered 0º.

quality of the considered domains. With respect to domains 3 and 4, the locations of such domains within the aligned array are worse than their locations within the staggered one. The geometry of the aligned blocks allows such domains to have three open boundaries, while in the staggered distribution they have four boundaries. Such geometry decreases the ventilation performance of the applied wind of these domains due to the lower inlet flux compared with the other five domains. In the case of $\theta = 45º$, the situation is reversed, where the staggered array show good removal efficiency compared with the aligned array for almost all domains. Such behavior can be attributed to the circulatory vortices that were established around the aligned blocks at such wind direction. These circulatory flows decrease the wind ventilation performance since it reduces the wind velocity within the array domains.

The results of such example show that the ventilation performance of the natural wind within a domain may be changed for the same domain at different conditions of the incident flow. In addition; the results shown confirm that the ventilation efficiency indices are able to reflect the flow characteristics within urban domains very well.
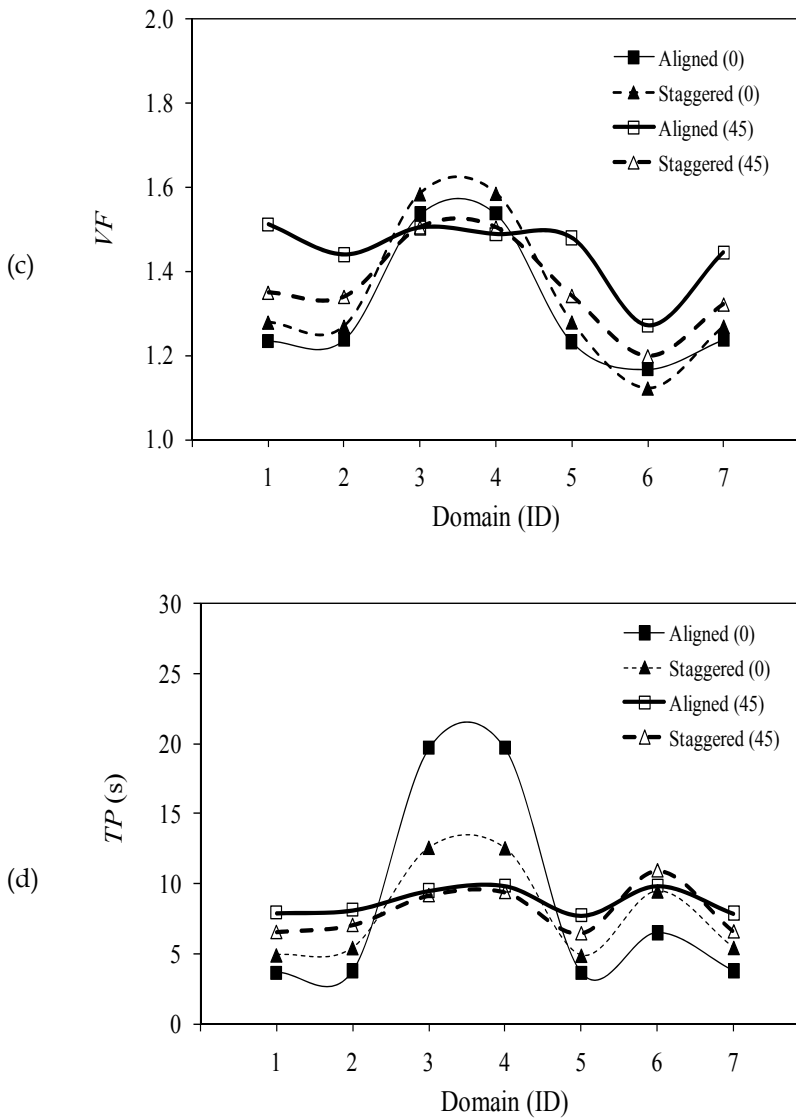
(a)

(b)
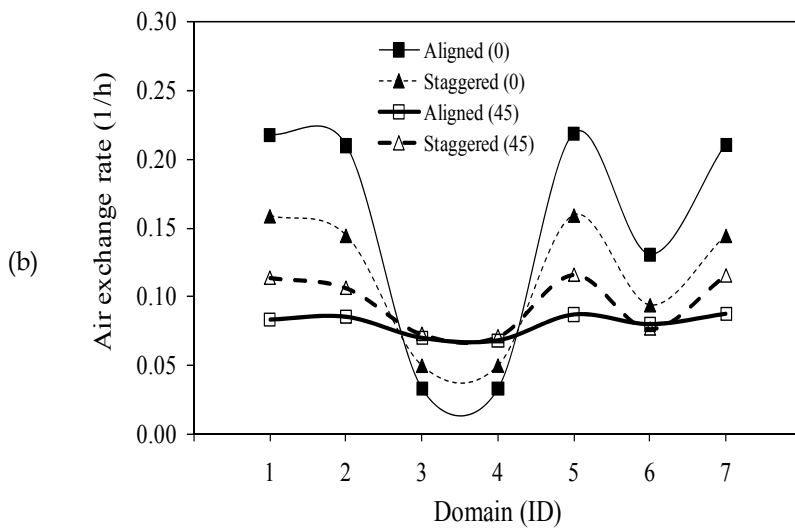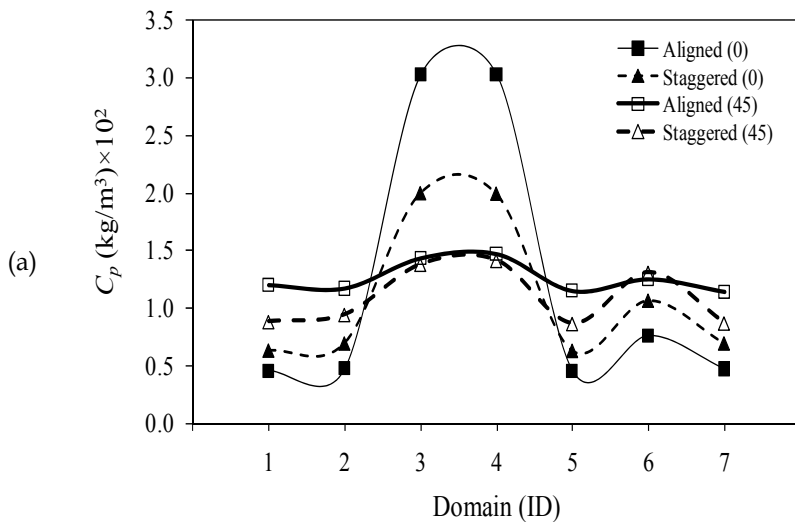
Fig. 18. Air quality parameters within selected domains for the two building arrays; (a) Domain averaged concentration, (b) Air exchange rate, (c) Visitation frequency, (b) Average staying time.

6. Conclusions

Ventilation efficiency indices of indoor environments were applied in evaluating the air quality of urban domains. There are many indices which represent the ventilation efficiency of indoor domains but three indices only are considered here: purging flow rate, visitation frequency and residence time. The calculations of these indices were carried out based on the average flow field analysis using computational fluid dynamics (CFD). Five case studies

for evaluating the air quality of urban domain in terms of the VE indices were considered. In the first and second cases, effects of the geometry of an isolated urban street (street width and street building height) on the air quality within the street domain were investigated. In the third one, the influence of wind direction on the air quality was investigated. In the fourth case, the effect of the computational domain height was investigated. Finally, in the fifth case, the effect of building arrangements on the air quality in dense urban areas was studied.

In conclusions, it can be said that the ventilation efficiency indices of indoor environments appear to be a promising tool in evaluating the air quality of urban domains as well. One of the features of applying these indices is that it is not necessary to consider the location of the pollutant source within the study domain. In addition, the VE indices are able to describe the pollutant behavior within the domain, which is very important for obtaining a complete assessment for the wind ventilation performance within urban domains.

7. References

Chock, D. (1977). A simple line-source model for dispersion near roadways, *Atmospheric Environment*, Vol. 12(4), pp. 823-829.

Sandberg, M. (1992). Ventilation effectiveness and purging flow rate – A review, *Proceedings of the International Symposium on Room Air Convection and Ventilation Effectiveness*; pp. 1-21, Tokyo, Japan.

Ito, K.; Kato S., & Murakami, S. (2000). Study of visitation frequency and purging flow rate based on averaged contaminant distribution–Study on evaluating of ventilation effectiveness of occupied space in room, *Japanese Journal of Architecture Planning and Environmental Engineering (Transaction of AIJ)*, Vol. 529, pp. 31-37, (in Japanese).

Kato, S.; Ito, K. & Murakami, S. (2003). Analysis of visitation frequency through particle tracking method based on LES and model experiment, *Indoor Air*, Vol. 13 (2), pp. 182-193.

Uehara, K.; Murakami, S.; Oikawa, S. & Wakamatsu, S. (1997). Wind tunnel test of concentration fields around street canyons within the stratified urban canopy layer, Part 3: Experimental studies on gaseous diffusion in urban areas; *Journal of Architecture Planning and Environmental Engineering (Transaction of AIJ)*, Vol. 499, pp. 9-16 (in Japanese).

Huang, H.; Ooka, R.; Kato, S. & Jiang, T. (2006). CFD analysis of ventilation efficiency around an elevated highway using visitation frequency and purging flow rate, *Journal of Wind and Structure*, Vol. 9 (4).

Sandberg, M. (1983). The use of moments for ventilation assessing air quality in ventilated Room, *Building and Environment*, Vol. 18 (4), pp. 181-197.

Kato, S. & Murakami, S. (1992). New scales for ventilation efficiency and their application based on numerical simulation and of room airflow, *Proceedings of ISRACVE*, The University of Tokyo, Japan, pp. 22-37.

Mfula, A.; Kukadia, V.; Griffiths, R. & Hall D (2005). Wind tunnel modelling of urban building exposure to outdoor pollution, *Atmospheric Environment*; Vol. 39 (15), pp. 2737-2745.

He, P.; Katayama, T.; Hayashi, T., Tanimoto, J. & Hosooka, I. (1997). Numerical simulation of air flow in an urban area with regularly aligned blocks, *Journal of Wind Engineering and Industrial Aerodynamics*, Vol. 67&68, pp. 281-291.

Lien, S.; Yee, E. & Cheng, Y. (2004). Simulation of mean flow and turbulence over a 2-D building array using high resolution CFD and a distributed drag force approach, *Journal of Wind Engineering and Industrial Aerodynamics*, Vol. 92, pp. 117-158.

Kim, J. & Baik, J. (2004). A numerical study of the effects of ambient wind direction on flow and dispersion in urban street canyon using the RNG k-ε turbulent model, *Atmospheric Environment*, Vol. 38, pp. 3039-3048.

Ferzigere, J. & Peric, M. (1997). Computational methods for fluid dynamics, Springer, Third Edition.

Xiaomin, X.; Zhen, H. & Jia, S. (2005). Impact of building configuration on air quality in street canyon, *Atmospheric Environment*, Vol. 39 (25), pp. 4519-4530.

Kanda, I.; Uehara, K.; Yamao, Y.; Yoshikawa, Y., & Morikawa, T. (2006). A wind tunnel study on exhaust gas dispersion from road vehicles -Part II: Effect of vehicle queues, *Journal of Wind Engineering and Industrial Aerodynamics*, Vol. 94(9), pp. 659-673.

Tsai, Y. & Chen, S. (2004). Measurements and three-dimensional modelling of air pollutant dispersion in an urban street canyon, *Atmospheric Environment*; Vol. 38(35), pp. 5911-5924.

Baker, C. J. & Hargreaves, D. M. (2001). Wind tunnel evaluation of a vehicle pollution dispersion model, *Journal of Wind Engineering and Industrial Aerodynamics*; Vol. 89(2), pp. 187-200.

Ahmad, K.; Khare, M. & Chaudhry, K. (2005). Wind tunnel simulation studies on dispersion at urban street canyons and intersections- A review, *Journal of Wind Engineering and Industrial Aerodynamics*; Vol. 93 (9), pp. 697-717.

Bady, M.; Kato, S.; Takahashi, T. & Huang, H. (2008). An experimental investigation of the wind environment and air quality within a densely populated urban street canyon. Submitted.

Bady, M.; Kato, S.; Ishida, Y.; Huang, H; & Takahashi, T. (2008). Exceedance probability as a tool to evaluate the wind environment within densely urban areas". *Journal of Wind and Structure*, Vol. 11(6).

Hui, S.; & Davidson, L. (1997). Towards the determination of the local purging flow rate, *Building and Environment*; Vol. 32(6), pp. 513-525.

Bady, M.; Kato, S.; & Huang, H. (2008). Towards the application of indoor ventilation efficiency indices to evaluate the air quality of urban areas, *Building and Environment*, Vol. 43(12).

Davidson, M.; Snyder, W.; Lawson R. & Hunt J. (1996). Wind tunnel simulation of plume dispersion through groups of obstacles, *Atmospheric Environment*; Vol. 30(22), pp. 3715-3731.

Nonlocal-closure schemes for use in air quality and environmental models

Dragutin T. Mihailović and Ana Firanj

Faculty of Agriculture, University of Novi Sad, Novi Sad, SERBIA
Dositeja Obradovića Sq. 8, 21000 Novi Sad

1. Introduction

The description of the atmospheric boundary layer (ABL) processes, understanding of complex boundary layer interactions, and their proper parameterization are important for air quality as well as many other environmental models. In that sense single-column vertical mixing models are comprehensive enough to describe processes in ABL. Therefore, they can be employed to illustrate the basic concepts on boundary layer processes and represent serviceable tools in boundary layer investigation. When coupled to 3D models, single-column models can provide detailed and accurate simulations of the ABL structure as well as mixing processes.

Description of the ABL during convective conditions has long been a major source of uncertainty in the air quality models and chemical transport models. There exist two approaches, local and nonlocal, for solving the turbulence closure problem. While the local closure assumes that turbulence is analogous to molecular diffusion in the nonlocal-closure, the unknown quantity at one point is parameterized by values of known quantities at many points in space. The simplest, most popular local closure method in Eulerian air quality and chemical transport models is the K-Scheme used both in the boundary layer and the free troposphere. Since it uses local gradients in one point of model grid, K-Scheme can be used only when the scale of turbulent motion is much smaller than the scale of mean flow (Stull, 1988), such as in the case of stable and neutral conditions in the atmosphere in which this scheme is consistent. However, it can not: (a) describe the effects of large scale eddies that are dominant in the convective boundary layer (CBL) and (b) simulate counter-gradient flows where a turbulent flux flows up to the gradient. Thus, K-Scheme is not recommended in the CBL (Stull, 1988). Recently, in order to avoid the K-scheme drawbacks, Alapaty (Alapaty, 2003; Alapaty & Alapaty, 2001) suggested a "nonlocal" turbulent kinetic energy (TKE) scheme based on the K-Scheme that was intensively tested using the EMEP chemical transport model (Mihailovic & Jonson, 2005; Mihailovic & Alapaty, 2007). In order to quantify the transport of a passive tracer field in three-dimensional simulations of turbulent convection, the nonlocal and non-diffusive behavior can be described by a transilient matrix whose elements contain the fractional tracer concentrations moving from one subvolume to another as a function of time. The approach was originally developed for and applied to geophysical flows known as turbulent transilient theory (T3) (Stull, 1988; Stull & Driedonks,

1987; Alapaty et al., 1997), but this formalism was extended and applied in an astrophysical context to three-dimensional simulations of turbulent compressible convection with overshoot into convectively stable bounding regions (Miesch et al., 2000). The most frequently used nonlocal-closure method is the asymmetric convective model (ACM) suggested by Pleim & Chang (1992). The design of this model is based on the Blackadar's scheme (Blackadar, 1976), but takes into account the important fact that, in the CBL, the vertical transport is asymmetrical (Wyngaard & Brost, 1984). Namely, the buoyant plumbs are rather fast and narrow, while downward streams are wide and slow. Accordingly, transport by upward streams should be simulated as nonlocal and transport by downward streams as local. The concept of this model is that buoyant plumbs rise from the surface layer and transfer air and its properties directly into all layers above. Downward mixing occurs only between adjacent layers in the form of a slow subsidence. The ACM can be used only during convective conditions in the ABL, while stable or neutral regimes for the K-Scheme are considered. Although this approach results in a more realistic simulation of vertical transport within the CBL, it has some drawbacks that can be elaborated in condensed form: (i) since this method mixes the same amount of mass to every vertical layer in the boundary layer, it has the potential to remove mass much too quickly out of the surface layer and (ii) this method fails to account for the upward mixing in layers higher than the surface layer (Tonnesen et al., 1998). Wang (Wang, 1998) has compared three different vertical transport methods: a semi-implicit K-Scheme (SIK) with local closure and the ACM and T3 schemes with nonlocal-closure. Of the three schemes, the ACM scheme moved mass more rapidly out of surface layer into other layers than the other two schemes in terms of the rate at which mass was mixed between different layers. Recently, this scheme was modified with varying upward mixing rates (VUR), where the upward mixing rate changes with the height, providing slower mixing (Mihailović et al., 2008).

The aim of this chapter is to give a short overview of nonlocal-closure TKE and ABL mixing schemes developed to describe vertical mixing during convective conditions in the ABL. The overview is supported with simulations performed by the chemical EMEP Unified model (version UNI-ACID, rv2.0) where schemes were incorporated.

2. Description of nonlocal-closure schemes

2.1. Turbulent kinetic energy scheme (TKE)

As we mentioned above the well-known issues regarding local-closure ABL schemes is their inability to produce well-mixed layers in the ABL during convective conditions. Holtslag & Boville (1993) using the NCAR Community Climate Model (CCM2) studied a classic example of artifacts resulting from the deficiencies in the first-order closure schemes. To alleviate problems associated with the general first-order eddy-diffusivity K-schemes, they proposed a nonlocal K-scheme. Hong & Pan (1996) presented an enhanced version of the Holtslag & Boville (1993) scheme. In this scheme the friction velocity scale (u_*) is used as a closure in their formulation. However, for moderate to strong convective conditions, u_* is not a representative scale (Alapaty & Alapaty, 2001). Rather, the convective velocity (w_*) scale is suitable as used by Hass et al. (1991) in simulation of a wet deposition case in Europe by the European Acid Deposition Model (EURAD). Depending on the magnitude of the scaling parameter h/L (h is height of the ABL, and L is Monin-Obukhov length), either

u_* or w_* is used in many other formulations. Notice that this approach may not guarantee continuity between the alternate usage of u_* and w_* in estimating K - eddy diffusivity. Also, in most of the local-closure schemes the coefficient of vertical eddy diffusivity for moisture is assumed to be equal to that for heat. Sometimes this assumption leads to vertical gradients in the simulated moisture fields, even during moderate to strong convective conditions in the ABL. Also, the nonlocal scheme considers the horizontal advection of turbulence that may be important over heterogeneous landscapes (Alapaty & Alapaty, 2001; Mihailovic et al. 2005).

The starting point of approach is to consider the general form of the vertical eddy diffusivity equation. For momentum, this equation can be written as

$$K_m = \frac{\overline{e}_* k z \left(1 - \frac{z}{h}\right)^p}{\Phi_m} \tag{1}$$

where K_m is the vertical eddy diffusivity, $\overline{e}_*$ is the mean turbulent velocity scale within the ABL to be determined (closure problem), k is the von Karman constant ($k = 0.41$), z is the vertical coordinate, p is the profile shape exponent coming from the similarity theory (Troen & Mahrt, 1986; usually taken as 2), and Φ_m is the nondimensional function of momentum. According to Zhang et al. (1996), we use the square root of the vertically averaged turbulent kinetic energy in the ABL as a velocity scale, in place of the mean wind speed, the closure to Eq. (1). Instead of using a prognostic approach to determine TKE, we make use of a diagnostic method. It is then logical to consider the diagnostic TKE to be a function of both u_* and w_*. Thus, the square root of diagnosed TKE near the surface serves as a closure to this problem (Alapaty & Alapaty, 2001). However, it is more suitable to estimate $\overline{e}_*$ from the profile of the TKE through the whole ABL.

According to Moeng & Sullivan (1994), a linear combination of the turbulent kinetic energy dissipation rates associated with shear and buoyancy can adequately approximate the vertical distribution of the turbulent kinetic energy, $e(z)$, in a variety of boundary layers ranging from near neutral to free convection conditions. Following Zhang et al. (1996) the TKE profile can be expressed as

$$e(z) = \frac{1}{2}\left(\frac{L_E}{h}\right)^{2/3}\left[0.4 w_*^3 + u_*^3 \left(h - z\right)\frac{\Phi_m}{kz}\right]^{2/3}, \tag{2}$$

where L_E characterizes the integral length scale of the dissipation rate. Here, $\Phi_m = \left(1 - 15 z / L\right)^{-1/4}$ is an empirical function for the unstable atmospheric surface layer (Businger et al., 1971), which is applied to both the surface and mixed layer. We used $L_E = 2.6h$ which is in the range $2.5h - 3.0h$ suggested by Moeng & Sullivan (1994). For the stable atmospheric boundary layer we modeled the TKE profile using an empirical function proposed by Lenschow et al. (1988), based on aircraft observations

$$\frac{e(z)}{u_*^2} = 6\left(1 - \frac{z}{h}\right)^{1.75}.$$

(3)

Following LES (Large Eddy Simulation) works of Zhang et al. (1996) and Moeng & Sullivan (1994), Alapaty (2003) suggested how to estimate the vertically integrated mean turbulent velocity scale $\overline{e}_*$ that within the ABL can be written as

$$e_* = \frac{1}{h}\int_0^h \sqrt{e(z)}\Psi(z)dz,$$

(4)

where $\Psi(z)$ is the vertical profile function for turbulent kinetic energy as obtained by Zhang et al. (1996) based on LES studies, later modified by Alapaty (personal communication), and dz is layer thickness.

The formulation of eddy-diffusivity by Eq. (1) depends on h. We follow Troen & Mahrt (1986) for determination of h using

$$h = \frac{Ri_c\left\{u(h)^2 + v(h)^2\right\}}{\frac{g}{\theta_0}\left\{\theta_v(h) - \theta_s\right\}},$$

(5)

where Ri_c is a critical bulk Richardson number for the ABL, $u(h)$ and $v(h)$ are the horizontal velocity components at h, g/θ_0, is the buoyancy parameter, θ_0 is the appropriate virtual potential temperature, and $\theta_v(h)$ is the virtual potential temperature of air near the surface at h, respectively. For unstable conditions $(L < 0)$, θ_s is given by (Troen & Mahrt (1986))

$$\theta_s = \theta_v(z_1) + C_0\frac{\overline{w\theta_{v0}}}{w_s},$$

(6)

where $C_0 = 8.5$ (Holtslag et al., 1990), w_s is the velocity while $\overline{w\theta_{v0}}$ is the kinematics surface heat flux. The velocity w_s is parameterized as

$$w_s = \left(u_*^3 + c_1 w_*^3\right)^{1/3}$$

(7)

and

$$w_* = \left[(g/\theta_0)w\theta_{v0}h\right]^{1/3}.$$

(8)

Using $c_1 = 0.6$. In Eq. (6), $\theta_v(z_1)$ is the virtual temperature at the first model level. The second term on the right-hand side of Eq. (6) represents a temperature excess, which is a measure in the lower part of the ABL. For stable conditions we use $\theta_s = \theta_v(z_1)$ with $z_1 = 2$ m.

On the basis of Eq. (5) the height of the ABL can be calculated by iteration for all stability conditions, when the surface fluxes and profiles of θ_v, u and v are known. The computation starts with calculating the bulk Richardson number Ri between the level θ_s and subsequent higher levels of the model. Once Ri exceeds the critical value, the value of h is derived with linear interpolation between the level with $Ri > Ri_c$ and the level underneath. We use a minimum of 100 m for h. In Eq. (5), Ri_c is the value of the critical bulk Richardson number used to be 0.25 in this study.

In the free atmosphere, turbulent mixing is parameterized using the formulation suggested by Blackadar (1979) in which vertical eddy diffusivities are functions of the Richardson number and wind shear in the vertical. This formulation can be written as

$$K_m = K_0 + S(kl)^2 \frac{Rc - Ri}{Rc} , \tag{9}$$

where K_0 is the background value (1 m² s⁻¹), S is the vertical wind shear, l is the characteristic turbulent length scale (100 m), Rc is the critical Richardson number, and Ri is the Richardson number defined as

$$Ri = \frac{g}{\theta_v S^2} \frac{\partial \theta_v}{\partial z} . \tag{10}$$

The critical Richardson number in Eq. (9) is determined as

$$Rc = 0.257 (\Delta z)^{0.175} , \tag{11}$$

where Δz is the layer thickness (Zhang & Anthes, 1982).

2.2. Nonlocal vertical mixing schemes

The nonlocal vertical mixing schemes were designed to describe the effects of large scale eddies, that are dominant in the CBL and to simulate counter-gradient flows where a turbulent flux flows up to the gradient. During convective conditions in the atmosphere, both small-scale subgrid and large-scale super grid eddies are important for vertical transport. In this section, we will consider three different nonlocal mixing schemes: the Blackadar's scheme (Blackadar, 1976), the asymmetrical convective model (Pleim & Chang, 1992) and the scheme with varying upward mixing rates (Mihailovic et al., 2008).

Transilient turbulence theory (Stull, 1988) (the Latin word *transilient* means to jump over) is a general representation of the turbulent flux exchange processes. In transilient mixing schemes, elements of flux exchange are defined in an $N \times N$ transilient matrix, where N is the number of vertical layers and mixing occurs not only between adjacent model layers, but also between layers not adjacent to each other. That means that all of the matrix elements are nonzero and that the turbulent mixing in the convective boundary layer can be written as

$$\frac{\partial c_i}{\partial t} = \sum_{j=1}^{N} M_{ij} c_j \quad , \tag{12}$$

where c is the concentration of passive tracer, the elements in the mixing matrix M represent mass mixing rates, and i and j refer to two different grid cells in a column of atmosphere. Some models specify mixing concepts with the idea of reducing the number of nonzero elements because of the cost of computational time during integration.

The Blackadar's scheme (Blackadar, 1976) is a simple nonlocal-closure scheme, that is designed to describe convective vertical transport by eddies of varying sizes. The effect of convective plumes is simulated by mixing material directly from the surface layer with every other layer in the convective layer. The schematic representation of vertical mixing simulated by the Blackadar's scheme is given in Fig. 1. The mixing algorithm can be written for the surface and every other layer as

$$\frac{\partial c_1}{\partial t} = -Mu c_1 \sum_{i=2}^{N} \frac{\Delta \xi_i}{\Delta \xi_1} + Mu \sum_{i=2}^{N} c_i \frac{\Delta \xi_1}{\Delta \xi_i} \quad , \tag{13}$$

and

$$\frac{\partial c_k}{\partial t} = Mu c_1 \frac{\Delta \xi_k}{\Delta \xi_1} + Mu c_k \frac{\Delta \xi_1}{\Delta \xi_i} \quad \left(2 < k \leq N\right), \tag{14}$$

respectively, where Mu represents the mixing rate, ξ is the vertical coordinate, and $\Delta \xi$ denotes the layer thickness. The mixing matrix which controls this model is nonzero only for the top row, the left most column, and the diagonal.
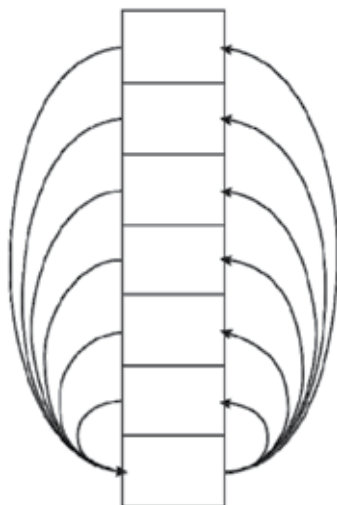
Fig. 1. A schematic representation of vertical mixing in a one dimensional column as simulated by the Blackadar's scheme.

The asymmetrical convective model (Pleim & Chang, 1992) is a nonlocal vertical mixing scheme based on the assumption of the vertical asymmetry of buoyancy-driven turbulence. The concept of this model is that buoyant plumes, according to the Blackadar's scheme, rise from the surface layer to all levels in the convective boundary layer, but downward mixing occurs between adjacent levels only in a cascading manner. The schematic representation of vertical mixing simulated by the ACM is presented in Fig. 2a. The mixing algorithm is driven by equations

$$\frac{\partial c_1}{\partial t} = Md_2 c_2 \frac{\Delta\xi_1}{\Delta\xi_2} - Muc_1 \sum_{i=2}^{N} \frac{\Delta\xi_i}{\Delta\xi_1} , \tag{15}$$

$$\frac{\partial c_k}{\partial t} = Muc_1 - Md_k c_2 + Md_{k+1} c_{k+1} \frac{\Delta\xi_{k+1}}{\Delta\xi_k} \left(2 < k \leq N\right) , \tag{16}$$

and

$$\frac{\partial c_N}{\partial t} = Muc_1 - Md_N c_N , \tag{17}$$

where Mu and Md are the upward and downward mixing rates, respectively. The downward mixing rate from level k to level $k-1$ is calculated as

$$Md_k = \frac{\xi_N - \xi_k}{\Delta\xi_k} Mu . \tag{18}$$

The mixing matrix controlling this model is non-zero only for the leftmost column, the diagonal and superdiagonal.

The scheme with varying upward mixing rates (VUR sheme), sugested by Mihailović et al. (2008) is a modified version of the ACM, where the upward mixing rate changes with the height, providing slower mixing. The schematic representation of vertical mixing simulated by this scheme is shown in Fig. 2b. The upward mixing rates are scaled with the amount of turbulent kinetic energy in the layer as

$$Mu_k = Mu_1 \frac{e_k \Delta\xi_k}{\sum_{i=1}^{N} e_i \Delta\xi_i} , \tag{19}$$

where Mu_1 is the upward mixing rate from surface layer to layer above and e_k denotes the turbulent kinetic energy in the considered layer. The upward mixing rate from surface
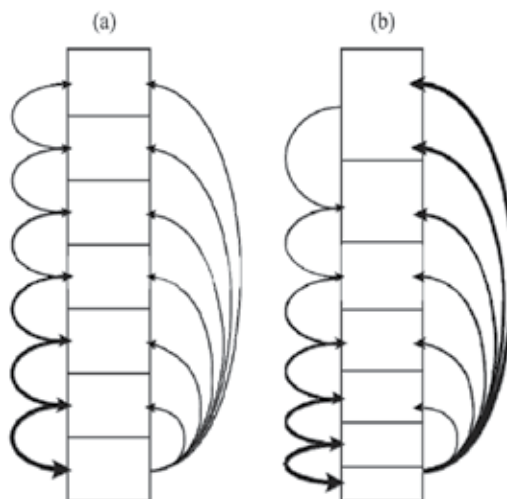
Fig. 2. Schematic representation of vertical mixing in a one-dimensional column as simulated by the (a) ACM and (b) VUR scheme.

layer to layer above is parameterized as

$$Mu_1 = \frac{\rho u_*^4 + H w_*}{h(\rho u_*^3 + H)} \ ,$$

(20)

where ρ is the air density while H represents the sensible heat flux. Using the VUR scheme, the mixing algorithm for the lowest layer can be written in the form

$$\frac{\partial c_1}{\partial t} = M d_2 c_2 \frac{\Delta \xi_1}{\Delta \xi_2} - Mu_1 c_1 - \sum_{k=3}^{N} Mu_k c_1 \ .$$

(21)

The algorithm for the other layers is very similar to the ACM algorithm [Eqs. (16) and (17)], with the upward mixing rate Mu substituted with varying upward mixing rates Mu_k.

3. Numerical simulations with nonlocal-closure schemes in the Unified EMEP chemical model

In the EMEP Unified model the diffusion scheme remarkably improved the vertical mixing in the ABL, particularly under stable conditions and conditions approaching free convection, compared with the scheme previously used in the EMEP Unified model. The improvement was particularly pronounced for NO_2 (Fagerli & Eliassen, 2002). However, with reducing the horizontal grid size and increasing the heterogeneity of the underlying surface in the EMEP Unified model, there is a need for eddy-diffusivity scheme having a higher level of sophistication in the simulation of turbulence in the ABL. It seems that the nonlocal eddy-diffusivity schemes have good performance for that. Zhang et al. (2001) demonstrated some advantages of nonlocal over local eddy-diffusivity schemes. The vertical

sub grid turbulent transport in the EMEP Unified model is modeled as a diffusivity effect. The local eddy-diffusivity scheme is designed following O'Brien (1970). (In further text this scheme will be referred to the OLD one). In the unstable case, K_m is determined as

$$K_m\left(z\right) = K_m\left(h\right) + \left(\frac{h-z}{h-h_s}\right)^2 \left\{\left[K_m\left(h_s\right) - K_m\left(h\right)\right] + \right.$$

$$\left. \left(z-h_s\right)\cdot\left[\frac{\delta}{\delta_z}\left(K_m\left(h_s\right)\right) + 2\cdot\frac{K_m\left(h_s\right) - K_m\left(h\right)}{h-h_s}\right]\right\} \quad h_s \leq z < h$$

(22)

where h_s is the height of the surface boundary layer. In the model calculation h_s is set to 4% of height of the ABL.

To compare performances of the proposed nonlocal-closure schemes TKE scheme (Eqs.(1)-(4)) and local OLD scheme (Eq. (22)), both based on the vertical eddy diffusivity formulation, in reproducing the vertical transport of pollutants in the ABL, a test was performed with the Unified EMEP chemical model (UNIT-ACID, rv2_0_9).

3.1 Short model description and experimental set up

The basic physical formulation of the EMEP model is unchanged from that of Berge & Jacobsen (1998). A polar-stereographic projection, true at 60°N and with the grid size of 50×50 km^2 was used. The model domain used in simulation had (101, 91) points covering the area of whole Europe and North Africa. The σ terrain-following coordinate was used with 20 levels in the vertical- from the surface to 100 hPa and with the lowest level located nearly at 92 m. The horizontal grid of the model is the Arakawa C grid. All other details can be found in Simpson et al. (2003). The Unified EMEP model uses 3-hourly resolution meteorological data from the dedicated version of the HIRLAM (HIgh Resolution Limited Area Model) numerical weather prediction model with a parallel architecture (Bjorge & Skalin, 1995). The horizontal and vertical wind components are given on a staggered grid. All other variables are given in the centre of the grid. Linear interpolation between the 3-hourly values is used to calculate values of the meteorological input data at each advection step. The time step used in the simulation was 600 s.

3.2 Comparison with the observations

The comparison of the TKE and VUR schemes with OLD eddy diffusion scheme has been performed, using simulated and measured concentrations of the pollutant NO_2 since it is one of the most affected ones by the processes in the ABL layer. The simulations were done for the years (i) 1999, 2001 and 2002 (TKE scheme) and (ii) 2002 (for VUR scheme) in the months when the convective processes are dominant in the ABL (April-September). The station recording NO_2 in air (μg(N) m^{-3}) concentration was considered for comparison when measurements were available for at least 75% of days in a year [1999 (80 stations), 2001 (78) and 2002 (82)]. We have calculated the bias on the monthly basis as (M-O)/O*100% where M and O denote the modeled and observed values, respectively. The comparison of the modeled and observed NO_2 in air (μg(N) m^{-3}) concentrations and corresponding biases for

both schemes (TKE and OLD) are shown in Fig. 3. The values used in calculations were averaged over the whole domain of integration. It can be seen that both schemes underestimate the observations. However, for all considered months, NO_2 concentrations calculated with the TKE scheme are in general higher and closer to the observations than those obtained by the OLD scheme (of the order of 10%). Correspondingly, the bias of the TKE scheme is lower than the OLD scheme. The comparison of the modeled and observed NO_2 in air ($\mu g(N)$ m^{-3}) concentrations between VUR and OLD schemes is shown in Fig. 4. The values used in the calculations were also averaged over the whole domain of integration. It can be seen that both schemes underestimate the observations. However, for all considered months, NO_2 concentrations calculated with the VUR scheme are in general higher and closer to the observations than those obtained using the eddy diffusion scheme (of the order of 15-20%). Accordingly, the bias of the VUR scheme is lower than the OLD eddy diffusion scheme.

To quantify the simulated values of the both schemes we have performed an error analysis of the NO_2 concentration outputs NO_2 based on a method discussed in Pielke (2002). Following that study, we computed several statistical quantities as follows

$$\nu = [\sum_{i=1}^{N} (\Gamma_i - \hat{\Gamma}_i)^2 / N]^{1/2} , \qquad (23)$$

$$\nu_{BR} = \{\sum_{i=1}^{N} [(\Gamma_i - \overline{\Gamma}) - (\hat{\Gamma}_i - \overline{\hat{\Gamma}})] / N\}^{1/2} , \qquad (24)$$

$$\eta = [\sum_{i=1}^{N} (\Gamma_i - \overline{\Gamma})^2 / N]^{1/2} , \qquad (25)$$

$$\hat{\eta} = [\sum_{i=1}^{N} (\hat{\Gamma}_i - \overline{\hat{\Gamma}})^2 / N]^{1/2} . \qquad (26)$$

Here, Γ is the variable of interest (aforementioned variables in this study) while N is the total number of data. An overbar indicates the arithmetic average, while a caret refers to an observation. The absence of a caret indicates a simulated value; ν is the rmse, while ν_{BR} is rmse after a bias is removed. Root-mean-square errors (rmse) give a good overview of a dataset, with large errors weighted more than many small errors. The standard deviations in the simulations and the observations are given by η and $\hat{\eta}$. A rmse that is less than the standard deviation of the observed value indicates skill in the simulation. Moreover, the values of η and $\hat{\eta}$ should be close if the prediction is to be considered realistic.
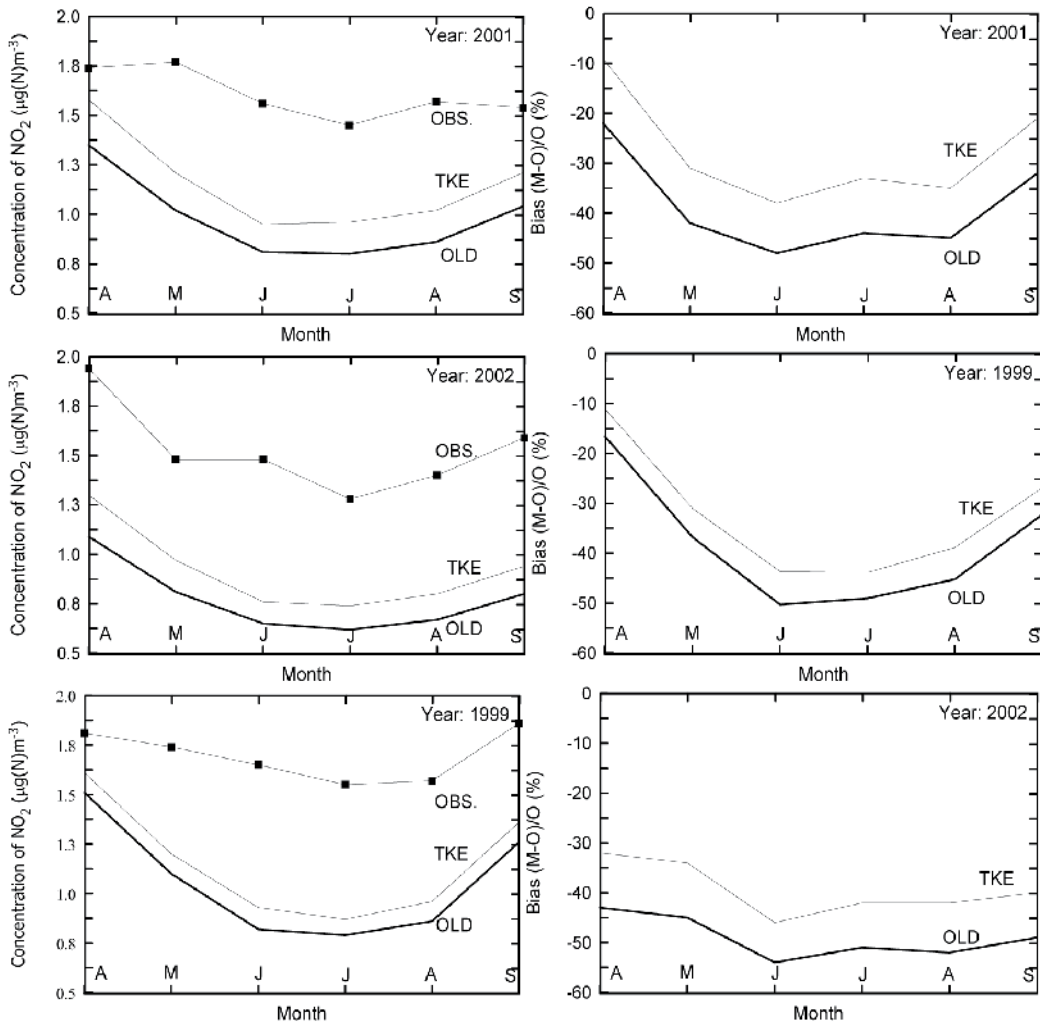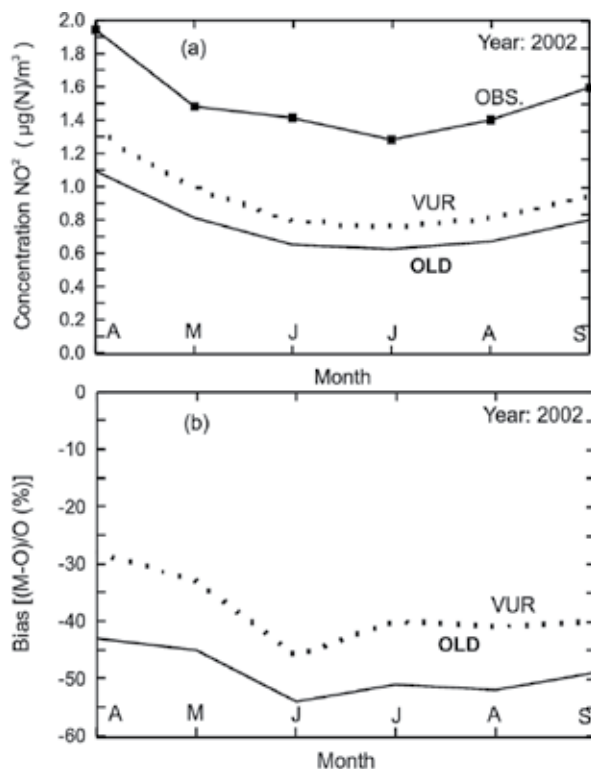
Fig. 3. The eddy diffusion (OLD) versus TKE scheme. Comparison of: the modeled and observed NO$_2$ in air (µg(N) m^{-3}) concentrations (left panels) and their biases (right panels) in the period April-September for the years 1999, 2001 and 2002. M and O denotes modeled and observed value, respectively.

The statistics gave the following values: (1) TKE ($v = 0.548$, $v_{BR} = 0.293$, $\eta = 0.211$, $\hat{\eta} = 0.147$) and OLD ($v = 0.802$, $v_{BR} = 0.433$, $\eta = 0.303$, $\hat{\eta} = 0.147$) and (2) VUR ($v = 0.571$ µg(N) m^{-3}, $v_{BR} = 0.056$ µg(N) m^{-3}, $\eta = 0.219$ µg(N) m^{-3}, $\hat{\eta} = 0.211$ µg(N) m^{-3}) and OLD ($v = 0.802$, $v_{BR} = 0.159$, $\eta = 0.303$, $\hat{\eta} = 0.211$). A comparison of η and $\hat{\eta}$, for (1) and (2), shows that difference between them, is evidently smaller with the TKE and VUR scheme schemes versus the OLD one.

Fig. 4. The eddy diffusion (OLD) versus the VUR scheme. Comparison of: (a) the modelled and observed NO_2 in air ($\mu g(N)$ m^{-3}) concentrations and (b) their biases in the period April-September for the year 2002. M and O denotes modelled and observed value, respectively.

4. Conclusions

In the ABL during convective conditions, when much of the vertical mixing is driven by buoyant plumes, we cannot properly describe mixing processes using local approach and eddy diffusion schemes. Nonlocal-closure schemes simulate much better vertical mixing than local ones. In this chapter, two nonlocal schemes (the TKE scheme and the VUR scheme) for applications in air quality and environmental models are described. The comparison of the TKE scheme and the VUR one with an eddy diffusion scheme (OLD) commonly used in chemical transport models was done. These comparisons were performed with the EMEP Unified chemical model using simulated and measured concentrations of the pollutant NO_2 since it is one of the most affected ones by the processes in the ABL layer. Nonlocal shemes gave better results than local one.

Acknowledgement

5. References

Alapaty, K.; Pleim, J.E.; Raman, S.; Niyogi, D.S. & Byun, D.W. (1997). Simulation of atmospheric boundary layer processes using local- and nonlocal-closure schemes, *Journal of Applied Meteorology*, 36, 214–233 ISSN 0894-8763

Alapaty, K. & Alapaty, M. (2001). Development of a diagnostic TKE schemes for applications in regional and climate models using MM5. *Research Note*, MCNC-North Carolina Supercomputing Center, Research Triangle Park, NC, pp. 5.

Alapaty, K. (2003). Development of two CBL schemes using the turbulence velocity scale. *4th WRF Users' workshop*, Boulder, Colorado, June 25-27.

Blackadar, A.K. (1976). Modeling the noctural bondary layer. *Proceedings of 4th Symposium of Atmospheric Turbulence, Diffusion and Air Quality*, pp. 46-49, Boston, American Meteorological Society

Blackadar, A.K. (1979). Modeling pollutant transfer during daytime convection. *4th Symposium on Atmospheric Turbulence Diffusion and Air Quality*, Reno, NV, American Meteorological Society, pp. 443-447.

Berge, E. & Jacobsen H.A. (1998). A regional scale multi-layer model for the calculation of long-term transport and deposition of air-pollution in Europe. *Tellus. Series B, Chemical and physical meteorology,* 50, 205-223, ISSN 0280-6509

Bjorge, D. & Skalin, R. (1995). PARLAM – the parallel HIRLAM version of DNMI. Research Report No. 27, Norwegian Meteorological Institute, Oslo, Norway, ISSN 0332-9879

Businger, J.A.; Izumi, Y. & Bradley, E.F. (1971). Flux profile relationships in the atmospheric surface layer. *Journal of the Atmospheric Sciences,* 28, 181-189.

Fagerli, H. & Eliassen, A. (2002). Modified parameterization of the vertical diffusion. In: Transboundary acidification, eutrophication and ground level ozone in Europe. EMEP Summary Status Report, *Research Report* No. 141, Norwegian Meteorological Institute, Oslo, Norway, pp. 74.

Hass, H.; Jacobs, H.J.; Memmesheimer, M.; Ebel, A. & Chang, J.S. (1991). Simulation a wet deposition case in Europe using European Acid Deposition Model (EURAD). In: *Air Pollution modeling and its Applications VIII*, pp. 205-213, Plenum Press, New York

Holtslag, A.A.M.; de Bruin, E.I.F. & Pan, H.-L. (1990). A high resolution air mass transformation model for short-range weather forecasting. *Monthly Weather Review,* 118, 1561-1575, ISSN 0027-0644

Holtslag, A.A.M. & Boville, B.A. (1993). Local versus nonlocal boundary layer diffusion in a global climate model. *Journal of Climate,* 6, 1825-1842, ISSN 0894-8755

Hong, S.Y. & Pan, H.L., (1996). Nonlocal boundary layer vertical diffusion in a medium-range forecast model. *Monthly Weather Review,* 124, 2322-2339, ISSN 0027-0644

Lenschow, D.H.; Li, X.S. & Zhu, C.J. (1988). Stably stratified boundary layer over the Great Plains. Part I: Mean and turbulent structure. *Boundary-Layer Meteorology*, 42, 95-121, ISSN 0006-8314

Miesch, M.S.; Brandenburg, A.; Zweibel, A. & Zweibel, E.G. (2000). Nonlocal transport of passive scalars in turbulent penetrative convection. *Physical Review E,* 61, 457–467, ISSN 1539-3755

Mihailovic D.T. & Jonson J.E. (2005). *Implementation of a TKE scheme in the Unified EMEP model. Air Pollution report* 5/2005, Norwegian Meteorological Institute, Oslo, ISSN 1503-8025.

Mihailovic, D.T.; Rao, S.T.; Alapaty, K.; Ku, J.Y.; Arsenic, I. & Lalic, B. (2005). A study of the effects of subgrid-scale representation of land use on the boundary layer evolution using 1-D model. *Environmental Modelling and Software,* 20, 705-714, ISSN 1364-8152

Mihailovic, D.T. & Alapaty, K. (2007). Intercomparison of two K-schemes: Local versus non-local in calculating concentrations of pollutants in chemical and air-quality models. *Environmental Modelling and Software*, 22, 1685-1689, ISSN 1364-8152

Mihailović, D.T.; Alapaty, K. & Sakradžija, M. (2008). Development of a nonlocal convective mixing scheme with varying upward mixing rates for use in air quality and chemical transport models *Environmental Software and Pollution Research*, 15, 296-302, ISSN 0944-1344

Moeng, C.-H. & Sullivan, P.P. (1994). A comparison of shear and buoyancy driven planetary-boundary-layer flows. *Journal of the Atmospheric Sciences,* 51, 999-1022, ISSN 0022-4928

O'Brien, J.J. (1970). A note on the vertical structure of the eddy exchange coefficient in the planetary boundary layer. *Journal of the Atmospheric Sciences*, 27, 1213-1215, ISSN 0022-4928

Pielke, R.A., Sr. (2002). *Mesoscale Meteorological Modeling.* 2nd ed. Academic Press, 676 pp. San Diego, CA.

Pleim, J.E. & Chang, J. S. (1992). A non-local closure model for vertical mixing in the convective boundary layer. *Atmospheric Environment*, A26, 965-981, ISSN 1352-2310

Simpson, D.; Fagerli, H.; Jonson, J.E.; Tsyro, S.; Wind, P. & Tuovinen, J.-P. (2003). Transboundary acidification, eutrophication and ground level ozone in Europe. Part I: Unified EMEP Model Description. *EMEP Status Report* 2003, pp. 74, The Norwegian Meteorological Institute, Norway

Stull, R.B. & Driedonks A.G.M. (1987) Applications of the transilient turbulence parameterization to atmospheric boundary-layer simulations. *Boundary-Layer Meteorology*, 40, 209-239, ISSN 0006-8314

Stull, R.B. (1988). *An Introduction to Boundary Layer Meteorology*, Dordrecht: Kluwer.

Tonnesen, G.; Olaguer, J.; Bergin, M.; Russell, T.; Hanna, A.; Makar, P.; Derwent, D. & Wang, Z. (1998). *Air quality models.* Draft as of 11/26/98, pp. 55.

Troen, I. & Mahrt, L. (1986). A simple model of the atmospheric boundary layer; sensitivity to surface evaporation. *Boundary-Layer Meteorology,* 37, 129-148 ISSN 0006-8314

Wang, Z. (1998). Computing volatile organic compound reactivities with a 3-D AQM *Proceedings of the photochemical Reactivity Workshop*, U.S. Environmental protection Agency, Durham, NC.

Wyngaard, J.C. & Brost, R.A. (1984). Top-down and bottom-up diffusion of a scalar in the convective boundary layer. *Journal of the Atmospheric Sciences,* 41, 102-112, ISSN 0022-4928

Zhang, D. & Anthes, R.C. (1982). A high-resolution model of the planetary boundary-layer-sensitivity tests and comparisons with SESAME-79 data. *Journal of Applied Meteorology*, 21, 1594-1609, ISSN 0894-8763

Zhang, C.; Randall, D.A.; Moeng, C.-H.; Branson, M.; Moyer, M. & Wang, Q. (1996). A surface parameterization based on vertically averaged turbulence kinetic energy. *Monthly Weather Review,* 124, 2521-2536, ISSN 0027-0644

Zhang, K.; Mao, H.; Civerolo, K.; Berman, S., Ku, J.-Y.; Rao, S.T.; Doddridge, B.; Philbrick, C.R. & Clark, R. (2001). Numerical investigation of boundary layer evolution and nocturnal low-level jets: local versus non-local PBL schemes. *Environmental Fluid Mechanic*, 1, 171-208, ISSN 1567-7419

Air quality monitoring in the Mediterranean Tunisian coasts

[a,b]Karim BOUCHLAGHEM, [a]Blaise NSOM and [b]Salem ELOURAGINI
[a]Université de Bretagne Occidentale. LBMS - EA 4325
Université Européenne de Bretagne
BP 93169. Rue de Kergoat. 29231. BREST Cedex 3 (France)
[b]Unité de recherche « Energétique et Environnement » (03/ UR 13-06)
Institut Supérieur des Sciences Appliquées et de Technologie de Sousse
Cité Taffala, 4003 Sousse Ibn Khaldoun, (Tunisia)

1. Introduction

The transfer from the liquid element (the sea) to the solid one (the land) engenderers thermal phenomena such breezes. During the day, the land heats up more rapidly than the sea. Over the land surface, the heat spreads in the low layers and gives birth to upward currents. This hot continental air rises up, and then is superseded by a colder air coming from the sea; it is the sea breeze. During the night, the phenomenon is reversed to become a land breeze.

If the synoptic wind is weak, the breezes will take their true size and result in the formation of convergent zones on the land and divergent zones over the sea. Some visual signs can help observe these phenomena. The low clouds of the cumulus type are a proof of the vertical movement. They are often related to the setting of the sea breeze (Simpson, 1994).

Many experimental and numerical studies have shown the impact of breeze circulations on the evolution of pollutant concentrations (Bouchlaghem et al., 2007; Srinivas et al., 2007; Baumgardner et al., 2006; Evtyugina et al., 2006; Flocas et al., 2006; Lim et al., 2006). The photochemical transformation also plays a crucial role in the production and destruction of pollutants. These transformations coupled with the dynamic circulations such as breezes represent the responsible process of the formation, transport and redistribution of reactive chemical species in the low layers of the atmosphere.

The study made by (Ma and Lyons, 2003) via a 3D version of RAMS model (Regional Atmospheric Modelling System) has shown that the recirculation of pollution is a Mediterranean characteristic. They have defined the recirculation as follows: in the presence of a weak synoptic wind, the heating and cooling of the land and the sea determine the local circulation which affects the transport and diffusion of emissions. In fact, during the night, emissions can be transported over the sea via a land breeze or an offshore synoptic wind just to return onshore to the land after the launching of the sea breeze. The study of (Nester, 1995) has shown that the phenomena of photochemical Smog are generally associated with this type of meteorological conditions such as, a weak synoptic wind and a recirculation of

land and sea breezes. He insists that the local recirculation, the topography, the coast shapes and the force of synoptic wind play important roles in the transport of pollution. The numerical study of (Liu et al., 2002) shows the effect of the recirculation of land and sea breezes on the ozone distribution. They demand that the ozone and its precursors be transported over the sea by the land breeze. Later on, the front breeze transports the ozone precursors on the land. A weak sea breeze and the intensification of solar radiations activate the photochemical process and contribute to the ozone increase of concentration.

A 3D model of air pollution TAPM (The Air Pollution Model) (Luhar and Hurley, 2004) second version has been applied to predict meteorological parameters and pollution field on the Mediterranean. The obtained results display that the development of a sea breeze during the day and a nocturnal land breeze due to the temperature contrast between the land and the sea may reduce the diffusion of air masses in the presence of the recirculation. Via a meso-scale model, (Ding et al., 2004) have explained that the late sea breeze development is due to the presence of an offshore synoptic wind. These breezes are generally characterized by the formation of a front breeze and a return current in the upper layers. They display that this dynamic nature contributes to the ozone concentration increase on the coasts. With reference to the experimental data of the MEDiterranean CAmpaign of PHOtochemical Tracers- TRansport and Chemical Evolution (MEDCAPHOT-TRACE), (Ziomas, 1998) has proved that the pollution problems are strictly interconnected with the launching and the steadiness of the sea breeze. Via the 3D version of RAMS Model (Regional Atmospheric Modelling System) and the experimental data analysis, [Millan et al., 2002] have proved that the sea breeze combines with the mountain breeze to create a recirculation over the Mediterranean basin with a residence time of few days. Under the impact of solar radiation, this recirculation takes the shape of photochemical reactor where the precursors give birth to ozone, acids and aerosols. They remarked that the problem of air quality on the Mediterranean basin is principally governed by diurnal meteorological process such as breezes.
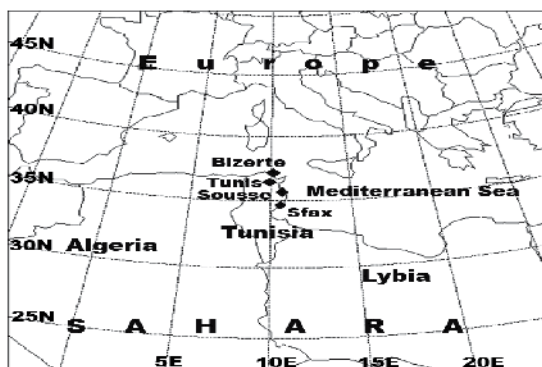
Fig. 1. North Africa map displaying Tunisia and Sousse region location (35° 48′ N, 10° 38′ E).

Several studies have pointed out, by using both in-situ and remote sensing observation, that dynamics of polluted air masses in the Mediterranean are influenced by local and mesoscale meteorological processes (Bouchlaghem et al., 2007; Helena et al., 2006; Viana et al., 2005; Puygrenier et al., 2005; Pérez et al., 2004; Gangoiti et al., 2001, 2002; Kassomenos et al., 1998;

Ziomas, 1998 and Millan et al., 1996). During summer, transport of polluted air masses is influenced by the sea-land breeze circulation (Millan et al., 2002). The later can affect urban areas along the coasts and further inland as it can penetrate up to hundred kilometres inland (Simpson et al., 1977; Simpson, 1994). Simultaneously, the Mediterranean climatic conditions (high temperatures and intensive solar radiation) especially in the summer period, promote the formation of photochemical secondary pollutants.

Synoptic scale meteorology induces frequent outbreaks of African Saharan dust reaching most Mediterranean regions (Lyamani et al., 2005; Alastuey et al., 2005; Querol et al., 2004; Rodriguez et al., 2002, 2004; Viana et al., 2002, 2003, 2007). The occurrence of dust outbreaks affecting the Mediterranean has a marked seasonal behaviour, and is generally driven by intense cyclone generated south of Atlas Mountain by the thermal contrast of cold marine Atlantic air and warm continental air that cross North Africa during summer (Meloni et al., 2007). Rodriguez et al., 2002) pointed out, through an analysis of experimental data recorded on the eastern sites of Spain, that the highest PM event recorded in the Mediterranean were frequently documented during outbreaks of African dust.

Annual pollution studies in the Mediterranean have pointed out that pollutant behaviour is a tracer of seasonal meteorology dynamic and becomes a common feature characterizing these regions (Simon et al., 2006; Marmer and Langmann, 2005).

Martin et al., 1991 suggest that the annual variation in meteorological conditions is a common feature in most of the Mediterranean areas and results in air pollution cycles different from those experienced in other latitudes.

Knowledge of the mechanisms that give rise to pollution episode in the Mediterranean regions is needed for the purpose of providing health advice to the public in events episodes.

To this end, local and seasonal variation of the main pollutants concentration and the meteorological conditions were studied in this chapter.

The studied regions are presented in sections 2. The instrumentation and methods are described in section 3. The seasonal behaviour derived from monthly average concentration and meteorological parameters at the coastal sites is presented in section 4. Summer evolution of Saharan dust and land-sea breeze events and relevant change in pollutants concentrations at a selected site are discussed in section 5 and 6. Pollutants evolution is presented in section 7.

2. Sites description

Tunisia country is located in the North part of Africa (Fig. 1). Its surface is 164.000 km2 with 10 millions inhabitants. Coastal cities share about 500 km of beach and are widely influenced by the Mediterranean Sea. The four sites presented in this study are Mediterranean coastal cities with relatively flat terrain.

Bizerte city is located at the North part of Tunisia (37° 16′ N, 9° 52′ E). Its urban area accounts about 114.000 inhabitants. The measurement station sample is classified as urban which is mainly influenced by residential, traffic and commercial activities. Tunis City (capital of Tunisia) is also located in the North part of Tunisia (36° 49′ N, 10° 11′ E). The urban area (750.000 inhabitants) is about 212.63 km2 surface. The sampling site is classified as urban, located in the vicinity of one of Tunis's major traffic Avenues (Bab Saadoun Ave.).

Sousse city is located at the Eastern central part of Tunisia (35° 49′ N, 10° 38′). The urban area (200.000 inhabitants) is about 45 km2 surface. The sampling site is urban under the influence of residential, traffic and commercial activities. The main industrial activities are a power plant and bricks work.

Finally, Sfax city is located at the south part of Tunisia (34° 44′ N, 10° 46′ E) with 270.000 inhabitants. The sampling site is industrial under the influence of intense chemical manufacturing activities.

3. Data and methods

It might be highlighted that there is a lack of knowledge in Tunisia on the pollution concentration, since the national monitoring stations operated by the ANPE (Agence Nationale de Protection de l'Environnement) is localised in the most urban zones. All instantaneous concentrations data can be controlled from the central station.

Surface O3 levels were continuously monitored using Environment model 41 M analysers. The concentrations of NOx (NO and NO2) were measured by using analysers Environment-AC, Models 31 M.

Other stations use standard NOx (NO & NO2), O3 and SO2 instruments designed by Teledyne Advanced Pollution Instrumentation Company (http://www.teledyne-api.com). Data processing techniques and standard methods are described in the analyser instruction manuals. Used Teledyne models are 200A, 400A and 100A for NOx, O3 and SO2 respectively. Additionally, all stations were equipped with automatic weather monitoring. A mobile laboratory is used to control pollutants levels in rural and urban sites. These measured pollutants are harmful both for the human health and the environment: Ozone is a major photo-oxide product of the atmosphere. It is manifested in the presence of UV radiation stemming from ozone precursors.

NO2 + UV radiation $\longrightarrow$ NO + O and O + O2 $\longrightarrow$ O3
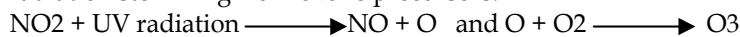
Then it is consumed by NO

NO + O3 $\longrightarrow$ NO2 + O2
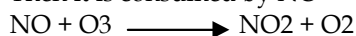
The high levels of ozone give birth to the formation of the Smog phenomena and the green house effect. The oxidization of NOx and SO2 in the atmosphere stimulates the formation of aerosols (e.g. H2SO4, HNO3…) which play a crucial role in the production of acid rain and the climatic and environmental change.

The influence of atmospheric transport scenarios on the levels of Particulate Matters was investigated by means of back-trajectories analysis using the Hysplit Model (www.arl.NOAA.gov) and information obtained from TOMS-NASA, NRL aerosol and dust maps (TOMS, www.jwocky.gsfc.nasa.gov; NRL www.nrlmry.navy.mil. Satellite images are provided by the NASA SEAWIFS project (www.seawifs.gsfc.nasa.gov).

4. Experimental results

4.1 Seasonal pollutants behavior

Fig. 2, 3, 4 and 5 show time series plots of the main pollutants concentrations (NO, NO2, NOx, O3, SO2 and PM10) and the local meteorological parameters at selected sites. A seasonal pattern of variation which completes one cycle per year is observed at all sites. NO, NO2 and NOx concentrations are lowest in summer (June, July and August) and peaking in

winter (December, January and February). In contrast, O3 concentration shows reversed tendency of seasonal variation. There is a clear indication of annual trend downward for NOx (NO and NO2) and SO2. This is may be due to the reduction of vehicle emission with the renew of the Tunisian vehicular troop during the last decade, the use of refined oil energies and the application of law decreasing industrial emissions by substituting heavy fuel for natural gas. Nevertheless there is no indication for annual O3 and PM10 levels decrease. O3 and PM10 are approximately stationary in their level and point out to the contribution of additional non local pollution sources during particular weather conditions.

NO, NO2 and NOx concentrations appear to be a common seasonal pattern across the sites. There is less air mixing in the lower boundary layer during the winter months and this could lead to elevated levels of this pollutants. Additionally, Derwent et al., (1995) suggest that high winter concentration of NO2 could be enhanced by reduced photochemical activity of the reaction in which NO2 and (OH) radicals combine to form nitric acid (HNO3). The winter highs could also be linked to increase industrial and home heating. The summer lows might be due to the enhanced photochemical activity on the presence of powerful solar radiation in which NO2 promotes ozone production.

Differences of concentration between locations can be described in terms of changes in the average level and the amplitude of the seasonal fluctuation. The main differences seem to be associated with the type of station (industrial, urban, traffic…) and the proximity to the main source emissions. The highest average levels (up to 45 ppb) and the larger seasonal amplitude of NOx concentration occur in Tunis City where the site is located in dense vehicular activity. The larger average levels (up to 40 ppb) and seasonal amplitude of SO2 appear in Sfax city where the measurement site is situated in the proximity of the industrial area. During the summer months, the lowest ozone average levels (up to 18 ppb) and the smallest seasonal amplitudes occur in Tunis City because of elevated levels of NO produced by exhausted fume of vehicles which deplete ozone concentration.

Simultaneously, the seasonal patterns of the weather variables appear to be much smoother than those of the pollution concentrations and show both negative and positive correlation according to pollutants type.

The negative correlation between the seasonal NOx concentrations and those of wind speed (Fig. 2 and Fig. 5) may suggest the effect of the increased air mixing. The curves show that weak wind conditions encourage pollutants accumulation over the measurement sites. Nevertheless, positive correlation between the seasonal O3 and PM10 concentrations and the meteorological variables (wind speed, temperature and solar radiation) may account for the meso-scale and long range transport phenomena which promote the increase of these pollutants concentration. The powerful UV radiation encourages photochemical activity and helps ozone production. Thus, O3 seasonal pattern consists of a roughly symmetric wave with summer peaks and winter troughs.

4.2 Summer pollutants variation

Saharan dust outbreaks over the Mediterranean Tunisian coasts represent the second summer phenomenon which results in a peak PM10 event reaching the highest annual values (by 200 µg /m3) (Fig. 7) and lower O3 concentration owing to the influence of the relatively clean Saharan air. It is important to note that by this period the daily average O3 concentration recorded in Sousse city drops to about 30 ppb.
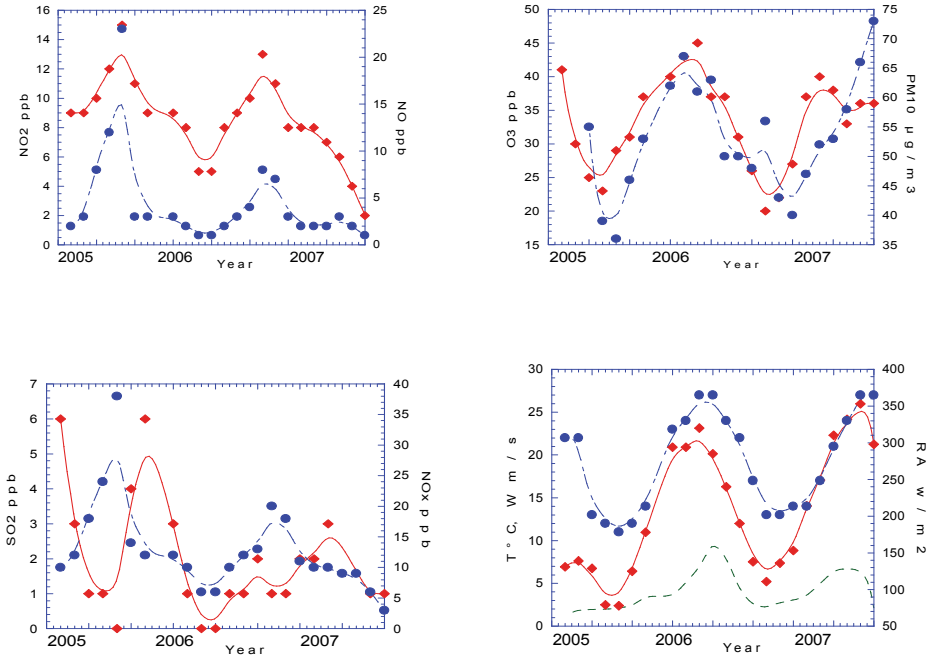
Fig. 2. Time series plots of pollutants concentrations (NO, NO2, O3, PM10, SO2 and NOx) and meteorological parameters (Temperature, Radiation and wind speed) ranging from September 2005 to August 2007 at Sousse site. Time evolution of the Left y-axis is plotted with Solid line and the right one is plotted with dashed line.
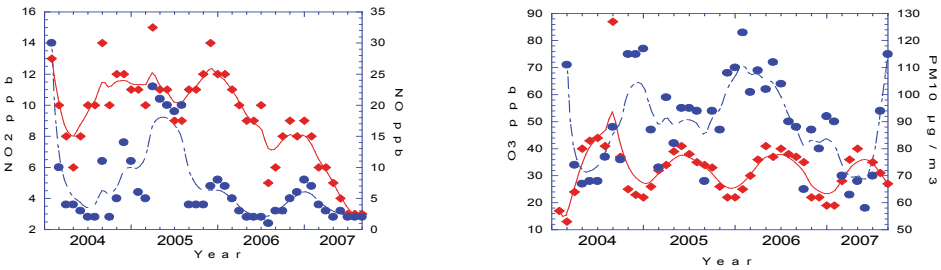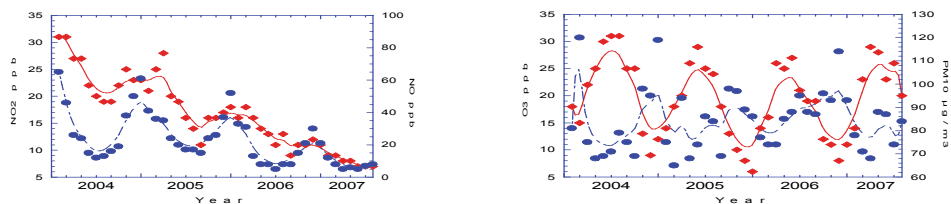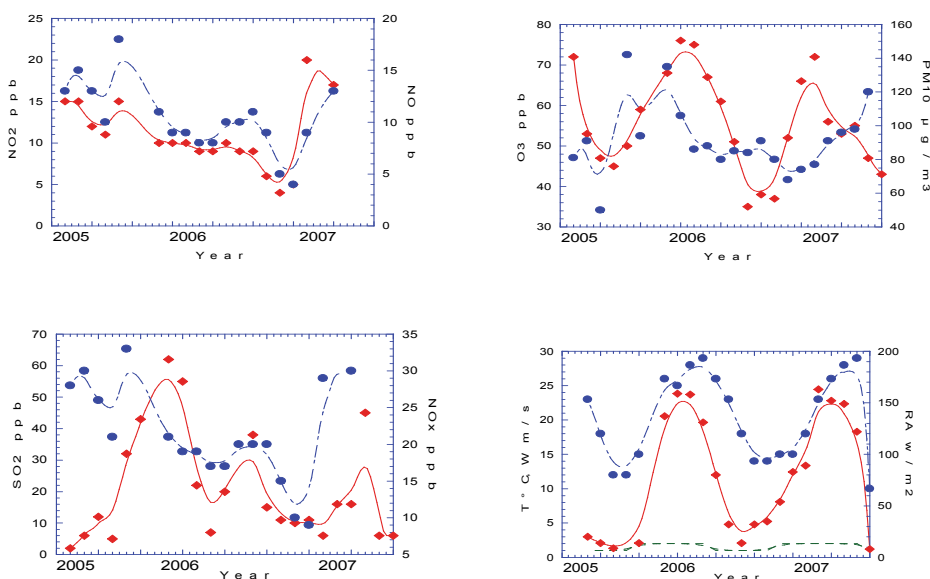

Fig. 3. Time series plots of pollutants concentrations (NO, NO2, O3 and PM10) ranging from January 2004 to August 2007 at Bizerte site. Time evolution of the Left y-axis is plotted with Solid line and the right one is plotted with dashed line.

Fig. 4. Time series plots of pollutants concentrations (NO, NO2, O3 and PM10) ranging from January 2004 to August 2007 at Tunis site. Time evolution of the Left y-axis is plotted with Solid line and the right one is plotted with dashed line.

Fig. 5. Time series plots of pollutants concentrations (NO, NO2, O3, PM10, SO2 and NOx) and meteorological parameters (Temperature, Radiation and wind speed) ranging from September 2005 to August 2007 at Sfax site. Time evolution of the Left y-axis is plotted with Solid line and the right one is plotted with dashed line.

Meloni et al., 2007 suggest that suspended Saharan air masses due to the mixing occurring there can reach 2000m altitude in winter season and 4000m in summer and travelling just above the mixing layer. They pointed out that the air masses loaded with desert dust is expected to become the main aerosol event when the trajectory interacts with the mixed layer.

Here, we presented a sampling PM events reaching Sousse city. During the summer period ranging from 21 June to 24 June 2006, peaks in the PM10 concentrations were reported (Fig. 7). Satellite observation showed a plume of Saharan dust (Fig. 8a) on 23 June 2006 over the Eastern Tunisian coast and the western Mediterranean. The back-trajectory air mass of the same day (Fig. 8b) shows that the air masses reaching the Tunisian costs have a long

range transport origin and the dust outbreaks start from south Algerian Sahara (Fig. 8c). In these conditions, the PM10 concentration at all sites increase rapidly. For instance, in Sousse city, the PM10 concentration increases to reach a level about two to three times the summer one (Fig. 7).

4.3 Winter pollutants variation

A sampling period ranging from 2 January to 5 January 2007 has been selected to study pollutants evolution during winter season. Fig. 9 displays time series of the meteorological parameters and pollutants concentration recorded at Sousse city during this period.

NO and NO2 peak is much higher in winter than in summer (up to 60 ppb on 04 January). In spite of higher traffic in summer than in winter (national statistics have shown that during the summer season, the vehicle number has doubled in Sousse region due to the increasing number of visitors.), NO and NO2 higher peak in winter can be explained on the basis of lower ventilation and lower mixing.

With respect to the NO2, in winter there is less O3 to oxidize the NO emissions and the NO2 peak in the morning is hardly detectable. While by the end of the day, there has been sufficient build-up of O3 to oxidize some of the NO and a peak is detected during that period.

The O3 concentrations are much higher in summer (up to 65 ppb) than in winter (up to 35 ppb). During summer, meteorological conditions such as high temperature and thermal convection often induce the mixing of the air masses and the photochemical reactions. Observed ozone concentration may be the result of photochemical reaction of primary pollutants (NOx from traffic). Furthermore, the sea breeze also brings O3 and the total concentration could result from a combination of local generation and regional transport. Nevertheless, in winter, the O3 values are limited to lesser photochemical activity and vertical mixing. With NO emissions in a stabilizing air layer, the nocturnal ozone concentration decreases rapidly reaching its minimum value (clear during 4 January) due to the fast reaction between NO and O3 to produce NO2 (This phenomenon requires calm wind condition to be clearly detected at the measuring site). Simultaneously, NO, NO2, SO2 and PM10 increase to their maximum values showing evidence of low mixing and low ventilation effect during weak wind condition.

With reference to the data of the National Institute of Meteorology, the data of the NOAA ARL model and to the air masses trajectories which come over Sousse region (HYSPLIT Model-Back trajectories) we have identified days during which the sea breeze is evident. In order to distinguish the sea breeze events, we have associated their development in a perpendicular wind direction to the coast (50°- 130°).
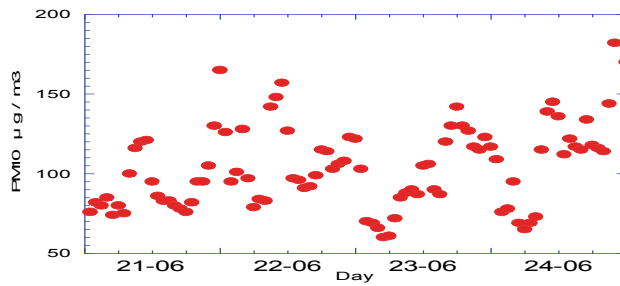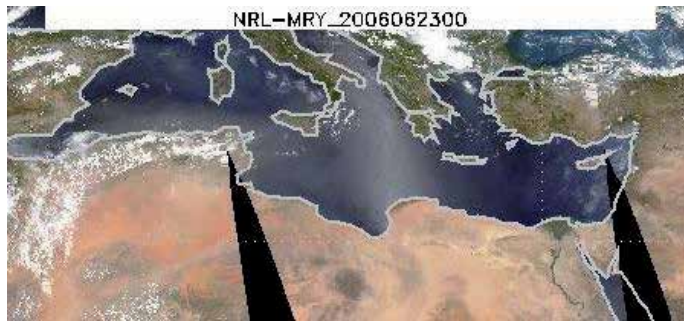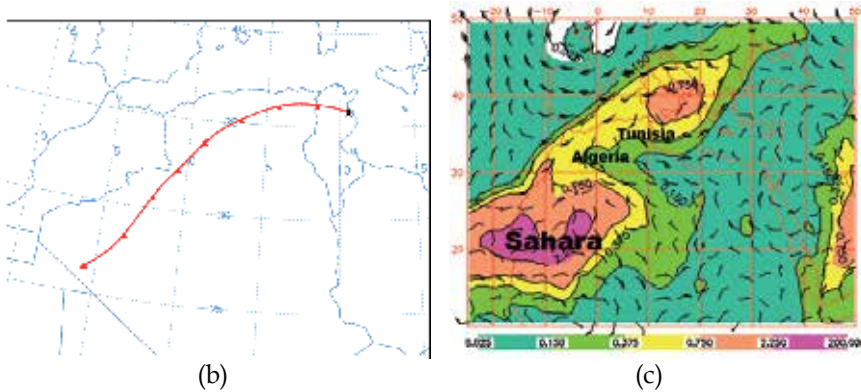
Fig. 7. Hourly averaged series of PM10 concentrations for the period ranging from 21 June 2006 to 24 June 2006.

(a)

(b)   (c)

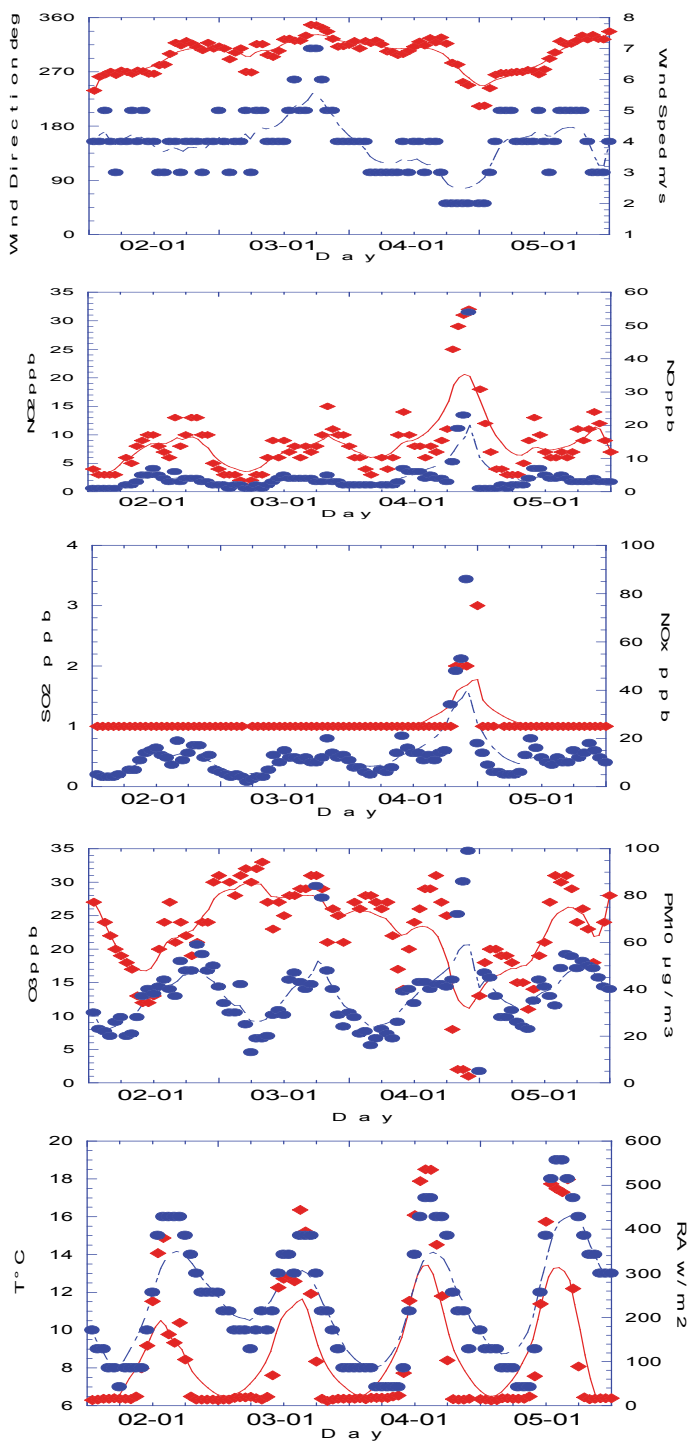Fig. 8. (a) Satellite image (b) backward trajectory and (c) Dust map for 23 June 2006.

Fig. 9. Hourly averaged series of meteorological parameters and pollutants concentrations for the period ranging from 2 January 2007 to 5 January 2007.

speed at night. On the synoptic scale, we have chosen anticyclonic situation as well as weak conditions of pressure gradient. The activation of the breeze varies between 0800 and 1600 Local Time (LT). We have come across two types of sea breeze: the early morning sea breeze characterized by a setting varying from 0800 LT to 1000 LT. This breeze type represents 35% (5 cases) of breeze days. The afternoon sea breeze characterized by a launching ranging between 1200 LT and 1600 LT representing 65% (10 cases) of breeze days. It is important to note that the sun rise time (ranging from 0500 to 0529 LT during the campaign) and the diurnal evolution of solar radiation intensity (Fig.8) which controls the setting of sea breeze remains nearly constant. This result shows that Sousse sea breeze launching doesn't only depend on the land sea temperature contrast but also on the direction and speed of the synoptic wind. Fig.10 illustrates air masses trajectories which reach Sousse region during the campaign. We distinguish three cases. First, an afternoon sea breeze (Fig.10a) in which we notice the recirculation of air masses and the switching of wind direction.

Second, early morning sea breeze (Fig.10b) in which we remark the steady South Eastern wind direction coming from the sea. Third, non-sea breeze (Fig.10c) in which the wind direction is maintained offshore during the day.

5. Afternoon sea breeze cases

The temporal evolution of the direction and speed of wind relative to afternoon sea breezes are regrouped in Fig.11.
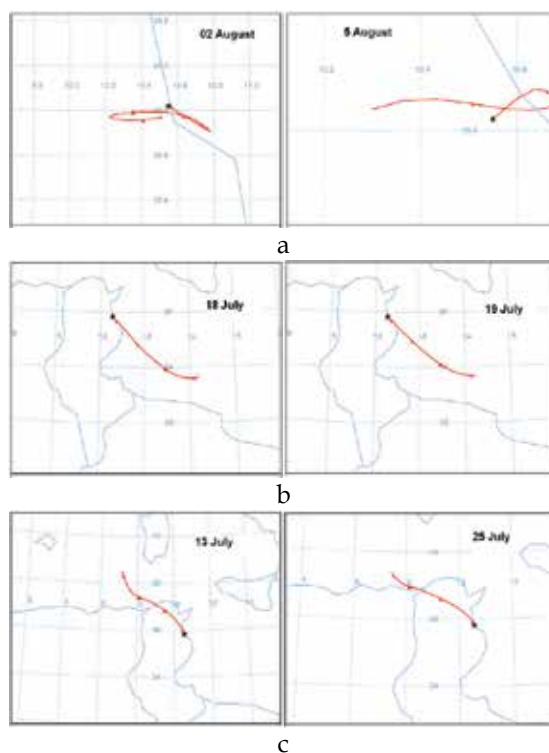

Fig. 10. Samples of surface air masses trajectories reaching Sousse region. (a) Afternoon sea breeze cases (b) Early morning sea breeze cases and (c) Non-sea breeze cases (NOAA ARL data).

The wind direction changes clockwise in a continuous, slow and progressive way starting from the North and the North West direction. The wind speed rises progressively during the period 00-1300 LT. It reaches its apogee between 5 and 7 m/s starting from 1300 LT until the end of the day (about 1900 LT). The maximum of wind speed is synchronized with the late change of the wind direction. The decrease of wind speed after the sun set points out to the disappearance of the sea breeze. This is due to the reduction of sea-land temperature contrast.

6. Early morning sea breeze cases

In order to visualize the early morning sea breeze variation, we have presented on Fig.12, the wind temporal evolution. In the morning (about 0900 LT), the wind direction switches about 30° South East vis-à-vis the synoptic wind direction (SSE). The wind progressively turns anticlockwise until it reaches the sea breeze direction. This rotation associated with a reinforcement of wind is carried out in such a way as the angle described is weak. We notice that the wind returns to its original sector (SSE) when the breeze vanishes. In order to distinguish the different effects which are due to two types of sea breeze, we have to compare the early morning wind direction and speed to the afternoon ones.
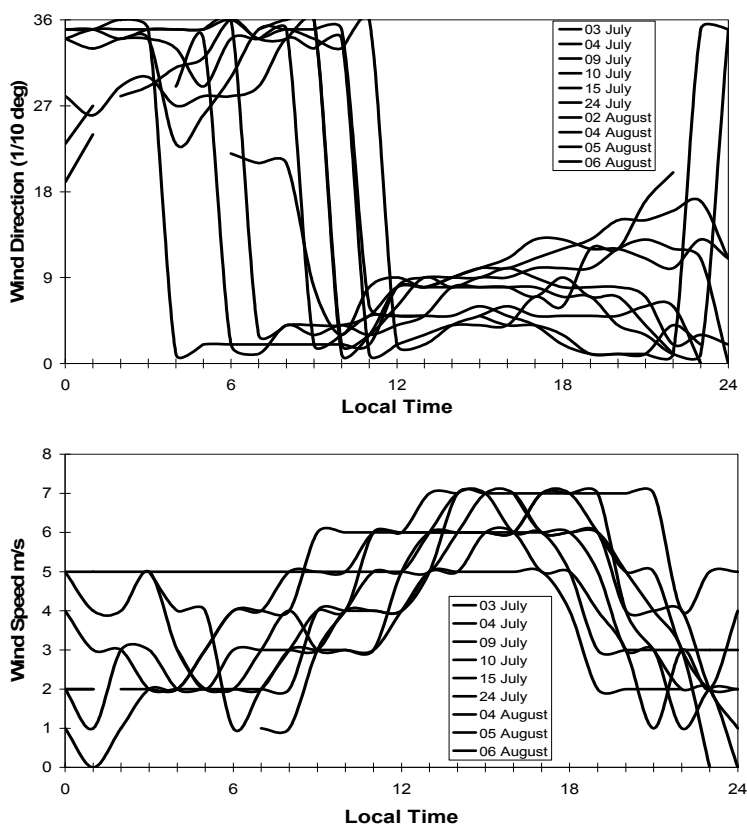
Fig. 11. Temporal variation of wind direction, and wind speed during the afternoon sea breeze days.
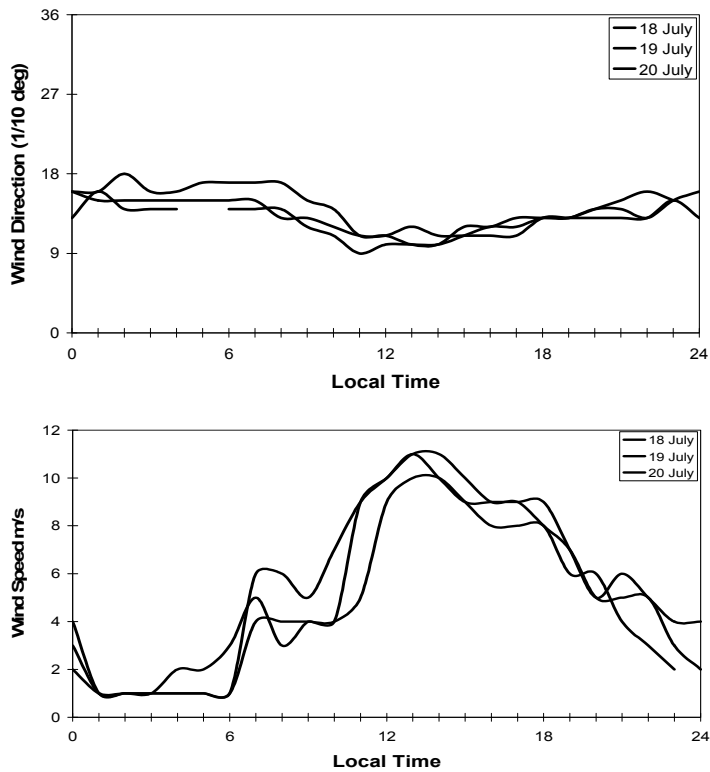
Fig. 12. Temporal variation of wind direction and wind speed, during the early morning sea breeze days.

These later curves are manifested in particular a limited late wind maximum (from 5 to 7 m/s). This wind is inferior to that of the morning sea breeze (11 m/s). This speed difference is attributed to the fact the late sea breeze is opposed by an offshore synoptic wind. Nevertheless, the onshore synoptic wind which characterizes the setting of the early morning sea breeze (about 0900 LT), triggers the wind direction change (anticlockwise) and its strengthening in the morning (11 m/s).

7. Evolution of pollutants concentration

In order to understand the photochemical potential coupled with the sea breeze dynamic circulations, we have carried out comparisons of ozone concentrations for early morning and late sea breeze cases vis-à-vis a non sea breeze case (Fig.13). According to these measurements, the region of Sousse is less polluted without breeze than with breeze. The temporal evolution of the ozone concentration related to late sea breeze days displays the ozone concentration reduction during the night which is due to the stability of air masses and to the decrease of the atmospheric boundary layer height. The polluted air is trapped in the upper layers (Millan et al., 2002). This thermal cover inhibits the upward and downward movements. Moreover, in the absence of UV radiation during the night, the ozone destruction is governed by the following active reaction:

$$NO + O_3 \longrightarrow NO_2 + O_2.$$
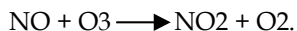
Just after the sunrise, the land surface heating gives birth to the appearance of a mixture of hot and cold air near the land surface and to the progressive increase of the atmospheric boundary layer height. The upper layers ozone is thus trapped on the surface level (Millan et al., 2002). This mechanism contributes to the concentration increase of early morning ozone. Starting from the fresh emissions in the presence of UV radiation, the ozone production notably intervenes in the early morning ozone concentration. As far as the sea breeze effects are concerned, their influence on O_3 concentration evolution is significant in the afternoon. It reaches a maximum concentration of 70 ppb and maintains the nocturnal ozone level. Now let's focus on the evolution of the pollutants concentration on the surface related to morning breeze days. As regards, the temporal evolution of the pollutants concentration, the influence of sea breeze setting is significant. The presence of South-East sea breeze causes the transport of the electric power plant emissions (orientation South-East according to our measurement site). This explains the rapid rise in the concentration of O_3 up to 50 ppb and of SO_2 up to 10 ppb at 0900 LT. Besides, the ozone concentration evolution indicates the presence of a second ozone maximum in the afternoon. The origin of this maximum is attributed to the powerful solar radiation. Now, let's compare ozone and sulfur dioxide during the two different breeze cases (Fig.14). The ozone maximum relative to afternoon sea breeze switches vis-à-vis that of morning breezes. This shift is due to the late wind direction change and to the relatively moderate wind speed. Contrary to the afternoon breeze concentration, the early morning SO_2 concentration is three times higher. This shows the pollutant advection stemming from the electric power plant as soon as the wind direction becomes parallel to direction made by the power plant and measurement site.

During the whole measurement campaign, the evolution of the solar radiation flux is of the same shape (Fig.15). Knowing that the powerful radiation is a dominant factor controlling the ozone production, the photochemical potential is not the unique factor responsible for the concentrations difference between the days of breeze. The late wind direction change, the relatively weak wind speed and the air masses recirculation highlight the afternoon ozone maximum. In fact, the ozone and its precursors are advected on the Mediterranean Sea via the nocturnal offshore synoptic wind just to return after the sea breeze setting.

The offshore synoptic wind opposes the sea breeze penetration causing the formation of an accumulation over the Mediterranean Sea. The ozone is far from the NO fresh emissions and thus can be saved. The ozone destruction mechanism is 3 to 7 times less rapid on the sea than in the land [Nester, 1995]. Due to the sea breeze setting, the ozone and its precursors return to joint the fresh emissions of Sousse region. This mechanism favours the appearance of an ozone maximum in the afternoon. The relatively weak wind traps the pollutants and promotes the photochemical production of ozone in the presence of intense solar radiation.
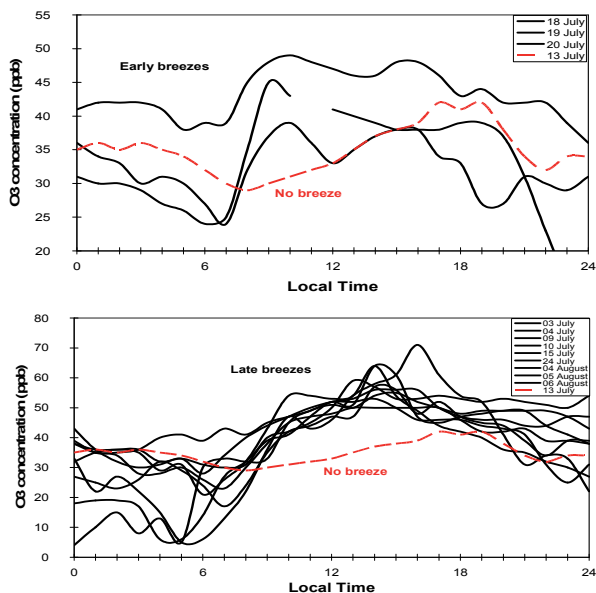
Fig.13. Comparison of the temporal evolution of pollutants concentration related to early morning sea breeze cases and the afternoon sea breeze cases vis-à-vis non-sea breeze cases
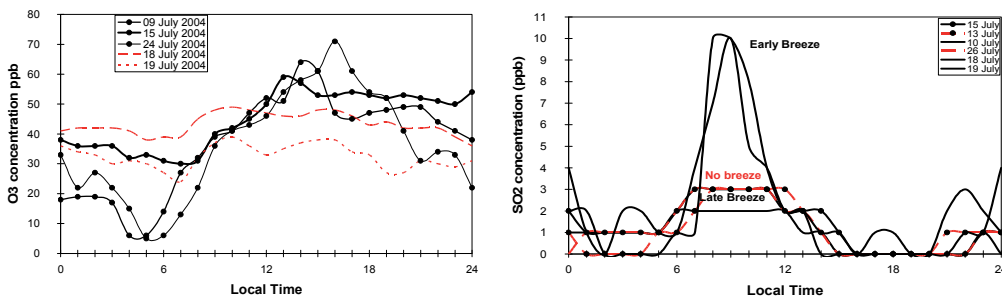

Fig. 14. Comparison of pollutants concentrations related to afternoon and early morning sea breezes. (Solid lines are afternoon sea breeze curve).
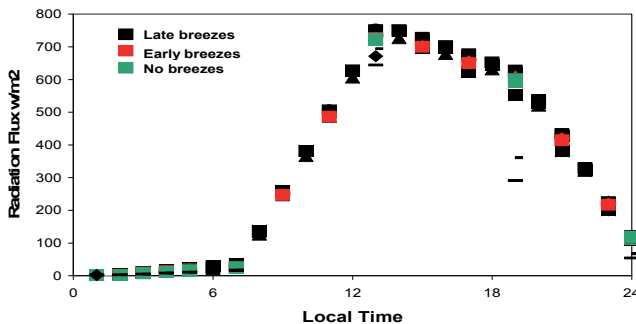

Fig. 15. Temporal variation of solar radiation flux at Sousse region (NOAA ARL data).

8. Conclusion

In this study we have shown that pollutants concentration behaviour depends on the influence of local, meso-scale and long ranges transport phenomenon.

During summer, Ozone concentration reaches its maximum values under the influence of land-sea breeze recirculation and powerful photochemical activity. Saharan dust outbreaks promote PM10 events over the Tunisian coastal sites. This phenomenon was shown to be linked to lower O3 concentration due to the influence of the relatively clean Saharan air.

In winter season, the O3 values are limited to lesser photochemical activity and vertical mixing. Primary pollutants peaks were much higher in winter than in summer which can be explained on the basis of lower ventilation in the winter and lower mixing.

In this paper, we point out that the Saharan dust outbreaks are expected to be an important natural event influencing Tunisian regions and so needs to be more detailed. To improve our understanding about this event and related synoptic phenomena on the Tunisian air quality, we planned to intensify our measurement campaign and to identify pollution episodes which underline the Tunisian pollutants concentrations.

9. References

Alastuey, A.; X., Querol, S., Castillo, M., Escudero, A., Avila, E., Cuevas, C., Torres, P- M., Romero, F., Exposito, O., García, J., Pedro Diaz, R., Van Dingenen, J-P. Putaud. (2005). Characterisation of TSP and PM2.5 at Izaña and Sta. Cruz de Tenerife (Canary Islands, Spain) during a Saharan Dust Episode (July 2002). Atmospheric Environment. 39, 26. 4715-4728.

Baumgardner D., Raga G.B., Grutter M., Lammel G., Evolution of anthropogenic aerosols in the coastal town of Salina Cruz, Mexico: Part I particle dynamics and land–sea interactions, Science of the Total Environment, Vol.367, No.1, 2006, pp. 288-301.

Bouchlaghem K., Ben Mansour F., Elouragini S., Impact of a sea breeze event on air pollution at the Eastern Tunisian coast, Atmospheric Research, Vol.86, 2007, pp. 162-172.

Derwent, R.G., D.R., Middleton, M.E., Goldstone, J.N., Lester, R., Perry. (1995). Analysis and interpretation of air quality data from an urban roadside location in central London over the period from July 1991 to July 1992. Atmospheric Environment. 29, 923-946.

Ding A., Wang T., Zhao M., Wang T., Li Z., Simulation of sea land breezes and a discussion of their implications on the transport of air pollution during a multi-day ozone episode in the Pearl River Delta of China, Atmospheric Environment, Vol.38, 2004, pp. 6737-6750. Evtyugina M.G., Pio T.N.C., Costa C.S., Photochemical pollution under sea breeze conditions, during summer, at the Portuguese West Coast, atmosp

heric Environment, Vol.40, No.33, 2006, pp. 6277-6293.

Flocas H.A., Assimakopoulos V.D., Helmis C.G., An experimental study of aerosol distribution over a Mediterranean urban area, Science of The Total Environment, Vol.367, No.2-3, 2006, pp. 872-887.

Gangoiti, G., M. M., Millán, R., Salvador, E., Mantilla. (2001). Long-range transport and re-circulation of pollutants in the western Mediterranean during the project Regional Cycles of Air Pollution in the West-Central Mediterranean Area. Atmospheric Environment. 35, 36. 6267-6276.

Gangoiti, G., L., Alonso, M., Navazo, A., Albizuri, G., Perez-Landa, M., Matabuena, V., Valdenebro, M., Maruri, J.A., García, M.M., Millán, (2002). Regional transport of pollutants over the Bay of Biscay: analysis of an ozone episode under a blocking anticyclone in west-central Europe. Atmospheric Environment. 36, 8. 1349-1361.

Helena Flocas, A., D., Vasiliki, C., Assimakopoulos, G., Helmis, (2006). An experimental study of aerosol distribution over a Mediterranean urban area. Science of The Total Environment. 367, 2-3. 872-887.

Kassomenos, P.A., H.A., Flocas, S., Lykoudis, A., Skouloudis, (1998). Spatial and temporal characteristics of the relationship between air quality status and mesoscale circulation over an urban Mediterranean basin. The Science of The Total Environment. 217, 1-2. 37-57.

Lim J-H., Sabin L.D., Schiff K.C., Stolzenbach K.D., Concentration, size distribution, and dry deposition rate of particle-associated metals in the Los Angeles region, Atmospheric Environment, Vol.40, No. 40, 2006, pp. 7810-7823.

Liu K.Y., Wang Z., Hsiao L.F., A modeling of a sea breeze and its impact on ozone distribution in northern Taiwan, Environmental Modelling and Software, Vol.17, 2002, pp. 21-27.

Luhar A.K., Hurley P.J., Application of a prognostic model TAPM to sea breeze flows, surface concentrations and fumigating plumes, Environmental Modelling and Software, Vol.19, 2004, pp. 591-601.

Lyamani, H., F.J., Olmo, L., Alados-Arboledas, (2005). Saharan dust outbreak over southeastern Spain as detected by sun photometer. Atmospheric Environment, 39, 38. 7276-7284.

Ma Y., Lyons T.J., Recirculation of coastal urban air pollution under a synoptic scale thermal through in Perth, Western Australia, Atmospheric Environment, Vol.37, 2003, pp. 443-454.

Marmer, E., B., Langmann, (2005). Impact of ship emissions on the Mediterranean summertime pollution and climate: A regional model study. Atmospheric Environment. 39, 26. 4659-4669.

Martín, M., J., Plaza, M. D., Andrés, J. C. Bezares, M.M., Millán, (1991). Comparative study of seasonal air pollutant behavior in a Mediterranean coastal site: Castellón (Spain) Atmospheric Environment. 25, 8. 1523-1535.

Meloni, D., A., Di Sarra, G., Biavati, J.J., De Luisi, F., Monteleone, G., Pace, S., Piacentino, D.M., Sferlazzo, (2007). Seasonal behavior of Saharan dust events at the Mediterranean island of Lampedusa in the Period 1999-2005. Atmospheric Environment. 41. 3041-3056.

Millán, M.M., R., Salvador, E., Mantilla, B., Artnano, (1996). Meteorology and photochemical air pollution in Southern Europe: Experimental results from EC research projects. Atmospheric Environment, 30, 12. 1909-1924.

Millan, M.M., M.J., Sanz, R., Salvador, E., Mantilla, (2002). Atmospheric dynamics and ozone cycles related to nitrogen deposition in the Western Mediterranean. Environmental Pollution. 118, 167-186.

Millan M.M., Sanz M.J., Salvador R., Mantilla E., Atmospheric dynamics and ozone cycles related to nitrogen deposition in the Western Mediterranean, Environmental Pollution, Vol.118, 2002, pp. 167-186.

Nair P.R., Chand D., Lal S., Modh K.S, Naja M., Parameswaran K., Ravindran S., Venkataramani S., Temporal variations in surface ozone at Thumba (8.6°N, 77°E) – a tropical coastal site in India, Atmospheric Environment, Vol.36, 2002, pp. 603-610.

Nester K., Influence of sea breeze flows on air pollution over the ATTIKA PENINSULA, Atmospheric Environment, Vol.29, No.24, 1995, pp. 3655-3670.

Puygrenier, V., F., Lohou, B., Campistron, F., Saïd, G., Pigeon, B., Bénech, D., Serça, (2005). Investigation on the fine structure of sea-breeze during ESCOMPTE experiment. Atmospheric Research. 74, 1-4, 329-353.

Pérez, C., M., Sicard, O., Jorba, A., Comerón, J.M., José, M., Baldasano, (2004). Summertime re-circulations of air pollutants over the north-eastern Iberian coast observed from systematic EARLINET lidar measurements in Barcelona. Atmospheric Environment. 38, 24. 3983-4000.

Rodríguez, S., X., Querol, A., Alastuey, E., Mantilla, (2002). Origin of high summer PM10 and TSP concentrations at rural sites in Eastern Spain. Atmospheric Environment. 36, 19. 3101-3112.

Rodríguez, S., X., Querol, A., Alastuey, M-M. Viana, M., Alarcón, E., Mantilla, C.R., Ruiz (2004). Comparative PM10–PM2.5 source contribution study at rural, urban and industrial sites during PM episodes in Eastern Spain. Science of The Total Environment. 328, 1-3. 95-113.

Simpson J.E., Sea breeze and local wind, Cambridge University, 1994.

Simpson, J.E., D.A., Mansfield, J.R. Milford, (1977). Inland penetration of sea breeze fronts. Quarterly .Journal of the Royal Meteorological Society. 103, 47-76.

Simon, V., L., Dumergues, J-L. Ponche, L.Torres, (2006). The biogenic volatile organic compounds emission inventory in France: Application to plant ecosystems in the Berre-Marseilles area (France). Science of The Total Environment. 372, 1. 164-182.

Srinivas C.V., Venkatesan R., Bagavath Singh A., Sensitivity of mesoscale simulations of land–sea breeze to boundary layer turbulence parameterization, Atmospheric Environment, Vol.41, No.12, 2007, pp. 2534-2548.

Viana, M., X., Querol, A., Alastuey, E., Cuevas, S., (2002). Rodríguez, Influence of African dust on the levels of atmospheric particulates in the Canary Islands air quality network. Atmospheric Environment. 36, 38. 5861-5875.

Viana, M., X., Querol, A., Alastuey, G., Gangoiti, M., Menéndez, (2003). PM levels in the Basque Country (Northern Spain): analysis of a 5-year data record and interpretation of seasonal variations. Atmospheric Environment. 37, 21. 2879-2891.

Viana, M., X., Querol, T., Götschi, A., Alastuey, J., Sunyer, B., Forsberg, J., Heinrich, D., Norbäck, F., Payo, J. A. Maldonado, N. Künzli, (2007). Source apportionment of ambient PM2.5 at five spanish centres of the european community respiratory health survey (ECRHS II). Atmospheric Environment. 41, 7. 1395-1406.

Viana, M., C., Pérez, X., Querol, A., Alastuey, S., Nickovic, J. M. Baldasano, (2005). Spatial and temporal variability of PM levels and composition in a complex summer atmospheric scenario in Barcelona (NE Spain). Atmospheric Environment. 39, 29. 5343-5361.

Ziomas, I.C., (1998). The Mediterranean campaign of photochemical tracers--transport and chemical evolution (MEDCAPHOT-TRACE): an outline. Atmospheric Environment. 32, 12. 2045-2053.

Secondary organic aerosol formation from the oxidation of a mixture of organic gases in a chamber

Marta G. Vivanco and Manuel Santiago
CIEMAT
Spain

1. Introduction

Particles suspended in the air can constitute a potential risk for human health and ecosystems (Pope and Dockery, 2006), specially the finest fraction. Although PM10 (particles with a maximum diameter of 10 μm) have been included in European directives for a longer time (Directive 1999/30/EC) air quality objectives for finer particles have been just very recently established. For particles with a mean diameter lower than 2.5 μm (PM2.5) the UE Directive 2008/50/EC has set a 25 μm/m^3 threshold for the annual mean concentration.

Although the term aerosol includes the particles and the gas in which they are suspended, commonly both terms, particles and aerosols, refer to particles in the atmosphere. A variety of inorganic and organic chemical compounds can be present in the particulate phase. The organic fraction can account for a 20 - 90 % of the finest fraction, according to some authors, such as (Kanakidou et al., 2005) and, therefore, the knowledge of this fraction is important to prevent human health risks. Both inorganic and organic aerosols can be directly emitted (primary aerosols) or can be formed in the atmosphere as a consequence of multiple physical and chemical processes (secondary aerosols). The presence of secondary organic aerosols (SOA) is specially relevant in urban areas (Zhang et al., 2007).

SOA is mainly produced from the oxidation of volatile organic compounds (VOCs), whose products present a sufficiently low volatility to partition into the particle phase according to the gas-particle partitioning theory (Odum et al., 1996) and then nucleate and grow to form organic particles. Presently, SOA is thought to be mainly constituted by polymers, formed through particle phase heterogeneous reactions (Kalberer et al., 2004). Other main components include organic nitrates, such as peroxynitrates and peroxyacylnitrates (Camredon et al., 2007; Kroll and Seinfeld, 2008), and carboxylic acids (Barsanti and Pankow, 2006). In spite of the fact that SOA formation has been the focus of many recent studies, some aspects continue to be not well understood. Simulation chambers represent an ideal vehicle to evaluate SOA formation potential by emitting selected VOCs in the presence of an oxidant under controlled conditions. Many studies in chambers have contributed to increase the knowledge of the oxidation processes of individual organic gases or simple mixes of them. VOCs related to anthropogenic emissions, such as substituted aromatics

(trimethylbenzenes, xylenes and toluene) and alkanes contained in gasolines, are potential SOA precursors in city areas, and they have been thoroughly studied in chamber experiments. Also VOCs related to biogenic emissions, such as isoprene and terpenes (limonene and pinenes) have been widely studied in chambers, as their contribution to global SOA formation is notorious (Claeys et al., 2004; Kleindienst et al., 2006; Leungsakul et al., 2005). OH-initiated is the most common oxidation pathway (Healy et al., 2008; Hu et al., 2007; Lim and Ziemann, 2005; Song et al., 2005; Weitkamp et al., 2007) and thus most of the studies in chambers have been focused on the reaction of the previously mentioned VOCs with this radical.

Recent publications suggest, however, that more complex VOCs mixtures should be used in chamber experiments in order to achieve a more realistic picture of the oxidative processes taking place in real polluted atmospheres (Hallquist et al., 2009). In this chapter SOA formation from a mixture of 1,3,5-TMB (1,3,5-trimethylbenzene), toluene, o-xylene and octane in the presence of an oxidant (nitrous acid, HONO) is evaluated at a 20% of relative humidity. For this purpose, a comprehensive gas phase chemistry and aerosol characterization is presented.

2. Experimental

The experiment was carried out in the EUPHORE facility located in CEAM (Valencia, Spain), a half-spherical Teflon outdoor chamber that allows the transmission of more than 80% of sunlight. Figure 1 illustrates de chamber when it is closed (left side of the picture), when it is being opened (central picture) and opened to sunlight (right side of the figure). The EUPHORE facility has been described in detail somewhere else (Becker, 1996; Volkamer et al., 2001).

Fig. 1. EUPHORE Photoreactor: closed (left side of the figure), while opening (middle of the figure), and opened to sunlight (right side of the figure).

Several analytical equipments provided information of some physical variables (temperature, radiation, humidity, pressure) and chemical concentration of many inorganic and organic gas compounds. Multiple measurement techniques, such as Gas Chromatography coupled with Mass Spectrometer (GC-MS), Fourier Transform Infrared Spectrometry (FTIR), High Pressure Liquid Chromatography (HPLC), Gas Chromatography (GC-ECD and GC-FID/PID), Absorptive Sampling Solid Phase Microextraction (SPME) were used to monitor the gas concentration of reactants and products.

Regarding the particle phase, aerosol concentration was monitored in an on-line way with a TEOM (Tappered Element Oscillating Monitor) and a SMPS (Scanning Mobility Particle Sizer).

This latter provides also information about the diameter particle distribution by classifying the aerosol particles by their electrical mobility. Also, three low volume samplings were taken during the experiment and one high volume once the chamber was closed, in order to analyze aerosol composition via gas chromatography and ion chromatography.

The experiment described in this chapter was performed on June, 17th, 2008, as a part of the campaign performed by the authors in 2008 described in recent publications (Vivanco et al., 2010). Experimental conditions are summarized in Table 1. A mixture of volatile organic compounds and HONO was introduced into the chamber.

	Time		Concentration (ppb)
Parents VOCs intro	7:11	1,3,5-TMB	151
HONO introduction	8:01	Toluene	99
Water introduction	8:48	o-xylene	17
Opening	10:33	Octane	80
Closure	15:23	HONO	98
		Relative Humidity	20%

Table 1. Experimental conditions

After the parent VOCs the oxidant was introduced. Also, humidity conditions were prepared by introducing pulverized water into the chamber. Then, the chamber was opened to the sunlight.

3. Gas phase chemistry of the parent VOCs

In this section, a study about the atmospheric photochemical reactions is done, focusing on the oxidation pathways of the parent VOCs. These pathways consist in multiple oxidation steps which lead to the formation of multiple compounds. A very useful source of knowledge for atmospheric oxidation pathways is the Master Chemical Mechansim, developed by the University of Leeds (Jenkin et al., 2003; Saunders et al., 2002). The latest version of this mechanism, MCM v3.1 (Bloss et al., 2005), takes into account most of the kinetic and mechanistic data avaliable to date.

The atmospheric oxidation of a certain compound is conditioned by its own structure and by the nature of the initial oxidant. Nitrous acid (HONO) was used as the oxidant compound and therefore, the major initial oxidant is the OH radical, formed by HONO photolysis. The reaction of the aromatic VOCs emitted in this experiment with the OH radical have been previously studied by several authors (Atkinson and Arey, 2003; Bloss et al., 2005; Hamilton et al., 2005; Huang et al., 2006; Johnson et al., 2004; Wagner et al., 2002). Two main reaction pathways can be identified in the oxidation of toluene, o-xylene or 1,3,5-TMB with OH: H-abstraction and OH-addition. The H-abstraction is considered as the minor route and leads to the formation of aromatic aldehydes. The OH-addition can occur in three differet ways: through the phenolic, the epoxy-oxy and the peroxy-bicyclic routes. The phenolic and epoxy-oxy routes lead to the formation of phenolic and epoxyde compounds respectively, while the peroxy-bicyclic route produces the opening of the aromatic rings and the formation of oxygenated products, which may lead to the formation of SOA if their volatility is low enough. This last route is considered as the major oxidation pathway according to the reactions included in the MCM v.3.1. A scheme of the oxidation pathways for toluene, o-xylene and 1,3,5-TMB is presented in figures 2a, 2b and 2c.
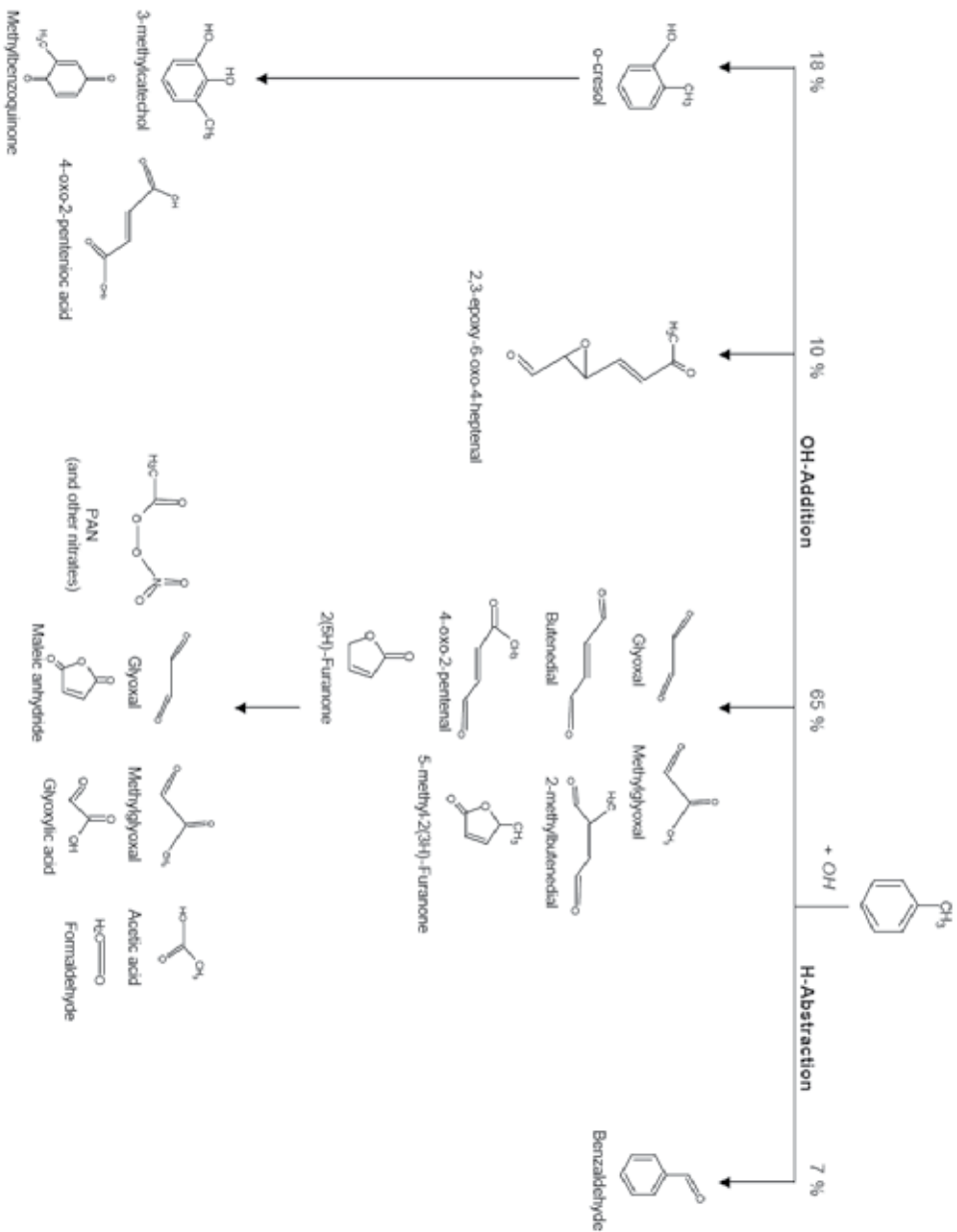
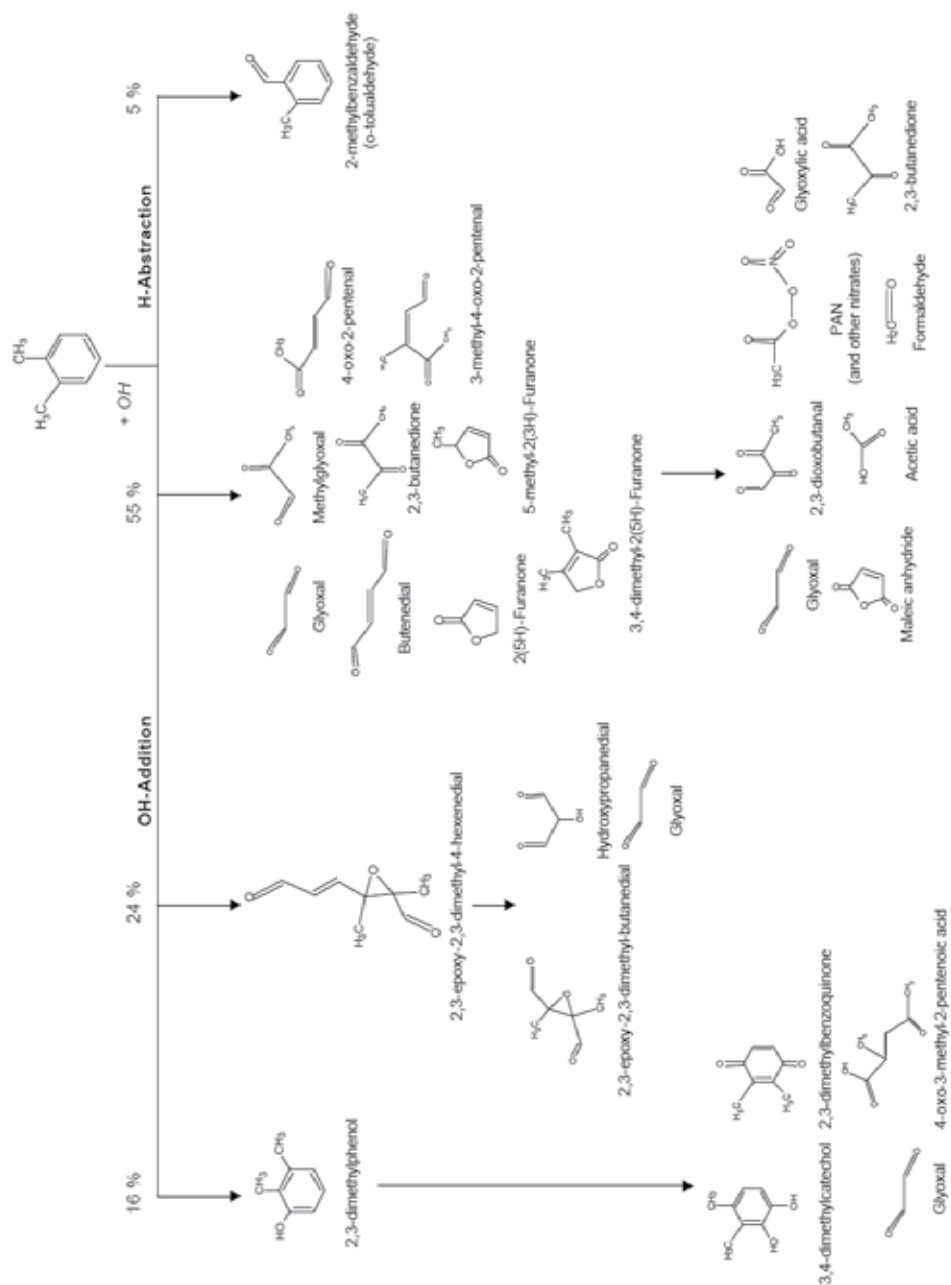Fig. 2a. Toluene oxidation pathways scheme (MCM v.3.1)

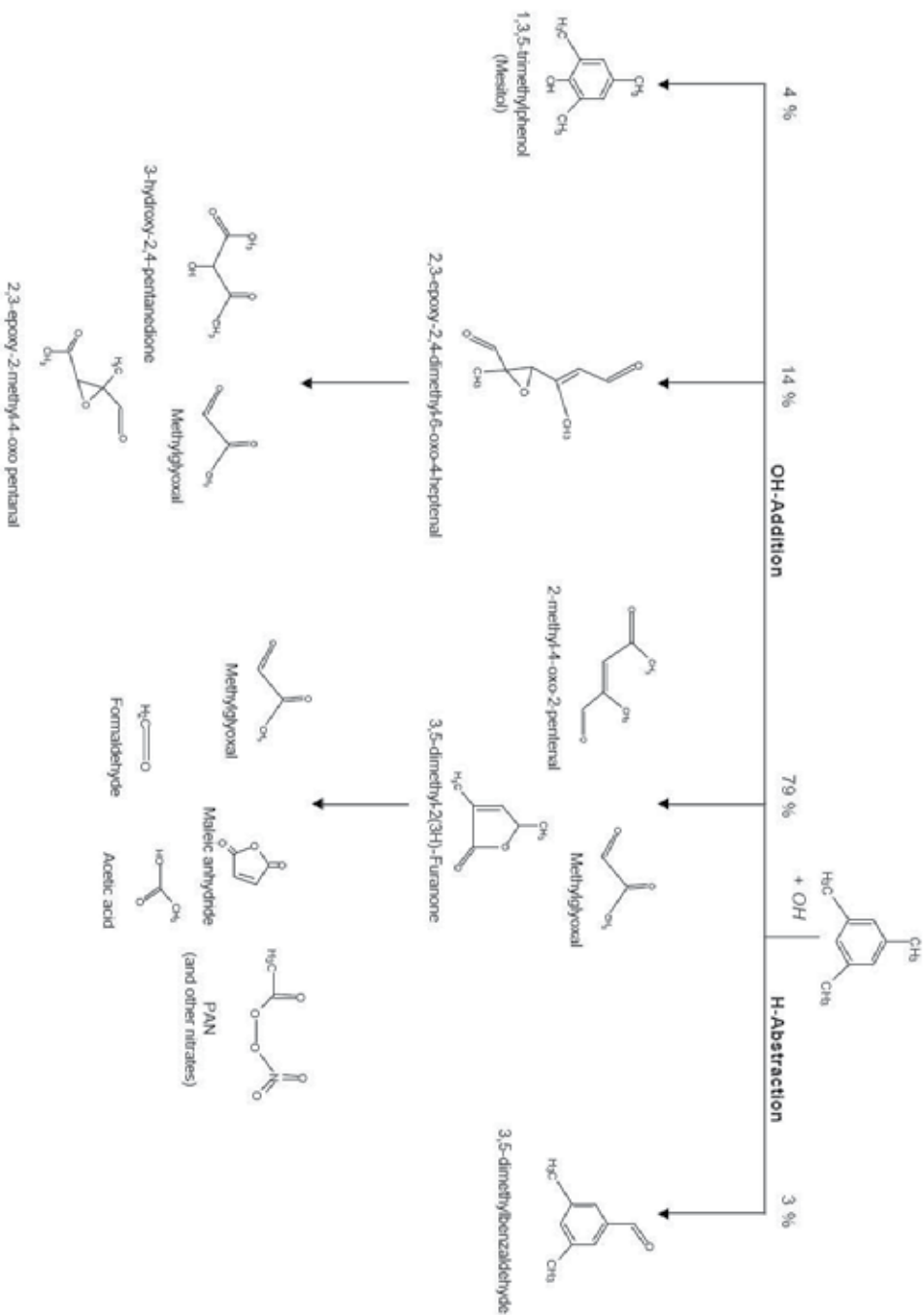Fig. 2b O-xylene oxidation pathways scheme (MCM v.3.1)

Fig. 2c. 1,3,5-TMB oxidation pathways scheme (MCM v.3.1)

In the case of octane, as for the rest of alkanes, the main oxidation pathway is the H-abstraction (Jordan et al., 2008; Lim and Ziemann, 2005). Figure 3 shows the main products formed during the octane oxidation, based on the reactions included in the MCM v.3.1:
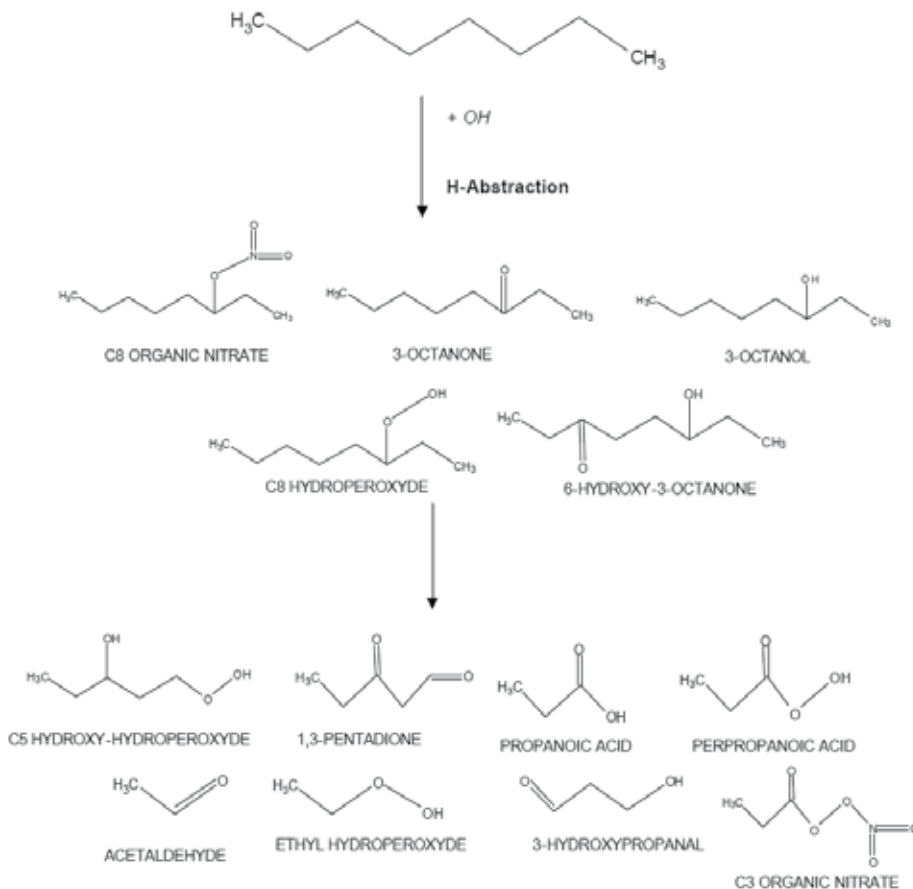

Fig. 3. Octane oxidation pathway scheme (based on MCM v3.1)

4. Results for the gas phase

Once the chamber is opened to the sunlight, the oxidation of the mixture of VOCs starts by reacting with the OH radical, formed from the photolysis of HONO:

$$HO\,NO + hv \rightarrow NO + OH \qquad (1)$$

OH radical is responsible for the initial oxidation of the VOCs by both OH-addition and H-abstraction. Although not presented in figures 3 and 4, an intermediate acyl peroxy radical is formed (RO_2), which may undergo several instantaneous reactions to form the resulting oxidation products.

Figure 4 illustrates a scheme of the overall processes expected to take place inside the chamber. Once the light enters the chamber new gas products and particles are formed due to oxidation processes occurring in both gas and particle phases.
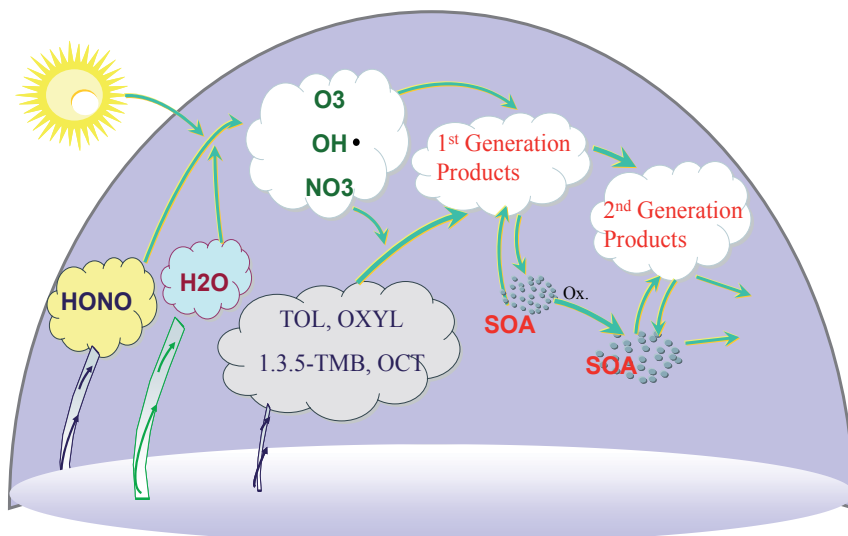

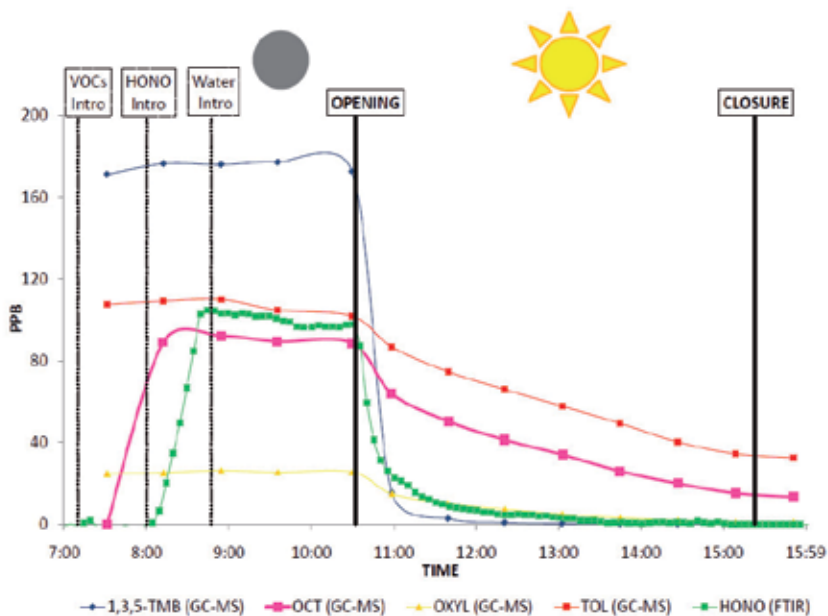Fig. 4 Illustration of processes expected to take place during the experiment

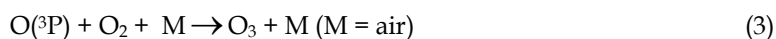Fig. 5. Time series showing HONO, toluene (TOL), o-xylene (OXYL), 1,3,5-TMB and octane (OCT) concentration

Time series showing the concentration of the initial reactants (the mixture of VOCs and HONO) are shown in Figure 5. The inmediate and pronounced decay of HONO concentration is clearly observed when light enters the chamber (green line).

Also, a very strong concentration decrease is observed for 1,3,5-TMB (blue line). This fact is related to the highest reactivity of this compound with the OH radical, compared to the other three organic gases. Table 2 includes the OH-reactivity constant for the four gases.

COMPOUND	kOH (10^{12} molecs/cm^3.s)
Toluene	5.74
o-xylene	13.6
Octane	8.61
1,3,5-TMB	56.7

Table 2. OH-reactivity constants for each parent VOC at 25º C (as given by MCM 3.1)

Ozone is a major product from the oxidation proccesses. In a clean atmosphere, there is a photoequilibrium between NO, NO_2 and O_3 and therefore no net ozone is produced (Atkinson, 2000):

$$NO_2 + hv \rightarrow NO + O(^3P) \tag{2}$$

$$O(^3P) + O_2 + M \rightarrow O_3 + M \ (M = air) \tag{3}$$

$$O_3 + NO \rightarrow NO_2 + O_2 \tag{4}$$

However, in the presence of VOCs, this equilibrium is broken due to reactions of NO with RO_2 and HO_2 radicals formed during the oxidation of VOCs:

$$RO_2 + NO \rightarrow RO + NO_2 \tag{5}$$

$$HO_2 + NO \rightarrow OH + NO_2 \tag{6}$$

consuming NO but not ozone and, therefore, leading to a net production of ozone, a well known atmospheric pollutant. Figure 6 shows the increasing ozone concentration and the strong decrease of 1,3,5-TMB concentration produced when the chamber is opened. This sudden growth of ozone concentration is clearly related to the broken equilibrium described above.
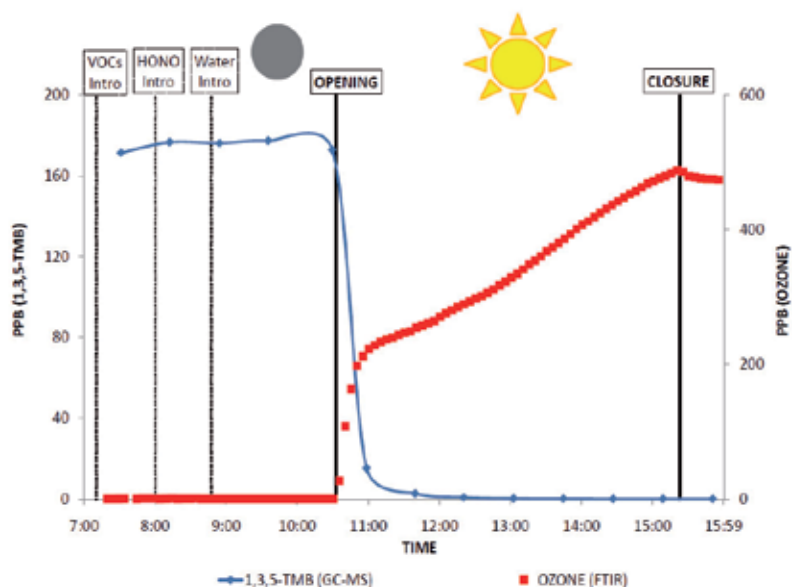
Fig. 6. Time series showing ozone and 1,3,5-TMB concentration

Besides ozone, a great variety of products were also identified during the experiment. Figure 7 shows the temporal evolution of the major products concentration. The parent VOCs and HONO have been also included in the figure in order to give a complete picture of the formation and decay times during the whole experiment.
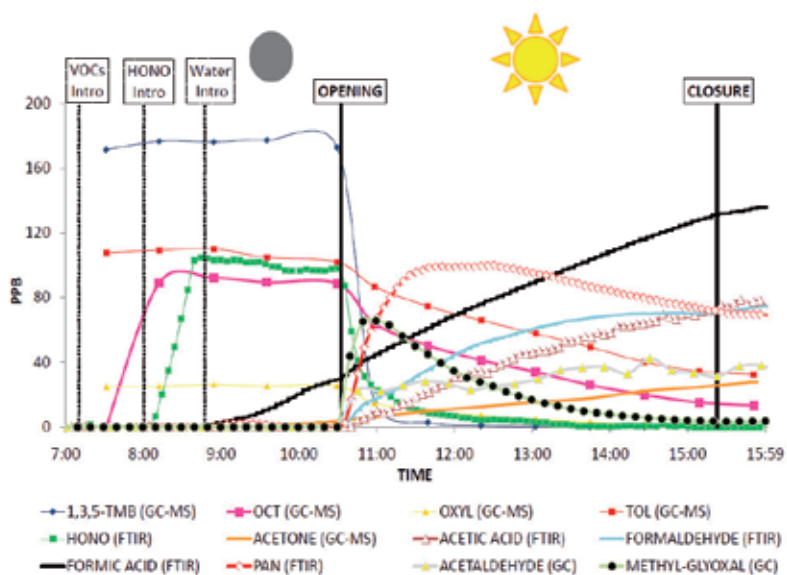

Fig. 7. Major products identified during the experiment (parent VOCs and HONO also included).

Peroxyacetyl nitrate (PAN) is one of main products formed inside the chamber. This nitrate is produced through the reaction of an acyl peroxy radical (RO2) with NO_2:

$$RO2 + NO_2 \rightarrow ROONO_2 \qquad (7)$$

and has a medium lifetime of 30 minutes, being thermal decomposition its major loss proccess at lower altitudes (Talukdar et al., 1995). PAN can partition to the particle phase and it has been previously identified as an important SOA constituent (Bonn et al., 2004; Johnson et al., 2004).

Methylglyoxal (2-oxopropanal) is a well known product from toluene, o-xylene and 1,3,5-TMB oxidation (Healy et al., 2008; Jang and Kamens, 2001; Volkamer et al., 2001). This dialdehyde can further react to form smaller compounds such as methanol, formadehyde, acetic acid and it can also produce PAN. In addition, methylglyoxal can partition into the particle phase. It has been reported that it can undergo accretion reactions (non-oxidative oligomer formation) to form hemiacetals due to the hydration of its aldehyde groups (Barsanti and Pankow, 2005; Loeffler et al., 2006). As a consequence of these proccesses, methylglyoxal presents an intermediate product concentration profile, with a clearly visible maximum peak.

Some other simple carbonyl products such as acetone, formaldehyde and acetaldehyde were also identified. In the case of formaldehyde, it can be produced from the oxidation of aromatic VOCs products (glyoxal, methylglyoxal, 2,3-butanedione or (5H)-2-furanone). Acetaldehyde can be mainly formed from the reaction of 3-octanone (an octane oxidation product) with OH radical. Acetone, however, is mainly formed from the ozonolysis of 3-methyl-4-oxo-2-pentenal, an o-xylene oxidation product. Ozonolysis reaction rates are very low (for a given compound, O3-reactivity constants are generally several orders of magnitude lower than OH-reactivity constants), so little quantities of acetone are produced in the experiment, as it can be seen in Figure 7.

Formic and acetic acids can be formed in the chamber from the aqueous phase oxidation of their respectives aldehydes (Chebbi and Carlier, 1996) and, in the case of acetaldehyde, also from the oxidation of aromatic VOCs oxidation products such as methylglyoxal, 2,3-butanedione and 3-methyl-4-oxo-2-pentenal. It has also been reported that formaldehyde reaction with hydroperoxyde radicals HO_2 can be a significant source of formic acid in the gas phase (Khwaja, 1995). However, the most remarkable aspect about the formic acid is that, as it can be seen in Figure 7, it starts to be formed before the opening of the chamber. The formation of this acid coincides with the introduction of water in the chamber, suggesting that there is an additional formic acid formation way that does not include a photochemical activation.

In addition to the products presented in Figure 7, some other compounds in much lower concentrations were identified (Figure 8).
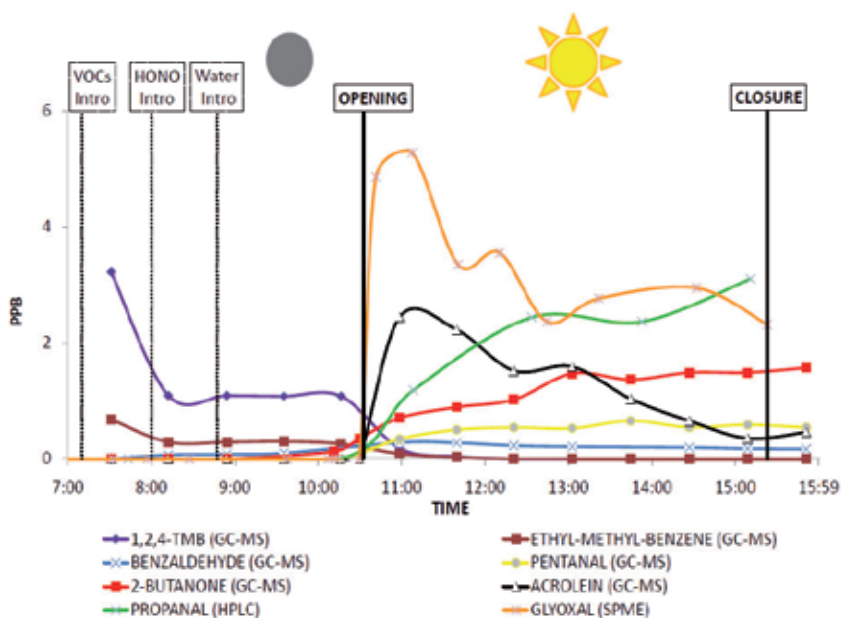
Fig. 8. Time series showing the concentration of some trace products

1,2,4-TMB and ethyl-methylbenzene (also known as ethyl-toluene) entered the chamber with the parent VOCs mixture in trace concentrations, while the presence of benzaldehyde in the chamber means that the H-abstraction pathway takes place at least for toluene, as benzaldehyde is its corresponding aromaldehyde. This is in concordance with the relative branching ratios predicted by MCM v.3.1 for the three gases, as toluene has the highest one (7 %) for the H-Abstraction route.

Glyoxal is a ring opening oxidation product from toluene and o-xylene (Volkamer et al., 2001). In the same way as methylglyoxal, this compound presents a high water solubility and can partition into the particle phase and form oligomers (Hastings et al., 2005; Hu et al., 2007; Volkamer et al., 2007). This fact could explain the low glyoxal gas phase concentration found in the experiment.

The small concentrations of acrolein, 2-butanone (butanone), propanal and pentanal measured through the experiment indicate that those are minor oxidation products from the parent VOCs.

5. Aerosol phase

The objective of the experiment was to determine the secondary organic formation from the mixture of the selected VOCs. As no aerosol was emitted all the aerosols recorded in the chamber have a secondary origin. Not only organic particles can be formed, but also some inorganic salts can be potential products of the reactant system. To identify these salts, ionic chromatography was applied. Figure 9 shows nitrates and sulfates contribution for the four samplings taken during the experiment (left side of the figure), as well as the characterization of the resulting organic mass (right side of the figure).
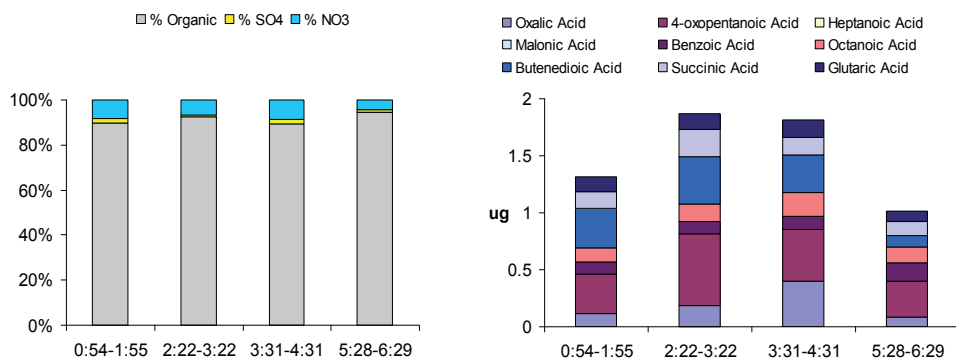
Fig. 9. Inorganic (left side) and organic (right side) filter characterization. The sampling time of each filter is presented in the x axis (time zero represents the opening of the chamber).

It can be seen that the inorganic contribution to the total aerosol mass is very low during the experiment. The small sulfate amount is similar to that found in blank filters. Nitrates can be formed due to the heterogeneous reaction of NO_2 with the water drops sticked on the chamber walls, driving to HNO_3 formation and, eventually, nitrates. Only a minimum quantity of the organic mass (about 60 – 90 μg in the first three filters and about 250 μg in the fourth) was identified, in a similar way to previous studies (Hamilton et al., 2005; Sato et al., 2007). Most of the acids identified were already detected in previous studies (Baltensperger et al., 2005; Hamilton et al., 2005; Jang and Kamens, 2001; Sato et al., 2007).
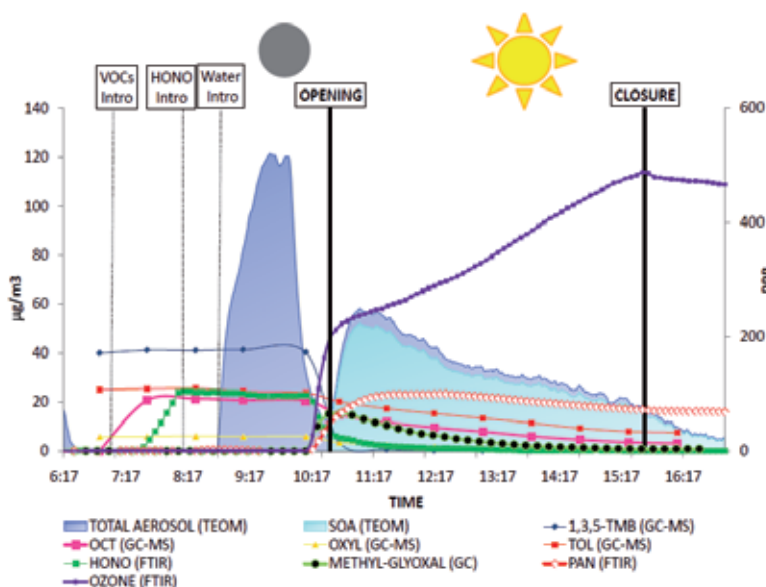

Fig. 10. Time series showing aerosol concentration measured with the TEOM (shaded blue area) and some other gases concentration.

Aerosol concentration measured with TEOM is presented in Figure 10 (dark blue area). Particles start to be formed once the chamber is opened. Inorganic contribution estimated

from the filters was discounted from the total aerosol concentration in order to take an idea of the organic content (SOA, light blue area in Figure 10). The particles formed before the opening of the chamber correspond to small drops of water that are introduced into the chamber to create the 20% of relative humidity conditions. Scale for gases is presented in the right y-axis (ppb) while particle concentration is presented in the left one, in $\mu g/m^3$.

While other gas products such as ozone present a continuously increasing behaviour, particles are mainly formed during the first hour of the experiment. The initial formed particles present a small diameter and start growing by coagulation processes due to collisions between them (Kulmala et al., 2004).

The results provided by SMPS regarding particle size are presented in Figure 11. They reveal a growth of the aerosols. It is important to notice that the formation of detectable particles (> 17 nm) starts approximately ten minutes after the opening of the chamber (purple band at 10:42). Because of the detection limit of SMPS, no smaller particles can be detected and therefore initial particle formation due to nucleation can not be monitored. For this reason, this analysis focuses on the particle growth once the first particles are formed.
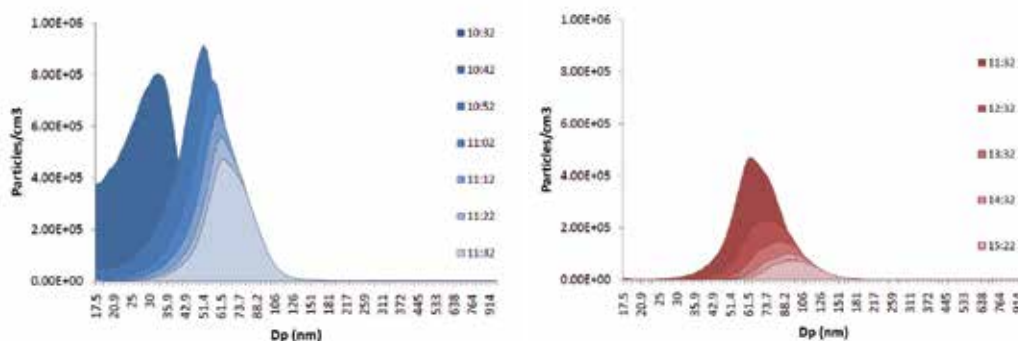

Fig. 11. Particle size distribution provided by SMPS

During the first hour after the opening of the chamber (left side of the figure) a quick growth in the particle diameter (Dp) takes place, coupled with a decrease in the number of particles, expressed as particles density (particles/cm³), which falls down from its maximum value (9E+5 particles/cm³). After this first hour, the particle diameter growth turns slower (right side of the figure). Coagulation and condensation of gas phase oxidation products can be the reason for this increase of the mean particle diameter (Sadezky et al., 2006). This increase in the mean particle diameter can be also inferred from Figure 12, where the temporal evolution of some selected diameters is presented.
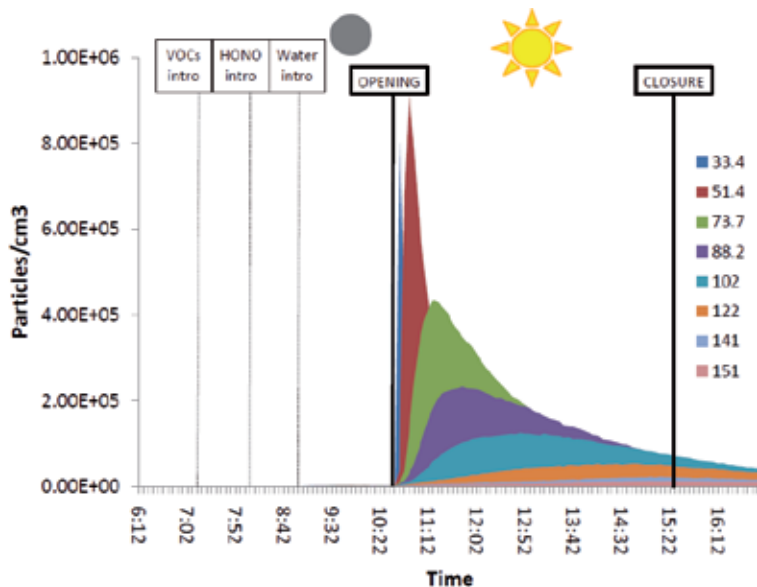
Secondary organic aerosol formation from
the oxidation of a mixture of organic gases in a chamber
279

Fig. 12. Evolution of some selected Dp (nm) with time

The smallest particles are formed in high quantities at the beginning of the experiment (in the figure, diameters 33.4 nm and 51.4 nm) and then their concentration falls, while higher particles appear gradually, but in lower concentrations.

6. Conclusions and future challenges

In this chapter, a study focused on SOA formation from a mixture of anthropogenic VOCs is presented. 1,3,5-TMB resulted to be the most reactive VOC and therefore the initial steps of the photooxidation in the chamber are governed by its degradation. During the experiment, several organic compounds were measured and identified as products from specific oxidation pathways, some of them also known as relevant SOA constituents (PAN, methylglyoxal). The influence of the mixture of VOCs in ozone formation is also corroborated by a progressive concentration increase of this compound in the chamber.

Regarding the aerosol phase, maximum concentration is reached during the first hour after the opening of the chamber, indicating the formation of particles via nucleation of the condensed oxidation products. After this initial formation, the aerosol particles evolve and growth, possibly by coagulation processes and by the uptake to the particle phase of further oxidation products.

The chemical characterization revealed the presence of several carboxylic acids, but only a minor fraction of the total mass collected was identified. This limitation constitutes a common problem in chamber studies, as a consequence of current analytical techniques. Therefore, a more complete organic characterization represents a challenge and a necessity to better understand organic aerosols formation.

7. Acknowledgement

8. References

Atkinson, R., (2000). Atmospheric chemistry of VOCs and NOx. *Atmospheric Environment,* 34, 2063-2101

Baltensperger, U., Kalberer, M., Dommen, J., Paulsen, D., Alfarra, M.R., Coe, H., Fisseha, R., Gascho, A., Gysel, M., Nyeki, S., Sax, M., Steinbacher, M., Prevot, A.S.H., Sjögren, S., Weingartner, E. and Zenobi, R., (2005). Secondary organic aerosols from anthropogenic and biogenic precursors. *Faraday Discussions,* 130, 265–278

Barsanti, K.C. and Pankow, J.F., (2006). Thermodynamics of the formation of atmospheric organic particulate matter by accretion reactions—Part 3: Carboxylic and dicarboxylic acids. *Atmospheric Environment,* 40, 6676–6686

Becker, K.H., EUPHORE final report. *Report of the EC-Project Contract EV5V-CT92-0059* (1996).

Bloss, C., Wagner, V., Jenkin, M.E., Volkamer, R., Bloss, W.J., Lee, J.D., Heard, D.E., Wirtz, K., Reviejo, M.M.-., Rea, G., Wenger, J.C. and Pilling, M.J., (2005). Development of a detailed chemical mechanism (MCMv3.1) for the atmospheric oxidation of aromatic hydrocarbons. *Atmospheric Chemistry and Physics,* 5, 641-664

Camredon, M., Aumont, B., Lee-Taylor, J. and Madronich, S., (2007). The SOA/VOC/NOx system: an explicit model of secondary organic aerosol formation. *Atmospheric Chemistry and Physics,* 7, 5599–5610

Claeys, M., Graham, B., Vas, G., Wang, W., Vermeylen, R., Pashynska, V., Cafmeyer, J., Guyon, P., Andreae, M.O., Artaxo, P. and Maenhaut, W., (2004). Formation of Secondary Organic Aerosols Through Photooxidation of Isoprene. *Science,* 303, 1173-1176

Chebbi, A. and Carlier, P., (1996). Carboxylic Acids in the Troposphere, Occurrence, Sources and Sinks: a Review. *Atmospheric Environment,* 30, 4233-4249

Hallquist, M., Wenger, J.C., Baltensperger, U., Rudich, Y., Simpson, D., Claeys, M., Dommen, J., Donahue, N.M., George, C., Goldstein, A.H., Hamilton, J.F., Herrmann, H., Hoffmann, T., Iinuma, Y., Jang, M., Jenkin, M.E., Jimenez, J.L., Kiendler-Scharr, A., Maenhaut, W., McFiggans, G., Mentel, T.F., Monod, A., Prevot, A.S.H., Seinfeld, J.H., Surratt, J.D., Szmigielski, R. and Wildt, J., (2009). The formation, properties and impact of secondary organic aerosol: current and emerging issues. *Atmospheric Chemistry and Physics,* 9, 5155–5236

Hamilton, J.F., Webb, P.J., Lewis, A.C. and Reviejo, M.M., (2005). Quantifying small molecules in secondary organic aerosol formed during the photo-oxidation of toluene with hydroxyl radicals. *Atmospheric Environment,* 39, 7263-7275

Healy, R.M., Wenger, J.C., Metzger, A., Duplissy, J., Kalberer, M. and Dommen, J., (2008). Gas/particle partitioning of carbonyls in the photooxidation of isoprene and 1,3,5-trimethylbenzene. *Atmospheric Chemistry and Physics,* 8, 3215-3220

Hu, D., Tolocka, M., Li, Q. and Kamens, R.M., (2007). A kinetic mechanism for predicting secondary organic aerosol formation from toluene oxidation in the presence of NOx and natural sunlight. *Atmospheric Environment,* 41, 6478–6496

Jang, M. and Kamens, R.M., (2001). Characterization of Secondary Aerosol from the Photooxidation of Toluene in the Presence of NOx and 1-Propene. *Environmental Science and Technology,* 35, 3626-3639

Jordan, C.E., Ziemann, P.J., Griffin, R.J., Lim, Y.B., R.Atkinson and Arey, J., (2008). Modeling SOA formation from OH reactions with C8-c17 n-alkanes. *Atmospheric Environment,* 42, 8015-8026

Kalberer, M., Paulsen, D., Sax, M., Steinbacher, M., Dommen, J., Prevot, A.S.H., Fisseha, R., Weingartner, E., Frankevich, V., Zenobi, R. and Baltensperger, U., (2004). Identification of Polymers as Major Components of Atmospheric Organic Aerosols. *Science,* 303, 1659-1662

Kanakidou, M., Seinfeld, J.H., Pandis, S.N., Barnes, I., Dentener, F.J., Facchini, M.C., Dingenen, R.V., Ervens, B., Nenes, A. and Nielsen, C.J., (2005). Organic aerosol and global climate modelling: a review. *Atmospheric Chemistry and Physics,* 5, 1053–1123

Khwaja, H.A., (1995). Atmospheric Concentrations of Carboxylic Acids and Related Compounds at a Semiurban Site. *Atmospheric Environment,* 29, 127-139

Kleindienst, T.E., Edney, E.O., Lewandowski, M., Offenberg, J.H. and Jaoui, M., (2006). Secondary Organic Carbon and Aerosol Yields from the Irradiations of Isoprene and alpha-Pinene in the Presence of NOx and SO2. *Environmental Science and Technology,* 40, 3807-3812

Kroll, J.H. and Seinfeld, J.H., (2008). Chemistry of secondary organic aerosol: Formation and evolution of low-volatility organics in the atmosphere. *Atmospheric Environment,* 42, 3593-3624

Kulmala, M., Laakso, L., Lehtinen, K.E.J., Riipinen, I., Maso, M.D., Anttila, T., Kerminen, V.-M., Horrak, U., Vana, M. and Tammet, H., (2004). Initial steps of aerosol growth. *Atmospheric Chemistry and Physics,* 4, 2553–2560

Leungsakul, S., Jeffries, H.E. and Kamens, R.M., (2005). A kinetic mechanism for predicting secondary aerosol formation from the reactions of d-limonene in the presence of oxides of nitrogen and natural sunlight. *Atmospheric Chemistry,* 39, 7063-7082

Lim, Y.B. and Ziemann, P.J., (2005). Products and Mechanism of Secondary Organic Aerosol Formation from Reactions of n-Alkanes with OH Radicals in the Presence of NOx. *Environmental Science and Technology,* 39, 9229-9236

Odum, J.R., Hoffmann, T., Bowman, F., Collins, D., Flagan, R.C. and Seinfeld, J.H., (1996). Gas/Particle Partitioning and Secondary Organic Aerosol Yields. *Environmental Science and Technology,* 30, 2580-2585

Pope, C.A. and Dockery, D.W., (2006). Health Effects of Fine Particulate Air Pollution: Lines that Connect. *Journal of Air and Waste Management,* 56, 709–742

Sadezky, A., Chaimbault, P., Mellouki, A., Römpp, A., R.Winterhalter, Bras, G.L. and Moortgat, G.K., (2006). Formation of secondary organic aerosol and oligomers from the ozonolysis of enol ethers. *Atmospheric Chemistry and Physics,* 6, 5009–5024

Sato, K., Hatakeyama, S. and Imamura, T., (2007). Secondary Organic Aerosol Formation during the Photooxidation of Toluene: NOx Dependence of Chemical Composition. *Journal of Physical Chemistry A,* 111, 9796-9808

Song, C., Na, K. and III, D.R.C., (2005). Impact of the Hydrocarbon to NOx Ratio on Secondary Organic Aerosol Formation. *Environmental Science and Technology,* 39, 3143-3149

Talukdar, R.K., Burkholder, J.B., Schmoltner, A.-M., Roberts, J.M., Wilson, R.R. and Ravishankara, A.R., (1995). Investigation of the loss processes for peroxyacetyl nitrate in the atmosphere: UV photolysis and reaction with OH. *Journal of Geophysical Research,* 100, 14163-14173

Vivanco, M.G., Santiago, M., Martínez-Tarifa, A., Borrás, E. García-Diego, C. and Sánchez, M., (2010). SOA Formation in a photoreactor from a mixture of organic gases and HONO for different experimental conditions. *Submitted to Atmospheric Environment on March 23th 2010,*

Volkamer, R., Platt, U. and Wirtz, K., (2001). Primary and Secondary Glyoxal Formation from Aromatics: Experimental Evidence for the Bicycloalkyl-Radical Pathway from Benzene, Toluene, and p-Xylene. *Journal of Physical Chemistry A,* 105, 7865-7874

Weitkamp, E.A., Sage, A.M., Pierce, J.R., Donahue, N.M. and Robinson, A.L., (2007). Organic aerosol formation from photochemical oxidation of diesel exhaust in a smog chamber. *Environmental Science and Technology,* 41, 6969-6975

Zhang, Q., Jimenez, J.L., Canagaratna, M.R., Allan, J.D., Coe, H., Ulbrich, I., Alfarra, M.R., Takami, A., Middlebrook, A.M., Sun, Y.L., Dzepina, K., Dunlea, E., Docherty, K., DeCarlo, P.F., Salcedo, D., Onasch, T., Jayne, J.T., Miyoshi, T., Shimono, A., Hatakeyama, S., Takegawa, N., Kondo, Y., Schneider, J., Drewnick, F., Borrmann, S., Weimer, S., Demerjian, K., Williams, P., Bower, K., Bahreini, R., Cottrell, L., Griffin, R.J., Rautiainen, J., Sun, J.Y., Zhang, Y.M. and Worsnop, D.R., (2007). Ubiquity and dominance of oxygenated species in organic aerosols in anthropogenically-influenced Northern Hemisphere midlatitudes. *Geophysical Research Letters,* 34, L13801

Algorithm for air quality mapping using satellite images

H. S. Lim, M. Z. MatJafri and K. Abdullah
School of Physics,
Universiti Sains Malaysia,
11800 Penang, Malaysia.
Tel: +604-6533888, Fax: +604-6579150
E-mail: hslim@usm.my, mjafri@usm.my, khirudd@usm.my

1. Introduction

Nowadays, air quality is a major concern in many countries whether in the developed or the developing countries. Environmental pollution is the major concern nowadays because all our daily activities are related to the environmental. Due to the high cost and limited number of air pollutant stations in each area, they cannot provide a good spatial distribution of the air pollutant readings over a city. Satellite observations can give a high spatial distribution of air pollution. The present study is dealing with a new developed algorithm for the determination of the concentration of particulate matter of size less than 10-micron (PM10) over Penang Island, Malaysia.

Air pollution in Asian cities has grown with the progressing industrialization and urbanization. This recent experience in Asia is predated by similar problems in the western countries at early stages of their economic development. Air quality in Chinese cities today is more closely resembles the London smog problem than the Los Angeles smog problem, although that could change as present problems with coal smoke are brought under control (UNEP Assessment Report).

Air pollution causes a number of health problems and it has been linked with illnesses and deaths from heart or lung diseases. Nowadays, air quality is a major problem in many developed countries and they having build up their own network for measuring the air quality levels. Malaysia also has build up our network for monitoring our environment. A network is composed of static measuring stations, which allow continuous measurements of air pollution parameters. Data are collected hourly which include five types of the air pollution constituently such as particulate matter less than 10 micron (PM10), sulphur dioxide (SO2), nitrogen dioxide (NO2), carbon monoxide (CO), and ozone (O3). This network is managed by Alam Sekitar Malaysia Sdn. Bhd. (ASMA), agency contracted by the Department of Environment Malaysia to measure air quality in the country.

Aerosols scatter incoming solar radiation and modify short-wave radiative properties of clouds by acting as cloud condensation nuclei (CCN) (Badarinath, et al.). Particulates matter

(PM), or aerosol, is the general term used for a mixture of solid particles and liquid droplets found in the atmosphere. Monitoring natural (dust and volcanic ash) and anthopogenic aerosols (biomass burning smoke, industrial pollution) has gained renewed attention because they influence cloud properties, alter the radiation budget of the earth-atmosphere system, affect atmospheric circulation patterns and cause changes in surface temperature and precipitation (Wang and Cgristopher, 2003).

The problem of particulate pollution in the atmosphere has attracted a new interest with the recent scientific evidence of the ill-health effects of small particles. Aerosol optical thickness in the visible (or atmospheric turbidity), which is defined as the linear integral of the extinction coefficient due to small airborne particles, can be considered as an overall air pollution indicator in urban areas. Several studies have shown the possible relationships between satellite data and air pollution. The monitoring of aerosol concentrations becomes a high environmental priority particularly in urban areas. Airborne particulate matter or aerosols, whether anthropogenic or of natural origin constitute a major environmental issue. At the regional level, aerosols are contributors to visibility degradation (haze) and to acid deposition; at the global level they play a role in climate change. At local level, epidemiological studies indicate that small sized aerosols are causal factors in mortality in urban areas. Therefore monitoring aerosol concentrations becomes a high priority at a variety of geographical scales.

Remote sensing technique was wide used for environment pollutant application such as water quality [Dekker, et al., (2002), Tassan, (1993) and Doxaran, et al., (2002)] and air pollutant (Ung, et al., 2001b). Several studies have shown the possible relationships between satellite data and air pollution [Weber, et al., (2001) and Ung, et al, (2001a)]. Other researchers used satellite data for such environment atmospheric studies such as NOAA-14 AVHRR (Ahmad and Hashim, 1997) and Landsat TM (Ung, et al., 2001b). In fact, air quality can be measure using ground instrument such as air sample. But these instruments are quite expensive and the coverage is limited by the number of the air pollutant station in each area. So, they cannot provide a good spatial distribution of air pollutant readings over a city. Compared to ground measurements, satellite imagery, due to their large spatial coverage and reliable repeated measurements, provide another important tool to monitor aerosols and their transport patterns (Wang and Christopher, 2003). The atmosphere affects satellite images of the Earth's surface in the solar spectrum. So, the signal observe by the satellite sensor was the sum of the effects from the ground and atmosphere. Tropospheric aerosols act to significantly alter the Earth's radiation budget, but quantification of the change in radiation is difficult because atmospheric aerosol distributions vary greatly in type, size, space and time (Penner, et al. 2002). Surface reflectance is a key to the retrieval of atmospheric components from remotely sensed data. Optical atmospheric effects may influence the signal measured by a remote sensor in two ways: radiometrically and geometrically. This means that they can modify the signal's intensity through scattering or absorption processes and its direction by refraction (Sifakis and Deschamps, 1992).

The objective of this study was to evaluate the developed algorithm for PM10 mapping by using Landsat visible bands. The corresponding PM10 data were measured simultaneously with the acquisition satellite scene for algorithm regression analysis. The algorithm was developed based on the atmospheric optical model. An algorithm was developed for PM10 determination. The independent variables are the visible wavelengths reflectance signals.
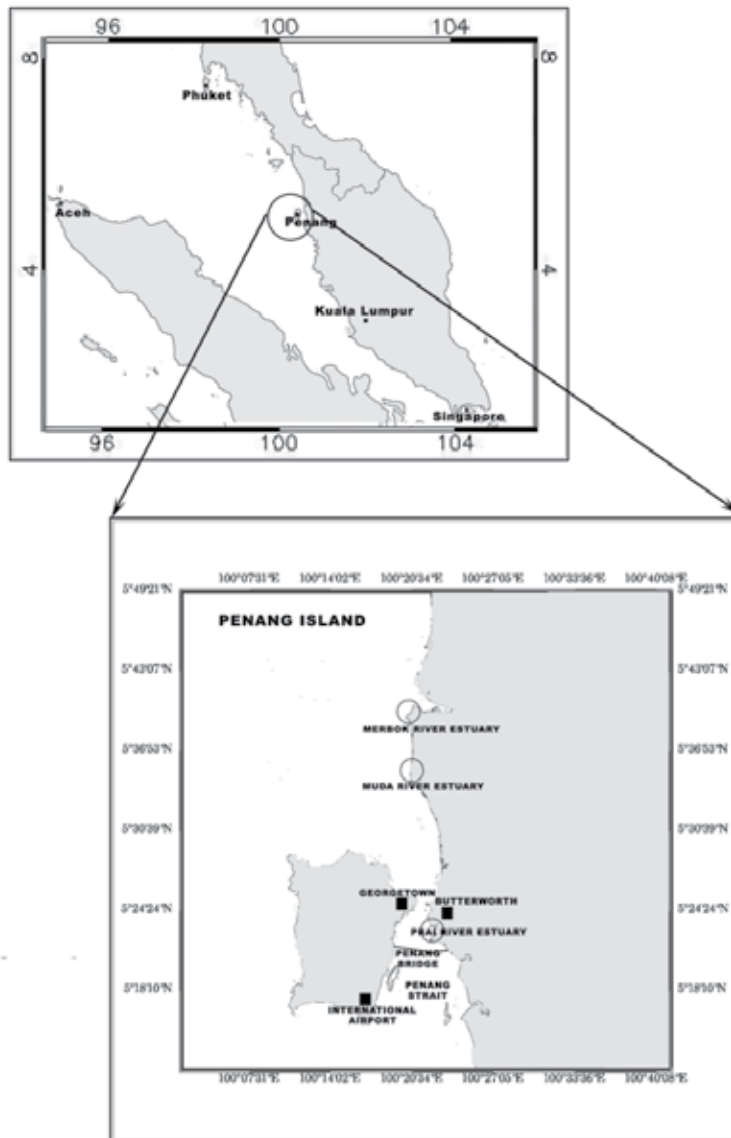
2. Study Area

Fig. 1. Study area.

The study area is the Penang Island, Malaysia, located within latitudes 5° 9′ N to 5° 33′ N and longitudes 100° 09′ E to 100° 30′ E (Figure 1). The map of the study area is shown in Figure 1. Penang Island is located in equatorial region and enjoys a warm equatorial weather the whole year. Therefore, it is impossible to get the 100 % cloud free satellite image over Penang Island. But, the satellite image chosen is less than 10 % of cloud coverage over the study area. Penang Island located on the northwest coast of Peninsular Malaysia.

Penang is one of the 13 states of the Malaysia and the second smallest state in Malaysia after Perlis. The state is geographically divided into two different entities - Penang Island (or "Pulau Pinang" in Malay Language) and a portion of mainland called "Seberang Perai" in Malay Language. Penang Island is an island of 293 square kilometres located in the Straits of Malacca and "Seberang Perai" is a narrow hinterland of 753 square kilometres (Penang-Wikipedia, 2009). The island and the mainland are linked by the 13.5 km long Penang Bridge and ferry.

Penang Island is predominantly hilly terrain, the highest point being Western Hill (part of Penang Hill) at 830 metres above sea level. The terrain consists of coastal plains, hills and mountains. The coastal plains are narrow, the most extensive of which is in the northeast which forms a triangular promontory where George Town, the state capital, is situated. The topography of "Seberang Perai" is mostly flat. Butterworth, the main town in "Seberang Perai", lies along the "Perai" River estuary and faces George Town at a distance of 3 km (2 miles) across the channel to the east (Penang-Wikipedia, 2009).

The Penang Island climate is tropical, and it is hot and humid throughout the year. with the average mean daily temperature of about 27oC and mean daily maximum and minimum temperature ranging between 31.4oC and 23.5oC respectively. However, the individual extremes are 35.7oC and 23.5oC respectively. The mean daily humidity varies between 60.9% and 96.8%. The average annual rainfall is about 267 cm and can be as high as 624 cm (Fauziah, et al, 2006).

3. Algorithm Model

The atmospheric reflectance due to molecule, R_r, is given by (Liu, et al., 1996)

$$R_r = \frac{\tau_r P_r(\Theta)}{4\mu_s \mu_v} \tag{1}$$

where
τ_r = Aerosol optical thickness (Molecule)
$P_r(\Theta)$ = Rayleigh scattering phase function
μ_v = Cosine of viewing angle
μ_s = Cosine of solar zenith angle
We assume that the atmospheric reflectance due to particle, R_a, is also linear with the τ_a [King, et al., (1999) and Fukushima, et al., (2000)]. This assumption is reasonable because other researchers also found the linear relationship between both aerosol and molecule scattering (Liu, et al., 1996).

$$R_a = \frac{\tau_a P_a(\Theta)}{4\mu_s \mu_v} \tag{2}$$

where
τ_a = Aerosol optical thickness (aerosol)
$P_a(\Theta)$ = Aerosol scattering phase function
Atmospheric reflectance is the sum of the particle reflectance and molecule reflectance, R_{atm}, (Vermote, et al., (1997).

$$R_{atm} = R_a + R_r \tag{3}$$

where
R_{atm}=atmospheric reflectance
R_p=particle reflectance
R_r=molecule reflectance

$$R_{atm} = \left[\frac{\tau_a P_a(\Theta)}{4\mu_s \mu_v} + K_1 + \frac{\tau_r P_r(\Theta)}{4\mu_s \mu_v} \right]$$

$$R_{atm} = \frac{1}{4\mu_s \mu_v} \left[\tau_a P_a(\Theta) + \tau_r P_r(\Theta) \right] \tag{4}$$

The optical depth is given by other researcher as in equation (5) (Camagni and Sandroni, 1983). From the equation, we rewrite the optical depth for particle and molecule as

$$\tau = \sigma \rho s \tag{5}$$

where
τ = optical depth
σ = absorption
s = finite path

$$\tau = \tau_a + \tau_r \qquad \text{(Camagni and Sandroni, 1983)}$$

$$\tau_r = \sigma_r \rho_r s \tag{6a}$$

$$\tau_p = \sigma_p \rho_p s \tag{6b}$$

Equations (6) are substituted into equation (4). The result was extended to a three bands algorithm as equation (8).
Form the equation; we found that PM10 was linearly related to the reflectance for band 1 and band 2. This algorithm was generated based on the linear relationship between τ and reflectance. Other Researcher also found that the PM10 was linearly related to the τ and the correlation coefficient for linear was better that exponential in their study (overall) (Retalis et al., 2003). This means that reflectance was linear with the PM10. In order to simplify the data processing, the air quality concentration was used in our analysis instead of using density, ρ, values.

$$R_{atm} = \frac{1}{4\mu_s \mu_v} \left[\sigma_a \rho_a s P_a(\Theta) + \sigma_r \rho_r s P_r(\Theta) \right]$$

$$R_{atm} = \frac{s}{4\mu_s \mu_v} \left[\sigma_a \rho_a P_a(\Theta) + \sigma_r \rho_r P_r(\Theta) \right]$$

$$R_{atm}(\lambda_1) = \frac{s}{4\mu_s\mu_v}\left[\sigma_a(\lambda_1)PP_a(\Theta,\lambda_1) + \sigma_r(\lambda_1)GP_r(\Theta,\lambda_1)\right]$$

$$R_{atm}(\lambda_2) = \frac{s}{4\mu_s\mu_v}\left[\sigma_a(\lambda_2)PP_a(\Theta,\lambda_2) + \sigma_r(\lambda_2)GP_r(\Theta,\lambda_2)\right]$$

$$P = a_0 R_{atm}(\lambda_1) + a_1 R_{atm}(\lambda_2) \tag{7}$$

The equation (8) was for two bands, so we rewrite the PM10 equation in three bands as

$$P = a_0 R_{atm}(\lambda_1) + a_1 R_{atm}(\lambda_2) + a_2 R_{atm}(\lambda_3) \tag{8}$$

Where

P = Particle concentration (PM10)
G = Molecule concentration
R_{atmi}= Atmospheric reflectance, i = 0, 1 and 3 are the number of the band
e_j= algorithm coefficient, j = 0, 1, 2, … (empirically determined).

4. Data Analysis and Results

Remote sensing satellite detectors exhibit linear response to incoming radiance, whether from the Earth's surface radiance or internal calibration sources. This response is quantized into 8-bit values that represent brightness values commonly called Digital Numbers (DN). To convert the calibrated digital numbers to at-aperture radiance, rescaling gains and biases are created from the known dynamic range limits of the instrument.

$$\text{Radiance, } L(\lambda) = \text{Bias}(\lambda) + [\text{Gain}(\lambda) \times DN(\lambda)] \tag{9}$$

where
λ = band number.
L is the radiance expressed in $Wm^{-2} sr^{-1}\mu m^{-1}$.
The spectral radiance, as calculated above, can be converted to at sensor reflectance values.

$$\rho^* = \frac{\pi L(\lambda)d^2}{E_0(\lambda)\cos\theta} \tag{10}$$

Where
ρ^* = Sensor Reflectance values
$L(\lambda)$ = Apparent At-Sensor Radiance ($Wm^{-2} sr^{-1}\mu m^{-1}$)
d   = Earth-Sun distance in astronomical units
             = {1.0-0.016729cos [0.9856(D-4)]} where (D = day of the year)
$E°(\lambda)$ = mean solar exoatmospheric irradiance ($Wm^{-2} sr^{-1}\mu m^{-1}$)
θ = solar Zenith angle (degrees)

The retrieval of surface reflectance is important to obtain the atmospheric reflectance in remotely sensed data and later used for algorithm calibration. In this study, we retrieve the surface reflectance using the relationship between the two visible bands (blue and red) and the mid infrared data at 2.1 μm. We use the assumption that the mid infrared band data is not significantly affected by atmospheric haze. An algorithm was developed based on the aerosol properties to correlate the atmospheric reflectance and PM10.

The surface reflectance can be obtained from mid-infrared band because the surface reflectances at various bands across the solar spectrum are correlated to each other to some extend. The surface reflectances of dark targets in the blue and red bands were estimated using the measurements in the mid-infrared band (Quaidrari and Vermote, 1999). Over a simple black target, the observed atmospheric reflectance is the sum of reflectance of aerosols and Rayleigh contributions (Equation 9). This simplification, however, is not valid at short wavelengths (less than 0.45 pm) or large sun and view zenith angles (Vermote and Roger, 1996). In this study, a simple form of the equation was used in this study (Equation 11). This equation also used by other research in their study (Popp, 2004).

$$Rs - TRr \qquad = Ratm \qquad\qquad (11)$$
$$Rs - Rr \qquad = Ratm \qquad\qquad (12)$$

where:
Rs   = reflectance recorded by satellite sensor
Rr   = reflectance from surface references
Ratm   = reflectance from atmospheric components (aerosols and molecules)
T   = transmittance

The surface reflectance in mid-infrared band is related to those in the visible bands. The surface reflectances were measured using a handheld spectroradiometer in the wavelength range of visible wavelengths (red and blue bands). The surface reflectances of dark targets in the visible bands are as follows:

$$\rho\,(TM1) = \rho\,(TM7)/3.846$$
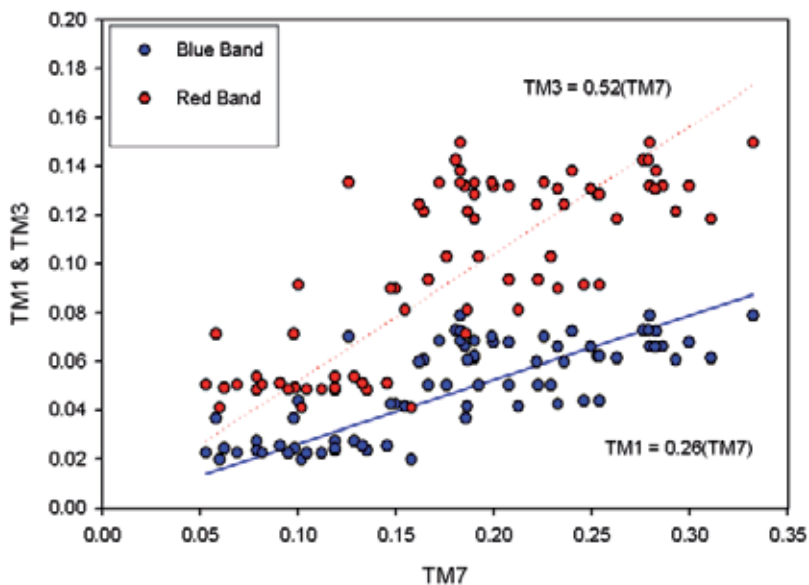$$\rho\,(TM3) = \rho\,(TM7)/1.923 \qquad\qquad (13)$$

Fig. 2. The relationship between band 1 (TM1) and band 3 (TM3) with band 7 (TM7) of Landsat.
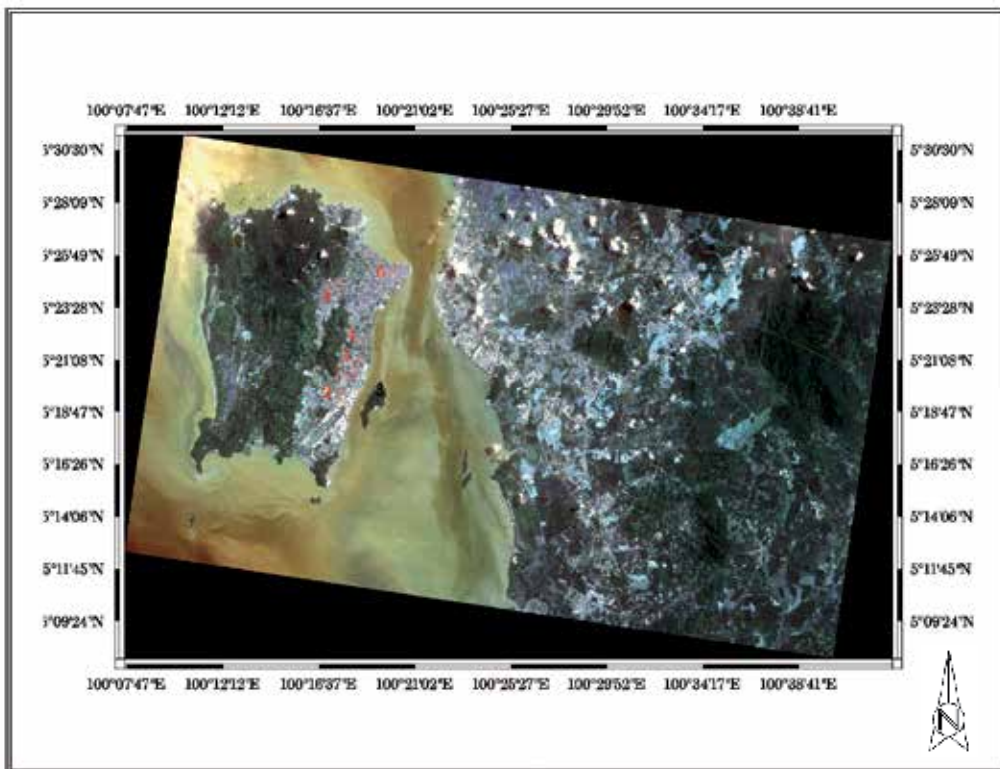

Fig. 3. Raw Landsat TM satellite image of 30/7/2000

Landsat satellite data set was selected corresponding to the ground truth measurements of the pollution levels. The PCI Geomatica version 10.1 image processing software was used in all the analyses. The Landsat satellite images were acquired on 30th July 2000 (Figure 3), 15th February 2001 (Figure 4), 17th January 2002 (Figure 5), 6th March 2002 (Figure 6), 5 February 2003 (Figure 7), 19th March 2004 (Figure 8) and 2nd February 2005 (Figure 9).
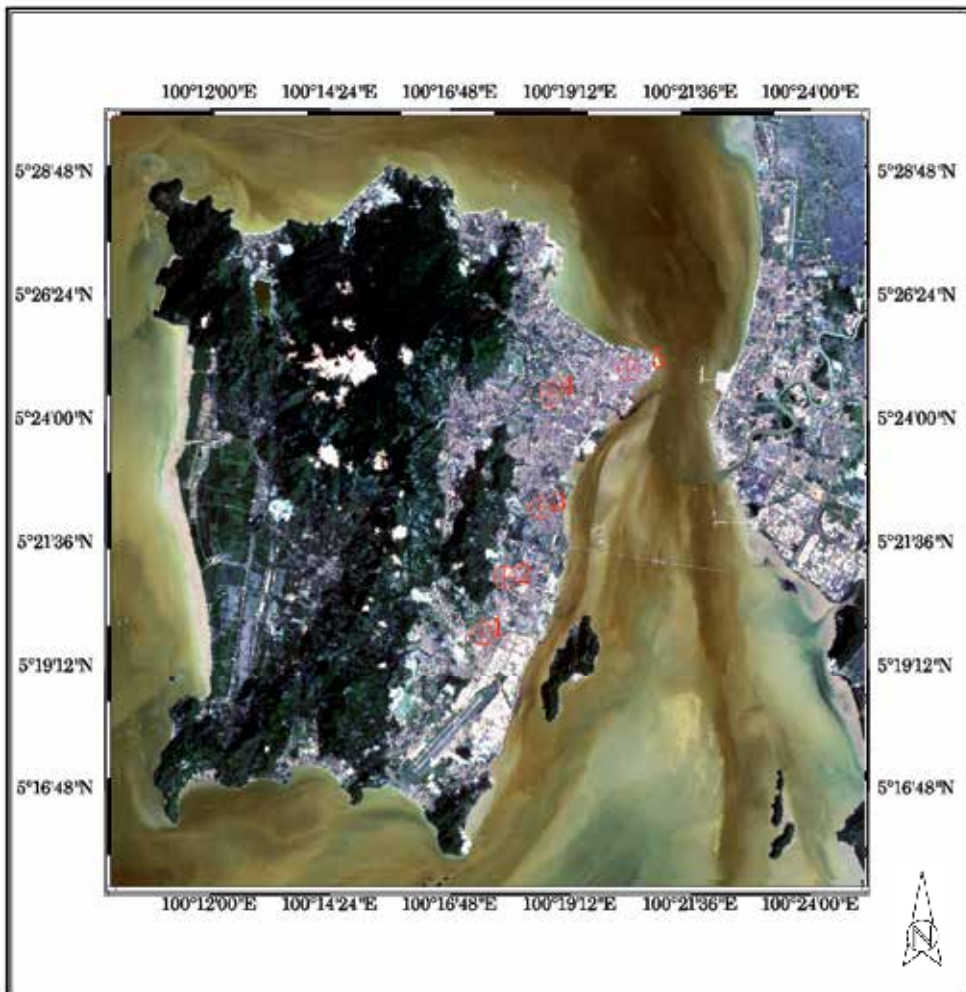

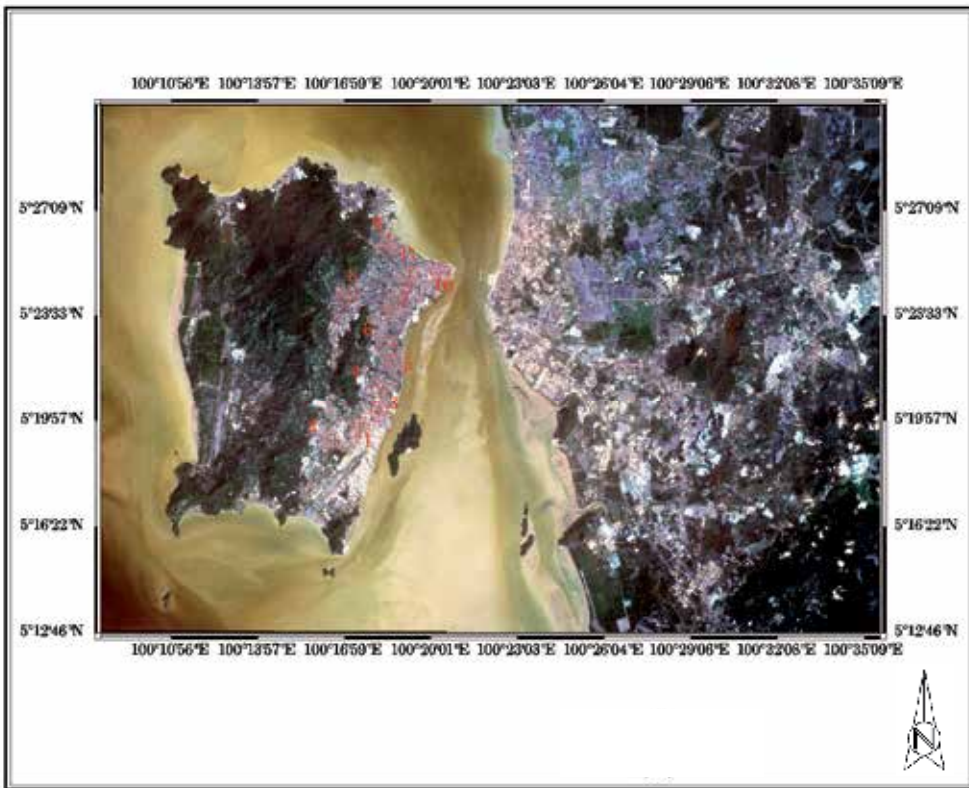Fig. 4. Raw Landsat TM satellite image of 15/2/2001
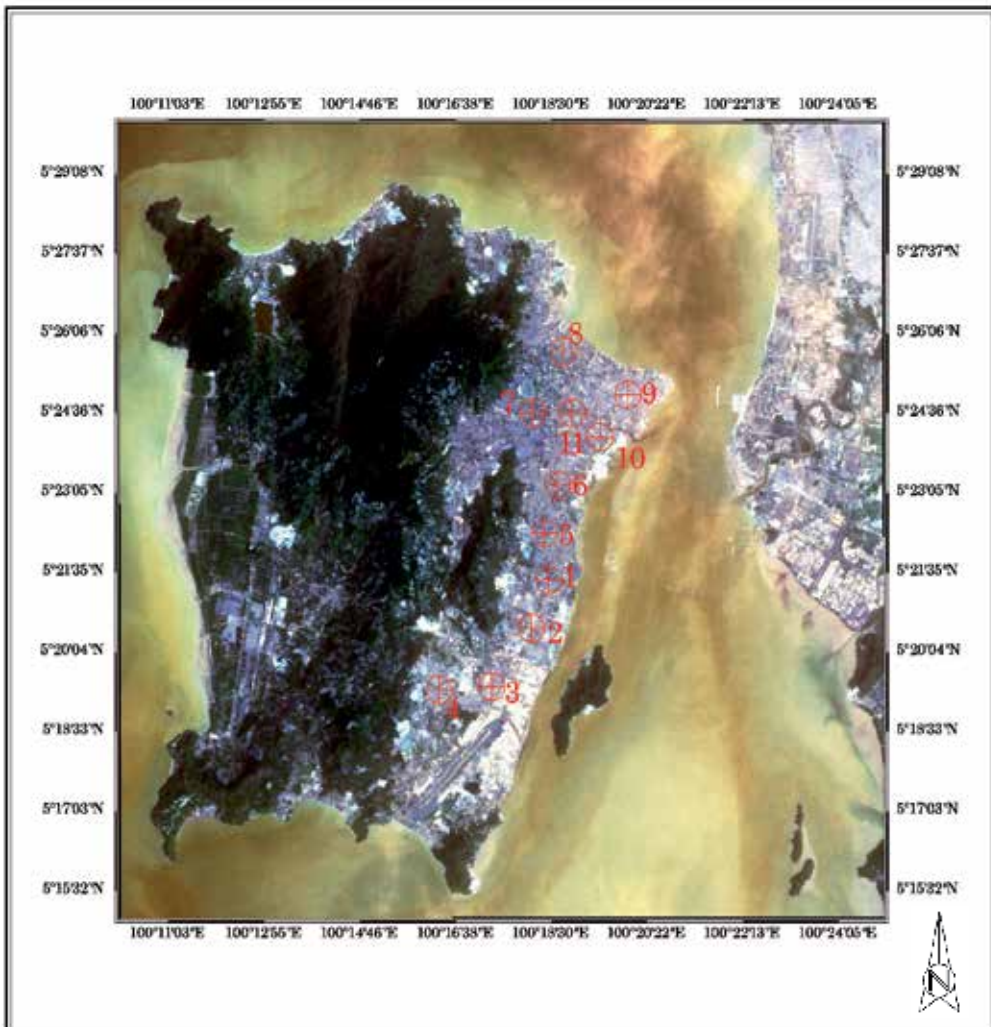
Fig. 5. Raw Landsat TM satellite image of 17/1/2002
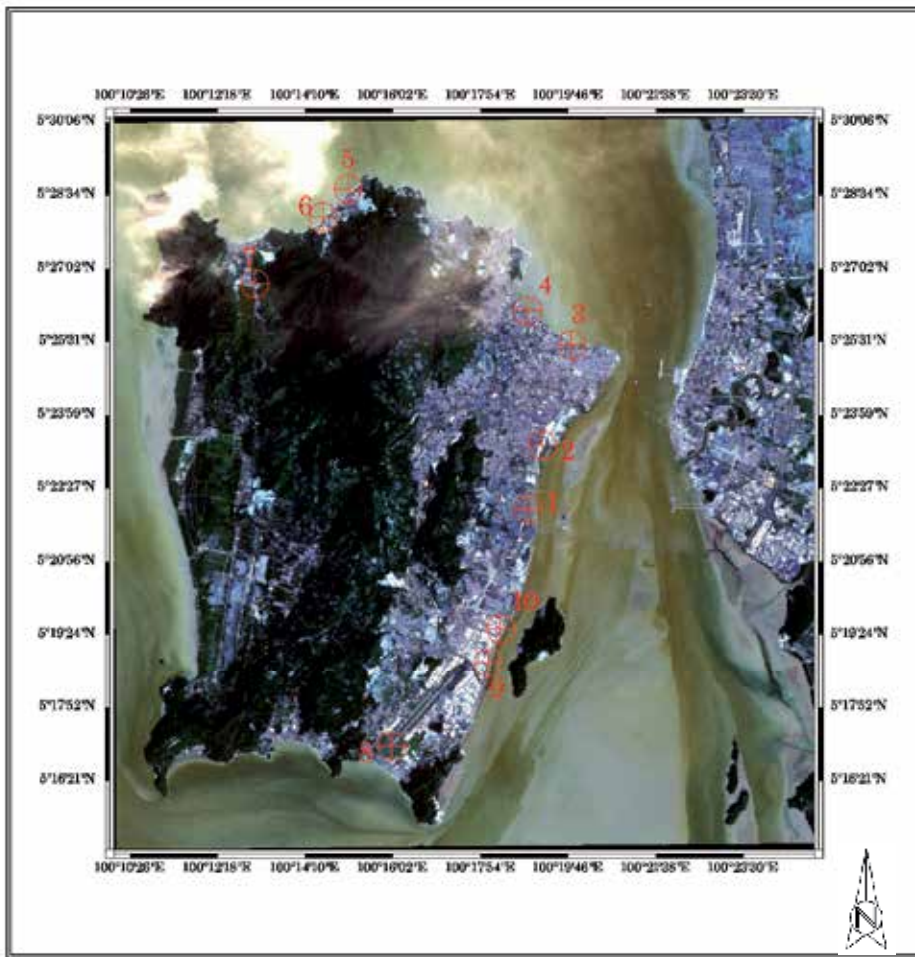
Fig. 6. Raw Landsat TM satellite image of 6/3/2002

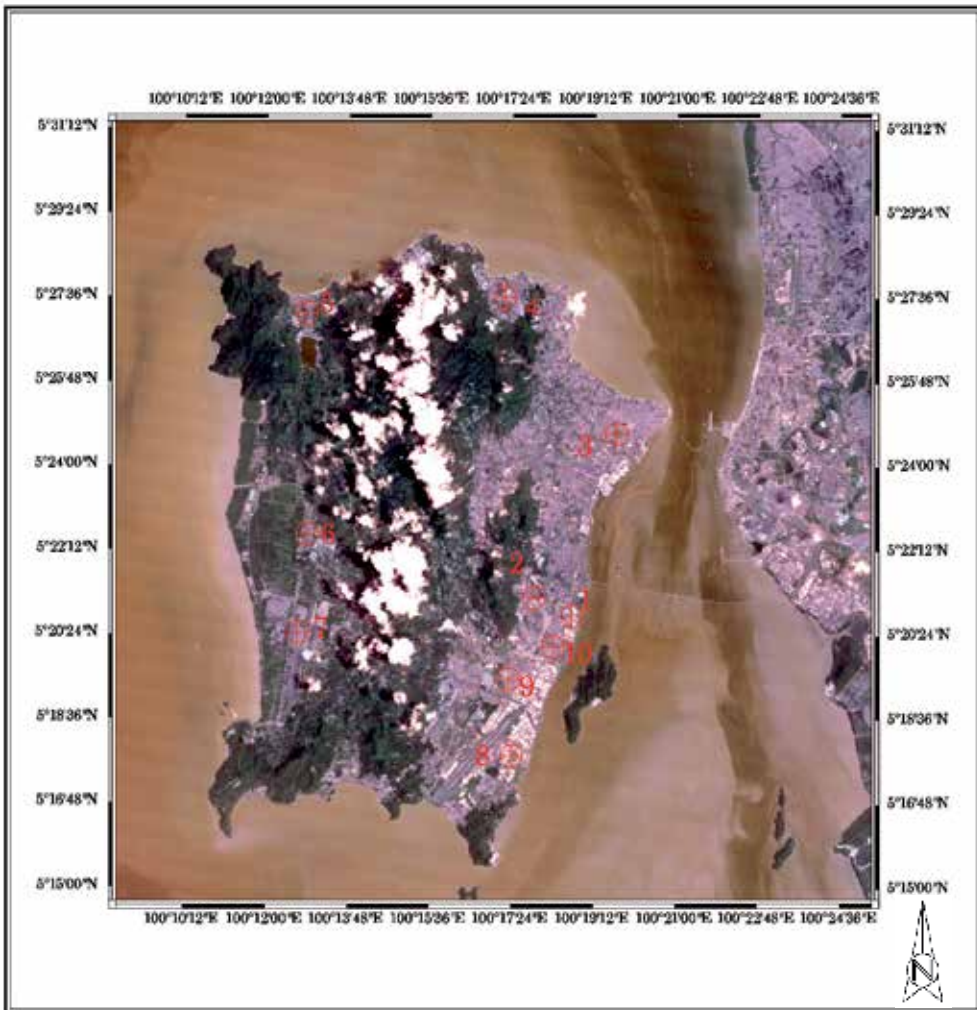Fig. 7. Raw Landsat TM satellite image of 5/2/2003

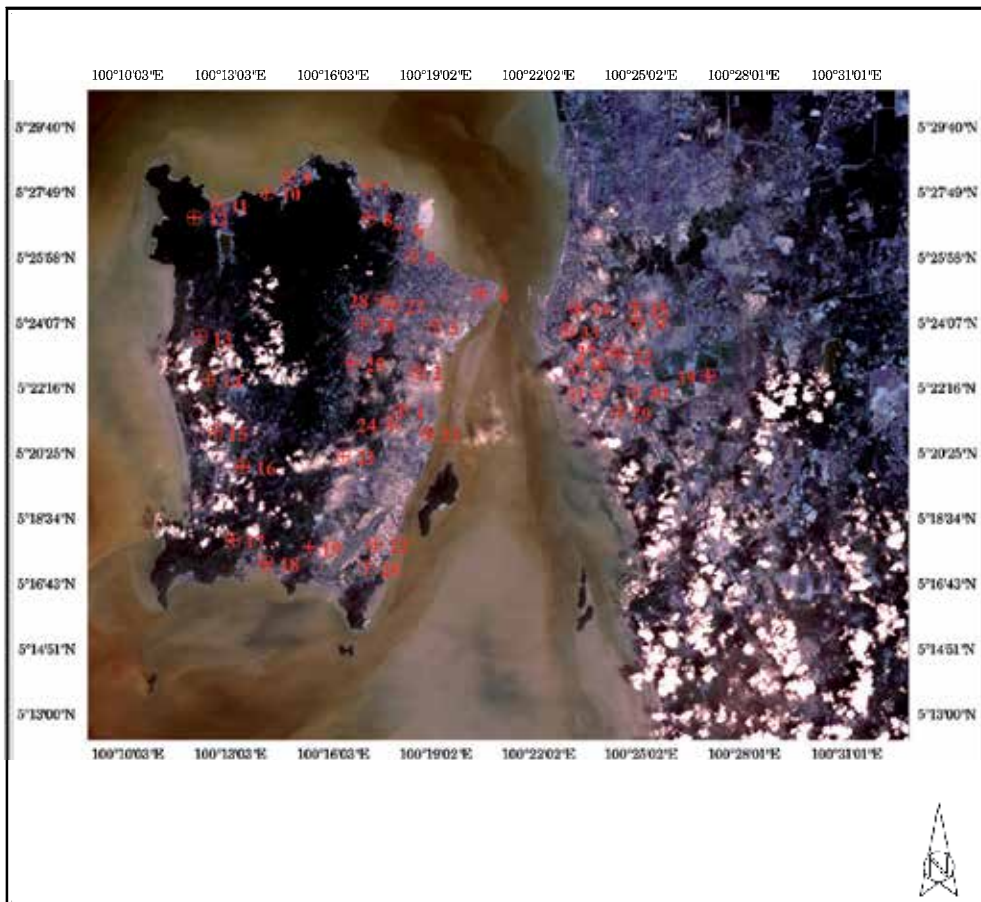Fig. 8. Raw Landsat TM satellite image of 19/3/2004

Fig. 9. Raw Landsat TM satellite image of 2/2/2005

Raw digital satellite images usually contain geometric distortion and cannot be used directly as a map. Some sources of distortion are variation in the altitude, attitude and velocity of the sensor. Other sources are panoramic distortion, earth curvature, atmospheric refraction and relief displacement. So, to correct the images, we have to do geometric correction. Image rectification was performed by using a second order polynomial transformation equation. The images were geometrically corrected by using a nearest neighbour resampling technique. Sample locations were then identified on these geocoded images. Regression technique was employed to calibrate the algorithm using the satellite multispectral signals.

PM10 measurements were collected simultaneously with the image acquisition using a DustTrak Aerosol Monitor 8520. The digital numbers of the corresponding in situ data were converted into irradiance and then reflectance. Our approach to retrieve the atmospheric component from satellite observation is by measuring the surface component properties. The reflectance measured from the satellite [reflectance at the top of atmospheric, ρ(TOA)] was subtracted by the amount given by the surface reflectance to obtain the atmospheric

reflectance. And then the atmospheric reflectance was related to the PM10 using the regression algorithm analysis. For each visible band, the dark target surface reflectance was estimated from that of the mid-infrared band. The atmospheric reflectance values were extracted from the satellite observation reflectance values subtracted by the amount given by the surface reflectance. The atmospheric reflectance were determined for each band using different window sizes, such as, 1 by 1, 3 by 3, 5 by 5, 7 by 7, 9 by 9 and 11 by 11. In this study, the atmospheric reflectance values extracted using the window size of 3 by 3 was used due to the higher correlation coefficient (R) with the ground-truth data.

The atmospheric reflectance values for the visible bands of TM1 and TM3 were extracted corresponding to the locations of in situ PM10 data. The relationship between the reflectance and the corresponding air quality data was determined using regression analysis. A new algorithm was developed for detecting air pollution from the digital images chosen based on the highest correlation coefficient, R and lowest root mean square error, RMS for PM10. The algorithm was used to correlate atmospheric reflectance and the PM10 values. The proposed algorithm produced high correlation coefficient (R) and low root-mean-square error (RMS) between the measured and estimated PM10 values. Finally, PM10 maps were generated using the proposed algorithm. This study indicates the potential of Landsat for PM10 mapping.

The data points were then regressed to obtain all the coefficients of equation (8). Then the calibrated algorithm was used to estimate the PM10 concentrated values for each image. The proposed model produced the correlation coefficient of 0.83 and root-mean-square error 18 $\mu g/m^3$. The PM10 maps were generated using the proposed calibrated algorithm. The generated PM10 map was colour-coded for visual interpretation [Figures 10 - 16]. Generally, the concentrations above industrial and urban areas were higher compared to other areas.

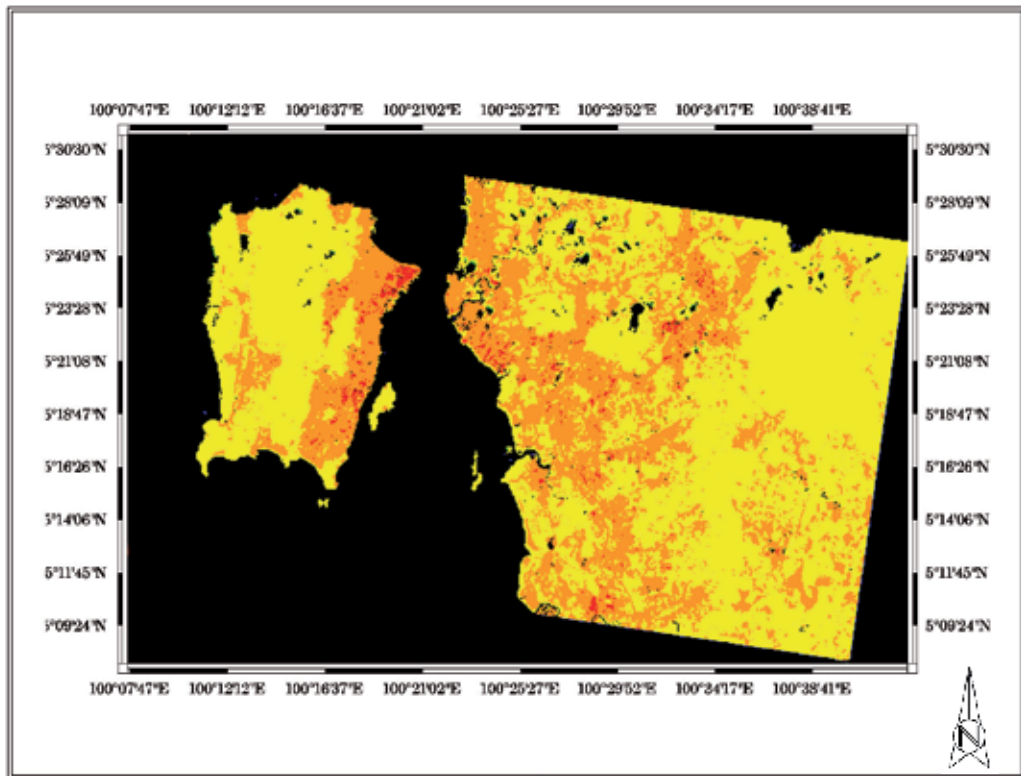| Algoritma	R							
	S1	S2	S3	S4	S5	S6	S7	S8
$PM10=a_0+a_1B_1+a_2B_1^2$	0.8670	0.8828	0.4893	0.6630	0.8596	0.8406	0.6256	0.6899
$PM10=a_0+a_1B_3+a_2B_3^2$	0.8773	0.9434	0.8415	0.7083	0.8884	0.8064	0.5965	0.8150
$PM10=a_0+a_1lnB_1+a_2(lnB_1)^2$	0.9196	0.8944	0.4860	0.6293	0.8698	0.8392	0.6264	0.7030
$PM10=a_0+a_1lnB_3+a_2(lnB_3)^2$	0.8897	0.9416	0.8418	0.7108	0.8954	0.8039	0.6156	0.8250
$PM10=a_0+a_1(B_1/B_3)+a_2(B_1/B_3)^2$	0.5655	0.8078	0.2038	0.4039	0.7896	0.1346	0.4703	0.6001
$PM10=a_0+a_1ln(B_1/B_3)+a_2ln(B_1/B_3)^2$	0.6494	0.8052	0.1676	0.3431	0.7955	0.1868	0.4709	0.6027
$PM10=a_0+a_1(B_1-B_3)+a_2(B_1-B_3)^2$	0.2663	0.1737	0.6507	0.3281	0.6903	0.5525	0.3051	0.6513
$PM10=a_1B_1+a_2B_3$ (Dicadangkan)	0.9250	0.9520	0.8834	0.8890	0.9042	0.8460	0.8043	0.8599

*B_1 and B_3 are the atmospheric reflectance values for red, green and blue band respectively.
Table 1 Regression results (R) using different forms of algorithms for PM10

Algoritma	RMS ($\mu g/m^3$)							
	S1	S2	S3	S4	S5	S6	S7	S8
$PM10=a_0+a_1B_1+a_2B_1^2$	10.6062	5.7532	13.5174	12.3583	8.7407	14.0650	14.8182	14.5665
$PM10=a_0+a_1B_3+a_2B_3^2$	10.2125	4.0631	8.4278	11.6537	7.8532	15.3573	15.2449	11.6584
$PM10=a_0+a_1lnB_1+a_2(lnB_1)^2$	8.3605	5.4773	13.5726	12.8299	8.4424	14.1245	15.0096	14.7498
$PM10=a_0+a_1lnB_3+a_2(lnB_3)^2$	9.7171	4.1251	8.4115	11.6123	7.6172	15.4450	15.1740	10.6088
$PM10=a_0+a_1(B_1/B_3)+a_2(B_1/B_3)^2$	17.5531	7.2187	16.7673	15.1016	10.4991	25.7333	16.9929	16.5911
$PM10=a_0+a_1ln(B_1/B_3)+a_2ln(B_1/B_3)^2$	16.1839	7.2633	16.9753	15.5062	10.3644	25.5122	16.9871	16.5500
$PM10=a_0+a_1(B_1-B_3) +a_2(B_1-B_3)^2$	20.5137	12.0613	11.0887	15.5941	12.3781	21.6464	18.3374	15.7390
$PM10=a_1B_1+a_2B_3$ (Dicadangkan)	9.9045	5.3033	9.2470	8.0795	7.3062	13.8448	11.0414	10.5886

*B_1 and B_3 are the atmospheric reflectance values for red, green and blue band respectively.
Table 2 Regression results (RMS) using different forms of algorithms for PM10

Legend

■ (blue)	<40 µg/m³	■ (orange)	120-160 µg/m³
■ (green)	40-80 µg/m³	■ (red)	>160 µg/m³
■ (yellow)	80-120 µg/m³	■ (black)	Air dan Kawasan Awan

Fig. 10. Map of PM10 around Penang Island, Malaysia-30/7/2000

Legend

🟦	<40 μg/m³	🟧	120-160 μg/m³
🟩	40-80 μg/m³	🟥	>160 μg/m³
🟨	80-120 μg/m³	⬛	Air dan Kawasan Awan

Fig. 11. Map of PM10 around Penang Island, Malaysia-15/2/2001

Fig. 12. Map of PM10 around Penang Island, Malaysia-17/1/2002

Legend

▮	<40 µg/m³	▮	120-160 µg/m³
▮	40-80 µg/m³	▮	>160 µg/m³
▮	80-120 µg/m³	▮	Air dan Kawasan Awan
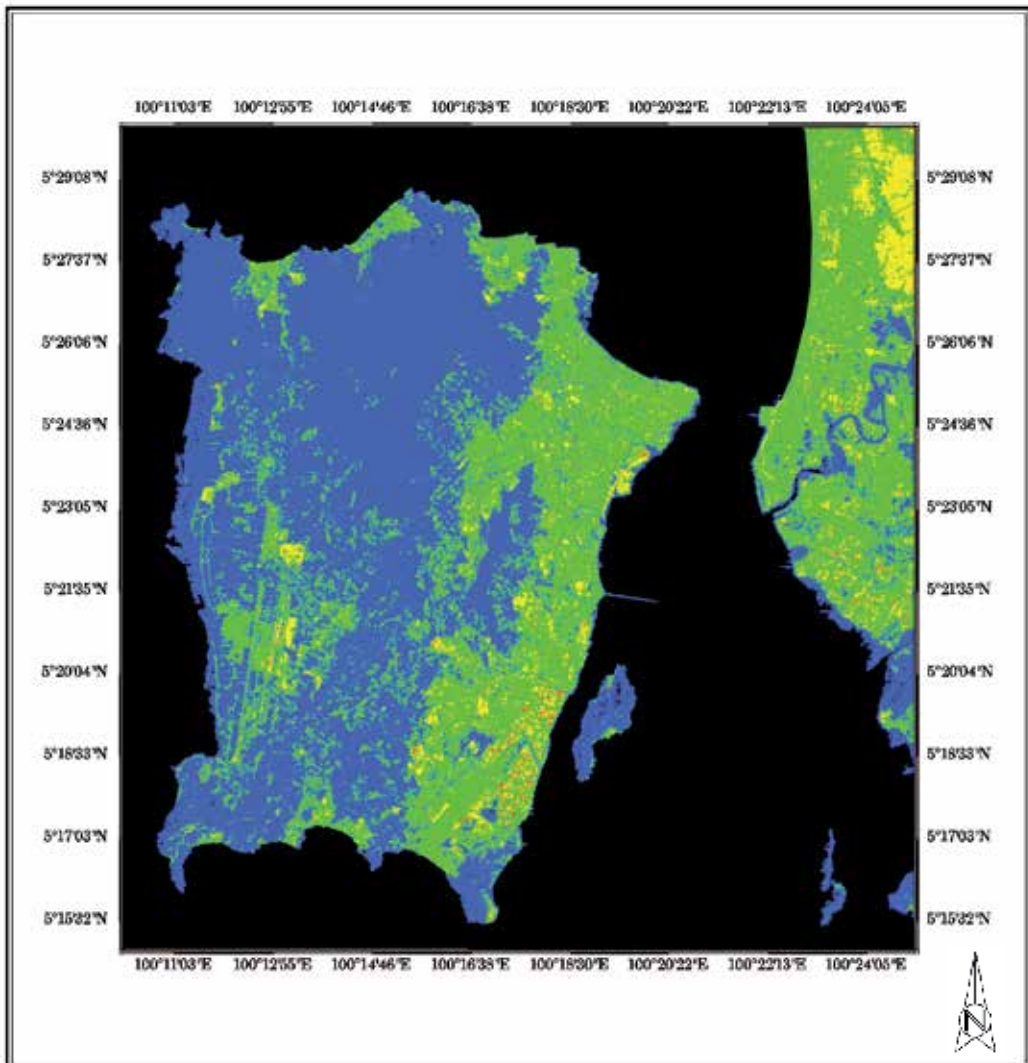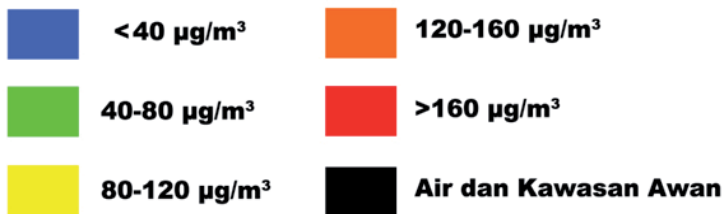
Fig. 13. Map of PM10 around Penang Island, Malaysia-6/3/2002

Legend

🟦	<40 µg/m³	🟧	120-160 µg/m³
🟩	40-80 µg/m³	🟥	>160 µg/m³
🟨	80-120 µg/m³	⬛	Air dan Kawasan Awan

Fig. 14. Map of PM10 around Penang Island, Malaysia-5/2/2003

Fig. 15. Map of PM10 around Penang Island, Malaysia-19/3/2004

Legend

<40 µg/m³	120-160 µg/m³
40-80 µg/m³	>160 µg/m³
80-120 µg/m³	Air dan Kawasan Awan
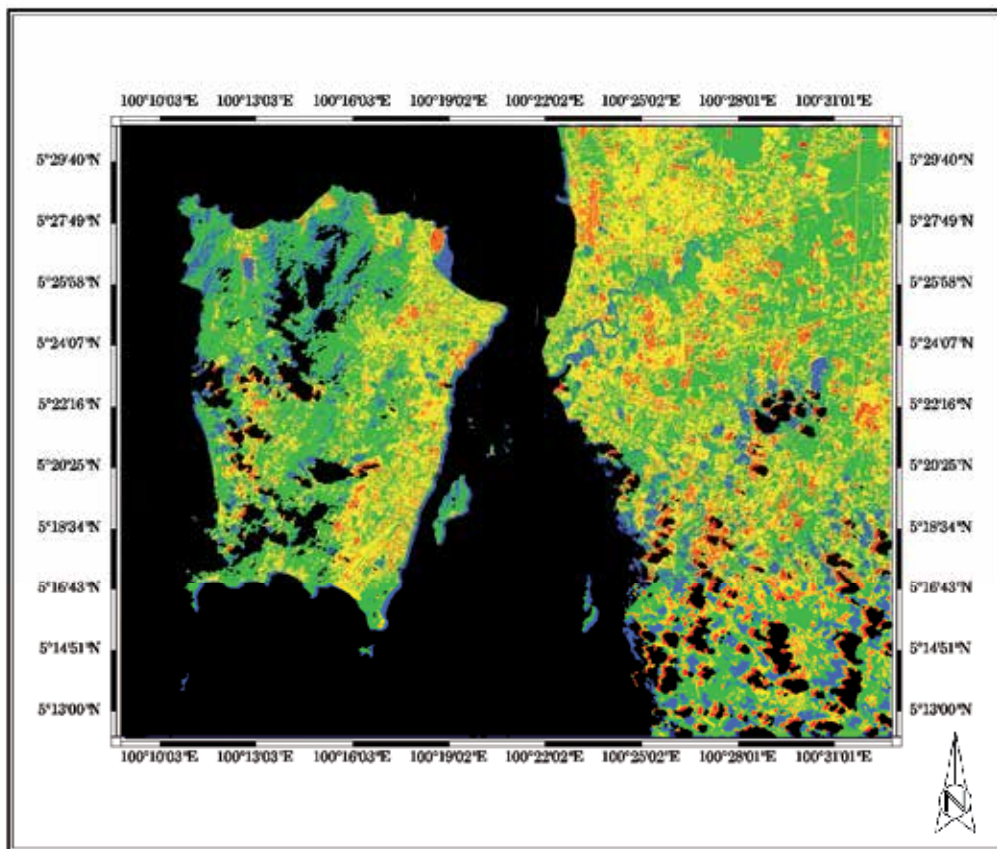
Fig. 16. Map of PM10 around Penang Island, Malaysia-2/2/2005

5. Conclusion

Image acquired from the satellite Landsat TM was successfully used for PM10 mapping over Penang Island, Malaysia. The developed algorithm produced a high correlation between the measured and estimated PM10 concentration. Further study will be carried out to verify the results. A multi regression algorithm will be developed and used in the

analysis. This study had shown the feasibility of using Landsat TM imagery for air quality study.

6. Acknowledgements

7. References

Asmala Ahmad and Mazlan Hashim, (2002). Determination of haze using NOAA-14 AVHRR satellite data, [Online] available:
http://www.gisdevelopment.net/aars/acrs/2002/czm/050.pdf

Badarinath, K. V. S., Latha, K. M., Gupta, P. K., Christopher S. A. and Zhang, J., Biomass burning aerosols characteristics and radiative forcing-a case study from eastern Ghats, India, [Online] available:
http://nsstc.uah.edu/~sundar/papers/conf/iasta_2002.pdf.

Camagni. P. & Sandroni, S. (1983). Optical Remote sensing of air pollution, Joint Research Centre, Ispra, Italy, Elsevier Science Publishing Company Inc

Dekker, A. G., Vos, R. J. and Peters, S. W. M. (2002). Analytical algorithms for lakes water TSM estimation for retrospective analyses of TM dan SPOT sensor data. International Journal of Remote Sensing, 23(1), 15−35.

Doxaran, D., Froidefond, J. M., Lavender, S. and Castaing, P. (2002). Spectral signature of highly turbid waters application with SPOT data to quantify suspended particulate matter concentrations. Remote Sensing of Environment, 81, 149−161.

Fauziah, Ahmad; Ahmad Shukri Yahaya & Mohd Ahmadullah Farooqi. (2006), Characterization and Geotechnical Properties of Penang Residual Soils with Emphasis on Landslides, American Journal of Environmental Sciences 2 (4): 121-128

Fukushima, H.; Toratani, M.; Yamamiya, S. & Mitomi, Y. (2000). Atmospheric correction algorithm for ADEOS/OCTS acean color data: performance comparison based on ship and buoy measurements. Adv. Space Res, Vol. 25, No. 5, 1015-1024

Liu, C. H.; Chen, A. J. ^ Liu, G. R. (1996). An image-based retrieval algorithm of aerosol characteristics and surface reflectance for satellite images, International Journal Of Remote Sensing, 17 (17), 3477-3500

King, M. D.; Kaufman, Y. J.; Tanre, D. & Nakajima, T. (1999). Remote sensing of tropospheric aerosold form space: past, present and future, Bulletin of the American Meteorological society, 2229-2259

Penang-Wikipedia, (2009). Penang, Available Online:
    http://en.wikipedia.org/wiki/Penang.

Penner, J. E.; Zhang, S. Y.; Chin, M.; Chuang, C. C.; Feichter, J.; Feng, Y.; Geogdzhayev, I. V.;
    Ginoux, P.; Herzog, M.; Higurashi, A.; Koch, D.; Land, C.; Lohmann, U.;
    Mishchenko, M.; Nakajima, T.; Pitari, G.; Soden, B.; Tegen, I. & Stowe, L. (2002). A
    Comparison of Model And Satellite-Derived Optical Depth And Reflectivity.
    [Online} available: http://data.engin.umich.edu/Penner/paper3.pdf

Popp, C.; Schläpfer, D.; Bojinski, S.; Schaepman, M. & Itten, K. I. (2004). Evaluation of
    Aerosol Mapping Methods using AVIRIS Imagery. R. Green (Editor), 13th Annual
    JPL Airborne Earth Science Workshop. JPL Publications, March 2004, Pasadena,
    CA, 10

Quaidrari, H. dan Vermote, E. F. (1999). Operational atmospheric correction of Landsat TM
    data, Remote Sensing Environment, 70: 4-15.

Retalis, A.; Sifakis, N.; Grosso, N.; Paronis, D. & Sarigiannis, D. (2003). Aerosol optical
    thickness retrieval from AVHRR images over the Athens urban area, [Online]
    available: http://sat2.space.noa.gr/rsensing/documents/IGARSS2003_AVHRR_
    Retalisetal_web.pdf.

Sifakis, N. & Deschamps, P.Y. (1992). Mapping of air pollution using SPOT satellite data,
    Photogrammetric Engineering & Remote Sensing, 58(10), 1433 – 1437

Tassan, S. (1997). A numerical model for the detection of sediment concentration in stratified
    river plumes using Thematic Mapper data. International Journal of Remote
    Sensing, 18(12), 2699−2705.

UNEP Assessment Report, Part 1: The South Asian Haze: Air Pollution, Ozone And
    Aerosols, [Online] available:
    http://www.rrcap.unep.org/issues/air/impactstudy/Part%20I.pdf.

Ung, A., Weber, C., Perron, G., Hirsch, J., Kleinpeter, J., Wald, L. and Ranchin, T., 2001a. Air
    Pollution Mapping Over A City – Virtual Stations And Morphological Indicators.
    Proceedings of 10th International Symposium "Transport and Air Pollution"
    September 17 - 19, 2001 – Boulder, Colorado USA. [Online] available: http://www-
    cenerg.cma.fr/Public/themes_de_recherche/teledetection/title_tele_air/title_tele_
    air_pub/air_pollution_mappin4043.

Ung, A., Wald, L., Ranchin, T., Weber, C., Hirsch, J., Perron, G. and Kleinpeter, J., 2001b. ,
    Satellite data for Air Pollution Mapping Over A City- Virtual Stations, Proceeding
    of the 21th EARSeL Symposium, Observing Our Environment From Space: New
    Solutions For A New Millenium, Paris, France, 14 – 16 May 2001, Gerard Begni
    Editor, A., A., Balkema, Lisse, Abingdon, Exton (PA), Tokyo, pp. 147 – 151, [Online]
    available: http://www-cenerg.cma.fr/Public/themes_de_recherche/teledetection/
    title_tele_air/title_tele_air_pub/satellite_data_for_t

Vermote, E. & Roger, J. C. (1996). Advances in the use of NOAA AVHRR data for land
    application: Radiative transfer modeling for calibration and atmospheric correction,
    Kluwer Academic Publishers, Dordrecht/Boston/London, 49-72

Vermote, E.; Tanre, D.; Deuze, J. L.; Herman, M. & Morcrette, J. J. (1997). 6S user guide
    Version 2, Second Simulation of the satellite signal in the solar spectrum (6S),
    [Online] available:
    http://www.geog.tamu.edu/klein/geog661/handouts/6s/6smanv2.0_P1.pdf

Weber, C., Hirsch, J., Perron, G., Kleinpeter, J., Ranchin, T., Ung, A. and Wald, L. 2001. Urban Morphology, Remote Sensing and Pollutants Distribution: An Application To The City of Strasbourg, France. International Union of Air Pollution Prevention and Environmental Protection Associations (IUAPPA) Symposium and Korean Society for Atmospheric Environment (KOSAE) Symposium, 12th World Clean Air & Environment Congress, Greening the New Millennium, 26 – 31 August 2001, Seoul, Korea. [Online] available: http://www-cenerg.cma.fr/Public/themes_de_recherche/ teledetection/title_tele_air/title_tele_air_pub/paper_urban_morpho.

Wang, J. and Christopher, S. A., (2003) Intercomparison between satellite-derived aerosol optical thickness and PM2.5 mass: Implications for air quality studies, Geophysics Research Letters, 30 (21).

A review of general and local thermal comfort models for controlling indoor ambiences

José Antonio Orosa García

University of A Coruña. Department of Energy and M.P.
Spain

1. Introduction

General thermal comfort is defined by certain thermal conditions that, on average, affect the environment in order to ensure comfort from its broader view. This expression is related with the general condition of an environment, but in each zone we can find parameters out of the mean value. As a result, it is necessary to study the localized effect of each thermal comfort variables over the human thermoregulation, to obtain an adequate thermal comfort. However, it is possible to improve indoor ambiences through relevant building structural modifications, particularly thermal inertia, air conditioning facilities and human habits.

In this chapter, a research about the principal works on general and local thermal comfort, to define the better models employed as control algorithm in Heating Ventilation and Air Conditioning Systems (HVAC) to improve energy saving, material conservancy and work risk prevention, was conducted.

2. Earlier Research Works

When we try to comprehend general thermal comfort, it is common to analyse Fanger's PMV model; this model is based on thermoregulation and heat balance theories. According to these theories, the human body employs physiological processes in order to maintain a balance between the heat produced by metabolism and heat lost from the body.

In 1967, Fanger investigated the body's physiological processes, when it is close to neutral to define the actual comfort equation. Investigations (Fanger, 2003) began with the determination that the only physiological processes influencing heat balance were sweat rate and mean skin temperature as a function of activity level. Later, he used data from the study by McNall et al. (1967), to derive a linear relationship between activity levels and sweat rate, and conducted a study to derive a linear relationship between activity level and mean skin temperature. These two linear relationships were substituted into heat balance equations to create a comfort equation and describe all combinations of the six PMV input variables that result in a neutral thermal sensation.

Once an initial comfort equation was obtained, it was validated against studies by Nevins et al. (1966) and McNall et al. (1967), in which participants rated their thermal sensation in response to specified thermal environments. To consider situations where subjects do not

feel neutral, the comfort equation was corrected by combining data from Nevins et al. (1966), McNall et al. (1967) and his own studies (Fanger, 1970). The resulting equation described thermal comfort as the imbalance between the actual heat flow from the body in a given thermal environment and the heat flow required for optimum comfort (i.e. neutral) for a given activity. This expanded equation related thermal conditions to the seven-point ASHRAE thermal sensation scale, the PMV index. Fanger (1970) also developed a related index, the Predicted Percentage Dissatisfied (PPD). This index is calculated from PMV and predicts the percentage of people who are likely to be dissatisfied with a given thermal environment.

Thermal comfort standards use the PMV model to recommend acceptable thermal comfort conditions. The recommendations made by ASHRAE 2004, ISO 7730:2005 and ISO 7726:2002 are seen in Table 1. These thermal conditions should ensure that at least 90% of occupants feel thermally satisfied.

	Operative	Acceptable
Winter	22ºC	20–23ºC
Summer	24.5ºC	23–26ºC

Table 1. ASHRAE standard recommendations.

When the general thermal comfort condition was defined by Scientifics, it developed research works to define the local comfort conditions related with air velocity, temperature and asymmetric radiation. In 1956, when Kerka and Humphreys began their studies on indoor environment, the first serious studies on local thermal comfort background began. However, man has had a special interest in controlling indoor environments. In these studies, they init to use panels to assess the intensity of smell of three different fumes and smoke to snuff. The main findings reveal that the intensity of the odour goes down slightly with a slight increase in atmospheric humidity. Another finding indicates that, in the presence of smoke snuff, the intensity of the odour goes down with increasing temperature for a constant partial vapour pressure.

In 1974, Cain explored the adaptation of man to four air components and to different concentrations over a period of time. The main conclusions revealed that there was no significant difference between pollutants. In 1979, Woods confirmed the results of Kerka and concluded that smell perception of odour intensity is linearly correlated with the enthalpy of air. In 1983, Cain et al. studied the impact of temperature and humidity on the perception of air quality. They concluded that the combination of high temperatures (more than 25.5ºC) and relative humidity (more than 70%) exacerbate odour problems. Six years later, in 1989, Berglund and Cain discussed the adaptation of pollutants over time for different humidities. This study concluded that air acceptability, for different ranges of humidity at 24ºC, is stable during the first hour. The subjective assessment of air quality was mainly influenced by temperature conditions and relative humidity and, second, by the polluted air. The linear effect of acceptance is more influenced by temperature than by relative humidity. In 1992, Gunnarsen et al. studied the possibility of adapting the perception of odour intensity; this adaptation was confirmed after a certain time interval. In 1996, Knudsen et al. carried out research into the air before accepting a full body and facial exposure. The problem with this test is that the process is carried out at a constant temperature equal to 22ºC and the relative humidity is not controlled.

In 1998, Fang and co-workers carried out an initial experiment in a chamber, with clean air heated to 18ºC and 30% relative humidity (see Fig. 1). In this experiment, 40 subjects without specific training were subjected to the conditions in these chambers (Fig. 1). As a precaution, they were warned not to use strong perfumes before the experiment. The subjects underwent a facial exposure and questioned about their first impression of the air quality inside the chamber. In this case, we consider the existence of clean air where there are no significant sources of pollution and the air has not been renewed with outdoor air. From these studies, it was concluded that there is a linear relationship between the acceptability and enthalpy of the air. At high temperature levels and humidity, the perception of air quality appears more influenced by these variables than by the air pollutants. These findings need further validation which involves the development of more experiences.

In a second experiment, Fang and co-workers carried out a study of the initial acceptability and subsequent developments. They used clean air and whole body exposure to different levels of temperature and humidity. This experiment was divided into two sets: one aimed at defining the feeling of comfort and the other at defining the perception of smell.
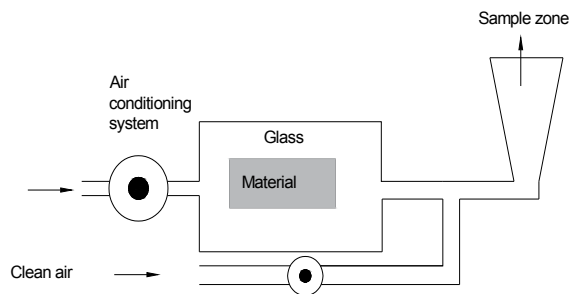
Fig. 1. House heated Climpaq designed by Albrectsen in 1988.

For these experiments, a system was developed based on two stainless steel chambers (3.60 x 2.50 x 2.55 m), independent and united by a door that allowed a camera to pass from one to the other; the individual who performs the test may turn to the second chamber at each stage of the experiment. The camera was subjected to a new odour level, temperature and/or humidity. (Fig. 2 reveals the shape of the chamber.) The experiment focused on conducting a survey on 36 students (26 males and 10 females) who had not been trained in issues of indoor environments. All were nearly 25 years old and had their whole body exposed in the chamber. The scale of values, employed during the survey, is seen in Fig. 3.
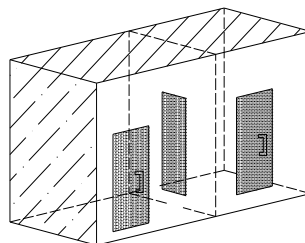
Fig. 2. New experimental chamber.

In these chambers, different temperatures and humidity within the ranges 18–28ºC and 30–70%, respectively, remained constant. The number of air changes in both chambers was the same and equal to 420 l/s. The existing pollutants came from the chamber or from the air renovation system.
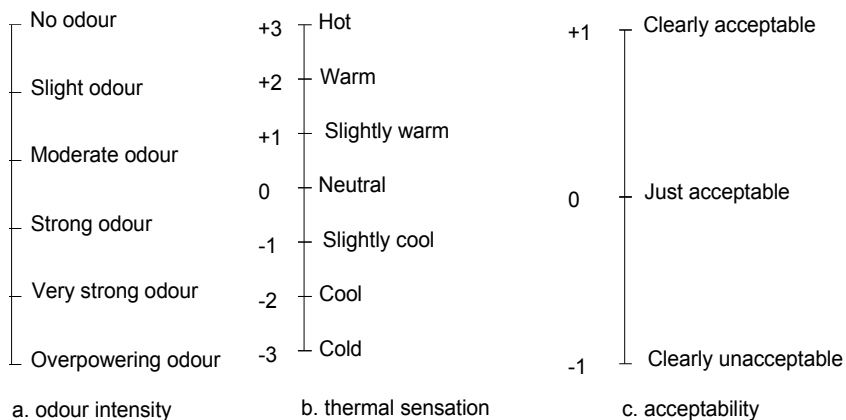
Fig. 3. Used survey.

Every 20 minutes, existing conditions were varied which prompted the individual to change camera. The questionnaires were filled in every 2.5, 5, 10, 15 and 20 minutes. Through the process, the subjects could adapt their clothing to the environment around them to achieve thermal neutrality.

During the second round of experiments, individuals were submitted to the same procedure as the earlier one. In this case, a contaminated source, particularly PVC, was introduced and air renovation descended to 200 l/s. The pollutants were hidden in the camera and individuals were introduced in groups of six to answer the survey. The findings from the first experiment indicated that, depending on the temperature and relative humidity in the new chamber, there was a sudden jump in the alarm. The alarm, after 20 minutes, does not depend on the conditions of initial temperature and relative humidity.
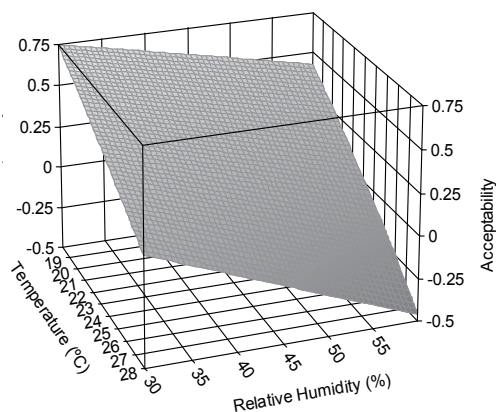
Fig. 4. Influence of temperature and relative humidity on the acceptability.

The results reveal that there is an increasing acceptability with the drop in temperature and relative humidity, and that cooling of the mucous membranes is essential to perceive the air as acceptable because it demonstrates the influence of the air enthalpy. The results indicated that, for a whole body exposure, there is a linear relationship of the acceptability with the enthalpy (for clean air as polluted, see Fig. 4). In conclusion, there is no difference between the initial acceptability and acceptability after 20 minutes of exposure. It also follows that the acceptability is independent of the environment conditions that surrounds the individual, before entering the camera.

The results of tests on odours indicate that the intensity of the odour varies little with temperature and relative humidity, and that there is some adjustment to smell after about 20 minutes. The studies by Berglund and Cain (1989) were proved in the absence of adaptation of acceptability in time. It also checks the result of Gunnarsen (1990), when it confirmed adaptation to the smell inside after a little while.

3. Results on General Thermal Comfort Models

3.1. P.O. Fanger model

Thermal comfort models were obtained from different bibliographic references (ISO and ASHRAE Standards), to determine which are more interesting.

The main object of heating, ventilation and air conditioning is to provide comfort to the occupants by removing or adding heat and humidity of the occupied space (ISO 7730:2005). Correspondingly, the main object of the study on the thermal comfort conditions is generally able to determine the conditions for achieving human internal thermal neutrality with minimal power consumption. To do this, the need to study a human body's response to certain environmental conditions arises.

It is considered a comfortable environment where there is no thermal perturbation, namely that the individual does not feel too cold or hot. This is achieved when the brain interprets the signals as two opposing forces, where the sensations of cold work in one direction and heat in the other. If the signals received in both directions are of the same magnitude, the resulting feeling is neutral. A person in thermal neutrality and completely relaxed is in a special situation, where the cold or heat sensors are not activated. To define the thermal comfort conditions of a climate, it must be given some characteristic parameters of the environment and its occupants. These parameters allow comparisons between the different environments of the study. Only after a thorough research, the thermal comfort and indoor air quality be judged the quality of the thermal environment and, consequently, the efficiency of the HVAC systems. Now, it can be revealed as the most important parameters in the design of the facilities of the air-conditioning systems.

To determine the thermal comfort rates of an environment, it can be found in two methods. One based on the study of thermal balance of the human body (Fiala et al., 2001) and the other based in empirical equations. This last method employs equations that define the same comfort rates with greater simplicity than the first. Another advantage is that they are expressed in terms of parameters much more easily in the sample for longer periods and, therefore, relate to the environment quality with energy savings.

The thermal balance is totally accepted and followed by ISO 7730:2005 for the study of comfort conditions, regardless of the climatic region. The thermal balance begins with two necessary initial conditions to maintain thermal comfort:

1) It must be obtained in a neutral thermal sensation from the combination of skin temperature and full body.

2) In a full body energy balance, the amount of heat produced by the metabolism must be equal to that lost to the atmosphere (steady state). Equation 3 was obtained by applying the above principles.

The rate of heat storage in the body was considered as two nodes (skin and core). The comfort equation can be obtained by setting the heat balance in thermally comfortable conditions for an individual. Based on these parameters, it can be established that the indices generally used to define a thermal environment (Equation 1) predicts the mean vote and 2 percent dissatisfaction.

$$PMV = \left(0.303 \cdot e^{-0.036 \cdot M} + 0.028\right) \cdot L \tag{1}$$

$$PPD = 100 - 95 \cdot e^{-\left(0.03353 PMV^4 + 0.2179 PMV^2\right)} \tag{2}$$

$$M - W = q_{sk} + q_{res} + S \tag{3}$$

$$M - W = (C + R + E_{sk}) + (C_{res} + E_{res}) + (S_{sk} + S_{cr}) \tag{4}$$

Where:

  M — rate of metabolic heat production (W/m²)
  W — rate of mechanical work accomplished (W/m²)
  q_{sk} — total rate of heat loss from skin (W/m²)
  q_{res} — total rate of heat loss through respiration (W/m²)
  C+R — sensible heat loss from skin (W/m²)
  C_{res} — rate of convective heat loss from respiration (W/m²)
  E_{res} — rate of evaporative heat loss from respiration (W/m²)
  S_{sk} — rate of heat storage in skin compartment (W/m²)
  S_{cr} — rate of heat storage in core compartment (W/m²)

PMV scale is a computational model for the evaluation of generic comfort conditions and predictions of its limits. It is constituted by seven thermal sensation points ranging from 3 (cold) to +3 (hot), where 0 represents the neutral thermal sensation.

To predict the number of persons who are dissatisfied in a given thermal environment, the PPD index is used. In this index, individuals who vote –3, –2, –1, 1, +2 and +3 on the PMV scale are considered thermally unsatisfied. Its evolution, as a function of PMV, is reflected in Fig. 5.

For a PMV value between –0.85 and +0.85, the percentage of dissatisfied (PPD) is 20 and the assumption of a stricter PPD of 10% corresponds to a PMV between –0.5 and +0.5.

As a result, it can be three kinds of comfort zones, depending on the admissible ranges PPD and PMV (Table 2).
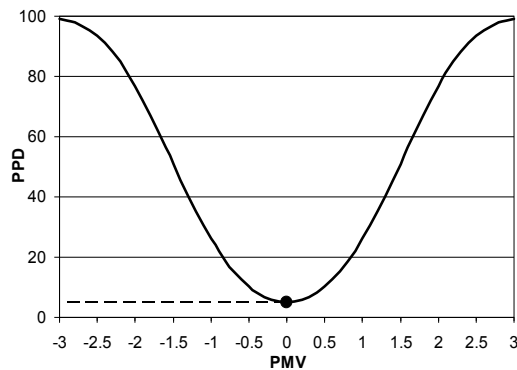
Fig. 5. Evolution of PPD on the basis of PMV.

Comfort	PPD	Range del PMV
A	<6	–0.2 < PMV < 0.2
B	<10	–0.5 < PMV < 0.5
C	<15	–0.7 < PMV < 0.7

Table 2. Predicted percentage of dissatisfied (PPD) based on the predicted mean vote (PMV).

One must remember that the evaporative heat loss from skin Esk depends on the amount of moisture on the skin, and the difference between the water vapour pressure on the skin and in the ambient environment. Finally, in the case of office workers, external work W can be considered zero. To deduce the comfort equation, the comfortable temperature of the skin and the sweat production equation with the full body thermal balance was combined (Stanton et al., 2005). This equation describes the relationship between measures of physical parameters and thermal sensation experienced by a person in an indoor environment. The comfort equation is an operational tool where physical parameters can be used to assess the thermal comfort conditions of an indoor environment. However, the comfort equation, obtained by Fanger, is too complicated to be solved through manual procedures.

On the sample of the thermal conditions of an interior environment, the human body does not feel the temperature of the compound; he feels the losses that occur with the thermal environment. Therefore, the parameters to be measured are those which affect the loss of heat: air temperature (ta), average temperature radiant ($\overline{t_r}$), relative humidity of the air (RH) and air velocity (v).

1. Metabolic rate (met): is the amount of energy emitted by an individual as a function of the level of muscle activity. Traditionally, metabolism has been estimated at met (1 met=58.15 W/m² surface of the body).

2. Cloth insulation (clo): is the unit used to measure the insulation of the clothing produced by clo, but the unit more technical and frequent use is m²ºC/W (1 clo=155 m²ºC/W). The scale is such that a naked person has a value of 0.0 clo and the typical street garment has 1.0 clo. The value of the clo, for people dressed, can be calculated as an addendum to the clo of each garment.

3. Mean radiant temperature: defines the radiant temperature of man, $\bar{t}_r$, as a uniform temperature in an imaginary black enclosure, in which a person would experience the same losses by radiation than in the real compound.

4. Operative Temperature: is the temperature in the walls and air of an equivalent compound that experiments the same heat transfer to the atmosphere by convection and radiation than in an enclosure where these temperatures are different.

5. Relative humidity: is defined as the relationship between the partial vapour pressures of water vapour in moist air and vapour pressure under saturated conditions. Often, it has been considered that the relative humidity of the interior environment is of little importance in the design of air conditioning elements. But now, the effect has become apparent on the comfort (ASHRAE; Fanger, 1970; Wargocki et al., 1999), perception of indoor air quality (Fang et al., 1998), health of the occupants (Molina, 2000) and energy consumption (Simonson, 2001).

6. Air velocity: No established clear link between air velocity and thermal comfort. For this reason, ASHRAE confirmed an air speed rise to a higher air temperature, but maintaining conditions within the comfort zone. In this, a series of curves of allowed temperature can be found for a given air speed, which is equivalent to those that produce the same heat loss through the skin.

After studying the equations that define the heat balance of a person, we can deduce the need of the sample for the instantaneous evolution of operative temperature, air velocity and relative humidity. To facilitate this procedure, it was summarised that the parameters must be measured directly or calculated (Table 3).

In Table 3, we found the term 'Equivalent Temperature', which is often used instead of Dry Heat Loss.

This equivalent temperature can be calculated from the dry heat loss and, by definition, is the uniform temperature of a radiant black enclosure with zero air velocity, in which an occupant would have the same dry heat loss as the actual non-uniform environment.

Method 1	Air velocity	Air temperature (t_a)	Mean radiant temperature ($\bar{t}_r$)	Humidity (w)
	Measure	Measure	Calculate	Measure
Method 2	Air velocity	Operative temperature (t_o)		Humidity (w)
	Measure	Measure		Measure
Method 3	Equivalent temperature (t_{eq})			Humidity (w)
	Measure			Measure
Method 4	Air velocity	Effective temperature (ET*)		
	Measure	Calculate		

Table 3. Methods to calculate general thermal comfort indexes.
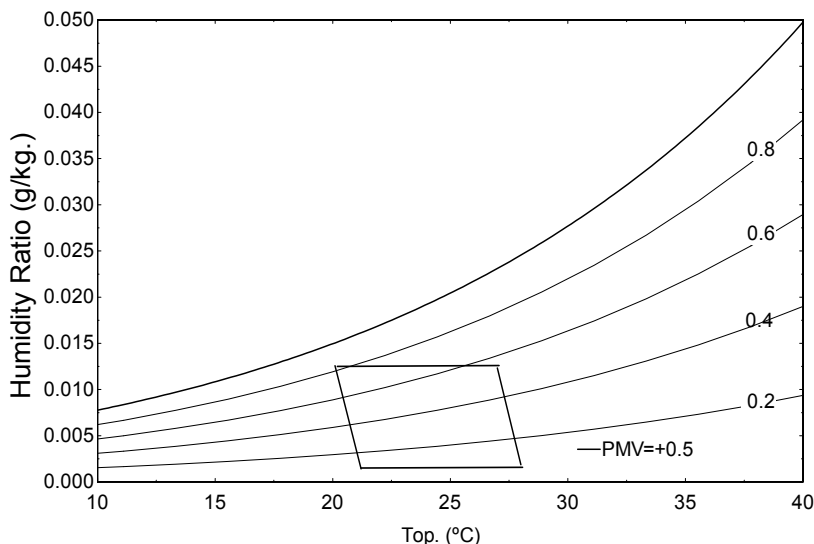
Fig. 6. Comfort zone.

Finally, it can be defined as a comfort zone for some given values of humidity, air speed, metabolic rate and insulation produced by clothing, in terms of operating temperature or the combination of air temperature and average radiant temperature. For air speeds not greater than 0.20 m/s, see Fig. 6.

3.2. Alternative PMV models

Among the thermal environment indices, the principal is the PMV. The conclusion on the work done by Oseland, subsequently reflected by ASHRAE, is that the PMV can be used to predict the neutral temperature with a margin of error of 1.4°C compared with the neutral temperature defined by the equation of thermal sensation. This thermal sensation expresses an equivalent index to the PMV. Its principal difference is that thermal sensation is obtained by regression of a survey to different individuals located in an environment. This survey presents a scale (Table 4).

An example, of a thermal sensation model that takes into account the effect of the clo, has been developed by Berglund (Equation 5).

Tsens	Thermal sensation
3	Warm
2	Heat
1	Soft
0	Neutral
–1	Soft freshness
–2	Freshness
–3	Cold

Table 4. Thermal sensation values.

$$T_{sens} = 0.305 \cdot T + 0.996 \cdot clo - 8.08$$

(5)

When Brager studied office buildings in San Francisco during the winter, he revealed that the PMV was found to be lower (colder) than the obtained thermal sensation. That defined a neutral temperature of 24.8°C, which was 2.4°C above the estimated value. After considering various UK offices with mechanical ventilation, it was demonstrated that the PMV differed by 0.5 points with the thermal sensation, which is equivalent to 1.5°C differences.

In Australia, Dear and Auliciems (1985), found a difference of 0.5–3.2° C between the neutral temperatures, estimated by surveys and determined by the PMV model of Fanger. Subsequently, Dear conducted a study in 12 Australian office buildings; it was defined that a temperature difference, between neutral temperatures proposed by surveys and PMV, was determined to about 1°C. Dear et al. extended their studies to those made by Brager. They returned to analyze and correct the data by the seat isolation. Again, discrepancies were found between the neutral temperature, based on the value obtained through surveys, and the value predicted by the equations. As a result, it seems that for real conditions, the thermal sensation of neutrality is in line with a deviation of the order of 0.2–3.3°C and an average of 1.4°C of the thermal neutrality conditions. The error was attributed to a PMV erroneous definition of the metabolic activity and the index of clo, or unable to take into account the isolation of the seat.

The Institute for Environmental Research of the State University of Kansas, under ASHRAE contract, has conducted extensive research on the subject of thermal comfort in sedentary regime. The purpose of this investigation was to obtain a model to express the PMV in terms of parameters easily sampled in an environment. As a result, an investigation of 1,600 school-age students revealed statistics correlations between the level of comfort, temperature, humidity, sex and exposure duration. Groups consisting of 5 men and 5 women were exposed to a range of temperatures between 15.6 and 36.7°C, with increases of 1.1°C at 8 different relative humidifies of 15, 25, 34, 45, 55, 65, 75 and 85% and for air speeds of lower than 0.17 m/s. During a study period of 3 hours and in intervals of half hours, subjects reported their thermal sensations on a ballot paper with 7 categories ranging between –3 and 3 (Table 4). These categories show a thermal sensation that varies between cold and warm, passing 0 that indicates thermal neutrality. The results have yielded to an expression of the form (Equation 6).

$$PMV = a \cdot t + b \cdot p_v - c$$

(6)

Time/sex	A	B	C
1 hour/man	0.220	0.233	5.673
Woman	0.272	0.248	7.245
Both	0.245	0.248	6.475
2 hours/man	0.221	0.270	6.024
Woman	0.283	0.210	7.694
Both	0.252	0.240	6.859
3 hours/man	0.212	0.293	5.949
Woman	0.275	0.255	8.620
Both	0.243	0.278	6.802

Table 5. The coefficients a, b and c are a function of spent time and the sex of the subject.

By using this equation and taking into account sex and exposure time to the indoor environment, it should be used as constants (Table 5).

With these criteria, a comfort zone is, on average, close to conditions of 26ºC and 50% relative humidity. The study subjects have undergone a sedentary metabolic activity, dressed in normal clothes and with a thermal resistance of approximately 0.6 clo. Its exposure to the indoor ambiences was for 3 hours.

4. Results on Local Thermal Comfort Models

For an indoor air quality study, there are a number of empirical equations used by some authors over the last few years (Simonson et al., 2001). Indices, such as the percentage of dissatisfaction with local thermal comfort, thermal sensation and indoor air acceptability, are determined in terms of some simple parameter measures, such as dry bulb temperature and relative humidity. For instance, the humidity ratio and relative humidity are the most important parameters to compare the effect of moisture in the environment, whereas temperature and enthalpy reflect the thermal energy of each psychometric process. Simonson revealed that moisture had a small effect on thermal comfort, but a lot more on the local thermal comfort. The current regulations (ISO 7730, ASHRAE and DIN 1946) do not coincide with the exact value of moisture in the environment for some conditions, but concludes that a very high or very low relative humidity worsens comfort conditions.

The agreement chosen by ANSI/ASHRAE and ISO 7730 to establish the comfort boundary conditions was about 10% of dissatisfaction. Other authors believe that the local thermal comfort is primarily a function of not only the thermal gradient at different altitudes and air speeds, but may be also owing to the presence of sweat on the skin or inadequate mucous membrane refrigeration. To meet the local thermal comfort produced by the interior air conditions, Toftum et al. (1998a, b) studied the response of 38 individuals who were provided with clean air in a closed environment. The air temperature conditions ranged between 20 and 29ºC and the humidity ratio between 6 and 19 g/kg, as from 20ºC and 45% RH to 29ºC and 70% RH. Individuals assessed the ambient air with three or four puffs, and thus the equation for the percentage of local dissatisfaction was developed (Equation 7). ASHRAE recommends keeping the percentage of local dissatisfaction below 15% and the percentage of general thermal comfort dissatisfaction below 10. This PD tends to decrease when the temperature decreases and, as a result, limited conditions can be employed to define the optimal conditions for energy saving in the air conditioning system.

$$PD = \frac{100}{1 + e^{(-3.58 + 0.18 \cdot (30 - t) + 0.14 \cdot (42.5 - 0.01 p_v))}}$$

(7)

Where:

p_v is the partial vapour pressure (Pa)

4.1. Air velocity models

Air velocity affects sensible heat dissipated by convection and latent heat dissipated by evaporation, because both the convection coefficient and the amount of evaporated water per unit of time depend on it; therefore, the restful feeling becomes affected by air drafts.

Aiming towards energy saving in summer, the ambient air temperature can be kept slightly higher than the optimum and achieve a more pleasant feeling by increasing air velocity. The maximum acceptable air speed is 0.9 m/s.

In winter, the air circulation causes a cold feeling and to keep air temperature above that needed to avoid a feeling of discomfort, with its corresponding energy consumption. In winter, considering that the dry air temperature tends to be in the low band of comfort, air conditions in inhabited areas must be carefully studied, in order to maintain the conditions of wellbeing without wasting energy. It is recommended that the winter air velocity in the inhabited zone should be lower than 0.15 m/s. Localized draft problems are more common in indoor environments, vehicles and aircraft, with air conditioning. Even without a speed-sensitive air, there may be dissatisfaction owing to excessive cooling somewhere in the body.

In principle, there is sensitivity to currents on the nude parts of the body; therefore, only noticeable current flows on the face, hands and lower legs. The amount of heat lost through the skin because of the flow depends on the average speed of air, temperature and turbulence. Owing to the behaviour of the cold sensors on the skin, the degree of discomfort depends not only on the loss of local heat, but also on the influence in temperature fluctuations. For equal thermal losses, there is a greater sense of dissatisfaction with high turbulence in the air flow.

Some studies exhibit the types of fluctuations that cause greater dissatisfaction. These have been obtained from groups of individuals subjected to various air speed frequencies. The oscillations with a frequency of 0.5 Hz are the most uncomfortable, whereas oscillations with a higher frequency of 2 Hz produce less sensitive effects.

According to the ISO 7730:2005, drafts produce an unwanted local cooling in the human body. The flow risk can be expressed as the percentage of annoyed individuals and calculated (Equation 8).

The draft risk model is based on studies of 150 subjects exposed to air temperatures between 20 and 26°C, with average air speed between 0.05 and 0.4 m/s and turbulence intensities from 0 to 70%. The model is also applicable to low densities of people, with sedentary activity and a neutral thermal sensation over the full body.

The draft risk is lower for non-sedentary activities and for people with neutral thermal sensation conditions. Fig. 7 reveals the relationship between air speed, temperature and the degree of turbulence, for a percentage of dissatisfaction of 10 or 20%. The different curves refer to a percentage of turbulence from 10 to 80.

$$DR = (34 - t)(v - 0.05)^{0.62}(0.37vT_u + 3.14)$$

$$(8)$$

Where:

      v is the air velocity (m/s)

      t is the air temperature (°C)

      Tu is turbulence intensity (%)
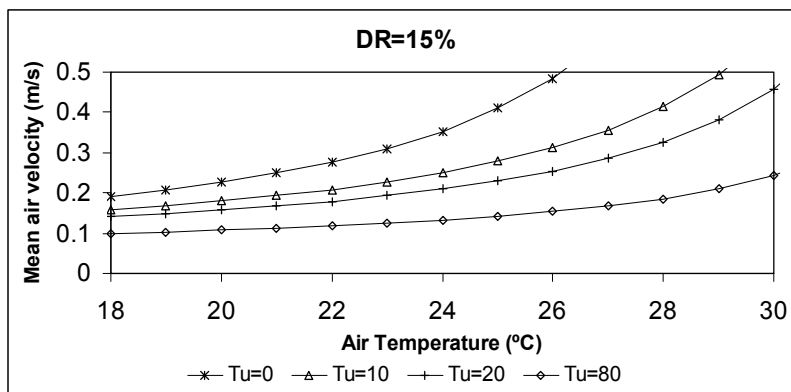
Fig. 7. Average air velocity, depending on temperature and the degree of turbulence thermal environments, for type A, B and C.

4.2. Asymmetric thermal radiation

A person located in front of an intense external heat source, in cold weather, may notice after a certain period of time some dissatisfaction. The reason is the excessive warm front and high cooling on the other side. This uncomfortable situation could be remedied with frequent changes in position to achieve a more uniform heating. This example reveals the uncomfortable conditions owing to a non-uniform radiant heat effect.

To evaluate the non-uniform thermal radiation, the asymmetric thermal radiation parameter ($\bar{t}_r$) is used. This parameter is defined on the basis of the difference between the flat radiation temperature (t_{pr}) of the two opposite sides of a small plane element. The experiences of individuals exposed to variations in asymmetrical radiant temperature, such as the conditions caused by warm roofs and cold windows, produce the greatest impact of dissatisfaction. During earlier experiences, the surface of the enclosure and air temperature was preserved.
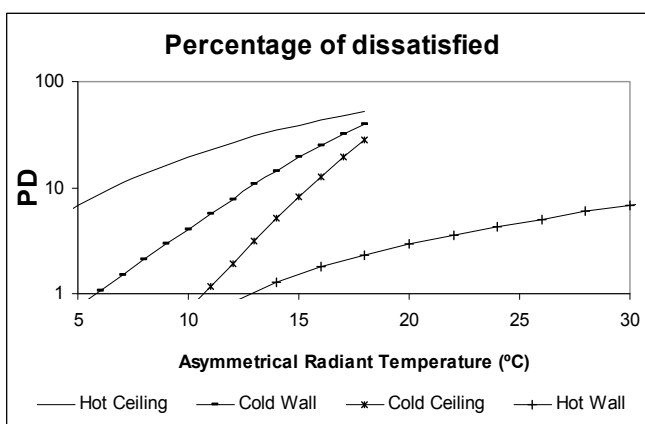
Fig. 8. Percentage of dissatisfied as a function of asymmetrical radiant temperature, produced by a roof or wall cold or hot.

The Parameter can be obtained by two methods: the first is based on the measure in two opposite directions, using a transducer to capture radiation that affects a small plane from the corresponding hemisphere. The second is to obtain temperature measurements from all surfaces of the surroundings and calculating the Δt_{pr}.

Equations 9, 10, 11 and 12 show the employed models for each case. Finally, the curves obtained are reflected in Fig. 8.

Hot ceiling ($\Delta t_{pr} < 23^\circ C$)

$$PD = \frac{100}{1 + \exp(2.84 - 0.174 \cdot \Delta t_{pr})} - 5.5$$

(9)

Cold wall ($\Delta t_{pr} < 15^\circ C$)

$$PD = \frac{100}{1 + \exp(6.61 - 0.345 \cdot \Delta t_{pr})}$$

(10)

Cold ceiling ($\Delta t_{pr} < 15^\circ C$)

$$PD = \frac{100}{1 + \exp(9.93 - 0.50 \cdot \Delta t_{pr})}$$

(11)

Hot wall ($\Delta t_{pr} < 35^\circ C$)

$$PD = \frac{100}{1 + \exp(3.72 - 0.052 \cdot \Delta t_{pr})} - 3.5$$

(12)

Where:

Δt_{pr} is the flat radiation temperature (ºC).

4.3. Vertical temperature difference

In general, there is an unsatisfied sensation with heat around the head and cold around the feet, regardless of whether the cause is convection or radiation. We can express the vertical temperature difference of the air existing at the ankle and neck height, respectively. Experiments on people's neutral thermal conditions have been conducted.

Based on these results, a temperature difference between head and feet of 3ºC produces a dissatisfaction of 5%. The curve obtained is reflected in Fig. 9. For a person in a sedentary activity, ISO 7730 is the acceptable value of 3ºC. The corresponding model is revealed in Equation 13.

$$PD = \frac{100}{1 + \exp(5.76 - 0.856 \cdot \Delta t)}$$

(13)
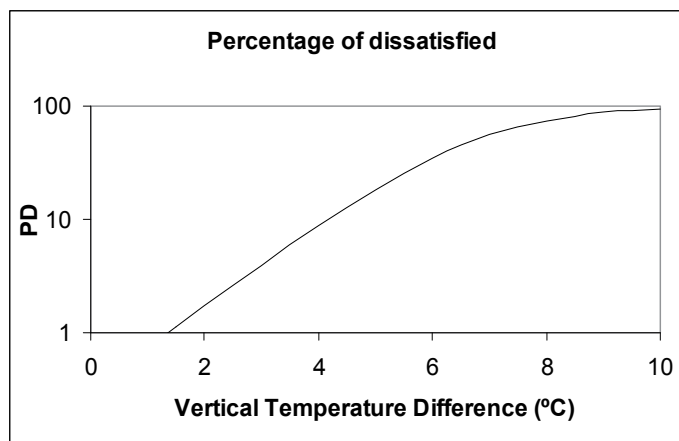
Fig. 9. Percentage of dissatisfied, depending on the vertical temperature difference.

4.4. Soil temperature

Direct contact between the feet and ground may cause local dissatisfaction, owing to a temperature which is either too high or low. Heat losses are dependent on other parameters, such as conductivity, heat capacity of the ground material and insulation capacity of the entire foot–footwear. ISO 7730 standard provides levels of comfort in sedentary activities for a 10% dissatisfied.

This leads to acceptable ground temperatures of between 19 and 29ºC. Studies have designated obtaining the curve (Fig. 10), and Equation 14 reflects the model of the percentage of dissatisfaction for different floor temperatures.

$$PD = 100 - 94 \cdot \exp(-1.387 + 0.118 \cdot t_f - 0.0025 \cdot t_f^2)$$

(14)

Where:

t_f is the floor temperature (ºC).
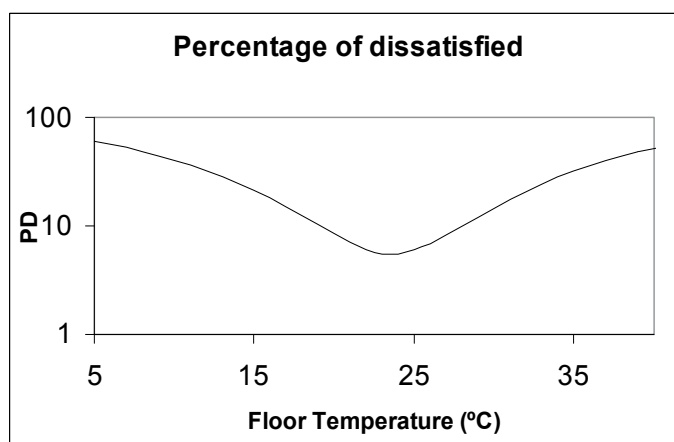
Fig. 10. Percentage of dissatisfied, depending on the temperature of the floor.

5. Conclusions and Future Research Works

Given the varied activities of international involvement in indoor environments, it was necessary for an intense research report about thermal comfort models, based on results of scientific research and actual ISO and ASHRAE Standards. From this research, it was concluded that, apart from the thermal comfort models, there are many more theoretical models, both deterministic and empirical. As a result, some empirical models (Equation 15) present an interesting application to building design and/or environmental engineering owing to its easy resolution. Furthermore, these models present a nearly similar prediction of thermal comfort than Fanger's model, if they are applied considering its respective conditions of special interest for engineering application. Regardless, Fanger's thermal comfort model presents an in-depth analysis that relates variables that act in the thermal sensation. As a result, this model is the principal tool to be employed as reference for future research (Orosa et al., 2009a, b) about indoor parameters on thermal comfort and indoor air quality.

$$PMV = a \cdot t + b \cdot p_v - c$$

(15)

However, different parameters can alter general thermal comfort in localized zones of the indoor environment, such as air velocity models, asymmetric thermal radiation, vertical temperature difference, soil temperature and humidity conditions.
All these variables are related with the local thermal discomfort by the percentage of dissatisfied that are expected to be found in this environment (PD). The result of the effect of relative humidity on local thermal comfort, in particular, is of special interest (Equation 16).

$$PD = \frac{100}{1 + e^{(-3.58 + 0.18 \cdot (30 - t) + 0.14 \cdot (42.5 - 0.01 p_v))}}$$

(16)

Finally, an important conclusion for this review is that it is possible to save energy if you lower the number of air changes, temperature and relative humidity (Orosa et al., 2008a, b, 2009c, d). These discussions, to maintain the PD with the corresponding energy savings, are ongoing. Cold, very dry air with high pollution causes the same number of dissatisfaction than clean, mild and more humid air. Of interest is that if there is a slight drop in temperature and relative humidity, pollutants emitted by each of the materials (Fang, 1996) will be reduced. However, field tests are recommended by the researchers, so that they can perform characterization of environments according to their varying temperature and relative humidity. This may start the validation of models that simulate these processes by computer and implement HVAC systems to reach better comfort conditions and, at the same time, other objectives, such as energy saving, materials conservancy or work risk prevention in industrial ambiences (Orosa et al., 2008c).

6. Acknowledgements

7. References

ASHRAE 55-2004. (2004). Thermal Environmental Conditions for Human Occupancy. *ASHRAE Standard.*

Berglund, L.; Cain, W.S. (1989). Perceived air quality and the thermal environment. In: *Proceedings of IAQ '89: The Human Equation: Health and Comfort*, San Diego, pp. 93–99.

Cain, W.S.; Leaderer, B.P.; Isseroff, R.; Berglund, L.G.; Huey, R.J.; Lipsitt, E.D.; Perlman, D. (1983). Ventilation requirements in buildings– I. Control of occupancy odour and tobacco smoke odour, *Atmospheric Environment*, 17, pp.1183–1197.

Cain, WS. (1974). Perception of odor intensity and the time-course of olfactory adaptatio. *ASHRAE Trans* 80, pp.53–75.

Charles, K.E. (2003). Fanger's Thermal Comfort and Draught Models. IRC-RR-162. Http://irc.nrc-cnrc.gc.ca/ircpubs. (Accessed July 2009)

Fanger, P.O.; (1970). Thermal comfort. Analysis and applications in environmental engineering. McGrawHill. ISBN:0-07-019915-9

Fang, L.; Clausen, G.; Fanger, P.O. (1998). Impact of Temperature and Humidity on Perception of Indoor Air Quality During Immediate and Longer Whole-Body Exposures. *Indoor Air.* Vol. 8, Issue 4. pp.276-284.

Fiala, D.; Lomas, K.J.; Stohrer, M. (2001). Computer prediction of human thermoregulatory and temperature responses to a wide range of environmental conditions. *Int. J. Biometeorol.* 45, 143-159.

Gunnarsen, L.; Fanger, P.O. (1992). Adaptation to indoor air pollution. *Environment International*. 18, pp. 43–54.

ISO 7730:2005. (2005). Ergonomics of the thermal environment -- Analytical determination and interpretation of thermal comfort using calculation of the PMV and PPD indices and local thermal comfort criteria.

ISO 7726:2002. (2002). Ergonomics of the thermal environment - Instruments for measuring physical quantities.

Knudsen, H.N.; Kjaer, U.D.; Nielsen, P.A. (1996). Characterisation of emissions from building products: long term sensory evaluation, the impact of concentration and air velocity. In: *Proceedings of Indoor Air '96*, Nagoya. International Conference on Indoor Air Quality and Climate, Vol. 3, pp. 551–556.

McNall, Jr; P.E., Jaax; J., Rohles, F. H.; Nevins, R. G.; Springer, W. (1967). Thermal comfort (and thermally neutral) conditions for three levels of activity. *ASHRAE Transactions,* 73.

Nevins, R.G.; Rohles, F. H.; Springer, W.; Feyerherm, A. M. (1966). A temperature-humidity chart for thermal comfort of seated persons. *ASHRAE Transactions*, 72(1), 283-295.

Molina M. (2000). Impacto de la temperatura y la humedad sobre la salud y el confort térmico, climatización de ambientes interiores (Tesis doctoral) . Universidad de A Coruña.

Orosa, J.A.; García-Bustelo, E. J. (2009) (a) Ashrae Standard Application in Humid Climate Ambiences". *European Journal of Scientific Research.* 27 , 1, pp.128-139.

Orosa, J.A.; Carpente, T. (2009) (b). Thermal Inertia Effect in Old Buildings. *European Journal of Scientific Research.* .27 ,2, pp.228-233.

Orosa, J.A.; Oliveira, A.C. (2009) (c). Energy saving with passive climate control methods in Spanish office buildings. *Energy and Buildings*, 41, 8, pp. 823-828.

Orosa, J.A.; Oliveira, A.C. (2009) (d). Hourly indoor thermal comfort and air quality acceptance with passive climate control methods. *Renewable Energy*, In Press, Corrected Proof, Available online 31 May.

Orosa, J.A.; Baaliña, A. (2008) (a). Passive climate control in Spanish office buildings for long periods of time. *Building and Environment*. doi:10.1016/j.buildenv.2007.12.001

Orosa, JA; Baaliña, A. (2008) (b). Improving PAQ and comfort conditions in Spanish office buildings with passive climate control. *Building and Environment*, doi:10.1016/j.buildenv.2008.04.013

Orosa, J.A., 2008 (c) University of A Coruña. Procedimiento de obtención de las condiciones de temperatura y humedad relativa de ambientes interiores para la optimización del confort térmico y el ahorro energético en la climatización. Patent number: P200801036.

Simonson, C.J.; Salonvaara, M.; Ojanen, T. (2001). Improving Indoor Climate and Comfort with Wooden Structures. Technical research centre of Finland. Espoo 2001.

Stanton, N.; Brookhuis, K.; Hedge, A.; Salas, E.; Hendrick, H.W. (2005). *Handbook of Human Factors and Ergonomics Methods*. CRC Press, 2005. ISBN 0415287006, 9780415287005.

Toftum, J.; Jorgensen, A.S.; Fanger, P.O. (1998). Upper limits for indoor air humidity to avoid uncomfortably humid skin. *Energy and Buildings*. 28, pp. 1-13.

Toftum, J.; Jorgensen, A.S.; Fanger, P.O. (1998). Upper limits of air humidity for preventing warm respiratory discomfort. *Energy and Buildings*. 28, pp.15-23.

Wargocki, P.; Wyon, D.P.; Baik, Y.K.; Clausen, G.; Fanger, P.O. (1999). Perceived air quality, Sick Building Syndrome (SBS) symptoms and productivity in an office with two different pollution loads. *Indoor Air*, 9, 165–179.

Woods, J.E. (1979). Ventilation, health & energy consumption: a status report, *ASHRAE Journal*, July, pp.23–27.

A new HVAC control system for improving perception of indoor ambiences

José Antonio Orosa García

University of A Coruña. Department of Energy and M.P.
Spain

1. Introduction

Thermal comfort plays a vital role in any working environment. However, it is a very ambiguous term and a concept that is difficult to represent on modern computers. It is best defined as a condition of the mind which expresses satisfaction with the thermal environment, and therefore, it is dependent on the individual's physiology and psychology.

Most often the set point and working periods of the Heating Ventilating and Air Conditioning system (HVAC) can be adjusted to suit the indoor conditions expected within a building. Despite this, as each building presents its own constructional characteristics and habits of its occupants, most common control systems do not factor in these variations. Consequently, the thermal comfort conditions are beyond the range of optimal behaviour, and further, of energy consumption.

To solve this problem several researchers have investigated the relationships between room conditions and thermal comfort. Normally, statistical approaches were employed, while recently, fuzzy and neural approaches have been proposed.

In this context, most control systems present an adequate accuracy in controlling indoor ambiences but, as mentioned earlier, this is insufficient. Therefore, a new algorithm is needed for this control system, which must necessarily consider the real construction characteristics of the indoor ambience as well as the occupants' habits. The comfort equation obtained by (Fanger, 1970) is observed to be too complicated to be solved using manual procedures, and more simplified models are needed as described in the following sections.

In this chapter a new methodology to control Heating Ventilating and Air Conditioning systems (HVAC) is discussed. This new methodology allows us to define the actual indoor ambiences, obtain an adequate model for each particular room, and employ this information to minimize the percentage of dissatisfaction, and simultaneously, reduce the energy consumption. Identical results can be obtained using expensive sampling apparatuses like thermal comfort modules and general HVAC control systems. Despite this, our new procedure, University of A Coruña patent P200801036, is based on the fact that simple models, adapted for each particular indoor ambience, will permit us to sample the principal related variables with low-cost sampling methods, such as data loggers. Finally, in this chapter the different ambiences where it can be employed will be dealt with.

2. Prior research

Thermal comfort can accurately be defined as the state of mind which expresses satisfaction with the thermal environment, and therefore, it depends on the individual's physiology and psychology (ISO 7730, 2005). This concept greatly influences any working environment; however, it remains a very vague term and a very difficult concept to represent on modern computers. Research conducted in the field of thermal comfort has proved that the required indoor temperature in a building is not a fixed value, and that the PMV index, which indirectly indicates satisfaction with the thermal comfort, is defined based on the six most important thermal variables: the human activity level, clothing insulation, mean radiant temperature, humidity, temperature and velocity of the indoor air, as seen in Fig. 1.
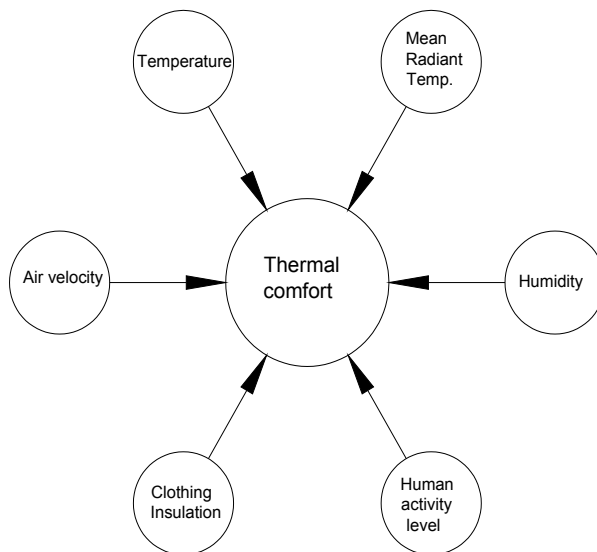
Fig. 1. Important variables that control thermal comfort.

In such a control scheme, the temperature and velocity of the indoor air have been commonly accepted as controlled variables for the HVAC system to keep the PMV index at comfort range. Energy saving was also reported to be achieved by this comfort-based control (Atthajariyakul and Leephakpreeda, 2004) and that a certain temperature range is sufficient to create a comfortable ambience.

Further, by controlling the heating and ventilation and by installing the air conditioning in that temperature zone, it will be interesting to obtain the lowest operating cost of the HVAC installation (Lute and van Paassen, 1995). To achieve these objectives different techniques like neuronal networks, adaptive models and regression models can be employed.

In the recent past, significant progress has been made in the fields of nonlinear pattern recognition, and thus a system control theory has been advanced in the branch of artificial neural networks (ANNs) (Mechaqrane and Zouak, 2004). It has also marked the progress of the neural network (FNN). However, most often, fuzzy logic controllers were employed because of their flexibility and intuitive uses. Basically, they have two control loops, one regulating the lighting and the other, the thermal aspects (Kristl *et al.*, 2008). In this case, the physical model of the chamber test with the measuring-regulation equipment was

constructed attempting to develop a control system using fuzzy logic control support, which would enable the harmonious operation of both the thermal and lighting systems.

The results of the experiments conducted by simultaneously running both the control loops prove that the system based on the fuzzy approach functions is much softer and closer to human reasoning than the classical Yes/No regime (Chen *et al.*, 2006).

Another method used was based on the climatic conditions. Humphrey and Nicol, 1998, established a strong relationship between comfort and the mean outdoor temperature by suggesting that, in office buildings, the occupants may fall back on a type of thermal memory to meet their comfort expectations. Humphreys concluded that particularly the daily exposure to outdoor and many indoor temperatures varies according to the climate zones and certain social factors, and that exposure to these temperatures in daily life is a key factor in establishing the perception of indoor thermal environments, and not solely based on the prevailing indoor parameters.

Finally, the regression models are the last method used to display the dynamic heat of a building. De Dear and Brager, 1998, suggested that thermal comfort can be related to the exposure thermal history (Chung *et al.*, 2008), the globe temperature (Leephakpreeda, 2008) and other indoor parameters by regression models.

Once the HVAC control techniques are described, a new procedure for controlling indoor ambience will be discussed in the sections that follow.

3. Materials and Methods

3.1. Standards

To investigate such types of environments, specific standards need to be considered. In this context, the ASHRAE Handbook Fundamentals, 2005, in chapter 40, titled "Codes and Standards" reminds us of the principal standards to be considered on HVAC Applications.

The first parameter is the comfort condition, defined by ASHRAE in the ANSI/ASHRAE 55-2004, "Thermal Environmental Conditions for Human Occupancy", which closely agrees with ISO Standards 7726:1998 "Ergonomics of the thermal environment-Instruments for measuring physical quantities" and the ISO 7730-1994 "Moderate Thermal Environments—Determination of the PMV and PPD Indices and specification of the Conditions for Thermal Comfort". These standards are principally based on Fanger's studies. ASHRAE emphasises that no lower humidity limits have been established for thermal comfort; consequently, this standard does not specify a minimum humidity level.

However, this same standard shows that systems designed to control humidity shall be able to maintain a humidity ratio at or below 0.012, which corresponds to a water vapour pressure of 1.910 kPa at standard pressure or a dew point temperature of 6.8 °C.

3.2. Sampling process

The methodology employed in this research work is based on sampling indoor comfort conditions, based on ISO 7730, and relates it with indoor the parameters like temperature and partial vapour pressure by curve fitting.

To collect the thermal comfort data, we can employ transducers similar to those utilised by the thermal comfort module of Innova Airtech 1221, 2009.

Using Gemini® dataloggers, air temperature and relative humidity monitoring has been conducted in a merchant vessel and buildings.

At the same time, outdoor data have been also obtained for comparison purposes. More than 11,000 measurements have been collected.

Later, the model thus obtained will be introduced in the HVAC control system of Simulink Ham Tools to simulate its behaviour in real buildings.

3.3. Thermal comfort models

Now, the principal models that enable us to define the thermal comfort in an indoor ambience will be analysed to select the one most adequate to be employed as the main algorithm of the HVAC control system.

3.3.1. Thermal balance model

Thermal balance is wholly accepted and followed by ISO 7730 for the study of comfort conditions, irrespective of the climatic region. Thermal balance begins with two mandatory initial conditions to maintain thermal comfort:

1) A neutral thermal sensation must be obtained from the combination of skin temperature and full body temperature.

2) In a full body energy balance, the amount of heat produced by metabolism must be equal to that lost to the atmosphere (steady state).

Applying the above principles, Equations 1 and 2 were obtained,

$$M - W = q_{sk} + q_{res} + S \tag{1}$$

$$M - W = (C + R + E_{sk}) + (C_{res} + E_{res}) + (S_{sk} + S_{cr}) \tag{2}$$

Where

M rate of metabolic heat production (W/m²)
W rate of mechanical work accomplished (W/m²)
qsk total rate of heat loss from skin (W/m²)
qres total rate of heat loss through respiration (W/m²)
C+R sensible heat loss from skin (W/m²)
Cres rate of convective heat loss from respiration (W/m²)
Eres rate of evaporative heat loss from respiration (W/m²)
Ssk rate of heat storage in skin compartment (W/m²)
Scr rate of heat storage in core compartment (W/m²)

The comfort equation can be obtained by setting the heat balance in thermally comfortable conditions for an individual, as Equation 1 shows. Based on these parameters the indices used in general to define a thermal environment can be established, as shown in Equation 3, that predicts the mean vote, and 4 of the percentage of dissatisfied.

$$PMV = \left(0.303 \cdot e^{-0.036 \cdot M} + 0.028\right) \cdot L \tag{3}$$

$$PPD = 100 - 95 \cdot e^{-\left(0,03353 PMV^4 + 0.2179 PMV^2\right)}$$

(4)

where L is the thermal load on the body, defined as the difference between the internal heat produced and the heat lost to the actual environment.

Once the equations were explained, the comfort equation obtained by Fanger is confirmed as being too complicated to be solved through manual procedures. Therefore, more simplified models are necessary as shown in the following sections.

3.3.2. Thermal sensation models

Of all the thermal environment indices, PMV is the principal one. The work done by Oseland, and subsequently reflected by ASHRAE, concluded that the PMV can be used to predict the neutral temperature, with a margin of error of 1.4°C compared with the neutral temperature, defined by the equation of thermal sensation. This thermal sensation expresses an index equivalent to the PMV, with the principal difference being that thermal sensation is obtained by a regression of surveys to different individuals located in an environment.

An example of a thermal sensation model that considers the effect of clothes (clo), has been developed by Berglund, 1978, and is shown in Equation 5.

$$T_{sens} = 0.305 \cdot T + 0.996 \cdot clo - 8.08$$

(5)

It is interesting to note that Brager and de Dear, 1998, also showed that the PMV was found to be lower (colder) than the obtained thermal sensation when they studied office buildings.

3.3.3. Adaptive models

Another group of alternative models used to define thermal comfort are the adaptive models. In their research, Nicol and Humphrey challenged the steady-state comfort theories by introducing the adaptive comfort theory (Kristl *et al.*, 2008). The theory proposes that occupants of an indoor ambience can support conditions over steady-state as they can adapt to their environment. Eight years later, in 1978, Humphrey introduced the argument that this comfort temperature is related to the external temperature at the location (Humphreys, 1976), as seen in Equation 6.

$$T_c = b + aT_o$$

(6)

Where T_c is the comfort temperature and T_o is the outside temperature index, and a, b are constants.

Nicol and Roaf, 1996, particularly recommended Equation 7 for occupants of naturally ventilated buildings. Several other adaptive models have also been proposed. For example, Humphreys, 1976, developed two models for neutral temperature, as given in Equation 8 and 9, and Auliciems and de Dear developed the relations to help predict group neutralities based on mean indoor and outdoor temperatures, as shown in Equations 10, 11 and 12, which were employed by the ASHRAE in Equation 13.

$$T_{n,o} = 17 + 0.38T_o \tag{7}$$

$$T_{n,1} = 2.6 + 0.831T_i \tag{8}$$

$$T_{n,o} = 11.9 + 0.534T_o \tag{9}$$

$$T_{n,i} = 5.41 + 0.731T_i \tag{10}$$

$$T_{n,o} = 17.6 + 0.31T_o \tag{11}$$

$$T_{n,i,o} = 9.22 + 0.48T_i + 0.14T_o \tag{12}$$

ASHRAE:

$$T_c = 17.8 + 0.31T_o \tag{13}$$

Where T_c is the comfort temperature, T_o is the outdoor air temperature, T_i is the mean indoor air temperature, $T_{n,i}$ is neutral temperature based on mean indoor air temperature and $T_{n,o}$ is neutral temperature based on mean outdoor air temperature.

Recent researches, however, such as 'Smart controls and thermal Comfort (SCATs)' project, funded by the European Commission in 1997–2000, sampled the indoor conditions in 26 offices in various countries, particularly France, Greece, Portugal, Sweden, and the United Kingdom. After relating the sampled values with the survey's results, it has concluded that comfort temperature (T_c) is a function of the exponentially weighted running mean of the daily mean outdoor temperature (T_{rm}) with $\alpha = 0.8$, as seen in Equations 14 and 15. This α is a constant between 0 and 1, which defines the speed at which the running mean responds to the outdoor temperature.

For running operation
$$T_c = 0.33 \cdot T_{rm} + 18.8 \tag{14}$$

For heated or cooled operation
$$T_c = 0.09 \cdot T_{rm} + 22.6 \tag{15}$$

3.3.4. Solution: selected model

The Institute for Environmental Research at Kansas State University, under ASHRAE contract, has conducted an extensive research on the subject of thermal comfort in the sedentary regime. The purpose of this investigation was to obtain a model to express the PMV in terms of parameters easily sampled in an environment.

Therefore, an investigation of 1600 school-age students revealed statistical correlations between the comfort level, temperature, humidity, gender, and exposure duration.

Groups of five men and five women were exposed to a range of temperatures between 15.6ºC and 36.7ºC, with increases of 1.1ºC at eight different relative humidities of 15, 25, 34, 45, 55, 65, 75 and 85%, and for air speeds of less than 0.17 m/s.

During a three-hour study period with half-hour intervals, subjects reported their thermal sensations on a ballot paper with seven categories ranging between -3 and 3. These categories show a thermal sensation that varies between cold to warm, passing through 0 that indicates thermal neutrality. The results have yielded an expression as shown in Equation 16.

$$PMV = a \cdot t + b \cdot p_v - c$$

(16)

By using this equation and considering gender and exposure time to the indoor environment, different constants need to be used. These constants were obtained by regression from the original PMV of the thermal balance model showed in Equation 3.
Now, this model can be implemented in the control system, and energy saving can be defined.

3.3.5. Solution: selected software

As shown, a host of commercially available computer tool models already exist for modelling single components or whole buildings. For modelling whole buildings, there are models for the hourly energy balance like Bsim1, ESP-r2, and EnergyPlus3 etc. While these tools are fully appropriate for designing standard buildings, they are not suitable for modelling innovative building elements such as building integrated heating and cooling systems, ventilated glass facades and solar walls, as these have not been defined in the program, 2008.

Thus far it has been observed that the major shortcomings of building energy simulation programs have been unable to accurately model HVAC systems that are not "standard". This argument can easily be extended to include advanced building elements. Modular models, however, have the advantage that the components and systems can be modelled as the need is encountered. Also, transparency of the existing components is essential, if the user/developer wishes to implement any modifications. A transparent, modular and open source system for modelling heat and moisture flows in buildings should therefore be a user-friendly tool that can be extended as needed in the future.

The above-mentioned concerns have given authors the impetus to develop an open and freely available building physics toolbox. The initiation of the International Building Physics Toolbox (IBPT) was thus begun by two groups of researchers working independently of each other, developing building physics models in Simulink.

For both groups, the reason for using Simulink as the development environment stemmed from the need to model, in great detail, the processes of heat, air and moisture transfer. In both groups, Simulink, which is part of the Matlab package, was chosen for its high degree of flexibility, modular structure, transparency of the models, and ease of use in the modelling process.

Simulink has earlier been used by other research communities (SIMBAD and CARNOT), but the models have either not been an open source, free of cost, or have not been directly applicable to building physics modelling.

Simulink's modular structure - using systems and subsystems - makes it easier to maintain an overview of the models, and new models can just as easily be added to the pool of existing models.

Another advantage of using Simulink is the graphical programming language based on blocks with different properties such as arithmetic functions, input/output, data handling, transfer functions, state space models etc. Further, Simulink has built-in state-of-the-art ordinary differential equation (ODE) solvers, which are automatically configured at the run-time of the model.

Therefore, only the physical model needs to be implemented, and not the solver. Further, models can be created using several different approaches, including assembling models directly in Simulink, using the standard blocks, Matlab m-files, S-functions, and Femlab9 models using one-, two-, or three-dimensional finite element calculations. This wide variety of modelling techniques with different advantages and disadvantages indicates that the optimal choice can always be made, to suit the task.

Finally, the graphical approach also makes it easy to express the very complex interaction between the different parts of the model. Besides, those unfamiliar with programming too can easily start building their own models or altering the existing ones. Therefore, the toolbox also represents a good method of teaching building physics.

Once the selected software is defined, the next step would be to define the mathematical model to be employed. The mathematical model employed in this simulation is the result of whole building Heat, Air and Moisture (HAM) (Kalagasidis, 2008 and 2009) balance, and depends on the moisture generated from occupant activities, moisture input or removed by ventilation, and moisture transported and exchanged between indoor air and the envelope (Nielsen *et al.*, 2002).

The mathematical model is based on the numerical resolution of the energy and moisture balance through the building. The obtained discretized heat and moisture balance equations are shown in Equations 17 and 18.

$$\frac{T_i^{n+1} - T_i^n}{\Delta t} = \frac{1}{C^n} \cdot \left\{ \left[\frac{(T_{i-1} - T_i)}{R_{i-1} + R_i} + \frac{(T_{i+1} - T_i)}{R_{i+1} + R_i} \right] - h_{evap} \cdot \left[\frac{(p_{i-1} - p_i)}{R_{p,i-1} + R_{p,i}} + \frac{(p_{i+1} - p_i)}{R_{p,i+1} + R_{p,i}} \right] \right\} \dots$$

$$+ \left\{ \begin{array}{l} m_a \cdot c_{pa} \cdot (T_{i-1} - T_i)^n, m_a > 0 \\ m_a \cdot c_{pa} \cdot (T_1 - T_{i+1})^n, m_a < 0 \end{array} \right\}$$

(17)

$$\frac{w_i^{n+1} - w_i^n}{\Delta t} = \frac{1}{d} \cdot \left\{ \left[\frac{(p_{i-1} - p_i)}{R_{p,i-1} + R_{p,i}} + \frac{(p_{i+1} - p_i)}{R_{p,i+1} + R_{p,i}} \right] - \left[\frac{(P_{suc,i-1} - P_{isuc,i})}{R_{suc,i-1} + R_{suc,i}} + \frac{(P_{suc,i+1} - p_{suc,i})}{R_{suc,i+1} + R_{suc,i}} \right] \right\} \dots$$

$$+ \left\{ \begin{array}{l} 6.21 \cdot 10^{-6} \cdot m_a \cdot (p_{i-1} - p_i)^n, m_a > 0 \\ 6.21 \cdot 10^{-6} \cdot m_a \cdot (p_i - p_{i+1})^n, m_a < 0 \end{array} \right\}$$

(18)

Where $_i$ is the objective node and $_{i+1}$ and $_{i-1}$ are the preceding and following nodes and $_n$ and $_{n+1}$ the previous and corresponding time steps.

To solve these balance equations, room models were created from the individual Building Physics Toolbox (Rode *et al.*, 2002). Ham–tools library is a Simulink model upgraded version of H-Tools with a similar structure and specially constructed for thermal system analysis in building physics.

The library contains blocks for 1-D calculation of Heat, Air and Moisture transfer throughout the building envelope components and ventilated spaces. The library is a part of the IBPT-International Building Physics Toolbox, and available as a free download.

This library presents two main blocks; a building envelope construction (walls, windows) and a thermal zone (ventilated spaces), enclosed by the building envelope. Component models provide detailed calculations of the hydrothermal state of each subcomponent in the structure, based on the surrounding conditions to which it is exposed.

In Fig. 2, we can see the principal blocks employed for a building simulation. Here, a block representing the different exterior/interior walls, floor, roof and windows components can be observed. These constructions are defined with respect to the physical properties (density of the dry material and open porosity), thermal properties (specific heat capacity of the dry material and thermal conductivity), and moisture properties (sorption isotherm, moisture capacity, water vapour permeability and liquid water conductivity) in line with the BESTEST structure.

Other parameters are also considered in the heat and moisture building balance, for example, internal gains (convective gains, radioactive gains and moisture gains), air change and heating/ cooling system.

The building's characteristics are defined in the thermal zone block, indicating the surface areas, orientations and tilts of each wall. Room volume, ambient air gain from the heat originated from solar energy and initial temperature is thus adjusted.

The Thermal model of the classroom is based on the WAVO model described by de Witt (2000), and developed assuming that long-wave radiation is equally distributed over the walls; room air has uniform temperature, the surface coefficients for convection and radiation are constant, and finally, that all radioactive heat input is distributed so that all the surfaces, except the windows, absorb the same amount of that energy per unit of surface area.

To introduce the PMV models obtained in the HVAC system, a diagram of a proposed control system is illustrated in Fig. 3. The controlled variables of indoor air are measured to be compared with the desired reference. By using the difference obtained, the controller manipulates the air-handling unit (AHU) to reduce the difference between the actual indoor air conditions and the reference ones.

The results showed that the optimal indoor-air condition for the HVAC system presented acceptable thermal comfort and indoor air quality with efficient energy consumption. Four controlled variables were specifically identified:

1. Indoor-air temperature

2. Indoor-air humidity

3. Indoor-air velocity

4. Air ventilation rate

These variables were determined for the indoor-air condition which efficiently provided the thermal comfort, and the indoor air quality, at the desired level and also reduced the cooling load in real-time implementation.

In our case, two different HVAC systems were proposed and simulated under real weather conditions.

One with a constant and another with a variable set point. In the variable set point HVAC control system each proposed set point temperature was observed to depend clearly on the indoor temperature, relative humidity and model constants for the heating and cooling periods.

Fig. 2. Matlab blocks for building simulations.

Fig. 3. Proposed implementation for HVAC control system.

3.4. Energy consumption

The energy performance aspect must always be considered. Once obtained, the neutral temperature proposed by the different models as set point-temperature must be simulated and compared with the variable set point temperatures proposed.

With these values, the perceptual increment of energy to air conditioning in indoor air can be calculated.

The methodology described (by Olalekan *et al.,* 2006) was employed to calculate the energy consumption needed to achieve ideal comfort conditions.

In this research work, the seasonal energy consumption is estimated as a function of the ventilation rate of outdoor air and enthalpy difference between the indoor and desired air conditions, as seen in Equations 19 and 20.

$$Q = \dot{m}_{ventilation} \int \Delta h \cdot dt \tag{19}$$

Where;

$$\Delta h = h_{indoor} - h_{desired} \tag{20}$$

h_{indoor} is the indoor enthalpy
$h_{desired}$ is the desired indoor enthalpy.

Finally, to study thermal neutral comfort conditions, comfort temperature-adapted index presented by ASHRAE has been used in Equation 3.

3.5. Indoor ambiences

3.5.1. Buildings

Two schools were sampled and simulated. One of the areas of the older school was built in 1890, and the other portion was built in 1960, and the new school was built in 1999, as seen in Fig. 4. Consequently, the old school presents 0.43 m of stone and 0.5 cm of concrete in the indoor side of the wall.

The wall of the new building consisted of insulation, brick, concrete and plaster arranged symmetrically in layers with respect to the middle of the wall, reaching 0.30 m of total thickness.

The classroom sampled in the old building is located on the second floor has a volume of 210 m³, while the new is located on the first floor with a volume of 150 m³.

All these buildings present a working period from February to June, and an unoccupied period during weekends and holidays.

During those periods, the classrooms are under natural ventilation and the central heating system was not employed. The active period ends in June, and therefore, energy saving during summer period was not of interest. Further, during the extreme conditions in winter, these schools do not function and therefore, the heating system will work only when the indoor conditions exceed the thermal comfort during winter and spring.

Fig. 4. A building in A Coruña.

3.5.2. Ships

An air conditioning control system in the control engine room is known to obviously lower the temperature to 20ºC, see Fig. 5.

Despite this, marine engineers will require that these values be corrected for each different indoor situation of the voyage, to reduce the workplace risk of thermal shock and heat stress in contrast to that in the engine room where the typical values of temperature are around 38ºC.

However, in practice this set point is almost never changed, and consequently, we find engineers suffering from headache and muscular pain.

Fig. 5. Control engine room of a ship.

4. Results and Discussion

This procedure was employed in two different ambiences; in a building and in a control engine room of a ship.

4.1. Buildings

To define the static set point in buildings adaptive methods are employed. In this context, the mean Galician outdoor temperature during the winter period ranges between 10 and 12 ºC, which represents a comfortable indoor temperature of 17.78ºC to 21.18ºC for each adapted model.

The highest value, which was obtained by the Nicol and Roaf model, shows the typical starting point temperature employed in indoor ambiences of this humid region.

On the contrary, the Humphreys' model showed an indoor temperature of 17.78ºC, which correlates with the energetic temperature suggested by the INEGA (Energetic Institute of Galicia) for energy saving in air conditioning during the winter period.

Once the fixed starting point temperatures were defined, along with the PMV index samples according to the partial vapour pressure and the indoor temperature, a curve was fitted based on the model of Equation 16.

This model was well adjusted with a correlation factor of 0.92 and it was introduced in the HVAC control system of HAM tools to fix a starting point according to a limit value. The limit value, during the winter season, will be of PMV=-0.5, indicating that the indoor temperature, which is the only controlled variable, will be set to reach a PMV value of –0.5 in a psychometric heating process of the moist air. In the summer this PMV value will change to 0.5.

The results obtained during the summer season showed that with a fixed starting point value of 20ºC, the indoor conditions will be automatically corrected from lower to equal or higher values than 20ºC, irrespective of the indoor comfort conditions being higher than the lower comfort limits.

Finally, the indoor relative humidity will experiment a similar behaviour when the indoor air is controlled with a fixed or a variable starting point. Despite this, the indoor relative humidity will reach, in both cases, a value higher than a 100% and therefore, there is a risk of condensation and mould.

This will happen particularly when the indoor air temperature drops to lower values. For example, with a variable starting point, the indoor temperature, which will differ from the fixed starting point, sometimes reaches values of 17.5ºC, while the indoor relative humidity will reach 100%. Despite this, with a fixed starting point the indoor conditions will show a similar relative humidity, and consequently, the solution will have a reduced margin in comfort limits, like PMV values of 0.4.

Once the hourly energy consumption is simulated, we can conclude that a variable starting point will reveal lower energy peaks than a fixed one, so such a control system will work for less time compared with the old method. Further, if the electricity cost in such buildings is assumed to be 0.09 €/kWh, we can conclude that during the winter months the energy consumption will be 33% lower than with a constant starting point value.

This result is related to the results (of Lute *et al.*, 1995) where a predictive control system (LPC) saves about 30% of energy consumption related to the conventional on/off and PI during the winter season, with the same type of comfort requirements.

To summarise, this methodology is noted to control indoor air conditions and is quite accurate as it suggests temperatures in line with the current HVAC standards. However, despite adaptive models showing adequate values for thermal neutralities, they are not at all suitable for energy saving.

4.2. Ship

As a possible solution to the extreme environment of an engine room and control engine room of a ship, a self-adjustment control system accounting for the indoor temperature and relative humidity is proposed, and the hottest set point temperature within the thermal comfort limits P.O. Fanger suggested was (PMV=+0.5). Matlab Simulink simulated this control system.

The indoor temperature and relative humidity at the control engine room were sampled and curve fitted to enable easy simulation in the software.

Once the control system was designed, it was used to simulate the sampled conditions representing the thermal comfort range within which work was possible in the control engine room, and compared them with the actual data generated by the samples.

This range is indirectly represented by the temperature and relative humidity curves of PMV=+0.5.

Results revealed that the new control system suggested a temperature of about 28°C and a relative humidity of 28% for a PMV of 0.5 and an initial fixed value of 20°C.

In our study, setting the control system to a PMV value of 0.5 appeared useful because it would reduce the operator's thermal shock when he came out after working in the engine room, and released the accumulated heat in the control engine room.

Besides, this set point adjustment would prevent physical hazards and could be expected to reduce the working hours of the HVAC system, and thereby extend the average life of the equipment. While these are the advantages, this high temperature was observed to reduce the environmental relative humidity to very low values, and despite this being beneficial for the electrical environment, the human occupants could be expected to suffer dehydration.

A solution attempted for this last problem was to reduce the adjusted PMV to a lower value like 0.4, which would in turn reduce the indoor temperature set point and, consequently, raise the indoor relative humidity.

Another possible solution was to increase the number of air changes per hour in the control engine room. Using outdoor air particularly, would be especially advantageous because of its low values of temperature and high values of relative humidity.

Finally, bibliographic conclusions suggest that future works must be conducted based on a variable operational starting point for air-conditioned buildings and they should also extend their research to more data samples such as other indoor ambiences during a whole year (Mechaqrane and Zouak, 2004).

5. Conclusions

A particular procedure was described and developed in this study, with the aim of presenting a new tool for energy saving in buildings, and workplace risk prevention for future use in international shipping worldwide.

This procedure is based on a new thermal comfort model which was advanced based on the P.O. Fanger PMV index, according to the Institute of the University of Kansa, and adapted to a specific indoor ambience, with a thermal comfort logger.

The results proved that this methodology was sufficiently accurate in buildings, and suggests temperatures according to the actual HVAC standards. The adaptive models also reveal adequate values for thermal neutralities, although they are not suitable for energy saving, due to their static value for a daily period. The Humphreys model alone shows a fixed starting point temperature similar to that proposed by the variable PMV model. Further, due to the mould risk under the higher indoor air relative humidity, it is interesting to define stricter PMV limits to reduce higher relative humidity values.

The indoor conditions of the engine room and the control engine room of a merchant ship, however, when investigated during a sea voyage, showed the following findings: the low indoor temperature conditions observed in the control engine room were a definite source of physical hazards for marine engineers who came in from the hot environment of the engine room.

Therefore, a new control system to reduce this workplace risk was developed, based on the general thermal comfort level and the conditions simulated. This simulation, based on real data generated by the sample, showed the new expected environment that could be obtained. For example, indoor temperatures of 28ºC were proposed by which a reduced thermal shock could be expected. Besides this, these modifications could be expected to reduce the working hours of the HVAC system, thus extending the average life of the equipment.

Finally, more research is warranted to define better PMV and adaptive models based on continuous sample data.

6. Acknowledgements

7. References

Atthajariyakul, S.; Leephakpreeda, T. (2004) . Real time determination of optimal indo-air condition fro thermal comfort, air quality and efficient energy usage. *Energy and Buildings*. 36 720-733.

Berglund, L. (1978). Mathematical Models for Predicting the Thermal Comfort Response of Building Occupants, *ASHRAE Transactions*. Vol.8.

Brager, G.S.; De Dear, R.J. (1998). Thermal adaptation in the built environment: a literature review. *Energy and Buildings*. 27:83-96.

Chen, K.; Jiao, Y.; Lee, E.S. (2006) . Fuzzy adaptive networks in thermal comfort. *Applied Mathematics Letters*. 19: 420-426.

Chung, C.; Kwok, A.; Mitamura, T.; Miwa, N.; Tamura A. (2008) . Thermal diary: Connecting temperature history to indoor comfort. *Building and Environment*. 43: 877-885.

De Dear, R.J.; Brager, G. S. (1998). Developing an adaptive model of thermal comfort and preference. *ASHRAE Transactions*. 104:145-167.

Fanger, P.O. (1970). Thermal Comfort. Danish Technical press. Doctoral Thesis. Copenhagen.

Humphreys, M.A. (1976). Comfortable indoor temperatures related to the outdoor air temperature. *Building Service Engineer*. 44: 5-27.

Humphreys, M. A., Nicol J. F. (1998) . Understanding the adaptive approach to thermal comfort. *ASHRAE Transaction*.104.

Innova Airtech Instruments company. http://www.pollutiononline.com. (Accessed February 2009).

International Building Physics web page. http:// www.ibpt.org. 2010. (Accessed February 2009).

ISO 7730:2005. Ergonomics of the thermal environment - Analytical determination and interpretation of thermal comfort using calculation of the PMV and PPD indices and local thermal comfort criteria.

Kalagasidis, A.S. BFTools H Building physiscs toolbox block documentation. Department of Building Physics. Chalmer Institute of Technology. Sweeden. 2002.

Kalagasidis, A.S. HAM-Tools. International Building Physics Toolbox. Block documentation. 2008.

Kristl, Z.; Kosir, M.; Lah, M.T.; Krainer, A. (2008). Fuzzy control system for thermal and visual comfort in building. *Renewable Energy.* 33: 694-702.

Leephakpreeda, T. (2008). Grey prediction on indoor comfort temperature for HVAC systems. *Expert systems with Applications*. 34: 2284-2289.

Lute, P.; van Paassen D. (1995). Optimal Indoor Temperature Control Using a Predictor. *IEEE Control Systems*.

Mechaqrane, A.; Zouak, M. (2004). A comparison of linear and neural network ARX models applied to a prediction of the indoor temperature of a building. *Neural Comput & Applications.* 13: 32-37.

Nicol, F.; Roaf, S. (1996). Pioneering new indoor temperature standard: the Pakistan project. *Energy and Buildings*. 23: 169-74.

Nielsen, T.R.; Peuhkuri, R.; Weitzmann, P.; Gudum, C. (2002). Modelling Building Physics in Simulink. BYG DTU Sr-02-03. ISSN 1601-8605.

Olalekan, F.; Osanyintola, O.F.; Simonson, C.J. (2006). Moisture buffering capacity on hygroscopic building materials: Experimental facilities and energy impact. *Energy and Buildings.* 38 1270-1282.

Orosa, J.A. University of A Coruña. Procedimiento de obtención de las condiciones de temperatura y humedad relativa de ambientes interiores para la optimización del confort térmico y el ahorro energético en la climatización. Patent number: P200801036.

Presentation of the international building physics toolbox for SIMULINK. (2008). Weitzmann, P.; Sasic Kalagasidis, A.; Nielsen, T.R.; Peuhkuri, R.; Hagentoft, C.

Rode C., Gudum, Weitzmann P., Peuhkuri R., Nielsen T.R., Sasic Kalagasidis A., Hagentoft C-E: International Building Physics Toolbox-General Report. Department of Building Physics. Chalmer Institute of Technology. Sweden. Report R-02: 2002. 4.

Weitzmann, P.; Kalagasidis, A. S.; Nielsen, T. R.; Peuhkuri, R.; Hagentoft, C (2008). Presentation of the international building physics toolbox for simulink.

Wit, M. WAVO. (2000). A simulation model for the thermal and hygric performance of a building.

Assessment of indoor air quality and heat stress exposure in an automotive assembly plant

Aziah Daud[1], Edimansyah Abdin[2]*, Azwan Aziz[1],
Lin Naing[3] and Rusli Nordin[4]

1. Division of Occupational Medicine, Department of Community Medicine, School of Medical Sciences, Health Campus, Universiti Sains Malaysia, Kelantan, 16150 Malaysia
2. (Correspondence author) Institute of Mental Health, Buangkok Green Medical Park, 10 Buangkok View, Singapore 539747
3. Institute of Medicine, National University of Brunei Darussalam, Jalan Tungku Link, Gadong BE 1410, Brunei Darussalam
4. Clinical School Johor Bahru, Tan Sri Jeffrey Cheah School of Medicine and Health Sciences, Monash University, Johor Bahru, Johor, 80100 Malaysia

1. Introduction

Indoor air quality and heat exposure have become an important occupational health and safety concern in the workplace. The indoor environment is important not only because of the amount of time spent inside buildings but because there are indoor sources of pollution, including, heating and cooking appliances, open fires, building and insulation materials, furniture, fabrics and furnishings, glues, cleaning products, other consumer products, and various biological sources, such as house dust mites, fungi, and bacteria. There is also the inflow of polluted outdoor air through windows, evaporation of substances from water, and, in some locations, infiltration of radon and other gases into the building from the underlying soil and bedrock (Harrison, 2002).

Indoor air quality is the result of an intricate series of interactions involving many indoor and outdoor ventilation, microbiological, toxicological, and physical systems (Jones, 2002). Exposure to indoor toxicants can potentially lead to a variety of adverse health outcomes (Bascom et al., 1995). The likelihood that an individual will become ill from the presence of a contaminant depends upon factors such as the individual's sensitivity to that contaminant, the contaminant concentration, the current state of their psychological and physical health and the duration and frequency of exposure (Seltzer, 1997). Indoor air pollutants have the potential to cause transient morbidity, disability, disease, and even death in extreme cases

(Berglund et al., 1992). Recent research into these health outcomes has involved human, animal, and in vitro studies (Maroni et al., 1995).

Heat stress is readily associated with high environmental temperatures and humidity. Many work environments expose workers to extremely hot and humid conditions. Heat-related illness is a problem for many types of workers: metal smelters, outdoor construction and law enforcement workers, plastics manufacturing workers, landscaping and recreation maintenance personnel, staff in warehouses without air conditioning, cooks and kitchen workers, and athletes. A number of human factors contribute to a worker's susceptibility to heat stress, such as medical conditions, increasing age, overall level of fitness, presence of other metabolically stressful illnesses, the use of certain medications, dehydration, alcohol intake, and individual ability to acclimatize to extreme temperatures. Environmental factors that can contribute to heat stress besides high ambient temperature are low convection currents, high humidity, low evaporative loss, and high insulation levels around the body (Ramphal, 2000).

Heat is a form of energy. It can be generated either endogenous or exogenous process (Simon, 1994). Heat stress from safety and health point of view is physical hazards which can cause health effects direct or indirect into certain industrial workers. Workers are potentially exposed to heat will facing heat stress symptoms if they are not protected. Environmental factors such as ambient temperature, relative humidity, radiant heat, conduction and air velocity plays a major roles contribute to heat stress problems (OSHA, 1999).

2. Important of the Study

The automotive assembly plant in the automotive industry is well known to be a stressful working environment. The automotive assembly plant is usually configured as three successive shops in which the body is constructed, painted, and then assembled together with all component parts into a finished vehicle (Figure 1). Kvarnström (1997) reported that an automotive assembly-line work is often perform in a workplace environment with physical problems, such as noise, vibrations and dangerous machines that can be important stress factors.

Fig. 1. Three stages of car manufacturing process

The automotive assembly plant is one of the main contributors to different types of pollutants. For instance, waste from plastics, aluminum, cooper, rags, sandpapers, solvents

and paints can be generated. In particular, automotive painting processes generates, among other issues, VOC emissions as paint solvents. Automotive painting and coating products are formulated by using resins, pigments, volatile organic solvents, and chemical additives. Unfortunately, the automotive coatings process ranks at the top of the emission volume hierarchy. For this reason, knowing the pollution sources and their characteristics in this sector is important for a proper prevention. Several initiatives have been developed worldwide to promote occupational health and safety, and environmental protection through regulations, code of practices, and guidelines for prevention (Esquer et al, 2009).

In an automotive assembly plant, exposure to indoor air pollutants and heat are probably one of the most dangerous health hazards for the workers. Workers involved in auto body repair are potentially exposed to a multitude of air contaminants. During structural repair, activities such as sanding, grinding, and welding generate aerosols that are released into the worker's breathing zone. If the surface of the car being repaired contains toxic metals, such as lead, cadmium, or chromium, exposure to these metals, is possible. Workers who paint cars can be exposed to organic solvents, hardeners that may contain isocyanate resins and pigments that may contain toxic components (NIOSH, 1993).

In Malaysia, IAQ has been recognized by the Department of Occupational Safety and Health (DOSH) as a critical issue (DOSH, 2006). In order to ensure all workers are protected from indoor air pollutants, the department has set forth a code of practice entitled "Code of Practice on Indoor Quality" (DOSH, 2005). This code of practice is applied to all industries in Malaysia including the automotive industry. One of the aims of the code was to establish a set of maximum exposure limits for common indoor air contaminants, such as carbon monoxide, carbon dioxide and respirable particulates (DOSH, 2005).

In Malaysia, although indoor air pollutants and heat exposure pose a risk to the worker's health, few studies have been conducted in this industry. This is a serious omission because the automotive industry is a key player in the manufacturing sector, a high income generating industry and a government-linked company in Malaysia. In 2004, Malaysia was the largest producer of passenger cars in the Association of Southeast Asian Nations (ASEAN), accounting for 24.4% of the total ASEAN motor vehicle production. For commercial vehicles, Malaysia was the third largest producer, accounting for 11.0% of the total ASEAN production (Prime Minister's Department, 2005). Therefore, the aim of this study was to determine the concentration of five common IAQ contaminants [carbon dioxide (CO_2), carbon monoxide (CO), respirable particulate matter (PM10), temperature and relative humidity (RH)] and pattern of heat stress in the paint shop and body shop sections of an automotive assembly plant in Malaysia.

3. Materials and Methods

3.1 Study design

A cross-sectional study of the two sections (paint and body shops) was conducted in 2005 at an automotive industry plant located in Rawang, Selangor. During the assessment, workers in paint shop section who were involved in study were worked in body preparation of car before sending the body car into the primer booth (drying oven). They started their work

from 8.00 a.m to 6.00 p.m. They had their morning break at 10.30 a.m to 10.45 a.m, lunch break at 1.00 p.m to   2.00 p.m and evening break at 4.30 p.m to 4.14 p.m. Workers in body shop section worked as welder (welding a car components using electronic spot gun welder). Their work times were almost the same as workers in paint shop section.

3.2 Indoor air quality (IAQ) monitoring

After walk-through surveys of the sites, data collection of IAQ was done using direct-reading instruments [the Q-TRAK™ Plus IAQ Monitor (TSI Inc, 2003a) and the DUST-TRAK™ aerosol monitor (TSI Inc, 2003b)] during an eight hour work shift from 9:30 AM to 5:30 PM during painting and sanding operations. The instruments were located in both sections (body and paint sections). The Q-TRAK™ Plus IAQ Monitor (TSI Inc, 2003a) was used to record the CO, CO_2, temperature and RH levels using a survey mode at one second intervals. This mode was used to display the real-time readings of all parameters simultaneously. Before sampling, the Q-TRAK™ Plus IAQ Monitor was calibrated for CO_2 and CO by running a span gas with a known concentration and a zero gas through the monitor by the local TSI distributor. The span gas concentrations for CO_2 and CO were 1,000 ppm and 35 ppm, respectively. If measurements were not within specifications, the instrument was recalibrated. The Q-TRAK™ Plus IAQ Monitor (TSI Inc, 2003a) uses a non-dispersive infrared sensor for measuring CO_2 concentration, an electrochemical sensor for measuring CO concentration, a thermistor for measuring temperature, and a thin-film capacitive element for measuring relative humidity (Ramachandran et al, 2002). A DUSTTRAK ™ aerosol monitor (TSI Inc, 2003b) was used to measure PM10. The DUSTTRAK ™ aerosol monitor measures PM10 at one minute intervals at a flow-rate of 1.7 l/minute. Before sampling, pre- and post-zero checks of the DUST-TRAK aerosol monitor were carried out. The DUST-TRAK aerosol monitor is an optical instrument that detects particles in the air matrix by optical scattering, using the optical diameter instead of the aerodynamic diameter (Guo et al, 2004). The data was analyzed using TrakProTM v3.41 software.

3.3 Heat stress monitoring

In this study, heat stress monitor (Model: QUESTempo34 Thermal Environment Monitor, Quest Technologies, USA) was used to measure the heat stress data. This data logging area heat stress monitor measures four parameter: ambient or dry temperature (DB), natural wet bulb temperature (WB), globe temperature (GB), and relative humidity (RH). The details of definition and calculation of WBGT were published elsewhere (NIOSH 1986). This study was used WBGT indoor ($WBGT_{indoor}$) index as results. Both of sections were in enclosure setting. Heat stress monitor was placed at the nearest position to the workers without interrupted their movements and job tasking. This machine was set at 1.1 meter height in stand position and supported by the standard photographic tripod. Tripod mounting is recommended to get the unit away from anything that might block radiant heat or airflow. Wet bulb reservoir is filled with distilled water. After adding water and placing the unit, all parameter were stabilizing in surrounding area for 10 minutes. The machine was calibrated before and after the measurements using calibration sensor module. After all procedure done, measurement started and the machine recorded automatically in data logger. Heat measurements took eight hours with interval one hour recorded all four parameter. All

setting was followed NIOSH (1986) standards. Eight hours exposure is a standard where calculation based time-weighted average WBGT (TWA-WBGT$_{indoor}$) with the equation below:

$$\frac{WBGT_1 \times t_1 + WBGT_2 \times t_2 + ... + WBGT_n \times t_n}{t_1 + t_2 + ... + t_n} \tag{1}$$

where:

WBGT$_1$ x t$_1$ + WBGT$_2$ x t$_2$ + ……. + WBGT$_n$ x t$_n$ = WBGT values per hour
t$_1$ + t$_2$ + …. + t$_n$ = duration of exposure per hour

Heat monitoring started at 10.00 a.m and end-up at 5.00 p.m. The results of heat measurements were printed directly from the machine and all parameter were analyzed. The workplace which had WBGT $_{indoor}$ more than 28oC (>28 ^{o}C) was considered hot and WBGT $_{indoor}$ less than 27.9 ^{o}C (≤27.9 ^{o}C) were considered normal (Granadillos, 1998).

3.4 Workload and work-rest regime evaluation

As described earlier, WBGT index can predict the severity of heat exposure. It is also can showed suggested allowable work-rest regime for given workload. The American Conference of Governmental Industrial Hygienists (ACGIH, U.S) published a standard time-limited values (TLVs) for WBGT indices (ACGIH, 1992).

For the purpose of the study, workers who worked in paint shop section were considered in acclimatized workers and workers in body shop section were considered in unacclimatized workers. Acclimatized workers means the workers were exposure gradually to the hot environment for 14 days or more (NIOSH, 1986) where else unacclimatized were verse versa . Over all, workers in the paint shop and body shop sections were in moderate workload and worked in 75% work / 25% rest in work-rest regime scales according to ACGIH standards (ACGIH, 2001). Below is the table of Screening Criteria for Heat Stress Exposure by ACGIH.

Work demand	Light	Moderate	Heavy	Very heavy
100% work	25.9 ^{o}C	27.5 ^{o}C	26.0 ^{o}C	
75% work 25% rest	30.5 ^{o}C	28.5 ^{o}C	27.5 ^{o}C	
50% work 50% rest	31.5 ^{o}C	29.5 ^{o}C	28.5 ^{o}C	27.5 ^{o}C
25% work 75% rest	32.5 ^{o}C	31.0 ^{o}C	30.0 ^{o}C	29.5 ^{o}C

Table 1. Screening criteria for heat stress exposure of acclimatized person

Work demand	Light	Moderate	Heavy	Very heavy
100% work	27.5 ºC	25.0 ºC	22.5 ºC	
75% work 25% rest	29.0 ºC	26.5 ºC	24.5 ºC	
50% work 50% rest	30.0 ºC	28.0 ºC	26.5 ºC	25.0 ºC
25% work 75% rest	31.0 ºC	29.0 ºC	28.0 ºC	26.5 ºC

Table 2. Screening criteria for heat stress exposure of unacclimatized person

4. Results

Parameters	DOSH Standard* in 8-TWA	Paint Shop Section				Body Shop Section			
		Mean	SD	Min	Max	Mean	SD	Min	Max
Temperature (ºc)	20-26	32.5	1.2	29.3	33.9	29.7	1.0	27.8	30.8
RH (%)	40-60	65.5	2.3	62.6	71.3	72.9	2.4	69.8	78.4
CO ppm	10	1.1	0.2	0.5	1.8	2.0	0.4	1.4	3.1
CO_2 ppm	C1000	252.8	30.7	204	360	252.5	28.3	204	339
PM_{10} mg/m³	0.15	0.4	0.1	0.2	1.6	0.4	0.1	0.2	2.4

Table 3. Descriptive summary of selected IAQ parameters in the paint shop section and body shop section
Note: C is the ceiling limit, mg/m³ is milligrams per cubic meter of air at 25⁰ Celsius and one atmosphere pressure, ppm is parts of vapors or gas per million parts of contaminated air by volume, 8-TWA is time-weighted average for up to 8 hours/day
* (DOSH, 1996) and (DOSH, 2005)

4.1 IAQ Parameters

4.1.1 Temperature and RH

Fig 2 shows the average temperature and RH obtained in the paint and body shop sections. The average temperature in the paint shop section was 32.5 $\pm$1.2ºC (29.7 - 33.9ºC and, in the body shop section the average temperature was 29.7 $\pm$1.0ºC (27.8 - 30.8ºC). The relative humidity in the body shop section ranged from 69.8 to 78.4% with an average of 72.9 $\pm$2.4%. The RH in the paint shop section was 65.5$\pm$2.3% (62.6-71.3), higher than that in the body shop. The temperature and RH of both sections exceeded those recommended by the DOSH (Table 3).

4.1.2 CO

Fig 3 shows the concentrations of CO in the paint and body shop sections. The results show that the concentration of CO in the body shop ranged from 1.4 to 3.1 with an average of 2.0 $\pm$0.4 ppm. In the paint shop, the concentration of CO ranged from 0.5 to 1.8 ppm with an average of 1.1 $\pm$0.2 ppm. The average concentration of CO in the body shop was higher than that in the paint shop. However, the concentrations of CO in both sections were within DOSH standard limits (Table 3).

4.1.3 CO2

Fig 4 shows the concentrations of CO2 in the paint and body shop sections. The results show the average concentration of CO2 in the paint shop was 252.8 $\pm$30.7 ppm, which was slightly higher than in the body shop (252.5 $\pm$ 28.3 ppm). The concentrations of CO2 in the paint and body shop sections were 204-360 and 204-339 ppm, respectively. These concentrations were within the DOSH standard limits (Table 3).

4.1.4 PM10

Fig 5 shows the concentrations of PM10 in the paint and body shop sections. The PM10 concentration in the paint shop section ranged from 0.2 to 1.6 ppm, with an average of 0.4 $\pm$ 0.1 ppm, in the body shop section it was 0.4 $\pm$ 0.1 ppm (0.2-2.4 ppm). The average PM10 in both sections exceeded the DOSH standard limits (Table 3).
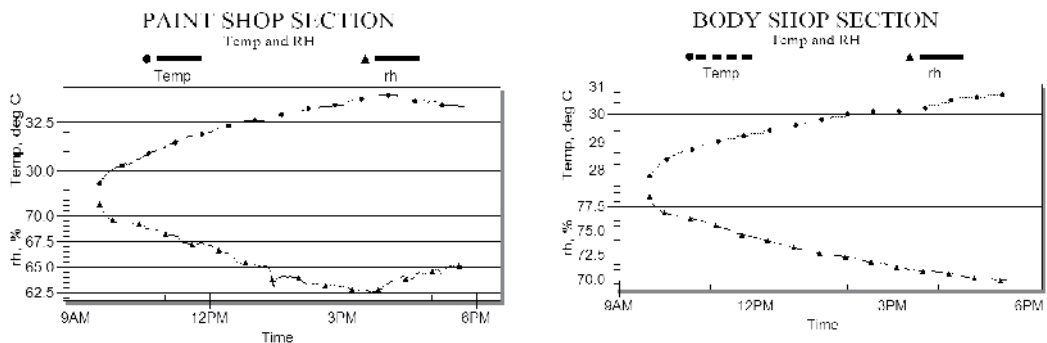
Fig. 2. Temperature and RH in the paint shop section (a) and body shop section (b)
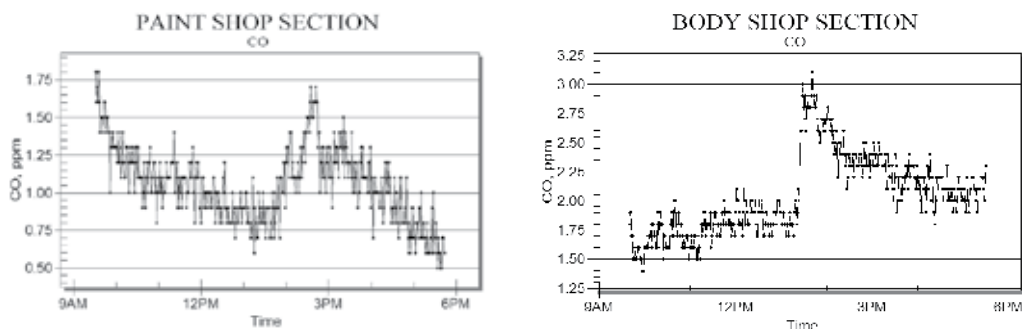
Fig. 3. The concentration of CO in the paint shop (a) and body shop section (b)
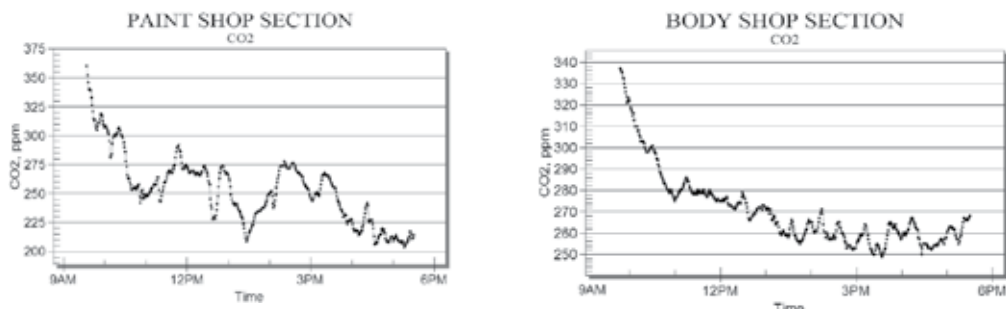
Fig. 4. Concentrations of CO_2 in the paint shop (a) and body shop section (b)
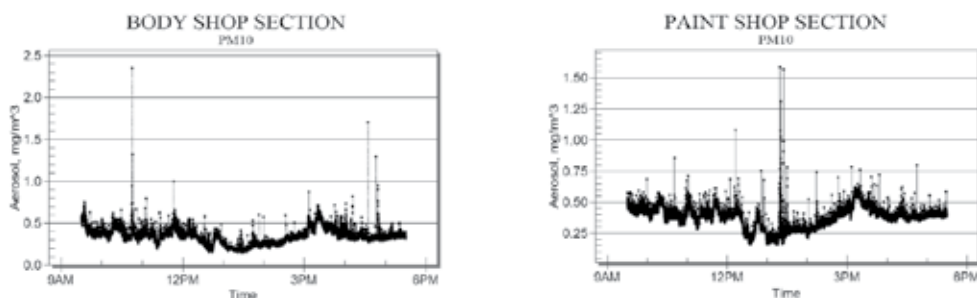
Fig. 5. Concentrations of PM10 in the paint shop (a) and body shop section (b)

4.2 Heat stress

All result of paint shop and body shop section were showed in Table 4. As over all, the study showed heat parameters in paint shop section (DB, WB and GB) were higher than heat parameter in body shop section. The TWA-WBGT$_{indoor}$ of paint shop was higher (28.3 ^{o}C) than TWA-WBGT$_{indoor}$ of body shop (27.0 ^{o}C). The min of relative humidity (RH%) of the paint shop was 48 RH% lower than RH% in body shop (55 RH%).

Heat parameters (min)	Section	
	Paint shop	Body shop
Dry temperature (DB) (in ^{o}C)	34.3	32.2
Wet bulb temperature (WB) (in ^{o}C)	25.5	24.8
Globe temperature (GB) (in ^{o}C)	34.8	32.2
TWA-WBGT$_{indoor}$ (in ^{o}C)	28.3	27.0
Relative humidity (RH%)	48	55

Table 3. Comparison of heat parameters in paint shop and body shop

Heat parameters (TWA-WBGT$_{indoor}$, DB, WB and GB) in paint shop were increased higher than heat parameters in body shop by time of measuring. By the way, both of the section

relatively showed all heat parameters were gradually increased by time (Figure 6). Meanwhile, RH% in paint shop was gradually decreased lower than RH% in body shop from start to end measuring (Figure 7). From the study, paint shop was considered "hot area" (>28 ºC) and body shop was considered "normal area" (≤27.9 ºC).

In paint shop section, workers were worked in moderate workload and worked in 75% work / 25%. From the TWA-WBGT$_{indoor}$ measured in   paint shop section (28.3 ºC), and compared with screening criteria for heat exposure in Table 3 (75% work / 25%: moderate: acclimatized: 28.5 ºC), workers were not exposed to heat stress. This condition was similar in workers in body shop when TWA-WBGT$_{indoor}$ measured was 27.0 ºC (75% work / 25%: moderate: unacclimatized: 26.5 ºC).
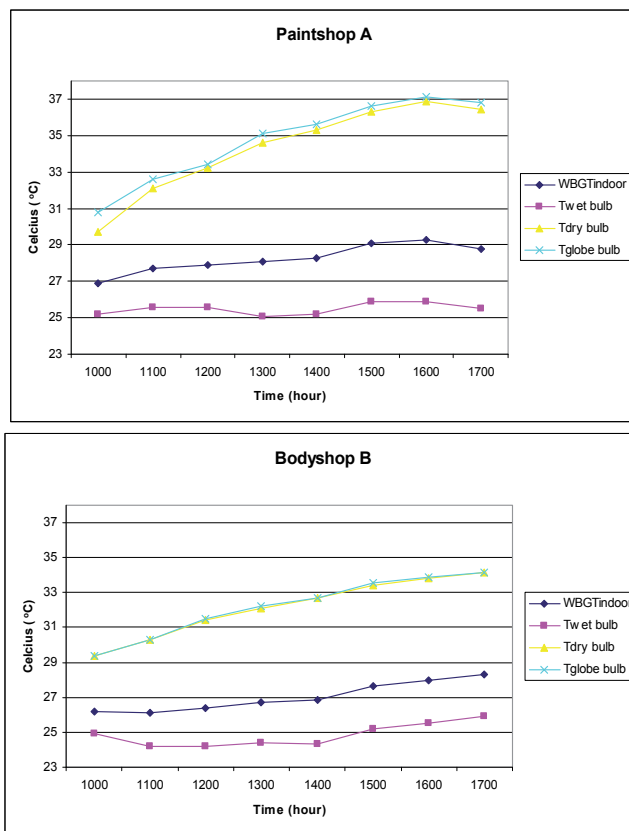
Fig. 6. The comparison heat parameters pattern in paint shop and body shop in 8 hours measuring time
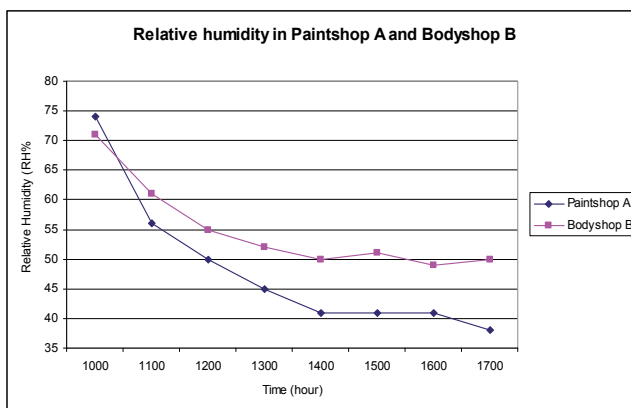
Fig. 7. The comparison relative humidity (RH%) pattern in paint shop and body shop in 8 hours measuring time

5. Discussion and Conclusion

The present study was aim to determine the concentration of five common IAQ contaminants [carbon dioxide (CO_2), carbon monoxide (CO), respirable particulate matter (PM10), temperature and relative humidity (RH)] and pattern of heat stress in the paint shop and body shop sections of an automotive assembly plant in Malaysia. We found that the temperature and RH in both sections exceeded the DOSH standard limits. The recommended optimum comfort range for RH according to DOSH is 40% to 60%. Low humidity can cause dryness of the eyes, nose and throat and may also increase the frequency of static electricity shocks. The relative humidity in the body shop ranged from 69.8 to 78.4% with an average of 72.9 ± 2.4%. High humidity, above 80%, can be associated with fatigue and "stuffiness" (DOSH, 1996).

We suggest the air-conditioning in this area should be monitored regularly. Humidity can result in the growth of mould and dust mites within the area if allowed to become too high. Rapid growth occurs when levels of humidity are above 60%, with a negative effect on respiratory illnesses such as asthma. If the level of humidity becomes too low, below 30%, this too can have adverse effects, with some people developing sore throats due to dryness of the air (DOSH, 1996). In this study, the concentration of CO and CO_2 were within the DOSH standard limits.

Our study found that the mean PM10 levels in both sections exceeded the DOSH recommendations at 0.15mg/m3. Inadequate ventilation of the sanders occurred during sanding in the body shop which probably contributed to increased levels of PM10 in the body shop. In the paint shop the high concentration of PM10 could be due to various organic solvents and paint overspraying. Thus, respirators need to be used properly to prevent worker exposure to air contaminants in the paint shop. Exhaust ventilation and process isolation are commonly used controls for PM10 reduction. In conclusion, the workers in the paint and body shop sections were exposed to high concentrations of RH, temperature and PM10. Therefore, IAQ management programs, engineering controls,

training and education should be conducted in these sections to minimize IAQ problem exposure.

In terms of heat stress monitoring, we found the heat environment in paint shop section was hot compared with body shop section. The study carried by Aziz (2003) in automobile found that, the TWA-WBGT$_{indoor}$ in paint shop was 29.2 °C and body shop was 24.7 °C. This condition happens because of the work process itself. In paint shop as a process, the work involved drying methods which painted car will have to dry in the oven booth before goes to assembly shop. The building itself was enclosed, so that the heat generated by oven booth will accumulated gradually through section. As a result, workers who worked nearest the heat source were potentially exposed to the hot environments. Environmental factors such as ambient temperature, relative humidity, radiant heat, conduction, air velocity and work process can cause heat stress problems to the workers in hot workplaces (OSHA, 1999).

Paint shop was consider in hot (WBGT >28 °C) compared with body shop (WBGT ≤27.9 °C). Its mean, the workers who worked in paint shop were potentially exposed to heat stress problems compared workers in body shop (Ramsey, 1999). A paint shop was considered hot-dry section (RH% >50) and body shop was considered hot-warm (%RH 50-70). A study by Aziz (2003) showed workers in paint shop section were pruned to have heat stress problems in hot-dry condition. The workers in body shop can also have heat stress problems in hot-warm condition. If there is not air movement, the rates of sweat evaporation on skin decreased if humidity increased. So, hot-warm can be stressful than hot-dry condition (BOHS, 1990). According to standard of screening criteria for heat stress exposure table 1 and table 2 by AGCIH, workers in both sections can worked in their work-rest regime schedule without having heat stress problems. Work-rest regime is very important in preventing heat stress in hot environment (OSHA, 1999). If the workers worked in very hot environment with unsuitable work-rest regime, heat stress may high to them.

Acclimatization program can increase the capability of heat tolerance to the workers who worked in hot condition (Graveling et al, 1998). Acclimatized workers can prevent the heat stress problems because their physiological system will responds immediately when they were exposed to hot environment. Acclimatization program in 7-14 days can improve the workers capability to the hot environment (Wildeboor and Camp, 1993). Therefore this program should be implemented in hot area like paint shop section.

Heat stress monitoring in potential hot workplace should be monitor regularly. Thermal indices like WBGT is the easiest way to predict the heat stress problem to the workers. Although, this index is not giving more information on physiological changes in workers who worked in hot environment, this is the effective way for early detection. The most important system to tackle heat stress problems is heat stress management program. Beside, the engineering control in workplace, training and education in heat stress management to the workers can create the awareness among them when working in hot situation. Then, heat stress problem can be reduced and safety and health of the workers will be protected.

6. References

ACGIH. (1992). *A manual of recommended practice*, American Conference of Govermental Industrial Hygienists

ACGIH. (2001). *American Conference of Governmental Industrial Hygienists - Threshold Limits Values and Biological Exposure Indices for 2001*, American Conference of Governmental Industrial Hygienists

Bascom, R. Kesavanathan, J. Swift, D.L. (1995). Human susceptibility to indoor contaminants. *Occupational Medicine* 10 (1), 119-132.

BOHS (1990). *The Thermal Environment*. Technical Guide # 8, British Occupational Hygiene Society

Berglund, B. Brunekreef, B. Knoppel, H. Lindvall, T. Maroni, M. L. Skov, P. (1992). Effects of indoor air pollution on human health. *Indoor Air* 2(1), 2-25.

DOSH. (1996). *Guidelines on occupational safety and health in the office*. Putrajaya: Department of Occupational Safety and Health, Ministry of Human Resource Malaysia.

DOSH. (2005). *Code of practice of indoor air quality*. Putrajaya: Department of Occupational Safety and Health, Ministry of Human Resource Malaysia

DOSH. (2006). *Annual report 2006*. Putrajaya: Department of Occupational Safety and Health, Ministry of Human Resource Malaysia

Esquer J, N. Elenesb, A. Zavala. (2009) Pollution Prevention in an Auto Assembly Plant in Mexico. In. *2nd International Workshop | Advances in Cleaner Production. Key Elements For A Sustainable World: Energy, Water And Climate Change*. São Paulo – Brazil – May 20th-22nd – 2009

Granadillos, N. G. (1998). A study on the assessment of heat stress among Filipino workers. Workshop on health and working conditions in South East Asia, Rangsit University, Thailand

Graveling, R. A., L. A. Morris, et al. (1998). *Working in hot conditions in mining: A literature review.* HSE Contract Reserach Report No. 10/1998. HSE, Institute of Occupational Medicine

Guo, S.C.L. Chan, L.Y. (2004). Indoor air quality in ice skating rinks in Hong Kong. *Environ Res*; 94: 327-35.

Harrison, P.T.C. (2002). Indoor air guidelines. *OccupEnviron Med*; 59: 73-4.

Jones, A.P. (2002). Indoor Air Quality. In. *Air Pollution Science for the 21st Century.* Edited by J. Austin, P. Brimblecombe and W. Sturges. Elsevier Science Ltd.

Kvarnström, S. (1997). *Stress prevention for blue-collar workers in assembly-line production,* 1–32, ILO, Geneva.

Maroni, M. Seifert, B. Lindvall, T. (1995). *Indoor Air Quality - a Comprehensive Reference Book*. Elsevier, Amsterdam.

NIOSH. (1986). *Criteria for a recommended standard...Occupational exposure to hot environments: Revised criteria.* Washington, D.C., National Institute for Occupational Safety and Health

NIOSH. (1993). *In-depth survey report: control technology for autobody repair and painting shops at Team Chevrolet, Colorado Springs, Colorado. Cincinnati.* US Department of Health and Human Services, Centers for Disease Control, National Institute for Occupational Safety and Health, DHHS-NIOSH.

OSHA. (1999). Heat stress: *OSHA Technical Manual*, U.S. Department of Labor.

Prime Minister's Department. (2005). *National automotive policy framework*. Putrajaya: Prime Minister's Department.

Ramachandran, G. Adgate, J.L. Church, T.R. (2002). Indoor air quality in two urban elementary schools: comfort parameters and microbial concentrations in air and carpets. California: *The 9th International Conference on Indoor Air Quality and* Climate, 2002.

Ramphal, L. (2000). Heat stress in the workplace. *BUMC PROCEEDINGS*; 13:349–350

Ramsey, J. D. (1999). Limiting injury/illness at the hot workplace. <u>*Safety Science Monitor*</u> Retrieved 27 July, 2005, from

http://www.monash.edu.au/muarc/ipso/vol3/oh1.pdf

Seltzer, J.M. (1997). Sources, concentrations, and assessment of indoor pollution. In: Bardana, E.J., Montanaro, A. (Eds.), *Indoor Air Pollution and Health*. Marcel Dekker, New York, pp. 11-60.

Simon, H.B. (1994) Hyperthermia and heatstroke. *Hosp Pract*. 29(8): p. 65-8, 73, 78-80.

TSI Inc. (2003a). *Q-Trak Plus IAQ Monitor Model 8552/8554: Operation and service manual*. Shoreview, MN: TSI Inc,

TSI Inc. (2003b). *DUSTTRAK Aerosol Monitor: operation and service manual Model 8520*. Shoreview, MN: TSC Inc,

Wildeboor, J. and J. Camp (1993). Heat stress: its effect and control. *AAOHN J* 41(6): 268-74

Fungal air quality in medical protected environments

Ricardo Araujo [1] and João P. Cabral [2]

1. IPATIMUP, Institute of Molecular Pathology and Immunology, University of Oporto

2. Department of Biology, Faculty of Science, and CIIMAR, University of Oporto Portugal

1. Introduction

Fungi are ubiquitous in indoor environments and are responsible for a wide range of diseases, from localized non-invasive pathologies to invasive and disseminated infections. These infections occur predominantly among highly immunosuppressed patients (patients with acute leukaemia, haematopoietic stem cell or solid organ transplantation) and can have devastating consequences. *Aspergillus* remains the most common mould to cause invasive infections, but other fungi are emerging as serious pathogens and threats in immunosuppressed patients. Most invasive fungal infections are acquired from air. It is therefore imperative to adopt, in clinical environments, preventive measures in order to reduce airborne fungal concentrations and, concomitantly, the risk for development of a fungal infection. At present, there are no methods and equipments that can completely eliminate fungi from indoor medical environments. Exposure to moulds in medical units is inevitable but the presence of air filtration systems, isolation, and adoption of environmental protective measures do mitigate patient exposure. Airborne mycological investigations should inform about indoor air quality and therefore should be routinely carried out in hospitals or other institutions where immunosuppressed individuals are treated. It is important to improve the methods already available to study indoor fungi in clean environments, and it is critical to define indicators of indoor air quality in medical environments. The present chapter deals with the biology of indoor fungi in medical environments, and the strategies and technical progresses that are at present available to prevent and control fungal diseases and to improve air quality in medical facilities.

2. Indoor fungi and medical environments

2.1 Main fungi in indoor environments

Fungi are ubiquitous in all atmospheres. In general, both outdoor and indoor atmospheres are dominated by species of *Cladosporium*, *Penicillium*, *Aspergillus* and *Alternaria*, and by yeasts and *Mycelia Sterilia*. *Cladosporium* is always the dominant fungus in outdoor atmospheres and in indoor atmospheres of normal and healthy buildings (except hospitals

where *Aspergillus* and *Penicillium* are usually dominant). The abundance of the other fungi varies with the season and place. In relation to outdoor environments, indoor atmosphere typically display lower diversity and abundance of fungi (Dacarro et al., 2003). The following genera can be represented indoors, but are always in clear minority: *Absidia*, *Acremonium*, *Arthrinium*, *Aureobasidium*, *Beauveria*, *Botrytis*, *Candida*, *Chaetomium*, *Chrysosporium*, *Epicoccum*, *Fusarium*, *Gliocladium*, *Mucor*, *Nigrospora*, *Paecilomyces*, *Phoma*, *Rhizopus*, *Scopulariopsis*, *Sporobolomyces*, *Stemphylium*, *Syncephalastrum*, *Trichoderma*, *Ulocladium* and *Verticillium* (Dacarro et al., 2003; Flannigan, 1997; Horner et al., 2004; Jo & Seo, 2005; Martinez et al., 2004; Sautour et al., 2009; Shelton et al., 2002).

Climate and human activities are the main factors that influence the composition of outdoor atmosphere. In the temperate climates, these display a typical pattern around the year. On the contrary, climate is not determinative in the mycoflora of indoor atmosphere, but human activities and the quality and maintenance of the building do play a major role in these environments. For these reasons, dominant fungi indoors vary between buildings and can be used as monitors of indoor air quality (Araujo et al., 2008a).

In the atmosphere, fungi are present in bioaerosols. Bioaerosols contain bacterial and fungal cells and cellular fragments, and products of microbial metabolism. Fungal spores constitute a significant fraction of bioaerosol microbial particles, and are often 100-1000 times more numerous than other bioparticles, like pollen grains. The particulate fraction in a bioaerosol is generally 0.3-100 μm in diameter. Fungal spores larger than 10 μm are deposited in the nasopharynx and can unchain nasal and ocular disorders. The respirable size fraction of 1-10 μm is of primary concern. Spores and fragments smaller than 10 μm (especially those smaller than 6 μm) can be transported to the lower airways and lungs, and trigger allergic reactions or infect tissues (Martinez et al., 2004; Stetzenbach et al., 2004). Bioaerosols that range in size from 1 to 5 μm generally remain in the air, whereas larger particles are deposited in the surfaces. Physical and environmental factors affect the settling of bioaerosols. Air currents, relative humidity and temperature are the most important environmental parameters affecting bioaerosol settling. The most significant physical parameters are particle size, density and shape (Martinez et al., 2004; Stetzenbach et al., 2004).

A human inhales on average 10 m³ of air per day, and spends 80-95 % of their time indoors. Indoor air pollution is therefore frequently reported to cause health problems (Dacarro et al., 2003).

2.2 The variability of indoor concentrations - outdoor air and other routes

Shelton et al. (2002) presented an exhaustive study of the mycoflora of outdoor and indoor atmospheres in all USA regions. More than 12,000 samplings were carried out, both in outdoor and indoor atmospheres in more than 1,700 buildings. The median of total indoor concentrations was 82 colony forming units (CFU) x m^{-3}, and of *Cladosporium*, *Penicillium*, *Aspergillus* and *Mycelia Sterilia*, was 40, 30, 20 e 30 CFU x m^{-3}, respectively. The median of the ratio indoor/outdoor was 0.16.

There are two main sources for indoor fungi. Outdoor sources are usually dominant. Most fungi present indoors come from outdoors (Flannigan, 1997; Horner et al., 2004). Another source is indoor environment itself. Fungi can grow in building materials, foodstuffs, flower pots, pet bedding materials, and house dust (Chao et al., 2001; Pasanen et al., 1992a, 1992b).

If suitable conditions exist, growth and sporulation in these substrates can be significant, and constitute a major source of fungi indoors (Pasanen et al., 1992a).

The mycoflora composition of outdoor and indoor atmosphere displays high variability. Fungi in the atmospheres vary along the year and during the day. For this reason, a reliable estimate of fungal levels in the atmosphere demands multiple determinations carried out in different seasons (Jantunen et al., 1997). Temporal variability is a major problem in assessing human exposure to indoor fungi. This variability is mainly due to the release of fungi from carpets and walls or other surfaces. This release depends on the type and degree of activity of occupants in the dwelling or building. All activities in buildings disturb settled fungal particles, but cleaning, constructional work and any other major dust-raising activities have a particular impact (Flannigan, 1997). To circumvent this temporal variability of indoor mycoflora, it has been suggested that floor dust should be sampled instead of the air, since it provides a long-term accumulation of previously airborne fungi. However, although house dust fungi reflect atmospheric populations, there are qualitative differences between these two mycofloras, probably resulting from the differences in the environments. Sampling of dust should not be used as a substitute for air sampling. In addition, viable counts for settled dust are much higher than corresponding air sampling counts for aerosolized dust, suggesting that many microbes in dust either form aggregates or are carried on dust particles which settle very rapidly (Flannigan, 1997).

2.3 Fungal growth, sporulation and adaptation to xerophylic conditions

Fungi from the atmosphere and indoor environments are influenced by temperature and humidity (atmospheric relative humidity and substrate moisture content). The optimum temperature for growth and sporulation is usually around 25-30 °C. Lower or higher temperatures result in lower growth and sporulation rates. A remarkable exception comprises fungi that can infect humans, such as those involved in aspergillosis and candidiasis, which display an optimum temperature around 37 °C (Araujo & Rodrigues, 2004). Temperature is usually not limiting in indoor environments, since most indoor fungi can grow in a wide range of temperatures (Douwes, 2009; Verhoeff, 1993).

Humidity is the most important factor determining fungal growth in indoor environments (Nielsen, 2003). Atmospheric relative humidity influences directly the release of conidia from conidiophores, and concomitantly, the concentration of spores in the atmosphere. Different patterns are displayed by *Cladosporium* and *Penicillium*. Whereas in *Cladosporium*, spore release is favoured by low humidity, the opposite behaviour is displayed by *Penicillium* (Pasanen et al., 1991). These differences influence the seasonal patterns of outdoor fungi. *Cladosporium* have maxima in the summer, but *Penicillium* display higher concentrations in the wetter months (Flannigan, 1997; Sautour et al., 2009; Verhoeff, 1993).

Fungal growth in building materials is more dependent on the moisture content of the substrate than on atmospheric relative humidity. The minimum moisture content of building materials allowing fungal growth is near 76 % (for atmospheric relative humidity, this value is near 82 %). Wood, wood composites (plywood, chipboard), and materials with a high starch content are capable of supporting fungal growth, at the lowest substrate moisture content. Plasterboard reinforced with cardboard and paper fibres, or inorganic materials coated with paint or treated with additives that offer an easily-degradable carbon source, are excellent substrates for fungal growth when substrate moisture content reaches 85-90 % (Nielsen, 2003; Pasanen et al., 1992b). All fungi need nutrients for growth and

sporulation. When growing in indoor substrates such as food, nutrients are not limiting, but on the surface of certain building materials, nutrients may limit fungal growth (Pasanen et al., 1992b). Local differences in ventilation and surface temperature can generate micro-climates with very high substrate moisture content, although the room can have a low atmospheric relative humidity. For this reason, a measurement of indoor atmospheric relative humidity is a poor predictor of indoor fungal growth (Nielsen, 2003).

Xerophilic fungi are well adapted to indoor environments, since these fungi grow and sporulate with low atmospheric relative humidity and substrates with low moisture content. Indeed, the majority of *Aspergillus* and *Penicillium* species are xerophilic and able to growth in substrates with water activity lower than 0.80 (Pasanen et al., 1992a; Verhoeff, 1993). Most of the other indoor fungi (namely *Cladosporium*, *Stachybotrys*, *Chaetomium*, *Trichoderma* and *Ulocladium*) are much less tolerant to xerophilic conditions (Pasanen et al., 1992b). Because of their low water activity requirements (compared with bacteria), fungi are the principal contaminant in various types of indoor substrates. They tend to colonize a wide variety of humid building materials wetted by floods or by plumbing leaks (Dacarro et al., 2003).

2.4 Fungal fragments and allergenicity

Until 1990-2000, it was thought that indoors fungi exist only as spores and hyphae. Work published by several teams showed that fungi from the atmosphere, growing in culture media or building materials, subjected to air currents, release cellular fragments (presumably hyphal and spore fragments). The presence of these fragments in indoor air was confirmed experimentally.

For three common species from the atmosphere, growing in culture medium or building material, Górny et al. (2002) showed that when the colonies were subjected to air currents, the number of released fragments was higher that the number of spores. Fragments released from fungi growing in culture medium were not influenced by air velocity. Kildesø et al. (2003) reported the release of spores and fragments from colonies of three different species. When *Penicillium chrysogenum* was subjected to air currents, only spores were released from the colonies, but with *Aspergillus versicolor*, 1 μm fragments were also released, in addition to individual spores. With *Trichoderma harzianum*, three types of particles were released from the colonies: groups of spores; individual spores; and fragments. The release of fragments and spores from indoor fungi (*A. versicolor* and *Stachybotrys chartarum*) growing on the surface of white ceiling tiles, wall-papered gypsum board and culture medium, and subjected to air currents, was recently reported by Seo et al. (2009). One month-old cultures released more spores than fragments, but after six month incubation, the number of released fragments exceeded the number of spores. The mass of released fragments and spores (assessed by the amount of (1,3)-β-D-glucan) generally increased with age of the cultures.

The presence of fungal fragments in indoor atmosphere, predicted by these studies carried out *in vitro* (in laboratory conditions), was confirmed by field determinations. Reponen et al. (2007) reported a study carried out in five mould-contaminated single houses in Louisiana and Southern Ohio. Indoor total spore concentrations were very high and higher than outdoor concentrations (both in winter and summer). Assessed by the 1,3-β-D-glucan concentration, the ratio between fragments and spores ranged from 0.011 to 2.163, the highest average (1.017) being for indoor samples collected in the winter. Considering that fragments are much smaller than spores, the corresponding number of fragments in indoor air in these houses was certainly much higher than the number of spores. It was concluded

that, in mouldy houses, fungal fragment mass can be as high as spore mass, and fragment number can exceed total spore number.

Long-term mould damage in buildings may increase the contribution of submicrometer-sized fungal fragments to the overall mould exposure. The health impact of these particles may be even greater than that of spores, considering the strong association between numbers of fine particles and adverse health effects reported in other studies (Reponen et al., 2007; Seo et al., 2009).

However, there are at present no detailed morphological and cultural studies of these fragments released by fungal colonies subjected to air currents, and therefore important questions remain open. Are these particles, fragments of spores or of hyphae? Are they viable and able to grow in culture media and in the respiratory tract?

It has been demonstrated that *in vitro*, depending of the fungal species and tested antibody, immunological reactivity of fungal fragments is 2 to 5 times higher than conidia, (Górny et al., 2002). In several moulds responsible for releasing airborne allergens, Green et al. (2005b) found that many of the allergens were in hyphal fragments. Germinated conidia and hyphae may be more allergenic than fungal conidia, but personal exposure to fungal allergens may be difficult to evaluate (Górny et al., 2002; Green et al., 2005a). Common fungal allergens described in the literature include *Aspergillus* Asp f 1, Asp f 3, Asp f 6, and *Alternaria* Alt a 1 (Chapman et al., 2001; Crameri & Blaser, 2002). Few enzyme-linked immunosorbent assays (ELISA) are commercially available for quantification of these allergens in environmental and house-dust samples. Very often, the allergens are not detected by available immunological methods and protocols. Chapman et al. (2001) reported that in order to detect allergens in spore suspensions, it was necessary to use heavily concentrated suspensions (>100,000 conidia x ml^{-1}). This may hampered the direct detection of allergens in atmospheric sampling.

In the human body, mucociliary clearance represents the first strategy for removal of airborne fungi from the respiratory tract. This can be followed by the activation of innate and adaptive immune responses. Occasionally, inflammation occurs and individuals may suffer mucous membrane irritation, chronic bronchitis and/or organic dust toxic syndrome. The most common inflammatory reactions to fungi are non-allergic, but an allergic response or a hypersensitivity pneumonitis can occur in individuals exposed to conidia, hyphae or fungal fragments (Eduard, 2009; Green et al., 2006).

More sensitized individuals may suffer from allergy following exposure to fungi. These patients usually present high IgE values and increased release of some inflammatory mediators. Houba et al. (1998) described baking workers with high IgE against common allergens. These professionals presented an increased risk for mould occupational allergy. Allergic bronchopulmonary aspergillosis (ABPA) is also an allergic response, but specific to *Aspergillus fumigatus* allergens present in the environment. The disease is more frequent among patients with asthma or with cystic fibrosis. The usual complains are breathless, pulmonary infiltrates, bronchiectasis and fibrosis (Stevens et al., 2003). Patients' serum display high levels of total IgE, specific *A. fumigatus* IgE and IgG antibodies, IL-2 receptor, and precipitins to *A. fumigatus*.

Besides an allergic response, hypersensitivity pneumonitis can occur upon exposure to fungi. This pathology, as described by the European Academy of Allergy and Clinical Immunology (www.eaaci.net), is generally associated with high IgG antibodies concentrations in response to alveolar or bronchiolar inflammation caused by fungi or other

allergens. On the contrary of allergy, this type of hypersensitivity to fungal allergens does not seem to be mediated by IgE. The patients may present neutrophilic inflammation with increased production of TNFα and IL-6, and symptoms such as fever, chilliness, dry cough, dyspnoea, changes in nodular bilateral x-ray, fatigue and headache (Eduard, 2009).

In some asthmatic patients, fungi seem to exacerbate symptoms, but in others this effect has not been found. Newson et al. (2000) described an association between airborne total fungal counts and incidence of severe asthma in England's Trent region. However, no specific fungal species were implicated. A twofold reduction of airborne exposure to allergens has been reported to reduce the risk of developing asthma and asthma severity (Peat & Li, 1999). Other studies reported no evidence of association between airborne fungi and asthma (Richardson et al., 2005). Thus, further studies are needed in order to clarify this problem.

2.5 Production of microbial volatile compounds and mycotoxins

Indoor atmosphere always contain a mixture of volatile organic compounds (VOCs), usually at low concentrations. It is not uncommon to detect 50 different compounds, each at a low concentration (usually below 5 µg x m^{-3}, but can exceed 100 µg x m^{-3}). Indoor atmosphere usually contain higher VOCs concentrations than outdoor atmospheres. VOCs belong to very different chemical groups, such as hydrocarbons, alcohols, acetones, S compounds, ethers, esters, N compounds, terpenes and acids (Jantunen et al., 1997; Portnoy et al., 2004).

Traditionally, sources for indoor VOCs were considered to be the outdoor air, the activities of people living and working inside the building, and the building materials and furniture. Modern buildings' atmosphere usually contain higher VOCs concentrations in relation to older constructions, due to VOCs' release from building materials (Jantunen et al., 1997). Studies carried out in the 1990s, showed that indoor fungi can also be a source for the production of VOCs. Some of the molecules produced by indoor fungi are not produced by other sources (Douwes, 2009; Verhoeff, 1993). Several authors have shown that fungi from the atmospheres growing in culture media, in building materials or in house dust, do produce an array of VOCs, and that these differed in the three growing conditions (Claeson et al., 2002; Fischer et al., 1999).

Far more difficult has been the detection and identification of fungal-produced VOCs directly in the atmosphere, due to their usually very low concentrations. The production of VOCs by fungi growing *in vitro* in the laboratory strongly suggests, but does not prove, that these compounds do exist in the atmospheres. Fischer et al. (2000) demonstrated that, in highly contaminated outdoor atmospheres, certain fungal-produced VOCs were detectable and identifiable. This was certainly related to the huge concentrations of fungi in the studied atmospheres.

When applied isolated, the negative effects on human body of several of these VOCs are known, and these could be used to establish safe limits, for indoor atmospheres. However, it is far more difficult to determine the effects of mixtures of compounds, the commonest situation in indoor atmospheres. For these there are no proposed safe limits (Jantunen et al., 1997).

A specific VOC fingerprint for each fungal species may be difficult to achieve, because emission patterns can vary between strains and the release of some compounds may be dependent on the growth phase. Using commercial materials (such as fibreglass, vinyl wallpaper, cork, ceiling tiles, and plasterboard) previously contaminated with conidial suspensions of *Aspergillus niger*, *Aspergillus versicolor* or *Penicillium brevicompactum*, Moularat

et al. (2008a) concluded that VOCs could be used for a preliminary characterization of the fungal diversity in air or dust samples. However, it was not possible to find VOCs specific for each fungal species (the profile changed with substrate). A second study with materials inoculated with conidial suspensions of the same three fungal species and placed in closed chambers showed that fungi, even before visible growth occurred, released 19 different VOCs, suggesting that identification of these molecules can be used for a rapid and reliable detection of the presence of fungal growth in materials (Moularat et al., 2008b). Schleibinger et al. (2005) studied the release of VOCs by *Penicillium brevicompactum*, *Aspergillus versicolor*, *Eurotium amstelodami* and *Chaetomium globosum* (two strains of each) growing in five different substrates. It was found that fungi released low amounts of VOCs, these encompassed a wide diversity of molecules, and there was a variation between the molecules released from the two strains tested for each species.

Mycotoxins are low molecular weight compounds, produced by fungi, toxic for animals and men, with no known function in fungal metabolism. Many mycotoxins are carcinogenic, teratogenic and mutagenic (Hintikka & Nikulin, 1998; Martinez et al., 2004; Portnoy et al., 2004). *Penicillium* and *Aspergillus* species are important fungi in indoor atmosphere, and many of these species were known mycotoxin-producers (Nielsen, 2003). It remained to be studied if *Penicillium* and *Aspergillus* present in the atmosphere also produce mycotoxins, and this was demonstrated from the beginning of the 1990s. When fungi common in the atmospheres and house dust were cultivated in building materials, several mycotoxins were produced *in vitro* (Nielsen, 2003; Nieminen et al., 2002). Mycotoxins have also been isolated directly from fungi-contaminated building materials and house dust (Hintikka & Nikulin, 1998).

However, the production of mycotoxins by indoor fungi growing in building materials is much lower (can be absent) than the production in culture medium, probably due to the much lower concentration of nutrients in the former conditions (Nielsen, 2003). Ren et al. (1999) even reported no mycotoxin production from several *Aspergillus* strains (isolated from indoor air) growing on building materials (although most of the strains did produce mycotoxins when grown in culture media).

As with the VOCs, it has been very difficult to detect, directly in the atmosphere, the presence of mycotoxins (Hintikka & Nikulin, 1998; Nielsen, 2003; Martinez et al., 2004). Papers by Fischer et al. (1999, 2000), among others (Hintikka & Nikulin, 1998), which are innovative in this subject, have since reported the detection directly in the filters of triptoquivaline and tripacidine, both produced by *A. fumigatus*, one of the most abundant fungi in the studied atmosphere. As for VOCs, the detection of these mycotoxins was most probably related to the very high concentration of spores in the analyzed atmosphere.

Trichothecenes are a family of mycotoxins produced by species of *Fusarium*, *Myrothecium*, *Trichoderma* and, specially important for indoor environments, *Stachybotrys*. Several tens of compounds have been described in this group. From these, stand out toxins T-2 and HT-2, nivalenol, desoxynivalenol and diacetoxyscirpenol. The effects of tricothecenes in humans and domestic and farm animals are well known for decades. The symptoms include internal burning, vomiting, diarrhoea with blood, cutaneous necrosis and internal haemorrhages, followed by death (Hintikka & Nikulin, 1998; Nielsen, 2003).

At high concentrations, mycotoxins induce acute intoxications, and the negative effects are relatively straightforward to examine and quantify. At low or very low concentrations, the problem is far more complicated. In very few cases (liver cancer induced by aflatoxins in

certain African regions, for instance), it has been possible to establish a correlation between the presence of a given mycotoxin in the human diet and the incidence of a certain disease. In comparison with food and fodder, mycotoxins concentrations in the atmosphere are expected to be very low. Moreover, the simultaneous presence of several adverse and negative factors in indoor atmosphere (mycotoxins and VOCs, for instance), is not uncommon. For these reasons, it has been difficult to establish a correlation between the presence of given mycotoxins in indoor environments and health problems of their occupants (Douwes, 2009; Mendell et al., 2009; Nielsen, 2003; Verhoeff, 1993).

However, in certain situations, the evidence for this association is substantial (Rea et al., 2003). Flappan et al. (1999) reported a case of infant pulmonary haemorrhage in a home in Missouri (USA). Inspection of the house revealed serious water infiltrations in the attic and in the baby's bedroom closet. Indoor air sampling (using a volumetric spore trap and microscopic total spore counts) carried out in five different rooms revealed huge air total spore concentrations in the baby's room (higher than 10,000 spores x m^{-3}), and very high concentrations in baby's bedroom closet, in the attic and in the family room (higher than 2,000 spores x m^{-3}). *Aspergillus* and *Penicillium* were largely dominant in the air of all rooms. *Stachybotrys* was detected only in the atmosphere of the baby's bedroom. Surface samples taken from water-damaged building materials from several rooms, and dust from baby's bedroom, contained *Stachybotrys*. In contaminated building materials were detected several trichothecene molecules. This case was similar to others reported in the Cleveland area in 1993-1998, which resulted in the death of 12 infants.

Additional research employing new technologies and modern equipments (particularly mass spectrometry and/or gas chromatography) will certainly be conducted on this subject in a near future (Schuchardt & Kruse, 2009).

3. Detection of fungi in indoor environments

3.1 Volumetric and sedimentary methods

Atmosphere sampling for bioaerosols has been conducted for decades with classical monitoring that relies on collection using forced air samplers and analysis by either culture media or microscopy (Stetzenbach et al., 2004).

Quantitative microbiological methods for atmosphere analysis witnessed important developments in the 1940s-1960s.

K. R. May's cascade impactor, described in 1945 (May, 1945), was one of the first instruments that allowed the detection of fungal cells, since collected all particles with 0.6-20 µm. The cascade impactor consisted of a system of four air-jets and sampling slides in series. The slits were progressively narrower, so that the speed jet and therefore the efficacy of impaction of particles increase from slide to slide. Particles impacted on glass slides covered with an adhesive substance, and, at the end, were counted by optical microscopy. The instrument allowed discrimination of the particles by size due to the four successive stages (Burge & Solomon, 1987; Davies, 1971).

An improvement of May's device was carried out by J. M. Hirst, in 1952 (Hirst, 1952). The instrument was also a slit sampler based on impaction on an adhesive surface, but allowed monitoring during a whole day (achieved by the slow and constant displacement of the slide underneath the slit) and with strong winds and rain. The equipment was reliable for

capturing large spores. Small spores such as those of *Aspergillus* and *Penicillium* were underestimated (Davies, 1971; Martinez et al., 2004).

May and Hirst slit impactors allowed no distinction between viable and dead cells, and, very importantly, did not enabled a rigorous identification of the fungal spores, since morphological characteristics of these cells only allow an identification at a genus level, and only for a restricted group of fungi (Stetzenbach et al., 2004). These drawbacks were resolved in the slit sampler developed by Bourdillon and collaborators in the 1940s (Bourdillon et al., 1941). Using the same principle of air suction through a narrow slit, a Petri dish with culture medium was placed underneath. The dish slowly rotated during sampling, so that an annular ring trace was formed in the agar. Bacteria were collected with very high efficiency (Davies, 1971; Henningson & Ahlberg, 1994).

A great step forward was given by Andersen in 1958, with the design of a six-stage impactor, with collection of particles on culture medium (Andersen, 1958). Air sucked passed six successive aluminium plates drilled with decreasing size holes. Underneath each plate was placed a Petri dish with culture medium. The decreasing size of the holes forced air to accelerate from the upper to the lower stage. The upper stage collected the biggest particles and the lowest stage the smallest cells. Between these, increasingly smaller cells were collected. Andersen sampler allowed discrimination of the particles by size, the determination of the concentration of culturable cells, and, after observation of the colonies, the identification of the fungi at species level (Eduard & Heederik, 1998; Flannigan, 1997; Henningson & Ahlberg, 1994; Martinez et al., 2004; Stetzenbach et al., 2004).

May, Hirst, Bourdillon and Andersen samplers were based on impaction on a solid surface - the projection of particles onto the surface of a glass slide or culture medium. By the time of design of these samplers, impingement - blowing the particles into a liquid by the use of glass impingers – was also improved in order to be used in microbiological analysis. Impingement is based on the suction of the air through a narrow capillary tube, and projection of the air jet into a liquid. Particles present in the atmosphere, such as fungi, are forced to enter the liquid.

From impinger models adapted to microbiological uses, stands out the all-glass impinger AGI-30 described by Malligo & Idoine (1964) and the three-stage impinger described by K. R. May, in a paper published in 1966 (May, 1966). AGI-30 impinger was developed from the AGI-4 model - the Porton impinger. The inlet was designed to simulate the human nose. The jet nozzle was raised above the liquid in order to get an impingement surface softer than the glass bottom of the flask. The collection efficiency for bacteria was very high (Eduard & Heederik, 1998; Henningson & Ahlberg, 1994).

The multi-stage liquid impinger of May (1966), built in thick walled Pyrex glass, had three superimposed chambers. In the first two chambers, air-jets impacted vertically on to glass discs filled with sampling liquid. The third chamber was a bowl-shaped swirling impinger (Eduard & Heederik, 1998; Henningson & Ahlberg, 1994; Martinez et al., 2004).

Impingement has some advantages over impaction on solid surfaces: 1) if the concentration is too high, the liquid can be diluted; 2) affords, simultaneously, total cell counting (by microscopy) and culturable cell counting (by culturing aliquots on nutrient media); 3) different culture media can be used, at the same time, to study a given sample; 4) collection of the cells in a liquid avoids desiccation resulting from impaction on solid surfaces, especially on glass slides; 5) cell clusters, kept intact when using impaction of agar medium, are dissociated in their individual cells; 6) the particle retention efficiency is very high; 7) the

equipment is compact and inexpensive (Martinez et al., 2004; May & Harper, 1957; Stetzenbach et al., 2004). The method has however some limitations: 1) it is not appropriate for clean atmosphere, since a reduced number of cells will be present in a relatively large volume of liquid; 2) after certain time of operation, the liquid, which is under low pressure, evaporates appreciably; 3) the efficiency for collecting bacteria is higher than for spores (Eduard & Heederik, 1998).

In addition to impaction and impingement, other methods have been used in the study of fungal populations in atmospheric bioaerosols. In filtration methods, filters collect particles through impaction and interception mechanisms. Filter materials commonly used for air microbiological sampling include glass fibre filters, mixed cellulose esters, polytetrafluoroethylene, polyvinyl chloride, gelatine, and polycarbonate (Eduard & Heederik, 1998; Martinez et al., 2004). Advantages of filter sampling include the simplicity of collection and sample handling procedures, the ability to perform different analyses on the same extraction solution, and the relatively inexpensive cost. Membrane filters can be placed directly on the surface of culture medium, or washed with a liquid, and this added to culture medium. Certain filters are dissolvable in warm liquids, and the resulting suspension can be platted on agarized medium. Two disadvantages for filter sampling are the low extraction efficiency from the filter material, and the dehydration of microorganisms, which reduces their cultivability (Martinez et al., 2004).

Sedimentary sampling is generally carried out using the settle plate method. Open Petri dishes with appropriate culture medium are left open during a given time (minutes, hours or days depending on the air contamination load). After a certain period of incubation, colonies are counted and identified. Sedimentary sampling has several advantages: 1) it is simple and inexpensive; 2) allow a cumulative assessment over a prolonged exposure times - «The cfu collected on settle plates are like a photocopy, or a mirror of what was going on at a particular point, during a period of time. Long sampling periods may increase measurement significance and reproducibility» (Pasquarella et al., 2000). The method suffers however from several limitations: 1) no known volume of air is analyzed, it is therefore not quantitative; 2) the rate of deposition of cells can be affected by air turbulence; 3) small cells tend to be under-estimated (Burge & Solomon, 1987; Pasquarella et al., 2000).

Pasquarella et al. (2000) argued extensively about the advantages of the sedimentary methods for hospital indoor microbial analysis. A new index was defined – the Index of Microbial Air Contamination (IMA), determined with the following procedure: «A standard Petri dish 9 cm in diameter containing plate count medium is left open to air according to the 1/1/1 scheme, for 1 h, 1 m from the floor, at least 1 m away from walls or any relevant physical obstacle. After 48 h incubation at 36±1 °C the colonies are counted. The number of colonies is the IMA». IMA classes and maximum acceptable levels of IMA were defined empirically. Five classes of IMA were devised: 0–5 very good; 6–25 good; 26–50 fair; 51–75 poor; >76 very poor. Maximum acceptable values of IMA were established, related to different infection or contamination risks. These were 5, 25 and 50, in places with very high, high and medium risk, respectively. For example, hospital operation rooms, with very high risk, should have a maximum IMA value of 5, corresponding to 9 CFU x dm^{-2} x h^{-1}. The authors also provided a comparison between IMA classes and several international standards.

Two standard incubation temperatures are used: 25-27 °C for growing the great majority of species, and 35-37 °C, for human-related species such as *Aspergillus fumigatus*, *A. flavus* and

A. niger (Araujo et al., 2008a). Spores of *Aspergillus* and *Penicillium* may survive for long periods, even years, whilst the cultivability or viability of others may decline very rapidly. The use of culture-based analysis methods underestimates populations in bioaerosols owing to the detection of only those fungi that grow in culture media, while non-culturable (live or dead) organisms go undetected. As with other environments, most of atmospheric fungi appear to be in a non-culturable sate (Flannigan, 1997).

Fungi are capable of causing health effects whether they are in the culturable or non-culturable but viable state. However, these effects are expected to be very different, but are poorly known. Can a live but non-culturable fungal spore, hypha or fragment grow on the surface of our respiratory epithelium? Enumeration of total fungi by microscopy lacks identification specificity, unless accompanied by specialized staining or immunological assay. Specific antibodies with heavy metals bind only to specific microbes that are viewed under scanning electron microscopy. Epifluorescence and electron microscopy has also been used. With fluorescence microscopy, microbes are stained with fluorochromes and are viewed with fluorescent light. Fluorescein diacetate (FDA) has been used for viable fungi. Scanning electron microscopy is useful for studying fungal spore surface characteristics, but is not routinely used for microbes' identification (Martinez et al., 2004).

In addition to these methods, biochemical assays that detect fungal specific molecules such as (1,3)-β-D-glucans, chitin, and ergosterol have been to estimate total fungal bioaerosol loads. These are particularly important for the quantification of fungal fragments, which are non-culturable and difficult to recognize by microscopy (Flannigan, 1997; Martinez et al., 2004; Stetzenbach et al., 2004). As Flannigan (1997) wisely remarked, most microbiological investigations of indoor air still employ culture-based methods, but sufficient attention is seldom given to four important issues: sampler performance, temporal variability, culture media and accurate identification. Too many studies identify only to the genus level and disregard the diversity of species, their ecology and potential significance for health, especially in important genera such as *Aspergillus* and *Penicillium*.

3.2 Molecular methods

Molecular biology has been increasingly applied in the evaluation of indoor air quality in medical environments. Quantitative PCR (QPCR) has been used for the detection of *Aspergillus*, *Penicillium* and *Paecilomyces* in the atmosphere of clinical wards (Haugland et al., 2004). Using this method, a comparative study carried out during and after construction works in clinical wards showed a generalized decrease in the atmospheric concentrations of these fungi (Morrison et al., 2004). QPCR has been employed for quantification of airborne fungi in other environments, such as allergic patients' homes. Whilst some studies could not find any correlation between the results using molecular and culture-based methodologies (Meklin et al., 2004; Pietarinen et al., 2008), others described, for some fungi (*Aspergillus*, *Penicillium* and *Cladosporium*) a significant correlation, but no association in other cases (*Acremonium*, *Aureobasidium* and *Wallemia*) (Lignell et al., 2008).

A consistent observation has been reported in all studies - molecular methods' sensitivity is considerably higher in comparison with traditional approaches based on culture methods (sometimes of several orders of magnitude). However, some fungi grow in culture but are not detected by molecular methods, and others do not grow in agarized media but are identified by molecular methods (Pietarinen et al., 2008). An example of differential results yielded by these two types of methods was recently presented by Bellanger et al. (2009) in a

study of allergic (with asthma, allergic rhinitis or conjunctivitis) patients' houses. *Aspergillus versicolor* grew well in culture media but went undetected by molecular methods. Molecular methods may not be able to detect all fungal species, particularly when large amounts of DNA of other fungi are present, or in presence of certain PCR inhibitors (those inhibitors can be present in the environment or be added through sample management). However, a wise selection of primers can detect many fungal species. Nevertheless, standardization of most procedures, such as extraction methodology, the selection of primers that should be employed for QPCR and amplification conditions, are still needed in order molecular methods be widely used and the results allow further comparisons.

3.3 Airborne fungal diversity and detection of rare taxa

Global assessment of the genetic diversity in a given environment has been studied using several molecular techniques. The metagenome description of the microbial communities in Sargasso Sea is still not concluded but a vast amount of new data was obtained (Venter et al., 2004). Metagenome fingerprinting techniques, such as automated ribosomal intergenic spacer analysis (ARISA), terminal restriction fragment length polymorphism (TRFLP) and denaturating gradient gel electrophoresis (DGGE), have been employed worldwide for measuring fungal species richness in communities. However, these methods may not reflect the actual microbial diversity, as they tend to identify only the dominant members of the community (Bent et al., 2007). ARISA is a high-resolution, highly reproducible, automated technique that uses the variability in the length of the intervening transcribed spacer regions (ITS) of rRNA genes in order to separate several samples into operational taxonomic units (OTUs). ARISA allows the characterization and distinction of fungal communities and has been employed to distinguish fungal soil communities from distinct cities and countries (Ranjard et al., 2001). The other two methods (TRFLP and DGGE) employ restriction enzymes or specific primers and non-automated gel electrophoresis for identification of microbial OTUs. TRFLP allowed a good characterization of fungal communities isolated from air samples collected from an urban area of Seoul (Korea) and soil samples in UK (Lee et al., 2010; Schütte et al., 2008).

Recently reported fungal metagenomic studies found that *Ascomycota* (*Dothideomycetes*, *Eurotiomycetes*, *Leotiomycetes*, and *Sordariomycetes*) and *Basidiomycota* (*Agaricomycetes)* were the most represented Divisions in outdoor atmospheres (Fröhlich-Nowoisky et al., 2009; Lee et al., 2010). Reports on fungal metagenome of indoor environments have been included in studies screening complete microbial communities (Angenent et al., 2005), but these are still very incomplete. The construction of metagenomic libraries is nowadays possible, although technically demanding and economically expensive. The future will bring new technologies and cheaper alternatives for sequencing large number of OTUs and these will allow knowledge of the composition of complete communities. The study of hospital metagenome can allow physicians, researchers and other medical staff a full knowledge of the microbial communities present inside medical wards. This is expected to give information on the presence of certain fungi in highly-restricted areas where critical patients are admitted, and therefore to have a considerable impact on public health.

Metagenomic strategies are not only an important tool for characterization of the genetic diversity in whole communities, but also represent an indispensable approach for detection of rare fungal taxa (by revealing new OTUs). Molecular methods such as QPCR are based on a previous selection of primers, and these are limited to *a priori* chosen taxa. These methods

cannot be used to find new taxa (Fröhlich-Nowoisky et al., 2009; Lee et al., 2010). The detection of rare taxa in the environment still remains a critical issue for the global understanding of the value and importance of each and all microorganisms. However, precautious should be taken against a simplistic interpretation of molecular data, since the presence of genetic material, even in good and preserved condition, is no guarantee that the organism is active (or alive) in the environment. In terms of interaction between the fungus and the human body, such active condition is probably indispensable for infection.

4. Air quality and fungal infections

4.1 Hospital indoor air quality and incidence of fungal infections

Many outdoor activities such as gardening, hunting, or camping, and few sports such as caving or cave diving, are associated with increased environmental exposure to pathogenic fungi and increased risk of invasive fungal diseases (IFDs) (Sipsas & Kontoyiannis, 2008). Inhalation of conidia and direct inoculation through minor skin lesions are the most common mechanisms for developing fungal disease. Some human practices, such as smoking tobacco or marijuana, use of illicit intravenous drugs, body piercing or tattooing, pet ownership, and travelling to endemic areas, are associated with an increased risk of IFD. Endemic mycoses usually occur in limited geographic areas and individuals outside the fungal ecological niche are not at risk of infection.

Immunocompromised patients are also at the highest risk for development of fungal infections in hospitals. The complete list of fungemia risk factors is vast, but the most relevant factors are: submission of patients to immunosuppressive treatments (such as chemotherapy, or corticosteroids therapy); neutropenia (<500 polymorphonuclear cells x ml^{-1}); treatment with antimicrobial agents; submission to bone marrow or solid organ transplants; previous colonization with fungal agents; presence of indwelling catheters; extensive surgery or burns; need of parenteral nutrition; assisted ventilation or haemodialysis; malnutrition; prolonged hospitalization particularly at intensive care units (De La Rosa et al., 2002; Fridkin & Jarvis, 1996). The most important fungal agents responsible for infection in these patients are *Candida*, *Aspergillus*, and several zygomycetes. In addition, emerging fungal pathogens (*Fusarium* sp., *Scedosporium* sp., *Thichosporon* sp. and *Malassezia* sp.) are becoming also a threat to these patients. Risk patients need to be protected from fungal pathogens, particularly by isolation in highly-restricted units, as most of these agents are airborne pathogens.

Aspergillus fumigatus is the main responsible for airborne infections in immunocompromised patients and one of the most common airborne moulds found indoors at clinical wards. The ability of the fungus to colonize and resist indoors, even under unfavourable conditions, and to germinate and grow faster under human internal milieu conditions (Araujo & Rodrigues, 2004) makes *A. fumigatus* one of the most serious fungal agents worldwide. The fungus is responsible for high mortality rates. Invasive aspergillosis generally involves inhalation of conidia or hyphae and further growth in human internal milieu. Vonberg & Gatsmeier (2006) reviewed all cases of invasive aspergillosis and concluded that the fungus is able to cause disease in environments with less than 1 CFU x m^{-3} of air. They recommended that risk patients should not be exposed to the fungus and concluded that prevention from all routes is critical. Patients staying long periods at clinical units with high degree and long duration of immunosuppression are at the highest risk for developing

invasive aspergillosis. In haematological patients, the incidence of fungal infections is higher in the group of patients suffering of acute leukaemia and aplastic anaemia malignancies (Araujo et al., 2008b; Pagano et al., 2006). In nosocomial aspergillosis, transmission occurs generally through the air, but the involvement of water (Warris et al., 2003), plants (Lass-Flörl et al., 2000), furniture (Menotti et al., 2005) or even person-to-person contact (Pegues et al., 2002) have been confirmed by molecular studies. In fungal infections caused by yeasts and other moulds, molecular studies have found a connection between the isolates collected from patients and from environmental samples (Cortez et al., 2008; Lupetti et al., 2002; Vos et al., 2006).

 Some studies have reported a decrease in the incidence of fungal infections in clinical units following a decrease in levels of airborne fungi (Alberti et al., 2001; Araujo et al., 2008b; Berthelot et al., 2006), but this improvement was not consistently found in all hospitals. One of the first studies reporting the absence of *A. fumigatus* infections in clinical environments with less than 0.1 CFU x m^{-3} was performed by Sherertz et al. (1987). No environmental breakpoints have been yet defined in order to completely prevent fungal infections in clinical units, nor it is well defined the frequency for collection of air samples and monitoring indoor air quality. Several measures have been described for protecting patients and decreasing the risk for acquisition of IFDs. Air filtration systems are the most used in clinical units, mostly the high efficiency particulate air (HEPA) filters, and they will be discussed in detail in the next topic.

4.2 Air filtration systems

As most indoor fungi came primarily from outdoors, it cannot be discarded the impact that an increase in outdoor fungi may have in increasing the risk of fungal diseases in clinical units. Some studies have tried to correlate outdoor fungal concentration and incidence of fungal diseases. However, other variables interfere with this relationship: the exact amount of fungi that in fact reach indoor air in clinical units; ventilation rates; protective measures present in wards (particularly the presence of air filtration systems); fungal colonization indoors; other routes for fungal access besides air; patient immune response; administration of prophylactic antifungal treatments. Nevertheless, some studies reported an association between outdoor fungi and incidence of indoor infections (Bouza et al., 2002; Radin et al., 1983; Srinivasan et al. 2002). The relationship between outdoor and indoor airborne fungi is much easier to find and has been observed by several researchers (Brenier-Pinchart et al., 2009; Curtis et al., 2005; Dassonville et al., 2008; Falvey & Streifel, 2007; Pini et al., 2004).

Air filters like F7-F9 retain around 90 % of the particles, while HEPA filters H13 retain 99.97 % of the particles with more than 0.3 μm. The installation of HEPA filters is commonly associated with positive pressure (>2.5 Pa) and air flow rates higher than 12 exchanges of air per hour (Sehulster et al., 2003). The complete HEPA filtration system is usually based upon a pre-filter G2-G4 (made of synthetic fibres, such as polyester, or glass fibre; with initial efficiency of around 70 %), a fine filter F5-F9 (several types are commercially available such as bag filters, rigid pocket, or cardboard filters), and a HEPA filter H10-H14. Pre-filters should be replaced often as they retain most part of airborne particles. The impact of filtration systems such as F8 or F9, and the presence of negative air flow, has been less studied than HEPA filters. F8 and F9 filtration systems may reduce significantly fungal air levels, but, as expected, are not as efficient as HEPA filters (Araujo et al., 2008a). Negative

air flow rates are presently forbidden in wards near renovation and construction sites (Sehulster et al., 2003).

Indoor levels of *Aspergillus* sp. can be greatly reduced by air filtration systems, such as the HEPA system, and this can result in a concomitant decrease in the incidence of invasive aspergillosis (Alberti et al., 2001; Araujo et al., 2008b; Vonberg & Gatsmeier, 2006). A significant reduction of *Candida* infections has been described after the installation of HEPA filters (Araujo et al., 2008b; Boswell & Fox, 2006). A systematic review focusing on the influence of HEPA filters in wards with immunosuppressed patients was recently reported by Eckmanns et al. (2006) who concluded that HEPA filters could be occasionally beneficial for patients. However, a significant decrease in fungal-related mortality rates was not found for HEPA protected areas.

All over the world, studies have been carried out in order to evaluate indoor air quality in medical facilities. The fungal airborne values in clinical wards without air filtration system are usually between 50 and 500 CFU x m^{-3} (Alberti et al., 2001; Brenier-Pinchart et al., 2009; Cooper et al., 2003; Curtis et al., 2005; Dassonville et al., 2008; Falvey & Streifel, 2007; Panagopoulou et al., 2002; Pini et al., 2004; Sautour et al., 2009). In clinical wards with air filtration, airborne fungal values are much lower ranging from 0 to 50 CFU x m^{-3}. Multiple factors may affect indoor concentrations, namely construction works, people's access to ward, the presence of additional protective barriers, and the implementation of water filtration (Anaissie et al., 2003; Araujo et al., 2008a; Carreras, 2006; Clark & de Calcina-Goff, 2009). In general, the major challenge in clinical wards is to prevent the entrance of fungi that are ubiquitous outside. By keeping lower fungal concentrations in areas around units with risk patients, it is also possible to find better air quality in clinical units.

Some outbreaks have been described following failures in air-filtration systems or by the presence of contaminated air-handling systems (Lutz et al., 2003; Muñoz et al., 2004). *A. fumigatus* was responsible for the fungal infections, in most cases. By repairing the air-filtration system and replacing old filters, it was possible to recover the unit and clinical department. The installation of portable HEPA filters may also be used in places where fixed HEPA filters are not possible to install. This strategy has been successfully described in some hospitals (Abdul Salam et al., 2010; Boswell & Fox, 2006; Engelhart et al., 2003). Verdenelli et al. (2003) have described that filters treated with antimicrobials displayed markedly less microbial colonization than untreated filters, resulting in less problems in the maintenance of filtration systems. However, this alternative is disputable, since it may enhance microbial resistance in clinical environments. The application of new materials for air filtration systems, such as silver- or cooper-impregnated materials, may represent an alternative to be tested (Clark & de Calcina-Goff, 2009).

In conclusion, regular and appropriate maintenance of air filtration systems is decisive for keeping excellent air quality in medical units. New engineering-made materials are expected in a near future and these hopefully will bring improvements in the air quality in hospital environments.

4.3 Recommendations for highly-protected medical environments

For highly-protected wards, a list of recommendations was issued in 2003 by the Center for Disease Control and Prevention (CDC) and Healthcare Infection Control Practices Advisory Committee (HICPAC) (Sehulster et al., 2003) and is currently available for free consulting (http://www.cdc.gov/mmwr/preview/mmwrhtml/rr5210a1.htm). In addition to the

recommendations already described in topic 4.2, routine hand hygiene taken by staff, patients, and visitors can prevent infections in health-care facilities (Carreras, 2006). Alcohol-based antiseptics (60-95 % alcohol) are recommended for hand washing. Similar procedures should be followed by people in contact with food, objects and other materials accepted in clinical units where risk patients are admitted. All objects admitted at units with risk patients should be kept clean and disinfected.

Wards are advised to be private (for single patients) and should be cleaned at least once a day and the high-touch surfaces cleaned much more frequently (Sehulster et al., 2003). Special attention should be given to bathrooms (carefully cleaned before patient's shower). Adequate temperature (22-24 °C) and humidity (30-60 %) should be maintained.

Other routes, like water, objects, beds (and pillows), plants or food, were shown to represent reservoirs of fungal agents and may be able to transfer conidia or hyphae to patients (Anaissie et al., 2003; Bouakline et al., 2000; Lass-Flörl et al., 2000; Potera, 2001; Warris et al., 2003; Woodcock et al., 2006). Hospital fabrics and plastics also act as reservoirs of medically important fungi. Some materials may influence the length of fungal survival (Neely & Orloff, 2001). Sodium hypochlorite is commonly used for cleaning walls and surfaces in wards, but other chemicals presenting fungicidal activity against most yeasts and moulds can be used as disinfectants (Araujo et al., 2006; Wilson et al., 2004). Chlorine is frequently recommended for routine treatment of the water and its recirculation in distribution systems is important (Sehulster et al., 2003). Alternatively, hot water can be maintained at temperatures ≥51 °C and cold water at <20 °C (a periodical increase to temperatures ≥66 °C is recommended in order to eliminate any microbial contamination). In order to prevent infections transmitted by contaminated foods, neutropenic patients are advised to consume low-microbial-content diets (Carreras, 2006; Remington & Schimpff, 1981). Abstention from pepper and other spices, tea, seeds, fruits and vegetables, which usually contain fungal conidia or hyphae (Bouakline et al., 2000), can restrict considerably patients' life and well being. Heating or irradiation (ultraviolet, gamma, microwave) can reduce or eradicate completely fungi present in water, food and some materials (Araujo et al., 2006; Gangneux et al., 2004).

Some cases of invasive aspergillosis have been associated with marijuana consumption. Therefore, smoking should be avoided by immunosuppressed patients (Verweij et al., 2000). Patients should remain isolated as long as their immune system is compromised and all treatments or diagnostic procedures should be conducted into the protected unit or ward. In occasions of leaving isolated wards, patients must wear facial mask (Raad et al., 2002).

Human movement may also be associated with an increase of indoor microbial contamination and the number of visitors should be restricted (Clark & de Calcina-Goff, 2009; Sehulster et al., 2003). Patients, visitors and unit staff should be continuous alerted to the procedures followed in restricted-environments. The implementation of educational programmes can result in a reduction of infections in clinical units (Jain et al., 2006).

Assessment of fungal genetic diversity may represent a useful tool for detecting the eventual presence of specific clonal populations in a clinical setting. *A. fumigatus* populations have been described as highly dynamic indoors, since new populations were found in just a few months (Araujo et al., 2010). Due to the high dispersion capability of moulds in indoor environments, more attention should be given to strains with increased pathogenic potential or reduced susceptibility to antifungal drugs. More attention will be given in coming years

to molecular epidemiological studies as they are becoming much cheaper and consistently more accepted and validated.

4.4 Prevention during hospital construction and renovation works

Construction and renovation of departments or hospitals have been carefully followed by medical administrations since these interventions can result in an increase of infections in clinical units. Inadequate ventilation and proximity to renovation and construction sites have been repeatedly implicated in the epidemiology of IFDs, mostly invasive aspergillosis (Cooper et al., 2003; Engelhart et al., 2003; Muñoz et al., 2004). Most hospitals surrounding construction sites are usually exposed to higher levels of airborne particles and additional protective measures should be followed. If large renovation works take place in units admitting risk patients, the patients should be transferred far from construction sites.

Airborne fungal levels are significantly higher when clinical units are subjected or close to construction or building demolition (Bouza et al., 2002; Cooper et al., 2003; Srinivasan et al., 2002). The adoption of all protected measures described in chapters 4.2 and 4.3 allows an efficient and protective environment to patients (Bouza et al., 2002; Cooper et al., 2003; Srinivasan et al., 2002). Additional attention should be given to the presence of barriers that limit the access of fungi and other particles to wards (doors that should be kept closed as long as possible, as well as tightly-closed windows). Different access routes for workmen, staff, patients and visitors have also been suggested (Cooper et al., 2003). Portable filtrations systems located in strategic places along the access to medical units can also be used (Abdul Salam et al., 2010; Engelhart et al., 2003). These systems are useful alternatives in emergencies following a complete breakdown of the fixed air filtration system (Sehulster et al., 2003). The use of facial masks by patients in close contact to risk environments can prevent IFDs (Raad et al., 2002).

Routine mycological assessment of the air and water should be carried out in hospitals, especially in areas where immunosuppressed patients are treated, aiming to detect anomalous situations and post alert warnings. These must be followed by a rapid intervention in order to avoid possible nosocomial infections. Such policies, in addition to educational programmes, are expected to result in a control and reduction of nosocomial infections and a promotion of patient's protection and well-being.

5. Conclusion and future perspectives

It is probably true to say that moulds cannot be completely eliminated from indoor environments. Normal buildings contain a diversity of materials and substrates that allow growth and sporulation of many species of fungi. Some strategies can be used to reduce indoor fungal load in wards receiving high-risk patients, namely by adding air filters and a positive air flow rate, by the presence of an anteroom, the use of protective clothes and of hair and shoe covers, the implementation of regular water filtration and the regular cleaning of walls and surfaces. The development of new engineering-made materials for air filtration systems may represent an alternative to be tested in a near future.

In hospitals or other institutions admitting immunosuppressed individuals, environmental reservoirs, namely air and water, should be routinely evaluated for the presence of fungi. Assessment of indoor fungal genetic diversity may represent a useful tool for studying the eventual presence of specific clones in clinical wards. Airborne fungal populations can

evolve fast, making difficult the study of the molecular epidemiology of fungal agents, but the use of intensive airborne sampling and genotype characterization can help to fulfil this desideratum. The era for characterization of hospital metagenome has been launched and fungal communities will certainly give us unexpected surprises and new perspectives regarding the quality of life for patients and staff at medical units.

6. References

Abdul Salam, Z. H.; Karlin, R. B.; Ling, M. L. & Yang, K. S. (2010). The impact of portable high-efficiency particulate air filters on the incidence of invasive aspergillosis in a large acute tertiary-care hospital. *American Journal of Infection Control,* 38, 4, e1-e7.

Alberti, C.; Bouakline, A.; Ribaud, P.; Lacroix, C.; Rousselot, P.; Leblanc, T.; Derouin, F. & *Aspergillus* Study Group. (2001). Relationship between environmental fungal contamination and the incidence of invasive aspergillosis in haematology patients. *Journal of Hospital Infection*, 48, 3, 198-206.

Anaissie, E. J.; Stratton, S. L.; Dignani, M. C.; Lee, C. K.; Summerbell, R. C.; Rex, J. H.; Monson, T. P. & Walsh, T. J. (2003). Pathogenic molds (including *Aspergillus* species) in hospital water distribution systems: a 3-year prospective study and clinical implications for patients with hematologic malignancies. *Blood*, 101, 7, 2542-2546.

Andersen, A. A. (1958). New sampler for the collection, sizing, and enumeration of viable airborne particles. *Journal of Bacteriology*, 76, 5, 471-484.

Angenent, L. T.; Kelley, S. T.; St Amand, A.; Pace, N. R. & Hernandez, M. T. (2005). Molecular identification of potential pathogens in water and air of a hospital therapy pool. *Proceedings of the National Academy of Sciences of the United States of America,* 102, 13, 4860-4865.

Araujo, R.; Amorim, A. & Gusmão, L. (2010). Genetic diversity of *Aspergillus fumigatus* in indoor hospital environments. *Medical Mycology: official publication of the International Society for Human and Animal Mycology*, doi: 10.3109/13693780903575360.

Araujo, R.; Cabral, J. P. & Rodrigues, A. G. (2008a). Air filtration systems and restrictive access conditions improve indoor air quality in clinical units: *Penicillium* as a general indicator of hospital indoor fungal levels. *American Journal of Infection Control,* 36, 2, 129-134.

Araujo, R.; Carneiro, A.; Costa-Oliveira, S.; Pina-Vaz, C.; Rodrigues, A. G. & Guimaraes, J. E. (2008b). Fungal infections after haematology unit renovation: evidence of clinical, environmental and economical impact. *European Journal of Haematology,* 80, 5, 436-443.

Araujo, R.; Gonçalves Rodrigues, A. & Pina-Vaz, C. (2006). Susceptibility pattern among pathogenic species of *Aspergillus* to physical and chemical treatments. *Medical Mycology: official publication of the International Society for Human and Animal Mycology*, 44, 5, 439-443.

Araujo, R. & Rodrigues, A. G. (2004). Variability of germinative potential among pathogenic species of *Aspergillus*. *Journal of Clinical Microbiology*, 42, 9, 4335-4337.

Bellanger, A. P.; Reboux, G.; Roussel, S.; Grenouillet, F.; Didier-Scherer, E.; Dalphin, J. C. & Millon, L. (2009). Indoor fungal contamination of moisture-damaged and allergic patient housing analysed using real-time PCR. *Letters in Applied Microbiology*, 49, 2, 260-266.

Bent, S. J.; Pierson, J. D.; Forney, L. J.; Danovaro, R.; Luna, G. M.; Dell'anno, A. & Pietrangeli, B. (2007). Measuring species richness based on microbial community fingerprints: the emperor has no clothes. *Applied and Environmental Microbiology, 73*, 7, 2399-2401.

Berthelot, P.; Loulergue, P.; Raberin, H.; Turco, M.; Mounier, C.; Tran Manh Sung, R.; Lucht, F.; Pozzetto, B. & Guyotat, D. (2006). Efficacy of environmental measures to decrease the risk of hospital-acquired aspergillosis in patients hospitalised in haematology wards. *Clinical Microbiology and Infection: the official publication of the European Society of Clinical Microbiology and Infectious Diseases, 12*, 8, 738-744.

Boswell, T. C. & Fox, P. C. (2006). Reduction in MRSA environmental contamination with a portable HEPA-filtration unit. *Journal of Hospital Infection*, 63, 1, 47-54.

Bouakline, A.; Lacroix, C.; Roux, N.; Gangneux, J. P. & Derouin, F. (2000). Fungal contamination of food in hematology units. *Journal of Clinical Microbiology*, 38, 11, 4272-4273.

Bourdillon, R. R.; Lidwell, O. M. & Thomas, J. C. (1941). A slit sampler for collecting and counting air-borne bacteria. *Journal of Hygiene*, 41, 2, 197-224.

Bouza, E.; Peláez, T.; Pérez-Molina, J.; Marín, M.; Alcalá, L.; Padilla, B.; Muñoz, P.; Adán, P.; Bové, B.; Bueno, M. J.; Grande, F.; Puente, D.; Rodríguez, M. P.; Rodríguez-Créixems, M.; Vigil, D.; Cuevas, O. & *Aspergillus* Study Team. (2002). Demolition of a hospital building by controlled explosion: the impact on filamentous fungal load in internal and external air. *Journal of Hospital Infection*, 52, 4, 234-242.

Brenier-Pinchart, M. P.; Lebeau, B.; Quesada, J. L.; Mallaret, M. R.; Borel, J. L.; Mollard, A.; Garban, F.; Brion, J. P.; Molina, L.; Bosson, J. L.; Cahn, J. Y.; Grillot, R. & Pelloux, H. (2009). Influence of internal and outdoor factors on filamentous fungal flora in hematology wards. *American Journal of Infection Control, 37*, 8, 631-637.

Burge, H. A. & Solomon, W. R. (1987). Sampling and analysis of biological aerosols. *Atmospheric Environment*, 21, 2, 451-456.

Carreras, E. (2006). Preventing exposure to moulds. *Clinical Microbiology and Infection: the official publication of the European Society of Clinical Microbiology and Infectious Diseases, 12*, 77-83.

Chao, H. J.; Miltom, D. K.; Schwartz, J. & Burge, H. A. (2001). Dustborne fungi in large office buildings. *Mycopathologia, 154*, 2, 93-106.

Chapman, M. D.; Tsay, A. & Vailes, L. D. (2001). Home allergen monitoring and control--improving clinical practice and patient benefits. *Allergy*, 56, 7, 604-610.

Claeson, A.-S.; Levin, J.-O.; Blomquist, G. & Sunesson, A.-L. (2002). Volatile metabolites from microorganisms grown on humid building materials and synthetic media. *Journal of Environmental Monitoring*, 4, 5, 667-672.

Clark, R. P. & de Calcina-Goff, M. L. (2009). Some aspects of the airborne transmission of infection. *Journal of the Royal Society, Interface / the Royal Society, 6*, 6, S767-S782.

Cooper, E. E.; O'Reilly, M. A.; Guest, D. I. & Dharmage, S. C. (2003). Influence of building construction work on *Aspergillus* infection in a hospital setting. *Infection Control and Hospital Epidemiology: the official journal of the Society of Hospital Epidemiologists of America, 24*, 7, 472-476.

Cortez, K. J.; Roilides, E.; Quiroz-Telles, F.; Meletiadis, J.; Antachopoulos, C.; Knudsen, T.; Buchanan, W.; Milanovich, J.; Sutton, D. A.; Fothergill, A.; Rinaldi, M. G.; Shea, Y. R.; Zaoutis, T.; Kottilil, S. & Walsh, T. J. (2008). Infections caused by *Scedosporium* spp. *Clinical Microbiology Reviews,* 21, 1, 157-197.

Crameri, R. & Blaser, K. (2002). Allergy and immunity to fungal infections and colonization. *The European Respiratory Journal: official journal of the European Society for Clinical Respiratory Physiology*, 19, 1, 151-157.

Curtis, L.; Cali, S.; Conroy, L.; Baker, K.; Ou, C. H.; Hershow, R.; Norlock-Cruz, F. & Scheff, P. (2005). *Aspergillus* surveillance project at a large tertiary-care hospital. *Journal of Hospital Infection*, 59, 3, 188-196.

Dacarro, C.; Picco, A. M.; Grisoli, P. & Redolfi, M. (2003). Determination of aerial microbiological contamination in scholastic sports environment. *Journal of Applied Microbiology*, 95, 5, 904-912.

Dassonville, C.; Demattei, C.; Detaint, B.; Barral, S.; Bex-Capelle, V. & Momas, I. (2008). Assessment and predictors determination of indoor airborne fungal concentrations in Paris newborn babies' homes. *Environmental research,* 108, 1, 80-85.

Davies, R. R. (1971). Air sampling for fungi, pollens and bacteria, In: *Methods in Microbiology*, *volume 4*, Booth. C., 367-404, Academic Press, London.

De La Rosa, G. R.; Champlin, R. E. & Kontoyiannis, D. P. (2002). Risk factors for the development of invasive fungal infections in allogeneic blood and marrow transplant recipients. *Transplant Infectious Disease: an official journal of the Transplantation Society,* 4, 1, 3-9.

Douwes, J. (2009). Building dampness and its effect on indoor exposure to biological and non-biological pollutants, In: *Dampness and Mould*, 7-29, WHO Europe, ISBN 978-92-890-4168-3, Copenhagen.

Eckmanns, T.; Rüden, H. & Gastmeier P. (2006). The influence of high-efficiency particulate air filtration on mortality and fungal infection among highly immunosuppressed patients: a systematic review. *The Journal of Infectious Diseases,* 193, 10, 1408-1418.

Eduard, W. & Heederik, D. (1998). Methods for quantitative assessment of airborne levels of noninfectious microorganisms in highly contaminated work environments. *Journal of the American Industrial Hygiene Association*, 59, 2, 113-127.

Eduard, W. (2009). Fungal spores: a critical review of the toxicological and epidemiological evidence as a basis for occupational exposure limit setting. *Critical Reviews in Toxicology*, 39, 10, 799-864.

Engelhart, S.; Hanfland, J.; Glasmacher, A.; Krizek, L.; Schmidt-Wolf, I. G. & Exner, M. (2003). Impact of portable air filtration units on exposure of haematology-oncology patients to airborne *Aspergillus fumigatus* spores under field conditions. *Journal of Hospital Infection*, 54, 4, 300-304.

Falvey, D. G. & Streifel, A. J. (2007). Ten-year air sample analysis of *Aspergillus* prevalence in a university hospital. *Journal of Hospital Infection*, 67, 1, 35-41.

Fischer, G.; Schwalbe, R.; Möller, M.; Ostrowski, R. & Dott, W. (1999). Species-specific production of microbial volatile organic compounds (MVOC) by airborne fungi from a composto facility. *Chemosphere*, 39, 5, 795-810.

Fischer, G.; Müller, T.; Schwalbe, R.; Ostrowski, R. & Dott, W. (2000). Exposure to airborne fungi, MVOC and mycotoxins in biowaste-handling facilities. *International Journal of Hygiene and Environmental Health*, 203, 2, 97-104.

Flannigan, B. (1997). Air sampling for fungi in indoor environments. *Journal of Aerosol Science*, 28, 3, 381-392.

Flappan, S. M.; Portnoy, J.; Jones, P. & Barnes, C. (1999). Infant pulmonary hemorrhage in a suburban home with water damage and mold (*Stachybotrys atra*). *Environmental Health Perspectives*, 107, 11, 927-930.

Fridkin, S. K. & Jarvis, W. R. (1996). Epidemiology of nosocomial fungal infections. *Clinical Microbiology Reviews,* 9, 4, 499-511.

Fröhlich-Nowoisky, J.; Pickersgill, D. A.; Després, V. R. & Pöschl, U. (2009). High diversity of fungi in air particulate matter. *Proceedings of the National Academy of Sciences of the United States of America,* 106, 31, 12814-12819.

Gangneux, J. P.; Noussair, L.; Bouakline, A.; Roux, N.; Lacroix, C. & Derouin, F. (2004). Experimental assessment of disinfection procedures for eradication of *Aspergillus fumigatus* in food. *Blood*, 104, 7, 2000-2002.

Górny, R. L.; Reponen, T.; Willeke, K.; Schmechel, D.; Robine, E.; Boissier, M. & Grinshpun, S. A. (2002). Fungal fragments as indoor air biocontaminants. *Applied and Environmental Microbiology*, 68, 7, 3522-3531.

Green, B. J.; Schmechel, D.; Sercombe, J. K. & Tovey, E. R. (2005a). Enumeration and detection of aerosolized *Aspergillus fumigatus* and *Penicillium chrysogenum* conidia and hyphae using a novel double immunostaining technique. *Journal of Immunological Methods*, 307, 1-2, 127-134.

Green, B. J.; Sercombe, J. K. & Tovey, E. R. (2005b). Fungal fragments and undocumented conidia function as new aeroallergen sources. *The Journal of Allergy and Clinical Immunology*, 115, 5, 1043-1048.

Green, B. J.; Tovey, E. R.; Sercombe, J. K.; Blachere, F. M.; Beezhold, D. H. & Schmechel, D. (2006). Airborne fungal fragments and allergenicity. *Medical Mycology: official publication of the International Society for Human and Animal Mycology*, 44, Suppl 1, S245-S255.

Haugland, R. A.; Varma, M.; Wymer, L. J. & Vesper, S. J. (2004). Quantitative PCR analysis of selected *Aspergillus*, *Penicillium* and *Paecilomyces* species. *Systematic and Applied Microbiology*, 27, 2, 198-210.

Henningson, E. W. & Ahlberg, M. S. (1994). Evaluation of microbiological aerosol samplers: a review. *Journal of Aerosol Science,* 25, 8, 1459-1492.

Hintikka, E.-L. & Nikulin, M. (1998). Airborne mycotoxins in agricultural and indoor environments. *Indoor Air*, 8, suppl. 4, 66-70.

Hirst, J. M. (1952). An automatic volumetric spore trap. *The Annals of Applied Biology*, 39, 2, 257-265.

Horner, W. E.; Worthan, A. G. & Morey, P. R. (2004). Air-and dustborne mycoflora in houses free of water damage and fungal growth. *Applied and Environmental Microbiology*, 70, 11, 6394-6400.

Houba, R.; Heederik, D. & Doekes, G. (1998). Wheat sensitization and work-related symptoms in the baking industry are preventable. An epidemiologic study. *American Journal of Respiratory and Critical Care Medicine*, 158, 5 Pt 1, 1499-1503.

Jain, M.; Miller, L.; Belt, D.; King, D. & Berwick, D. M. (2006). Decline in ICU adverse events, nosocomial infections and cost through a quality improvement initiative focusing on teamwork and culture change. *Quality & Safety in Health Care,* 15, 4, 235-239.

Jantunen, M.; Jaakola, J. J. K. & Krzyzanowski, M. (1997). *Assessment of exposure to indoor air pollutants,* WHO Regional Publications, European Series, no. 78, Copenhagen.

Jo, W.-K. & Seo, Y.-J. (2005). Indoor and outdoor bioaerosol levels at recreation facilities, elementary schools, and homes. *Chemosphere*, 61, 11, 1570-1579.

Kildesø, J.; Würtz, H.; Nielsen, K. F.; Kruse, P.; Wilkins, K.; Thrane, U.; Gravesen, S.; Nielsen, P. A. & Schneider, T. (2003). Determination of fungal spore release from wet building materials. *Indoor Air*, 13, 2, 148-155.

Lass-Flörl, C.; Rath, P.; Niederwieser, D.; Kofler, G.; Würzner, R.; Krezy, A. & Dierich, M. P. (2000). *Aspergillus terreus* infections in haematological malignancies: molecular epidemiology suggests association with in-hospital plants. *Journal of Hospital Infection*, 46, 1, 31-35.

Lee, S. H.; Lee, H. J.; Kim, S. J.; Lee, H. M.; Kang, H. & Kim, Y. P. (2010). Identification of airborne bacterial and fungal community structures in an urban area by T-RFLP analysis and quantitative real-time PCR. *Science of the Total Environment*, 408, 6, 1349-1357.

Lignell, U.; Meklin, T.; Rintala, H.; Hyvärinen, A.; Vepsäläinen, A.; Pekkanen, J. & Nevalainen, A. (2008). Evaluation of quantitative PCR and culture methods for detection of house dust fungi and streptomycetes in relation to moisture damage of the house. *Letters in Applied Microbiology*, 47, 4, 303-308.

Lupetti, A.; Tavanti, A.; Davini, P.; Ghelardi, E.; Corsini, V.; Merusi, I.; Boldrini, A.; Campa, M. & Senesi, S. (2002). Horizontal transmission of *Candida parapsilosis* candidemia in a neonatal intensive care unit. *Journal of Clinical Microbiology*, 40, 7, 2363-2369.

Lutz, B. D.; Jin, J.; Rinaldi, M. G.; Wickes, B. L. & Huycke, M. M. (2003). Outbreak of invasive *Aspergillus* infection in surgical patients, associated with a contaminated air-handling system. *Clinical Infectious Diseases: an official publication of the Infectious Diseases Society of America*, 37, 6, 786-793.

Malligo, J. E. & Idoine, L. S. (1964). Single-stage impaction device for particle sizing biological aerosols. *Applied Microbiology*, 12, 1, 32-36.

Martinez, K. F.; Rao, C. Y. & Burton, N. C. (2004). Exposure assessment and analysis for biological agents. *Grana*, 43, 4, 193-208.

May, K. R. & Harper, G. J. (1957). The efficiency of various liquid impinger samplers in bacterial aerosols. *British Journal of Industrial Medicine*, 14, 4, 287-297.

May, K. R. (1945). The cascade impactor: an instrument for sampling coarse aerosols. *Journal of Scientific Instruments*, 22, 10, 187-195.

May, K. R. (1966). Multistage liquid impinger. *Bacteriological Reviews*, 30, 3, 559-570.

Meklin, T.; Haugland, R. A.; Reponen, T.; Varma, M.; Lummus, Z.; Bernstein, D.; Wymer, L. J. & Vesper, S. J. (2004). Quantitative PCR analysis of house dust can reveal abnormal mold conditions. *Journal of Environmental Monitoring*, 6, 7, 615-620.

Mendell, M. A.; Mirer, A. G.; Cheung, K.; Douwes, J.; Sigsaard, T.; Bønløkke, J.; Meyer, H. W.; Hirvonen, M.-R. & Roponen, M. (2009). Building dampness and its effect on indoor exposure to biological and non-biological plollutants, In: *Dampness and Mould*, 63-92, WHO Europe, ISBN 978-92-890-4168-3, Copenhagen.

Menotti, J.; Waller, J.; Meunier, O.; Letscher-Bru, V.; Herbrecht, R. & Candolfi, E. (2005). Epidemiological study of invasive pulmonary aspergillosis in a haematology unit by molecular typing of environmental and patient isolates of *Aspergillus fumigatus*. *Journal of Hospital Infection*, 60, 1, 61-68.

Morrison, J.; Yang, C.; Lin, K. T.; Haugland, R. A.; Neely, A. N. & Vesper, S. J. (2004). Monitoring *Aspergillus* species by quantitative PCR during construction of a multi-storey hospital building. *Journal of Hospital Infection*, 57, 1, 85-87.

Moularat, S.; Robine, E.; Ramalho, O. & Oturan, M. A. (2008a). Detection of fungal development in a closed environment through the identification of specific VOC: demonstration of a specific VOC fingerprint for fungal development. *Science of the Total Environment*, 407, 1, 139-146.

Moularat, S.; Robine, E.; Ramalho, O. & Oturan, M. A. (2008b). Detection of fungal development in closed spaces through the determination of specific chemical targets. *Chemosphere*, 72, 2, 224-232.

Muñoz, P.; Guinea, J.; Peláez, T.; Durán, C.; Blanco, J. L. & Bouza, E. (2004). Nosocomial invasive aspergillosis in a heart transplant patient acquired during a break in the HEPA air filtration system. *Transplant Infectious Disease: an official journal of the Transplantation Society*, 6, 1, 50-54.

Neely, A. N. & Orloff, M. M. (2001). Survival of some medically important fungi on hospital fabrics and plastics. *Journal of Clinical Microbiology*, 39, 9, 3360-3361.

Newson, R.; Strachan, D.; Corden, J. & Millington, W. (2000). Fungal and other spore counts as predictors of admissions for asthma in the Trent region. *Occupational and Environmental Medicine*, 57, 11, 786-792.

Nielsen, K. F. (2003). Mycotoxin production by indoor molds. *Fungal Genetics and Biology*, 39, 2, 103-177.

Nieminen, S. M.; Kärki, R.; Auriola, S.; Toivola, M.; Laatsch, H.; Laatikainen, R.; Hyvärinen, A. & von Wright, A. (2002). Isolation and identification of *Aspergillus fumigatus* mycotoxins on growth medium and some building materials. *Applied and Environmental Microbiology*, 68, 10, 4871-4875.

Pagano, L.; Caira, M.; Candoni, A.; Offidani, M.; Fianchi, L.; Martino, B.; Pastore, D.; Picardi, M.; Bonini, A.; Chierichini, A.; Fanci, R.; Caramatti, C.; Invernizzi, R.; Mattei, D.; Mitra, M. E.; Melillo, L.; Aversa, F.; Van Lint, M. T.; Falcucci, P.; Valentini, C. G.; Girmenia, C. & Nosari, A. (2006). The epidemiology of fungal infections in patients with hematologic malignancies: the SEIFEM-2004 study. *Haematologica*, 91, 8, 1068-1075.

Panagopoulou, P.; Filioti, J.; Petrikkos, G.; Giakouppi, P.; Anatoliotaki, M.; Farmaki, E.; Kanta, A.; Apostolakou, H.; Avlami, A.; Samonis, G. & Roilides, E. (2002). Environmental surveillance of filamentous fungi in three tertiary care hospitals in Greece. *Journal of Hospital Infection*, 52, 3, 185-191.

Pasanen, A.-L.; Pasanen, P.; Jantunen, M. J. & Kalliokski, P. (1991). Significance of air humidity for fungal spore release into the air. *Atmospheric Environment*, 25, 2, 459-462.

Pasanen, A.-L.; Heinonen-Tanski, H.; Kalliokoski, P. & Jantunen, M. J. (1992a). Fungal microcolonies on indoor surfaces – an explanation for the base-level fungal spore counts in indoor air. *Atmospheric Environment*, 26B, 1, 117-120.

Pasanen, A.-L.; Juutinen, T.; Jantunen, M. J. & Kalliokoski, P. (1992b). Occurrence and moisture requirements of microbial growth in building materials. *International Biodeterioration & Biodegradation*, 30, 4, 273-283.

Pasquarella, C.; Pitzurra, O. & Savino, A. (2000). The index of microbial air contamination. *Journal of Hospital Infection*, 46, 4, 241-256.

Peat, J. K. & Li, J. (1999). Reversing the trend: reducing the prevalence of asthma. *The Journal of Allergy and Clinical Immunology*, 103, 1 Pt 1, 1-10.

Pegues, D. A.; Lasker, B. A.; McNeil, M. M.; Hamm, P. M.; Lundal, J. L. & Kubak, B. M. (2002). Cluster of cases of invasive aspergillosis in a transplant intensive care unit: evidence of person-to-person airborne transmission. *Clinical Infectious Diseases: an official publication of the Infectious Diseases Society of America*, 34, 3, 412-416.

Pietarinen, V. M.; Rintala, H.; Hyvärinen, A.; Lignell, U.; Kärkkäinen, P. & Nevalainen, A. (2008). Quantitative PCR analysis of fungi and bacteria in building materials and comparison to culture-based analysis. *Journal of Environmental Monitoring*, 10, 5, 655-663.

Pini, G.; Donato, R.; Faggi, E. & Fanci, R. (2004). Two years of a fungal aerobiocontamination survey in a Florentine haematology ward. *European Journal of Epidemiology,* 19, 7, 693-698.

Portnoy, J. M.; Barnes, C. S. & Kennedy, K. (2004). Sampling for indoor fungi. *Current Reviews of Allergy and Clinical Immunology*, 113, 2, 189-198.

Potera, C. (2001). Clothing spreads spores. *Environmental Health Perspectives*, 109, 8, A365.

Raad, I.; Hanna, H.; Osting, C.; Hachem, R.; Umphrey, J.; Tarrand, J.; Kantarjian, H. & Bodey, G. P. (2002). Masking of neutropenic patients on transport from hospital rooms is associated with a decrease in nosocomial aspergillosis during construction. *Infection Control and Hospital Epidemiology: the official journal of the Society of Hospital Epidemiologists of America,* 23, 1, 41-43.

Radin, R. C.; Greenberger, P. A.; Patterson, R. & Ghory, A. (1983). Mould counts and exacerbations of allergic bronchopulmonary aspergillosis. *Clinical Allergy,* 13, 3, 271-275.

Ranjard, L.; Poly, F.; Lata, J. C.; Mougel, C.; Thioulouse, J. & Nazaret, S. (2001). Characterization of bacterial and fungal soil communities by automated ribosomal intergenic spacer analysis fingerprints: biological and methodological variability. *Applied and Environmental Microbiology,* 67, 10, 4479-4487.

Rea, W. J.; Didriksen, N.; Simon, T. R.; Pan, Y.; Fenyves, E. J. & Griffiths, B. (2003). Effects of toxic exposure to molds and mycotoxins in building-related illness. *Archives of Environmental Health*, 58, 7, 399-405.

Remington, J. S. & Schimpff, S. C. (1981). Occasional notes. Please don't eat the salads. *The New England Journal of Medicine*, 304, 7, 433-435.

Ren, P.; Ahearn, D. G. & Crow, S. A. (1999). Comparative study of *Aspergillus* mycotoxin production on enriched media and construction material. *Journal of Industrial Microbiology & Biotechnology*, 23, 3, 209-213.

Reponen, T.; Seo, S.-C.; Grimsley, F.; Lee, T.; Crawford, C. & Grinshpun, S. A. (2007). Fungal fragments in moldy houses: a field study in homes in New Orleans and Southern Ohio. *Atmospheric Environment*, 41, 37, 8140-8149.

Richardson, G.; Eick, S. & Jones, R. (2005). How is the indoor environment related to asthma?: literature review. *Journal of Advanced Nursing*, 52, 3, 328-339.

Sautour, M.; Sixt, N.; Dalle, F.; L'Ollivier, C.; Fourquenet, V.; Calinon, C.; Paul, K.; Valvin, S.; Maurel, A.; Aho, S.; Couillault, G.; Cachia, C.; Vagner, O.; Cuisenier, B.; Caillot, D. & Bonnin, A. (2009). Profiles and seasonal distribution of airborne fungi in indoor and outdoor environments at a French hospital. *Science of the Total Environment*, 407, 12, 3766-3771.

Schleibinger, H.; Laussmann, D.; Brattig, C.; Mangler, M.; Eis, D. & Ruden, H. (2005). Emission patterns and emission rates of MVOC and the possibility for predicting hidden mold damage? *Indoor Air*, 15, Suppl 9, 98-104.

Schuchardt, S. & Kruse, H. (2009). Quantitative volatile metabolite profiling of common indoor fungi: relevancy for indoor air analysis. *Journal of Basic Microbiology,* 49, 4, 350-362.

Schütte, U. M.; Abdo, Z.; Bent, S. J.; Shyu, C.; Williams, C. J.; Pierson, J. D. & Forney, L. J. (2008). Advances in the use of terminal restriction fragment length polymorphism (T-RFLP) analysis of 16S rRNA genes to characterize microbial communities. *Applied Microbiology and Biotechnology,* 80, 3, 365-380.

Sehulster, L.; Chinn, R. Y.; CDC & HICPAC. (2003). Guidelines for environmental infection control in health-care facilities. Recommendations of CDC and the Healthcare Infection Control Practices Advisory Committee (HICPAC). *MMWR. Recommendations and Reports: Morbidity and mortality weekly report. Recommendations and reports / Centers for Disease Control,* 52, RR-10, 1-42.

Seo, S.-C.; Reponen, T.; Levin, L. & Grinshpun, S. A. (2009). Size-fractionated (1→3)-β-D-glucan concentrations aerosolized from different moldy building materials. *Science of the Total Environment*, 407, 2, 806-814.

Shelton, B. G.; Kirkland, K. H.; Flanders, W. D. & Morris, G. K. (2002). Profiles of airborne fungi in building and outdoor environments in the United States. *Applied and Environmental Microbiology*, 68, 4, 1743-1753.

Sherertz, R. J.; Belani, A.; Kramer, B. S.; Elfenbein, G. J.; Weiner, R. S.; Sullivan, M. L.; Thomas, R. G. & Samsa, G. P. (1987). Impact of air filtration on nosocomial *Aspergillus* infections. Unique risk of bone marrow transplant recipients. *The American Journal of Medicine,* 83, 4, 709-718.

Sipsas, N. V. & Kontoyiannis, D. P. (2008). Occupation, lifestyle, diet, and invasive fungal infections. *Infection*, 36, 6, 515-525.

Srinivasan, A.; Beck, C.; Buckley, T.; Geyh, A.; Bova, G.; Merz, W. & Perl, T. M. (2002). The ability of hospital ventilation systems to filter *Aspergillus* and other fungi following a building implosion. *Infection Control and Hospital Epidemiology: the official journal of the Society of Hospital Epidemiologists of America,* 23, 9, 520-524.

Stetzenbach, L. D.; Buttner, M. P. & Cruz, P. (2004). Detection and enumeration of airborne biocontaminants. *Current Opinion in Biotechnology*, 15, 3, 170-174.

Stevens, D. A.; Moss, R. B.; Kurup, V. P.; Knutsen, A. P.; Greenberger, P.; Judson, M. A.; Denning, D. W.; Crameri, R.; Brody, A. S.; Light, M.; Skov, M.; Maish, W.; Mastella, G. & Participants in the Cystic Fibrosis Foundation Consensus Conference. (2003). Allergic bronchopulmonary aspergillosis in cystic fibrosis--state of the art: Cystic Fibrosis Foundation Consensus Conference. *Clinical Infectious Diseases: an official publication of the Infectious Diseases Society of America*, 37, Suppl 3, S225-S264.

Venter, J. C.; Remington, K.; Heidelberg, J. F.; Halpern, A. L.; Rusch, D.; Eisen, J. A.; Wu, D.; Paulsen, I.; Nelson, K. E.; Nelson, W.; Fouts, D. E.; Levy, S.; Knap, A. H.; Lomas, M. W.; Nealson, K.; White, O.; Peterson, J.; Hoffman, J.; Parsons, R.; Baden-Tillson, H.; Pfannkoch, C.; Rogers, Y. H. & Smith, H. O. (2004). Environmental genome shotgun sequencing of the Sargasso Sea. *Science*, 304, 5667, 66-74.

Verdenelli, M. C.; Cecchini, C.; Orpianesi, C.; Dadea, G. M. & Cresci, A. (2003). Efficacy of antimicrobial filter treatments on microbial colonization of air panel filters. *Journal of Applied Microbiology,* 94, 1, 9-15.

Verhoeff, A. (1993). *Biological particles in indoor environments*, European collaborative action, Indoor Air Quality & its impact on man, report no. 12, EUR 14988 EN, Commission of The European Communities, Luxembourg.

Verweij, P. E.; Kerremans, J. J.; Voss, A. & Meis, J. F. (2000). Fungal contamination of tobacco and marijuana. *JAMA: the Journal of the American Medical Association,* 284, 22, 2875.

Vonberg, R. P. & Gastmeier, P. (2006). Nosocomial aspergillosis in outbreak settings. *Journal of Hospital Infection*, 63, 3, 246-254.

Vos, M. C.; Endtz, H. P.; Horst-Kreft, D.; Doorduijn, J.; Lugtenburg, E.; Verbrugh, H. A.; Löwenberg, B.; de Marie, S.; van Pelt, C. & van Belkum, A. (2006). *Candida krusei* transmission among hematology patients resolved by adapted antifungal prophylaxis and infection control measures. *Journal of Clinical Microbiology*, 44, 3, 1111-1114.

Warris, A.; Klaassen, C. H.; Meis, J. F.; De Ruiter, M. T.; De Valk, H. A.; Abrahamsen, T. G.; Gaustad, P. & Verweij, P. E. (2003). Molecular epidemiology of *Aspergillus fumigatus* isolates recovered from water, air, and patients shows two clusters of genetically distinct strains. *Journal of Clinical Microbiology*, 41, 9, 4101-4106.

Wilson, S. C.; Brasel, T. L.; Carriker, C. G.; Fortenberry, G. D.; Fogle, M. R.; Martin, J. M.; Wu, C.; Andriychuk, L. A.; Karunasena, E. & Straus, D. C. (2004). An investigation into techniques for cleaning mold-contaminated home contents. *Journal of Occupational and Environmental Hygiene,* 1, 7, 442-447.

Woodcock, A. A.; Steel, N.; Moore, C. B.; Howard, S. J.; Custovic, A. & Denning, D. W. (2006). Fungal contamination of bedding. *Allergy*, 61, 1, 140-142.

Edited by Ashok Kumar

Air pollution is about five decades or so old field and continues to be a global concern. Therefore, the governments around the world are involved in managing air quality in their countries for the welfare of their citizens. The management of air pollution involves understanding air pollution sources, monitoring of contaminants, modeling air quality, performing laboratory experiments, the use of satellite images for quantifying air quality levels, indoor air pollution, and elimination of contaminants through control. Research activities are being performed on every aspect of air pollution throughout the world, in order to respond to public concerns. The book is grouped in five different sections. Some topics are more detailed than others. The readers should be aware that multi-authored books have difficulty maintaining consistency. A reader will find, however, that each chapter is intellectually stimulating. Our goal was to provide current information and present a reasonable analysis of air quality data compiled by knowledgeable professionals in the field of air pollution.

Photo by sinemaslow / iStock

IntechOpen